Boron-Containing Aromatics as Communicating and Communicative Units in π-Conjugated Systems

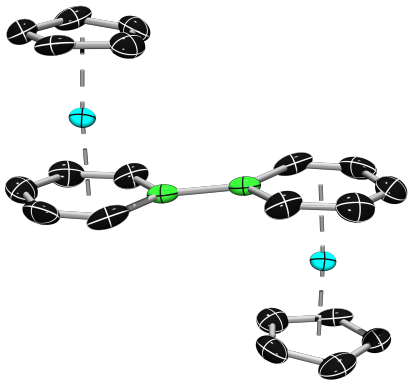

Bret B. Macha

Dissertation zur Erlangung des naturwissenschaftlichen Doktorgrades der Julius-Maximilians-Universität Würzburg

Mai 2016

Boron-Containing Aromatics as Communicating and Communicative Units in π-Conjugated Systems

Dissertation zur Erlangung des naturwissenschaftlichen Doktorgrades
der
Julius-Maximilians-Universität Würzburg

vorgelegt von

Bret B. Macha
aus Hungerford, Texas
Vereinigte Staaten von Amerika
Würzburg 2016

Eingereicht bei der Fakultät für Chemie und Pharmazie am .....

Gutachter der schriftlichen Arbeit:

1. Gutachter: Prof. Dr. Holger Braunschweig
2. Gutachter: Prof. Dr. Todd B. Marder

Prüfer des öffentlichen Promotionskolloquiums:

1. Prüfer: Prof. Dr. Holger Braunschweig
2. Prüfer: Prof. Dr. Todd B. Marder
3. Prüfer: Prof. Dr. Matthias Lehmann

Datum des öffentlichen Promotionskolloquiums: .....

Doktorurkunde ausgehändigt am: .....

For Leroy and Ann Macha

Consider your origin. You were not formed to live like brutes, but to follow virtue and knowledge.

The Divine Comedy
Dante Alighieri

The experiments within this presented work were carried out from 15.02.2012 to 1.05.2016 at the Institute of Inorganic Chemistry of the Julius-Maximilians-Universität Würzburg under the guidance of Prof. Dr. Holger Braunschweig.

Research presented in this thesis was subsequently published within the following publications:

Cover Picture: Platinum *trans*-Bis(borirene) Complexes Displaying Coplanarity and Communication Across a Platinum Metal Center

H. Braunschweig, A. Damme, R. D. Dewhurst, H. Kelch, B. B. Macha, K. Radacki, A. Vargas, Q. Ye

Chem. Eur. J. **2015**, *21*, 2273.

Author Profile: Platinum *trans*-Bis(borirene) Complexes Displaying Coplanarity and Communication Across a Platinum Metal Center

H. Braunschweig, A. Damme, R. D. Dewhurst, H. Kelch, B. B. Macha, K. Radacki, A. Vargas, Q. Ye

Chem. Eur. J. **2015**, *21*, 2277.

Platinum *trans*-Bis(borirene) Complexes Displaying Coplanarity and Communication Across a Platinum Metal Center

H. Braunschweig, A. Damme, R. D. Dewhurst, H. Kelch, B. B. Macha, K. Radacki, A. Vargas, Q. Ye

Chem. Eur. J. **2015**, *21*, 2377–2386.

A Bimetallic 1,1'-Bis(boratabenzene) Complex: Unprecedented Intramolecular Metal-Metal Communication Through a B–B Bond

H. Braunschweig, S. Demeshko, W. C. Ewing, I. Krummenacher, B. B. Macha, J. D. Mattock, F. Meyer, J. Mies, M. Schäfer, A. Vargas

Angew. Chem. Int. Ed. **2016**, *55,* 7708–7711.

Ein Zweikerniger 1,1'-Bis(boratabenzol)-Komplex: Beispiellose Intramolekulare Metall-Metall-Kommunikation durch eine B–B-Bindung

H. Braunschweig, S. Demeshko, W. C. Ewing, I. Krummenacher, B. B. Macha, J. D. Mattock, F. Meyer, J. Mies, M. Schäfer, A. Vargas

Angew. Chem. **2016**, *128,* 7839–7842.

Copyright permission was obtained to reproduce diagrams and figures from the following sources:

Chem. Eur. J. **2015**, *21*, 2273. (License #3866451506795)

Chem. Eur. J. **2015**, *21*, 2277. (License #3866460161226)

Chem. Eur. J. **2015**, *21*, 2377–2386. (License #3866460237753)

Figure 1 from the article: J. P. Carpenter, C. M. Lukehart, *Inorg. Chim. Acta* **1991**, *190*, 7–10,[421] was used in this thesis (Figure 3-11) because the full set of X-ray structural data deposited in the CCDC was not available. (License #3866460877179)

Acknowledgements

First and foremost, I would like to thank Prof. Dr. Holger Braunschweig for providing the best work environment any chemist could ever ask for. Throughout my time in Germany and during the period of my doctoral research he has never failed to be a dependable educator, guide, and inspiration for me. I would also like to thank my previous professors at Texas A&M University (USA) and Université Laval (Canada), especially Profs. Drs. François Gabbaï, John Gladysz, and Frédéric-Georges Fontaine as well as the late Prof. Dr. John Hogg.

I would secondly like to thank the European Research Council for their generous award of an advanced grant for the "borylenefun" project as well as the government of Bavaria and the Julius-Maximilians-Universität Würzburg for providing financial support for the research presented in this thesis. A tremendous debt of gratitude is owed to the Julius-Maximilians-Universität Würzburg Institut für Anorganische Chemie building maintenance staff (Alfred Schertzer, Manfred Reinhart, Berthold Fertig, Liselotte Michels, Gertrud Wunderling, and Christoph Mahler) as well as the secretarial staff (Birgit Zepke, Sabine Timmroth, and Cornelia Walter) for their help during my time in the laboratory. For technical help, I would like to graciously thank all of the members of the Institut für Anorganische Chemie research staff especially Dr. Rüdiger Bertermann and Marie-Luise Schäfer for their aid in NMR spectroscopy. I would also specifically like to thank Dr. Krzysztof Radacki and Marius Schäfer for their help interpreting data from X-ray crystallography. Thanks are also due to Dr. Alfredo Vargas, Prof. Dr. Ashwini K. Phukan and James D. Mattock for their work with DFT calculations.

I would like to especially thank all the Braunschweig group technicians for their work and patience with me during my study at the university. It is a well-known fact that nothing in the lab could be accomplished without the work of Kai Hammond, Sascha Stellwag-Konertz, Christine Werner, and Felix Weißenberger. I would also like to thank the senior scientists (Drs. Justin Wolf and Carsten Kollann) and postdoctoral researchers of our group (Drs. Jan Mies and William C. Ewing) for their highly useful discussion and suggestions made during my research project.

To the members of Lab 417 (Christina Claes and senior scientists Drs. Rian D. Dewhurst and Ivo Krummenacher), who I had the utmost pleasure in pestering during the completion phase of my thesis, I cannot thank you enough. It has been an absolute blast coming to "work" day in and day out. All of the suggestions and

corrections given during this time have made my thesis something I know I will be proud of for the rest of my life. I also would like to thank you all for the help in preparation and writing of my manuscripts and data interpretation during the completion of my doctoral projects.

I would also like to thank all the members (past and present) of the Braunschweig group with whom I have had such a great time working with. I would especially like to thank my laboratory colleagues (Lab 221): Dr. Bernd Pfaffinger, Stefan Ullrich, Dominic Auerhammer, Jonas Müssig, and Anna Rempel for many wonderful memories and discussions concerning mutual research projects and interests. I would also like to thank my former Master's student Falco Claus for his work on the boratabenzene project. My time in Germany was short, but the memories were profound! I wish you all the best and may our paths cross soon in the future.

Special thanks are also due to all the people who have contributed as authors on the publications reported in this thesis. During my doctoral studies I have relied upon the help of Hauke Kelch and Drs. Alex Damme, and Qing Ye for key spectroscopic interpretation and work. I would also like to thank the collaborative efforts of the group of Prof. Dr. Franc Meyer, especially the work of Dr. Serhiy Demeshko.

Finally, I would like to take some time to thank the members of my family who have proven an ever-reliable source of inspiration and guidance for me while living outside of the United States. To my parents (Gene and Nancy Macha), grandparents (Don and Ann Strouhal), and sister (Lauren Macha), I can never thank you enough for the support you have given me through the years I have been abroad. Also I would like to thank all of my uncles and aunts (Gene and Stacey Strouhal, Donny and Ann Strouhal, Margaret Macha, and Judy Macha Brown) for their support over the past four years. It has been quite difficult being away from home for so long, but the patience shown by all of you has made my journey both easier and less stressful. The completion of my doctoral studies shows that your dedication has paid off and will hopefully result in wonderful things to come for the future of our family.

Abbreviations

2c2e	two-center, two-electron (bond)
3c2e	three-center, two-electron (bond)
Å	Angstrøm (bond length)
Ar	aryl-
ATRP	atom transfer free radical polymerization
BCat	catecholatoboryl-, (1,3,2-benzodioxaborol-3-yl)
bp	boiling point
br	broad (spectral resonance)
Bu	butyl-
Bz	benzyl-
CCDC	Cambridge Crystallographic Data Centre
COD	1,5-cyclooctadiene-, (C_8H_{12})
COE	cyclooctene-, (C_8H_{14})
Cp	cyclopentadienyl-, (η^5-C_5H_5)
Cp*	pentamethyl-cyclopentadienyl-, (η^5-C_5Me_5)
Cp’	methyl-cyclopentadienyl-, (η^5-C_5H_4Me)
Cy	cyclohexyl-
d	doublet (spectral resonance)
d^n	electron configuration
DEPT	distortionless enhancement by polarization transfer (spectroscopy)
DFT	density functional theory
Dipp	2,6-di-*iso*propylphenyl-
Dur	duryl-, (2,3,5,6-tetramethylphenyl)
e^-	electron
eq.	molar equivalent
Et	ethyl-
E	main group element
Fc	ferrocenyl-
FLP	frustrated Lewis pair
h	hour
HSQC	heteronuclear single-quantum correlation (spectroscopy)
HMBC	heteronuclear multiple-bond correlation (spectroscopy)
HOMO	highest occupied molecular orbital
I	nuclear spin
IMe	1,3-dimethylimidazol-2-ylidene
IMeMe	1,3,4,5-tetramethyl imidazol-2-ylidene
IMes	1,3-*bis*(2,4,6,-trimethylphenyl) imidazol-2-ylidene
*i*Pr	*iso*propyl-
IR	infrared
J	coupling constant (Hz)

L	neutral (2-electron) donor ligand
LUMO	lowest unoccupied molecular orbital
m-	*meta*-
M	metal, molar
Me	methyl-
Mes	mesityl-, (2,4,6-trimethylphenyl)
min	minute
MLCT	metal-to-ligand charge transfer
mp	melting point
MS	mass spectroscopy
mt	2-sulfanyl-1-methylimidazolyl-
o-	*ortho*-
OLED	organic light-emitting diode
n-Bu	*n*-butyl-
NHC	*N*-heterocyclic carbene
NLO	nonlinear optic(al) (properties)
NMR	nuclear magnetic resonance
NOESY	nuclear overhauser effect spectroscopy
Nu	nucleophile
ORTEP	Oak Ridge Thermal Ellipsoid Plot
p-	*para*-
Ph	phenyl-
ppm	parts per million
Py	pyridinyl-
q	quartet (spectral resonance)
R	alkyl-
r.t.	room temperature
ROESY	rotating frame nuclear overhauser effect spectroscopy
s	singlet (spectral resonance)
t	triplet (spectral resonance)
t-Bu	*tert*-butyl-
THF	tetrahydrofuran
Tipp	2,4,6-tri-*iso*propylphenyl-
TMS	trimethylsilyl-
Tol	tolyl-, (4-methylphenyl)
UV	ultraviolet
vt	virtual triplet
vq	virtual quintet
X	halogen, anionic (1-electron) ligand
Z	Lewis acidic (2-electron acceptor) ligand
Δ	heating
δ	chemical shift (ppm)
η	hapticity (π-coordination)
κ	denticity (σ-coordination)
λ	wavelength
μ	bridging
ν	frequency
π	pi (symmetry)
σ	sigma (symmetry)

Table of Contents

Chapter 1 – Introduction 1

1.1 Transition Metal Complexes of Boron 1

1.1.1 General 1
1.1.2 Transition Metal-Borane Complexes 5
1.1.3 Transition Metal-Boryl Complexes 9
1.1.4 Transition Metal-Borylene Complexes 14

1.1.4.1 Synthesis of Borylene Complexes 17
1.1.4.2 Reactivity of Borylene Complexes 21

1.2 Boron-Containing π-Conjugated Systems 25

1.2.1 Monomeric Systems and Boron 27
1.2.2 Oligomeric and Polymeric Systems and Boron 32

1.2.2.1 Main-Chain Functionalized Organoboron Polymers 33
1.2.2.2 Side-Chain Functionalized Organoboron Polymers 34
1.2.2.3 Transition Metals Incorporated into Organoboron Polymers 35

1.3 Cyclic Mono-Boron Containing Heterocyclic Aromatic and Antiaromatic Systems 36

1.3.1 General 37
1.3.2 Borirenes 41
1.3.3 Borabenzene-Boratabenzene 47

Chapter 2 – Project Borylene 55

2.1 First Generation Borylene Synthesis 55

2.1.1 Previous Work 57
2.1.2 Unsymmetrical Aminoborylene Synthesis 59

2.1.2.1 $[(OC)_5Cr\{BN(SiMe_3)(t\text{-}Bu)\}]$ 60
2.1.2.2 $[(OC)_5Mo\{BN(SiMe_3)(t\text{-}Bu)\}]$ 62
2.1.2.3 $[(OC)_5W\{BN(SiMe_3)(t\text{-}Bu)\}]$ 64

2.1.3 Synthetic Attempts at a Group 4 Terminal Borylene 68
2.1.4 Synthetic Attempts at a Group 6 Terminal Phosphinoborylene 70

2.2 Second Generation Borylene Synthesis 78

2.2.1 Previous Work 78
2.2.2 Synthesis of Unsymmetrical Terminal Aminoborylene Complexes by Intermetallic Borylene Transfer 80

2.2.2.1 $[(\eta^5\text{-}C_5H_5)(OC)_3V\{BN(SiMe_3)(t\text{-}Bu)\}]$ 80
2.2.2.2 $[(\eta^5\text{-}C_5Me_5)Ir\{BN(SiMe_3)(t\text{-}Bu)\}_2]$ 83

2.2.3 Synthesis of Unsymmetrical Bridging Aminoborylene Complexes by Intermetallic Borylene Transfer 86

2.2.3.1 [{(η^5-C_5H_4Me)Co}$_2${μ-(CO)}$_2${μ-BN(SiMe$_3$)(*t*-Bu)}] 86
2.2.3.2 [{(η^5-C_5H_5)Ni}$_2$(μ-CO){μ-BN(SiMe$_3$)(*t*-Bu)}] 88
2.2.3.3 [(Pt{μ-BN(SiMe$_3$)$_2$}$_2$){Cr(μ-CO)(CO)$_4$}{Cr(μ-CO)(CO)$_3$(PEt$_3$)}] 91

2.3 M=B-B=M Synthesis Attempts 95

2.4 Reactions of a Base Stabilized Diborene with Grubb's Catalyst 97

2.5 Project Borylene Summary 98

2.6 Project Borylene Appendices 100

Chapter 3 – Project Borirene 103

3.1 Borirene Conjugation 103

3.1.1 Previous Work 107
3.1.2 Platinum *bis*-σ-Alkynyl Precursors 112

3.1.2.1 Synthesis of *trans*-[Pt(C≡C-Ph)$_2$(PEt$_3$)$_2$] and General Remarks 112
3.1.2.2 *trans*-[Pt(C≡C-*p*-C_6H_4OMe)$_2$(PEt$_3$)$_2$] 115
3.1.2.3 *trans*-[Pt(C≡C-*p*-$C_6H_4CF_3$)$_2$(PEt$_3$)$_2$] 117
3.1.2.4 *trans*-[Pt(C≡C-9-$C_{14}H_9$)$_2$(PEt$_3$)$_2$] 120
3.1.2.5 *cis*-[Pt(C≡C-Ph)$_2$(DCPE)] 122
3.1.2.6 *trans*-[Pt{(C≡C)$_3$-Tr*}$_2$(PEt$_3$)$_2$] 123
3.1.2.7 Discussion and Theory 127

3.1.3 Borylene Transfer Reactions onto *trans*-Platinum *bis*-σ-Alkynyl Complexes 132

3.1.3.1 General Synthetic Routes and Considerations 132
3.1.3.2 *trans*-[Pt{(μ-{B=N(SiMe$_3$)$_2$}C=C)-Ph}$_2$(PEt$_3$)$_2$] 134
3.1.3.3 *trans*-[Pt{(μ-{B=N(SiMe$_3$)$_2$}C=C)-*p*-C_6H_4OMe}$_2$(PEt$_3$)$_2$] 140
3.1.3.4 *trans*-[Pt{(μ-{B=N(SiMe$_3$)$_2$}C=C)-*p*-$C_6H_4CF_3$}$_2$(PEt$_3$)$_2$] 142
3.1.3.5 Discussion and Theory 144
3.1.3.6 Attempted Borylene Transfer onto *trans*-[Pt(C≡C-9-$C_{14}H_9$)$_2$(PEt$_3$)$_2$] 152
3.1.3.7 Transfer attempts onto *cis*-[Pt(C≡C-Ph)$_2$(DCPE)] 153
3.1.3.8 Attempted Borylene Transfer onto *trans*-[Pt{(C≡C)$_3$-Tr*}$_2$(PEt$_3$)$_2$] 155

3.2 Gladysz-Type Platinum End-Capped Alkynyl Species 157

3.2.1 Synthesis of Platinum Butadiynyl Precursors 157

3.2.1.1 *trans*-[PtCl(*p*-tol)(PCy$_2$Me)$_2$] 159
3.2.1.2 *trans*-[Pt{(C≡C)$_2$-H}(*p*-tol)(PCy$_2$Me)$_2$] 160
3.2.1.3 *trans,trans*-[(*p*-tol)(Cy$_2$MeP)$_2$Pt(C≡C)$_4$Pt(PCy$_2$Me)$_2$(*p*-tol)] 162

3.2.2 Borylene Transfer Attempts 164

3.3 Synthesis of Monoborirene Adducts 166

3.4 Expansion Reaction of a Borirene to a Borole 169

3.5 Alkynylborane Oligomerization Studies 172

3.6 Project Borirene Summary 176

Chapter 4 – Project Boratabenzene 179

4.1 *bis*(Boratabenzene) Synthesis 179

4.1.1 Previous Work 180
4.1.2 Synthesis and Purification of a 1,1'-*bis*(Boratabenzene) Complex 183

4.1.2.1 $[\{(\eta^5\text{-}C_5H_5)Co\}_2\{\mu{:}\eta^6,\eta^6\text{-}(BC_5H_5)_2\}]$ 184

4.1.3 Oxidation Studies of $[\{(\eta^5\text{-}C_5H_5)Co\}_2\{\mu{:}\eta^6,\eta^6\text{-}(BC_5H_5)_2\}]$ 190

4.1.3.1 $[\{(\eta^5\text{-}C_5H_5)Co\}_2\{\mu{:}\eta^6,\eta^6\text{-}(BC_5H_5)_2\}][PF_6]_2$ 190
4.1.3.2 $[\{(\eta^5\text{-}C_5H_5)Co\}_2\{\mu{:}\eta^6,\eta^6\text{-}(BC_5H_5)_2\}][PF_6]$ 191

4.2 Reactivity Studies of $[\{(\eta^5\text{-}C_5H_5)Co\}_2\{\mu{:}\eta^6,\eta^6\text{-}(BC_5H_5)_2\}]$ 193

4.2.1 $[\{(\eta^5\text{-}C_5H_5)Co\}_2\{\mu{:}\eta^6,\eta^6\text{-}(BC_5H_5)_2\}]$ Ring-Cobalt Cleavage Attempts with MCN 194
4.2.2 Attempted Boron-Boron Bond Cleavage by Oxidative Addition of $[\{(\eta^5\text{-}C_5H_5)Co\}_2\{\mu{:}\eta^6,\eta^6\text{-}(BC_5H_5)_2\}]$ to Transition Metals 195

4.3 Project Boratabenzene Summary 197

Chapter 5 – Summary 199

Chapter 6 – Zusammenfassung 207

Chapter 7 – Experimental 215

7.1 General Considerations 215

7.2 Project Borylene Experimental 217

7.3 Project Borirene Experimental 226

7.4 Project Boratabenzene Experimental 242

7.5 Computational Details 245

7.6 Published X-ray Structural Data 246

Chapter 8 – References 249

Chapter 1 – Introduction

1.1 Transition Metal Complexes of Boron

1.1.1 General

Boron, as a consequence of its possession of only three valence electrons, readily adopts an electron deficient state when covalently bonded to main group elements and transition metals.[1] This characteristic propensity makes the reactivity of boron both interesting and exploitable as a fundamental tool for functionalization of a wide range of chemical substrates.[2-13] Coordination of a simple Lewis base is typically thought of as the simplest stabilization mechanism boron must undergo to complete its valence shell, but recent research into this "humble" mechanism has fostered a renaissance of novel "frustrated Lewis pair" (FLP) reactions and small molecule activations.[14-17] Boron's electron deficient nature also gives rise to many interesting coordinative properties of the element when involved in interactions with transition metals,[18-23] and for applications in transition metal-catalyzed hydroboration, diborations, C-F bond activations, and C-H bond activations.[11,12,14-17,24-27] From the pioneering work of Stock on B_2H_6,[2] to the multiple Nobel prizes in chemistry (most recently for catalytic cross-coupling),[28-31] the chemistry of boron has continually been refined over its one hundred year history for applicability within the fields of catalysis,[8,10-12,24-27] metal-free small molecule activations,[13-17] polyhedral borane chemistry,[6,7,9] medicinal applications,[32,33] and materials sciences.[34,35]

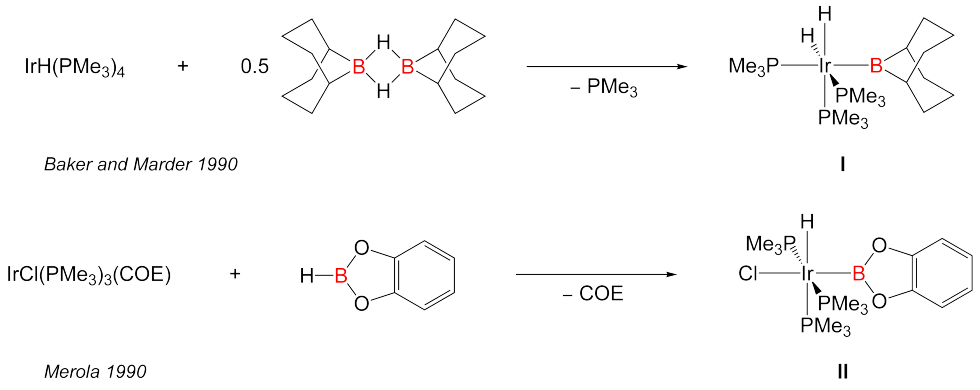

Figure 1-1. The first structurally confirmed transition metal-boron interactions reported concurrently by the groups of Baker, Marder *et al.* (**I**)[38] and by Merola *et al.* (**II**)[39] (COE = cyclooctene) in 1990.

Although the proposal of a "boryl"-transition metal interaction was derived from Nöth's seminal work in 1963,[36,37] such complexes were not structurally elucidated until 1990 when transition metal boryl structures were published concurrent by Baker, Marder, Westcott and coworkers[38] (Figure 1-1, **I**) as well as by Merola and

coworkers (Figure 1-1, **II**).[39] Figure 1-1 showcases both of these transition metal-boryl species synthesized *via* oxidative additions of borane B-H bonds to iridium centers. In recent years, many different transition metal-boron interactions have been reported and quantified; however, for the purpose of this thesis, focus will be limited to three primary transition metal-boron interactions.

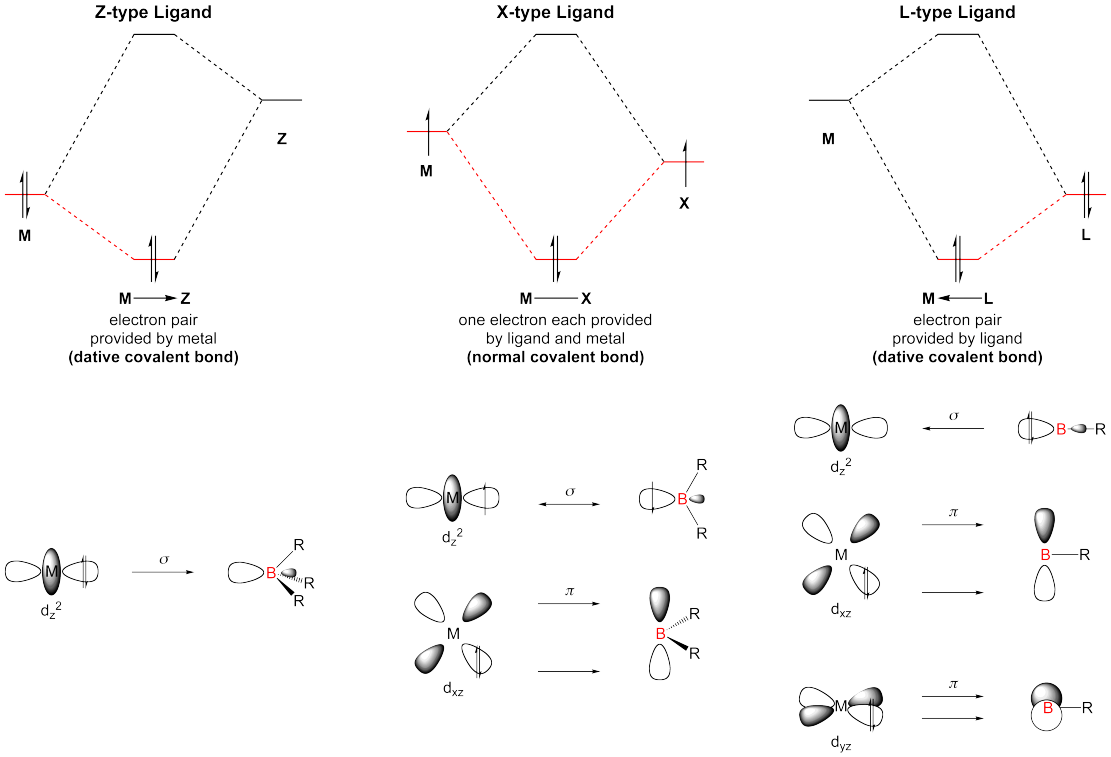

Figure 1-2. Generalized orbital schematics for common boron-metal interactions.[23]

The three fundamental transition metal-boron interactions consisting of electron precise two-center, two-electron (2c2e) M-B bonds are typically classified by the following nomenclatures: boranes, boryls, and borylenes.[18-23] The stability and reactivity of these compounds has been shown to differ drastically from other transition-metal boron interactions such as borides and metallaboranes primarily due to variation in the 2c2e ligand bonding situations (see Figure 1-2) as well as the resonance structures that can subsequently be proposed from the main group substituents bound to boron.[18,19] Examination of the variety of published crystallographic data on these three types of bonding environments reveal a startling amount of variance attainable in the geometry at the boron center from these borane, boryl, and borylene interactions, which correspond to the archetypal Z- (Figure 1-2, left), X- (Figure 1-2, center), and L-type (Figure 1-2, right) ligand definitions, respectively.[40,41]

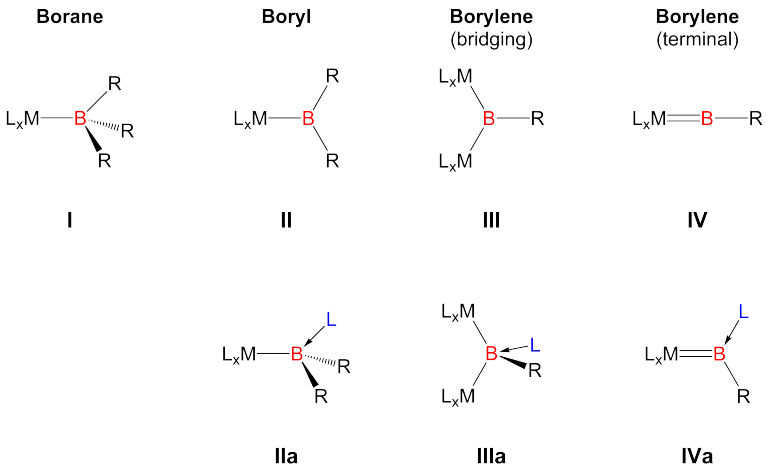

Figure 1-3. Generalized molecular orbital diagrams and nomenclatures for common transition metal-boron bonding interactions.[41]

For explanation of these bonding systems, the geometry will first be discussed in terms of transition metal-boron terminal interactions, followed by transition metal-boron bridging interactions. The borane and borylene coordination modes of the boron ligands essentially represent the two extremes of dative bonding for a 2c2e interaction with a transition metal (Figure 1-2, left and right). The transition metal-boryl interaction represents a covalent electron sharing interaction and as such is counted as a X-type ligand in formal electron counting analysis of the complex[41,42] The geometry of transition metal-borane (Figure 1-3, **I**) complexes (L_xM-BR_3) are closely related to the geometry of simple Lewis acid-base adducts and are typically thought of as such, with the metal center donating a pair of electrons into the vacant p_z orbital of the boron center (Z-type ligand).[43-45] Crystallographically these species feature sp^3-hybridized tetrahedral geometry at the boron center with elongated B-R bond distances relative to the free uncoordinated BR_3 compounds.[46] Transition metal-boryl (Figure 1-3, **II**) complexes (L_xM-BR_2) feature a planar three-coordinate sp^2-hybridized boron center manifested *via* a boron-transition metal σ-bond (X-type ligand). These boryl interactions are supremely important in the field of transition metal catalysis as they constitute the most commonly proposed active intermediates in most boron-transition metal catalytic cycles.[47-50] The final class of transition metal-boron 2c2e bonds is the transition metal-borylene (Figure 1-3, **IV**) complex (L_xM-BR), which is typically classified as a boron-centered two-electron donation (:B-R) into the transition metal's d_{z^2} orbital with two-electron back-donation from the core d_{xz} and d_{yz} transition metal orbitals into the π^*-orbital of the :B-R ligand.[51-57] This transition metal-borylene interaction can be rationalized as an isoelectronic

analog of the ubiquitous transition metal-carbonyl, -cyano, -dinitrogen, and linear -nitrosyl ligand interactions.[40]

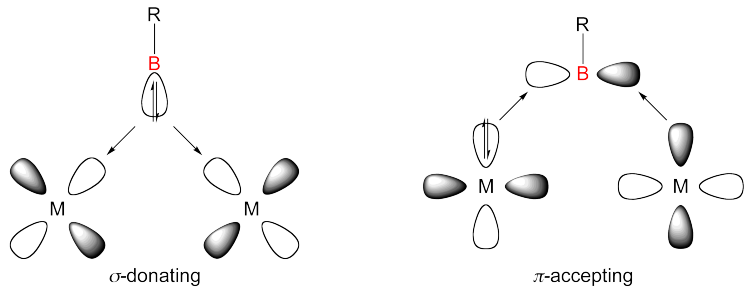

Figure 1-4. Generalized molecular orbital schematics for common transition metal-borylene bridging interactions.[40]

In the case of borylene ligands, the possibility to bridge multiple transition metals exists and has been well documented (Figure 1-3, **III**).[18-23,58] In these three-center, two-electron (3c2e) bridging interactions the boron typically maintains a trigonal planar geometry and is thought of as a neutral ligand based on detailed crystallographic and theoretical studies.* This bonding situation for boron is rationalized as a 3c2e σ-donation to the metal centers with metal d orbital back-donation into the π*-orbital of the (:B-R) fragment (see Figure 1-4).[59,60] Another key aspect of the chemistry of boryl and both terminal and bridging borylene bonding interactions is the ability for the boron to still be electron deficient while coordinated to transition metals. These highly Lewis acidic boron sites possess sufficient reactivity to coordinate Lewis bases, depending on the stabilizing substituents bound to boron and the steric bulk of the Lewis base.[18-23] Coordination of a Lewis base will inherently increase the dimensionality of the boron's geometry and can significantly alter the electronic delocalization between the boron substituents and the transition metal.[58,61]

* See Section 1.1.4 for more information on this bonding analysis.

1.1.2 Transition Metal-Borane Complexes

Although it is believed that transition metals possess the capability to function as simple Lewis bases[62,63] in the formation of dative bonds with boranes, the existence of a true unsupported transition metal-borane (L_xM-BR_3) dative interaction has never been structurally confirmed.[23,43-45,57] Beginning with Shriver's initial 1963[64] publication, the tungsten dihydride complex [(η^5-C_5H_5)$_2$$WH_2$] (Figure 1-5, **I**) was believed to react with BF_3 forming the transition metal-borane product [(η^5-C_5H_5)$_2$$WH_2$($BF_3$)] (Figure 1-5, **II**). Later research pursuing similar haloborane (BF_3 and BCl_3) reactivity with the transition metal hydrides [(η^5-C_5H_5)$_2$$MoH_2$], [($\eta^5$-$C_5H_5$)$_2$$WH_2$], and [($\eta^5$-$C_5H_5$)$_2$ReH], led to the report of the formal Lewis pair adducts [(η^5-C_5H_5)$_2$$WH_2$($BCl_3$)], [($\eta^5$-$C_5H_5$)$_2$$MoH_2$($BF_3$)], [($\eta^5$-$C_5H_5$)$_2$ReH($BF_3$)], and [($\eta^5$-$C_5H_5$)$_2$ReH($BCl_3$)].[65] These reported transition metal-borane dative interactions were later found to be based essentially on infrared spectroscopic evidence and X-ray powder diffraction studies,[66] which led to their later refutation without crystal structure elucidation. Research published by Braunschweig and coworkers, starting in 1994,[67] showed structural evidence contradicting these reports, with the zwitterionic complexes [(η^5-C_5H_4{B(*i*Pr)Cl_2})(η^5-C_5H_5)WH_3] and [(η^5-C_5H_4{B(*t*-Bu)Cl_2})(η^5-C_5H_5)WH_3] (Figure 1-5, **III**) being the only isolable species from reactions of [(η^5-C_5H_5)$_2$$WH_2$] with the dihaloboranes B(*i*Pr)Cl_2 and B(*t*-Bu)Cl_2 respectively. Formation of these products was verified from previous research published by Siebert and coworkers in which C-H activation of [(η^5-C_5H_5)$_2$Fe] is observed by reaction with BI_3.[68] This C-H activation subsequently leads to migration of the borane onto the cyclopentadienyl ring forming a 1:1 ratio of [(η^5-C_5H_5)$_2$FeH][BI_4] and [(η^5-C_5H_4{BI_2})(η^5-C_5H_5)Fe]. Studies by Braunschweig and coworkers (Figure 1-5, **IV**) aimed specifically at reproducing the tungsten-borane complex [(η^5-C_5H_5)$_2$$WH_2$($BF_3$)] reported by Shriver were crystallographically shown to produce only the ion pair [(η^5-C_5H_5)$_2$$WH_3$][$BF_4$].[69,70] To date, the best case for synthesis of an unsupported transition metal-borane complex is the reaction of the anionic iron complex [NEt_4][(η^5-C_5H_5)Fe(CO)$_2$] with BPh_3 as reported by Burlitch, Hughes, and coworkers.[71] The purported product complex [NEt_4][(η^5-C_5H_5)Fe(BPh_3)(CO)$_2$] displays a ^{11}B NMR resonance of –29 ppm, which is indicative of a tetracoordinate environment for a boron nucleus.[23] However, crystallographic data for this complex was not obtained, and the species is known to be unstable upon solvation with dissociation of the borane, thus the validity of this complex is still debatable.

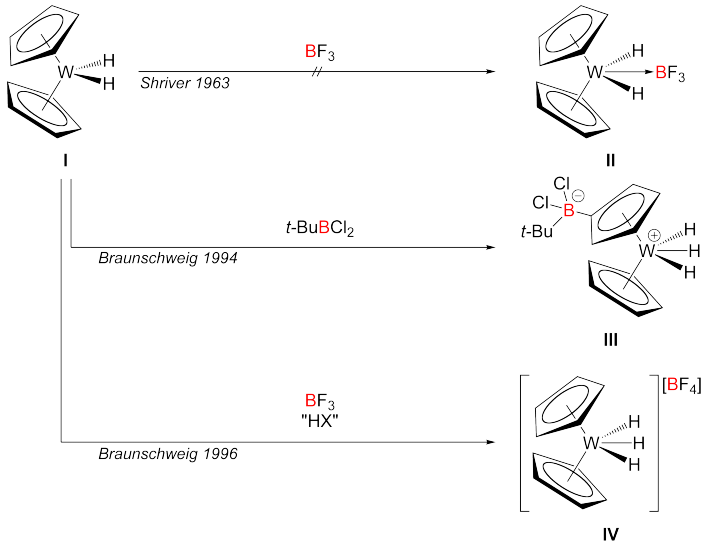

Figure 1-5. Reaction schemes showcasing Shriver's purported borane complex relative to the actual reaction products: ion pair formation and zwitterion formation.[64,67,69,70]

The successful formation of a metal-borane bond was reported by the Hill group in 1999[72,73] using a multidentate L_3Z ligand scaffold to stabilize the transition metal-borane interaction and prevent dissociation of the borane upon solvation of the complex. Using this route (Figure 1-6), the anionic tridentate *tris*(azolyl)borate ligand Na[HB(mt)$_3$] (mt = 2-sulfanyl-1-methylimidazolyl) was coordinated to the ruthenium precursor [Ru(CH=CHCPh$_2$OH)Cl(CO)(PPh$_3$)$_2$] by salt elimination reaction followed by intramolecular elimination of the alkene to yield the ruthenaboratrane complex [Ru{B(mt)$_3$}(CO)(PPh$_3$)] (Figure 1-6, **I**). This ruthenaboratrane complex exhibited a ^{11}B NMR spectroscopic resonance at 17 ppm and a Ru-B bond distance of 2.161(5) Å. This information, combined with tetrahedral geometry at the boron center and an infrared carbonyl stretching frequency ($\tilde{\nu}$(C≡O) = 1,888 cm^{-1}) is consistent with a Ru(0) complex, and provided sufficient evidence for the initial report of a Z-type borane ligand bound to a transition metal scaffold. This ligand scaffold has retrospectively been shown to be adaptable for coordination to all member of Group 8 and 9 resulting seminal transition metal-borane complexes of the elements: Fe,[74] Os,[75] Co,[76] Rh,[77] and Ir.[78]

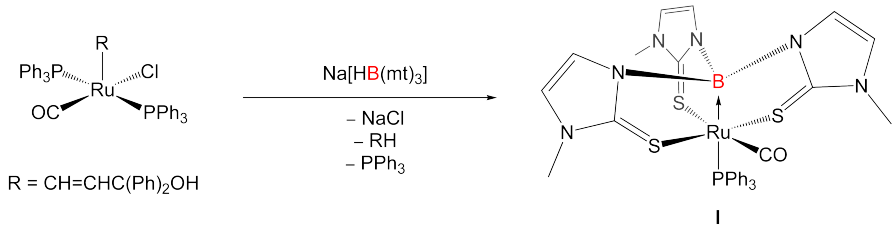

Figure 1-6. Reaction forming the first structurally confirmed metalloboratrane complex as reported by Hill *et al.* in 1999 (mt = 2-sulfanyl-1-methylimidazolyl).[72,73]

Recent collaborative work by the groups of Bourissou, Ozerov, and Maron have allowed for in depth comparative results, both experimental and theoretical, on a transition metal tetradentate *tris*(phosphine) κ^4-*PPPB* boratrane scaffold.[79-81] In concurrent publications from 2008 the *tris*(phosphino)borane B{*ortho*-*i*Pr$_2$P(C$_6$H$_4$)}$_3$ or TPB (Figure 1-7, **I**,) ligand's coordinative properties were evaluated by comparison between the Ni(0), Pd(0), and Pt(0) metalloboratrane scaffolds (Group 10, d^{10} systems, Figure 1-7, **II**, **III**, and **IV** respectively) and Cu(I), Ag(I), and Au(I) *trans*-chlorometalloboratrane scaffolds (Group 11, d^{10} systems, Figure 1-7, **V**, **VI**, and **VII** respectively). These six complexes are all formally 16-electron and 18-electron d^{10} configurations featuring C_3 rotational symmetry around the metalloboratrane and differ only in the presence of a boron *trans*-halide ligand. The simplicity of these species make comparisons possible for trend establishment of group, oxidation state, and *trans*-halide influences upon the metal-boron bonding environment.[79]

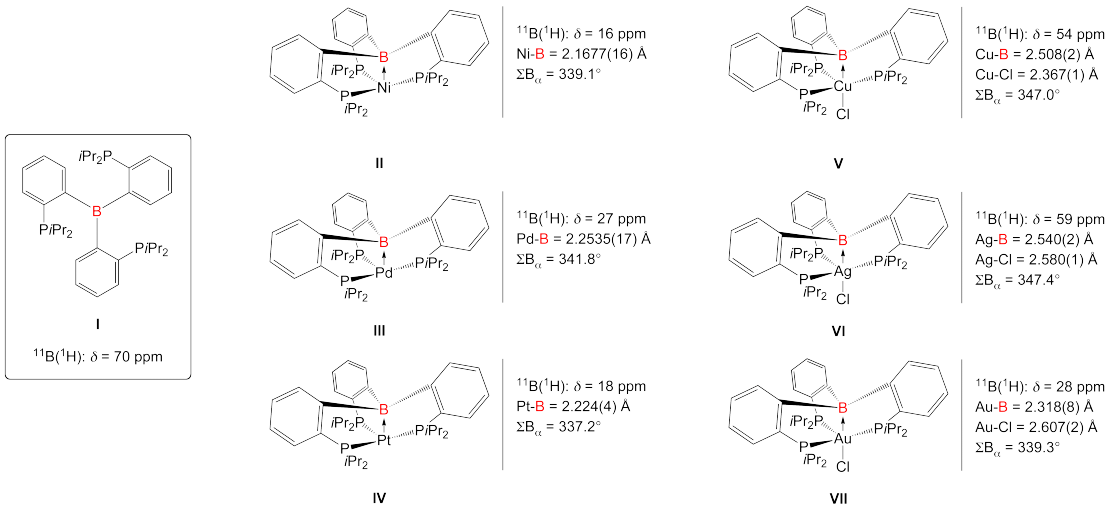

Figure 1-7. Structural and experimental data reported by Bourissou, Ozerov, and Maron *et al.* pertaining to Group 10 and 11 d^{10} metalloboratrane species.[79-81]

Treatment of the metal precursors [Ni(COD)$_2$], [Pd(P*t*-Bu$_3$)$_2$], [Pt(P*t*-Bu$_3$)$_2$], [CuCl], [AgCl], and [AuCl(SMe$_2$)] with the TPB ligand afforded the tetradentate κ^4-*PPPB* metalloboratrane complexes: [Ni(TPB)], [Pd(TPB)], [Pt(TPB)], [Cu(TPB)Cl],

[Ag(TPB)Cl], and [Au(TPB)Cl] respectively.[79] As reported in the publications by Bourissou, Ozerov, and Maron, analysis of three specific parameters, M-B bond distances, ^{11}B NMR spectroscopy, and bond angle summation (ΣB_α) around the boron center, were all used to quantify that the platinum and gold (5d transition metal) adducts exhibited the greatest Lewis basicity towards this particular borane (Z-type) ligand scaffold. The table seen in Figure 1-7 lists all three of these parameters for each complex.[79-81]

1.1.3 Transition Metal-Boryl Complexes

A transition metal-boryl interaction (L_xM-BR_2) is typically classified as a covalent 2c2e bond between a transition metal and boron-centered ligand.[23] This bonding motif enables the boron ligand to function as an anionic (X-type) ligand in the coordination sphere of the transition metal scaffold and influences the formal oxidation state of the metal as such (Figure 1-8, left). Boryl ligands often possess trigonal planar geometry at the boron center as a result of a vacant or partially vacant p_z orbital.[47-50] The flanking substituents bound to the boron center often contain additional lone pairs of electrons to stabilize this p_z orbital by formal resonance structures similar to those of *N*-heterocyclic carbene (NHC) transition metal complexes. The transition metal's d_{xz} and d_{yz} orbitals also possess the ability to π-backdonate into this vacant p_z (π-acidic) orbital, enabling a direct competition between metal and boron flanking substituents for stabilization of this system depending upon the degree of rotation around the M-B bond (Figure 1-8, right).[49,82-85] The boryl ligand's ability to function as a strong σ-donor combined with this metal-substituent competition for the p_z orbital on boron is believed to give the boryl ligand an exceedingly high *trans*- influence. Experimentally this high *trans*-influence has been verified and can be roughly estimated to be equal or slightly greater than transition metal hydride interactions.[49] As consequence of this property, boryl ligands are typically found to adopt geometries where they are *trans*- to traditional L-type ligands as well as anionic cyclopentadienyl ligands.[47-50,82]

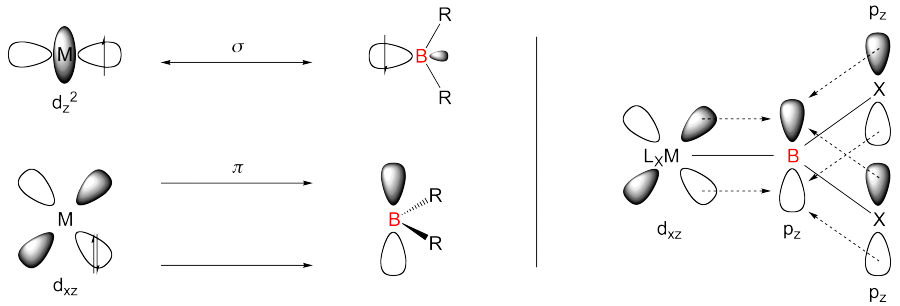

Figure 1-8. Diagram showing competition for the p_z orbital at the boron center of a boryl ligand.[47,49]

As an anionic ligand, the boryl interaction is vital to most transition metal-catalyzed hydroboration, diboration, C-H borylation, and C-halide borylation reactions due to the reliance these systems have upon B-B and B-E oxidative addition and reductive elimination chemistry to achieve turnover of catalytic cycles.[11,12,47-50,86-90] Starting with the structurally unconfirmed "boryl" complexes published in the 1960's[91,92] to the first confirmed transition metal-boryl interactions published by the groups of

Baker, Marder, Westcott and coworkers[38] as well as Merola and coworkers,[39] the first transition metal boryl complexes were successfully synthesized from oxidative additions of haloboranes (B-X), hydroboranes (B-H), and diboranes (B-B) to transition metals.[47-50] Figure 1-9 lists a selection of first transition metal boryl and diboryl complexes as well as M-B bond distances and ^{11}B NMR resonances.[38,39,93-99]

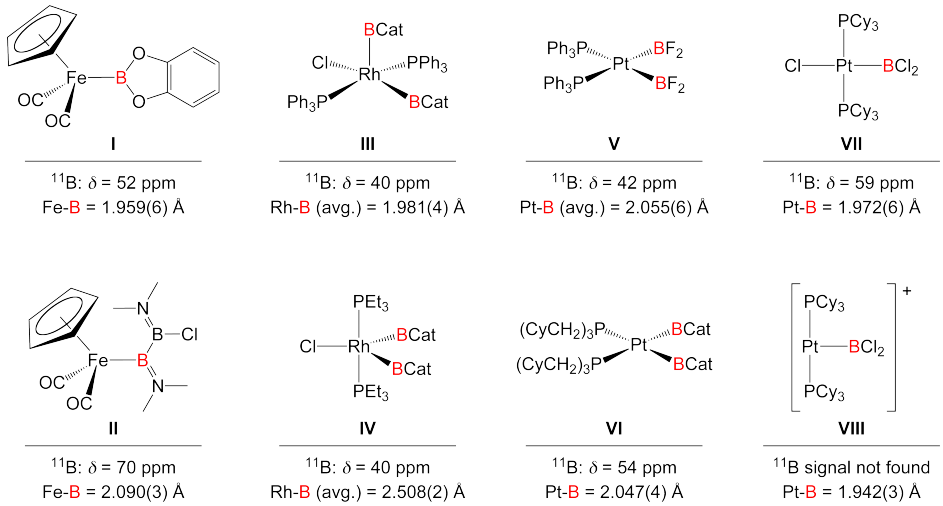

Figure 1-9. Reported transition metal-boryl species derived from oxidative additions of boranes and diboranes to transition metals (BCat = 1,3,2-benzodioxaborol-3-yl).*

The transition metal-boryl bond allows for variable rotation around the M-B axis, which can be stabilized *via* overlap of the boron p_z orbital with the metal's core d orbitals in multiple separate confirmations (Figure 1-10, left). The stability of this d_π-p_π backdonation into the boryl substituent is a dynamic process, which can be perturbed *via* coordination of a Lewis base to the boryl center. Work published in 1996 by Braunschweig and coworkers was able to experimentally show this d_π-p_π backdonation by structural study of metal-boron distances in the iron boryl complex $[(\eta^5\text{-}C_5H_5)_2Fe(CO)_2BCl_2]$ *vs.* that of the Lewis-base-quarternized version with 4-methylpyridine $[(\eta^5\text{-}C_5H_5)_2Fe(CO)_2BCl_2(NC_5H_4\text{-}4\text{-}Me)]$ (Figure 1-10, **I** and **II**).[61,100] The iron dihaloboryl complex shown below in its unquarternized state exhibits a Fe-B bond distance of 1.942(3) Å *vs.* 2.1326(14) Å in its quarternized state, accounting for a weakened metal-boron bond. Carbonyl stretching frequencies under infrared radiation also showed significantly lower resonant frequencies for the base-quarternized version ($\tilde{\nu}$(C≡O) = 1,976 and 1,916 cm^{-1}) compared to the base-free version ($\tilde{\nu}$(C≡O) = 2,026 and 1,974 cm^{-1}), indicative of a significant increase of electron density at the iron center due to lack of π-overlap with the boron center. Also

* Individual references for compounds reported in Figure 1-9: **I**,[93] **II**,[95] **III**,[94] **IV**,[97] **V**,[96] **VI**,[99] **VII**,[98] and **VIII**.[98]

of interest are the B-Cl distances, which lengthen from 1.782 Å (avg.) to 1.881 Å (avg.) as would be expected with an increase in dimensionality of the boron geometry.[61]

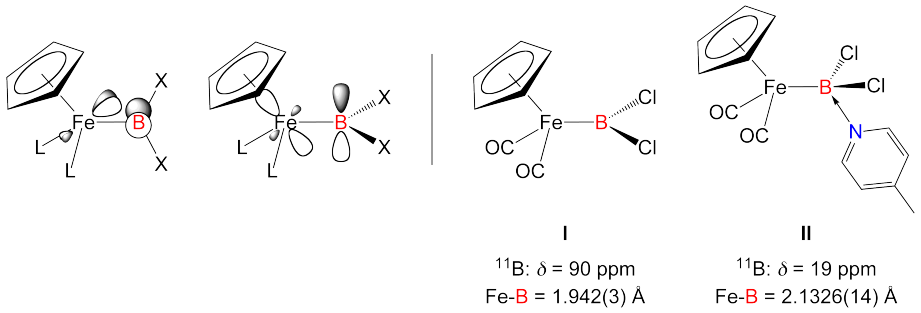

Figure 1-10. Experimental data published by Braunschweig *et al.* pertaining to divergent M-B bonding environments between an unquarternized and quarternized boryl transition metal species.[61,100]

Traditionally, boryl species were best suited for incorporation into mid-transition metal scaffolds, with fewer known examples from either extreme of the d block. However, in recent years the group of Yamashita, Nozaki, and coworkers have extended the synthesis of 1,3,2-diazaboroles, reported previously by Weber,[101] to the generation and isolation of 1,3,2-diazaborolyl anions bound to s block metals cations (Figure 1-11, **II**).[102] These lithium[103] and magnesium[104] salts of anionic borolyl ligands are isostructural and isoelectronic to traditional *N*-heterocyclic carbenes, save the carbon atom at the 2-position of the ring is exchanged for an anionic boron atom. The borolyl ligand salts are observed to display nucleophilic characteristics and reactivity, allowing for their incorporation into metal scaffolds usually ill-suited for traditional metal-boryl complexes synthesized *via* oxidative additions. This nucleophilicity also allows for synthesis of "boryl" complexes of transition metals (*via* salt eliminations) in lower oxidation states. Starting with Group 3 and 4[105] transition metal-boryl complexes (Figure 1-11, **III** and **V**) to Group 11 and 12 transition metal-boryl complexes (Figure 1-11, **IV**),[106-109] many new bonding environments have recently been reported and studied. Figure 1-11 shows reported borolyl ligand synthesis and coordination onto a variety of highly Lewis acidic and basic metal scaffolds.

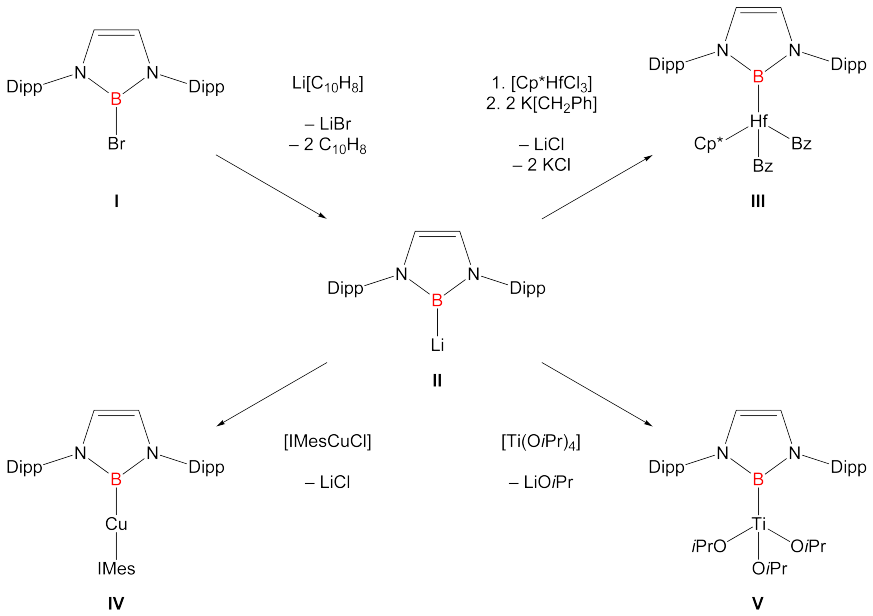

Figure 1-11. Synthesis of an alkali metal salt of a borolyl ligand (top left to center) (Dipp = 2,6-di-*iso*propylphenyl) followed by coordination to elements of Groups 4 and 11 *via* salt elimination reactions as reported by Yamashita *et al.* from 2006 to 2009 (IMes = 1,3-dimesitylimidazol-2-ylidene).*

Additionally, Braunschweig and coworkers have recently published platinum oxoboryl,[110,111] iminoboryl,[112-114] and alkylideneboryl[115,116] complexes synthesized from oxidative addition and subsequent halosilane elimination (Figure 1-12). Oxidative addition of the dibromosiloxyborane $Br_2BOSiMe_3$ to the Pt(0) complex $[Pt(PCy_3)_2]$ (^{31}P: δ = 62 ppm, $^1J_{Pt\text{-}P}$ = 4,161 Hz) yielded the Pt(II) haloboryl complex *trans*-$[(Cy_3P)_2BrPt\{B(Br)OSiMe_3\}]$ (^{31}P: δ = 21 ppm, $^1J_{Pt\text{-}P}$ = 2,777 Hz). This complex was subject to subsequent elimination of the bromosilane $BrSiMe_3$ *in situ* to successfully give the platinum oxoboryl species *trans*-$[(Cy_3P)_2BrPt(BO)]$ (Figure 1-12, **II**) as a linear anionic B-O ligand isoelectronic to a σ-alkynyl ligand. The platinum center is still rationalized to be in the +2 oxidation state based on its ^{31}P-^{195}Pt NMR satellite coupling constants (^{31}P: δ = 33 ppm, $^1J_{Pt\text{-}P}$ = 2,294 Hz) and the linear geometry of the oxoboryl ligand. The iminoboryl platinum complex *trans*-$[(Cy_3P)_2BrPt(BNSiMe_3)]$ (^{31}P: δ = 31 ppm, $^1J_{Pt\text{-}P}$ = 2,389 Hz) was also prepared under similar conditions and showcased the Pt-B-N-Si linkage to be essentially linear, further lending evidence to this ligand species functioning as isoelectronic mimics to transition metal σ-alkynyl coordination (Figure 1-12, **III**).[117] Later publication of the platinum alkylideneboryl complex *trans*-$[(Cy_3P)_2BrPt\{BCH(SiMe_3)\}]$ (^{31}P: δ = 30 ppm, $^1J_{Pt\text{-}P}$ = 2,482 Hz) synthesized in a similar manner of oxidative addition and

* Individual references for compounds reported in Figure 1-11: **I**,[102,103] **II**,[102,103] **III**,[105] **IV**,[106,107] and **V**.[105]

halosilane elimination of $Br_2BCHSiMe_3$ with $[Pt(PCy_3)_2]$ provided further data for this series of complexes (Figure 1-12, **IV**).[115,116]

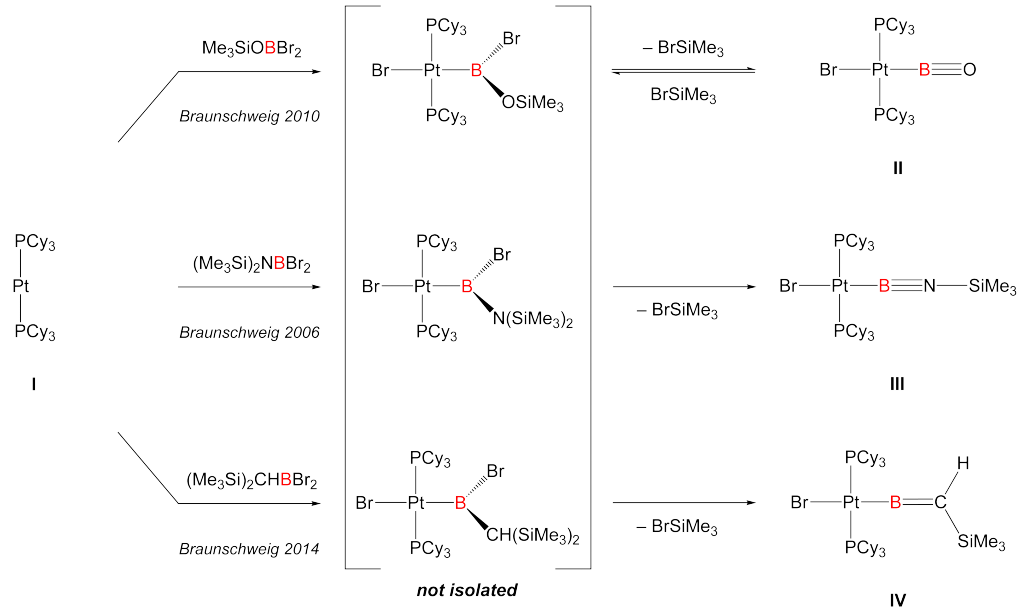

Figure 1-12. Examples from Braunschweig *et al.* of the synthesis of oxoboryl-, iminoboryl-, and alkylideneboryl- adducts bound to a platinum scaffold.[110-116]

1.1.4 Transition Metal-Borylene Complexes

Transition metal-borylene complexes of the type L_xM=B-R, where :B-R is considered a linear 2-electron σ-donating terminal ligand, have been known since 1998.[118,119] Although it is believed that "free" mono-substituted borylene species can be generated, and in some cases be stable enough to transfer between metals and organic fragments at ambient temperatures,[48,51-57] structural evidence for a non-coordinated mono-substituted borylene fragment has eluded isolation. Bertrand, Stephan, and coworkers have shown that reduction of a cyclic (alkyl)-(amino)carbene-dihaloborane adduct leads to an isolable allenic species that displays some free borylene reactivity through rearrangement to a proposed bent borylene species in solution.[120-122] Recent publication by Braunschweig and coworkers of a "masked" borylene shows the ability of a terphenyl-substituted (Figure 1-13, left) borylene to be isolated *via* coordination to carbonyls and isonitriles (Figure 1-13, right).[123]

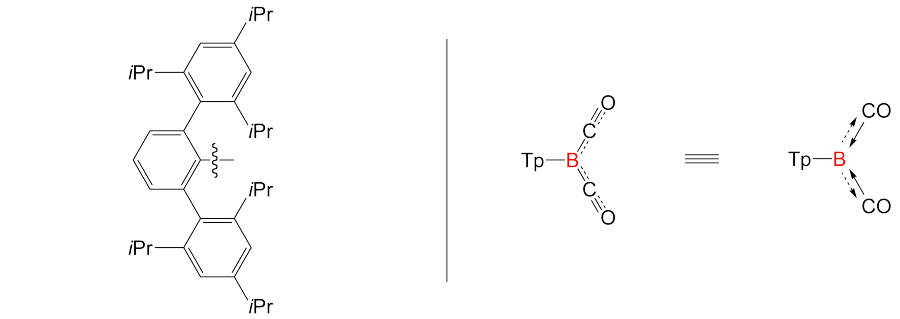

Figure 1-13. Examples from Braunschweig *et al.* of characterized terphenyl borylene adducts bound to stabilizing ligands, which are not known to be isolable in the absence of these influences.[123]

Starting with the initial work performed by Timms in 1967,[124] successful characterization of a ":B-F" fragment was published based on infrared spectroscopy of the species generated *in situ* from matrix isolation.[125] Subsequent research by West and coworkers in 1984 showed the ability to trap the products formed from *in situ* synthesis of a :B-$SiPh_3$ silylborylene* at –196 °C; however, the free silylborylene was never isolated.[126,127] The conclusion from nearly 50 years of attempted syntheses of a free borylene species is that their extreme reactivity combined with low thermal stability inhibits their isolation without stabilizing influences such as transition-metal or Lewis-base coordination.

* See Section 1.3.2, Figure 1-47, for full reaction details.

However, stable borylenes can be readily synthesized by exploiting their strong affinity for transition metals and carbonyls.[23,57] With the boron coordinated to these stabilizing fragments, ambient temperature decomposition is severely limited and alternative reactivity can be explored. As linear isoelectronic analogs of traditional carbonyl and dinitrogen ligands, the :B-F "fluoroborylene" species was a likely candidate for attempts to synthesize stable borylene ligands within the coordination sphere of transition metals. Justification for the stability of a transition metal fluoroborylene complex was taken from theoretical analysis of the frontier orbitals.[128-140] Orbital diagrams for the CO, N_2, and BF ligands all show the HOMOs in σ-sp lobal geometry combined with doubly degenerate π^* LUMOs (Figure 1-14).[57,60,141]

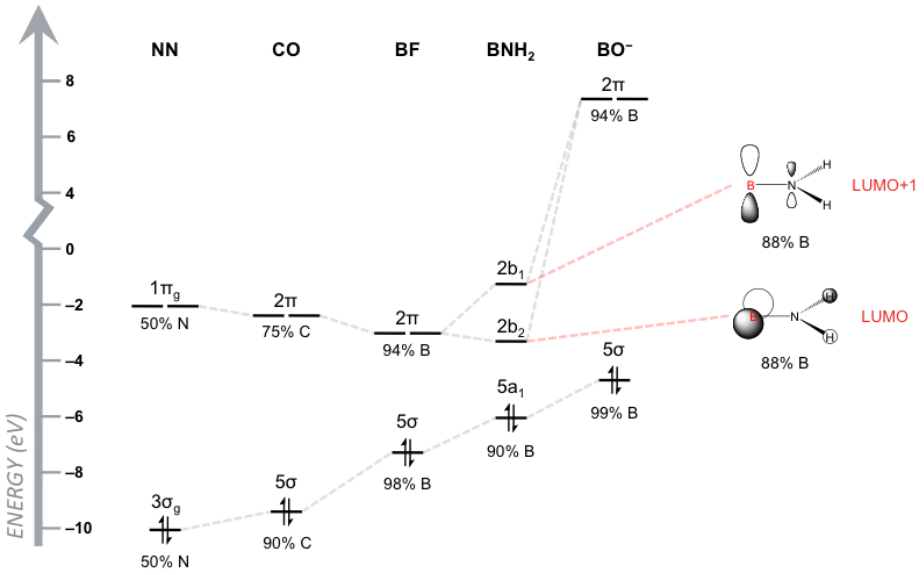

Figure 1-14. Valence orbital energies of borylene fragments relative to carbonyl, dinitrogen, and oxoboryl ligands with reported percentages of each atom listed below.[128]

Computational studies of the binding energies of the fluoroborylene (:BF) and aminoborylene ($:BNH_2$) ligands compared to the isoelectronic carbonyl (:CO), dinitrogen (:NN), and oxoboryl ($[:BO]^-$) ligand analogs show these two borylene ligands to possess significantly higher HOMO energies but only slightly lower LUMO energies.[128] These characteristics allow the ligand to stabilize bonds between transition metals to a greater degree than the other three comparative species primarily because of the borylenes' ability to function as stronger σ-donors (energetically higher HOMO) and more effective π-acceptors (energetically lower LUMOs) (Figure 1-14). Of the two borylene ligands computed, the aminoborylene ($:BNH_2$) species is projected to be the more effective ligand of the two by having split

LUMO degeneracy in contrast to the doubly degenerate LUMO levels of the fluoroborylene (:BF) species and an overall lower-lying LUMO (see Figure 1-14). This increased aminoborylene ligand $2b_2$ orbital stability is symmetry justified due to the C_{2v} symmetry of $:BNH_2$ as opposed to the linear fluoroborylene (:BF), which possesses $C_{\infty v}$ symmetry.[128,142]

Another key piece of evidence that terminal monosubstituted borylene ligands act solely as mimics of the ubiquitous carbonyl ligands is their pronounced ability to bridge more than one (identical or different) metal atom. Two distinct possibilities exist to rationalize this bridging interaction: as either a neutral L-ligand donating one electron to each metal center in a $L_{0.5}$ electron-counting description, or as a bridging "boryl" interaction where the boron center is covalently bound to the two metal centers in accordance with a formal X-ligand electron-counting description. To quantify these interactions, a series of theoretical calculations and high-resolution X-ray structural studies were performed by the groups of Braunschweig, Stalke,[143,144] and Kaupp[145] indicating that the bridging interaction of the monosubstituted borylenes does not alter the formal oxidation state of the bound metals. As a result of these studies, bridging monosubstituted boron ligands are formally rationalized in electron-counting and nomenclature as bridging borylenes and not bridging boryls.

1.1.4.1 Synthesis of Borylene Complexes

In terms of transition metal chemistry the first known borylene species were synthesized by Braunschweig and coworkers in 1995,[146,147] however these species were crystallographically shown to be bridging two metal centers in a fashion analogous to a bridging carbonyl motif. As seen in Figure 1-15, the reported bimetallic manganese system [μ-BNMe$_2${(η^5-C$_5$H$_5$)Mn(CO)$_2$}$_2$] (Figure 1-15, **II**) was isolated from the salt elimination reaction of the halodiborane B$_2$(NMe$_2$)$_2$Cl$_2$ with two equivalents of the mono-anionic silylmanganese precursor K[(η^5-C$_5$H$_5$)Mn(CO)$_2$(SiPh$_2$Me)] (Figure 1-15, **I**). The species featured Mn-B and Mn-Mn bond distances of 2.03(1) Å and 2.790(2) Å respectively, with three reported infrared carbonyl stretching frequencies ($\tilde{\nu}$(C≡O) = 1,960, 1,917, and 1,883 cm^{-1}) and an ^{11}B NMR spectroscopic resonance of δ = 103 ppm.

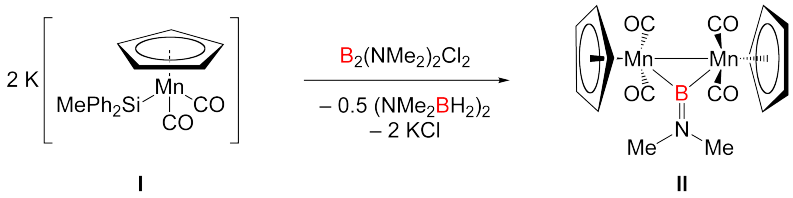

Figure 1-15. Reaction published by Braunschweig *et al.* forming the first bridging transition metal borylene species.[146,147]

Synthesis of a "terminal" borylene fragment bound to a transition metal was reported by Cowley and coworkers in 1998.[148] In his work, [(OC)$_4$Fe{B(η^5-C$_5$Me$_5$)}] (Figure 1-16, **III**) was reported as containing a ":BCp*" or :B(η^5-C$_5$Me$_5$) ligand which would be isoelectronic to a terminal :B-F species and would as such constitute a definitive terminal borylene moiety. This species was prepared by reacting the dianionic iron tetracarbonyl complex K$_2$[Fe(CO)$_4$] (Figure 1-16, **I**) with the dihaloborane analog of pentamethylcyclopentadiene ((*cyclo*-C$_5$Me$_5$)BCl$_2$) (Figure 1-16, **II**). In a following report, Cowley was also able to synthesize the cationic iron half sandwich complex with a pendant ":BCp*" borylene fragment [(η^5-C$_5$Me$_5$)Fe(CO)$_2${B(η^5-C$_5$Me$_5$)}][AlCl$_4$].[149] However, analysis of the bonding situation of this boron-pentamethylcyclopentadienyl fragment from both reported complexes concluded that the boron atom has zero π-accepting ability, as the L$_2$X nature of the pentamethylcyclopentadienyl fragment effectively saturates the boron center, preventing any formal M-B multiple bond character from being established. Analysis of the NMR spectra of these complexes (^{11}B: δ = –35 and –38 ppm respectively) revealed hypervalent character of the boron atoms and X-ray structural data for the Fe-B bond distances (2.010(3) Å and 1.977(3) Å respectively) indicated that a more

accurate representation for this bonding system would be as an iron *nido*-pentacarbohexaborane complex.[57]

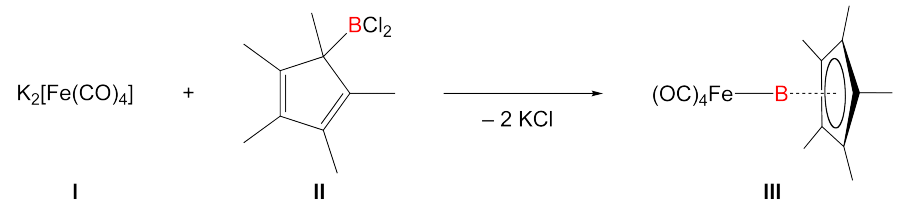

Figure 1-16. Synthesis by Cowley *et al.* of transition metal terminal pentamethylcyclopentadienyl-borylene species.[148]

In stark contrast to the behavior of this species is the tungsten terminal borylene published by Braunschweig and coworkers in 1998.[118,119] Although the synthesis is quite similar to Cowley's reported borylene (Figure 1-17), the spectroscopic data for the complex is markedly different. The tungsten pentacarbonyl aminoborylene species $[(OC)_5W{=}BN(SiMe_3)_2]$ (Figure 1-17, **III**) was prepared by dual salt elimination reaction of the corresponding tungsten pentacarbonyl dianion $Na_2[W(CO)_5]$ (Figure 1-17, **I**) with the dibromoaminodihaloborane ($Br_2BN(SiMe_3)_2$) (Figure 1-17, **II**). This reaction has been shown to be valid for all members of Group 6 and successful synthesis and structural characterization were reported in a series of concurrent publications.[150-152] Crystallographically, the closest comparable M-B bond distance to that of the iron borylene $[(OC)_4Fe\{B(\eta^5\text{-}C_5Me_5)\}]$ species published by Cowley would be the terminal chromium aminoborylene species $[(OC)_5Cr{=}BN(SiMe_3)_2]$ (most similar covalent radii), which displays a similar M-B bond distance (1.996(6) Å compared to 2.010(3) Å).[150,151] In addition, the ^{11}B NMR spectrum shows the resonance for the boron environment to occur at 92 ppm (compared to −35 ppm for $[(OC)_4Fe\{B(\eta^5\text{-}C_5Me_5)\}]$), lending further evidence to the divergent bonding environments between the Cr-B-N and Fe-B-Cp* systems.

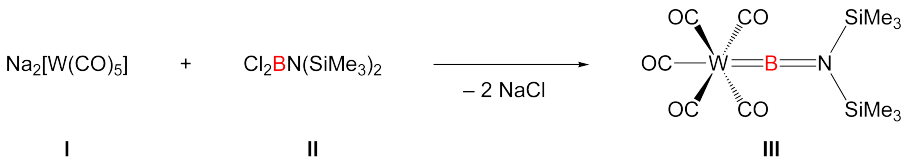

Figure 1-17. Reaction forming the first terminal transition metal borylene species.[118,119]

The group of Braunschweig and coworkers have successfully synthesized two borylene complexes with extreme steric bulk at the boron center. Publication of the terminal hypersilyl-[152-154] and terphenyl-[155,156] borylene species

$[(OC)_5Cr{=}BSi(SiMe_3)_3]$ (Figure 1-18, **I**) and $[(OC)_5Cr{=}B\{2,6\text{-}(2,4,6\text{-}i Pr_3C_6H_2)_2C_6H_3\}]$ (Figure 1-18, **II**) have shown extreme bonding environments of the boron center to transition metals (shorter M-B bond distances) and have allowed for unprecedented reactivity patterns of terminal borylene complexes.[123,157,158] Analysis of the NMR spectroscopic (^{11}B: δ = 204 and 150 ppm respectively) and structural data (Cr-B bond distances of 1.878(10) Å and 1.904(5) Å, respectively) pertaining to the M-B bond both point to markedly different boron environments for these two species. These species both forego the amino-stabilization of the boron center, resulting in much greater metal-boron bonding interactions as well as further electronic deshielding of the boron nucleus. As can be seen below in Figure 1-18, the terminal borylene species have both been prepared *via* dual salt elimination closely akin to the terminal aminoborylene species.

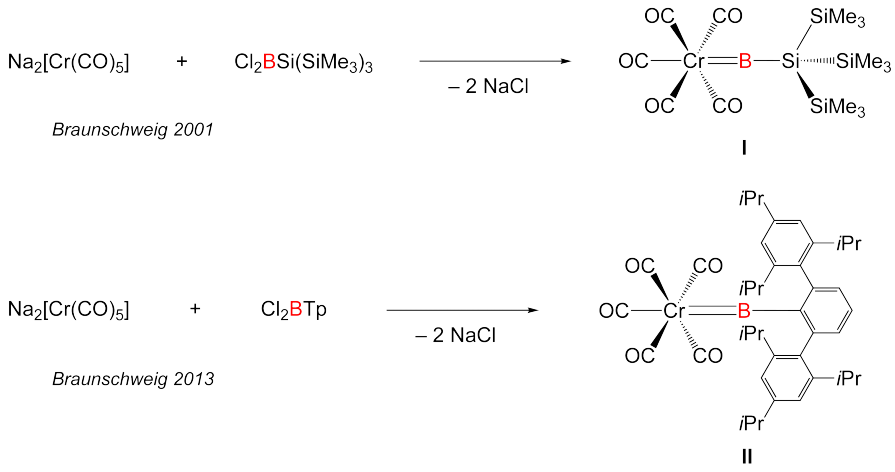

Figure 1-18. Reactions aimed at incorporation of extreme steric bulk for further stabilization of terminal transition metal borylene species.[152-156]

Another reported route for the synthesis of transition metal borylene complexes is through elimination of two equivalents of dihydrogen from reaction of a transition metal σ-dihydrogen complex with a H_2B-R borane as reported in 2008 by Sabo-Etienne and coworkers. This method was initially discovered during a reactivity study of the ruthenium dihydrogen complexes $[RuH_2(\sigma\text{-}H_2)_2(PCy_3)_2]$[159] and $[RuHCl(H_2)(PCy_3)_2]$[160] (Figure 1-19, **I**) with H_2BMes. The reactions respectively yielded the *bis*-σ-B-H bridged borane complex and the terminal borylene complex $[RuHCl(BMes)(PCy_3)_2]$ (Figure 1-19, **III**) *via* double elimination of dihydrogen through the *bis*-σ-B-H intermediate complex $[RuHCl(bis\text{-}\sigma\text{-}H_2BMes)(PCy_3)_2]$ (Figure 1-19, **II**) as proposed in Figure 1-19. The ruthenium borylene species reported displayed an ^{11}B NMR resonance at 106 ppm and a Ru-B bond distance of 1.780(4) Å. The reaction for this particular species was successful in yielding the parent borylene

complex, however, a significant lack of follow up research has indicated this method to not be universally applicable, often yielding the transition metal *bis*-σ-B-H complexes as a byproduct in equilibrium with the metal borylene species.

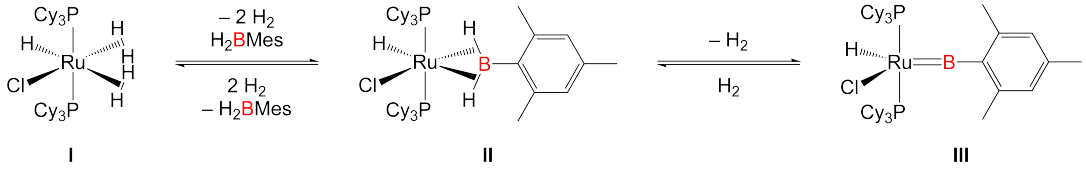

Figure 1-19. Synthesis of a terminal transition metal borylene species *via* a transition metal dihydrogen complex published by Sabo-Etienne *et al.*[160]

One last group of borylene transition metal complexes that merit discussion are the cationic transition metal borylene species. These complexes can be successfully synthesized *via* halide abstractions from transition metal haloboryl species, as initially reported by Aldridge and coworkers in 2003 (Figure 1-20) in several concurrent publications.[161-165] The initially-reported complex [(η^5-C_5Me_5)Fe(CO)$_2$(BMes)][BAr$^f_4$] (Figure 1-20, **II**) was synthesized from reaction of the neutral iron-haloboryl complex [(η^5-C_5Me_5)Fe(CO)$_2${BBr(Mes)}] (Figure 1-20, **I**) with Na[BAr$^f_4$].[161] Spectroscopically this complex displays data similar to traditional arylborylene complexes with a Fe-B bond distance of 1.79 Å and a ^{11}B NMR resonance of 145 ppm. The infrared spectrum of [(η^5-C_5Me_5)Fe(CO)$_2$(BMes)][BAr$^f_4$] shows two stretching frequencies in the carbonyl range ($\tilde{\nu}$(C≡O) = 2,055 and 2,013 cm^{-1}), which are significantly shifted to higher frequency relative to the bromoboryl precursor ($\tilde{\nu}$(C≡O) = 2,006 and 1,961 cm^{-1}). This experimental finding can be dually justified by the creation of a stronger Fe-B bond in the borylene complex rather than in the boryl complex. Computational analysis shows the bonding situation of the cationic iron complex (Figure 1-20, **II**) to also be closely akin to Fischer carbene systems, which would allow for increased Fe→B π-backdonation from the metal center into the boron p orbitals.[162]

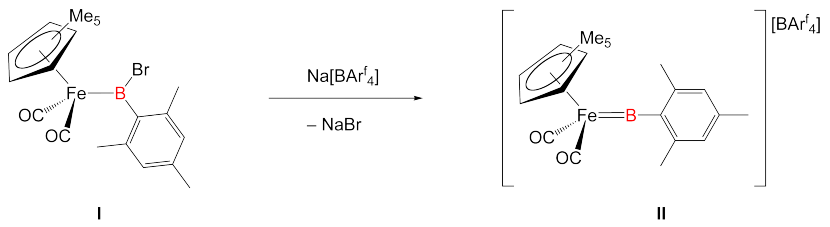

Figure 1-20. Reaction published by Aldridge *et al.* for the synthesis of a cationic transition metal terminal borylene species synthesized *via* halide abstraction from a transition metal-boryl species.[161]

1.1.4.2 Reactivity of Borylene Complexes

Although the synthesis of terminal borylene species is still vitally important for transition metal chemistry, the reactivity of these borylene species also provides extremely valuable information pertaining to the M-B-R electronic environment and merits a full discussion in this introduction. Typical reactions of terminal borylene complexes proceed through two routes: (A) coordination of Lewis bases to the boron atom and subsequent reactivity and metathesis reactions, or (B) transfer of the borylene ligand to other metals and organic substituents (Figure 1-21).[23,54,56] The first reaction pathway simply relies on the highly Lewis acidic boron site to allow for coordination and subsequent reactivity of organic substrates[56] while the second pathway typically depends on the strong *trans*- influence of the borylene ligand destabilizing the bonding environment of the *trans*- ligand within the metal complex and allowing for ligand dissociation and coordination of organic or organometallic substituents. These coordinated substituents can then react with the borylene and yield coupled products.[54]

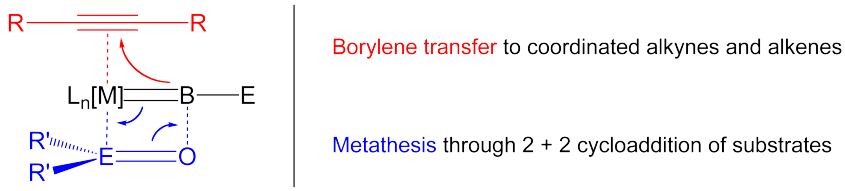

Figure 1-21. Two reactivity pattern observed in transition metal borylene complexes.

Examination of the first possible reaction mechanism involves coordination of a Lewis base to the Lewis acidic boron site as seen in Figure 1-21. Although this coordination can often be used to stabilize the boron center and make isolation of these highly reactive transition metal-borylene species possible, other reactions can take place through this initial step.[56,163-165] Figure 1-22 shows an overview of Lewis base transition metal-borylene interactions that are used to: (A) stabilize the boron electron deficient environment (Figure 1-22, **I**),[163-165] (B) force migration of carbonyls to the boron center (Figure 1-22, **II**),[166,167] or (C) liberate the borylene moiety from the metal center by coordination of multiple bases (Figure 1-22, **III**).[123]

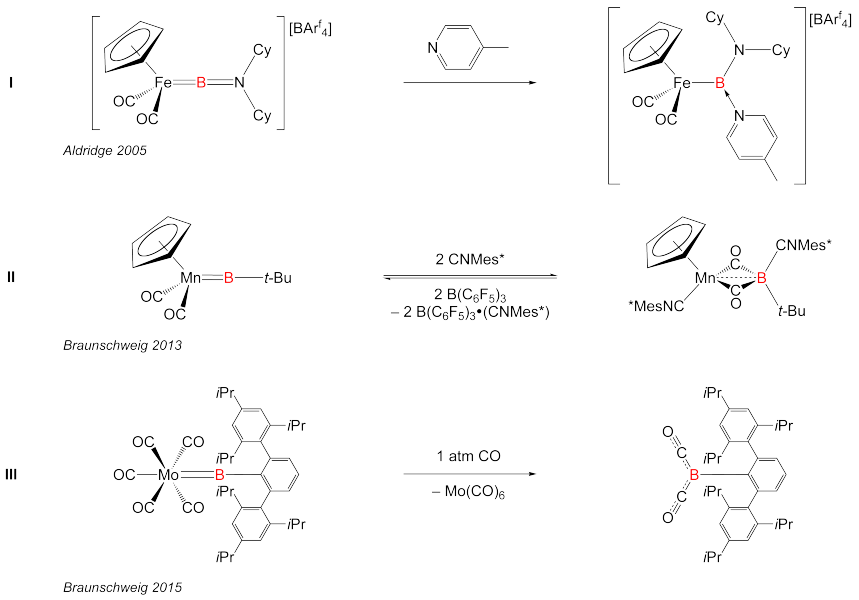

Figure 1-22. Reactions for base stabilized borylene species.[123,163-167]

Another possible route for reactivity of the coordinated Lewis base is for it to participate in metathesis reactions through a [2+2] cycloaddition type intermediate (Figure 1-21, bottom). The first known example of this type of reactivity was shown by Aldridge and coworkers[164,165] from examination of the reactivity of a cationic terminal iron aminoborylene species with phosphine and arsine chalcogenides. Reaction of $[(\eta^5\text{-}C_5H_5)Fe(CO)_2(BN\textit{i}Pr_2)][BAr^f{}_4]$ (Figure 1-23, **I** and **III**) with Ph_3PS and Ph_3AsO successfully led to the metathesis of the Fe=B bond with either the P-S or As-O bonds, yielding the transition metal-chalcogen products $[(\eta^5\text{-}C_5H_5)Fe(CO)_2(EPh_3)][BAr^F{}_4]$ (E = P (Figure 1-23, **IV**), As (Figure 1-23, **V**)). Incidentally, the reaction failed when attempted with the phosphine oxide species Ph_3PO (presumably due to the higher stability of the phosphine oxide bond), yielding only phosphine oxide coordination to the boron center (Figure 1-23, **II**). Precedence for this metathesis was also published by Braunschweig and coworkers[168-170] shortly afterwards from the reaction of a terminal manganese *tert*-butyl borylene species $[(\eta^5\text{-}C_5H_5)(CO)_2Mn{=}B(t\text{-}Bu)]$ (Figure 1-23, **VI**)[171,172] with benzophenone, yielding the manganese carbene product $[(\eta^5\text{-}C_5H_5)(CO)_2Mn{=}CPh_2]$ (Figure 1-23, **VII**) and the boroxine $(B(t\text{-}Bu)O)_3$ as a side product. In following studies this reaction has been witnessed to proceed with many organic carbonyl species, always yielding the transition metal-carbene[170] and the *tert*-butyl borylene substituent coupled to the Lewis basic fragment. Figure 1-23 lists these published reactions and their isolated products.

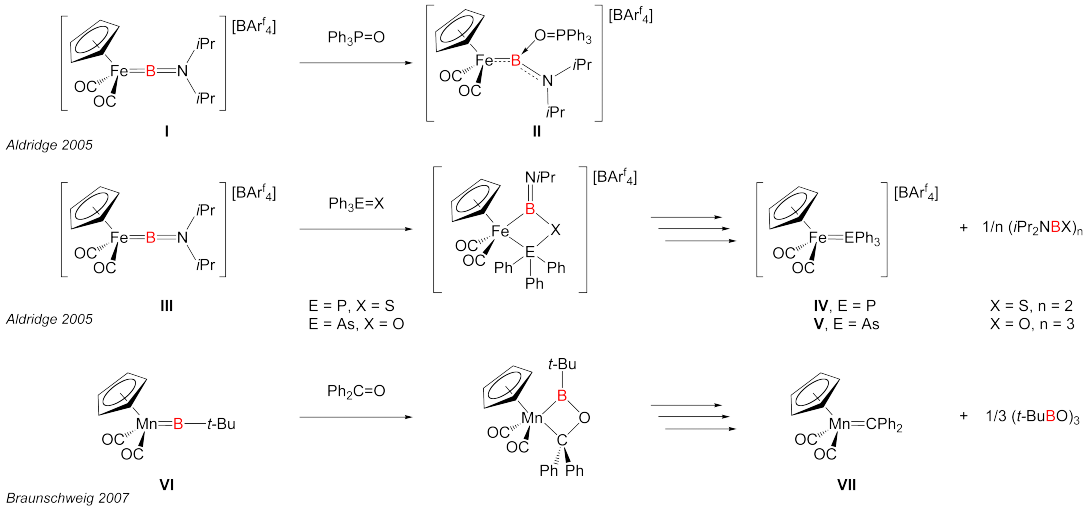

Figure 1-23. Reactions published by Aldridge and Braunschweig detailing metathesis *via* [2+2] cycloadditions of substrates with terminal transition metal-borylene species.[164,165,168,169]

As can also be seen in Figure 1-21, the strong *trans*- influence of the borylene ligand of Group 6 pentacarbonyl terminal borylenes (Figure 1-24, **I**) can be exploited to eject a *trans*- carbonyl ligand. Once this coordination site has successfully been created, coordination of alkynyl[173-176] and alkenyl[177,178] species is proposed followed by subsequent rearrangement leading to elimination of the borylene ligand coupled to the organic fragments. The characterized products isolated from these published reactions show formation of borirene products (Figure 1-24, **III**) from reactions of alkynes while reactions with alkenes have shown to lead to C-H activation products (Figure 1-24, **II**).[54] Figure 1-24 shows a general review of these reactions.* For in depth discussion see Section 1.3.2.

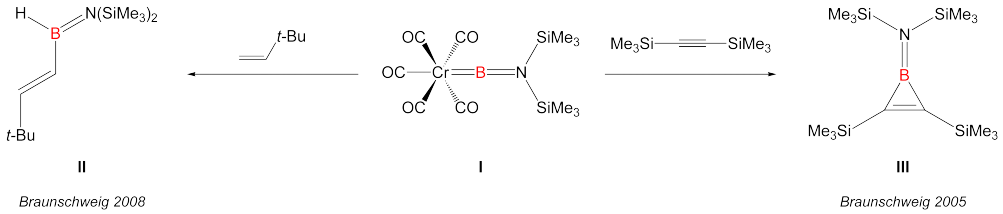

Figure 1-24. Reactions of organic unsaturated substituents with terminal borylene species yielding the borylene fragment coupled to the organic substituent in two motifs.[173-178]

Borylene species can also be synthesized by transfer of the borylene fragment from one metal center to another by either photolytic or thermolytic mechanisms.[23,54] These transfer reactions are said to yield second generation borylene species as the

* See Section 1.3.2 for more in depth discussion.

borylene ligands are not directly synthesized on the metal center, only transferred from existing borylene species. These transfer reactions are typically performed by mixing a Group 6 transition metal-aminoborylene pentacarbonyl species (*i.e.* $[(OC)_5Cr{=}BN(SiMe_3)_2]$) with another transition metal carbonyl species and photolysing or thermolysing the mixtures. Thermolysis or photolysis of the reaction mixtures results in equilibrium exchange of the borylene and carbonyl ligands on the metal scaffolds. This equilibrium is eventually driven to one specific product by the poor solubility of the metal hexacarbonyl species subsequently formed (*i.e.* $[Cr(CO)_6]$, Figure 1-25, **I**) Thus these transfer reactions are possible despite the transferred borylene species being more thermodynamically stable as the equilibrium will eventually drive the reaction to the transferred product as long as the solubility remains higher than the metal hexacarbonyl byproduct. Using this method, mono-borylene transition metal complexes have been synthesized featuring terminal (Figure 1-25, **II**)[179,180] and bridging (Figure 1-25, **III**)[181] borylene interactions as well as *bis*(borylene) transition metal complexes incorporating homo- (Figure 1-25, **IV**),[182,183] and hetero-borylene (Figure 1-25, **V**)[184-186] ligands. Figure 1-25 shows examples of transfer reactions used to prepare new transition metal-borylene complexes.

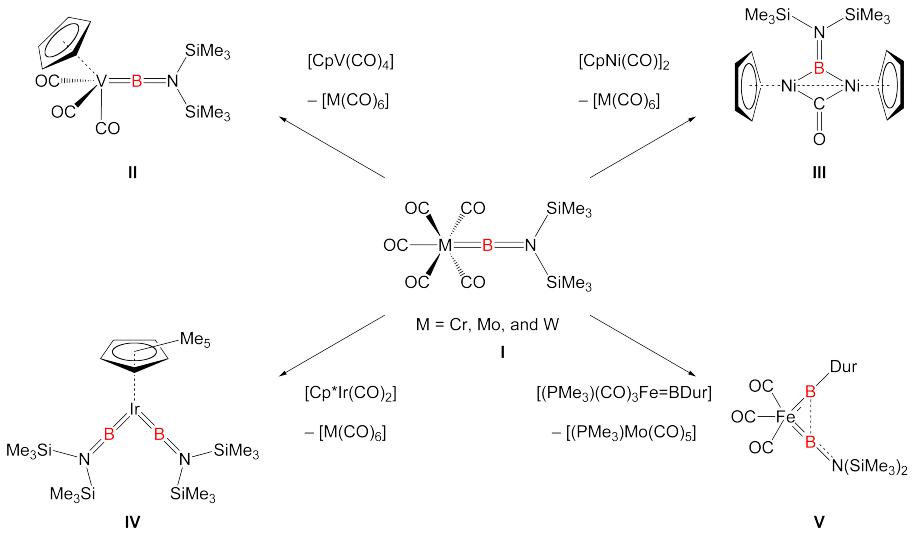

Figure 1-25. Synthesis of second-generation transition metal borylene species synthesized by Braunschweig and coworkers from 1998 to 2013.*

* Individual references for compounds reported in Figure 1-25: **I**,[118,119] **II**,[179,180] **III**,[181] **IV**,[182,183] and **V**.[184-186]

1.2 Boron-Containing π-Conjugated Systems

As previously discussed, three-coordinate boron species possess an empty $2p_z$ orbital (Figure 1-26, **I**) which enables coordination with Lewis bases. This coordination typically increases the geometric dimensionality of the system from a trigonal planar geometry to a four-coordinate pseudo-tetrahedral geometry (Figure 1-26, **II**).[187-192] Since coordination of Lewis bases can also lead to decomposition of the system (*i.e.* from air and moisture), steric protection of the boron center is often incorporated into the system to increase its robustness against decomposition.[193,194] Alternatively, this highly π-acidic vacant orbital can be stabilized *via* other mechanisms, depending on the nature of the substituents bound to the three-coordinate boron center. Resonance structures can be drawn from substituents bearing free lone pairs of electrons (*i.e.* oxo or amino) to a boron center that can increase the stability of these compounds (Figure 1-26, **III**) relative to boranes with non-conjugated substituents. Another stabilization interaction common between boron and π-conjugated aromatic substituents (*i.e.* aryl, vinyl, or alkynyl) is an overlap of the boron p_z orbital with the π-orbitals of these substituents (Figure 1-26, **IV**). In these two particular three-coordinate stabilization interactions (Figure 1-26, **III** and **IV**), the boron center remains planar allowing for aromatic delocalization across the boron center instead of terminating with a sp^3-hybridized boron center.[187-192,195]

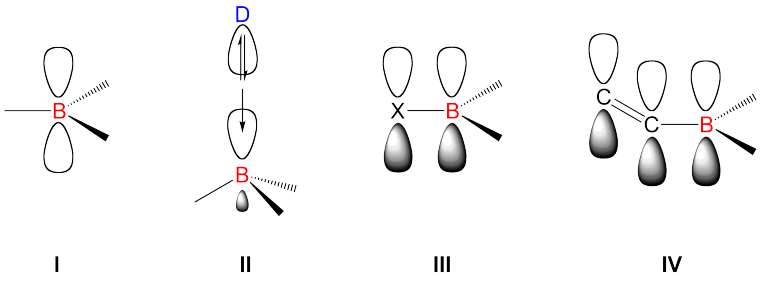

Figure 1-26. Representation of boron's vacant p_z orbital (**I**), and three interactions for electronic stabilization of this orbital (**II**, **III**, and **IV**).

The three-coordinate nature of the boron atom can also be thought of as an isoelectronic and isostructural analog of a carbocationic center in a π-conjugated polymeric or aromatic framework and as such can function as an electron-deficient polymeric unit. In this manner, use of the "electron hole" of the boron center can further promote delocalization of the aromatic electron density over the boron in a manner closely akin to doped P-type semiconductors.[187,188] This vacant $2p_z$ orbital also gives the boron center the ability to stabilize photoexcited electron density from ground state conjugated systems.[192] As can be seen in Figure 1-26, these three

stabilizing interactions combine to make conjugated borane systems uniquely exploitable for their photophysical abilities,[196,197] specifically: nonlinear optics (NLO),[198-202] anion sensing,[203-206] and organic light-emitting diodes (OLEDs).[207,208]

1.2.1 Monomeric Systems and Boron

Internal and external augmentation of small π-conjugated monomeric systems with boron substituents has been shown in a variety of manners.[187-192,209-213] As depicted in Figure 1-27, functionalization of these π-conjugated systems can occur in two manners: (A) either dually boron substituted in an effort to expand the delocalization across two three-coordinate boron centers (Figure 1-27, **I**), or (B) substituted with one boron moiety and a Lewis base that results in a "donor-acceptor" system across the π-conjugated substituent (Figure 1-27, **II**).[187-192]

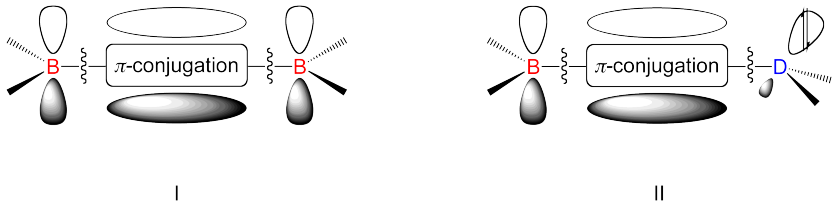

Figure 1-27. Two types of boron augmentation of π-conjugated systems: (**I**), functionalization of both sides with a three-coordinate boron center, and (**II**), functionalization with a three-coordinate boron center and an electron pair donor (donor-acceptor system).

Starting with the synthesis of *para*-phenylenediboranes by Kaim and coworkers in 1984,[214,215] borane moieties have been shown to be useful in augmenting the photoluminescent properties of the parent π-conjugated (phenylene) system. Functionalization with the sterically bulky $BMes_2$ group (Figure 1-28, **I**) resulted in a stable system which could be reversibly reduced twice electrochemically to a dianionic diborataarene (Figure 1-28, **III**). The cyclic voltammogram for the reduction of compound **I** by one- (Figure 1-28, **II**) and two-electron (Figure 1-28, **III**) processes shows a potential difference of 0.69 V between the mono- and dianionic forms. This data indicates electronic delocalization across the phenylene bridge in the monoanionic form, where the oxidation state of one boron radical center impacts the reduction potential for the other boron center due to its high π-acidity. Marder and coworkers, through their extensive studies on chromophore-borane functionalization, have developed knowledge for augmenting the photophysical abilities of these chromophores with monoborane- and diborane-substituents.[216-218]

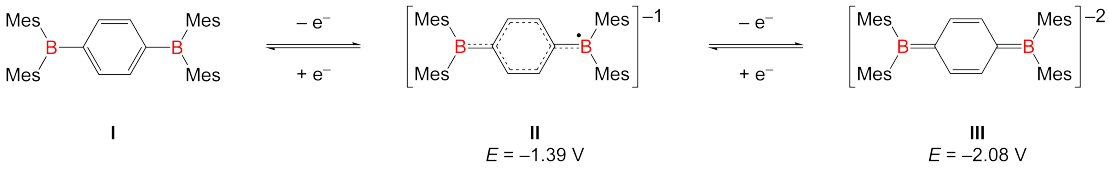

Figure 1-28. Single electron stepwise reduction of the $BMes_2$-functionalized *para*-phenylenediborane (**I**) to the mono- (**II**) and dianionic (**III**) forms with reduction potentials for transitions referenced to the saturated calomel electrode (SCE).[214,215]

Shirota and coworkers were able to synthesize $BMes_2$-functionalized conjugated oligothiophenes and use them as electron transports in the construction of multilayer OLED-type devices.[219-221] These systems displayed stable amorphous glass-type polymeric properties with high glass-transition temperatures (T_g). In the initial 1998 report,[219] a bathochromic shift was observed in the absorption data from UV-vis spectroscopic characterization of three-linked (Figure 1-29, **II**) *vs.* two-linked (Figure 1-29, **I**) thiophene chains functionalized with -$BMes_2$ terminal groups (Figure 1-29). This data was used to justify an increase in π-conjugation for the LUMO of the system and was extrapolated to predict a further energetic lowering of the LUMO as the thiophene chain length is increased. Concurrent work by Corriu, Siebert, and coworkers have also reported absorption red-shifting (bathochromic) for borane-functionalized oligothiophenes when incorporated into polymeric forms *vs.* their monomeric forms.[222] This bathochromic absorption shifting also indicated an increase in the electronic delocalization between the thiophene moieties and the three-coordinate boron centers; however, the reported characterization of these systems was severely limited due to the lack of stability of the polymer against oxygen and moisture.

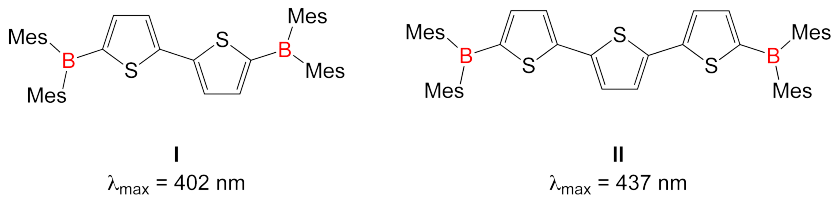

Figure 1-29. Examples of $BMes_2$-functionalized thiophene chains as reported by Shirota *et al.* UV-vis spectroscopy shows a bathochromic absorption shift from **I** to **II**, indicating an expansion of the electronic delocalization of the LUMO.[219]

Terminal three-coordinate borane end-caps on π-conjugated systems have been shown by photophysical and electrochemical studies to extend the π-conjugated delocalization due to the boron atom's high π-acidity.[222,223] Another manner of borane monomer functionalization depends upon synthesis of a single borane end-

cap in combination with a Lewis basic end-cap on the alternate side of the π-conjugated system. This system results in a donor-acceptor type of conjugated system[187-192] informally known as a "push-pull" interaction where the π-acidity of the boron center is used to "pull" electron density from the Lewis base across the entire delocalized system. This creates a dipole over the π-conjugated system inducing conjugation across the compound. As can be seen in Figure 1-30, the structure of the compound is represented by two mesomeric forms in equilibrium. Compound **I** can be considered a state where the lone pair of electrons resides formally on the donor substituent, while compound **II** shows the electron pair conjugated into an aromatic interaction over the π-conjugated system, boron atom, and donor atom. This delocalization also results in formal charged states for the boron and donor substituents.

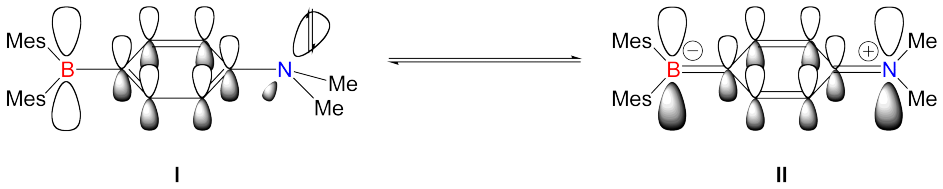

Figure 1-30. The first reported donor-acceptor functionalized π-conjugated system, synthesized by Williams and Glogowski *et al.*, in equilibrium between a formal Lewis acid/Lewis base compound (**I**) and electron-delocalized compound (**II**).[224,225]

Williams and Glogowski were the first group to report donor-acceptor functionalized compounds with their synthesis of *para*-donor-functionalized aryl(dimesityl)boranes (see Figure 1-30, **II** for one example) in 1972.[224] As can be seen in Figure 1-31, the groups of Marder, Shirota, Yamaguchi, and Wang have reported Lewis basic variants adapted for use as electron pair donors for these push-pull systems.[225-229] Electronically these systems show a decrease in the degree of hybridization of the Lewis basic center (increase in planarity of the three-coordinate donor) proportional to the strength of the Lewis acidic side of the π-conjugated system.

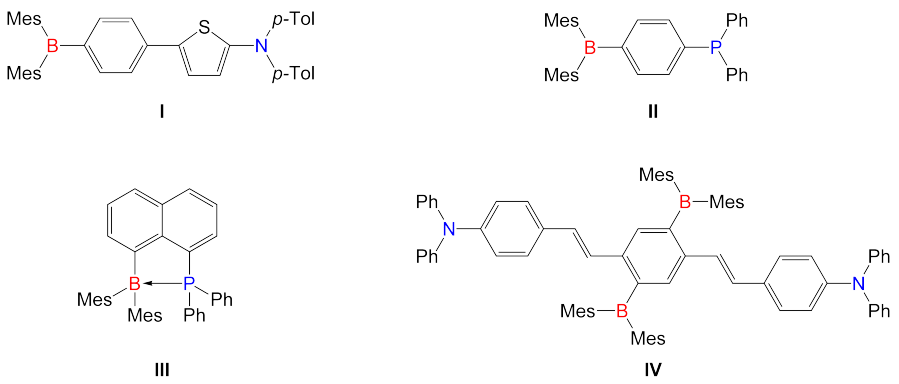

Figure 1-31. Selection of reported donor-acceptor π-conjugated systems.*

Transition metal complexes can also be integrated into this donor-acceptor format, further increasing the range of functionalized substituents available for incorporation into these photoluminescent devices.[226] In particular, the use of triarylborane-functionalized ligands in transition metal complexes has been shown to enhance the metal-to-ligand charge transfer (MLCT) and phosphorescent abilities of these complexes.[230,231] As can be seen in Figure 1-32, numerous examples of incorporation of a three-coordinate boron center into Fe(II), Hg(II), Ru(II), and Pt(II) complexes have been reported by the groups of Marder, Wang, and Gabbaï.[226,232-234]

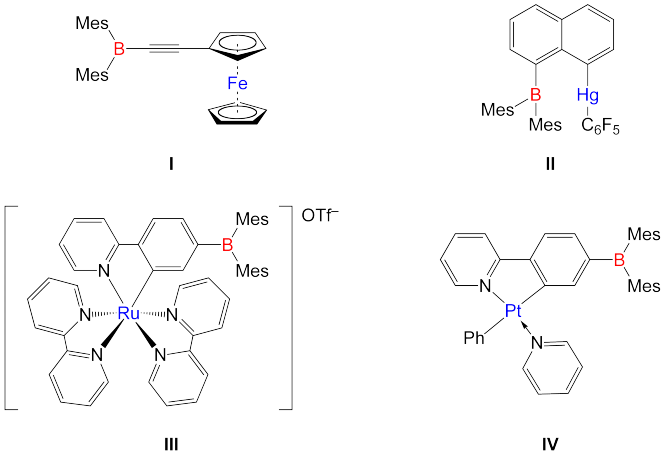

Figure 1-32. Selection of reported donor-acceptor π-conjugated systems in which transition metal centers act as the electron-donating group.†

Marder and coworkers were able to incorporate a transition metal into the middle of a donor-acceptor framework by synthesizing a Pt(II) complex with *trans*-coordination of functionalized phenylacetylenyl moieties (Figure 1-33, **I** and **II**). This format can be rationalized as a simple transition-metal-containing mimic of the

* Individual references for compounds reported in Figure 1-31: **I**,[227] **II**,[226] **III**,[229] and **IV**.[228]
† Individual references for compounds reported in Figure 1-32: **I**,[226] **II**,[232] **III**,[234] and **IV**.[233]

aforementioned donor-acceptor system (Figure 1-30), however, in this particular case, the metal's d orbitals provide the conjugation between the two phenylacetylene units.[235] Wang and coworkers later reported similar species incorporating platinum centers into the periphery of the π-conjugated system (Figure 1-33, **III** and **IV**).[236,237]

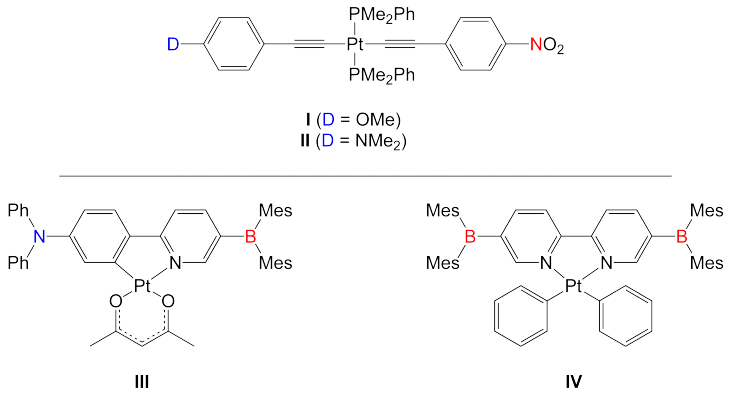

Figure 1-33. A donor-acceptor system incorporating a transition metal as a mimic of traditional π-conjugated systems as reported by Marder *et al.* (top, **I** and **II**).[235] Two examples by Wang *et al.* showcasing the a transition metal in the periphery of a π-conjugated donor-acceptor (bottom, **III**) and diborane (bottom, **IV**) system.[236,237]

1.2.2 Oligomeric and Polymeric Systems and Boron

Incorporation of π-conjugated borane groups into polymeric and oligomeric forms has resulted in materials that possess many photophysical aspects similar to their smaller monomeric forms.[192] Starting from 1992[238] until the early 2000's,[239-248] reports by Chujo and coworkers detailed the synthesis of boron-containing polymers prepared *via* reactions of dihydroboranes (H_2BR) with dicyano monomers resulting in the hydroboration and polymerization of the substrates.[238-248] These reports spurred concurrent research into new methods for incorporation of three-coordinate boron centers within polymeric frameworks. Another common polymerization technique published by Chujo and coworkers was the hydroboration of dialkynyl monomers with singly-substituted boranes.[249-252] As can be seen from Figure 1-34, the position of the three-coordinate boron centers in these polymers can be summarized in three ways: (**I**) main-chain functionalized conjugated polymers, (**II**) side-chain functionalized conjugated polymers, and (**III**) side-chain functionalized polyolefins.[192] These three different boron orientations in polymeric materials have all been experimentally observed and result in dramatically different physical and electronic properties of these polymers. Although the initial reports by Chujo on polymerization studies of boranes continued until the mid 2000's, the main problem associated with the characterization of all these polymers is the high reactivity of the boron center towards air and moisture, leading to decomposition before accurate chain lengths and masses could be estimated. Incorporation of steric bulk at the boron center alleviates some of this chain decomposition, but the characterization of these species in detail still remains an important problem if these polymers are to be integrated into industrially feasible synthesis.

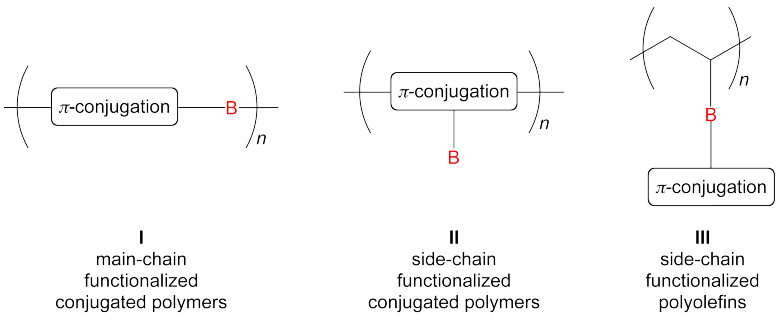

Figure 1-34. The three main representations for the incorporation of boron functionalities and π-conjugated systems into a polymer.[192]

1.2.2.1 Main-Chain Functionalized Organoboron Polymers

Although a plethora of polymerization reactions using boron-containing functional groups were reported by Chujo and coworkers in the early 1990's,[238-241] the first π-conjugated system was not reported until 1998.[249,253] Initially, the most commonly explored techniques developed for incorporation of three-coordinate boron systems into π-conjugated polymers were hydroborations, haloborations, and phenylborations of monomeric substrates with boranes. Later, incorporation of alkynyl or arylenyl substituents into a polymer framework was developed using techniques centered around organolithium, organotin, and Grignard coupling reactions in order to keep an unsaturated backbone intact.[192] Sterically encumbering aryl substituents such as Mes (2,4,6-tri-methylphenyl) or Tipp (2,4,6-tri-*iso*propylphenyl) groups can be appended to the boron center to increase the stability of the polymer framework from decomposition. Polymerization reactions can be monitored by examination of the ^{11}B NMR spectra. Typical NMR data for these reactions show a broadening of the ^{11}B resonance, with an accompanying upfield shift as higher degrees of polymerization are realized. This upfield shift and broad ^{11}B NMR resonance is indicative of higher degrees of conjugation within the polymer and an extension of the degree of π-overlap of the aromatic linkers and the boron centers (π^*-p_z overlap).

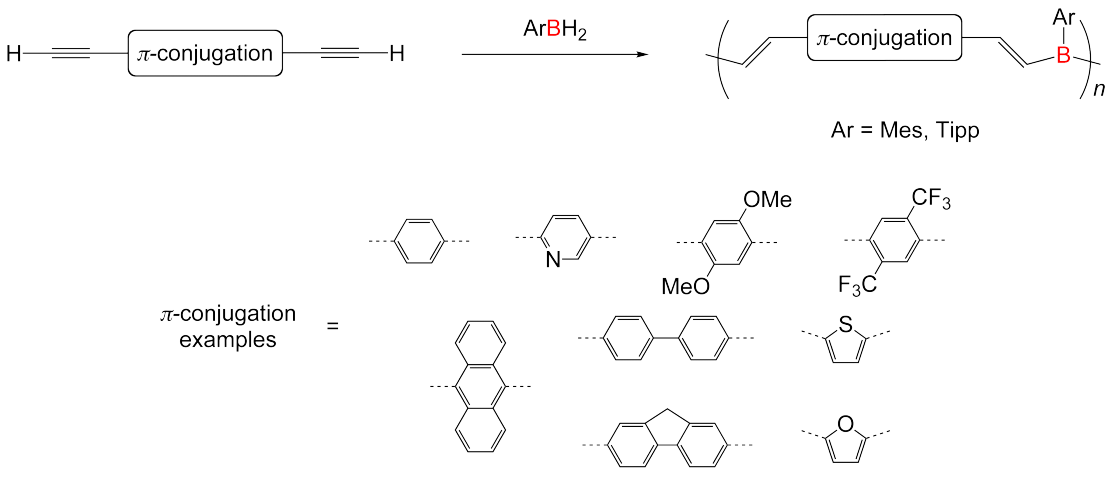

Figure 1-35. Selection of π-conjugated dialkynyl systems incorporated into a polymer by hydroboration of alkynyl functionalities with aryl boranes ($ArBH_2$).[192,249,250]

1.2.2.2 Side-Chain Functionalized Organoboron Polymers

Integration of boron functionalities into the side chains of a monomeric unit allows these systems to impart significantly beneficial properties to these polymeric systems relative to main-chain boron functionalization. Firstly, the integration of the boron unit into the side chains of a polymeric unit allows for only one of the boron's valence electrons to be tied up in proper bonding to the polymeric backbone with the other two available for further electronic tuning of the system (Figure 1-36). Secondly, functionalization of the side chains on polymeric systems with boron substituents can be achieved by first forming a fully π-conjugated main chain polymer. Functionalization of the monomers with silyl substituents allows for further post-polymerization reactions with haloboranes to initiate silicon-boron exchange and functionalize the side chains of the system with boron units (Figure 1-37). This method has another benefit as the initial polymerization reaction does not have any air- or moisture-sensitive boron substituents, so the reactions can be run in wet solvents and under air if appropriate.

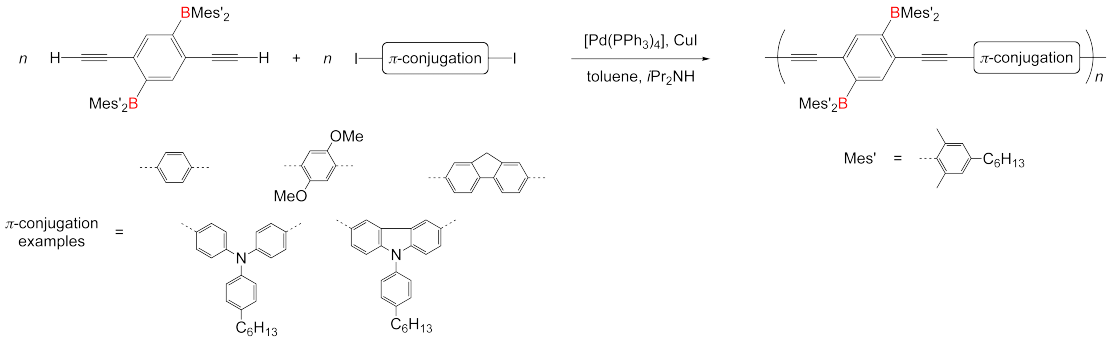

Figure 1-36. Selection of π-conjugated systems and a peripherally boron-functionalized aryl dialkyne incorporated into a polymer under palladium-catalyzed Sonogashira-Hagihara coupling conditions as reported by Yamaguchi *et al.*[192,254]

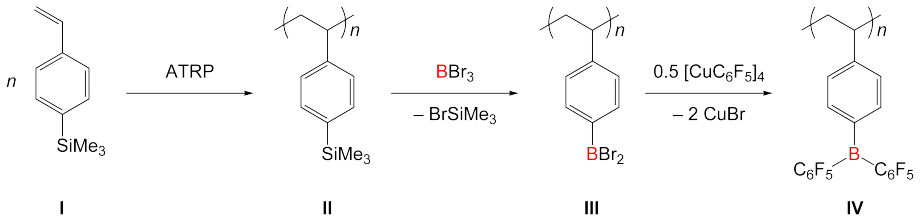

Figure 1-37. Functionalization of polymers with peripheral boron functionalities by silicon-boron exchange as reported by Jäkle *et al.*[192,255]

1.2.2.3 Transition Metals Incorporated into Organoboron Polymers

Incorporation of transition metals into boron-containing π-conjugated polymeric frameworks was originally reported by Chujo and coworkers (Figure 1-38) in two publications from 2001.[251,252] After these initial publications, Jäkle and coworkers reported several examples of main chain as well as side chain functionalization of boron-containing polymeric systems with ferrocenyl derivatives.[256-258] In addition to the obvious d_π-p_π overlap between the metal and its ligands, the system can also relax excited electronic states through metal-to-ligand charge transfer (MLCT) mechanisms. The systems reported by Chujo and coworkers used several key photoactive transition metal systems including Pt(II) and Ru(II) units as metal scaffolds for this chemistry. The polymers are typically built from hydroboration of the transition metal *bis*(alkynyl) monomers with aryl boranes as previously outlined in Figure 1-35.

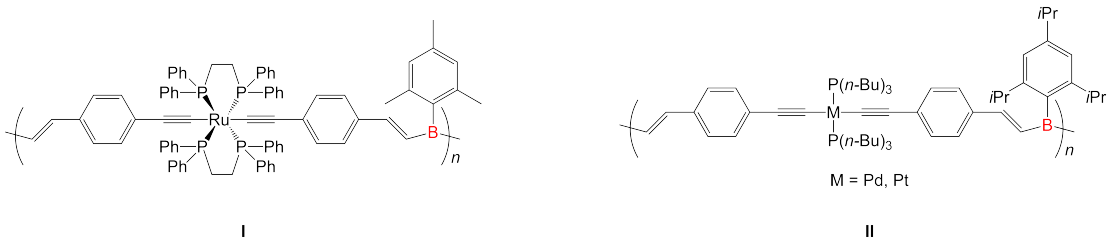

Figure 1-38. Three examples of transition metal polymeric structures synthesized by hydroboration reaction of groups 8[251] (**I**) and 10[252] (**II**, **III**) transition metal *bis*(alkynyl) monomers with aryl boranes as reported by Chujo *et al.*

1.3 Cyclic Mono-Boron Containing Heterocyclic Aromatic and Antiaromatic Systems

The construction of boron-containing aromatic and antiaromatic heterocycles constitutes another method for the incorporation of an empty p_z orbital into π-conjugated systems. As covered in the previous chapter, the ability of a three-coordinate boron center to allow for conjugation between aromatic units is a key feature of the development of these species for materials applications.[187-192] Unfortunately, polymeric species often feature C-C and C-B bonds that have low rotational energy barriers which prevent proper alignment of the boron p_z orbital with the π-conjugated systems. Integration of three-coordinate boron centers into aromatic and antiaromatic heterocycles allows for a forced planar geometry within the ring and helps to prevent loss of conjugation due to bond rotation. Figure 1-39 illustrates two simple comparative compounds possessing three-coordinate boron centers and phenyl-substituted organic backbones (both linear and cyclic). The linear three-coordinate boron species[259] (Figure 1-39, **I**) is observed to have free rotation around the boron-vinyl bonds, while the cyclic three-coordinate boron species[260,261] (Figure 1-39, **II**) is locked into a planar geometry due to the cyclic nature of the system.

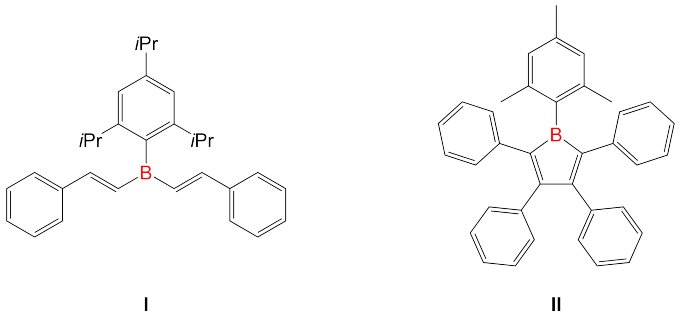

Figure 1-39. Mono-boron π-conjugated systems incorporating the boron in a linear[259] (**I**) and a cyclic antiaromatic form[260,261] (**II**).

1.3.1 General

For the purpose of this introduction, discussion will be limited to only mono-boron heterocycles. Specifically these systems constitute the borirenes (Figure 1-40, **I**), boroles (Figure 1-40, **II**), borabenzene/boratabenzenes (Figure 1-40, **III** and **IV** respectively), and borepines (Figure 1-40, **V**) classes of aromatic and antiaromatic systems.[262-268] These systems all display drastically different photophysical characteristics from their carbon analogs as well as the ability to function as potential ligands with transition metals.[269-271]

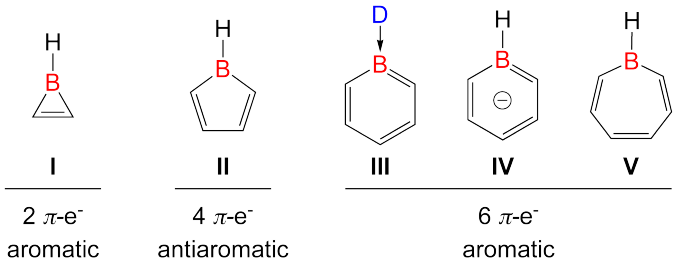

Figure 1-40. Five mono-boron aromatic and antiaromatic systems. Borirene (**I**), borabenzene (**III**), boratabenzene (**IV**), and borepine (**V**) systems are considered aromatic under Hückel rules while the borole (**II**) system is considered antiaromatic under Breslow rules.[262-268]

Of these five classes of compounds, three examples (borirene (Figure 1-40, **I**),[272] borabenzene (Figure 1-40, **III**)[273] and borepine (Figure 1-40, **V**)[274] are known to obey the Hückel rules for aromaticity[275] by possessing cyclic planar geometries and π-conjugated electron counts equal to $4n + 2$ (where n is greater than or equal to zero). In the case of the borepine (Figure 1-40, **V**), some discussion still exists whether all species are truly aromatic due to the non-planar ring geometries of certain examples;[276-278] however, the majority of crystallographically-characterized borepine species are shown to exhibit planar geometry. Consequently, compounds that possess cyclic planar geometries and an electron count of only $4n$ electrons (as defined by Breslow)[279-281] are classified as antiaromatic in nature and typically possess high instability and increased reactivity when compared to their aromatic analogues. This classification has been applied to many bicyclic ring systems such as pentalene and biphenylene; however, the most common monocyclic boron-containing system that has been experimentally characterized and satisfies these requirements is the borole (Figure 1-40, **II**) class of compounds.[282]

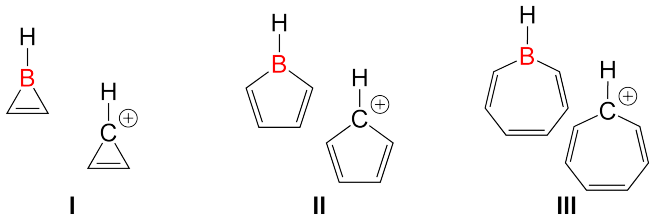

Figure 1-41. Mono-boron aromatic and antiaromatic systems (top) and their respective isoelectronic and isostructural boron-free cationic analogs (bottom).[283,284]

As boron possesses one fewer valence electron than carbon, many of these boron-containing systems are isostructural and isoelectronic with cationic cyclic hydrocarbons.[268] As seen above in Figure 1-41 the borirene (Figure 1-41, **I** top), borole (Figure 1-41, **II** top), and borepine (Figure 1-41, **III** top) are all isostructural and isoelectronic analogues of the respective cyclopropenylium (Figure 1-41, **I** bottom), cyclopentadienylium (Figure 1-41, **II** bottom), and cycloheptatrienylium (Figure 1-41, **III** bottom) aromatic and antiaromatic systems.[283,284]

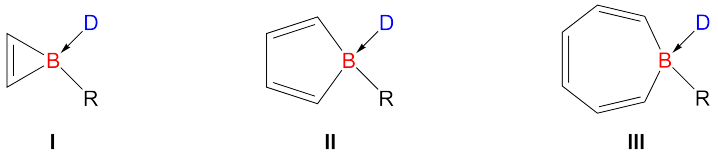

Figure 1-42. Simple base coordination reactivity for all boron containing aromatic and antiaromatic systems resulting in a four-coordinate boron center.[176,278,285,286]

The reactivity of these boron containing aromatic and antiaromatic systems is similar to other π-conjugated boron containing systems, which feature primary reactivity (and decomposition) based on coordination of bases at the boron p_z orbital (Figure 1-42, **I**, **II**, and **III**).[176,278,285,286] This typical coordination requires strong Lewis bases (*i.e.* carbenes, phosphines, and amines) to disrupt the aromatic or antiaromatic electron delocalization of the system. The ability of Lewis bases to interrupt the aromatic delocalization and alter the HOMO-LUMO energetic gaps of these systems can be witnessed by UV-vis absorption spectroscopy with the absorption spectrum of the four-coordinate boron compound typically being hypsochromically shifted relative to those of the three-coordinate boron aromatic or antiaromatic systems.[176,278,285,286]

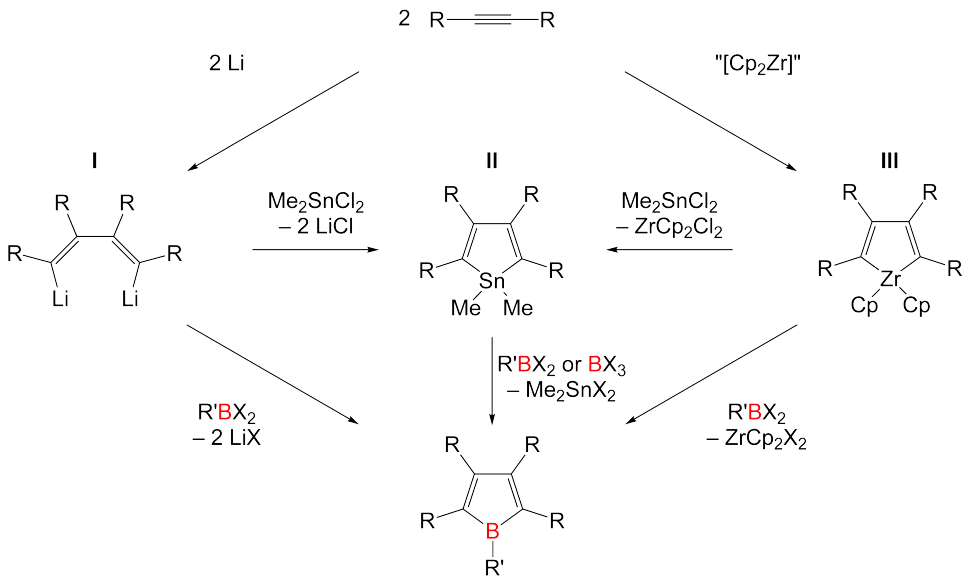

Figure 1-43. Outline of the main synthetic routes for the preparation for boroles.[287]

Borirenes and borabenzenes/boratabenzenes and their complexes will occupy a formal section of this introduction, so a short synthetic discussion will follow concerning antiaromatic borole systems. These systems are typically synthesized by tin-boron exchange (Figure 1-43, **II**) or zirconium-boron exchange (Figure 1-43, **III**) reactions from stannacyclic or zirconacyclic precursors with functionalized dihaloboranes or trihaloboranes.[287] It should be noted that some species of boroles can be synthesized directly from reactions of the 1,4-dilithio-1,3-butadienes with functionalized dihaloboranes (Figure 1-43, **I**).[287] A similar synthetic strategy for insertion of a boron atom into an aromatic ring system is commonly used for borabenzene and borepine systems as well.[270,273] Due to the high reactivity of the borole systems, the use of sterically encumbering aryl substituents is typically employed to yield boroles of sufficient stability for controlled reactivity studies and X-ray structural characterization.[287]

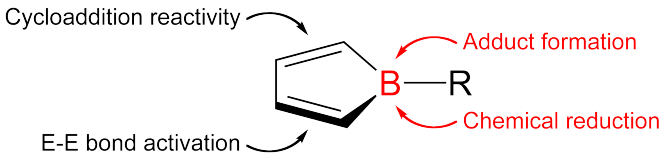

Figure 1-44. Generic diagram detailing the known reactivity patterns displayed by borole systems.[287]

Besides the aforementioned reactivity of boroles with Lewis bases, boroles are known to react through either the unsaturated backbone of the system (Figure 1-44, black arrows), or directly at the boron center (Figure 1-44, red arrows). Boroles are known

to perform Diels-Alder type cycloadditive reactions with unsaturated organic substrates as well as main-group E-E bond activations through the backbone of the system. Besides the aforementioned base coordination, the boron center is also capable of being electrochemically reduced, resulting in monoanionic and dianionic 5-electron and 6-electron systems respectively.[287]

1.3.2 Borirenes

The three-membered borirene system (*cyclo*-BC_2R_3) constitutes the smallest mono-boron heteronuclear aromatic system allowed by the Hückel rule.[275,288] Borirenes possess two π-electrons delocalized over all three-ring atoms (*cyclo*-BC_2) and are typically classified as isoelectronic with the well-known cyclopropenylium cations (Figure 1-45, top).[271] The degree of aromaticity in the ring is known to vary to a great extent based upon the nature of the substituents bound to the boron center (Figure 1-45, bottom). Base coordination to the boron atom is still possible with strong bases (*i.e.* pyridines and carbenes, Figure 1-45, **III**),[176] and the resulting four-coordinate boron species is rationalized to have zero π-electron delocalization over the boron atom and has negligible aromaticity based upon experimental monitoring of the UV-vis data for the absorption spectroscopy. Borirenes with exocyclic substituents at the boron atom bearing no lone pairs of electrons (*i.e.* aryl, Figure 1-45, **I**)[289] to stabilize the boron center are thought to have the greatest degree of aromatic delocalization. Finally, species bearing exocyclic boron substituents covalently bound to the boron center that bear free pairs of electrons (*i.e.* amino, Figure 1-45, **II**)[173,174] are typically rationalized to lie in between these two extremes based upon UV-vis absorption spectroscopy.

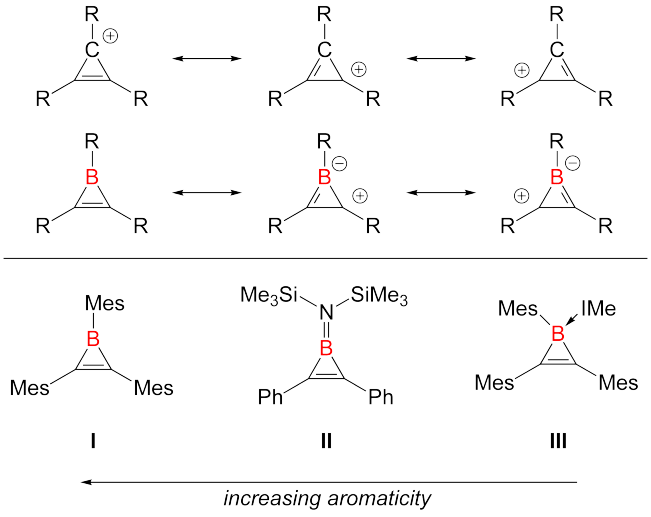

Figure 1-45. Comparison between cyclopropenylium cation and borirene resonance structures (top). Variance between functionalized borirenes and the degree of π-electron aromaticity over all three (*cyclo*-BC_2) atoms of the ring (bottom).[173,174,176,289]

Borirenes have traditionally been difficult to prepare under laboratory conditions due to their propensity for dimerization in solution to 1,4-diboracyclohexa-2,5-dienes (Figure 1-46, **IV**).[290] Borirenes possess high degrees of ring strain and are ill-suited to be synthesized by traditional tin-boron or silicon-boron exchange routes *via*

stannacyclic and zirconacyclic reactions with trihaloboranes. Starting with the publication by Timms and coworkers of an *in situ* haloborylene capture by acetylene in 1968 (Figure 1-46),[290] the halide-functionalized borirene species (Figure 1-46, **III**) was reported to be difficult to isolate from reaction mixtures due to instability of the borirene at room temperature. In this publication, use of extremely high temperatures (>2,000 °C) led to the liberation of "free" :B-F and :B-Cl haloborylenes[124,125,290] in the presence of acetylene gas, allowing for the trapping of the free borylene by borirene formation. This process was successful in yielding borirene intermediates; however, these intermediates were found to dimerize into 1,4-diboracyclohexa-2,5-diene species as outlined in Figure 1-46. Use of more sterically bulky alkynyl substituents was later developed to allow for increased ease of isolation of the synthesized borirenes and increased resistance of these borirenes towards dimerization.

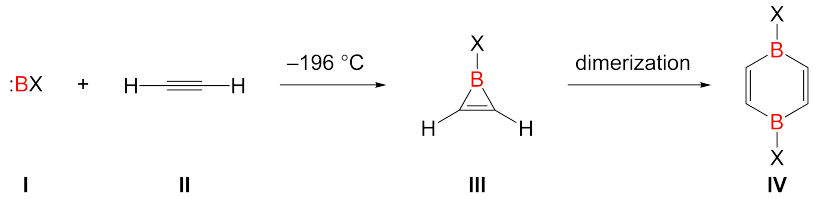

Figure 1-46. Reaction to trap free haloborylenes (**I**) by *in situ* reaction with alkynes (**II**) resulting in a haloborirene (**III**); however, the species is not stable and will dimerize to the 1,4-diboracyclohexa-2,5-diene species (**IV**).[290]

1984 stands as a remarkable year for the synthesis of borirenes with three different routes being published by the groups of West,[126,127] Berndt,[291,292] and Meller.[293] West was able to successfully adapt the work published by Timms for alkyne capture of a liberated borylene[290] into a successful route to capture a liberated silylborylene (:B-$SiPh_3$, Figure 1-48, **II**) by formation of the 1-triphenylsilyl-2,3-*bis*(trimethylsilyl)borirene (Figure 1-48, **III**). The route employed photolytic ejection of a free silylborylene in frozen solvent matrix and capture by the sterically bulky *bis*(trimethylsilyl)acetylene to prevent dimerization of the species in solution.[126,127]

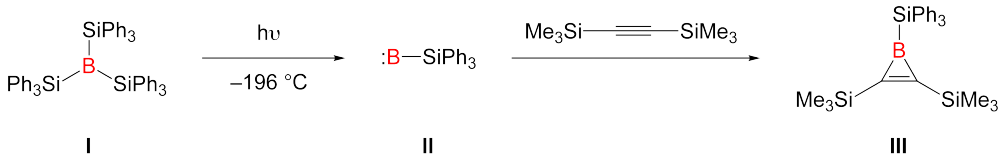

Figure 1-47. Borirene synthesis by liberation of a free borylene and its trapping with an alkyne by West and coworkers.[126,127]

Berndt and coworkers reported an elegant synthesis of *tert*-butyl-functionalized borirenes from reaction of a dihalodiborane (1,2-di-*tert*-butyl-1,2-dichlorodiborane, Figure 1-48, **II**) with *bis*(trimethylstannyl)acetylene (Figure 1-48, **I**). The reaction results in the non-reversible loss of chlorotrimethylstannane and formation of a boryl-functionalized borirene (Figure 1-48, **III**) in near quantitative crude yields.

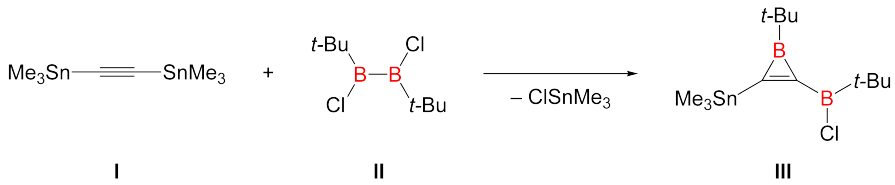

Figure 1-48. Synthesis of a borirene unit in solution *via* halostannane elimination by Berndt and coworkers.[291,292]

Meller and coworkers published a reduction of a dithiaborole with sodium metal resulting in formation of a borirene. The synthetic method involved reaction of 3-*bis*(trimethylsilyl)amino-1,2,3-dithiaborole (Figure 1-49, **I**) with excess sodium metal resulting in a "ring contraction" to form the *bis*(trimethylsilyl)aminoborirene species (Figure 1-49, **II**). An intermediate oligomeric precursor is reported in this publication, which could be isolated by an "oligocondensation" process and characterized by mass spectroscopy. Heating of this oligocondensate under high vacuum allows for the final isolation of the borirene species as shown in Figure 1-49.

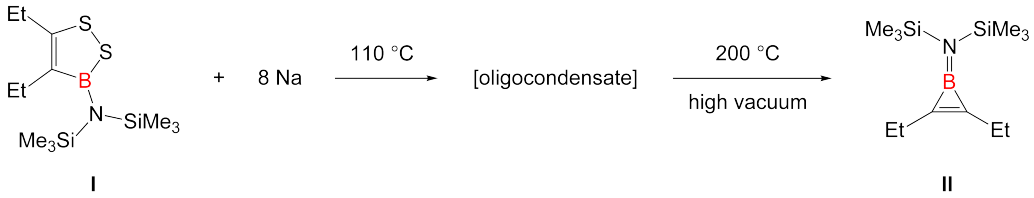

Figure 1-49. Synthesis by Meller and coworkers involving the isolation of an oligocondensate which could be converted to a borirene by heating.[293]

Another route for borirene synthesis was published by Eisch and coworkers through a series of publications starting from 1987 where a trimesityl-functionalized alkynylborane (Figure 1-50, **I**) was irradiated photolytically (λ = 300 nm)[294] to force mesityl migration from the boron to the α-carbon of the alkynyl substituent and alkynylborane rearrangement to a *cyclo*-BC_2 ring system where the boron is covalently bonded to the formerly α- and β-carbons of the alkyne (Figure 1-50, **II**). It should be noted that continued irradiation of the borirene can lead to reversion back to the alkynyl species.

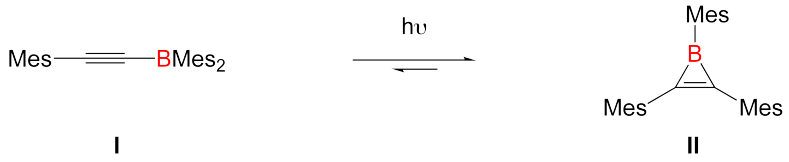

Figure 1-50. Photorearrangement of a diarylalkynylborane to force migration of one aryl substituent to the *α*-carbon resulting in a stable borirene.[294]

With the development of increased steric bulk on terminal transition metal borylene complexes, another route was eventually developed that utilized photolysis or thermolysis of transition metal terminal group 6 borylene complexes in the presence of free alkynes.[173,174] This process led to transfer of the terminal :BN(SiMe$_3$)$_2$ fragment from the metal pentacarbonyl scaffold to the alkynyl compound resulting in an aromatization of the *cyclo*-BC$_2$ system and release of a free borirene. Modification of this route with other alkynes and diynes, as well as *σ*-alkynyl transition metal complexes, has been subsequently published. Figure 1-51 displays a selection of these alkynyl species that have been used to create borirenes from the Group 6 terminal transition metal borylenes (Figure 1-51, **I**).[173-175,295,296]

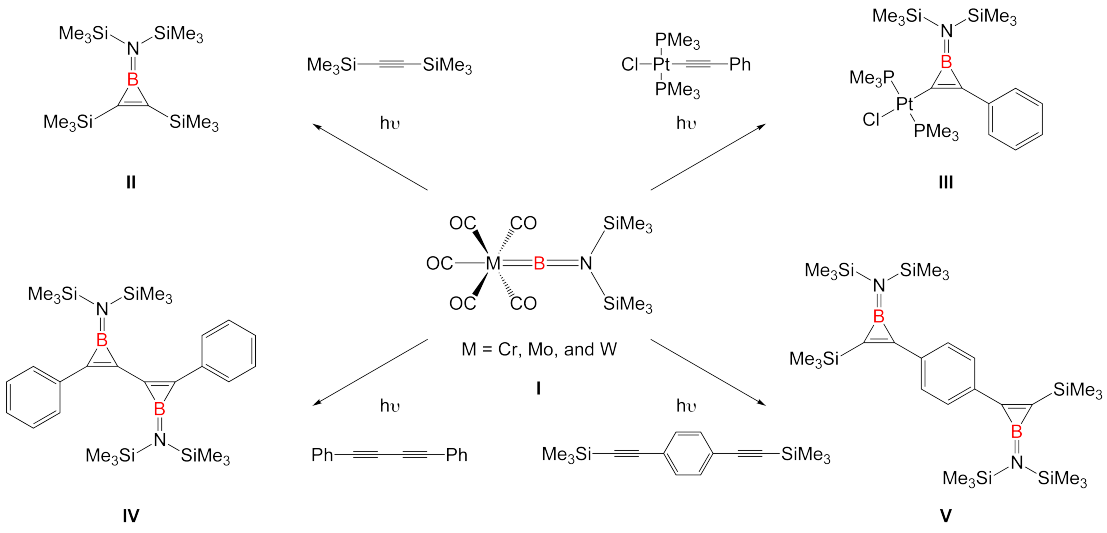

Figure 1-51. Photolytic reactions used to generate monoborirenes and *bis*(borirenes) from terminal transition metal borylenes resulting in a variety of functionalized species.*

Augmentation of the alkynes can also be accomplished with transition metal-alkynyl species, resulting in transition metal-functionalized borirenes. These species incorporate a transition metal's d orbitals into the borirene system and allow for augmentation of the electronic structure of the borirene with a significant amount of electronic donation into the system. As can be seen in the photolytic or thermolytic

* Individual references for compounds reported in Figure 1-51: **I**,[118,119] **II**,[173,174] **III**,[295] **IV**,[175] and **V**.[175]

reactions of transition metal alkynyl species in the presence of terminal transition metal borylenes, the transition metal-functionalized borirenes can be successfully isolated (Figure 1-51, **III** and Figure 1-52, **III**). As can be seen in Figure 1-52, the iron-functionalized borirene continues to dissociate and re-coordinate a carbonyl ligand, allowing for rearrangement of the complex to form a product where the boron atom has inserted into the Fe-C bond (Figure 1-52, **IV** and **V**).[297] This rearrangement process is constantly occurring while the mixture is under photo-irradiation and all three species have been isolated and structurally characterized from reaction mixtures.

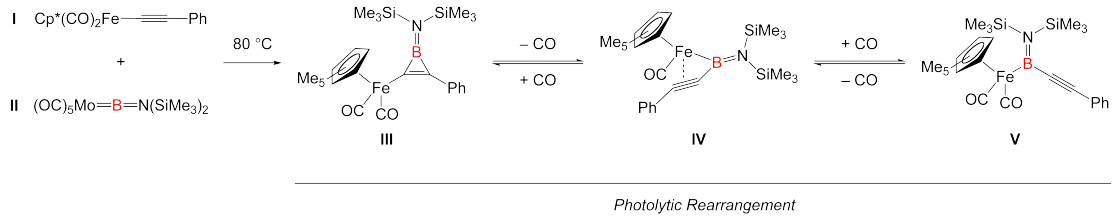

Figure 1-52. Synthesis of a *σ*-bonded transition metal borirene complex and subsequent photolytic rearrangement of the ring with dissociation of a carbonyl ligand.[297]

Functionalization of the boron atom of a borirene *cyclo*-BC_2 system by a transition metal can also occur from irradiation of an alkynyl species with a transition metal-functionalized borylene complex (see Figure 1-53).[283,284] Irradiation of a $FeCp^*(CO)_2$-functionalized chromium pentacarbonyl borylene species (Figure 1-53, **I**) in the presence of *bis*(trimethylsilyl)acetylene led to the transfer of the ferroborylene fragment to the alkyne, resulting in an isolable ferroborirene (Figure 1-53, **III**).[283,284]

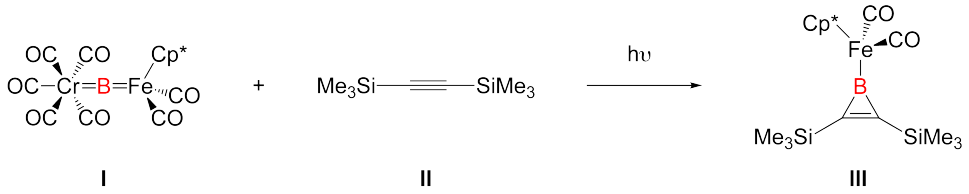

Figure 1-53. Synthesis of a "ferroborirene" species as reported by Braunschweig *et al.* in which an iron-substituted borylene fragment is used to augment a borirene by incorporation of a transition metal *σ*-bond to the boron.[283,284]

The reactivity of these borirene species can be summarized by Figure 1-54. To generalize all of the reactivity studies that have been performed on borirene species, the species are known to react with O_2, resulting in insertion of dioxygen between the boron and the carbons of the *cyclo*-BC_2 ring (Figure 1-54, **II**). The species is known to

react with methanol and other alcohols to lead to the ring-opened borirene with the methoxy substituent bound to boron and protonation of the *β*-carbon (Figure 1-54, **III**). Reactions with glacial acetic acid lead to cleavage of both boron-carbon bonds, resulting in (Z)-dimesitylethene (Figure 1-54, **IV**). As previously discussed in Figure 1-45, base coordination can occur at the boron center to lead to the quarternized borirene, a product that is often in equilibrium with the non-coordinated precursor.

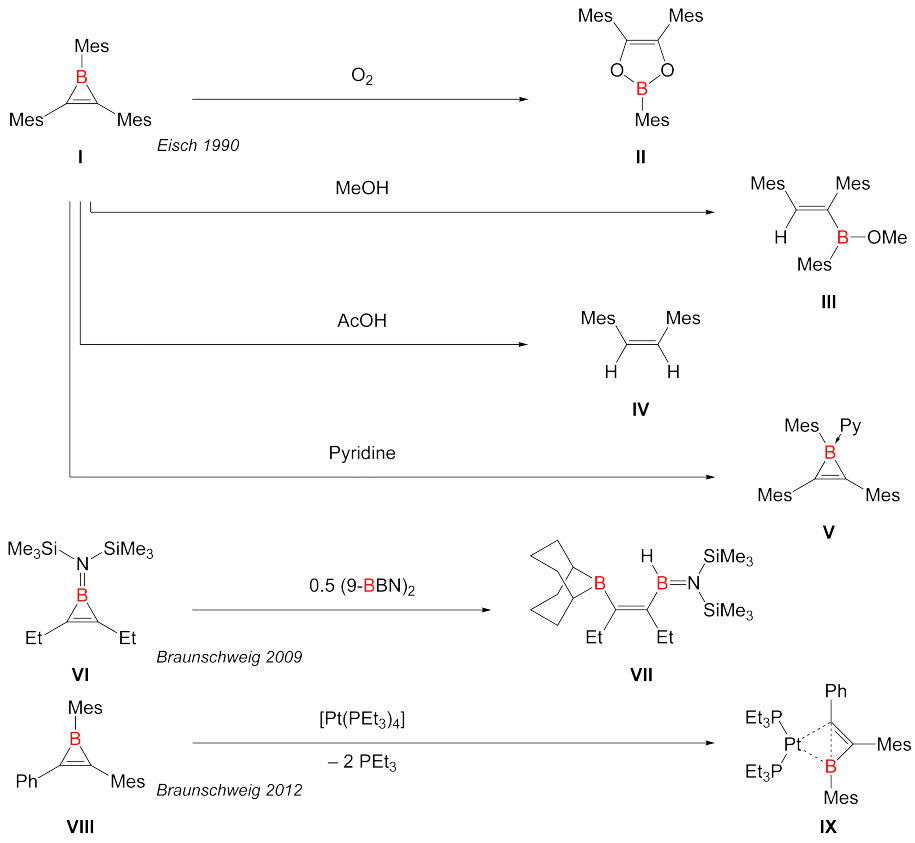

Figure 1-54. Selected reactivity of borirenes.[289,298,299]

Hydroboration of the borirene system has been reported[298] with 9-BBN, resulting in ring opening and boron functionalization of the *β*-carbon atom with protonation of the (formerly borirene) boron atom (Figure 1-54, **VI**). In 2012 Braunschweig and coworkers published a reaction in which the *in-situ* generated Pt(0) complex ($Pt(PEt_3)_2$) is used to partially activate the B-C bond of a borirene *cyclo*-BC_2 system, resulting in a four-membered platinacycle.[299] Spectroscopic and structural study of the system found that it stands as a snapshot of a partial B-C bond activation (Figure 1-54, **VII**).

1.3.3 Borabenzene-Boratabenzene

Among the multitude of systems characterized in the introduction of this section, the borabenzene/boratabenzene system possesses the ability to be stable in both neutral and anionic states, both of which have been shown to be viable bound in an η^6-manner to transition metals.[300,301] In both of these systems, the boron atom is σ-bound to neighboring carbon atoms within the ring with a π-electron involved in the aromatic system. Borabenzene/boratabenzene systems are classified based on the nature of the bond between the boron and the exocyclic ring substituent. As can be seen in Figure 1-55, borabenzene compounds are stabilized by a dative bond (Figure 1-55, **I**), provided by a Lewis base donating into the empty sp^2-hybridized orbital on boron (Lewis acid) in the plane of the ring. This arrangement allows for the boron center to possess an octet of electrons and be a neutral compound. Boratabenzene species possess a covalent bond between the boron and the exocyclic unit (Figure 1-55, **II**). In this bonding situation the boron center is σ-bound to three substituents with one π-electron involved in the aromatic system. This bonding situation denotes an anionic charge upon the boron.[300,301]

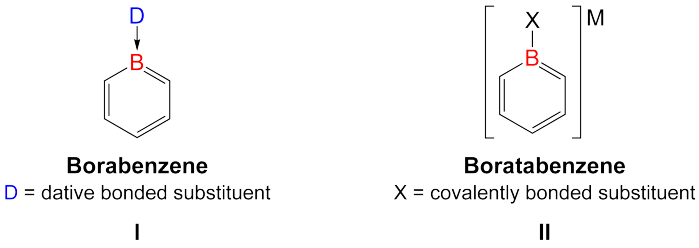

Figure 1-55. Comparison between nomenclature of a borabenzene compound (**I**), which features a Lewis base bound to boron, and a boratabenzene compound (**II**), which features a covalently-bound exocyclic substituent resulting in an negatively charged ring system.[300,301]

As a neutral six π-electron isoelectronic and isostructural mimic of the aromatic benzene (Figure 1-56, **II**) and pyridine systems (Figure 1-56, **III**), the borabenzene ring (Figure 1-56, **I**) possesses near perfect sp^2-hybridized geometry across all six atoms within the cycle with minimal ring strain.[300,301] Although they are stable and aromatic by DFT calculations *sans* Lewis base coordination to the boron center, no characterized examples have ever been reported for base-free borabenzene systems.[300-310]

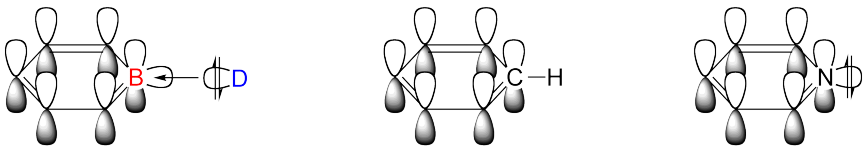

I II III

Figure 1-56. π-orbitals of benzene (**II**) compared to a base-stabilized borabenzene (**I**) and pyridine (**III**).

Fontaine and coworkers have published a detailed study of borabenzene exchange reactions between various Lewis bases. Data from this publication shows exchange of phosphine-borabenzene systems (Me_3P-, Ph_3P-, and Cy_3P-borabenzene) with carbenes to form carbene-borabenzene adducts (IMes-borabenzene) (IMes = 1,3-*bis*(2,4,6,-trimethylphenyl)imidazol-2-ylidene) that indicates that the species could be exchanged through an associative mechanistic pathway.[311] In an earlier study by Maier and coworkers (Figure 1-57), flash thermolysis experiments were conducted at 770 °C on a boracyclohexadiene compound (Figure 1-57, **I**) to determine if any methoxysilane elimination could be forced with generation of an donor-free borabenzene species. These studies failed to identify any donor-free borabenzene species by condensation of the thermalized products on a 10 K cold window. A condensed species was characterized by infrared spectroscopy and rationalized as a borabenzene adduct with dinitrogen (Figure 1-57, **II**), however X-ray structural evidence for the compound was not obtained.[312,313]

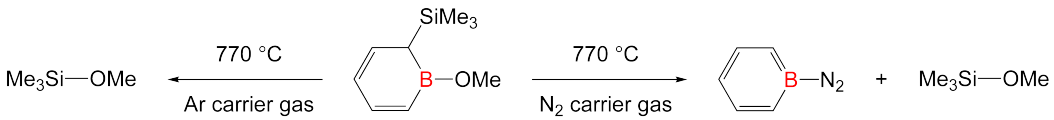

I II

Figure 1-57. Flash thermolysis study of a 1-boracyclohexa-2,4-diene (**I**) under N_2 carrier gas atmosphere, yielding a borabenzene-dinitrogen species (**II**) characterized by infrared spectroscopy.[312,313]

A metal-free neutral borabenzene species was first isolated bound to pyridine in 1985 by Schmid and coworkers.[314] The species was synthesized by tin-boron exchange of a stannacyclohexadiene precursor with BBr_3 to yield a boracyclohexadiene compound (Figure 1-58, **I**). Compound **I** was methoxylated with dimethylether (Figure 1-58, **II**) and deprotonated to form the anionic boratabenzene species shown in Figure 1-58 (**III**). This boratabenzene species could then be silylated with trimethylsilylchloride to form a silylboracyclohexadiene species (Figure 1-58, **IV**), which reacts with Lewis

bases (pyridine in this case, Figure 1-58, **V**) to force elimination of the siloxane and aromatization of the borabenzene ring system with pyridine, stabilizing the boron center by donation into the vacant sp²-hybridized orbital.[314,315]

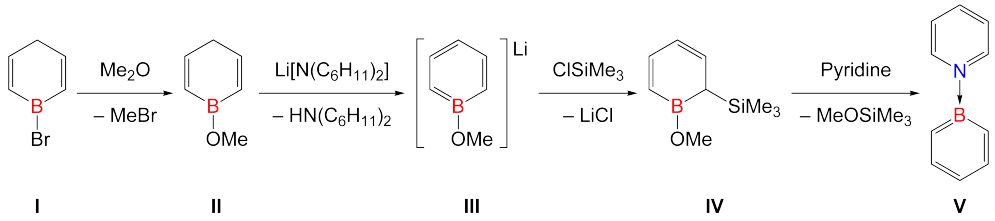

Figure 1-58. Synthesis of the first structurally-characterized metal-free borabenzene compound reported by Schmid *et al.* by utilizing a siloxane elimination aromatization reaction on a silylboracyclohexadiene precursor.[314]

When η^6-bound to transition metals, the borabenzene species is typically thought of as analogous to traditional arene-like coordination of a neutral six π-electron aromatic ring with a transition metal in a manner similar to the classic η^6-benzene-chromiumtricarbonyl species as shown below (Figure 1-59, **I**). Schmid and coworkers were able to coordinate their neutral borabenzene-pyridine adduct (Figure 1-58, **V**) to Group 6 transition metal fragments[315] in a similar η^6-manner to the benzene ligand in Figure 1-59 (**I**) and Fu and coworkers later published a borabenzene-THF adduct η^6-bound to a chromium fragment,[316,317] as can be seen in Figure 1-59 (**II**).

Figure 1-59. Arene (**I**) and borabenzene (**II**) ligand coordination onto a chromium transition metal ($Cr(CO)_3$) complex.[316,317]

Boratabenzene systems are typically thought of as analogs to the ubiquitous cyclopentadienyl ligands in that they contain six π-electrons in an anionic ring system. The species are most often isolated bound in an η^6-manner to transition metals with alkali metal counter cations.[300,301] The exocyclic substituent bound to boron can have an impact on the aromatic conjugation of the ring by its possession of exocyclic electron pairs that can form π-interactions with the boron's p_z orbital (Figure 1-60).[318-324] Fu and coworkers were able to show variable geometry in boratabenzene systems possessing exocyclic amino- (Figure 1-60, **I**) and phosphino- (Figure 1-60, **II**) substituents, resulting in sp²- and sp³-hybridized geometries of the nitrogen and phosphorus atoms, respectively.[321] Coordination of

aminoboratabenzene and phosphinoboratabenzene ligands to transition metals also showed that they possess the ability to coordinate through different parts of the ligand. Aminoboratabenzene species typically ring-coordinate[325] (Figure 1-61, **III**) while the phosphinoboratabenzene species possess the ability to coordinate through the phosphine lone pair of electrons (Figure 1-61, **I**) as well as the boratabenzene ring (Figure 1-61, **II**).[326]

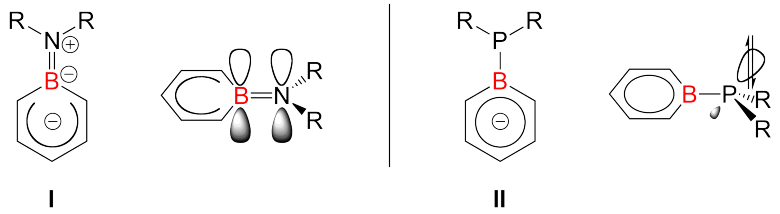

Figure 1-60. Examples of boron-bound exocyclic substituents influencing the delocalization of the aromatic delocalization within the *cyclo*-BC_5H_5 ring.[321,325]

Study of boratabenzene transition metal complexes by the groups of Ashe,[325] Fu,[326] Heck,[327] Fontaine[328] and others have shown the boratabenzene ring coordination to posses a variety of bonding interactions (η^3, η^5, and η^6) with the transition metal. Figure 1-61 lists several noteworthy examples of these coordination modes. Through study of X-ray characterized examples of boratabenzene complexes, the charge of the ring is predicted to lie predominantly on the boron-flanking carbon atoms. This results in η^6-coordination of the system to transition metals resulting in a bonding mode that has been termed “slip-distorted”, where the boratabenzene ring does not sit directly on the metal center, but rather slips off the metal center with the boron lying furthest from the metal atom (Figure 1-61, **III**). The variety of interactions make these boratabenzene ligands of high interest in polymerization catalysis as they have the ability to open metal coordination sites through ligand shifting in a manner similar to ubiquitous indenyl- systems.[300,301,325-343]

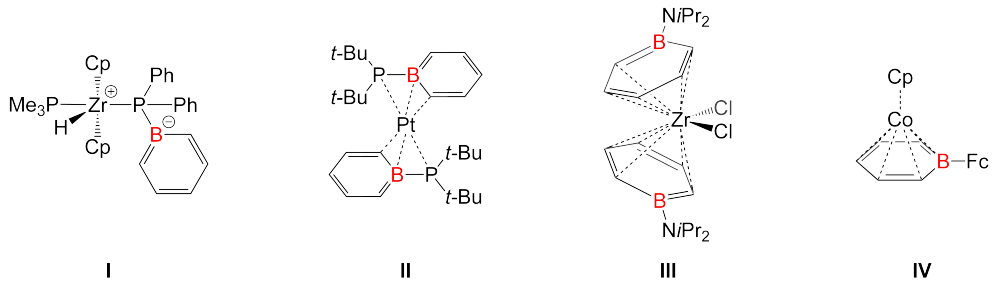

Figure 1-61. Examples of η^3-, η^5-, and η^6-coordination modes of boratabenzene ligands.*

In 1970, Herberich and coworkers reported the first synthetic route to boratabenzene complexes[344,345] by utilizing a "ring-expansion" reaction of cobaltocene with phenyldibromoborane (Figure 1-62). In the reaction cobaltocene plays a dual role of reductant as well as reagent (Figure 1-62, **I**). Two equivalents of cobaltocene are added to the reaction with one equivalent functioning as a reducing agent and the second undergoing ring expansion. Analysis of this cobaltocene aromatic system led to the theory that the boratabenzene ring was isoelectronic to the cyclopentadienyl ring. In a series of concurrent publications, the groups of Herberich and Ashe were able to develop the synthesis of boratabenzene complexes and salts into reliable protocols.[346-349]

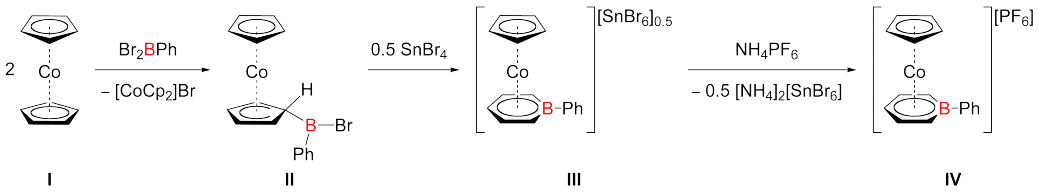

Figure 1-62. Reaction reported by Herberich *et al.* in which the first boratabenzene complex was synthesized from a "ring-expansion" reaction of cobaltocene with dibromoboranes.[344,345]

A year later, Ashe reported the synthesis of lithium phenylboratabenzene (Figure 1-63) through an alternative route in which a stannacycle precursor (Figure 1-63, **II**) is prepared, followed by tin-boron exchange to form the parent boracyclohexadiene species (Figure 1-63, **III**).[350] Reaction of this boracyclohexadiene with *tert*-butyllithium led to deprotonation and aromatization of the ring in a lithium-stabilized salt complex (Figure 1-63, **IV**). Both of these synthetic routes are still employed today in the synthesis of boratabenzene species; however, the one that has become more favorable and adaptable for augmentation is the stannacyclic route, which is also applicable to other boron containing heterocycle synthesis.

* Individual references for compounds reported in Figure 1-61: **I**,[330] **II**,[332] **III**,[329] and **IV**.[331]

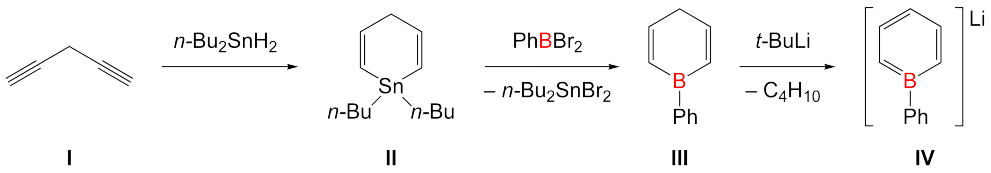

Figure 1-63. Reaction reported by Ashe *et al.* providing an alternate route to lithium salts of the phenylboratabenzene anion.[350]

In 1976, Herberich was able to provide a key step in the generation of cation-bound boratabenzene salts with report of cleavage of the boratabenzene ring system from the cobalt metal center (Figure 1-64, **I**). The reported reaction used KCN and NaCN in acetonitrile to strip the boratabenzene from the cobalt center. The reaction yields the cobalt cyanide complex (Figure 1-64, **IV**) with release of the potassium or sodium boratabenzene salt (Figure 1-64, **III**).[351]

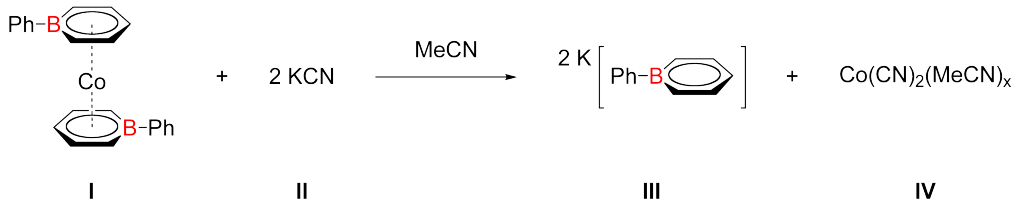

Figure 1-64. Cleavage of the boratabenzene ligand from cobalt as reported by Herberich *et al.* using KCN in acetonitrile to provide sodium salts of boratabenzenes.[351]

Within this same 1976 publication, these sodium and potassium boratabenzene salts were subsequently reacted with Group 8, 9, and 10 transition metal halides (Figure 1-65) resulting in η^6-coordination of the boratabenzene ring to the transition metal and the salt-elimination byproduct.[351] These species all feature η^6-coordination of the mono- (Figure 1-65, **IV** and **V**) and di-boratabenzene ligands (Figure 1-65, **II** and **III**) to the transition metal centers and were characterized by elemental analysis, ^{11}B NMR spectroscopy, and mass spectroscopy; however, no X-ray structures were reported.[351]

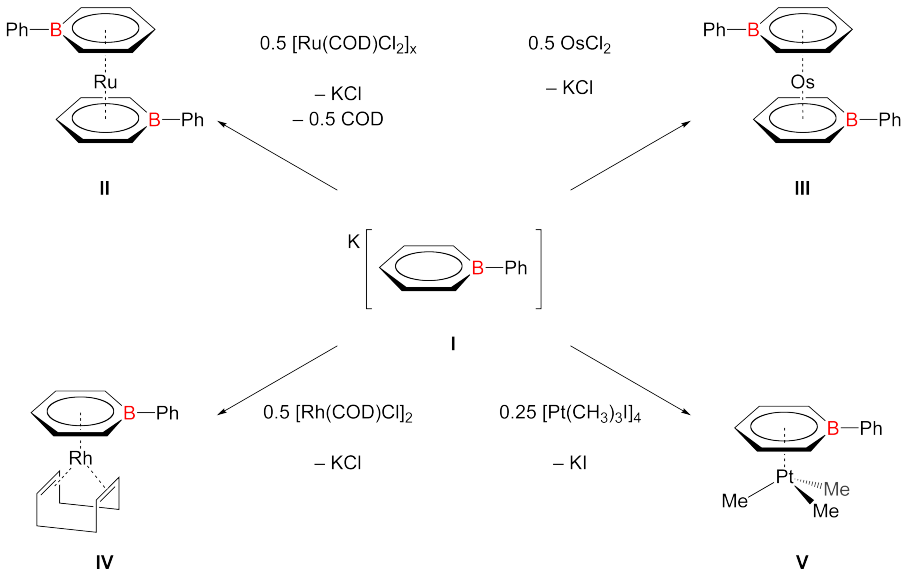

Figure 1-65. Practical applications of salt elimination reactions using boratabenzene salts with transition metal halides resulting in η^6-coordination of the boratabenzene to transition metals.[351]

Chapter 2 – Project Borylene

2.1 First Generation Borylene Synthesis

As previously discussed,[*] the first terminal borylene ligand coordinated to a transition metal scaffold was published by our research group in 1998.[118,119] The development of new "first generation borylene complexes" or borylene ligands constructed on the transition metal centers (as opposed to being transferred to the metal centers) over the resulting years has provided information pertaining to the stability and reactivity of this ligand system.[48,51-57] However, after nearly 18 years of research, the cumulative number of characterized examples of first generation terminal borylene transition metal complexes shows that there is still much to be learned regarding their synthesis, reactivity, and stability. As only a few examples of these ligands are known, the value of new terminal borylene species cannot be understated, especially if the ligand can display the ability to transfer between metal scaffolds, as only one such example of this borylene ligand reactivity is known, the *bis*(trimethylsilyl)aminoborylenes.[179,180]

Of key interest in this research project was the synthesis and characterization of new "first generation" terminal borylene species that could extend the experimental knowledge regarding the structural and electronic properties of the ligand's bonding environment. Previous borylene research has shown the propensity of the systems to prefer two main reactivity pathways: either (A) the ability to transfer to other organometallic species, or (B) complexation of unsaturated substrates and subsequent metathesis reactivity.[†] As an example of a terminal borylene ligand displaying both of these reactivity profiles has yet to be found, the ultimate goal of this borylene synthetic study was to engineer a species which could exhibit both transfer and metathesis reactivity.

Also of importance during this research project was the synthesis of terminal borylene complexes of highly Lewis acidic transition metal-ligand fragments. The vanadium terminal *bis*(trimethylsilyl)aminoborylene species [(η^5-C_5H_5)$(OC)_3$V{$BN(SiMe_3)_2$}] reported in 2003[179-180] still stands as a benchmark complex, because it features a borylene ligand terminally bound to the earliest transition metal species known (Group 5). The transfer of borylene ligands to more Lewis acidic complexes has been attempted, but the few isolated examples have thus far eluded structural confirmation. Given this unexplored realm of the periodic table

[*] See Section 1.1.4 for an introduction to first generation synthesis of transition metal borylene complexes.
[†] See Section 1.1.4.2 for an introduction to transfer and metathesis reactions of transition metal borylene complexes.

in borylene chemistry, the creation of a terminal borylene ligand complex with a Group 4 transition metal was attempted during this research project.

2.1.1 Previous Work

The synthesis of transition metal complexes bearing bridging and terminal borylene ligands has been developed by our research group *via* two main routes.[48,51-57] As the synthesis of a first generation borylene complex requires the generation of two M-B bonds, these species are most often synthesized through: (A) double salt elimination reactions which generate both M-B bonds, or (B) a salt elimination reaction to generate an initial M-B bond followed by a subsequent halosilane elimination to generate the second M-B bond. Other routes for borylene synthesis have been explored, however for preparatory scale borylene synthesis, these two predominant routes have been incorporated into standard laboratory protocols for our group and serve as the basis for the generation of the majority of our first generation borylene reagents.

As can be seen in Figure 2-1, the sterically bulky terphenyl-substituted terminal arylborylene complex $[(OC)_5Mo{=}B\{2,6\text{-}(2,4,6\text{-}i Pr_3C_6H_2)_2C_6H_3\}]$ (**3**) can be readily synthesized *via* double salt elimination reaction from Group 6 transition metal dianion ($Na_2[Mo(CO)_5]$) (**1**) with a dihaloterphenylborane ($Cl_2B\{2,6\text{-}(2,4,6\text{-}i Pr_3C_6H_2)_2C_6H_3\}$) (**2**).[123] This reaction showcases an example of reaction pathway A, whereby the stable terminal borylene product can be generated by reaction of a transition metal dianion with a functionalized dihaloborane. The reaction yield is compromised due to the high thermal instability of the Group 6 transition metal dianion; however, large reaction scales enable generation of the product in practical yields and the stability of the product in solution enables purification by multiple recrystallization steps to achieve an analytical quality reagent.

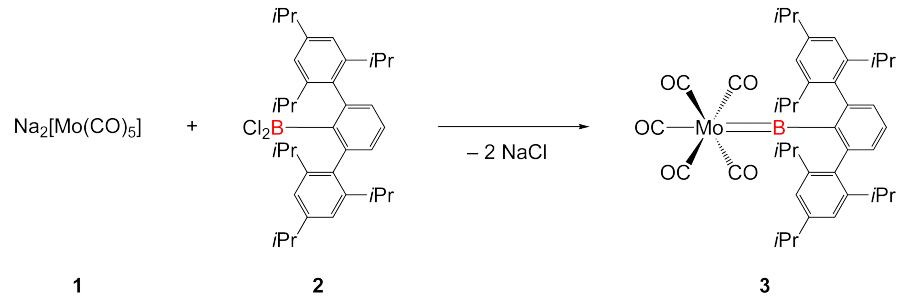

Figure 2-1. $[(OC)_5Mo{=}B\{2,6\text{-}(2,4,6\text{-}i Pr_3C_6H_2)_2C_6H_3\}]$ (**3**) synthesis from $Na_2[Mo(CO)_5]$ (**1**) and $Cl_2B\{2,6\text{-}(2,4,6\text{-}i Pr_3C_6H_2)_2C_6H_3\}$ (**2**).[123]

An alternative route for the preparatory scale synthesis of terminal transition metal-borylene complexes was also developed incorporating a halosilane elimination for generation of the second M-B bond in the complex. This route employs the synthesis

of an initial metastable transition metal-boryl complex that can subsequently undergo halosilane elimination generating the transition metal-borylene complex as the final species. As can be seen in Figure 2-2, the terminal iron-borylene complex [$(Me_3P)(OC)_3Fe{=}B\{2,3,5,6\text{-}C_6Me_4H\}$] (**7**) can be readily generated *via* a combination of a salt-elimination reaction with a halosilane elimination reaction by mixing the iron monoanion $K[(Me_3P)(OC)_3Fe(SiMe_3)]$ (**4**) with the duryl dihaloborane $Cl_2B\{2,3,5,6\text{-}C_6Me_4H\}$ (**5**) to generate the metastable iron-boryl complex [$(Me_3P)(Me_3Si)(OC)_3Fe\text{-}BCl\{2,3,5,6\text{-}C_6Me_4H\}$] (**6**) *via* salt-elimination reaction. Subsequent halosilane elimination from this metastable intermediate yields the terminal iron borylene complex [$(Me_3P)(OC)_3Fe{=}B\{2,3,5,6\text{-}C_6Me_4H\}$] (**7**) in sufficient yields to use the species as a reagent in subsequent synthesis.[352,353]

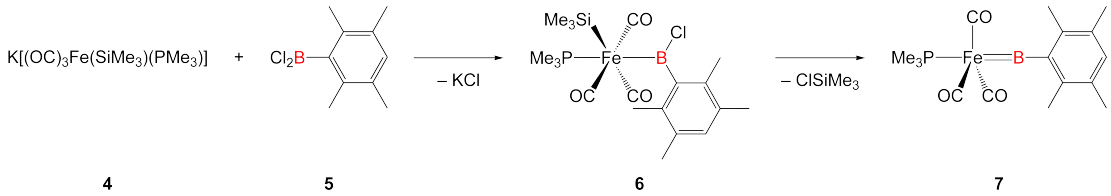

Figure 2-2. Synthesis of [$(Me_3P)(OC)_3Fe{=}B\{2,3,5,6\text{-}C_6Me_4H\}$] (**7**) from $K[(Me_3P)(OC)_3Fe(SiMe_3)]$ (**4**) and $Cl_2B\{2,3,5,6\text{-}C_6Me_4H\}$ (**5**) through the intermediate iron-boryl complex [$(Me_3P)(Me_3Si)(OC)_3Fe\text{-}BCl\{2,3,5,6\text{-}C_6Me_4H\}$] (**6**).[352,353]

The known reactivity patterns displayed by characterized examples of transition metal-borylene complexes have unto this point involved either transfer or metathesis type processes. Our research group has sought to synthesize and characterize an example of a transition metal-borylene complex that could display both of these distinct reactivity patterns. Synthetic studies were conducted on dihaloborane precursors previously shown to generate borylene species from transition metal mono- and dianions. Augmented versions of these previously discussed synthetic procedures were implemented in attempts to synthesize new novel transition metal-borylene complexes which could display new reactivity patterns and be able to yield data pertaining to the ligand's preference towards either photolytic/thermolytic transfer or metathesis type reactivity.

2.1.2 Unsymmetrical Aminoborylene Synthesis

As an initial prerequisite for the synthesis of the Group 6 terminal transition metal-borylene complexes, the synthesis of the corresponding Group 6 transition metal dianions ($Na_2[M(CO)_5]$, M = Cr (**11**), Mo (**1**), and W (**12**)) must first be achieved, which are then mixed with the dihaloborane $Cl_2BN(SiMe_3)_2$.[354] As can be seen in Figure 2-3, the synthetic procedures developed by our group for the synthesis of the Group 6 transition metal pentacarbonyl terminal borylene complexes ($[(OC)_5M\{BN(SiMe_3)_2\}]$, M = Cr (**13**), Mo (**14**), and W (**15**)) all depend upon the initial synthesis of the corresponding Group 6 pentacarbonyl amine complexes ($[(OC)_5M(NMe_3)]$, M = Cr (**8**), Mo (**9**), and W (**10**)) as starting materials.[355] Treatment of these Group 6 pentacarbonyl amines with two equivalents of sodium naphthalenide ($Na[C_{10}H_8]$) leads to generation of the corresponding dianion in solution. These dark brown/red solutions can be subsequently purified by centrifugation of the suspended dianion and removal of the supernatant to yield the reagent as an analytically pure species. The high thermal instability of these Group 6 pentacarbonyl dianions inhibit their storage and all three examples (Cr (**11**), Mo (**1**), and W (**12**)) must be synthesized immediately prior to reaction with the corresponding dihaloboranes. The synthesis of these dianionic species must be conducted at low temperatures (–78 °C) and the generated Group 6 transition metal dianions ($Na_2[M(CO)_5]$, M = Cr (**11**), Mo (**1**), and W (**12**)) must be kept at temperatures below –40 °C to inhibit decomposition.

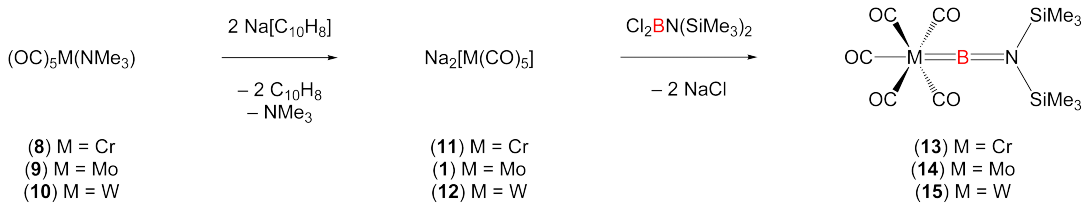

Figure 2-3. $[(OC)_5M\{BN(SiMe_3)_2\}]$ synthesis by reaction of the corresponding transition metal dianionic complexes with $Cl_2BN(SiMe_3)_2$.[118,119,152]

As the synthesis of the Group 6 pentacarbonyl terminal *bis*(trimethylsilyl)aminoborylene complexes ($[(OC)_5M\{BN(SiMe_3)_2\}]$, M = Cr (**13**), Mo (**14**), and W (**15**)) are possible through reaction of $Cl_2BN(SiMe_3)_2$ with the corresponding Group 6 transition metal dianion ($Na_2[M(CO)_5]$, M = Cr (**11**), Mo (**1**), and W (**12**)), a similar dihaloborane ($Br_2BN(SiMe_3)(t\text{-}Bu)$) (**18**) was employed in the synthesis of three new first generation terminal borylene species (see Section 2.1.2.1). The synthesis of this particular dihaloborane is shown in Figure 2-4 and proceeds through a modified route inspired by Rochow and coworkers.[356,357] The secondary

amine $HN(SiMe_3)(t\text{-Bu})$ (**16**) was deprotonated with *n*-BuLi in solution to yield the lithium amido salt $Li[N(SiMe_3)(t\text{-Bu})]$ (**17**). Mixing of $Li[N(SiMe_3)(t\text{-Bu})]$ (**17**) with one equivalent of BBr_3 successfully generated the dihaloborane $Br_2BN(SiMe_3)(t\text{-Bu})$ (**18**) in near quantitative yield along with the salt elimination product LiBr.[356,357]

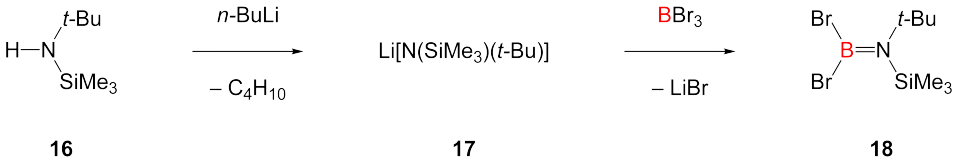

Figure 2-4. $Br_2BN(SiMe_3)(t\text{-Bu})$ (**18**) synthesis *via* deprotonation of $HN(SiMe_3)(t\text{-Bu})$ followed by salt elimination reaction with BBr_3.[356,357]

The dihaloborane ($Br_2BN(SiMe_3)(t\text{-Bu})$) (**18**) was observed *via* ^1H, ^{11}B, ^{13}C and ^{29}Si NMR spectroscopy and easily be distinguished as a sharp resonance in $^{11}B\{^1H\}$ NMR spectra appearing at δ = 36 ppm. ^1H NMR spectra of the compound displayed two prominent resonances at 0.405 and 1.485 ppm corresponding to the trimethylsilyl and *tert*-butyl protons respectively (9H for each resonance). The trimethylsilyl proton resonance at 0.405 ppm was assigned by 2D ^1H-^{13}C (HSQC) ($^{13}C\{^1H\}$: δ = 5.76 ppm, $^1J_{C\text{-}Si}$ = 58 Hz) correlation spectroscopy as well as the interpreted $^2J_{H\text{-}Si}$ coupling value of 6.6 Hz. Unfortunately the $^{29}Si\{^1H\}$ NMR resonance ($^{29}Si\{^1H\}$: δ = 7.8 ppm) was too broad to verify this coupling constant.

2.1.2.1 $[(OC)_5Cr\{BN(SiMe_3)(t\text{-Bu})\}]$ (19)

$[(OC)_5Cr\{BN(SiMe_3)(t\text{-Bu})\}]$ (**19**) was prepared by modification of the literature procedure * for the preparation of the chromium pentacarbonyl *bis*(trimethylsilyl)aminoborylene complex $[(OC)_5Cr\{BN(SiMe_3)_2\}]$ (**13**).[118,119] $Na_2[Cr(CO)_5]$ (**11**) was freshly prepared by two-electron reduction of $[(OC)_5Cr(NMe_3)]$ (**8**) with two equivalents of $Na[C_{10}H_8]$ in a THF solution held at low temperature (–78 °C) (Figure 2-5). Workup of the reaction crude gave the chromium dianion, $Na_2[Cr(CO)_5]$ (**11**), as a light yellow, thermally unstable powder which was immediately suspended in toluene and cooled to –78 °C. Neat $Br_2BN(SiMe_3)(t\text{-Bu})$ (**18**) was then added to the reaction mixture at –78 °C (Figure 2-5). The product was subsequently purified out of the crude mixture by solvent removal *in vacuo* and extraction from the two equivalents of salt byproduct (NaBr) by pentane extraction. Crystallization of this pentane extract at –40 °C yielded $[(OC)_5Cr\{BN(SiMe_3)(t\text{-Bu})\}]$ (**19**) as a colorless solid in approximately 39% yield. The compound readily crystallizes as air and moisture sensitive transparent light yellow (almost colorless)

* See Section 2.1.2 for reaction literature and details.

crystalline blocks. Differential thermal analysis of these crystalline solids showed a melting point for [(OC)$_5$Cr{BN(SiMe$_3$)(*t*-Bu)}] (**19**) at 60 °C with decomposition in excess of 211 °C.

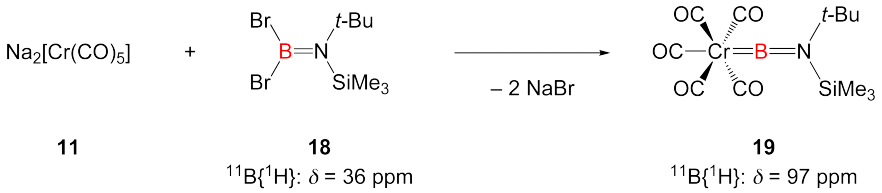

Figure 2-5. [(OC)$_5$Cr{BN(SiMe$_3$)(*t*-Bu)}] (**19**) synthesis from Na$_2$[Cr(CO)$_5$] (**11**) and Br$_2$BN(SiMe$_3$)(*t*-Bu) (**18**).

[(OC)$_5$Cr{BN(SiMe$_3$)(*t*-Bu)}] (**19**) was characterized by ^{1}H, ^{11}B, ^{13}C, and ^{29}Si NMR spectroscopy. ^{1}H NMR spectra of the complex display two prominent resonances at 0.159 and 1.148 ppm corresponding to the trimethylsilyl and *tert*-butyl protons, respectively (9H for each resonance). The trimethylsilyl proton resonance at 0.159 ppm was assigned through 2D ^{1}H-^{13}C (^{13}C{^{1}H}: δ = 3.27 ppm, $^1J_{C\text{-}Si}$ = 58 Hz) correlation spectroscopy (HSQC) as well as the interpreted $^2J_{H\text{-}Si}$ coupling value of 6.7 Hz. Unfortunately the ^{29}Si{^{1}H} NMR resonance (^{29}Si{^{1}H}: δ = 3.4 ppm) is too broad to verify this coupling constant. The ^{11}B{^{1}H} NMR spectra of the complex features a resonance for the boron environment at 97 ppm, which is slightly downfield-shifted from the reported resonance of [(OC)$_5$Cr{BN(SiMe$_3$)$_2$}] (**13**) (^{11}B{^{1}H}: δ = 92 ppm).[118,119] ^{13}C{^{1}H} NMR spectroscopy of the compound revealed carbonyl carbon environments at 218.44 ppm (*trans*- to {BN(SiMe$_3$)(*t*-Bu)}) and 217.93 ppm (*cis*- to {BN(SiMe$_3$)(*t*-Bu)}) which is in agreement with the ^{13}C{^{1}H} carbonyl environments reported previously for [(OC)$_5$Cr{BN(SiMe$_3$)$_2$}] (**13**) (218.0 ppm (*trans*- to {BN(SiMe$_3$)$_2$}) and 217.6 ppm (*cis*- to {BN(SiMe$_3$)$_2$})); however, these values are slightly shifted downfield from the reference compound.[118,119] It is generally accepted that an downfield shift of carbonyl carbon NMR resonances can be an indicator for increased π-backdonation of the metal to the carbonyl ligand.[358,359] Analysis of [(OC)$_5$Cr{BN(SiMe$_3$)(*t*-Bu)}] (**19**) by infrared spectroscopy shows three observable bands that could correlate to the $\tilde{\nu}$(C≡O) stretching modes at 2,058, 1,969, and 1,900 cm^{-1}, which correlates to the data published for [(OC)$_5$Cr{BN(SiMe$_3$)$_2$}] (**13**) ($\tilde{\nu}$(C≡O) = 2,064, 1,981, and 1,942 cm^{-1}).[118,119] The three observed carbonyl stretching modes found in [(OC)$_5$Cr{BN(SiMe$_3$)(*t*-Bu)}] (**19**) and [(OC)$_5$Cr{BN(SiMe$_3$)$_2$}] (**13**) correspond to the three stretching modes that would be expected for a C_{4v}-symmetric {M(CO)$_5$} transition metal center with a terminal borylene ligand.[360-363] This infrared data is consistent with an octahedral geometry for [(OC)$_5$Cr{BN(SiMe$_3$)(*t*-

Bu)}] (**19**) as well as the stronger σ-donor and/or weaker π-acceptor ability of the {BN(SiMe$_3$)(*t*-Bu)} ligand compared to {BN(SiMe$_3$)$_2$} due to the decreased energies of the carbonyl stretching bands.[60,141,364]

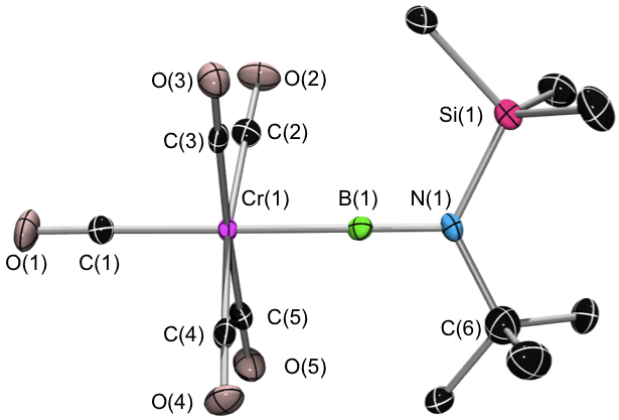

Figure 2-6. ORTEP-rendered structure of [(OC)$_5$Cr{BN(SiMe$_3$)(*t*-Bu)}] (**19**). Thermal ellipsoids set at 50% probability. All hydrogen atoms have been omitted for clarity. Selected bond distances (Å) and angles (°): Cr(1)–B(1) 1.980(2), Cr(1)–C$_{ax}$ 1.908(2), Cr(1)–C$_{eq}$ (avg.) 1.893, B(1)–N(1) 1.359(3), C$_{ax}$–O$_{ax}$ 1.137(3), C$_{eq}$–O$_{eq}$ (avg.) 1.142, B(1)–Cr(1)–C(1) 178.74(9), B(1)–Cr(1)–C$_{eq}$ (avg.) 87.54, N(1)–B(1)–Cr(1) 179.8(2), ΣN_α 360.0.

Crystals suitable for X-ray diffraction were grown from saturated solutions of [(OC)$_5$Cr{BN(SiMe$_3$)(*t*-Bu)}] (**19**)* in hexane. An ORTEP diagram for the structure as well as some key bond distances for [(OC)$_5$Cr{BN(SiMe$_3$)(*t*-Bu)}] (**19**) are shown in Figure 2-6. The [(OC)$_5$Cr{BN(SiMe$_3$)(*t*-Bu)}] (**19**) species displays Cr-B, B-N, Cr-C$_{ax}$, and Cr-C$_{eq}$ (avg.) bond distances of 1.980(2), 1.359(3), 1.908(2), and 1.893 (avg.) Å respectively. These data are comparable† to those of [(OC)$_5$Cr{BN(SiMe$_3$)$_2$}] (**13**), which displays Cr-B, B-N, Cr-C$_{ax}$, and Cr-C$_{eq}$ (avg.) bond distances of 1.995(6), 1.353(7), 1.908(6), and 1.891 (avg.) Å respectively.[150,151]

2.1.2.2 [(OC)$_5$Mo{BN(SiMe$_3$)(*t*-Bu)}] (20)

[(OC)$_5$Mo{BN(SiMe$_3$)(*t*-Bu)}] (**20**) was prepared according to a modification of the preparation of the molybdenum pentacarbonyl *bis*(trimethylsilyl)aminoborylene complex [(OC)$_5$Mo{BN(SiMe$_3$)$_2$}][152] (**16**).‡ Na$_2$[Mo(CO)$_5$] (**1**) is freshly prepared from two-electron reduction of [(OC)$_5$Mo(NMe$_3$)] (**9**) with two equivalents of Na[C$_{10}$H$_8$] in a THF solution held at low temperature (–78 °C) (Figure 2-3). Workup of the reaction crude gave the molybdenum dianion Na$_2$[Mo(CO)$_5$] (**1**) as a light yellow

* C$_{12}$H$_{18}$BCrNO$_5$Si, *M* = 347.17, monoclinic, space group = *P2$_1$/n*.
† C$_{11}$H$_{18}$BCrNO$_5$Si$_2$, *M* = 363.24, triclinic, space group = *P–1*.
‡ See Section 2.1.2 for reaction literature and details.

thermally unstable powder which was immediately suspended in toluene and cooled to –78 °C. Neat $Br_2BN(SiMe_3)(t\text{-Bu})$ (**18**) was then added to the reaction mixture at –78 °C (Figure 2-7). The product was subsequently purified out of the crude mixture by solvent removal *in vacuo* and extraction from the two equivalents of salt byproduct (NaBr) by pentane extraction. Crystallization of this pentane extract at –40 °C yielded $[(OC)_5Mo\{BN(SiMe_3)(t\text{-Bu})\}]$ (**20**) as a colorless solid in very poor (<10%) yield. The low yield can attributed to the low thermal stability of both $Na_2[Mo(CO)_5]$ (**1**) and $[(OC)_5Mo\{BN(SiMe_3)(t\text{-Bu})\}]$ (**20**) while in solution and in the solid state. The compound readily crystallizes as air and moisture sensitive transparent light yellow (almost colorless) crystalline blocks. Differential thermal analysis was not performed on the species as it will readily decompose at temperatures above 0 °C.

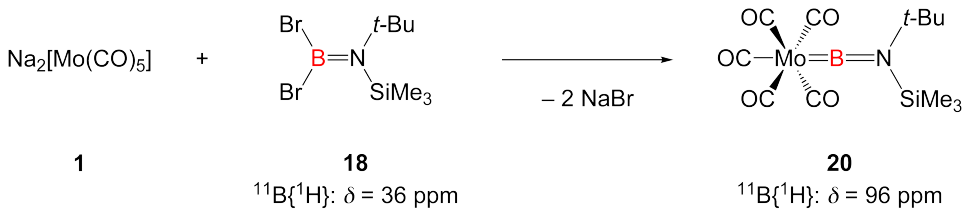

Figure 2-7. $[(OC)_5Mo\{BN(SiMe_3)(t\text{-Bu})\}]$ (**20**) synthesis from $Na_2[Mo(CO)_5]$ (**1**) and $Br_2BN(SiMe_3)(t\text{-Bu})$ (**18**).

$[(OC)_5Mo\{BN(SiMe_3)(t\text{-Bu})\}]$ (**20**) was characterized by ^1H, ^{11}B, ^{13}C, and ^{29}Si NMR spectroscopy. ^1H NMR spectra of the complex display two prominent resonances at 0.141 and 1.137 ppm corresponding to the trimethylsilyl and *tert*-butyl protons, respectively (9H for each resonance). The trimethylsilyl proton resonance at 0.141 ppm is assigned through 2D ^1H-^{13}C ($^{13}C\{^1H\}$: δ = 3.51 ppm, $^1J_{C\text{-}Si}$ = 58 Hz) correlation spectroscopy (HSQC) as well as the interpreted $^2J_{H\text{-}Si}$ coupling value of 6.6 Hz. Unfortunately the $^{29}Si\{^1H\}$ NMR resonance ($^{29}Si\{^1H\}$: δ = 3.4 ppm) is too broad to verify this coupling constant. The $^{11}B\{^1H\}$ NMR spectra of the complex witnesses the resonance of the boron environment to appear at 96 ppm, which is slightly downfield shifted from the reported resonance of $[(OC)_5Mo\{BN(SiMe_3)_2\}]$ (**14**) ($^{11}B\{^1H\}$: δ = 90 ppm).[152] $^{13}C\{^1H\}$ NMR spectroscopy for the compound displays the carbonyl carbon environments at 206.86 ppm (*trans*- to $\{BN(SiMe_3)(t\text{-Bu})\}$) and 207.50 ppm (*cis*- to $\{BN(SiMe_3)(t\text{-Bu})\}$), which is in agreement with the $^{13}C\{^1H\}$ carbonyl environments reported previously for $[(OC)_5Mo\{BN(SiMe_3)_2\}]$ (**14**) (206.8 ppm (*trans*- to $\{BN(SiMe_3)_2\}$) and 207.7 ppm (*cis*- to $\{BN(SiMe_3)_2\}$)).[152] Analysis of $[(OC)_5Mo\{BN(SiMe_3)(t\text{-Bu})\}]$ (**20**) by infrared spectroscopy shows two bands attributable to the $\tilde{\nu}$(C≡O) stretching modes at 2,065 and 1,896 cm^{-1}. For this

compound, repeated IR spectroscopic data collection could only identify two stretching modes for the carbonyl ligands, in contrast to three carbonyl stretching modes ($\tilde{\nu}$(C≡O) = 2,071, 1,982, and 1,945 cm^{-1}) observed for [(OC)$_5$Mo{BN(SiMe$_3$)$_2$}] (**14**).[152]

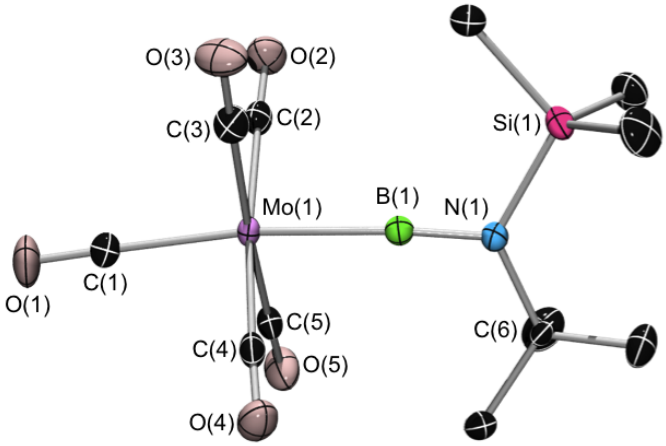

Figure 2-8. ORTEP-rendered structure of [(OC)$_5$Mo{BN(SiMe$_3$)(*t*-Bu)}] (**20**). Thermal ellipsoids set at 50% probability. All hydrogen atoms have been omitted for clarity. Selected bond distances (Å) and angles (°): Mo(1)–B(1) 2.145(3), Mo(1)–C$_{ax}$ 2.078(2), Mo(1)–C$_{eq}$ (avg.) 2.056, B(1)–N(1) 1.363(3), C$_{ax}$–O$_{ax}$ 1.141(3), C$_{eq}$–O$_{eq}$ (avg.) 1.146, B(1)–Mo(1)–C(1) 173.55(8), B(1)–Mo(1)–C$_{eq}$ (avg.) 88.15, N(1)–B(1)–Mo(1) 175.9(2), ΣN$_\alpha$ 359.7.

Crystals suitable for X-ray diffraction were grown from saturated solutions of [(OC)$_5$Mo{BN(SiMe$_3$)(*t*-Bu)}] (**20**)* in hexane. An ORTEP diagram for the structure as well as some key bond distances for [(OC)$_5$Mo{BN(SiMe$_3$)(*t*-Bu)}] (**20**) are shown in Figure 2-8. The [(OC)$_5$Mo{BN(SiMe$_3$)(*t*-Bu)}] (**20**) species displays Mo-B, B-N, Mo-C$_{ax}$, and Mo-C$_{eq}$ (avg.) bond distances of 2.145(3), 1.363(3), 2.078(2), and 2.056 (avg.) Å respectively. This data is comparable † to the distances of [(OC)$_5$Mo{BN(SiMe$_3$)$_2$}] (**14**), which displays Mo-B, B-N, Mo-C$_{ax}$, and Mo-C$_{eq}$ (avg.) bond distances of 2.152(2), 1.355(2), 2.075(2), and 2.056 (avg.) Å, respectively.[152]

2.1.2.3 [(OC)$_5$W{BN(SiMe$_3$)(*t*-Bu)}] (21)

[(OC)$_5$W{BN(SiMe$_3$)(*t*-Bu)}] (**21**) was prepared according to a modification of the preparation of the tungsten pentacarbonyl *bis*(trimethylsilyl)aminoborylene complex [(OC)$_5$W{BN(SiMe$_3$)$_2$}][118,119] (**15**).‡ Na$_2$[W(CO)$_5$] (**12**) is freshly prepared from two-electron reduction of [(OC)$_5$W(NMe$_3$)] (**10**) with two equivalents of Na[C$_{10}$H$_8$] in a

* C$_{12}$H$_{18}$BMoNO$_5$Si, *M* = 391.11, monoclinic, space group = *P*2$_1$/*c*.
† C$_{11}$H$_{18}$BMoNO$_5$Si$_2$, *M* = 407.19, triclinic, space group = *P*–*1*.
‡ See Section 2.1.2 for reaction literature and details.

THF solution held at low temperature (–78 °C) (Figure 2-3). Workup of the reaction crude gave the tungsten dianion, $Na_2[W(CO)_5]$ (**12**), as a light yellow thermally unstable powder which was immediately suspended in toluene and cooled to –78 °C. Neat $Br_2BN(SiMe_3)(t\text{-Bu})$ (**18**) then was added to the reaction mixture at –78 °C (Figure 2-9). The product was subsequently purified out of the crude mixture by solvent removal *in vacuo* and extraction from the two equivalents of salt byproduct (NaBr) by pentane extraction. Crystallization of this pentane extract at –40 °C yielded $[(OC)_5W\{BN(SiMe_3)(t\text{-Bu})\}]$ (**21**) as a colorless solid in approximately 35% yield.

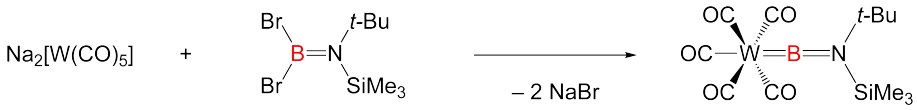

12 **18** $^{11}B\{^1H\}$: δ = 36 ppm **21** $^{11}B\{^1H\}$: δ = 92 ppm

Figure 2-9. $[(OC)_5W\{BN(SiMe_3)(t\text{-Bu})\}]$ (**21**) synthesis from $Na_2[W(CO)_5]$ (**12**) and $Br_2BN(SiMe_3)(t\text{-Bu})$ (**18**).

$[(OC)_5W\{BN(SiMe_3)(t\text{-Bu})\}]$ (**21**) was characterized by ^1H, ^{11}B, ^{13}C, and ^{29}Si NMR spectroscopy. ^1H NMR spectra of the complex display two prominent resonances at 0.143 and 1.152 ppm corresponding to the trimethylsilyl and *tert*-butyl protons, respectively (9H for each resonance). The trimethylsilyl proton resonance at 0.152 ppm is assigned through 2D ^1H-^{13}C ($^{13}C\{^1H\}$: δ = 3.50 ppm, $^1J_{C\text{-}Si}$ = 58 Hz) correlation spectroscopy (HSQC) as well as the interpreted $^2J_{H\text{-}Si}$ coupling value of 6.8 Hz. Unfortunately the $^{29}Si\{^1H\}$ NMR resonance ($^{29}Si\{^1H\}$: δ = 2.5 ppm) is too broad to verify this coupling constant. The $^{11}B\{^1H\}$ NMR spectra of the complex witnesses the resonance of the boron environment to appear at 92 ppm, which is slightly downfield shifted from the reported resonance of $[(OC)_5W\{BN(SiMe_3)_2\}]$ (**15**) ($^{11}B\{^1H\}$: δ = 87 ppm).[118,119] $^{13}C\{^1H\}$ NMR spectroscopy for the compound displays the carbonyl carbon environments at 191.16 ppm (*trans*- to $\{BN(SiMe_3)(t\text{-Bu})\}$) and 197.68 ppm (*cis*- to $\{BN(SiMe_3)(t\text{-Bu})\}$), which is in agreement with the $^{13}C\{^1H\}$ carbonyl environments reported previously for $[(OC)_5W\{BN(SiMe_3)_2\}]$ (**15**) (196.5 ppm (*trans*- to $\{BN(SiMe_3)_2\}$) and 197.2 ppm (*cis*- to $\{BN(SiMe_3)_2\}$)). Both of these $^{13}C\{^1H\}$ carbonyl resonances display prominent tungsten satellites correlating to ^{183}W (I = ½, 14.3% natural abundance) coupling ($^1J_{C\text{-}W}$) values of 126 and 121 Hz (*trans*-/*cis*- to $\{BN(SiMe_3)(t\text{-Bu})\}$ respectively). Analysis of $[(OC)_5W\{BN(SiMe_3)(t\text{-Bu})\}]$ (**21**) by infrared spectroscopy shows two observable bands assignable to the $\tilde{\nu}(C\equiv O)$ stretching modes at 2,065 and 1,898 cm^{-1}. For this compound, repeated IR

spectroscopic data collection could only identify two stretching modes for the carbonyl ligands, in contrast to three carbonyl stretching modes ($\tilde{\nu}$(C≡O) = 2,075, 1,967, and 1,941 cm^{-1}) observed for [(OC)$_5$W{BN(SiMe$_3$)$_2$}] (**15**).[118,119]

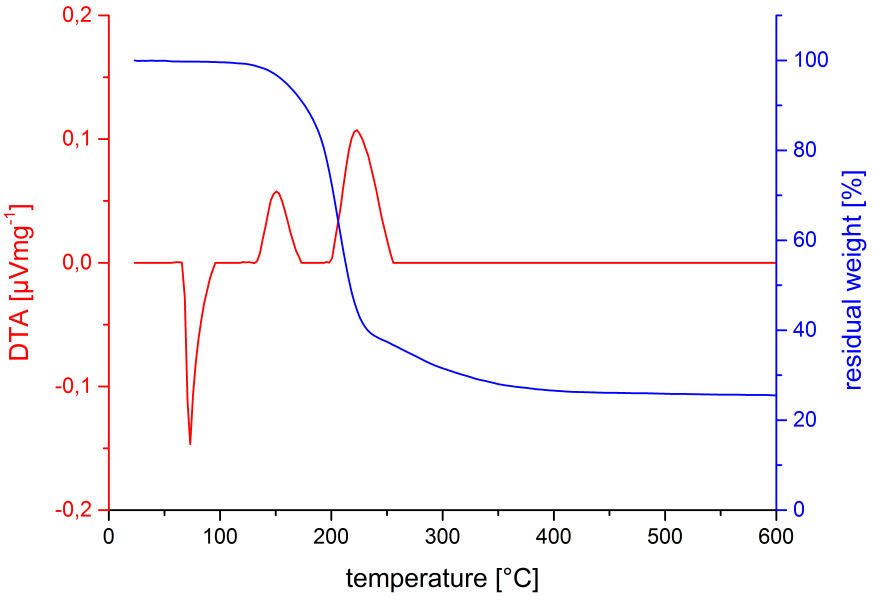

Figure 2-10. Thermogravimetric analysis plot (thermogram) of [(OC)$_5$W{BN(SiMe$_3$)(*t*-Bu)}] (**21**). Graph lines display DSC data (red) and TGA data (blue) relative to temperature along the x-axis for comparison.

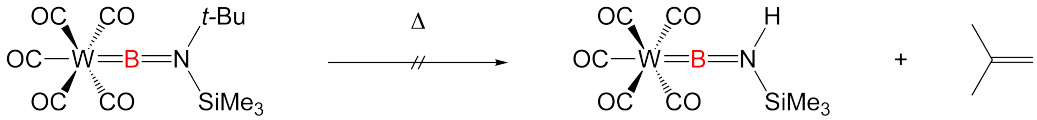

21 **22** **23**

Figure 2-11. Possible thermal decomposition pathway proposed by the TGA thermogram of [(OC)$_5$W{BN(SiMe$_3$)(*t*-Bu)}] (**21**).[365-370]

The compound readily crystallizes as air and moisture sensitive transparent light yellow (almost colorless) crystalline blocks. Differential thermal analysis (Figure 2-10) of these crystalline solids showed a melting point for [(OC)$_5$W{BN(SiMe$_3$)(*t*-Bu)}] (**21**) at 73 °C with two exothermic peaks at 150 °C and 233 °C (decomposition in excess of 233 °C). Originally, this first endothermic peak was thought to correspond to the possible thermal elimination (thermolysis) of *iso*butene from the complex[365-370] (as shown in Figure 2-11) or the elimination of the five carbonyl ligands resulting in a metal borylene residue.[140] The compound was analyzed using thermogravimetric methods and a metastable intermediate could be detected at approximately ~230 °C; however, the mass loss is already approaching complete destruction of the compound and does not appear to correlate to either of these two

possible complex decomposition pathways. After repeated attempts at heating the $[(OC)_5W\{BN(SiMe_3)(t\text{-}Bu)\}]$ (**21**) compound in the solid state, no other species could be detected other than decomposition products (tungsten black).

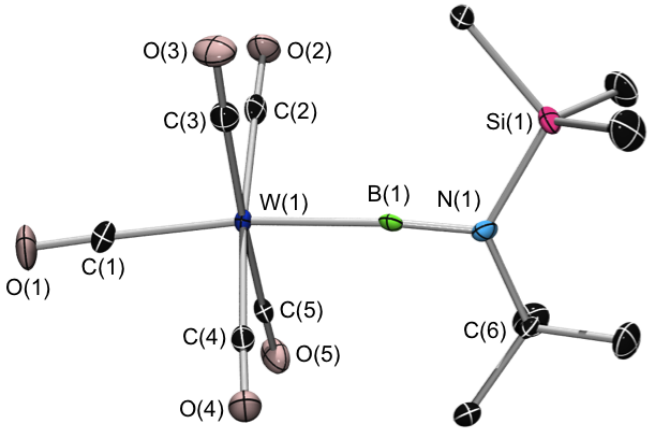

Figure 2-12. ORTEP-rendered structure of $[(OC)_5W\{BN(SiMe_3)(t\text{-}Bu)\}]$ (**21**). Thermal ellipsoids set at 50% probability. All hydrogen atoms have been omitted for clarity. Selected bond distances (Å) and angles (º): W(1)–B(1) 2.154(4), W(1)–C_{ax} 2.061(3), W(1)–C_{eq} (avg.) 2.048, B(1)–N(1) 1.350(5), C_{ax}–O_{ax} 1.142(4), C_{eq}–O_{eq} (avg.) 1.145, B(1)–W(1)–C(1) 173.5(1), B(1)–W(1)–C_{eq} (avg.) 88.35, N(1)–B(1)–W(1) 176.0(3), ΣN_{α} 359.6.

Crystals suitable for X-ray diffraction were grown from saturated solutions of $[(OC)_5W\{BN(SiMe_3)(t\text{-}Bu)\}]$ (**21**) [*] in hexane. An ORTEP diagram for the structure as well as some key bond distances for $[(OC)_5W\{BN(SiMe_3)(t\text{-}Bu)\}]$ (**21**) are shown in Figure 2-12. The $[(OC)_5W\{BN(SiMe_3)(t\text{-}Bu)\}]$ (**21**) species displays W-B, B-N, W-C_{ax}, and W-C_{eq} (avg.) bond distances of 2.154(4), 1.350(5), 2.061(3), and 2.048 (avg.) Å respectively. This data is comparable[†] to the distances of $[(OC)_5W\{BN(SiMe_3)_2\}]$ (**15**), which displays W-B, B-N, W-C_{ax}, and W-C_{eq} (avg.) bond distances of 2.151(6), 1.338(8), 2.039(6), and 2.035 (avg.) Å respectively.

[*] $C_{12}H_{18}BWNO_5Si$, M = 479.01, monoclinic, space group = $P2_1/c$.
[†] $C_{11}H_{18}BWNO_5Si_2$, M = 495.09, triclinic, space group = $P\bar{1}$.

2.1.3 Synthetic Attempts at a Group 4 Terminal Borylene

Dr. Stefanie Bertsch wrote extensively in her thesis[371] on strategies and attempts to synthesize and characterize a stable Group 4 transition metal borylene species.* The reactions attempted in her thesis focused on two main synthetic routes: (A) photolytic and thermolytic borylene transfers, and (B) oxidative additions of boranes and haloboranes onto Group 4 scaffolds (Ti(II), Zr(II), and Hf(II)) generated from reductive eliminations or ligand dissociations of metastable Group 4 transition metal complexes in the II and IV oxidation states.[371]

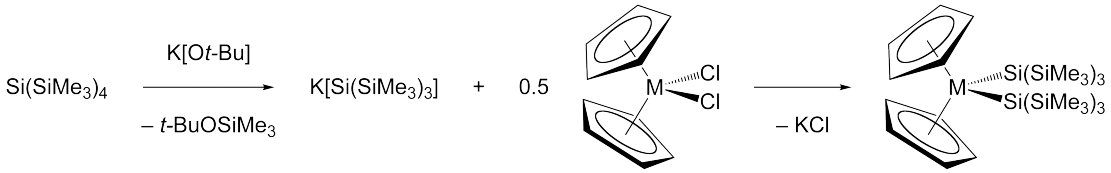

Figure 2-13. $[(\eta^5\text{-}C_5H_5)_2Zr(Si(SiMe_3)_3)_2]$ (**28**) and $[(\eta^5\text{-}C_5H_5)_2Hf(Si(SiMe_3)_3)_2]$ (**29**) synthesis from $K[Si(SiMe_3)_3]$ (**25**) and the dihalometallocenes $[(\eta^5\text{-}C_5H_5)_2ZrCl_2]$ (**26**) and $[(\eta^5\text{-}C_5H_5)_2HfCl_2]$ (**27**).

As the halosilane elimination reaction between a transition metal-silyl complex and a functionalized haloborane has been shown to be a valid method for the synthesis of the second M-B bond in terminal first generation transition metal borylene complexes,[352,353] a project was conceived where Group 4 transition metal *bis*(hypersilyl) (hypersilyl = $\{Si(SiMe_3)_3\}$) complexes were synthesized and reacted with a variety of dihaloboranes and the quarternized trihaloborane $BF_3{\bullet}OEt_2$. Literature precedence for the generation of Group 4 *bis*(hypersilyl) species[372-374] show them to be remarkably stable thermally and photochemically due to the sterically blocked inter- and intramolecular C-H activation decomposition pathways and decreased reactivity with oxygen substituents that are prevalent with other Group 4 transition metal-silyl complexes.[375-382] As Figure 2-13 shows, these Group 4 *bis*(hypersilyl) complexes can be easily generated through salt elimination reactions of Group 4 dihalometallocenes ($[(\eta^5\text{-}C_5H_5)_2ZrCl_2]$ (**26**) and $[(\eta^5\text{-}C_5H_5)_2HfCl_2]$ (**27**)) with two equivalents of $K[Si(SiMe_3)_3]$ (**25**). Using the above route in Figure 2-13, both $[(\eta^5\text{-}C_5H_5)_2Zr(Si(SiMe_3)_3)_2]$ (**28**) and $[(\eta^5\text{-}C_5H_5)_2Hf(Si(SiMe_3)_3)_2]$ (**29**) species were successfully prepared in this manner.[372]

* See the thesis of Dr. Stefanie Bertsch Sections 3.4-3.6 (pages 47-60) and Section 5 (pages 126-127) for a list of transition metal scaffolds used during these reported reaction studies.

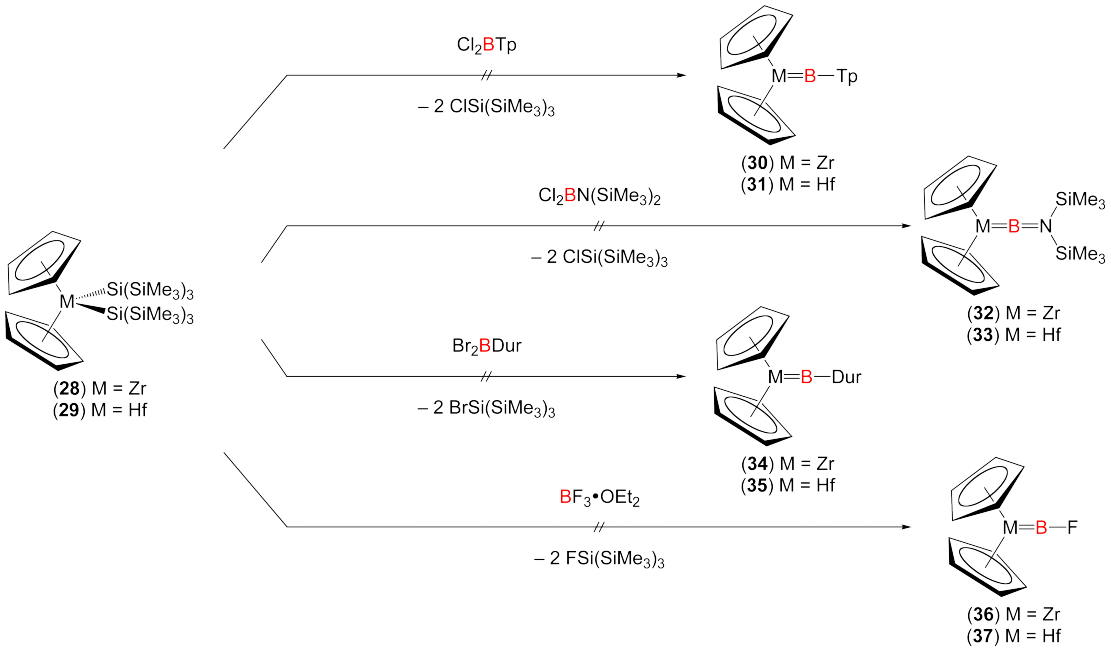

Figure 2-14. [(η^5-C_5H_5)$_2$Zr(Si(SiMe$_3$)$_3$)$_2$] (**28**) and [(η^5-C_5H_5)$_2$Hf(Si(SiMe$_3$)$_3$)$_2$] (**29**) test reactions with dihaloboranes Cl$_2$BTp (Tp = 2,6-(2,4,6-*i*Pr$_3$C$_6$H$_2$)$_2$C$_6$H$_3$)), Cl$_2$BN(SiMe$_3$)$_2$ and Br$_2$BDur, and the quarternized trihaloborane BF$_3$•OEt$_2$. None these reactions yielded discernable terminal borylene species through halosilane elimination reactions.

As can be seen in Figure 2-14, the reactions of the Group 4 transition metal *bis*(hypersilyl) species [(η^5-C_5H_5)$_2$Zr(Si(SiMe$_3$)$_3$)$_2$] (**28**) and [(η^5-C_5H_5)$_2$Hf(Si(SiMe$_3$)$_3$)$_2$] (**29**) with dihaloboranes Cl$_2$B{2,6-(2,4,6-*i*Pr$_3$C$_6$H$_2$)$_2$C$_6$H$_3$} (Cl$_2$BTp), Cl$_2$BN(SiMe$_3$)$_2$, and Br$_2$B{2,3,5,6-C$_6$Me$_4$H} (Br$_2$BDur), as well as the trihaloborane BF$_3$•OEt$_2$, were attempted. These reactions were all performed on small test reaction scales using freshly prepared Group 4 *bis*(hypersilyl) complexes as they are not stable over prolonged periods of time (even in a glovebox). These test reactions all showed no generation of borylene species at room temperature and all four reactions either displayed (A) unselective decomposition of the Group 4 transition metal *bis*(hypersilyl) complex or (B) no reactivity upon heating of the reaction mixtures to temperatures of 80 °C. The outcomes of these test reactions suggest hypersilyl transfer from the metal to the boron, resulting in the formation of silylboranes and the dihalometallocenes [(η^5-C_5H_5)$_2$ZrX$_2$] and [(η^5-C_5H_5)$_2$HfX$_2$] (X = F, Cl, or Br). This proposed silylborane formation was witnessed in the reactions with the dihaloboranes Cl$_2$BN(SiMe$_3$)$_2$, and Br$_2$B{2,3,5,6-C$_6$Me$_4$H} (Br$_2$BDur) as well as the trihaloborane BF$_3$•OEt$_2$, while the bulky terphenyl substituted dihaloborane Cl$_2$B{2,6-(2,4,6-*i*Pr$_3$C$_6$H$_2$)$_2$C$_6$H$_3$} (Cl$_2$BTp) showed no discernable reactivity.

2.1.4 Synthetic Attempts at a Group 6 Terminal Phosphinoborylene

In an attempt to synthesize a terminal borylene species which could exhibit two distinct reactivity patterns in which the borylene ligand: (A) transfers to other transition metal scaffolds or unsaturated organic substrates and (B) undergoes metathesis through 2+2 cycloadditions, a new borylene ligand scaffold was proposed.* Figure 2-15 displays the rationale used to arrive at the envisioned transition metal-borylene ligand system that could combine these two principles. The key for this proposed scaffold is in the Group 6 pentacarbonyl framework, which seems to be a prerequisite for borylene transfer under photolytic or thermolytic conditions. The metathesis reactivity route is dependent upon a partially saturated boron environment that could still be accessible by small Lewis bases to initiate the required 2+2 cycloaddition.

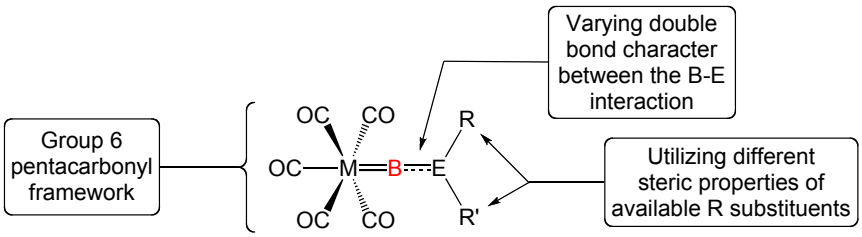

Figure 2-15. Diagram detailing the rationale for creating a transition metal terminal borylene species that could photolytically transfer the borylene fragment to other transition metal species as well as undergo metathesis type reactivity.

A prime candidate for the required "E" substituent would be a phosphino substituent, given the well-documented reduced overlap of the phosphorus lone pair of electrons with an electronically unsaturated three-coordinate boron center.[324,328,383,384] Utilizing this scaffold, sufficient steric bulk could be incorporated into the "R" substituents on a phosphino-substituted terminal borylene to allow for protection of the boron center. This structural motif satisfies both of the requirements of borylene complexes (A) the terminal Group 6 pentacarbonyl *bis*(trimethylsilyl)aminoborylenes ($(OC)_5M\{BN(SiMe_3)_2\}$, M = Cr (**13**), Mo (**14**), and W(**15**)) as well as the manganese cyclopentadienyl *bis*(carbonyl) terminal *tert*-butylborylene [(η^5-C_5H_5)$(OC)_2$Mn{B*t*-Bu}][168,169] understood to impose their respective reactivity patterns.

* See Sections 1.1.4 and 2.1.1 for details on the duality of terminal borylene reactivity.

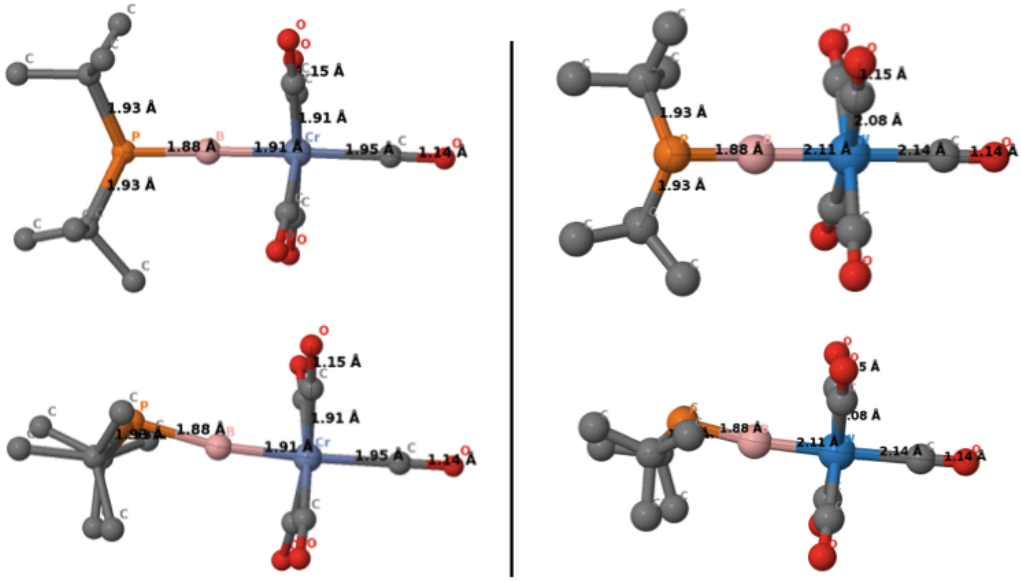

$(OC)_5Cr{=}B{-}P(t\text{-}Bu)_2$
(38)

$(OC)_5W{=}B{-}P(t\text{-}Bu)$
(39)

Figure 2-16. Structural geometry and predicted bond lengths for ([$(OC)_5Cr\{BP(t\text{-}Bu)_2\}$] (**38**) and [$(OC)_5W\{BP(t\text{-}Bu)_2\}$] (**39**)).

Geometry optimizations and Density Functional Theory (DFT) calculations were performed at the B3LYP/6-311G* level of theory to predict the geometry and electronic structures of two proposed terminal Group 6 pentacarbonyl phosphinoborylene species ([$(OC)_5Cr\{BP(t\text{-}Bu)_2\}$] (**38**) and [$(OC)_5W\{BP(t\text{-}Bu)_2\}$] (**39**)) utilizing *tert*-butyl substituents flanking the terminal phosphinoborylene for steric protection. Figures 2-16 shows the predicted geometry of [$(OC)_5Cr\{BP(t\text{-}Bu)_2\}$] (**38**) and [$(OC)_5W\{BP(t\text{-}Bu)_2\}$] (**39**), which clearly show a longer B-P bond distance (1.88 Å and 1.88 Å respectively) than the B-N distances of [$(OC)_5Cr\{BN(SiMe_3)_2\}$] (**13**) and [$(OC)_5W\{BN(SiMe_3)_2\}$] (**15**) (1.35 Å and 1.34 Å respectively) (Table 2-1). These elongated bond lengths in the complexes [$(OC)_5Cr\{BP(t\text{-}Bu)_2\}$] (**38**) and [$(OC)_5W\{BP(t\text{-}Bu)_2\}$] (**39**) also result in a tetrahedral geometry of the phosphorus centers (ΣP_α = 323.1° for [$(OC)_5Cr\{BP(t\text{-}Bu)_2\}$] (**38**)) in both species, in contrast to the trigonal planar geometry observed in [$(OC)_5Cr\{BN(SiMe_3)_2\}$] (**13**) (ΣN_α = 359.8°) and [$(OC)_5W\{BN(SiMe_3)_2\}$] (**15**). Complexes **38** and **39** also feature dramatically shorter M-B bond distances (1.91 Å and 2.11 Å respectively) and longer M-C_{ax} bond distances (1.95 Å and 2.14 Å respectively) relative to complexes **13** and **15**, further indicating that the bonding situation for this theoretical phosphinoborylene ligand to the metal center is dramatically more stable than the *bis*(trimethylsilyl)aminoborylene ligand. As can be seen in Figure 2-17, the frontier orbital projections (HOMO–1, HOMO, and LUMO) for [$(OC)_5Cr\{BP(t\text{-}Bu)_2\}$] (**38**)

show a clear indication that the HOMO resides primarily on the phosphorus center (phosphorus lone pair of electrons), with the LUMO observed to be primarily on the boron substituent. The frontier orbital projections for the complex [(OC)$_5$W{BP(*t*-Bu)$_2$}] (**38**) are almost identical in geometry to those of [(OC)$_5$Cr{BP(*t*-Bu)$_2$}] (**38**) and have subsequently been omitted to save space. Direct comparison between these two calculated terminal phospinoborylene species ([(OC)$_5$Cr{BP(*t*-Bu)$_2$}] (**38**) and [(OC)$_5$W{BP(*t*-Bu)$_2$}] (**39**)) with corresponding structural data of the aminoborylene species ([(OC)$_5$Cr{BN(SiMe$_3$)$_2$}] (**13**) (ΣN_α = 359.8°) and [(OC)$_5$W{BN(SiMe$_3$)$_2$}] (**15**)) indicates that the orbital overlap between the phosphorus lone pair and the unsaturated boron center is much less pronounced in the phophino-substituted borylene complexes, even though the comparisons are between calculated structures in the gas phase and solid state X-ray crystallographic data (Table 2-1).

(OC)$_5$Cr{BN(SiMe$_3$)$_2$} (**13**)[153,154] [Å]		(OC)$_5$Cr{BP(*t*-Bu)$_2$} (**38**) [Å]		(OC)$_5$W{BN(SiMe$_3$)$_2$} (**15**)[118,119] [Å]		(OC)$_5$W{BP(*t*-Bu)$_2$} (**39**) [Å]	
N–B	1.35	**P–B**	1.88	**N–B**	1.34	**P–B**	1.88
B–Cr	1.98	**B–Cr**	1.91	**B–W**	2.15	**B–W**	2.11
Cr–C$_{ax}$	1.91	**Cr–C$_{ax}$**	1.95	**W–C$_{ax}$**	2.04	**W–C$_{ax}$**	2.14

Table 2-1. Comparison between the calculated bond lengths of the proposed terminal Group 6 pentacarbonyl phosphinoborylenes (Cr = **38** and W = **39**) and the published solid-state X-ray crystal structures of terminal Group 6 pentacarbonyl *bis*(trimethylsilyl)aminoborylenes (Cr = **13** and W = **15**).

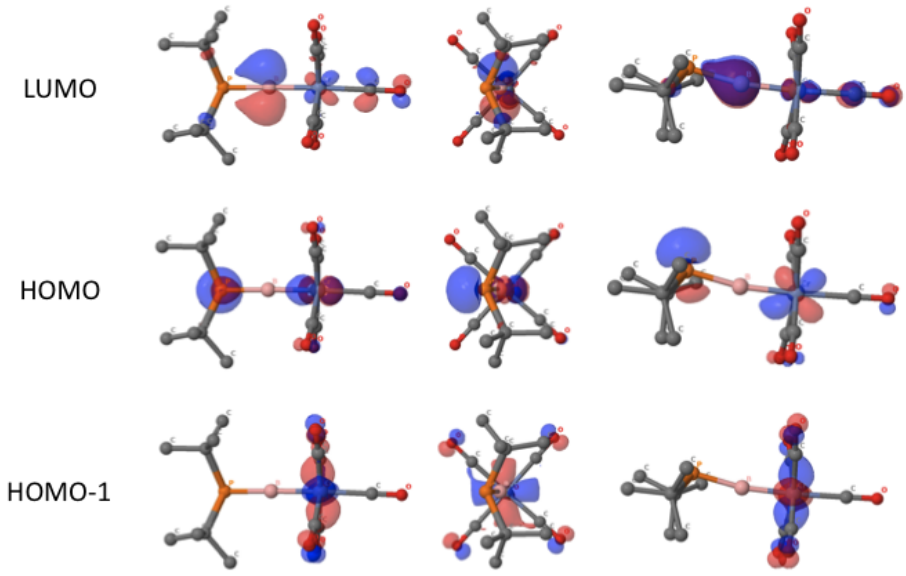

Figure 2-17. Frontier orbital projections (HOMO–1, HOMO, and LUMO) for ([(OC)$_5$Cr{BP(*t*-Bu)$_2$}] (**38**) aligned along the three principle (x, y, and z) axes.

Since the reaction of a *bis*(trimethylsilyl)aminodihaloborane ($X_2BN(SiMe_3)_2$, X = Cl, Br) with a Group 6 transition metal dianion ($Na_2[M(CO)_5]$, M = Cr (**11**), Mo (**1**), or W (**12**)) provided the corresponding borylene complexes in adequate yields (Figure 2-3), attempts were made to prepare a terminal phosphinoborylene species by reaction of these same Group 6 transition metal dianion species ($Na_2[M(CO)_5]$, M = Cr (**11**), Mo (**1**), or W (**12**)) with a phosphinodihaloborane reagent. Initially, as can be seen in Figure 2-18, the dimeric diphenyldibromoborane ($[Br_2BPPh_2]_2$ (**42**)) was synthesized[385] *via* quarternization of diphenylphosphine (**40**) with BBr_3 and deprotonation *via* mixing with one equivalent of triethylamine. The synthesis of this dimeric phosphinodihaloborane was possible; however, when reacted with the chromium and tungsten dianions ($Na_2[M(CO)_5]$, M = Cr (**11**) and W (**12**)), no isolable chromium or tungsten pentacarbonyl phosphinoborylene products could be observed. The failure of these reactions was attributed to the quarternized dimer preventing salt elimination reactions in solution with the dianions at low temperatures (the dianions are not stable at temperatures above –40 °C).

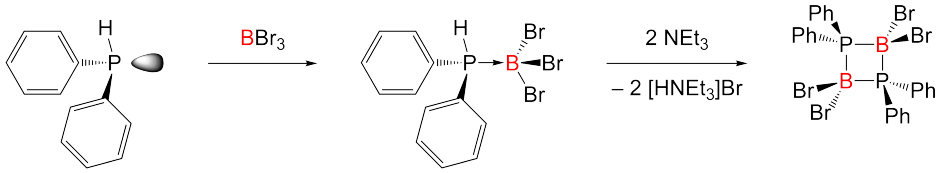

Figure 2-18. Synthesis of the diphenylphosphinodibromoborane dimer $[Br_2BPPh_2]_2$ (**42**) *via* quarternization of BBr_3 with diphenylphosphine (**40**) to yield the isolable Lewis pair $HPh_2P{\bullet}BBr_3$ (**41**), followed by deprotonation with triethylamine (NEt_3).

An ideal precursor phosphinodihaloborane would be a species with sterically bulky groups at the P atom to prevent dimerization in solution. An idea proposed by Dr. Justin Wolf led to the conception of a dibromo(dicyclohexylphosphino)borane, which was predicted to be monomeric in solution. Conceptually, the reaction of this new phosphine would be achieved in a similar manner to the previously reported Group 6 pentacarbonyl *bis*(trimethylsilyl)aminoborylenes ($(OC)_5M\{BN(SiMe_3)_2\}$, M = Cr (**13**), Mo (**14**), and W(**15**)) as can be seen in Figure 2-19.

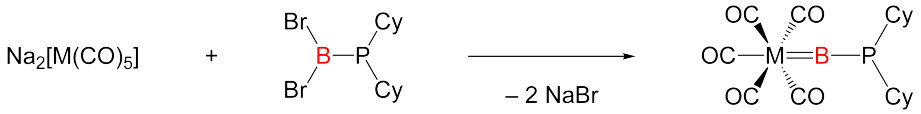

(**11**) M = Cr
(**1**) M = Mo
(**12**) M = W

(**43**)

(**44**) M = Cr
(**45**) M = Mo
(**46**) M = W

Figure 2-19. Proposed synthesis of $[(OC)_5M\{BPCy_2\}]$ (M = Cr (**44**), Mo (**45**), and W(**46**)) *via* salt elimination of a monomeric phosphinohaloborane (**43**) with the Group 6 pentacarbonyl dianions $Na_2[M(CO)_5]$ (M = Cr (**11**), Mo (**1**), and W (**12**)).

Phosphinoborane $Br_3B{\bullet}PHCy_2$ (**48**) was used as a precursor for deprotonation towards the monomeric phosphinoborane species Br_2BPCy_2 (**43**) displayed in Figures 2-19 and 2-20. Synthesis of this starting material was achieved by reaction of dicyclohexylphosphine (**47**) with tribromoborane (BBr_3) in near quantitative yields; however, the deprotonation of the phosphine adduct (**48**) was not possible using standard laboratory bases (several examples are shown). This failure was attributed to the higher pK_a values for the dialkylphosphine (pK_a: $HPCy_2$ = 35.7) relative to the diaryl phosphines (pK_a: $HPPh_2$ = 21.7).[386]

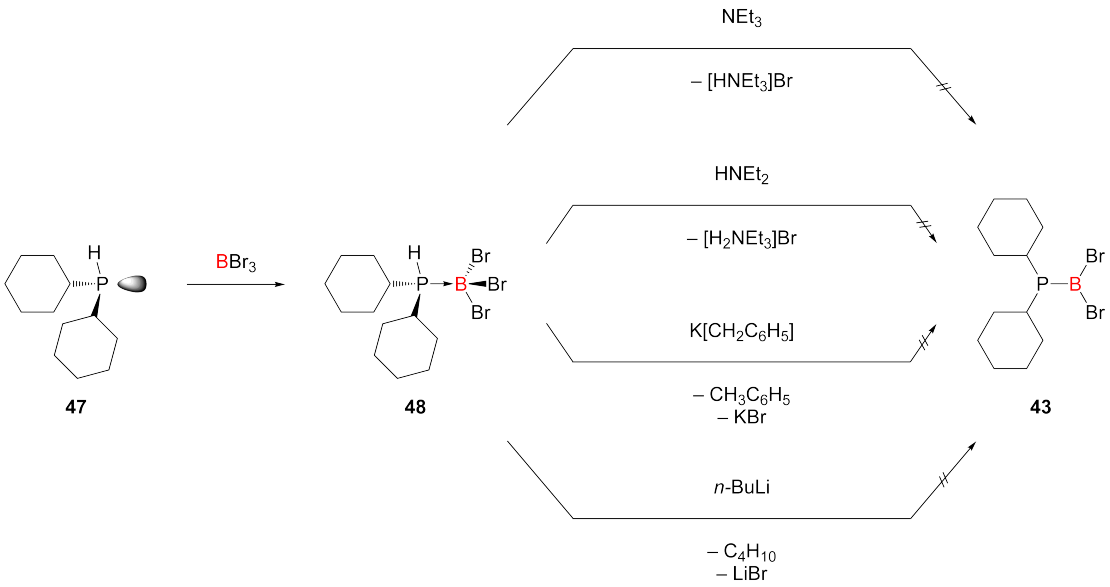

Figure 2-20. Synthesis of the Lewis pair $HCy_2P{\bullet}BBr_3$ (**42**) followed by attempted deprotonation reactions with the amine bases NEt_3 and $HNEt_2$ as well as the anionic bases *n*-BuLi and $K[CH_2C_6H_5]$. All four of these bases failed to yield the desired monomeric phosphidodihaloborane Cy_2PBBr_2 (**43**).

Mixing of $HPCy_2$ (**47**) with one equivalent of tribromoborane (BBr_3) gave the Lewis pair $HCy_2P{\bullet}BBr_3$ (**48**) (^{31}P: δ = 1.7 ppm, $^1J_{P\text{-}B}$ = 138 Hz) in near quantitative yield. The Lewis pair precipitates out of solution as a white crystalline solid, which has a melting point at approximately 168 °C with no observable decomposition under 300 °C. $HCy_2P{\bullet}BBr_3$ (**48**) can also be witnessed by ^1H, ^{11}B, and ^{13}C NMR spectroscopy. $^1H\{^{31}P\}$ NMR spectra of the adduct display one prominent resonance at 4.313 ppm corresponding to the phosphine P-H proton, which is observed as a doublet in the non-phosphorus decoupled ^1H NMR spectra of the complex which shows a coupling constant for the P-H interaction ($^1J_{P\text{-}H}$) equal to 405 Hz. The $^{11}B\{^1H\}$ NMR spectra of the complex display a coupling constant for the B-P interaction ($^1J_{B\text{-}P}$) equal to 137 Hz (matching the data found in the $^{31}P\{^1H\}$ NMR spectra).

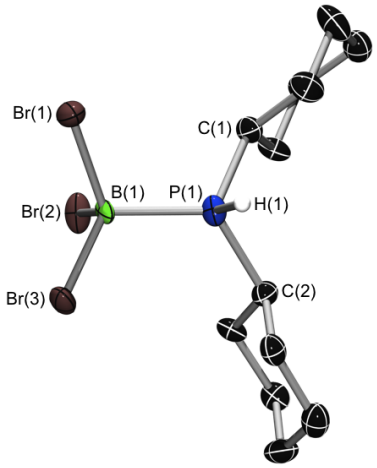

Figure 2-21. ORTEP-rendered structure of $HCy_2P{\bullet}BBr_3$ (**48**). Thermal ellipsoids set at 50% probability. Selected bond distances (Å) and angles (°): P(1)–B(1) 1.96(1), P(1)–C(1) and P(1)–C(2) 1.84 (avg.), P(1)–H(1) 1.4(1), B(1)–Br(1), B(1)–Br(2), and B(1)–Br(3) 2.00 (avg.), B(1)–P(1)–C 114.7 (avg.), P(1)–B(1)–Br 107.8 (avg.).

Crystals suitable for X-ray diffraction were grown from saturated solutions of $HCy_2P{\bullet}BBr_3$ (**48**)* in benzene. An ORTEP diagram for the structure as well as some key bond distances for $HCy_2P{\bullet}BBr_3$ (**48**) are shown in Figure 2-21. The $HCy_2P{\bullet}BBr_3$ (**48**) species displays P-B, P-C (avg.), and B-Br (avg.) bond distances of 1.96(1), 1.84 (avg.), and 2.00 (avg.) Å respectively.

Deprotonation reactions were attempted with the amine bases NEt_3 and $HNEt_2$ (Figure 2-20) but failed to yield the desired monomeric dibromo(dicyclohexylphosphino)borane (**43**). Deprotonation reactions were also attempted with the lithium- and potassium-stabilized anionic bases *n*-BuLi and $K[CH_2C_6H_5]$, but these reagents were also found to be unable to deprotonate the phosphine.

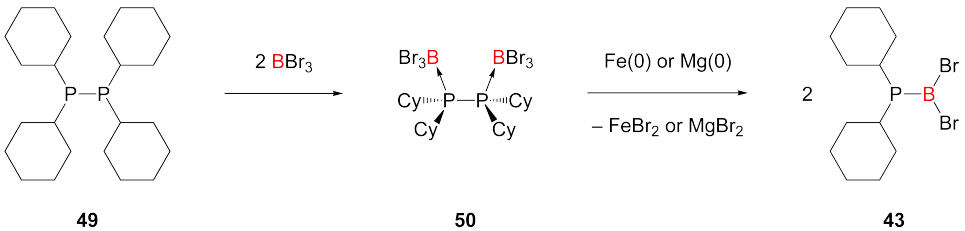

Figure 2-22. Proposed synthetic route to the desired monomeric phosphinodihaloborane Cy_2PBBr_2 (**43**).

Since synthetic attempts failed to yield the monomeric dibromo(dicyclohexylphosphino)borane by mimicking previous literature

* $C_{12}H_{23}BBr_3P$, M = 448.81, monoclinic, space group = $P2_1/n$.

deprotonation reactions for diarylphosphines,[385] an alternative route was proposed in order to achieve this target dihaloborane based on previously reported work by Issleib, Nöth, and coworkers.[387-396] As can be seen in Figure 2-22, the dicyclohexyldiphosphine (**49**) could be quarternized with one or two equivalents of tribromoborane to yield the diphosphine with two equivalents of quarternized tribromoborane $Br_3B{\bullet}PCy_2Cy_2P{\bullet}BBr_3$ (**50**). This species could subsequently be reacted with Fe(0) or Mg(0) in solution to cleave the diphosphine P-P bond by two-electron reduction. Subsequent elimination of two equivalents of bromide in solution should result in precipitation of the MBr_2 salt with formation of the monomeric dibromo(dicyclohexylphosphino)borane (**43**).

2.2 Second Generation Borylene Synthesis

2.2.1 Previous Work

As previously discussed,* the first intermetallic terminal borylene transfer was published by our group in 2003 (Figure 2-23).[179,180] These borylene transfer reactions are performed either under photo- or thermolytic conditions in order to initiate ligand dissociation and complex rearrangement. As only a few examples of these ligand transfers are known, the nature of the complexes accepting the borylene ligand must be analyzed to predict further success in transfer reactions. All of these transfer reactions require the generation of an open coordination site on the target transition metal complex and subsequent exchange of a carbonyl (or L type) ligand for a borylene ligand. The driving force for these transfer reactions is typically understood to be the inherent stability (and decreased solubility) of the Group 6 hexacarbonyl complexes formed as a byproduct of carbonyl exchanges. The decreased solubility of these Group 6 pentacarbonyl species successfully inhibits the reverse reaction once borylene transfer has been successfully accomplished. Decomposition of the Group 6 terminal borylene complex in solution also liberates up to five equivalents of free CO with one equivalent of elemental transition metal (M(0)). This small excess of free CO in solution in turn drives the formation of the group 6 hexacarbonyl complexes by further pushing the equilibrium towards the products.

As can be seen in Figure 2-23, the first synthesis of a "second generation" terminal borylene complex was achieved by borylene transfer from the chromium pentacarbonyl *bis*(trimethylsilyl)aminoborylene ([$(OC)_5Cr\{BN(SiMe_3)_2\}$] (**13**)) onto a vanadium cyclopentadienyl tetracarbonyl scaffold [$(\eta^5\text{-}C_5H_5)V(CO)_4$] (**51**)) resulting in borylene/carbonyl exchange with formation of the vanadium cyclopentadienyl tricarbonyl terminal *bis*(trimethylsilyl)aminoborylene complex ([$(\eta^5\text{-}C_5H_5)(CO)_3V\{BN(SiMe_3)_2\}$] (**52**)).

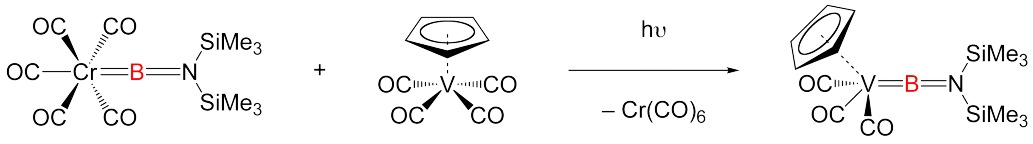

13 51 52

Figure 2-23. [$(\eta^5\text{-}C_5H_5)(CO)_3V\{BN(SiMe_3)_2\}$] (**52**) synthesis by borylene transfer from [$(OC)_5Cr\{BN(SiMe_3)_2\}$] (**13**) to [$(\eta^5\text{-}C_5H_5)V(CO)_4$] (**51**).

* See Section 1.1.4 for an introduction to transfer of terminal borylene ligands to transition metal complexes.

In an analogous synthetic route the terminal borylene ligand is also known to transfer to a transition metal scaffold in a bridging fashion, as published by our group in 2009.[181] These reactions also proceed under photolytic or thermolytic conditions, however in these cases, the final bridging borylene complex can be either achieved directly as depicted in Figure 2-24, or formed by a subsequent rearrangement of an initially formed terminal borylene species. As can be seen below in Figure 2-24, this particular synthesis of a "second generation" bridging borylene complex was achieved by borylene transfer from the tungsten pentacarbonyl *bis*(trimethylsilyl)aminoborylene ($[(OC)_5W\{BN(SiMe_3)_2\}]$ (**15**)) onto a dinuclear nickel cyclopentadienyl carbonyl scaffold, ($[\{(\eta^5\text{-}C_5H_5)Ni\}_2\{\mu\text{-}(CO)\}_2]$ (**53**)), resulting in borylene/carbonyl exchange with formation of the dinickel complex $[\{(\eta^5\text{-}C_5H_5)Ni\}_2\{\mu\text{-}(CO)\}\{\mu\text{-}BN(SiMe_3)_2\}]$ (**54**).

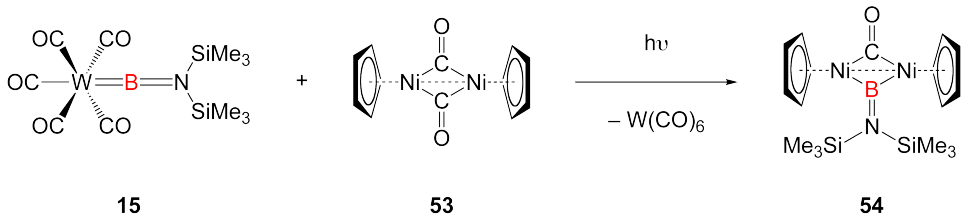

15 53 54

Figure 2-24. $[\{(\eta^5\text{-}C_5H_5)Ni\}_2\{\mu\text{-}(CO)\}\{\mu\text{-}BN(SiMe_3)_2\}]$ (**54**) synthesis by borylene transfer from $[(OC)_5W\{BN(SiMe_3)_2\}]$ (**15**) to $[\{(\eta^5\text{-}C_5H_5)Ni\}_2\{\mu\text{-}(CO)\}_2]$ (**53**).

2.2.2 Synthesis of Unsymmetrical Terminal Aminoborylene Complexes by Intermetallic Borylene Transfer

To further test the reactivity of the new terminal unsymmetrical borylene complexes, attempts were made to transfer the borylene ligand to transition metal carbonyl scaffolds previously shown to be borylene ligand acceptors. These reactions can proceed under photo- or thermolytic conditions and borylene transfer was successful regardless of the Group 6 metal used (photolytic conditions for $[(OC)_5Cr\{BN(SiMe_3)(t\text{-}Bu)\}]$ (**19**) and $[(OC)_5W\{BN(SiMe_3)(t\text{-}Bu)\}]$ (**21**), thermolytic conditions for $[(OC)_5Mo\{BN(SiMe_3)(t\text{-}Bu)\}]$ (**20**)). Borylene complex $[(OC)_5Cr\{BN(SiMe_3)(t\text{-}Bu)\}]$ (**19**) was used as a standard reagent for these transfer studies, as it can be synthesized with the highest yield, and provides the best yields in photolytic syntheses of the target "second generation" borylene complexes.

2.2.2.1 $[(\eta^5\text{-}C_5H_5)(OC)_3V\{BN(SiMe_3)(t\text{-}Bu)\}]$ (55)

$[(\eta^5\text{-}C_5H_5)(OC)_3V\{BN(SiMe_3)(t\text{-}Bu)\}]$ (**55**) was prepared by borylene transfer under photolytic conditions from the unsymmetrical terminal "first generation" chromium borylene complex, $[(OC)_5Cr\{BN(SiMe_3)(t\text{-}Bu)\}]$ (**19**), to the vanadium cyclopentadienyl tetracarbonyl complex ($[(\eta^5\text{-}C_5H_5)V(CO)_4]$ (**51**)) with formal reciprocal transfer of one carbonyl ligand from $[(\eta^5\text{-}C_5H_5)V(CO)_4]$ (**51**) back to $[(OC)_5Cr\{BN(SiMe_3)(t\text{-}Bu)\}]$ (**19**) resulting in the formation of one equivalent of $[Cr(CO)_6]$ (Figure 2-25). The reaction can be monitored *via* $^{11}B\{^1H\}$ NMR spectroscopy with consumption of the starting terminal borylene species, $[(OC)_5Cr\{BN(SiMe_3)(t\text{-}Bu)\}]$ (**19**) (δ = 97 ppm) and growth of the slightly downfield shifted resonance corresponding to product complex $[(\eta^5\text{-}C_5H_5)(OC)_3V\{BN(SiMe_3)(t\text{-}Bu)\}]$ (**55**) (δ = 100 ppm). The product complex $[(\eta^5\text{-}C_5H_5)(OC)_3V\{BN(SiMe_3)(t\text{-}Bu)\}]$ (**55**) can also be subsequently monitored *via* ^1H NMR spectroscopy with observation of a resonance corresponding to the cyclopentadienyl protons ($\eta^5\text{-}C_5H_5$) at δ = 4.636 ppm (δ = 4.66 ppm for $[(\eta^5\text{-}C_5H_5)(CO)_3V\{BN(SiMe_3)_2\}]$[179,180] (**52**)). This photolytic reaction seems to progress in a much faster manner than the synthesis of the reported $[(\eta^5\text{-}C_5H_5)(CO)_3V\{BN(SiMe_3)_2\}]$ (**52**) complex (6 h *vs.* 96 h). For this particular species the best way to conduct the reaction in order to easily monitor progress is to use the tungsten terminal unsymmetrical borylene complex $[(OC)_5W\{BN(SiMe_3)(t\text{-}Bu)\}]$ (**21**) as its $^{11}B\{^1H\}$ resonance is found at 92 ppm, which does not overlap as completely with the $^{11}B\{^1H\}$ NMR resonance of the formed product $[(\eta^5\text{-}C_5H_5)(OC)_3V\{BN(SiMe_3)(t\text{-}Bu)\}]$ (**55**) at 100 ppm (δ = 98 ppm for $[(\eta^5\text{-}C_5H_5)(CO)_3V\{BN(SiMe_3)_2\}]$[179,180] (**52**)). Workup of the complex can be achieved by removal of all volatiles *in vacuo* and sublimation of the $[M(CO)_6]$ (M = Cr or W)

byproduct by heating at 60 °C under high vacuum (0.001 Torr). Purification of the yellow/orange residue can subsequently be accomplished by extraction of the crude material with hexane and filtration of this extract through a small column of pacified silica gel (SiO_2)[397] to yield the product as a yellow fraction. Storage of this solution in the glovebox freezer (–40 °C) for one week yielded [(η^5-C_5H_5)(OC)$_3$V{BN(SiMe$_3$)(*t*-Bu)}] (**55**) as a yellow air and moisture sensitive crystalline solid in 84% yield. Differential thermal analysis of this yellow crystalline solid showed a melting point for [(η^5-C_5H_5)(OC)$_3$V{BN(SiMe$_3$)(*t*-Bu)}] (**55**) at 74 °C with decomposition above 259 °C.

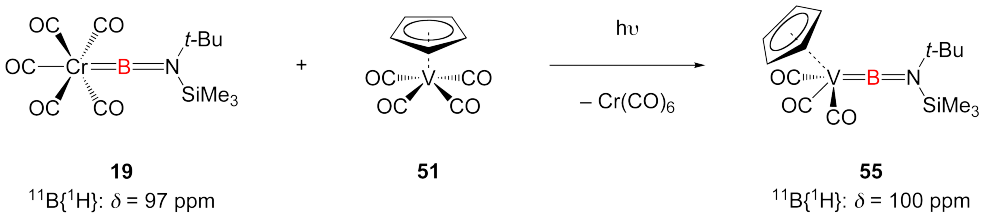

Figure 2-25. [(η^5-C_5H_5)(OC)$_3$V{BN(SiMe$_3$)(*t*-Bu)}] (**55**) synthesis by a borylene transfer reaction from [(OC)$_5$Cr{BN(SiMe$_3$)(*t*-Bu)}] (**19**) to [(η^5-C_5H_5)V(CO)$_4$] (**51**).

[(η^5-C_5H_5)(CO)$_3$V{BN(SiMe$_3$)(*t*-Bu)}] (**55**) can be witnessed by ^{1}H, ^{11}B, ^{13}C, and ^{29}Si NMR spectroscopy. ^{1}H NMR spectra of the complex display two prominent resonances at 0.264 and 1.273 ppm corresponding to the trimethylsilyl and *tert*-butyl protons respectively (9H for each resonance). Both of these values are slightly downfield shifted from the reported values of the chromium pentacarbonyl terminal unsymmetrical borylene [(OC)$_5$CrBN(SiMe$_3$)(*t*-Bu)] (**19**) (0.159 and 1.148 ppm for the trimethylsilyl and *tert*-butyl protons, respectively). The trimethylsilyl proton resonance at 0.264 ppm was assigned through 2D ^{1}H-^{13}C NMR (^{13}C{^{1}H}: δ = 2.84 ppm, $^1J_{C\text{-}Si}$ = 58 Hz) correlation spectroscopy (HSQC) as well as the interpreted $^2J_{H\text{-}Si}$ coupling value of 6.7 Hz. This value for the trimethylsilyl NMR spectroscopic resonance is in agreement with published data for the similar *bis*(trimethylsilyl)aminoborylene complex [(η^5-C_5H_5)(CO)$_3$V{BN(SiMe$_3$)$_2$}] (**52**) (^{1}H: δ = 0.21 ppm, N-Si(C*H*$_3$)$_3$).[179,180] Unfortunately the ^{29}Si{^{1}H} NMR resonance (^{29}Si{^{1}H}: δ = 3.55 ppm) is too broad to verify this coupling constant. ^{13}C{^{1}H} NMR spectra for the compound shows the carbonyl carbon environments at δ = 197.67 ppm (all three are equivalent on the NMR timescale), which is not in agreement with the data reported for [(η^5-C_5H_5)(CO)$_3$V{BN(SiMe$_3$)$_2$}] (**52**) (^{13}C{^{1}H}: δ = 211.47 ppm, M-*C*O).[179,180] This environment for the carbonyl ligands seems to be significantly high-field shifted from the previously reported similar compound [(η^5-C_5H_5)(CO)$_3$V{BN(SiMe$_3$)$_2$}] (**52**); however, this is the only carbonyl environment

observed in the spectra of the compound (the scanning width for the $^{13}C\{^{1}H\}$ NMR spectrum was from –40 to 240 ppm).

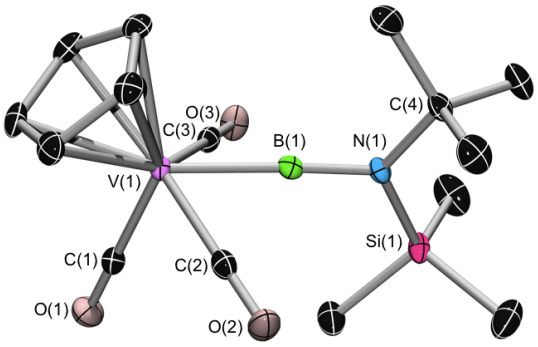

Figure 2-26. ORTEP-rendered structure of [(η^5-C_5H_5)$(OC)_3$V{BN($SiMe_3$)(*t*-Bu)}] (**55**). Thermal ellipsoids set at 50% probability. All hydrogen atoms have been omitted for clarity. Selected bond distances (Å) and angles (°): V(1)–B(1) 1.968(1), V(1)–$C_{proximal}$ (avg.) 1.899, V(1)–C_{distal} 1.940(1), B(1)–N(1) 1.373(2), $C_{proximal}$–$O_{proximal}$ (avg.) 1.163, C_{distal}– O_{distal} 1.147(2), V(1)–B(1)–N(1) 177.6(1), B(1)–V(1)–$C_{proximal}$ (avg.) 62.96, N(1)–B(1)–C_{distal} 110.47(6), ΣN_α 359.9.

Crystals suitable for X-ray diffraction were grown from saturated solutions of [(η^5-C_5H_5)$(OC)_3$V{BN($SiMe_3$)(*t*-Bu)}] (**55**) in hexane.[*] An ORTEP diagram of the structure as well as some key bond distances for [(η^5-C_5H_5)$(OC)_3$V{BN($SiMe_3$)(*t*-Bu)}] (**55**) are shown in Figure 2-26. The [(η^5-C_5H_5)$(OC)_3$V{BN($SiMe_3$)(*t*-Bu)}] (**55**) species displays V-B, B-N, V-$C_{proximal}$ (avg.), and V-C_{distal} (proximal and distal in relation to the {BN($SiMe_3$)(*t*-Bu)} ligand) distances of 1.968(1), 1.373(2), 1.899 (avg.), and 1.940(1) Å, respectively. The cyclopentadienyl ligand centroid is approximately 1.925 Å from the vanadium center. These data are comparable[†] to the distances of [(η^5-C_5H_5)$(OC)_3$V{BN($SiMe_3$)$_2$}] (**52**), which displays V-B, B-N, V-$C_{proximal}$ (avg.), and V-C_{distal} (proximal and distal in relation to the {BN($SiMe_3$)$_2$} ligand) distances of 1.960(6), 1.378(7), 1.886 (avg.), and 1.936(6) Å respectively.[179,180] One structural aspect of the [(η^5-C_5H_5)$(OC)_3$V{BN($SiMe_3$)$_2$}] (**52**) complex that was discussed in the original publication was the abnormally short carbonyl $C_{proximal}$-B distances (C-B) of 1.997(8) Å and 2.037(8) Å, which indicate an interaction with the boron similar to other recent published species by our group.[155,156] The carbonyl $C_{proximal}$-B distances of [(η^5-C_5H_5)$(OC)_3$V{BN($SiMe_3$)(*t*-Bu)}] (**55**) are found to be 2.022 Å and 2.019 Å, respectively.

[*] $C_{15}H_{23}BNO_3SiV$, M = 355.19, orthorhombic, space group = *Pbca*.
[†] $C_{14}H_{23}BNO_3Si_2V$, M = 371.26, monoclinic, space group = $P2_1/c$.

2.2.2.2 [(η^5-C_5Me_5)Ir{BN(SiMe$_3$)(*t*-Bu)}$_2$] (58)

The iridium *bis*(borylene) complex [(η^5-C_5Me_5)Ir{BN(SiMe$_3$)(*t*-Bu)}$_2$] (**58**) was prepared by borylene transfer under photolytic conditions from the unsymmetrical terminal "first generation" chromium borylene complex, [(OC)$_5$Cr{BN(SiMe$_3$)(*t*-Bu)}] (**19**), to the iridium pentamethylcyclopentadienyl dicarbonyl complex [(η^5-C_5Me_5)Ir(CO)$_2$] (**56**) with formal reciprocal transfer of two carbonyl ligands from [(η^5-C_5Me_5)Ir(CO)$_2$] (**56**) back to [(OC)$_5$Cr{BN(SiMe$_3$)(*t*-Bu)}] (**19**), resulting in the formation of two equivalents of [Cr(CO)$_6$] (Figure 2-27). Monitoring of the reaction by $^{11}B\{^1H\}$ NMR spectroscopy showed consumption of one equivalent of the starting terminal borylene species, [(OC)$_5$Cr{BN(SiMe$_3$)(*t*-Bu)}] (**19**), observed at δ = 97 ppm, and formation of the monoborylene-substituted iridium monoborylene complex [(η^5-C_5Me_5)(OC)Ir{BN(SiMe$_3$)(*t*-Bu)}] (**57**) ($^{11}B\{^1H\}$: δ = 69 ppm). The $^{11}B\{^1H\}$ NMR spectroscopic data for [(η^5-C_5Me_5)(OC)Ir{BN(SiMe$_3$)(*t*-Bu)}] (**57**) is in good agreement with the previously published iridium pentamethylcyclopentadienyl carbonyl *bis*(trimethylsilyl)aminoborylene complex [(η^5-C_5Me_5)(OC)Ir{BN(SiMe$_3$)$_2$}] ($^{11}B\{^1H\}$: δ = 67 ppm).[182,183] The intermediary iridium monoborylene complex, [(η^5-C_5Me_5)(OC)Ir{BN(SiMe$_3$)(*t*-Bu)}] (**57**), was not isolated and the photolytic reaction was continued until conversion to the iridium *bis*(borylene) complex [(η^5-C_5Me_5)Ir{BN(SiMe$_3$)(*t*-Bu)}$_2$] (**58**) was complete. Following this initial transfer, the consumption of the second equivalent of the starting terminal borylene complex [(OC)$_5$Cr{BN(SiMe$_3$)(*t*-Bu)}] (**19**) ($^{11}B\{^1H\}$: δ = 97 ppm) is subsequently observed with formation of the final disubstituted transition metal *bis*(borylene) species, [(η^5-C_5Me_5)Ir{BN(SiMe$_3$)(*t*-Bu)}$_2$] (**58**), observed at δ = 71 ppm. The $^{11}B\{^1H\}$ NMR resonance of [(η^5-C_5Me_5)Ir{BN(SiMe$_3$)(*t*-Bu)}$_2$] (**58**) is slightly downfield shifted of that of the previously published iridium pentamethylcyclopentadienyl *bis*(trimethylsilyl)amino-*bis*(borylene) complex [(η^5-C_5Me_5)Ir{BN(SiMe$_3$)$_2$}$_2$] ($^{11}B\{^1H\}$: δ = 69 ppm).[182,183] The product complex [(η^5-C_5Me_5)Ir{BN(SiMe$_3$)(*t*-Bu)}$_2$] (**58**) can also be subsequently monitored *via* ^{1}H NMR spectroscopy with observation of a resonance corresponding to the pentamethylcyclopentadienyl protons (η^5-C_5Me_5) at δ = 2.346 ppm (δ = 2.34 ppm for [(η^5-C_5Me_5)Ir{BN(SiMe$_3$)$_2$}$_2$]).[182,183] This photolytic reaction seems to progress more rapidly than the synthesis of the *bis*(borylene) [(η^5-C_5Me_5)Ir{BN(SiMe$_3$)$_2$}$_2$] (12 h *vs.* 20 h). Workup of the complex can be achieved by removal of all volatiles *in vacuo* and sublimation of the [Cr(CO)$_6$] byproduct by heating at 60 °C under high vacuum (0.001 Torr). Purification of the yellow/black residue can subsequently be accomplished by extraction of the crude material with hexane and filtration of this extract through a small column of pacified

silica gel (SiO_2)[397] to yield the product as a light yellow (almost colorless) fraction. Storage of this solution in the glovebox freezer (–40 °C) for one week yielded [(η^5-C_5Me_5)Ir{BN($SiMe_3$)(*t*-Bu)}$_2$] (**58**) as a colorless air and moisture sensitive crystalline solid in 58% yield. Differential thermal analysis of these yellow crystalline solids showed a melting point at 128 °C with decomposition above 301 °C.

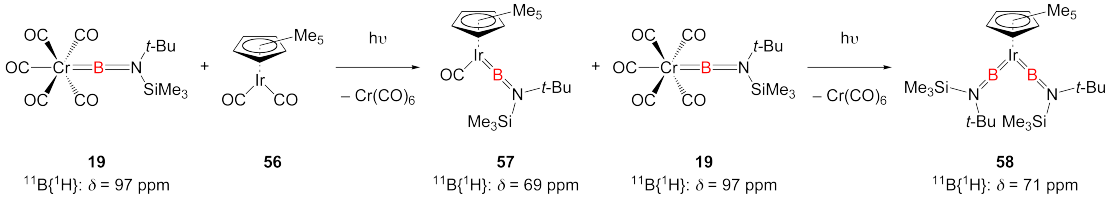

Figure 2-27. [(η^5-C_5Me_5)Ir{BN($SiMe_3$)(*t*-Bu)}$_2$] (**58**) synthesis by twofold borylene transfer reactions from [(OC)$_5$Cr{BN($SiMe_3$)(*t*-Bu)}] (**19**) to [(η^5-C_5Me_5)Ir(CO)$_2$] (**56**) *via* the observed monoborylene species [(η^5-C_5Me_5)Ir{BN($SiMe_3$)(*t*-Bu)}(CO)] (**57**).

[(η^5-C_5Me_5)Ir{BN($SiMe_3$)(*t*-Bu)}$_2$] (**58**) was characterized by ^{1}H, ^{11}B, ^{13}C, and ^{29}Si NMR spectroscopy. ^{1}H NMR spectra of the complex show two prominent resonances at 0.442 and 1.452 ppm corresponding to the trimethylsilyl and *tert*-butyl protons respectively (18H for each resonance). Both of these values are slightly downfield shifted from the reported values of the chromium pentacarbonyl terminal borylene complex [(OC)$_5$Cr{BN($SiMe_3$)(*t*-Bu)}] (**19**) (0.159 and 1.148 ppm for the trimethylsilyl and *tert*-butyl protons respectively). The trimethylsilyl proton resonance at 0.442 ppm was assigned through 2D ^{1}H-^{13}C NMR (^{13}C{^{1}H}: δ = 4.47 ppm, $^1J_{C\text{-}Si}$ = 57 Hz) correlation spectroscopy (HSQC) as well as the interpreted $^2J_{H\text{-}Si}$ coupling value of 6.7 Hz. This value for the trimethylsilyl NMR spectroscopic resonance is in agreement with published data for the similar *bis*(trimethylsilyl)amino-*bis*(borylene) iridium complex [(η^5-C_5Me_5)Ir{BN($SiMe_3$)$_2$}$_2$] (^{1}H: δ = 0.37 ppm, N-Si(CH_3)$_3$).[182,183] Unfortunately the ^{29}Si{^{1}H} NMR resonance (^{29}Si{^{1}H}: δ = –1.22 ppm) is too broad to verify this coupling constant. Analysis of [(η^5-C_5Me_5)Ir{BN($SiMe_3$)(*t*-Bu)}$_2$] (**58**) by infrared spectroscopy shows multiple observable bands assignable to possible $\tilde{\nu}$(B=N) stretching modes at 2,002 and 1,653 cm^{-1}.

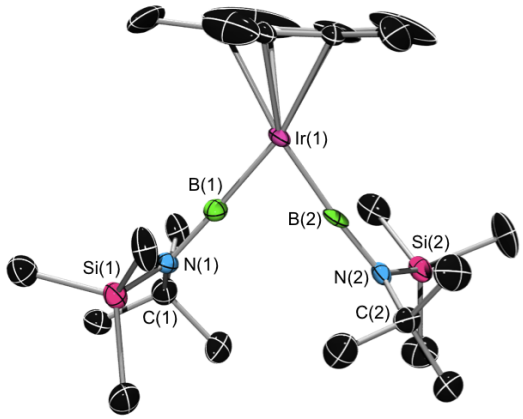

Figure 2-28. ORTEP-rendered structure of [(η^5-C_5Me_5)Ir{BN($SiMe_3$)(*t*-Bu)}$_2$] (**58**). Thermal ellipsoids set at 50% probability. All hydrogen atoms have been omitted for clarity. Selected distances (Å) and angles (°): Ir(1)–B(1) 1.857(6), Ir(1)–B(2) 1.881(5), B(1)–N(1) 1.404(7), B(2)–N(2) 1.372(7), Ir–Cp* centroid (Cp* = η^5-C_5Me_5) 1.935, B(1)–Ir(1)–B(2) 79.13, Ir(1)–B(1)–N(1) 178.3(4), Ir(1)–B(2)–N(2) 176.1(4).

Crystals suitable for X-ray diffraction were grown from saturated solutions of [(η^5-C_5Me_5)Ir{BN($SiMe_3$)(*t*-Bu)}$_2$] (**58**) in hexane.* An ORTEP diagram of the structure as well as some key bond distances for [(η^5-C_5Me_5)Ir{BN($SiMe_3$)(*t*-Bu)}$_2$] (**58**) are shown in Figure 2-28. The [(η^5-C_5Me_5)Ir{BN($SiMe_3$)(*t*-Bu)}$_2$] (**58**) species displays Ir-B (avg.) and B-N (avg.) bond distances of 1.869 (avg.) and 1.388 (avg.) Å respectively with an Ir-Cp* centroid (Cp* = η^5-C_5Me_5) distance of 1.935 Å. The angle between the borylene ligands (∠ B-Ir-B) is found to be 79.13°. This data is comparable† to those of [(η^5-C_5Me_5)Ir{BN($SiMe_3$)$_2$}$_2$], which displays Ir-B (avg.) and B-N (avg.) bond distances of 1.863 Å and 1.396 Å respectively with an Ir-Cp* centroid (Cp* = η^5-C_5Me_5) distances of 1.955 Å. The angle between the borylenes (∠ B-Ir-B) was reported to be 78.33°.[182,183]

* $C_{24}H_{51}B_2IrN_2Si_2$, M = 637.68, monoclinic, space group = $P2_1/n$.
† $C_{22}H_{51}B_2IrN_2Si_4$, M = 669.83, monoclinic, space group = $P2_1/n$.

2.2.3 Synthesis of Unsymmetrical Bridging Aminoborylene Complexes by Intermetallic Borylene Transfer

2.2.3.1 [{(η^5-C_5H_4Me)Co}$_2${μ-(CO)}$_2${μ-BN(SiMe$_3$)(*t*-Bu)}] (61)

[{(η^5-C_5H_4Me)Co}$_2$(μ-CO)$_2${μ-BN(SiMe$_3$)(*t*-Bu)}] (**61**) was prepared by borylene transfer under photolytic conditions from the unsymmetrical terminal "first generation" chromium borylene complex, [(OC)$_5$Cr{BN(SiMe$_3$)(*t*-Bu)}] (**19**), to the cobalt methylcyclopentadienyl (Cp') dicarbonyl complex [(η^5-C_5H_4Me)Co(CO)$_2$] (**59**) with formal reciprocal transfer of a carbonyl ligand from [(η^5-C_5H_4Me)Co(CO)$_2$] (**59**) back to the [(OC)$_5$Cr{BN(SiMe$_3$)(*t*-Bu)}] (**19**) complex resulting in the formation of one equivalent of [Cr(CO)$_6$] (Figure 2-29). Monitoring of the reaction can be undertaken *via* $^{11}B\{^1H\}$ NMR spectroscopy with consumption of one equivalent of the starting terminal borylene species, [(OC)$_5$Cr{BN(SiMe$_3$)(*t*-Bu)}] (**19**), observed at δ = 97 ppm and formation of the monoborylene-substituted cobalt methylcyclopentadienyl carbonyl complex, [{(η^5-C_5H_4Me)(OC)Co{BN(SiMe$_3$)(*t*-Bu)}] (**60**) ($^{11}B\{^1H\}$: δ = 81 ppm). The $^{11}B\{^1H\}$ NMR spectroscopic data for [{(η^5-C_5H_4Me)(OC)Co{BN(SiMe$_3$)(*t*-Bu)}] (**60**) is in agreement with the previously published cobalt *bis*(trimethylsilyl)aminoborylene complex [{(η^5-C_5H_4Me)(OC)Co{BN(SiMe$_3$)$_2$}] ($^{11}B\{^1H\}$: δ = 79 ppm).[181] This complex is unfortunately unstable and will slowly convert to the Co-B-Co bridging borylene ({μ-BN(SiMe$_3$)(*t*-Bu)}) species after isolation with loss of one borylene ligand and recombination of two individual [{(η^5-C_5H_4Me)(OC)Co{BN(SiMe$_3$)(*t*-Bu)}] (**60**) complexes to form the final, thermally stable, complex [{(η^5-C_5H_4Me)Co}$_2${μ-(CO)}$_2${μ-BN(SiMe$_3$)(*t*-Bu)}] (**61**) ($^{11}B\{^1H\}$: δ = 104 ppm). The $^{11}B\{^1H\}$ NMR spectroscopic data for the [{(η^5-C_5H_4Me)Co}$_2${μ-(CO)}$_2${μ-BN(SiMe$_3$)(*t*-Bu)}] (**61**) complex is also in agreement with the previously published dicobalt methylcyclopentadienyl dicarbonyl *bis*(trimethylsilyl)aminoborylene complex [{(η^5-C_5H_4Me)Co}$_2$(μ-CO)$_2${μ-BN(SiMe$_3$)$_2$}] ($^{11}B\{^1H\}$: δ = 104 ppm).[181] Formation of [{(η^5-C_5H_4Me)Co}$_2${μ-(CO)}$_2${μ-BN(SiMe$_3$)(*t*-Bu)}] (**61**) can also be monitored *via* ^1H NMR spectroscopy with observation of a resonance corresponding to the methylcyclopentadienyl (η^5-C_5H_4Me) protons (-CH_3) at δ = 1.937 ppm (δ = 1.92 ppm for [{(η^5-C_5H_4Me)Co}$_2$(μ-CO)$_2${μ-BN(SiMe$_3$)$_2$}]).[181] Workup of the complex can be achieved by removal of all volatiles *in vacuo* and sublimation of the [Cr(CO)$_6$] byproduct by heating at 60 °C under high vacuum (0.001 Torr). Purification of the red/black residue can subsequently be accomplished by extraction of the crude material with hexane and filtration of this extract over a small column of pacified

silica gel (SiO_2)[397] to yield the product as a dark red fraction. Storage of this solution in the glovebox freezer (–40 °C) for one week yielded [{(η^5-C_5H_4Me)Co}$_2$(μ-CO)$_2${μ-BN($SiMe_3$)(*t*-Bu)}] (**61**) as a dark red air and moisture sensitive crystalline solid in 65% yield. It should be noted that no crystals of the proposed terminal monoborylene species [{(η^5-C_5H_4Me)(OC)Co{BN($SiMe_3$)(*t*-Bu)}] (**60**) were ever grown from solution, only crystals of [{(η^5-C_5H_4Me)Co}$_2$(μ-CO)$_2${μ-BN($SiMe_3$)(*t*-Bu)}] (**61**) were able to be collected even though NMR data taken from these solutions indicated the presence of a proposed monoborylene species (the complex [{(η^5-C_5H_4Me)(OC)Co{BN($SiMe_3$)(*t*-Bu)}] (**60**) is probably an oil).[181]

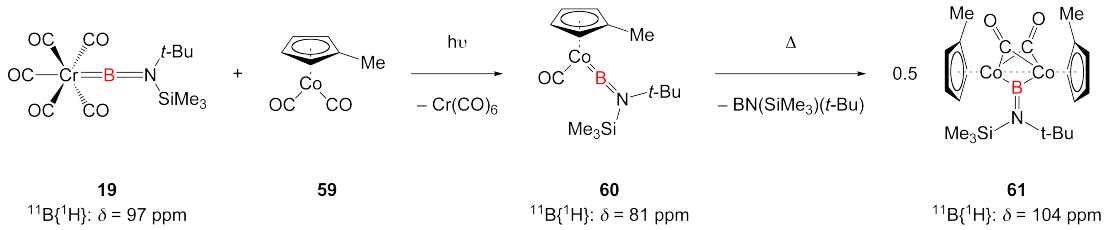

Figure 2-29. [{(η^5-C_5H_4Me)Co}$_2$(μ-CO)$_2${μ-BN($SiMe_3$)(*t*-Bu)}] (**61**) synthesis by borylene transfer reaction from [$(OC)_5$Cr{BN($SiMe_3$)(*t*-Bu)}] (**19**) to [(η^5-C_5H_4Me)Co$(CO)_2$] (**59**).

[{(η^5-C_5H_4Me)Co}$_2$(μ-CO)$_2${μ-BN($SiMe_3$)(*t*-Bu)}] (**61**) can be witnessed by ^{1}H, ^{11}B, ^{13}C, and ^{29}Si NMR spectroscopy. ^{1}H NMR spectra of the complex display two prominent resonances at 0.335 and 1.404 ppm corresponding to the trimethylsilyl and *tert*-butyl protons, respectively (9H for each resonance). Both of these values are slightly downfield-shifted from the reported values of the chromium pentacarbonyl terminal borylene [$(OC)_5$CrBN($SiMe_3$)(*t*-Bu)] (**19**) (0.159 and 1.148 ppm for the trimethylsilyl and *tert*-butyl protons respectively). The trimethylsilyl proton resonance at 0.335 ppm was assigned through 2D ^{1}H-^{13}C NMR (^{13}C{^{1}H}: δ = 5.90 ppm, $^1J_{C\text{-}Si}$ = 57 Hz) correlation spectroscopy (HSQC). This value for the trimethylsilyl NMR spectroscopic resonance is in agreement with published data for the similar *bis*(trimethylsilyl)aminoborylene complex [{(η^5-C_5H_4Me)Co}$_2$(μ-CO)$_2${μ-BN($SiMe_3$)$_2$}] (^{1}H: δ = 0.31 ppm, N-Si(C*H*$_3$)$_3$).[181] Unfortunately the ^{29}Si{^{1}H} NMR resonance (^{29}Si{^{1}H}: δ = –2.83 ppm) is too broad to verify this coupling constant. Analysis of [{(η^5-C_5H_4Me)Co}$_2$(μ-CO)$_2${μ-BN($SiMe_3$)(*t*-Bu)}] (**61**) by infrared spectroscopy shows multiple observable bands assignable to the $\tilde{\nu}$(C≡O) stretching modes at 1,762, 1,713, and 1,686 cm^{-1}.

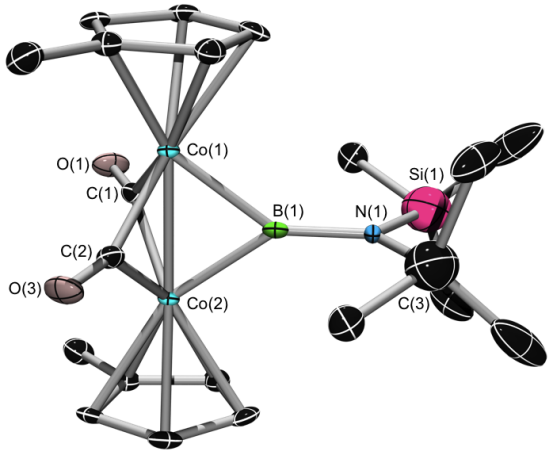

Figure 2-30. ORTEP-rendered structure of [{(η^5-C_5H_4Me)Co}$_2$(μ-CO)$_2${μ-BN($SiMe_3$)(*t*-Bu)}] (**61**). Thermal ellipsoids set at 50% probability. All hydrogen atoms have been omitted for clarity. Selected distances (Å) and angles (º): Co(1)–B(1) 1.959(9), Co(1)–C(1) 1.864(9), B(1)–N(1) 1.41(1), Co(1)–Co(2) 2.350(2), C(1)–O(1) 1.171(9), Co(1)–Cp' centroid (Cp = η^5-C_5H_4Me) 1.750, Co(1)–B(1)–Co(2) 73.71, B(1)–Co(1)–Cp' centroid (Cp' = η^5-C_5H_4Me) 126.3, Co(1)–Co(2)–Cp' centroid (Cp = η^5-C_5H_4Me) 176.1, ΣN_α 360.0 Si(1)–N(1)–B(1)–Co(1) 83.82.[*]

Crystals suitable for X-ray diffraction were grown from saturated solutions of [{(η^5-C_5H_4Me)Co}$_2$(μ-CO)$_2${μ-BN($SiMe_3$)(*t*-Bu)}] (**61**) in hexane.[†] An ORTEP diagram of the structure as well as some key bond distances for [{(η^5-C_5H_4Me)Co}$_2${μ-(CO)}$_2${μ-BN($SiMe_3$)(*t*-Bu)}] (**61**) are shown in Figure 2-30. The [{(η^5-C_5H_4Me)Co}$_2${μ-(CO)}$_2${μ-BN($SiMe_3$)(*t*-Bu)}] (**61**) species displays Co-B, B-N, Co-C, and C-O bond distances of 1.959(9), 1.41(1), 1.864(9), and 1.171(9) Å respectively with a Co-Cp' centroid (Cp' = η^5-C_5H_4Me) distance of 1.750 Å. The angle between the Co(1)-Co(2)-B and Co(1)-Co(2)-C(1) planes was found to be 117.08º and is identical to the other Co(1)-Co(2)-C(2) plane by symmetry definition. This data is comparable[‡] to those of [{(η^5-C_5H_4Me)Co}$_2${μ-(CO)}$_2${μ-BN($SiMe_3$)$_2$}], which displays Co-B, B-N, Co-C, and C-O bond distances of 1.963(2), 1.389(3), 1.867(2), and 1.170(2) Å respectively with a Co-Cp' centroid (Cp' = η^5-C_5H_4Me) distance of 1.745 Å.[181]

2.2.3.2 [{(η^5-C_5H_5)Ni}$_2$(μ-CO){μ-BN($SiMe_3$)(*t*-Bu)}] (62)

[{(η^5-C_5H_5)Ni}$_2$(μ-CO){μ-BN($SiMe_3$)(*t*-Bu)}] (**62**) was prepared by borylene transfer under photolytic conditions from the unsymmetrical terminal "first generation" chromium borylene complex, [(OC)$_5$Cr{BN($SiMe_3$)(*t*-Bu)}] (**19**), to the nickel

[*] It should be noted that the complex is symmetrical and was solved crystallographically as if the silicon Si(1) and the carbon C(3) atoms were electronically equivalent (hence the large ellipsoids). They are not and this is the reason that the structure shows all atoms as unique (no "prime" notation to distinguish between the two symmetrical parts).
[†] $C_{21}H_{32}BCo_2NO_2Si$, M = 487.25, monoclinic, space group = *C2/c*.
[‡] $C_{20}H_{32}BCo_2NO_2Si_2$, M = 503.32, monoclinic, space group = *C2/c*.

cyclopentadienyl monocarbonyl dimer ([{(η^5-C_5H_5)Ni}$_2${μ-(CO)$_2$}] (**53**)) with formal reciprocal transfer of a carbonyl ligand from [{(η^5-C_5H_5)Ni}$_2${μ-(CO)$_2$}] (**53**) back to [(OC)$_5$Cr{BN(SiMe$_3$)(*t*-Bu)}] (**19**) resulting in the formation of one equivalent of [Cr(CO)$_6$] (Figure 2-31). Monitoring of the reaction can be undertaken *via* ^{11}B{^{1}H} NMR spectroscopy with consumption of the starting terminal borylene species, [(OC)$_5$Cr{BN(SiMe$_3$)(*t*-Bu)}] (**19**), observed at δ = 97 ppm and the product complex [{(η^5-C_5H_5)Ni}$_2${μ-(CO)}{μ-BN(SiMe$_3$)(*t*-Bu)}] (**62**) observed at δ = 94 ppm. The ^{11}B{^{1}H} NMR spectroscopic data for the [{(η^5-C_5H_5)Ni}$_2${μ-(CO)}{μ-BN(SiMe$_3$)(*t*-Bu)}] (**62**) complex is in agreement with the previously published nickel cyclopentadienyl monocarbonyl bridging borylene dimeric complex [{(η^5-C_5H_5)Ni}$_2$(μ-CO){μ-BN(SiMe$_3$)$_2$}] (**54**) (^{11}B{^{1}H}: δ = 92 ppm).[181] During the course of the reaction, no terminal borylene species was ever observed besides the precursor [(OC)$_5$CrBN(SiMe$_3$)(*t*-Bu)] (**19**) either in solution or in the solid state, indicating that this particular reaction proceeds through transfer of the terminal borylene directly to the bridging position of the nickel dimer reagent [{(η^5-C_5H_5)Ni}$_2$(μ-CO)$_2$] (**53**). Formation of the product complex [{(η^5-C_5H_5)Ni}$_2$(μ-CO){μ-BN(SiMe$_3$)(*t*-Bu)}] (**62**) can also be subsequently monitored *via* ^{1}H NMR spectroscopy with observation of a resonance corresponding to the cyclopentadienyl (η^5-C_5H_5) protons at δ = 5.323 ppm (δ = 5.30 ppm for [{(η^5-C_5H_5)Ni}$_2$(μ-CO){μ-BN(SiMe$_3$)$_2$}] (**54**)).[181] Workup of the complex can be achieved by removal of all volatiles *in vacuo* and sublimation of the [Cr(CO)$_6$] byproduct by heating at 60 °C under high vacuum (0.001 Torr). Purification of the red/black residue can subsequently be accomplished by extraction of the crude material with hexane and filtration of this extract over a small column of pacified silica gel (SiO$_2$)[397] to yield the product as a dark red fraction. Storage of this solution in the glovebox freezer (–40 °C) for one week yielded [{(η^5-C_5H_5)Ni}$_2$(μ-CO){μ-BN(SiMe$_3$)(*t*-Bu)}] (**62**) as a red air and moisture sensitive crystalline solid in 74% yield. Differential thermal analysis of these red crystalline solids showed a melting point for [{(η^5-C_5H_5)Ni}$_2$(μ-CO){μ-BN(SiMe$_3$)(*t*-Bu)}] (**62**) at 114 °C with decomposition above 235 °C.

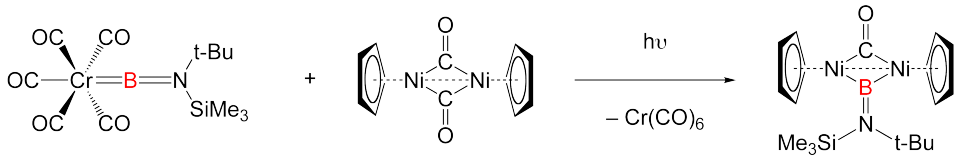

19
$^{11}B\{^{1}H\}$: δ = 97 ppm

53

62
$^{11}B\{^{1}H\}$: δ = 94 ppm

Figure 2-31. [{(η^5-C_5H_5)Ni}$_2$(μ-CO){μ-BN(SiMe$_3$)(*t*-Bu)}] (**62**) synthesis by a borylene transfer from [(OC)$_5$Cr{BN(SiMe$_3$)(*t*-Bu)}] (**19**) to [{(η^5-C_5H_5)Ni}$_2$(μ-CO)$_2$] (**53**).

[{(η^5-C_5H_5)Ni}$_2$(μ-CO){μ-BN(SiMe$_3$)(*t*-Bu)}] (**62**) was characterized by ^{1}H, ^{11}B, ^{13}C, and ^{29}Si NMR spectroscopy. ^{1}H NMR spectra of the complex display two prominent resonances at 0.236 and 1.179 ppm corresponding to the trimethylsilyl and *tert*-butyl protons respectively (9H for each resonance). Both of these values are slightly downfield shifted from the reported values of the chromium pentacarbonyl terminal unsymmetrical borylene [(OC)$_5$CrBN(SiMe$_3$)(*t*-Bu)] (**19**) (0.159 and 1.148 ppm for the trimethylsilyl and *tert*-butyl protons respectively). The trimethylsilyl proton resonance at 0.236 ppm was assigned through 2D ^{1}H-^{13}C NMR ($^{13}C\{^{1}H\}$: δ = 4.04 ppm, $^{1}J_{C\text{-}Si}$ = 57 Hz) correlation spectroscopy (HSQC) as well as the interpreted $^{2}J_{H\text{-}Si}$ coupling value of 6.6 Hz. This value for the trimethylsilyl NMR spectroscopic resonance is in agreement with published data for the similar *bis*(trimethylsilyl)aminoborylene complex [{(η^5-C_5H_5)Ni}$_2$(μ-CO){μ-BN(SiMe$_3$)$_2$}] (**54**) (^{1}H: δ = 0.17 ppm, N-Si(C*H*$_3$)$_3$).[181] Unfortunately the $^{29}Si\{^{1}H\}$ NMR resonance ($^{29}Si\{^{1}H\}$: δ = −2.81 ppm) is too broad to verify this coupling constant. Analysis of [{(η^5-C_5H_5)Ni}$_2$(μ-CO){μ-BN(SiMe$_3$)(*t*-Bu)}] (**62**) by infrared spectroscopy shows a band assignable to the $\tilde{\nu}$(C≡O) stretching mode at 1,817 cm^{-1}.

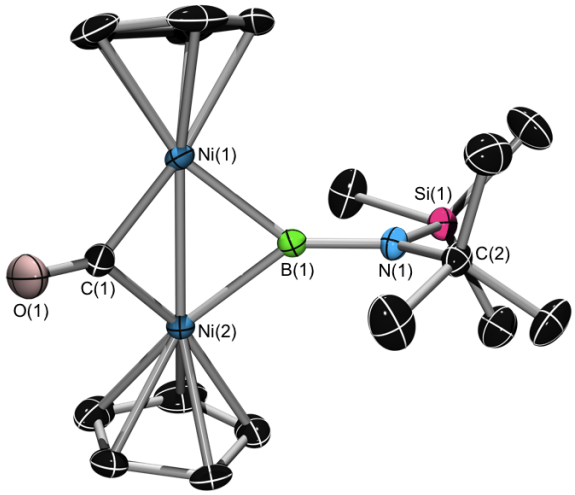

Figure 2-32. ORTEP-rendered structure of [{(η^5-C_5H_5)Ni}$_2$(μ-CO){μ-BN(SiMe$_3$)(*t*-Bu)}] (**62**). Thermal ellipsoids set at 50% probability. All hydrogen atoms have been omitted for clarity. Selected distances (Å) and angles (°): Ni(1)–B(1) 1.936(4), Ni(1)–C(1) 1.841(5), B(1)–N(1) 1.390(6), Ni(1)–Ni(2) 2.3710(7), C(1)–O(1) 1.168(6), Ni–Cp centroid (Cp = η^5-C_5H_5) 1.761 (avg.), Ni(1)–B(1)–Ni(2) 75.79, B(1)–Ni(1)–Cp centroid (Cp = η^5-C_5H_5) 131.97, Ni(1)–Ni(2)–Cp centroid (Cp = η^5-C_5H_5) 166.51, ΣN_α 360.0 Si(1)–N(1)–B(1)–Ni(1) 86.05.

Crystals suitable for X-ray diffraction were grown from saturated solutions of [{(η^5-C_5H_5)Ni}$_2$(μ-CO){μ-BN(SiMe$_3$)(*t*-Bu)}] (**62**) in hexane.* An ORTEP diagram of the structure as well as some key bond distances for [{(η^5-C_5H_5)Ni}$_2$(μ-CO){μ-BN(SiMe$_3$)(*t*-Bu)}] (**62**) are shown in Figure 2-32. The [{(η^5-C_5H_5)Ni}$_2$(μ-CO){μ-BN(SiMe$_3$)(*t*-Bu)}] (**62**) species displays Ni-B, Ni-C, B-N, and C-O bond distances of 1.931 (avg.), 1.840 (avg.), 1.390(6), and 1.168(6) Å respectively with a Ni-Cp centroid (Cp = η^5-C_5H_5) distances of 1.761 Å (avg.). The angle between the Ni(1)-Ni(2)-B(1) and the Ni(1)-Ni(2)-C(1) planes was found to be 138.34°. This data is comparable† to those of [{(η^5-C_5H_5)Ni}$_2${μ-(CO)}{μ-BN(SiMe$_3$)$_2$}] (**54**), which displays Ni-B, Ni-C, B-N, and C-O bond distances of 1.929 (avg.), 1.846 (avg.), 1.384(2), and 1.173(2) Å respectively with a Ni-Cp centroid (Cp = η^5-C_5H_5) distances of 1.758 Å (avg.).[181]

2.2.3.3 [(Pt{μ-BN(SiMe$_3$)$_2$}$_2$){Cr(μ-CO)(CO)$_4$}{Cr(μ-CO)(CO)$_3$(PEt$_3$)}] (64)

In a reaction that will be discussed in detail later,‡ a *trans*-platinum *bis*-σ-alkynyl complex, *trans*-[Pt(C≡C-9-$C_{14}H_9$)$_2$(PEt$_3$)$_2$] (**63**), was prepared and irradiated in the presence of two equivalents of the terminal chromium

* $C_{18}H_{28}BNNi_2OSi$, M = 430.70, monoclinic, space group = $C2/c$.
† $C_{17}H_{28}BNNi_2OSi_2$, M = 446.78, monoclinic, space group = $P2_1/c$.
‡ See Section 3.1.2.4 for the synthetic details regarding the preparation of *trans*-[Pt(PEt$_3$)$_2$(C≡C-9-$C_{14}H_9$)$_2$] (**63**).

bis(trimethylsilyl)aminoborylene complex, $[(OC)_5Cr\{BN(SiMe_3)_2\}]$ (**13**). The expected product for this reaction was the *trans*-platinum *bis*-σ-borirenyl complex *trans*-$[Pt\{(\mu\text{-}\{B{=}N(SiMe_3)_2\}C{=}C)\text{-}9\text{-}C_{14}H_9\}_2(PEt_3)_2]$, however, workup of the reaction mixture failed to yield this product and unexpectedly provided a Cr-Pt-Cr bowtie complex containing two bridging borylene and two bridging carbonyl ligands, similar to other recently reported species by our group (Figure 2-33).[398-405] NMR spectroscopic data (^1H, ^{11}B, ^{13}C, and ^{31}P) for this reaction mixture indicate that the reaction proceeds by photolytic reductive elimination of the alkynyl substituents in a fashion similar to recent work published by Jones and coworkers[406] subsequently forming a Pt(0) complex in solution. Workup of the complex was achieved by removal of all volatiles *in vacuo* and extraction of the dark yellow residue with hexane. Filtration of this extract over pacified silica gel (SiO_2)[397] yielded a yellow fraction which displayed two $^{11}B\{^1H\}$ NMR resonances at 92 ppm and 47 ppm, however it is unclear if these NMR resonances correlate to the isolated species. Storage of this solution in the glovebox freezer (–40 °C) for one week yielded $[(Pt\{\mu\text{-}BN(SiMe_3)_2\}_2)\{Cr(\mu\text{-}CO)(CO)_4\}\{Cr(\mu\text{-}CO)(CO)_3(PEt_3)\}]$ (**64**) as a yellow air and moisture sensitive crystalline solid in very poor (isolated crystals) yield (<10% yield). The quality of the crystal structure is not sufficient for publication (see B(2) ellipsoid); however, the connectivity and bond distance comparison with a similar published structure is shown ($[(OC)_4Cr(\mu\text{-}CO)\{\mu\text{-}BN(SiMe_3)_2\}Pd(PCy_3)]$).[398,399]

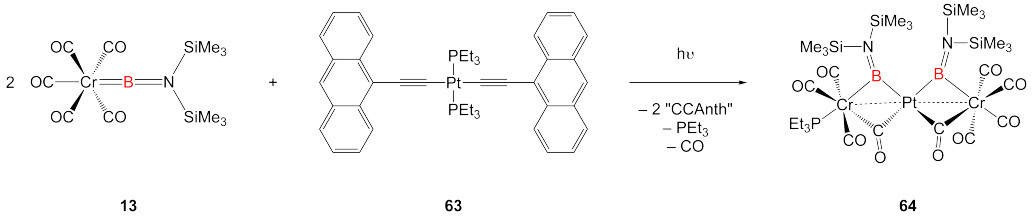

Figure 2-33. $[(Pt\{\mu\text{-}BN(SiMe_3)_2\}_2)\{Cr(\mu\text{-}CO)(CO)_4\}\{Cr(\mu\text{-}CO)(CO)_3(PEt_3)\}]$ (**64**) synthesis *via* photolytic rearrangement of the platinum *bis*-σ-alkynyl species *trans*-$[Pt(C{\equiv}C\text{-}9\text{-}C_{14}H_9)_2(PEt_3)_2]$ (**63**) in the presence of two equivalents of $[(OC)_5Cr\{BN(SiMe_3)_2\}]$ (**13**).

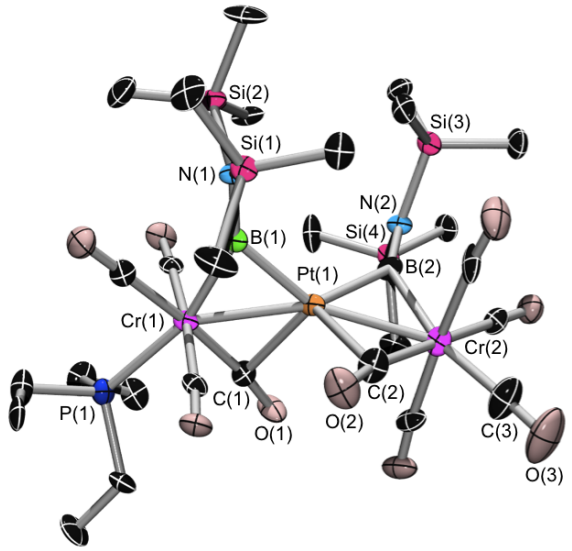

Figure 2-34. ORTEP-rendered structure of [(Pt{μ-BN(SiMe$_3$)$_2$}$_2$){Cr(μ-CO)(CO)$_4$}{Cr(μ-CO)(CO)$_3$(PEt$_3$)}] (**64**). Thermal ellipsoids set at 50% probability. All hydrogen atoms have been omitted for clarity.

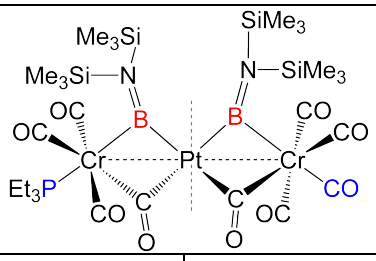

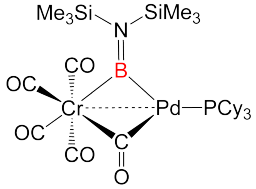

Cr(1)–Pt(1)	2.636(2)	Cr(2)–Pt(1)	2.689(3)	Cr(1)–Pd(1)	2.623(1)
Cr(1)–B(1)	2.05(1)	Cr(2)–B(2)	2.16(2)	Cr(1)–B(1)	2.0842(18)
B(1)–Pt(1)	2.09(2)	B(2)–Pt(1)	2.04(1)	B(1)–Pd(1)	2.0425(18)
Cr(1)–C(1)	1.90(1)	Cr(2)–C(2)	1.89(2)	Cr(1)–C(1)	1.936(2)
C(1)–Pt(1)	2.39(1)	C(2)–Pt(1)	2.32(2)	C(1)–Pd(1)	2.165(2)
B(1)–N(1)	1.38(2)	B(2)–N(2)	1.38(2)	B(1)–N(1)	1.377(2)
C(1)–O(1)	1.16(2)	C(2)–O(2)	1.17(2)	C(1)–O(1)	1.155(2)
Cr(1)–P(1)	2.359(3)	Cr(2)–C(3)	1.87(2)	Cr(1)–C(3)	1.868(2)
		C(3)–O(3)	1.13(3)	C(3)–O(3)	1.138(2)
				Pd(1)–P(1)	2.3470(10)
N(1)–B(1)–Cr(1)	149.35	N(2)–B(2)–Cr(2)	144.32	N(1)–B(1)–Cr(1)	152.33
N(1)–B(1)–Pt(1)	131.35	N(2)–B(2)–Pt(1)	135.93	N(1)–B(1)–Pd(1)	128.74
O(1)–C(1)–Cr(1)	171.77	O(2)–C(2)–Cr(2)	167.07	O(1)–C(1)–Cr(1)	165.49
O(1)–C(1)–Pt(1)	113.15	O(2)–C(2)–Pt(1)	114.37	O(1)–C(1)–Pd(1)	115.2

Table 2-2. Selected bond distances (Å) and angles (°) for the two borylene bridging modes of [(Pt{μ-BN(SiMe$_3$)$_2$}$_2$){Cr(μ-CO)(CO)$_4$}{Cr(μ-CO)(CO)$_3$(PEt$_3$)}] (**64**) (left) compared to previously published data for [(OC)$_4$Cr(μ-CO){μ-BN(SiMe$_3$)$_2$}Pd(PCy$_3$)] (right).[398,399]

Crystals suitable for X-ray diffraction were grown from saturated solutions of [(Pt{μ-BN(SiMe$_3$)$_2$}$_2$){Cr(μ-CO)(CO)$_4$}{Cr(μ-CO)(CO)$_3$(PEt$_3$)}] (**64**) in hexane. An ORTEP

diagram of the structure as well as some key bond distances for [(Pt{μ-BN(SiMe$_3$)$_2$}$_2$){Cr(μ-CO)(CO)$_4$}{Cr(μ-CO)(CO)$_3$(PEt$_3$)}] (**64**) are shown in Figure 2-34 and Table 2-2 with bond distances from the previously published complex [(OC)$_4$Cr(μ-CO){μ-BN(SiMe$_3$)$_2$}Pd(PCy$_3$)] shown for comparison.[398,399] Although it is difficult to directly compare two borylene ligands bridging between 3d-5d transition metals to a borylene ligand bridging between a 3d-4d transition metal, the Cr-M, Cr-B, and M-B bond distances for all three of these bridging borylene ligands are observed to be similar. This is probably due to the comparable covalent radii of the metals. The largest discrepancy between these three bridging borylene interactions seems to be the M-C bond distances, which indicate a stronger affinity for the carbonyl ligand with the palladium center compared to the platinum species.

2.3 M=B-B=M Synthesis Attempts

Utilizing the same reaction conditions for the successful synthesis of the Group 6 pentacarbonyl *bis*(trimethylsilyl)aminoborylene species $[(OC)_5M\{BN(SiMe_3)_2\}]$ (M = Cr (**13**), Mo (**14**), and W (**15**)) (see Figure 2-3) from Group 6 transition metal dianions ($Na_2[M(CO)_5]$ (M = Cr (**11**), Mo (**1**), and W (**12**)), reactions were performed with 0.5 equivalents of B_2Br_4 (**65**) at −100 °C in attempts to prepare a bridging diborylene transition metal (M=B-B=M) complex of the type $[(OC)_5M\{=B-B=\}M(CO)_5]$ (M = Cr (**66**) and W (**67**)). These test reactions were conducted using the standard preparatory scales (~1.2 g $[(OC)_5M(NMe_3)]$ (M = Cr (**8**) and W (**10**)) used in the generation of the Group 6 pentacarbonyl *bis*(trimethylsilyl)aminoborylene species $[(OC)_5M\{BN(SiMe_3)_2\}]$ (M = Cr (**13**), and W (**15**)) (Figure 2-35, top). Workup of the complexes was attempted by solvent removal *in vacuo* and product extraction with benzene; however, workup of the reactions did not indicate any product formation and typically witnessed complete decomposition of all identifiable species in solution. NMR spectroscopic monitoring of the resultant reaction solutions or extractions also failed to confirm the successful synthesis of either mono- or diborylene species.

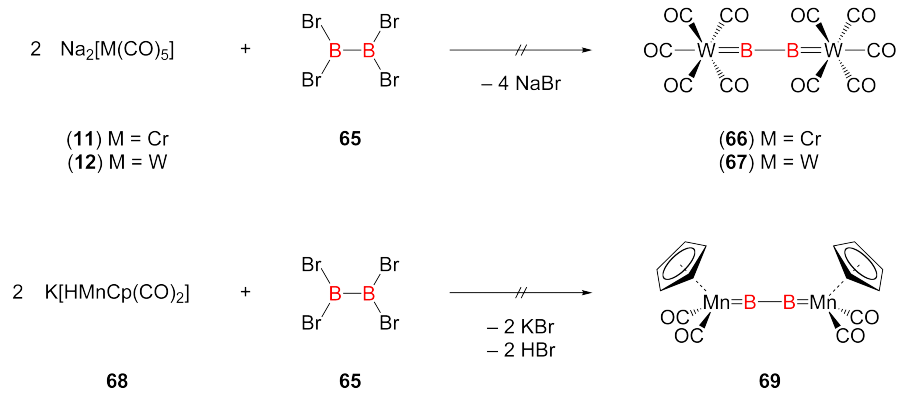

Figure 2-35. Attempted synthesis of M=B-B=M type diborylenes (M = Cr (**66**), W (**67**), and Mn (**69**)) from salt elimination reactions of the transition metal mono- and dianions $K[(\eta^5\text{-}C_5H_5)Mn(CO)_2H]$ (**68**), $Na_2[Cr(CO)_5]$ (**11**), and $Na_2[W(CO)_5]$ (**12**) with tetrabromodiborane (**65**).

A similar reaction was also attempted using the potassium metallate complex $K[(\eta^5\text{-}C_5H_5)Mn(CO)_2H]$ (**68**). This species is commonly used as a reagent in the synthesis of the manganese borylene species $[\{(\eta^5\text{-}C_5H_5)Mn(CO)_2\}_2(\mu\text{-B}t\text{-Bu})]$.[171,172] This reagent was tested to see if a combination of salt-elimination and HBr elimination could yield a M=B-B=M species of the form $[\{(\eta^5\text{-}C_5H_5)(OC)_2Mn\}(=B-B=)\{Mn(CO)_2(\eta^5\text{-}C_5H_5)\}]$ (**69**). This reagent was chosen because it is slightly more

sterically bulky than the group 6 transition metal pentacarbonyl dianions ($Na_2[M(CO)_5]$ (M = Cr (**11**) and W (**12**)) and would also incorporate two terminal Cp rings for added stability of the target borylene complex (Figure 2-35, bottom), however, the reaction unfortunately also yielded no identifiable product by NMR spectroscopic monitoring of the reaction mixtures and extractions.

2.4 Reactions of a Base Stabilized Diborene with Grubb's Catalyst

Finally, a reaction was conceived using an *N*-heterocyclic carbene (NHC-stabilized (1,3-dimethylimidazol-2-ylidene, IMe) diborene species (**70**)[407,408] with Grubb's catalyst, in an attempt to directly generate a transition metal borylene species by Ru=C/B=B metathesis. This reaction was attempted with treatment of $[(Cy_3P)_2Cl_2Ru\{=CHCH_3\}]$ (**71**) (a derivative of Grubb's 1st Generation catalyst) with the IMe-stabilized dithiophenyl diborene (**70**). Unfortunately this reaction typically led to complete destruction of the Ru complex after multiple attempts and no identifiable species besides free tricyclohexylphosphine (PCy_3) in the NMR analysis of the reaction mixture.

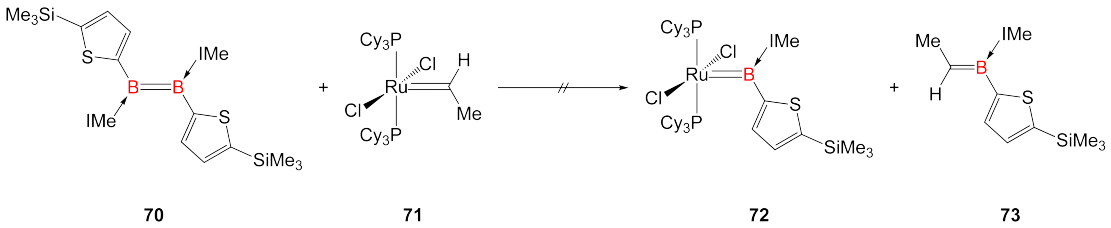

70 **71** **72** **73**

Figure 2-36. Attempted synthesis of transition metal terminal borylene complex **72** from 1:1 reaction of Grubb's 1st Generation catalyst **71** with the NHC (IMe)-stabilized diborene **70**.

2.5 Project Borylene Summary

To summarize the work reported in this chapter, a new borylene ligand ({BN(SiMe$_3$)(*t*-Bu)}) has been successfully synthesized ("first generation borylene") bound in a terminal manner to the base metal scaffolds of the kind [M(CO)$_5$] (M = Cr, Mo, and W). This new unsymmetrical borylene ligand is closely akin to the *bis*(trimethylsilyl)aminoborylene ligand and displays similar structural characteristics and reactivity. The unsymmetrical borylene ligand {BN((SiMe$_3$)(*t*-Bu)} does display some individual characteristics of note and undergoes photolytic transfer to transition metal scaffolds in a more rapid manner, and appears to be a more reactive borylene ligand, than the previously published symmetrical *bis*(trimethylsilyl)aminoborylene ligand based on NMR and IR spectroscopy.

Photolytic transfer attempts with this new borylene ligand were conducted with other metal scaffolds, resulting in either complete or partial transfer and the formation of either terminal or bridging borylene complexes. The unsymmetrical ligand's coordination to early transition metals (up to Group 6) indicates a preference for a terminal coordination motif while bound to these highly Lewis acidic species. The ligand also appears to bind in more energetically stable bridging coordination modes when bound to transition metals with high Lewis basicity and has been witnessed to transfer to transition metal scaffolds in a terminal manner and subsequently rearrange in order to achieve a more energetically stable final state.

Analysis of the accumulated data for all of the terminal borylene species discussed in this section, particularly bond distances, infrared spectroscopy, and ^{11}B{^{1}H} NMR spectroscopic data, has been performed, and a trend in the data has been established. Section 2.6 has been included below to elucidate these trends for the unsymmetrical borylene {BN(SiMe$_3$)(*t*-Bu)} ligand when bound to different families of transition metals, leading to the following conclusions:

[1] NMR spectroscopic data for the ^{11}B{^{1}H} boron and ^{13}C{^{1}H} carbonyl environments of the first generation borylene species ([(OC)$_5$M{BN(SiMe$_3$)(*t*-Bu)}] (M = Cr (**19**), Mo (**20**), and W (**21**))) all show progressive up-field shifting as the Group 6 metal becomes heavier (Cr (**19**) to Mo (**20**) to W (**21**)), indicating maximum deshielding for these nuclei in the [(OC)$_5$Cr{BN(SiMe$_3$)(*t*-Bu)}] (**19**) complex.

[2] The boron-metal-*trans*-carbon (B-M-C$_{trans}$) axes of the first generation borylene complexes [(OC)$_5$M{BN(SiMe$_3$)(*t*-Bu)}] (M = Mo (**20**), and W (**21**)) are not

completely linear in the solid state, preventing direct (solid) IR spectroscopic comparison. The chromium analog [$(OC)_5Cr\{BN(SiMe_3)(t\text{-}Bu)\}$] (**19**), however, is essentially linear and displays the expected three carbonyl IR stretching frequencies, all at higher energy than those of the chromium *bis*(trimethylsilyl)aminoborylene complex [$(OC)_5Cr\{BN(SiMe_3)_2\}$] (**13**), indicating that the ($\{BN(SiMe_3)(t\text{-}Bu)\}$) ligand is a stronger σ-donor to the chromium metal center.

[3] In transfer reactions, the $\{BN(SiMe_3)(t\text{-}Bu)\}$ fragment appears to be more stable as a terminal ligand when bound to more Lewis acidic first row transition metals and appears to prefer coordination in a bridging motif when coordinated to more Lewis basic first row transition metals.

Finally, several other reactions were attempted not only to synthesize new borylene ligands, but also to elucidate alternative routes to the synthesis of transition metal borylene complexes unto this point not attempted (to our knowledge). These studies, while unsuccessful, have been included in this thesis in an effort to seed these ideas and possible mechanisms for future success in these projects. More importantly, this data has been included for the more economical usage of time and resources for any researchers who may continue these projects in the future.

2.6 Project Borylene Appendices

	$[(OC)_5Cr\{BN(SiMe_3)(t\text{-}Bu)\}]$ (**19**)	$[(OC)_5Mo\{BN(SiMe_3)(t\text{-}Bu)\}]$ (**20**)	$[(OC)_5W\{BN(SiMe_3)(t\text{-}Bu)\}]$ (**21**)
X-ray Structural Data (100 K) [Å]			
M–B	1.980(2)	2.145(3)	2.154(4)
M–C_{ax}	1.908(2)	2.078(2)	2.061(3)
M–C_{eq} (avg.)	1.893	2.056	2.048
B–N	1.359(3)	1.363(3)	1.350(5)
C–O_{ax}	1.137(3)	1.141(3)	1.142(4)
^{1}H NMR (500.13 MHz, C_6D_6, 297 K) [ppm]			
s, 9H, C-(CH_3)$_3$	1.148 (s)	1.137 (s)	1.143 (s)
s, 9H, Si-(CH_3)$_3$	0.159 (s, $^2J_{H\text{-}Si}$ = 6.7 Hz)	0.141 (s, $^2J_{H\text{-}Si}$ = 6.6 Hz)	0.152 (s, $^2J_{H\text{-}Si}$ = 6.8 Hz)
^{13}C{^{1}H} NMR (125.77 MHz, C_6D_6, 297 K) [ppm]			
***trans*-*C*O to B**	218.44 (s)	207.50 (s)	197.68 (s, $^1J_{C\text{-}W}$ = 121 Hz)
***cis*-*C*O to B**	217.93 (s)	206.86 (s)	191.16 (s, $^1J_{C\text{-}W}$ = 126 Hz)
***C*-(CH_3)$_3$**	58.43 (s)	58.29 (s)	57.96 (s)
C-(*C*H$_3$)$_3$	33.55 (s)	33.93 (s)	33.96 (s)
Si-(*C*H$_3$)$_3$	3.27 (s) (s, $^1J_{C\text{-}Si}$ = 58 Hz)	3.51 (s) (s, $^1J_{C\text{-}Si}$ = 58 Hz)	3.50 (s) (s, $^1J_{C\text{-}Si}$ = 58 Hz)
^{13}C{^{1}H}-DEPT135 NMR (125.77 MHz, C_6D_6, 297 K) [ppm]			
C-(*C*H$_3$)$_3$	33.55 (s)	33.93 (s)	33.96 (s)
Si-(*C*H$_3$)$_3$	3.27 (s)	3.51 (s)	3.50 (s)
^{11}B{^{1}H} NMR (160.47 MHz, C_6D_6, BF_3•OC_4H_{10}, 297 K) [ppm]			
{*B*N(SiMe$_3$)(*t*-Bu)}	97.03 (br s)	95.74 (br s)	91.68 (br s)
^{29}Si{^{1}H} NMR (79.49 MHz, C_6D_6, $C_4H_{12}Si$, 297 K) [ppm]			
N-*Si*-(CH_3)$_3$	3.42 (s)	3.35 (s)	2.49 (s)
Solid State IR Spectroscopy [cm^{-1}]			
$\tilde{\nu}$(stretch)	2,058	2,065	2,065
$\tilde{\nu}$(stretch)	1,969	–	–
$\tilde{\nu}$(stretch)	1,900	1,896	1,898

Table 2-3. Comparison of spectroscopic data (X-ray, NMR, and IR) for "first generation" terminal borylenes of the type $[(OC)_5M\{BN(SiMe_3)(t\text{-}Bu)\}]$ (M = Cr (**19**), Mo (**20**), and W(**21**)).

	[(η^5-C_5H_5)(OC)$_3$V{BN(SiMe$_3$)(*t*-Bu)}] (**55**)	[(η^5-C_5Me_5)Ir{BN(SiMe$_3$)(*t*-Bu)}$_2$] (**58**)
X-ray Structural Data (100 K) [Å]		
M–B	1.968(1)	1.869 (avg.)
M–C$_{proximal}$	1.899 (avg.)	–
M–C$_{distal}$	1.940(1)	–
B–N	1.373(2)	1.388 (avg.)
C–O$_{proximal}$	1.163 (avg.)	–
C–O$_{distal}$	1.147(2)	–
M–Cp$_{centroid}$	1.925	1.935
^{1}H NMR (500.13 MHz, C_6D_6, 297 K) [ppm]		
s, 9H, C-(C*H*$_3$)$_3$	1.373 (s)	1.452 (s)
s, 9H, Si-(C*H*$_3$)$_3$	0.264 (s, $^2J_{H\text{-}Si}$ = 6.7 Hz)	0.442 (s, $^2J_{H\text{-}Si}$ = 6.7 Hz)
^{13}C{^{1}H} NMR (125.77 MHz, C_6D_6, 297 K) [ppm]		
***C*-(CH$_3$)$_3$**	57.83 (s)	52.03 (s)
C-(*C*H$_3$)$_3$	33.12 (s)	34.00 (s)
Si-(*C*H$_3$)$_3$	2.84 (s, $^1J_{C\text{-}Si}$ = 58 Hz)	4.47 (s, $^1J_{C\text{-}Si}$ = 57 Hz)
^{13}C{^{1}H}-DEPT135 NMR (125.77 MHz, C_6D_6, 297 K) [ppm]		
C-(*C*H$_3$)$_3$	33.12 (s)	34.00 (s)
Si-(*C*H$_3$)$_3$	2.84 (s)	4.47 (s)
^{11}B{^{1}H} NMR (160.47 MHz, C_6D_6, BF_3•OC_4H_{10}, 297 K) [ppm]		
{*B*N(SiMe$_3$)(*t*-Bu)}	100.32 (br s)	70.78 (br s)
^{29}Si{^{1}H} NMR (79.49 MHz, C_6D_6, $C_4H_{12}Si$, 297 K) [ppm]		
N-*Si*-(CH$_3$)$_3$	3.55 (s)	–1.22 (s)

Table 2-4. Comparison of spectroscopic data (X-ray and NMR) for "second generation" terminal borylenes [(η^5-C_5H_5)(OC)$_3$V{BN(SiMe$_3$)(*t*-Bu)}] (**55**) and [(η^5-C_5Me_5)Ir{BN(SiMe$_3$)(*t*-Bu)}$_2$] (**58**).

	[{(η^5-C_5H_4Me)Co}$_2$(μ-CO)$_2$ {μ-BN($SiMe_3$)(*t*-Bu)}] (**61**)	[{(η^5-C_5H_5)Ni}$_2$(μ-CO) {μ-BN($SiMe_3$)(*t*-Bu)}] (**62**)
X-ray Structural Data (100 K) [Å]		
M–B	1.959(9)	1.936(4)
M–C$_{bridging}$	1.864 (avg.)	1.841(5)
M–M	2.350(2)	2.3710(7)
B–N	1.41(1)	1.390(6)
C–O$_{bridging}$	1.171 (avg.)	1.168(6)
M–Cp$_{centroid}$	1.75	1.761
^{1}H NMR (500.13 MHz, C_6D_6, 297 K) [ppm]		
C-(C*H*$_3$)$_3$	1.404 (s)	1.179 (s)
Si-(C*H*$_3$)$_3$	0.335 (s)	0.236 (s, $^2J_{H\text{-}Si}$ = 6.6 Hz)
^{13}C{^{1}H} NMR (125.77 MHz, C_6D_6, 297 K) [ppm]		
***C*-(CH$_3$)$_3$**	56.83 (s)	56.91 (s)
C-(*C*H$_3$)$_3$	33.62 (s)	33.21 (s)
Si-(*C*H$_3$)$_3$	5.90 (s, $^1J_{C\text{-}Si}$ = 57 Hz)	4.04 (s, $^1J_{C\text{-}Si}$ = 57 Hz)
^{13}C{^{1}H}-DEPT135 NMR (125.77 MHz, C_6D_6, 297 K) [ppm]		
C-(*C*H$_3$)$_3$	33.62 (s)	33.21 (s)
Si-(*C*H$_3$)$_3$	5.90 (s)	4.04 (s)
^{11}B{^{1}H} NMR (160.47 MHz, C_6D_6, BF_3•OC_4H_{10}, 297 K) [ppm]		
{*B*N(SiMe$_3$)(*t*-Bu)}	103.63 (br s)	94.07 (br s)
^{29}Si{^{1}H} NMR (79.49 MHz, C_6D_6, $C_4H_{12}Si$, 297 K) [ppm]		
N-*Si*-(CH$_3$)$_3$	–2.83 (s)	–2.81 (s)
Solid State IR Spectroscopy [cm^{-1}]		
$\tilde{\nu}$(stretch)	1,762	2,002
$\tilde{\nu}$(stretch)	1,713	1,817
$\tilde{\nu}$(stretch)	1,686	–

Table 2-5. Comparison of spectroscopic data (X-ray and NMR) for "second generation" bridging borylenes [{(η^5-C_5H_4Me)Co}$_2$(μ-(CO)$_2${μ-BN($SiMe_3$)(*t*-Bu)}] (**61**) and [{(η^5-C_5H_5)Ni}$_2$(μ-CO){μ-BN($SiMe_3$)(*t*-Bu)}] (**62**).

Chapter 3 – Project Borirene

3.1 Borirene Conjugation

As stated in the introduction,* heterocyclic mono-boron containing aromatic and antiaromatic systems are of active interest to materials chemists for their potential to be integrated into electronically conjugated materials.[187-192] Initially, the goal of this research into borirene systems was to explore methods of chaining borirene heteroaromatic systems together in an effort to force conjugation between usually independent aromatic borirene units. Previous work by our group in synthesizing borirene systems either: (A) directly bound to one another as in the case of [{μ-$BN(SiMe_3)_2$(MeO-4-C_6H_4-C=C-)}$_2$] (**75**),[173-175] or (B) interspaced with π-conjugated linking intermediates ([1,4-*bis*-{μ-$BN(SiMe_3)(Me_3SiC{=}C)$}C_6H_4] (**77**)),[175] showed little proof of exocyclic conjugation between either the borirene-borirene or borirene-linker-borirene systems. Structural data taken from single crystal X-ray diffraction studies (Figure 3-1) pertaining to these borirene-borirene or borirene-linker-borirene systems indicated non-coplanarity between the borirene three membered ring systems and the exocyclic substituents without exception.[175]

* See Section 1.3 for an introduction to boron-containing heterocyclic aromatic and antiaromatic chemistry.

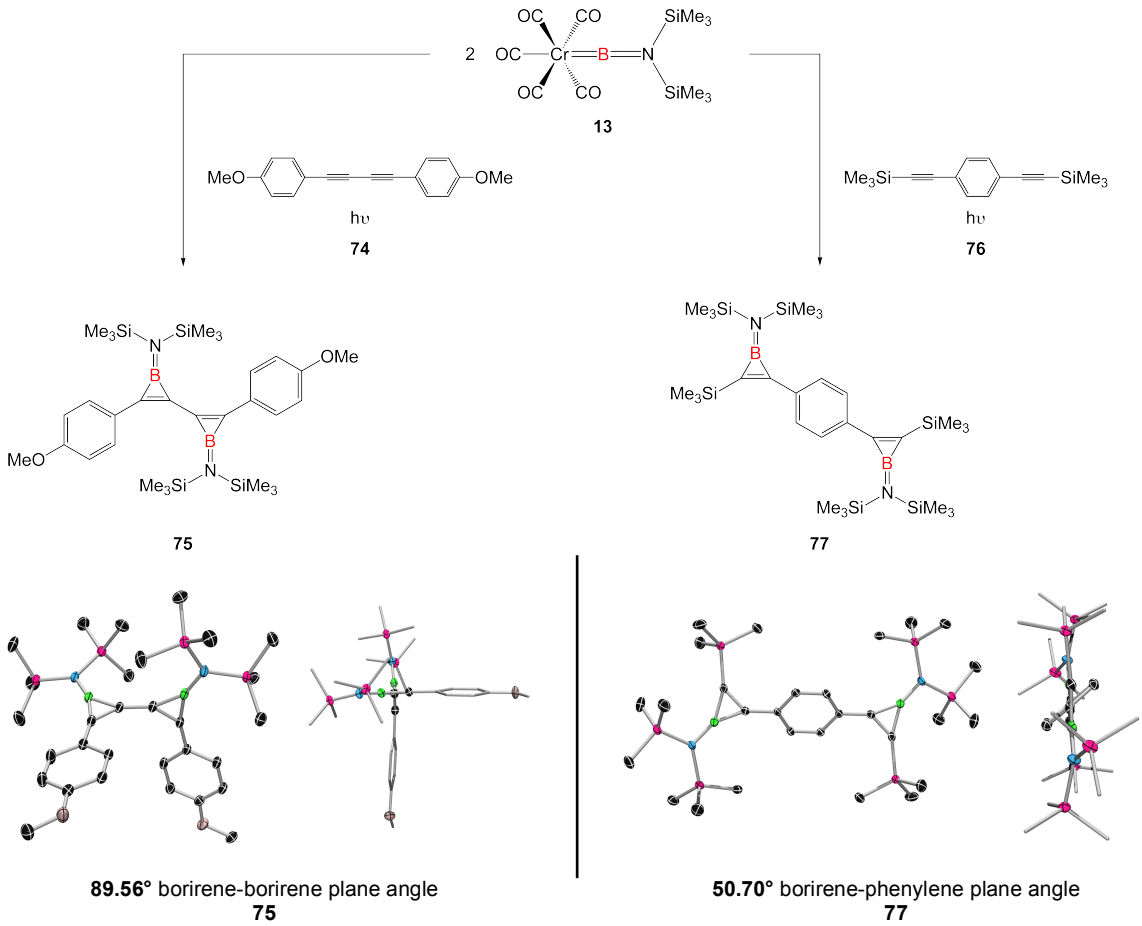

Figure 3-1. Synthesis of two different diborirene compounds by photolytic borylene transfer from two equivalents of $[(OC)_5Cr\{BN(SiMe_3)_2\}]$ (**13**) onto the respective diynes (**74**) and (**76**) (top). Single-crystal X-ray diffraction structures for the two different orientations of diborirene systems: directly linked (**75**), or interspaced with π-conjugated linking intermediates (**77**) (bottom).[175]

By forcing conjugation between linked borirene systems, it was hypothesized that a similar bathochromic shift (or red-shift) in the UV-vis absorption spectrum would be observed in a similar manner to that reported by Shirota and coworkers in their study of conjugated thienyl bridging substituents* with three-coordinate boron end-caps.[219-221] This data corresponds to a decrease in the HOMO-LUMO gap of the compounds as higher degrees of electronic delocalization are implied when in oligomeric and polymeric forms. Recently Scheschkewitz and coworkers[409-411] have also used π-conjugated linkers (phenylene) to induce a variance in communication between silicon-silicon double bond units (disilenes) and to manifest their solid-state coplanarity or non-coplanarity depending upon the positions of the aromatic phenylene ring that are substituted (*para*- (**80**) *vs. meta*- (**79**)) by the disilene moieties (Figure 3-2).[409-411] The tunability of the HOMO-LUMO gaps in these

* See Section 1.2.1, Figure 1-29 for more details on these π-conjugated systems.

molecules was also demonstrated by examination of the UV-vis spectra of the *para*- (**80**) *vs*. *meta*- (**79**) ring positions occupied by the disilenes to assess differing degrees of π-communication between the systems when compared to the mono-substituted phenylene disilene (**78**). Work published by our group has also shown coplanarity between two heterocyclic moieties across diborole[412,413] and diborene[407,408] linkers. Structural and spectroscopic data from these systems has been used as an indicator for heterocyclic communication with the central π-conjugated systems of these thiophene-augmented diborene and diborole systems.[407,408,412,413]

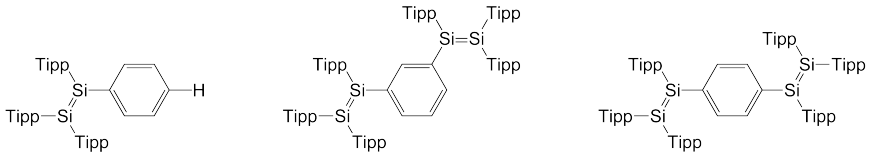

Figure 3-2. Functionalized silene (**78**) and disilene (*meta*- (**79**) and *para*- (**80**)) compounds prepared by Scheschkewitz and coworkers displaying prominent bathochromic shifting (red-shifting) of the UV-vis absorption maxima dependent upon the specific ring positions occupied by the disilene moieties (Tipp = 2,4,6-iPr$_3$C$_6$H$_2$).[409-411]

Organometallic linkers have also been reported to aid in conjugation between independent delocalized units* in both polymeric[251,252,414-416] and monomeric[235,417,418] systems, and can increase communication between these systems when incorporated in a direct A-B sequential order. Utilization of this A-B copolymer arrangement also allows for further tuning of the photophysical profile of the overall polymer as well as to increase solvent tolerance.[251,252,414-416] Reports by the groups of Low and Wang have recently shown application for a platinum intermediate in manifesting coplanarity between normally independent heterocyclic and aromatic chromophores in the solid state.[417,418] Figure 3-3 shows two examples of chromophores featuring nitrogen- (**81**) and boron-containing (**82**) chromophoric moieties that were shown to display coplanarity in the solid state *vs*. non-coplanar arrangements when free of a *trans*-platinum *bis*(alkynyl) intermediary.[417,418]

* See Section 1.2 for an introduction to monomeric and polymeric three-coordinate boron chemistry.

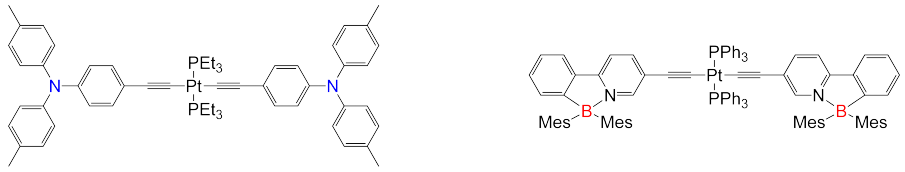

Figure 3-3. Use of a *trans*-platinum *bis*(alkynyl) intermediary to force coplanar arrangement in the solid state of chromophoric systems containing nitrogen (**81**) and boron (**82**) substituents that have traditionally been difficult to conjugate exocyclically.[417,418]

3.1.1 Previous Work

As previously covered in the introduction,* the synthesis of borirenes (heteroaromatic three-membered *cyclo*-BC_2R_3 rings) has been shown[294] to be possible *via* photolytic rearrangement of a alkynyldiarylborane (dimesityl(mesitylethynyl)borane (**83**)) to form trimesitylborirene (**84**) (Figure 3-4, top). This route has also been shown to be feasible for preparatory scale synthesis of these triarylborirene species;[294] however, the route is severely limited by the scope and difficulty in preparing these alkynyl boranes, and is not known to be a valid route for the synthesis of non-aryl substituted borirenes. Using this known photolytic rearrangement route, the synthesis of transition metal σ-borirenyl complexes would be theoretically possible by photolytic irradiation of an alkyne-functionalized transition metal-boryl species. This route (rearrangement) has been shown to be feasible and has been previously published by our group in the synthesis of [(η^5-C_5Me_5)$(OC)_2$Fe(μ-{$BN(SiMe_3)_2$}C=C)-Ph] (**86**) from photolytic irradiation of [(η^5-C_5Me_5)$(OC)_2$Fe$BN(SiMe_3)_2$C≡C-Ph] (**85**) under a carbon monoxide atmosphere (Figure 3-4, bottom);[297] however, the reaction is reversible and has never been shown to be feasible for preparatory scale synthesis of a transition metal σ-borirenyl complex (**86**).

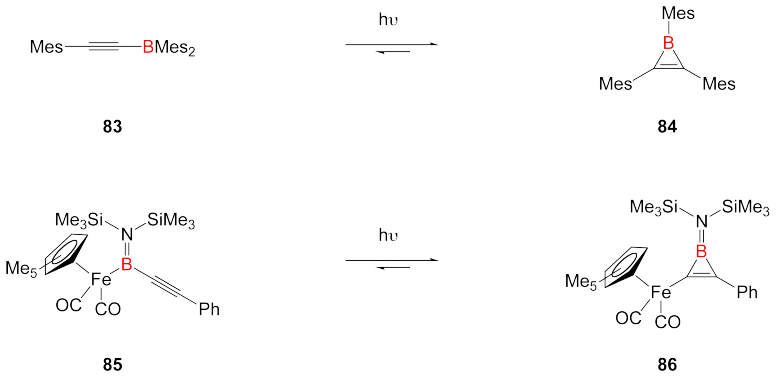

Figure 3-4. Photolytic precedence for the synthesis of trimesitylborirene (**84**) from dimesityl(mesitylethynyl)borane (**83**) (top)[294] and a similar rearrangement of an alkyne functionalized transition metal-boryl complex, [(η^5-C_5Me_5)$(OC)_2$Fe$BN(SiMe_3)_2$C≡C-Ph] (**85**), to form the iron-borirenyl species [(η^5-C_5Me_5)$(OC)_2$Fe(μ-{$BN(SiMe_3)_2$}C=C)-Ph] (**86**) (bottom).[297]

To date, the most efficient manner for borirene synthesis appears to be photolytic and thermolytic terminal borylene transfer from a Group 6 pentacarbonyl transition metal scaffold (M = Cr (**13**) and Mo (**14**)) to the alkyne functionality of a transition metal σ-alkynyl species (M = Pt (**87**) and Fe (**89**)) resulting in formation of the transition metal σ-borirenyl species (M = Pt (**88**) and Fe (**86**)) (Figure 3-5).[295,297]

* See Section 1.3.2 for an introduction to photolytic generation of borirenes.

This method has been proven to be successful for many "borylenation" reactions of C-C triple bonds using these mildly reactive, thermally stable, group 6 pentacarbonyl terminal *bis*(trimethylsilyl)aminoborylene complexes ([(OC)$_5$M{BN(SiMe$_3$)$_2$}], M = Cr (**13**), Mo (**14**), and W (**15**)). This later route has many benefits relative to the photo-rearrangement route because once the successful synthesis of the borylene complexes has been achieved, the borylene transfer to alkynyl reagents is possible with almost any non-sterically bulky alkyne. The yield of the borylene transfer reactions is typically lower, but still preferable due to the expanded range of transferable substituents available. This transfer methodology has been shown to be viable for the synthesis of borirenes from both organic[173-175] and organometallic[295,297] alkynyl species with relatively high yields and under relatively mild conditions both thermally and photolytically.

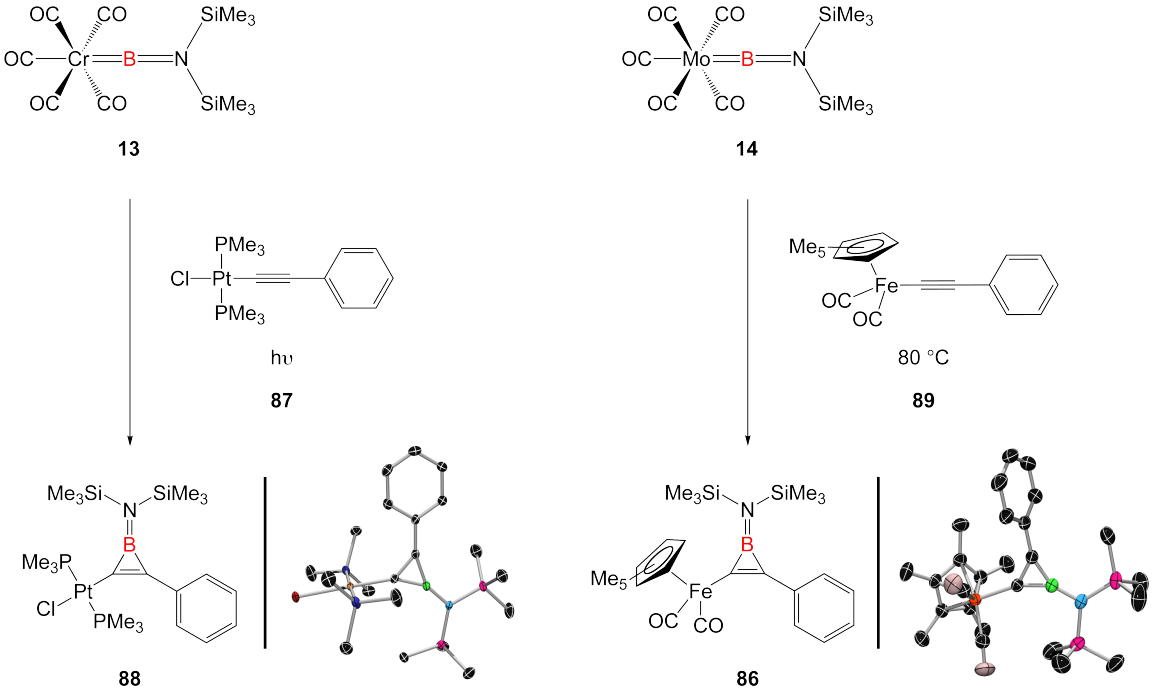

Figure 3-5. Photolytic and thermolytic transfers of the terminal transition metal-borylene ligand of [(OC)$_5$M{BN(SiMe$_3$)$_2$}] (M = Cr (**13**) and Mo (**14**)) to the alkynyl substituent of the transition metal σ-alkynyl precursors **87** and **89** to yield the transition metal σ-borirenyl complexes **88** and **86**, respectively.[295,297]

In 2009[295] and 2011,[297] our research group published the first successful synthesis of the transition metal σ-borirenyl complexes of platinum (**88**) and iron (**86**), respectively. These systems were synthesized *via* photolytic and thermolytic transfers of a terminal borylene ligand {BN(SiMe$_3$)$_2$} from a group 6 transition metal pentacarbonyl scaffold ([(OC)$_5$M{BN(SiMe$_3$)$_2$}], M = Cr (**13**) and Mo (**14**)) onto their respective transition metal σ-alkynyl precursors (Figure 3-5). Publication of the

platinum σ-borirenyl species *trans*-[PtCl{(μ-{BN(SiMe$_3$)$_2$}C=C)-Ph}(PMe$_3$)$_2$] (**88**) and the subsequent reactivity studies showed the ability of the platinum σ-borirenyl system to shift the UV-vis spectroscopic absorption (maxima) profile when compared to the platinum σ-alkynyl precursor *trans*-[PtCl(C≡C-Ph)(PMe$_3$)$_2$] (**87**) (Figure 3-6).[295] The presence of spectral overtones due to the C-C triple bond in the spectrum of the platinum σ-alkynyl complex *trans*-[PtCl(C≡C-Ph)(PMe$_3$)$_2$] (**87**) overshadows any exact calculations pertaining to the absorption maxima for the complex, but what is apparent by viewing the spectra of the platinum σ-borirenyl complex *trans*-[PtCl{(μ-{BN(SiMe$_3$)$_2$}C=C)-Ph}(PMe$_3$)$_2$] (**88**) is that the spectral profile is drastically changed and now displays one specific absorption maxima which was predicted to be dependent upon the substituents exocyclically bound to the borirene (*cyclo*-BC$_2$) system.

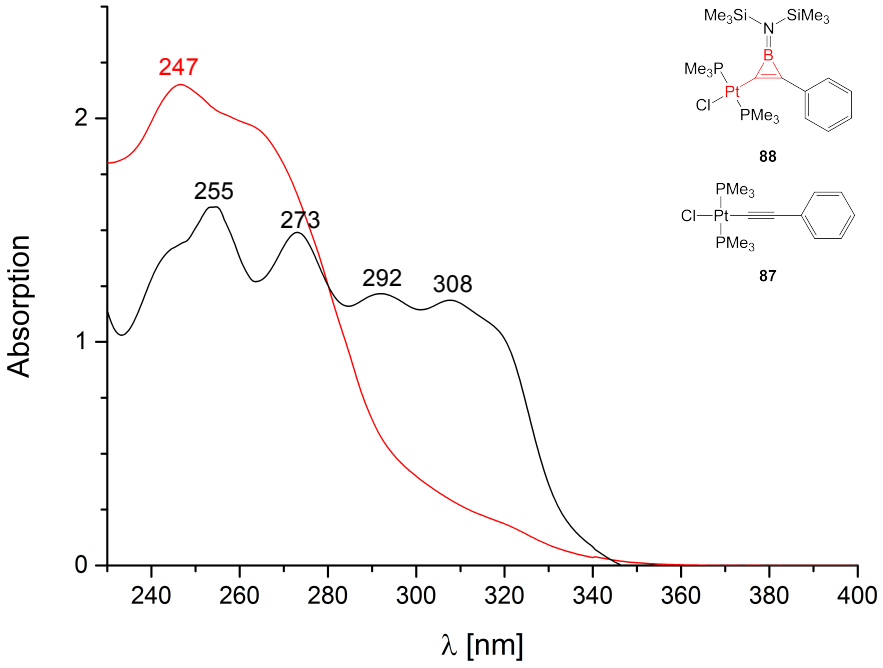

Figure 3-6. Plotted UV-vis absorption spectroscopic data comparing (maxima) of the platinum σ-alkynyl complex, *trans*-[PtCl(C≡C-Ph)(PMe$_3$)$_2$] (**87**, black), and the platinum σ-borirenyl complex *trans*-[PtCl{(μ-{BN(SiMe$_3$)$_2$}C=C)-Ph}(PMe$_3$)$_2$] (**88**, red).

Time-dependent density functional theory (TD-DFT) calculations provided by Dr. Alfredo Vargas were used to model the major electronic transitions observed in the absorption spectra of three proposed mono-borirene compounds and complexes: *cyclo*-C(H)C(Ph)BN(SiMe$_3$)$_2$ (**90**), *trans*-[PtCl{(μ-{BN(SiMe$_3$)$_2$}C=C)-

Ph}$(PMe_3)_2$][295] (**88**), and *cyclo*-C(Ph)C(Ph)BN$(SiMe_3)_2$ (**91**).[173-175] * A key determinant of π-communication between two electronically communicating centers is the bathochromic shifting or red-shifting of absorption transitions, which has been associated with an increase of delocalization in the π-conjugated orbitals of the complexes and compounds.[219-221] The rationalization of this effect stems from the fact that increasing delocalization splits both empty and filled orbitals into further non-degenerate molecular orbitals. This increased splitting narrows the gap between the highest relevant filled orbital (HOMO) and the lowest relevant unoccupied orbital (LUMO), thus decreasing the energy of transition between the orbitals (HOMO-LUMO gap) and resulting in a bathochromic shift of the absorption maximum (lower energy of transition). Indeed, the predicted TD-DFT calculated transitions for the complexes are: *cyclo*-C(H)C(Ph)BN$(SiMe_3)_2$ (**90**) (262 nm), *trans*-[PtCl{(μ-{BN$(SiMe_3)_2$}C=C)-Ph}$(PMe_3)_2$] (**88**) (276 nm), and *cyclo*-C(Ph)C(Ph)BN$(SiMe_3)_2$ (**91**) (295 nm). This calculated data shows that expansion of the π-conjugated system from integration of a transition metal or aryl substituent results in a further lowering of the HOMO–1 to LUMO transition energy. Figure 3-7 displays data corroborating a calculated redshift of 14 nm for replacement of the R = H (**90**) fragment with a R = *trans*-{PtCl$(PMe_3)_2$} fragment (**88**), and a calculated redshift of 33 nm upon replacement of R = H (**90**) by extension of the conjugated system over a second phenyl ring (**91**).

* Geometry optimizations were conducted at the B3LYP/6-311+G* and OLYP/TZP levels of theory using the Gaussian03 and ADF programs.

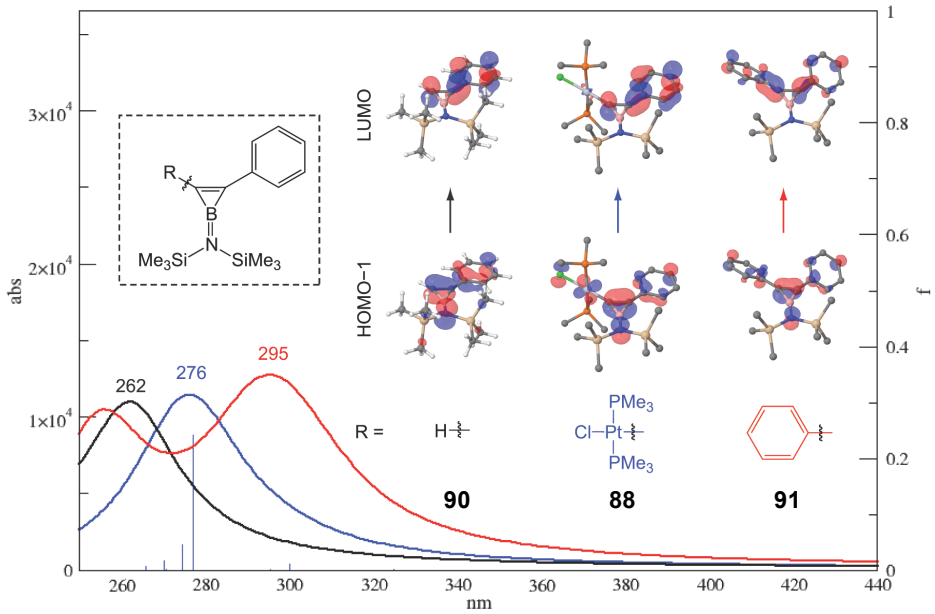

Figure 3-7. TD-DFT analysis for the augmentation of a monoborirene system by modification of one of the carbon exocyclic substituents resulting in calculated absorption maxima profiles for the theoretically proposed complexes and compounds: (**90**) (black, λ_{max} = 262 nm), (**88**) (blue, λ_{max} = 276 nm), and (**91**) (red, λ_{max} = 295 nm).

With the publication of the first platinum-substituted monoborirene system *trans*-[PtCl{(μ-{BN(SiMe$_3$)$_2$}C=C)-Ph}(PMe$_3$)$_2$] (**88**) by our research group in 2009,[295] a secondary project was developed to create a *trans*-platinum *bis*(borirene) system which could allow the platinum atom to serve as a bridge for significant electron delocalization across the two normally independent heteroaromatic borirene rings ({*cyclo*-BC$_2$}-Pt-{*cyclo*-BC$_2$}). Experimentally, this strong delocalizing influence of platinum has been confirmed by observation of a planar arrangement of these subsequently reported *trans*-platinum *bis*(borirene) systems in the solid state and the data reported in this section of this thesis stands as the first experimentally confirmed result of this nature.

3.1.2 Platinum *bis*-*σ*-Alkynyl Precursors

Platinum *σ*-alkynyl complexes have been known to be synthesized in mono- (**87**) and *bis*- (**95**) forms through modification of a reaction published by Sonogashira and coworkers (Figure 3-8).[235,419-422] From the 2009 report for the *trans*-[PtCl(C≡C-Ph)$(PMe_3)_2$] (**87**) species[295,423] and the aforementioned Sonogashira publication,[419] the platinum mono-*σ*-alkynyl and *bis*-*σ*-alkynyl precursors were synthesized by treatment of the platinum *bis*(phosphine) dichloride complexes [$PtCl_2(PR_3)_2$] (R = Me (**92**) or Et (**93**)) with phenylacetylene (**94**) in a solvent/reagent mixture of THF and diethylamine. The reaction mixture can be separated from the diethylammonium chloride salt byproduct by column chromatography under normal atmospheric conditions as the platinum *σ*-alkynyl complexes are predominantly observed to be air stable. The platinum *σ*-alkynyl complexes also are well suited as borylene transfer acceptors as they are typically robust enough to survive UV irradiation.

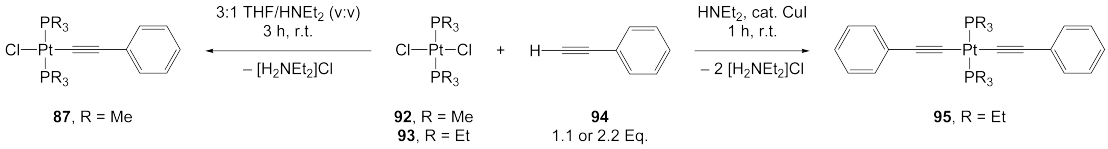

Figure 3-8. Manipulation of reaction conditions published by the groups of Schanze[423] and Sonogashira[419] for the synthesis of mono- (**87**, left) and *bis*- (**95**, right) platinum *σ*-alkynyl complexes from the respective *trans*-platinum dichloride *bis*(phosphine) complexes [$PtCl_2(PR_3)_2$] (R = Me (**92**) or Et (**93**)) and phenylacetylene (**94**).

3.1.2.1 Synthesis of *trans*-[Pt(C≡C-Ph)$_2$(PEt_3)$_2$] (95) and General Remarks

cis-[$PtCl_2(PEt_3)_2$] (**98**) was used as a base reagent for the construction of all *trans*-platinum *bis*-*σ*-alkynyl precursors. Synthesis of this precursor was conducted as outlined by Parry and Parshall[424-427] by mixing potassium tetrachloroplatinate (**96**) with triethylphosphine (**97**) (2.0 eq. minimum) in degassed 1:1 (v:v) EtOH/H_2O to liberate two equivalents of KCl and yield *cis*-[$PtCl_2(PEt_3)_2$] (**98**). The [$PtCl_2(PEt_3)_2$] platinum precursor is known to exist in the *cis*-[$PtCl_2(PEt_3)_2$] conformation (**98**)* at room temperature, but undergoes isomerization to the *trans*-[$PtCl_2(PEt_3)_2$] (**93**)† species at temperatures in excess of 80 °C[427] (Figure 3-9). Consequently, all alkyne-metal coupling reactions were performed at temperatures in excess of 80 °C in order to yield the desired *trans*- isomers of the platinum *bis*-*σ*-alkynyl species.

* Literature value for ^{31}P NMR Spectrum (CH_2Cl_2, H_3PO_4) [ppm]: δ = 9.75 (s, $^1J_{P\text{-}Pt}$ = 3,509 Hz).[427]
† Literature value for ^{31}P NMR Spectrum (CH_2Cl_2, H_3PO_4) [ppm]: δ = 12.98 (s, $^1J_{P\text{-}Pt}$ = 2,399 Hz).[427]

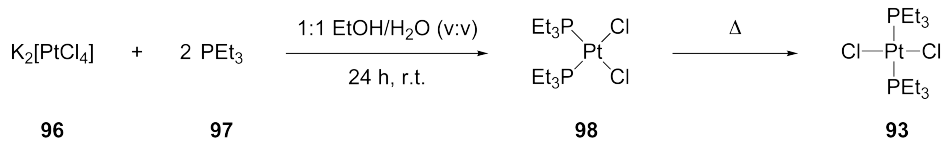

Figure 3-9. Synthesis of *cis*-[$PtCl_2(PEt_3)_2$] (**98**).[424-427] Conversion from the *cis*-[$PtCl_2(PEt_3)_2$] (**98**) isomer to the *trans*-[$PtCl_2(PEt_3)_2$] (**93**) isomer is known to take place in excess of an 80 °C thermal barrier.[427]

The synthesis of all of the *trans*-platinum *bis*-*σ*-alkynyl precursors reported in this thesis stems from the seminal 1978 publication by Sonogashira, Hagihara, and coworkers of *trans*-[$Pt(C{\equiv}C\text{-}Ph)_2(PEt_3)_2$] (**95**).[419] In this publication, *trans*-[$PtCl_2(PEt_3)$] (**93**) was mixed with phenylacetylene (**94**) (2.0 eq. minimum) in diethylamine and was allowed to react in the presence of CuI for one hour at room temperature to afford *trans*-[$Pt(C{\equiv}C\text{-}Ph)_2(PEt_3)_2$] (**95**) in 90% yield. The CuI in these reactions acts as a catalyst and increases the speed of formation of these *trans*-platinum *bis*-*σ*-alkynyl species; however, the routes reported in this thesis are all copper-free in order to isolate clean NMR spectroscopic data for the intermediary platinum mono-*σ*-alkynyl species. For faster reaction rates, catalytic amounts of CuI can be incorporated into the reaction mixtures. NMR spectroscopic data for the reported complexes in this section will be predominantly taken from the *in situ* reaction mixtures for accurate description of the intermediary platinum monoalkynyl species. The $^{31}P\{^1H\}$ NMR data and prominent platinum satellites correlating to ^{195}Pt (I = ½, 33.8% natural abundance) coupling ($^1J_{P\text{-}Pt}$) are also noted in order to differentiate between species with similar NMR resonances. Stepwise, the modified reaction shown below in Figure 3-10 requires the base diethylamine to deprotonate phenylacetylene forming the diethylammonium phenylacetylenide ion pair [H_2NEt_2][C≡C-Ph]. The presence of [H_2NEt_2][C≡C-Ph] in solution with *trans*-[$PtCl_2(PEt_3)_2$] (**93**) ($^{31}P\{^1H\}$: δ = 13.0 ppm, $^1J_{P\text{-}Pt}$ = 2,399 Hz) at 80 °C slowly ushers in a double salt elimination reaction, forming the *trans*-platinum *bis*-*σ*-alkynyl species *trans*-[$Pt(C{\equiv}C\text{-}Ph)_2(PEt_3)_2$] (**95**) ($^{31}P\{^1H\}$: δ = 10.7 ppm, $^1J_{P\text{-}Pt}$ = 2,387 Hz) with two equivalents of diethylammonium chloride as byproducts.

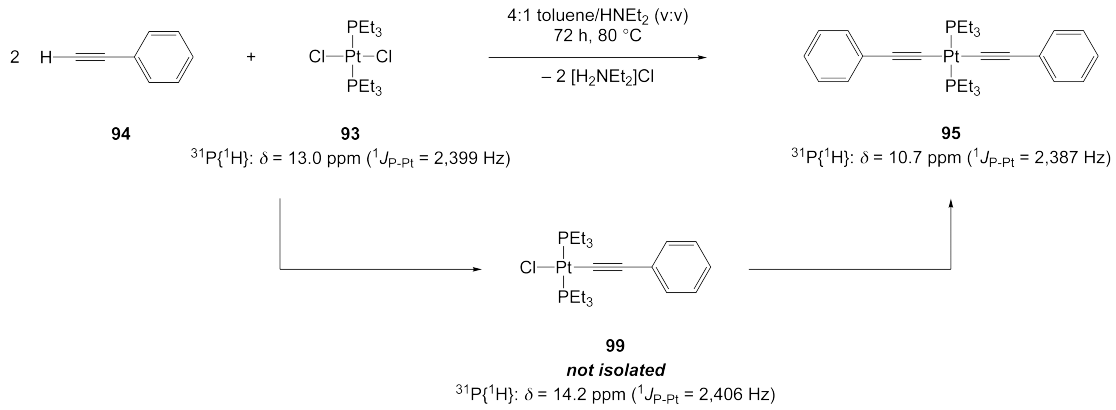

Figure 3-10. *trans*-[Pt(C≡C-Ph)$_2$(PEt$_3$)$_2$] (**95**) synthesis from *trans*-[PtCl$_2$(PEt$_3$)$_2$] (**93**) with the non-isolated intermediate *trans*-[PtCl(C≡C-Ph)(PEt$_3$)$_2$] (**99**).*

Monitoring the solution *via* $^{31}P\{^1H\}$ NMR spectroscopy also shows the intermediate mono-*σ*-alkyne *trans*-[PtCl(C≡C-Ph)(PEt$_3$)$_2$] (**99**) ($^{31}P\{^1H\}$: δ = 14.2 ppm, $^1J_{P\text{-}Pt}$ = 2,406 Hz) in solution; however, the species was not isolated. The reaction mixtures are typically observed to start off colorless and evolve into light yellow solutions as more of the *trans*-[Pt(C≡C-Ph)$_2$(PEt$_3$)$_2$] (**95**) species is formed. Continued heating of the reaction at 80 °C mixture typically allows for full conversion of the precursor *trans*-[PtCl$_2$(PEt$_3$)$_2$] (**93**) to *trans*-[Pt(C≡C-Ph)$_2$(PEt$_3$)$_2$] (**95**) over 72 h (Figure 3-10), however, longer reaction times at 80 °C can be utilized to ensure product conversion with no observable decomposition of the product or starting material. The *trans*-[Pt(C≡C-Ph)$_2$(PEt$_3$)$_2$] (**95**) product is witnessed *via* $^{195}Pt\{^1H\}$ NMR spectroscopy as a triplet appearing at −4,755 ppm ($^1J_{Pt\text{-}P}$ = 2,376 Hz). *trans*-[Pt(C≡C-Ph)$_2$(PEt$_3$)$_2$] (**95**) is air stable (as are most of the platinum *bis*-*σ*-alkynyl species studied) and can be purified by silica gel (SiO$_2$) column chromatography. Toluene is typically used as an eluent and the R$_f$ values for the collection fraction are in the 0.5-0.75 range. As a general rule, crystallization by saturated toluene or benzene solution atmospheric diffusion is a reliable way to accrue material of sufficient purity for analytical characterization of the platinum *bis*-*σ*-alkynyl precursors. The crystallized *trans*-[Pt(C≡C-Ph)$_2$(PEt$_3$)$_2$] (**95**) product can readily be witnessed as bright yellow colored crystalline blocks which melt within the range of 187-189 °C.[419] Analysis of *trans*-[Pt(C≡C-Ph)$_2$(PEt$_3$)$_2$] (**95**) by infrared spectroscopy was previously reported[419] with one observable band for the Pt-C stretching mode at 549 cm^{-1} and one reported $\tilde{\nu}$(C≡C) absorption at 2,107 cm^{-1}.

* NMR spectroscopic data taken directly from reaction mixtures: $^{31}P\{^1H\}$ NMR (161.98 MHz, 4:1 (v:v) $C_6H_5CH_3$/HNEt$_2$, H_3PO_4, 297 K).

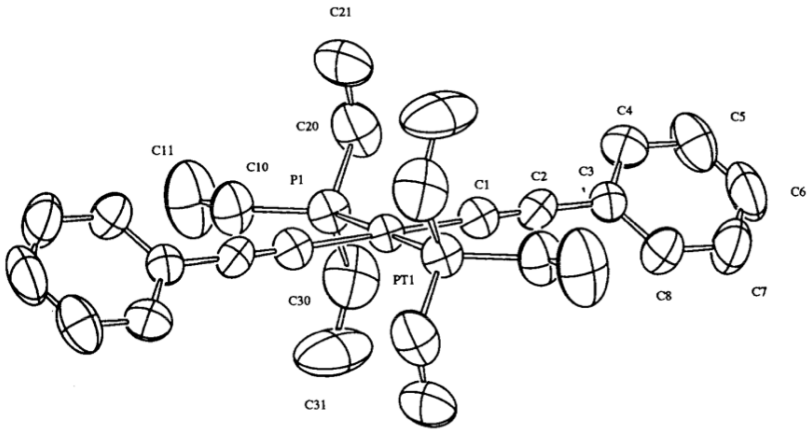

Figure 3-11. *trans*-[Pt(C≡C-Ph)$_2$(PEt$_3$)$_2$] (**95**) X-ray structure as reported by Lukehart and coworkers. Thermal ellipsoids set at 50% probability. All hydrogen atoms have been omitted for clarity. Selected bond distances (Å) and angles (º): Pt(1)–P(1) 2.289(3), Pt(1)–C(1) 1.98(1), C(1)–C(2) 1.21(1), C(2)–C(3) 1.43(1), P(1)–Pt(1)–P(1) 180.00, C(1)–Pt(1)–C(1) 180.00, P(1)–Pt(1)–C(1) 87.7(3), Pt(1)–C(1)–C(2) 177.8(9), C(1)–C(2)–C(3) 176(1).[421]

An X-ray crystal structure for *trans*-[Pt(C≡C-Ph)$_2$(PEt$_3$)$_2$] (**95**) has been previously reported.[421] The reported bond distances will be used to compare with the other platinum *bis*-*σ*-alkynyl species reported in this section. An ORTEP diagram for the structure as well as some key bond distances for *trans*-[Pt(C≡C-Ph)$_2$(PEt$_3$)$_2$] (**95**) are shown in Figure 3-11. The Pt-C(1) and the C(1)-C(2) bond distances (1.98(1) and 1.21(1) Å, respectively) are of particular interest and will be discussed comparatively to other structures in Section 3.1.2.7. It should also be noted that the symmetry for the reported X-ray structure of *trans*-[Pt(C≡C-Ph)$_2$(PEt$_3$)$_2$] (**95**) is different* than the other platinum *bis*-*σ*-alkynyl species reported in this section of the thesis and make direct comparison difficult.

3.1.2.2 *trans*-[Pt(C≡C-*p*-C$_6$H$_4$OMe)$_2$(PEt$_3$)$_2$] (102)

trans-[Pt(C≡C-*p*-C$_6$H$_4$OMe)$_2$(PEt$_3$)$_2$] (**102**) was prepared according to the modified literature procedure previously discussed† in which *trans*-[PtCl$_2$(PEt$_3$)$_2$] (**93**) is mixed with 4-ethynylanisole (**100**) (2.0 eq. minimum) in a 4:1 (v:v) mixture of toluene/HNEt$_2$ (Figure 3-12). The reaction was heated for 72 h at 80 ºC during which time full consumption of *trans*-[PtCl$_2$(PEt$_3$)$_2$] (**93**) (^{31}P{^{1}H}: δ = 13.0 ppm, $^1J_{P\text{-}Pt}$ = 2,399 Hz) is witnessed *via* ^{31}P{^{1}H} NMR spectroscopy with formation of the *trans*-platinum mono-*σ*-alkynyl species *trans*-[PtCl(C≡C-*p*-C$_6$H$_4$OMe)(PEt$_3$)$_2$] (**101**) (^{31}P{^{1}H}: δ = 13.9 ppm, $^1J_{P\text{-}Pt}$ = 2,437 Hz) firstly (not isolated), and formation of the

* C$_{28}$H$_{40}$P$_2$Pt, *M* = 750.47 reported (633.64 calculated), monoclinic, space group = *P*2$_1$/*c*.
† See Section 3.1.2.1.

trans-platinum *bis*-*σ*-alkynyl species *trans*-[Pt(C≡C-*p*-$C_6H_4OMe)_2(PEt_3)_2$] (**102**) ($^{31}P\{^1H\}$: δ = 11.3 ppm, $^1J_{P\text{-}Pt}$ = 2,424 Hz) secondly (Figure 3-12). The resulting light yellow reaction mixture was purified *via* silica gel (SiO_2) column chromatography to yield the *trans*-platinum *bis*-*σ*-alkynyl species *trans*-[Pt(C≡C-*p*-$C_6H_4OMe)_2(PEt_3)_2$] (**102**) as air-stable light yellow crystalline solids in 96 % yield. The compound readily crystallized in large, light-yellow blocks. Differential thermal analysis of these light-yellow crystalline solids showed a melting point for (**102**) at 156 °C, but no decomposition below 300 °C.

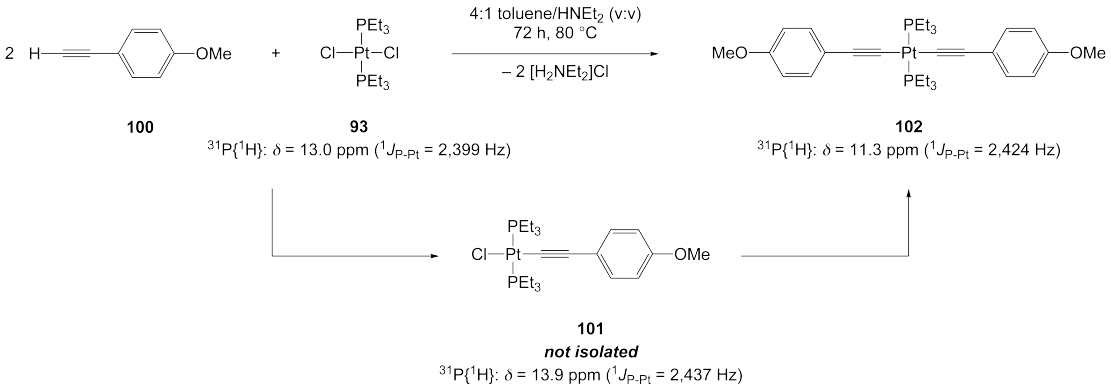

Figure 3-12. *trans*-[Pt(C≡C-*p*-$C_6H_4OMe)_2(PEt_3)_2$] (**102**) synthesis from *trans*-$[PtCl_2(PEt_3)_2]$ (**93**) with the non-isolated intermediate *trans*-[PtCl(C≡C-*p*-$C_6H_4OMe)(PEt_3)_2$] (**101**).*

The *trans*-[Pt(C≡C-*p*-$C_6H_4OMe)_2(PEt_3)_2$] (**102**) product is witnessed *via* $^{195}Pt\{^1H\}$ NMR spectroscopy as a triplet appearing at −4,759 ppm ($^1J_{Pt\text{-}P}$ = 2,390 Hz). Analysis of *trans*-[Pt(C≡C-*p*-$C_6H_4OMe)_2(PEt_3)_2$] (**102**) by infrared spectroscopy shows multiple observable bands that could correlate to the Pt-C stretching mode at 641, 536, and 509 cm^{-1} and one observable $\tilde{\nu}$(C≡C) absorption at 2,102 cm^{-1}.

* NMR spectroscopic data taken directly from reaction mixtures: $^{31}P\{^1H\}$ NMR (161.98 MHz, 4:1 (v:v) $C_6H_5CH_3/HNEt_2$, H_3PO_4, 297 K).

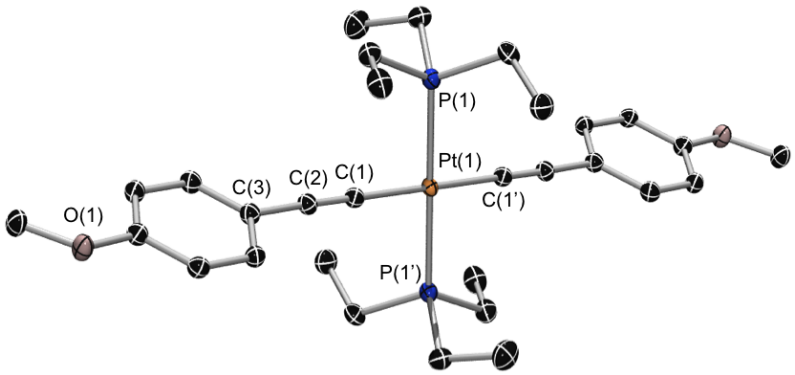

Figure 3-13. ORTEP-rendered structure of *trans*-[Pt(C≡C-*p*-$C_6H_4OMe)_2(PEt_3)_2$] (**102**). Thermal ellipsoids set at 50% probability. All hydrogen atoms have been omitted for clarity. Selected bond distances (Å) and angles (°): Pt(1)–P(1) 2.305(1), Pt(1)–C(1) 2.000(9), C(1)–C(2) 1.20(1), C(2)–C(3) 1.468(6), P(1)–Pt(1)–P(1') 180.00(4), C(1)–Pt(1)–C(1') 180.0(3), P(1)–Pt(1)–C(1) 84.7(2), Pt(1)–C(1)–C(2) 175.1(6), C(1)–C(2)–C(3) 177.8(6).

Crystals suitable for X-ray diffraction were grown from saturated solutions of (**102**) in benzene. An ORTEP diagram for the structure as well as some key bond distances for (**102**) are shown in Figure 3-13. The *trans*-[Pt(C≡C-*p*-$C_6H_4OMe)_2(PEt_3)_2$] (**102**) species displays Pt-C(1) and C(1)-C(2) bond distances of 1.20(1) Å and 2.000(9) Å respectively. This data is comparable [*] to the distances of the *trans*-[$Pt(C{\equiv}C\text{-}Ph)_2(PEt_3)_2$] (**95**) species and the values for the C(1)-C(2) bond distance are as expected for a C-C triple bond.

3.1.2.3 *trans*-[Pt(C≡C-*p*-$C_6H_4CF_3)_2(PEt_3)_2$] (106)

The trimethylsilyl-protected alkyne 1-[(trimethylsilyl)ethynyl]-4-(trifluoromethyl)benzene (**103**) was used as the starting material for the synthesis of *trans*-[Pt(C≡C-*p*-$C_6H_4CF_3)_2(PEt_3)_2$] (**106**). The alkyne was deprotected by the reaction shown in Figure 3-14 according to similar literature precedence[428] in which the trimethylsilyl-protected alkyne is deprotected through reaction with a strong base (NaOH). The reaction mixture is biphasic and requires the use of a phase-transfer catalyst (benzyltriethylammonium chloride) to properly combine the two reagents. The reaction can easily be monitored by $^{19}F\{^1H\}$ NMR spectroscopy with the deprotected alkyne appearing at –63.6 ppm. Protonation was performed according to literature and purification was achieved *via* silica gel column chromatography (SiO_2) to yield 4-ethynyl-α,α,α-trifluorotoluene (**104**) as a clear oil. The alkyne is not light-

[*] $C_{30}H_{44}O_2P_2Pt$, M = 693.68, triclinic, space group = P–1.

stable and must be used immediately after deprotection or stored in brown glassware at low temperatures (<0 °C).

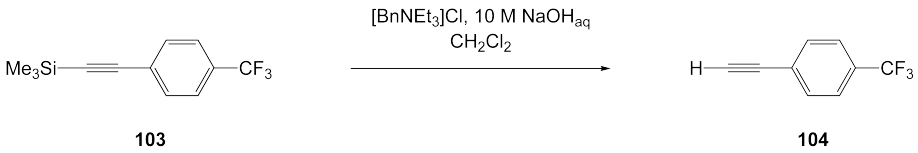

Figure 3-14. Deprotection of Me_3Si-C≡C-*p*-$C_6H_4CF_3$ (**103**) with NaOH to form the H-C≡C-*p*-$C_6H_4CF_3$ alkyne (**104**) starting material.[428]

trans-[Pt(C≡C-*p*-$C_6H_4CF_3$)$_2$(PEt_3)$_2$] (**106**) was prepared according to the modified literature procedure previously discussed* in which *trans*-[$PtCl_2$(PEt_3)$_2$] (**93**) is mixed with 4-ethynyl-α,α,α-trifluorotoluene (**104**) (minimum 2.0 eq.) in a 4:1 v:v mixture of toluene/$HNEt_2$ (Figure 3-15). The reaction was heated for 72 h at 80 °C during which time full consumption of *trans*-[$PtCl_2$(PEt_3)$_2$] (**93**) ($^{31}P\{^1H\}$: δ = 13.0 ppm, $^1J_{P\text{-}Pt}$ = 2,399 Hz) is witnessed *via* $^{31}P\{^1H\}$ NMR spectroscopy with formation of the *trans*-platinum mono-*σ*-alkynyl species *trans*-[PtCl(C≡C-*p*-$C_6H_4CF_3$)(PEt_3)$_2$] (**105**) ($^{31}P\{^1H\}$: δ = 14.6 ppm, $^1J_{P\text{-}Pt}$ = 2,404 Hz) firstly (not isolated), and formation of the *trans*-platinum *bis*-*σ*-alkynyl species *trans*-[Pt(C≡C-*p*-$C_6H_4CF_3$)$_2$(PEt_3)$_2$] (**106**) ($^{31}P\{^1H\}$: δ = 11.3 ppm, $^1J_{P\text{-}Pt}$ = 2,375 Hz) secondly (Figure 3-15). The resulting light yellow reaction mixture was purified *via* silica gel (SiO_2) column chromatography to yield the *trans*-platinum *bis*-*σ*-alkynyl species *trans*-[Pt(C≡C-*p*-$C_6H_4CF_3$)$_2$(PEt_3)$_2$] (**106**) as air-stable light yellow crystalline solids in 86% yield. The compound is very difficult to crystallize out of solution and readily will form yellow powdery solid material when dried. Differential thermal analysis of this light yellow solid material showed a melting point for **106** at 138 °C with no decomposition below 300 °C.

* See Section 3.1.2.1.

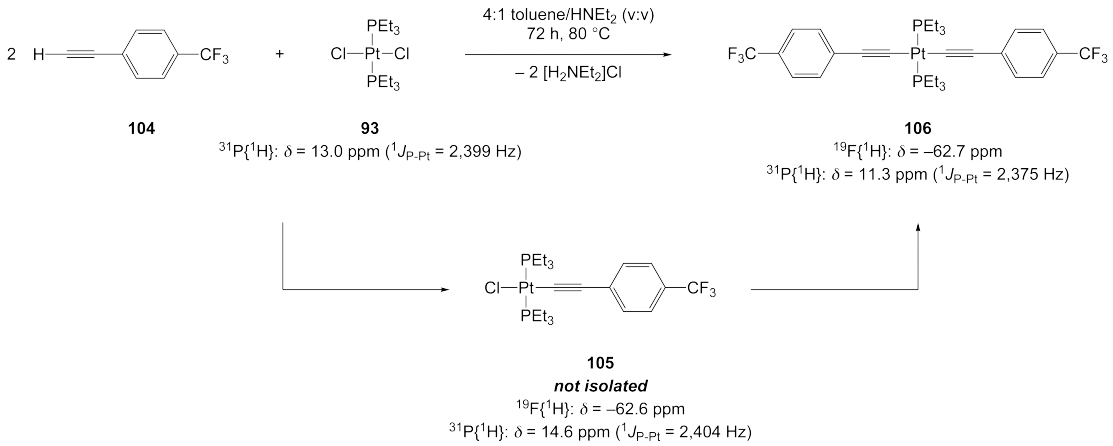

Figure 3-15. *trans*-[Pt(C≡C-*p*-$C_6H_4CF_3$)$_2$(PEt_3)$_2$] (**106**) synthesis from *trans*-[$PtCl_2$(PEt_3)$_2$] (**93**) with the non-isolated intermediate *trans*-[PtCl(C≡C-*p*-$C_6H_4CF_3$)(PEt_3)$_2$] (**105**).*

Spectroscopically, the *trans*-[Pt(C≡C-*p*-$C_6H_4CF_3$)$_2$(PEt_3)$_2$] (**106**) product is witnessed *via* ^{195}Pt{^{1}H} NMR spectroscopy as a triplet appearing at –4,748 ppm ($^1J_{Pt\text{-}P}$ = 2,350 Hz). Analysis of *trans*-[Pt(C≡C-*p*-$C_6H_4CF_3$)$_2$(PEt_3)$_2$] (**106**) by infrared spectroscopy shows multiple observable bands that could correspond for the Pt-C stretching mode at 656, 633, and 605 cm^{-1} and one observable $\tilde{\nu}$(C≡C) absorption at 2,100 cm^{-1}.

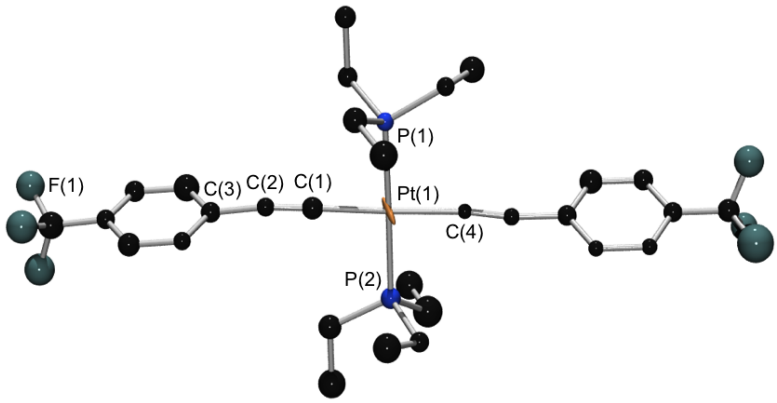

Figure 3-16. ORTEP-rendered isotropic structure of *trans*-[Pt(C≡C-*p*-$C_6H_4CF_3$)$_2$(PEt_3)$_2$] (**106**). All hydrogen atoms have been omitted for clarity.

Crystals of *trans*-[Pt(C≡C-*p*-$C_6H_4CF_3$)$_2$(PEt_3)$_2$] (**106**) suitable for X-ray diffraction were grown from saturated benzene solutions of the compound (Figure 3-16). The structure† has low completeness and is highly disordered due to the presence of the

* NMR spectroscopic data taken directly from reaction mixtures: ^{31}P{^{1}H} NMR (161.98 MHz, 4:1 (v:v) toluene/$HNEt_2$, H_3PO_4, 297 K).
† $C_{30}H_{38}F_6P_2Pt$, M = 769.63, triclinic, space group = P–1.

two trifluoromethyl groups on periphery of the compound. Because of the highly disordered nature of the structure, isotropic representations for the non-platinum thermal ellipsoid plot must be used. The structural details can not be used in any direct geometric comparison to other *trans*-platinum *bis*-*σ*-alkynyl species used in this section of the thesis and the structure is used to only display atom connectivity.

3.1.2.4 *trans*-[Pt(C≡C-9-$C_{14}H_9$)$_2$(PEt_3)$_2$] (63)

As with the reaction for *trans*-[Pt(C≡C-*p*-$C_6H_4CF_3$)$_2$(PEt_3)$_2$] (**106**), the reaction for *trans*-[Pt(C≡C-9-$C_{14}H_9$)$_2$(PEt_3)$_2$] (**63**) required synthesis of a protected alkyne which should be stored until use as the deprotonated species is not stable under ambient light and temperature environments. For this purpose, 4-(anthracen-10-yl)-2-methylbut-3-yn-2-ol (**109**) was synthesized from 9-bromoanthracene (**107**) and 2-methyl-but-3-yn-2-ol (**108**) according to literature protocol.[429] The alkyne was deprotected by the reaction shown in Figure 3-17 using the strong base (KOH).[429] Purification of the deprotected alkyne was achieved *via* silica gel column chromatography (SiO_2) to yield 10-ethynylanthracene (**110**) as a bright yellow solid. The alkyne is not light-stable and must be used immediately after deprotection or stored in brown glassware at low temperatures (<10 °C).

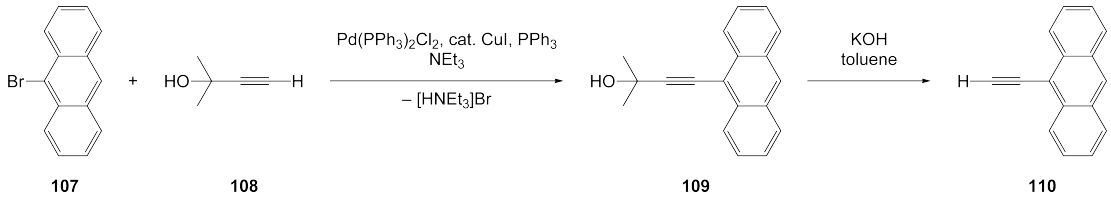

Figure 3-17. Synthesis of 4-(anthracen-10-yl)-2-methylbut-3-yn-2-ol (**109**) from 9-bromoanthracene (**107**) and 2-methyl-but-3-yn-2-ol (**108**) followed by the deprotection with KOH to form 10-ethynylanthracene (**110**).[429]

trans-[Pt(C≡C-9-$C_{14}H_9$)$_2$(PEt_3)$_2$] (**63**) was prepared according to the modified literature procedure previously discussed* in which *trans*-[$PtCl_2$(PEt_3)$_2$] (**93**) is mixed with 10-ethynylanthracene (**110**) (minimum 2.0 eq.) in a 4:1 v:v mixture of toluene/$HNEt_2$ (Figure 3-18). The reaction was heated for 48 h at 80 °C during which time full consumption of *trans*-[$PtCl_2$(PEt_3)$_2$] (**93**) ($^{31}P\{^1H\}$: δ = 13.0 ppm, $^1J_{P\text{-}Pt}$ = 2,399 Hz) is witnessed *via* $^{31}P\{^1H\}$ NMR spectroscopy with formation of the *trans*-platinum *bis*-*σ*-alkynyl species *trans*-[Pt(C≡C-9-$C_{14}H_9$)$_2$(PEt_3)$_2$] (**63**) ($^{31}P\{^1H\}$: δ = 12.2 ppm, $^1J_{P\text{-}Pt}$ = 2,366 Hz). In this reaction no species that could be characterized as the *trans*-platinum mono *σ*-alkynyl intermediate was witnessed. The resulting dark

* See Section 3.1.2.1.

brown reaction mixture was purified *via* silica gel (SiO_2) column chromatography to yield the *trans*-platinum *bis*-*σ*-alkynyl species *trans*-[Pt(C≡C-9-$C_{14}H_9$)$_2$(PEt_3)$_2$] (**63**) as an air and light sensitive yellow crystalline solid in 27% yield. The compound is very difficult to crystallize from solution and readily will form a yellow powder when isolated.

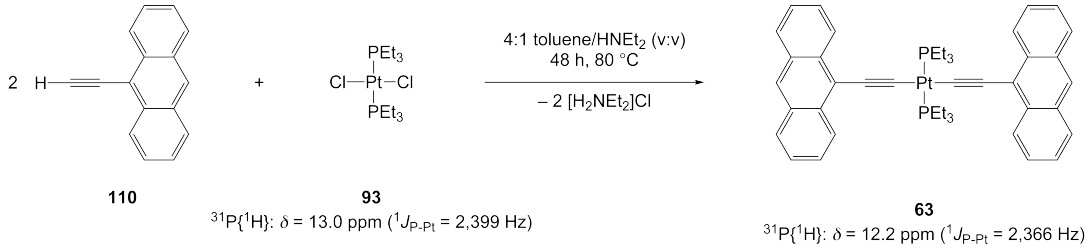

110 **93**

$^{31}P\{^1H\}$: δ = 13.0 ppm ($^1J_{P\text{-}Pt}$ = 2,399 Hz)

63

$^{31}P\{^1H\}$: δ = 12.2 ppm ($^1J_{P\text{-}Pt}$ = 2,366 Hz)

Figure 3-18. *trans*-[Pt(C≡C-9-$C_{14}H_9$)$_2$(PEt_3)$_2$] (**63**) synthesis from 10-ethynylanthracene (**110**) and *trans*-[$PtCl_2$(PEt_3)$_2$] (**93**).*

Spectroscopically, the *trans*-[Pt(C≡C-9-$C_{14}H_9$)$_2$(PEt_3)$_2$] (**63**) product is witnessed *via* $^{195}Pt\{^1H\}$ NMR spectroscopy as a triplet appearing at −4,721 ppm ($^1J_{Pt\text{-}P}$ = 2,356 Hz). Crystals suitable for X-ray diffraction were grown from saturated solutions of **63** in benzene. An ORTEP diagram for the structure as well as some key bond distances for *trans*-[Pt(C≡C-9-$C_{14}H_9$)$_2$(PEt_3)$_2$] (**63**) are shown in Figure 3-19. The *trans*-[Pt(C≡C-9-$C_{14}H_9$)$_2$(PEt_3)$_2$] (**63**) species displays Pt-C(1) and the C(1)-C(2) bond distances of 2.011(9) Å and 1.18(1) Å, respectively. This data is comparable† to the distances of the *trans*-[Pt(C≡C-Ph)$_2$(PEt_3)$_2$] (**95**) species and the values for the C(1)-C(2) bond distance are as expected for a C-C triple bond.

* NMR spectroscopic data taken directly from reaction mixtures: $^{31}P\{^1H\}$ NMR (161.98 MHz, 4:1 (v:v) toluene/$HNEt_2$, H_3PO_4, 297 K).

† $C_{44}H_{48}P_2Pt$, M = 833.88, triclinic, space group = $P\bar{1}$.

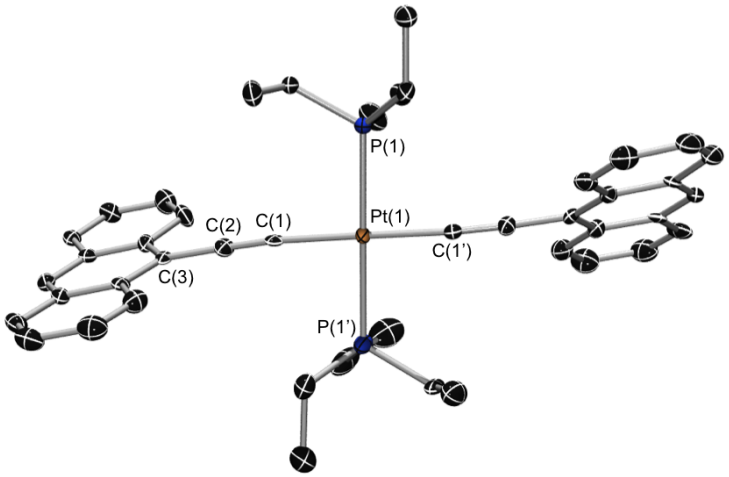

Figure 3-19. ORTEP-rendered structure of *trans*-[Pt(C≡C-9-$C_{14}H_9$)$_2$(PEt_3)$_2$] (**63**). Thermal ellipsoids set at 50% probability. All hydrogen atoms have been omitted for clarity. Selected bond distances (Å) and angles (°): Pt(1)–P(1) 2.295(3), Pt(1)–C(1) 2.011(9), C(1)–C(2) 1.18(1), C(2)–C(3) 1.44(1), P(1)–Pt(1)–P(1) 177.3(1), C(1)–Pt(1)–C(1) 174.8(4), P(1)–Pt(1)–C(1) 93.7(3), Pt(1)–C(1)–C(2) 174.5(9), C(1)–C(2)–C(3) 179(1).

3.1.2.5 *cis*-[Pt(C≡C-Ph)$_2$(DCPE)] (112)

trans-[Pt(C≡C-Ph)$_2$(PEt_3)$_2$] (**95**) was prepared according to the modified literature procedure previously discussed.* The *trans*-[Pt(C≡C-Ph)$_2$(PEt_3)$_2$] (**95**) species was then mixed with *bis*(dicyclohexylphosphino)ethane (**111**) (DCPE) ($^{31}P\{^1H\}$: δ = 0.3 ppm) in toluene and heated for 24 h at 80 °C during which time full consumption of *trans*-[Pt(C≡C-Ph)$_2$(PEt_3)$_2$] (**95**) is witnessed *via* $^{31}P\{^1H\}$ NMR spectroscopy with formation of the *cis*-platinum *bis*-σ-alkynyl species *cis*-[Pt(C≡C-Ph)$_2$(DCPE)] (**112**) ($^{31}P\{^1H\}$: δ = 61.3 ppm, $^1J_{P\text{-}Pt}$ = 2,227 Hz) and evolution of free triethylphosphine (**97**) ($^{31}P\{^1H\}$: δ = −20.5 ppm) (Figure 3-20). The resulting light yellow reaction mixture was purified *via* silica gel (SiO_2) column chromatography to yield the *cis*-platinum *bis*-σ-alkynyl species *cis*-[Pt(C≡C-Ph)$_2$(DCPE)] (**112**) as a light-sensitive light yellow crystalline solid in 72% yield. Spectroscopically, the *cis*-[Pt(C≡C-Ph)$_2$(DCPE)] (**112**) product is witnessed *via* $^{195}Pt\{^1H\}$ NMR spectroscopy as a triplet appearing at −4,891 ppm ($^1J_{Pt\text{-}P}$ = 2,220 Hz).

* See Section 3.1.2.1.

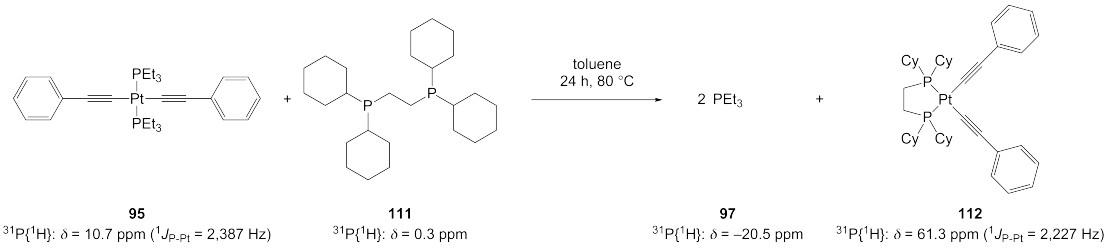

Figure 3-20. *cis*-[Pt(C≡C-Ph)$_2$(DCPE)] (**112**) synthesis from 1,2-*bis*(dicyclohexylphosphino)ethane (**111**) and *trans*-[Pt(C≡C-Ph)$_2$(PEt$_3$)$_2$] (**95**).*

3.1.2.6 *trans*-[Pt{(C≡C)$_3$-Tr*}$_2$(PEt$_3$)$_2$] (115)

As part of a collaboration with the group of Prof. Dr. Rik R. Tykwinski (Friedrich-Alexander-Universität Erlangen-Nürnberg), a gift of the hexatriyne H-(C≡C)$_3$-Tr* (**113**) (Tr* = *tris*-(3,5-di-*tert*-butylphenyl)methyl) was used in the synthesis of a *trans*-platinum *bis*-*σ*-hexatriynyl species, *trans*-[Pt{(C≡C)$_3$-Tr*}$_2$(PEt$_3$)$_2$] (**115**). Synthesis and characterization data for the hexatriyne were taken from literature report of the compound.[430] The presence of the large sterically protecting Tr* (*tris*-(3,5-di-*tert*-butylphenyl)methyl) groups instead of the aryl substituents used in the previous reported studies of these *trans*-platinum *bis*-*σ*-alkynyl compounds allowed the H-(C≡C)$_3$-Tr* (**113**) alkyne to be stable under ambient conditions and was used directly as received without the deprotection reactions needed for some of the aryl alkynes.

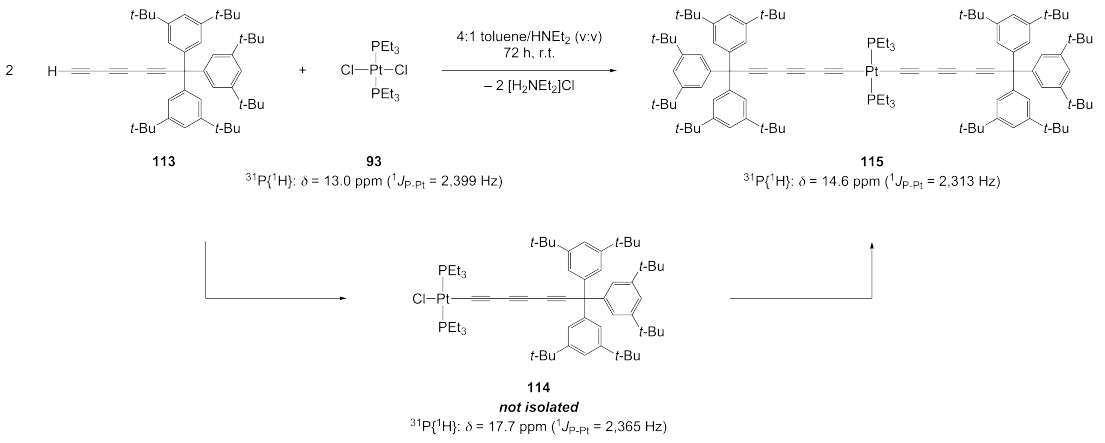

Figure 3-21. *trans*-[Pt{(C≡C)$_3$-Tr*}$_2$(PEt$_3$)$_2$] (**115**) synthesis from *trans*-[PtCl$_2$(PEt$_3$)$_2$] (**93**) with the non-isolated intermediate *trans*-[PtCl{(C≡C)$_3$-Tr*}(PEt$_3$)$_2$] (**114**).†

* NMR spectroscopic data taken directly from reaction mixtures: ^{31}P{^{1}H} NMR (161.98 MHz, 4:1 (v:v) toluene/HNEt$_2$, H_3PO_4, 297 K).
† NMR spectroscopic data taken directly from reaction mixtures: ^{31}P{^{1}H} NMR (161.98 MHz, 4:1 (v:v) toluene/HNEt$_2$, H_3PO_4, 297 K).

trans-[Pt{(C≡C)$_3$-Tr*}$_2$(PEt$_3$)$_2$] (**115**) was prepared according to the modified literature procedure previously discussed* in which *trans*-[PtCl$_2$(PEt$_3$)$_2$] (**93**) is mixed with H-(C≡C)$_3$-Tr* (**113**) (minimum 2.0 eq.) in a 4:1 v:v mixture of toluene/HNEt$_2$ (Figure 3-21). The reaction was kept at room temperature for 72 h during which time full consumption of *trans*-[PtCl$_2$(PEt$_3$)$_2$] (**93**) (^{31}P{^{1}H}: δ = 13.0 ppm, $^1J_{P\text{-}Pt}$ = 2,399 Hz) is witnessed *via* ^{31}P{^{1}H} NMR spectroscopy with initial formation of the *trans*-platinum mono-σ-hexatriynyl species *trans*-[PtCl{(C≡C)$_3$-Tr*}(PEt$_3$)$_2$] (**114**) (^{31}P{^{1}H}: δ = 17.7 ppm, $^1J_{P\text{-}Pt}$ = 2,365 Hz) (not isolated), and subsequent formation of the *trans*-platinum *bis*-σ-hexatriynyl species *trans*-[Pt{(C≡C)$_3$-Tr*}$_2$(PEt$_3$)$_2$] (**115**) (^{31}P{^{1}H}: δ = 14.6 ppm, $^1J_{P\text{-}Pt}$ = 2,313 Hz) (Figure 3-21). The resulting bright yellow reaction mixture was purified *via* silica gel (SiO$_2$) column chromatography to yield the *trans*-platinum *bis*-σ-hexatriynyl species *trans*-[Pt{(C≡C)$_3$-Tr*}$_2$(PEt$_3$)$_2$] (**115**) as an air and light stable yellow crystalline solid in 72% yield. The compound is very difficult to crystallize out of solution and readily will form a yellow powder when dried.

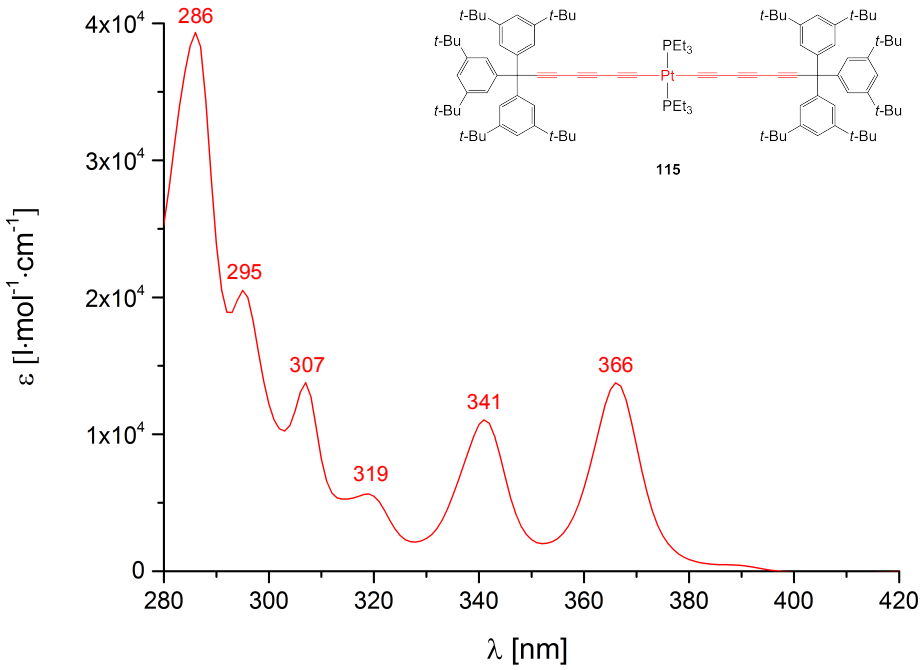

Figure 3-22. UV-vis absorption spectrum of *trans*-[Pt{(C≡C)$_3$-Tr*}$_2$(PEt$_3$)$_2$] (**115**) as measured in benzene. Data is plotted as wavelength [λ] *vs.* extinction coefficient [ε].

* See Section 3.1.2.1.

The complex *trans*-[Pt{(C≡C)$_3$-Tr*}$_2$(PEt$_3$)$_2$] (**115**) is witnessed *via* ^{195}Pt{^{1}H} NMR spectroscopy* as a triplet appearing at −4,743 ppm ($^1J_{Pt\text{-}P}$ = 2,283 Hz). Analysis of *trans*-[Pt{(C≡C)$_3$-Tr*}$_2$(PEt$_3$)$_2$] (**115**) by infrared spectroscopy shows two observable bands that could correspond to $\tilde{\nu}$(C≡C) absorptions at 2,137 cm^{-1} and 2,031 cm^{-1}. The UV-vis absorption spectrum of the compound can be seen in Figure 3-22 and displays absorption maxima at 286, 295, 307, 319, and 341 nm with the lowest energetic absorption maxima being 366 nm. The UV-vis profile corresponds to the reported absorption spectra of the H-(C≡C)$_3$-Tr* (**113**) homocoupled product Tr*-(C≡C)$_6$-Tr* (**116**) as reported by Tykwinski and coworkers (λ_{max} = 310 nm), however the presence of a platinum linker induces a bathochromic shift of the maximum absorption by 56 nm (λ_{max} = 366 nm).

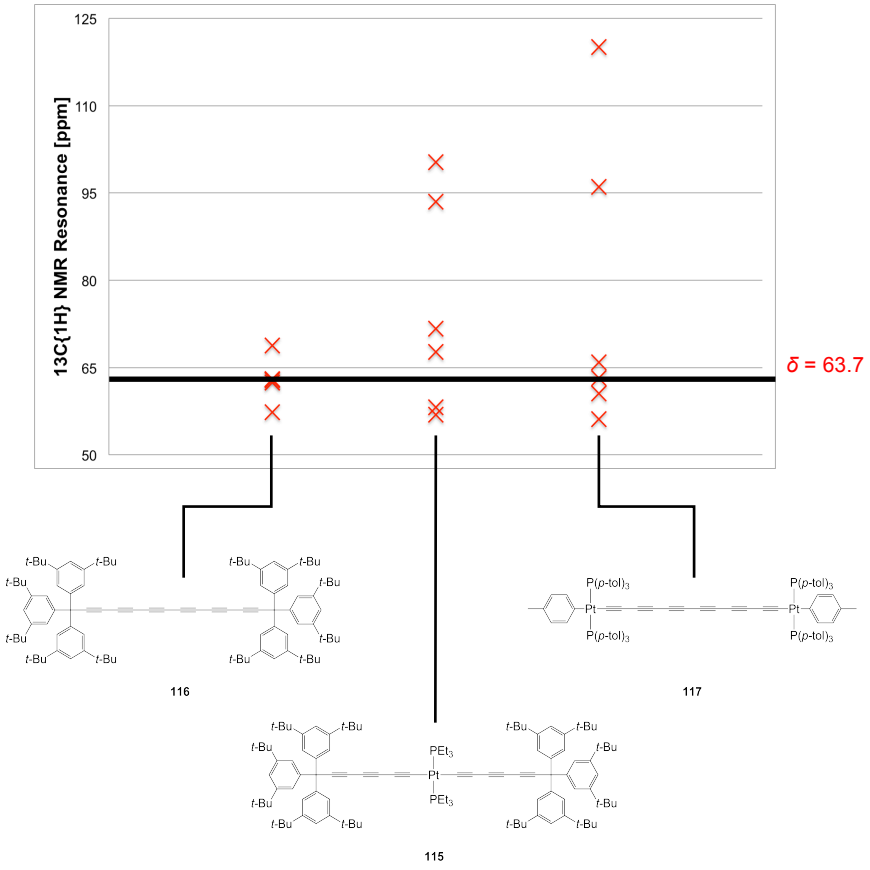

Figure 3-23. Plot of the alkynyl ^{13}C NMR resonances for *trans*-[Pt{(C≡C)$_3$-Tr*}$_2$(PEt$_3$)$_2$] (**115**) *vs.* the ^{13}C NMR resonances for **116** and **117** as reported by Tykwinski[430] and Gladysz[431] respectively displaying a well-defined region for carbon resonances within C-C triple bond chains.

Comparative spectroscopic analysis of the ^{13}C NMR data for the Tr*-(C≡C)$_6$-Tr* (**116**) compound reported by Tykwinski and a platinum end-capped 12 sp-carbon

* ^{195}Pt{^{1}H} NMR (107.00 MHz, C_6D_6, K_2PtCl_6, 297 K).

bimetallic bridging alkyne reported by Gladysz and coworkers (**117**)[431] relative to *trans*-[Pt{(C≡C)$_3$-Tr*}$_2$(PEt$_3$)$_2$] (**115**) also shows correlation of the interior alkyne carbon resonances (Figure 3-23). The data for all three of these species pertaining to the 12 interior sp-carbon nuclei show two divergent resonances for species **115** and **117** corresponding to the two platinum α-carbons and β-carbons ($^{13}C\{^1H\}$: δ = 100.2 ppm and 93.5 ppm) and ($^{13}C\{^1H\}$: δ = 120.1 ppm and 96.0 ppm) respectively. The rest of the carbon resonances are observed to appear in a very distinctive band centered around 63.7 ppm (observed in species **116**),[430] which is to date the best estimate for the $^{13}C\{^1H\}$ NMR chemical shifts for the linear carbon allotrope carbyne.[432-434] Figure 3-23 shows the plot of **115** relative to the reported data for **117** by Gladysz and coworkers as well as **116** reported by Tykwinski and coworkers.[430,431]

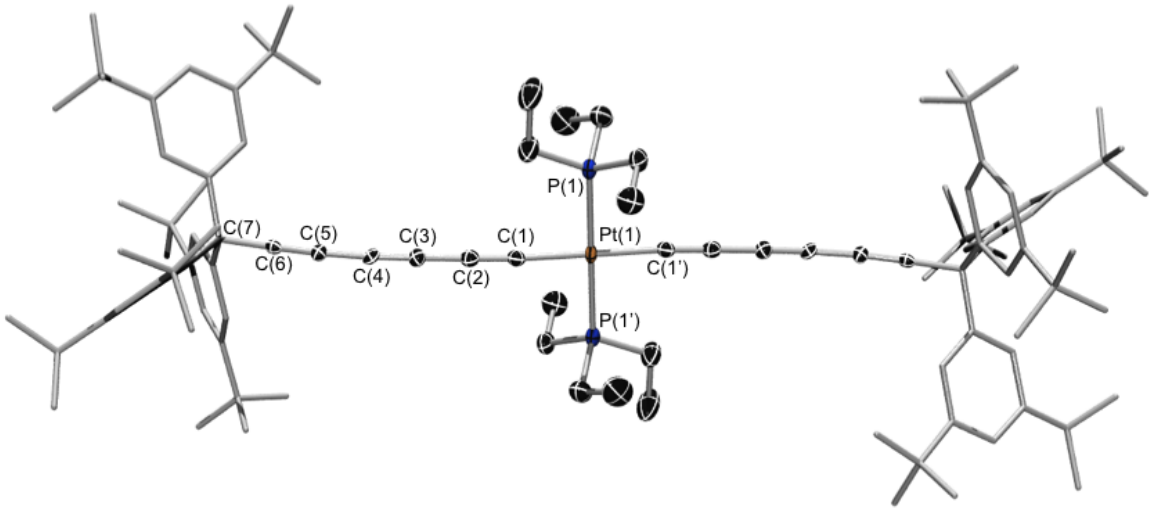

Figure 3-24. ORTEP-rendered structure of *trans*-[Pt{(C≡C)$_3$-Tr*}$_2$(PEt$_3$)$_2$] (**115**). Thermal ellipsoids set at 50% probability. All hydrogen atoms have been omitted for clarity.

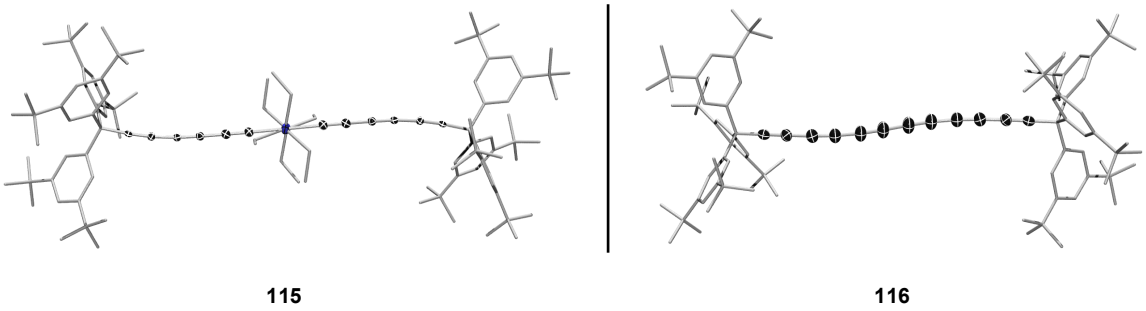

Figure 3-25. Structural comparison between **116** as reported by Tykwinski and coworkers[340] and *trans*-[Pt{(C≡C)$_3$-Tr*}$_2$(PEt$_3$)$_2$] (**115**) showcasing the classic bending of the structure in the oligoalkynes of exceptional length.

Crystals suitable for X-ray diffraction were grown from saturated solutions of **115** in benzene. An ORTEP diagram for the solid-state structure of *trans*-[Pt{(C≡C)$_3$-Tr*}$_2$(PEt$_3$)$_2$] (**115**) is shown in Figure 3-24. The complex *trans*-[Pt{(C≡C)$_3$-Tr*}$_2$(PEt$_3$)$_2$] (**115**) displays Pt-P and the Pt-C(1) bond distances of 2.299(1) Å and 1.975(4) Å respectively. Direct structural observation of *trans*-[Pt{(C≡C)$_3$-Tr*}$_2$(PEt$_3$)$_2$] (**115**) and **116** as reported by Tykwinski and coworkers[430] shows the classic oligoalkyne bending (Figure 3-25) as also noted by Gladysz and coworkers in their study of platinum-stabilized oligoalkynes.[431] The observed alkyne bond distances of the two structures show the expected alternating bond distances between the formal C-C triple bonds and the C-C single bonds; however, as the structure reported by Tykwinski possesses an inversion center in the middle of the molecule the Pt-C(1) distances cannot be accurately discussed. Direct comparisons (Table 3-1) between the two structures (**115** *vs.* **116**, respectively) show similar C-C bond distances for the *trans*-[Pt{(C≡C)$_3$-Tr*}$_2$(PEt$_3$)$_2$] (**115**) complex for the C(1)-C(2) (1.219(6) *vs.* 1.201(4) Å), C(2)-C(3) (1.378(6) *vs.* 1.353(4) Å), C(3)-C(4) (1.203(6) *vs.* 1.205(4) Å), and C(4)-C(5) (1.369(6) *vs.* 1.363(4) Å) atoms which all fit to the reported data published by Tykwinski and coworkers.[430]

	Pt–C$_1$	**C$_1$–C$_2$**	**C$_2$–C$_3$**	**C$_3$–C$_4$**	**C$_4$–C$_5$**	**C$_5$–C$_6$**	**C$_6$–C$_7$**
115	1.975(4)	1.219(6)	1.378(6)	1.203(6)	1.369(6)	1.217(6)	1.407(6)
	–	**C$_1$–C$_2$**	**C$_2$–C$_3$**	**C$_3$–C$_4$**	**C$_4$–C$_5$**	**C$_5$–C$_6$**	**C$_6$–C$_7$**
116	–	1.201(4)	1.353(4)	1.205(4)	1.363(4)	1.192(3)	1.483(3)

Table 3-1. Bond distance comparison between **116** as reported by Tykwinski and coworkers[430] and *trans*-[Pt{(C≡C)$_3$-Tr*}$_2$(PEt$_3$)$_2$] (**115**).

3.1.2.7 Discussion and Theory

Because of their similarity, comparisons between the spectroscopic data for the species *trans*-[Pt(C≡C-Ph)$_2$(PEt$_3$)$_2$] (**95**), *trans*-[Pt(C≡C-*p*-C$_6$H$_4$OMe)$_2$(PEt$_3$)$_2$] (**102**), and *trans*-[Pt(C≡C-*p*-C$_6$H$_4$CF$_3$)$_2$(PEt$_3$)$_2$] (**106**) will be directly compared to each other, while general data for the other three compounds mentioned in this section will be included where applicable. Of greatest importance to this study is the spectroscopic profile shifting for the incorporation of electron-withdrawing (CF$_3$) and electron-donating (OMe) substituents on the scaffold of the *trans*-[Pt(C≡C-Ph)$_2$(PEt$_3$)$_2$] (**95**) system.

	$^{31}P\{^{1}H\}$ (202.46 MHz, C_6D_6, H_3PO_4) [ppm]	$^{195}Pt\{^{1}H\}$ (107.00 MHz, C_6D_6, K_2PtCl_6) [ppm]
95	11.41 $^{1}J_{P\text{-}Pt}$ = 2,387 Hz $^{1}J_{P\text{-}C}$ = 18 Hz	−4,755 $^{1}J_{Pt\text{-}P}$ = 2,376 Hz $^{1}J_{Pt\text{-}C}$ = 957 Hz $^{2}J_{Pt\text{-}C}$ = 266 Hz
102	11.43 $^{1}J_{P\text{-}Pt}$ = 2,402 Hz $^{1}J_{P\text{-}C}$ = 18 Hz	−4,759 $^{1}J_{Pt\text{-}P}$ = 2,390 Hz $^{1}J_{Pt\text{-}C}$ = 952 Hz
106	11.55 $^{1}J_{P\text{-}Pt}$ = 2,360 Hz $^{1}J_{P\text{-}C}$ = 14 Hz	−4,747 $^{1}J_{Pt\text{-}P}$ = 2,350 Hz $^{1}J_{Pt\text{-}C}$ = 959 Hz
63	12.08 $^{1}J_{P\text{-}Pt}$ = 2,364 Hz	−4,721 $^{1}J_{Pt\text{-}P}$ = 2,356 Hz
112	61.91 $^{1}J_{P\text{-}Pt}$ = 2,231 Hz	−4,891 $^{1}J_{Pt\text{-}P}$ = 2,220 Hz
115	12.46 $^{1}J_{P\text{-}Pt}$ = 2,283 Hz	−4,742 $^{1}J_{Pt\text{-}P}$ = 2,281 Hz

Table 3-2. Heteronuclear NMR spectroscopic data ($^{31}P\{^{1}H\}$ and $^{195}Pt\{^{1}H\}$) for platinum *bis*-*σ*-alkynyl species reported in Section 3.2.1.

Spectroscopically, all of the six reported platinum *bis*(phosphine) *bis*-*σ*-alkynyl systems can be observed *via* $^{31}P\{^{1}H\}$ NMR spectroscopy with $^{1}J_{P\text{-}Pt}$ coupling constants that can be verified by $^{195}Pt\{^{1}H\}$ NMR spectra of the compounds ($^{1}J_{Pt\text{-}P}$). The $^{195}Pt\{^{1}H\}$ NMR spectroscopic data for compounds **95**, **102**, and **106** not only displayed simple $^{1}J_{Pt\text{-}P}$ coupling, but also were able to show $^{1}J_{Pt\text{-}C}$ coupling and in one case $^{2}J_{Pt\text{-}C}$ coupling (**95**). $^{195}Pt\{^{1}H\}$ NMR spectroscopic findings for the values of the $^{1}J_{Pt\text{-}C}$ interactions were reported as 957 Hz (**95**), 952 Hz (**102**) and 959 Hz (**106**) and a $^{2}J_{Pt\text{-}C}$ coupling constant of 266 Hz (**95**). $^{13}C\{^{1}H\}$ NMR spectroscopy for the *trans*-platinum *bis*-*σ*-alkynyl systems revealed the *α*-carbon-platinum coupling constants ($^{1}J_{C\text{-}Pt}$) to be 961 Hz (**95**), 958 Hz (**102**), and 969 Hz (**106**) while the *β*-carbon-platinum coupling constants were found to be $^{2}J_{C\text{-}Pt}$ 270 Hz (**95**), 270 Hz (**102**) and 272 Hz (**106**) (Table 3-3). It should be noted that a decrease in $^{1}J_{Pt\text{-}P}$ and $^{1}J_{Pt\text{-}P}$ coupling constants would be expected for the *cis*-[Pt(C≡C-Ph)$_2$(DCPE)] (**112**) species; however, the coupling values remained relatively constant when compared to *trans*-[Pt(C≡C-Ph)$_2$(PEt$_3$)$_2$] (**95**). Literature review of similar *cis*-platinum *bis*(alkynyl) compounds bearing chelating bidentate phosphines confirmed this trend and the reported coupling constants for *cis*-[Pt(C≡C-Ph)$_2$(DCPE)] (**112**) were found to match with published results for *cis*-[Pt(C≡C-Ph)$_2$(DEPE)] ($^{1}J_{P\text{-}Pt}$ = 2,209 Hz and $^{1}J_{Pt\text{-}P}$ = 2,209 Hz) as reported by Wrackmeyer and coworkers (DEPE =

bis(diethylphosphino)ethane).[435] It should also be noted that ^{31}P-^{13}C coupling with the alkynyl carbon nuclei could also be detected in the $^{13}C\{^1H\}$ NMR spectra, showing interaction with both *α*- and *β*-carbon nuclei as well as the *ipso*- and *ortho*-carbon nuclei of the aryl substituents. Table 3-3 lists these resonances and their observed heteronuclear coupling values (*ipso*- and *ortho*-carbon coupling values were too poorly resolved to report accurately).

	$^{13}C_{\alpha}$ [ppm]	$^{1}J_{C\text{-}Pt}$ [Hz]	$^{2}J_{C\text{-}P}$ [Hz]	$^{13}C_{\beta}$ [ppm]	$^{2}J_{C\text{-}Pt}$ [Hz]	$^{3}J_{C\text{-}P}$ [Hz]
95	108.5	961	15	110.1	270	1.3
102	105.7	958	15	109.3	270	2.5
106	113.1	969	15	109.6	272	–

Table 3-3. Heteronuclear $^{13}C\{^1H\}$ NMR coupling data for C_{α} and C_{β} carbon interactions with ^{31}P and ^{195}Pt nuclei observed in the platinum *bis*-*σ*-alkynyl species reported in Section 3.2.1.

The X-ray data for *trans*-[Pt(C≡C-*p*-$C_6H_4CF_3$)$_2$(PEt_3)$_2$] (**106**) is difficult to use for data comparison due to the disorder present in the system from the trifluoromethyl groups; however, the data is presented along with data for species **102** and **63** to try to establish a trend for the substitution of the base *trans*-[Pt(C≡C-Ph)$_2$(PEt_3)$_2$] (**95**) compound. What is immediately apparent is that the functionalized ring systems *trans*-[Pt(C≡C-*p*-C_6H_4OMe)$_2$(PEt_3)$_2$] (**102**), *trans*-[Pt(C≡C-*p*-$C_6H_4CF_3$)$_2$(PEt_3)$_2$] (**106**), and *trans*-[Pt(C≡C-9-$C_{14}H_9$)$_2$(PEt_3)$_2$] (**63**) all display slightly elongated platinum-phosphorus bonds (2.305(1), 2.308 (avg.), and 2.293 (avg.) Å, respectively) compared to the base *trans*-[Pt(C≡C-Ph)$_2$(PEt_3)$_2$] (**95**) species (2.289(3) Å). Substitution of the *para*- position of the aryl systems seems to have very little effect upon the Pt(1)-C(1) and C(1)-C(2) bond distances as all four species essentially display equivalent bond distances. Structurally, *trans*-[Pt(C≡C-Ph)$_2$(PEt_3)$_2$] (**95**) and *trans*-[Pt(C≡C-9-$C_{14}H_9$)$_2$(PEt_3)$_2$] (**63**) display essentially the same C(2)-C(3) bond distances (1.43(1), and 1.438 (avg.) Å, respectively); however, the *trans*-[Pt(C≡C-*p*-C_6H_4OMe)$_2$(PEt_3)$_2$] (**102**) species displays a much longer bond distance of 1.468(6) Å indicating that the methoxy-functionalized aryl substituent has greatest effect upon the C(2) environment.

	95[421]	**102**	**106***	**63**†
Space Group	$P2_1/c$	$P\bar{1}$	$P\bar{1}$	$P\bar{1}$
Pt–P [Å]	2.289(3)	2.305(1)	2.308	2.293
Pt–C(1) [Å]	1.98(1)	2.000(9)	1.978	2.006
C(1)–C(2) [Å]	1.21(1)	1.20(1)	–	1.195
C(2)–C(3) [Å]	1.43(1)	1.468(6)	–	1.438

Table 3-4. Comparative X-ray structural data for the platinum *bis*-*σ*-alkynyl species *trans*-[Pt(C≡C-Ph)$_2$(PEt$_3$)$_2$] (**95**),[421] *trans*-[Pt(C≡C-*p*-C$_6$H$_4$OMe)$_2$(PEt$_3$)$_2$] (**102**), *trans*-[Pt(C≡C-*p*-C$_6$H$_4$CF$_3$)$_2$(PEt$_3$)$_2$] (**106**), and *trans*-[Pt(C≡C-9-C$_{14}$H$_9$)$_2$(PEt$_3$)$_2$] (**63**) reported in Section 3.2.1.

The UV-vis data for compounds *trans*-[Pt(C≡C-Ph)$_2$(PEt$_3$)$_2$] (**95**), *trans*-[Pt(C≡C-*p*-C$_6$H$_4$OMe)$_2$(PEt$_3$)$_2$] (**102**), and *trans*-[Pt(C≡C-*p*-C$_6$H$_4$CF$_3$)$_2$(PEt$_3$)$_2$] (**106**) were recorded (in hexane) for trend establishment of the absorption spectra with the addition of electron-donating (OMe) and electron-withdrawing (CF$_3$) substituents upon the *trans*-[Pt(C≡C-Ph)$_2$(PEt$_3$)$_2$] (**95**) scaffold. The data will also be used for comparison to the *trans*-platinum *bis*-*σ*-borirenyl species reported in Section 3.1.3. Unfortunately, due to the presence of spectral overtones resulting from the C-C triple bond stretches typical for this class of compounds, species *trans*-[Pt(C≡C-Ph)$_2$(PEt$_3$)$_2$] (**95**), *trans*-[Pt(C≡C-*p*-C$_6$H$_4$OMe)$_2$(PEt$_3$)$_2$] (**102**), and *trans*-[Pt(C≡C-*p*-C$_6$H$_4$CF$_3$)$_2$(PEt$_3$)$_2$] (**106**) all display three pseudo-maxima within their UV-vis absorption spectra. The presence of these triple-bond vibrational artifacts make discussion of the fine differences in the absorption maxima for all *bis*-*σ*-alkynyl precursors impossible and also renders trend establishment for the bathochromic and hypochromic influences of these substituents inaccurate for projection to the final *bis*-*σ*-borirenyl spectral profiles. As can be seen below in Figure 3-26 and Table 3-5, the absorption maxima are reported for the augmented *trans*-[Pt(C≡C-*p*-C$_6$H$_4$OMe)$_2$(PEt$_3$)$_2$] (**102**) and *trans*-[Pt(C≡C-*p*-C$_6$H$_4$CF$_3$)$_2$(PEt$_3$)$_2$] (**106**) variants of the *trans*-[Pt(C≡C-Ph)$_2$(PEt$_3$)$_2$] (**95**) scaffold.

* Structure is highly disordered and data is not reliable. The bond distances are averaged for trend establishment.
† Values are taken from an average for the two independent molecules in the asymmetric unit. The estimated standard deviations have subsequently been removed.

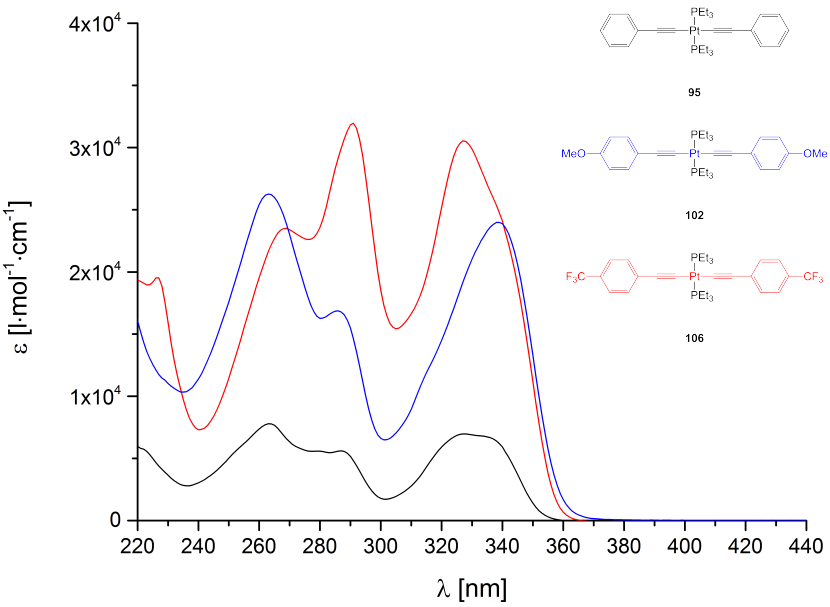

Figure 3-26. UV-vis absorption spectra of *trans*-platinum *bis*-*σ*-alkynyl species *trans*-[Pt(C≡C-Ph)$_2$(PEt$_3$)$_2$] (**95**, black), *trans*-[Pt(C≡C-*p*-C$_6$H$_4$OMe)$_2$(PEt$_3$)$_2$] (**102**, blue), and *trans*-[Pt(C≡C-*p*-C$_6$H$_4$CF$_3$)$_2$(PEt$_3$)$_2$] (**106**, red) as measured in hexane. Data is plotted as wavelength [λ] *vs.* extinction coefficient [ε].

	95 (ε)	**102 (ε)**	**105 (ε)**
λ [nm]	263 (7,790)	263 (26,260)	269 (23,510)
λ [nm]	287 (5,609)	286 (16,870)	291 (31,960)
λ [nm]	327 (6,969)	339 (23,980)	327 (30,540)

Table 3-5. UV-vis absorption maxima [λ] and extinction coefficients [ε] for the compounds *trans*-[Pt(C≡C-Ph)$_2$(PEt$_3$)$_2$] (**95**), *trans*-[Pt(C≡C-*p*-C$_6$H$_4$OMe)$_2$(PEt$_3$)$_2$] (**102**), and *trans*-[Pt(C≡C-*p*-C$_6$H$_4$CF$_3$)$_2$(PEt$_3$)$_2$] (**106**) in hexane solutions.

3.1.3 Borylene Transfer Reactions onto *trans*-Platinum *bis*-*σ*-Alkynyl Complexes

Borylene ligand transfer reactions were attempted for all platinum *bis*-*σ*-alkynyl complexes reported in Section 3.1.2. Although the synthesis of these species is possible under thermolytic conditions, the optimal route (highest yielding) for synthesis of these platinum *bis*-*σ*-borirenyl complexes was found to be photolytic transfer of the terminal borylene ligand from a group 6 transition metal pentacarbonyl scaffolds ([$(OC)_5M\{BN(SiMe_3)_2\}$], M = Cr (**13**), Mo (**14**), and W (**15**)) onto the platinum *bis*-*σ*-alkynyl precursors. Data accrued from the characterization of platinum *bis*-*σ*-borirenyl complexes was used to demonstrate the ability of the platinum linker in aiding the individual borirene units in becoming exocyclically delocalized and will be discussed at length in Section 3.1.3.5.

3.1.3.1 General Synthetic Routes and Considerations

Mechanistically, these borylene transfer reactions are thought to proceed according to the route outlined in Figure 3-27 in which the high *trans*-influence of the terminal borylene ligand is used to eject the *trans*-carbonyl in the complex [$(OC)_5M\{BN(SiMe_3)_2\}$] (**A**), freeing a ligand coordination site (**B**). This ejection of a carbonyl ligand is how the CO atmosphere is generated (combined with a small amount of inherent decomposition of [$(OC)_5M\{BN(SiMe_3)_2\}$], which can generate up to 5 equivalents of free carbon monoxide). Coordination of an alkyne to this open site (2 e^- π-donation to the metal center) is thought to occur (**C**) followed by a *cis*-/*trans*-isomerization to put the alkynyl species *cis*- to the terminal borylene ligand (**D**). Elimination of the coupled alkyne and borylene ligands results in formation of the borirene species which can dissociate through coordination of free carbon monoxide to the metal and formation of the independent transition metal *σ*-borirenyl complex (**E**). The final step is coordination of another equivalent of free carbon monoxide in solution to yield [$M(CO)_6$] as a poorly soluble byproduct, which precipitates out of solution.

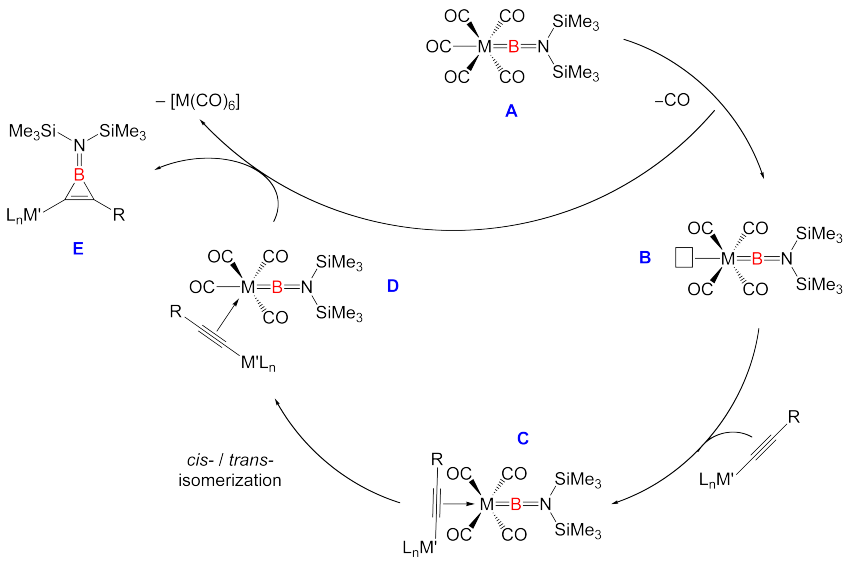

Figure 3-27. Generalized mechanism for the formation of a transition metal *σ*-borirenyl complex from photolytic irradiation of a group 6 pentacarbonyl terminal borylene complex and a transition metal *σ*-alkynyl complex.

All reactions reported in this section of the thesis were run with a minimum of 2.2 equivalents of the terminal borylene complex $[(OC)_5CrBN(SiMe_3)_2]$ (**13**) to ensure full conversion to the platinum *bis*-*σ*-borirenyl products (and at a faster rate). Excesses of borylene ligand will not affect the purification of the products as the unreacted borylene complex along with the $[Cr(CO)_6]$ byproduct can readily be sublimed out of the dried reaction solids. It should also be noted that over-irradiation of the sample will decompose the platinum *bis*-*σ*-borirenyl product. Maximum irradiation times for these reactions should be no longer than 12 h and high ratios (greater than 2.2 eq.) of $[(OC)_5Cr\{BN(SiMe_3)_2\}]$ (**13**) compared to the platinum *bis*-*σ*-alkynyl precursor allow for faster conversion rates before product decomposition becomes too severe. Also, as the product decomposes because of over-irradiation, the reaction mixture becomes increasingly cloudy (formation of chromium black) and the rate of photolytic transfer decays as a consequence. Pale yellow benzene or hexane solutions of $[(OC)_5Cr\{BN(SiMe_3)_2\}]$ (**13**) were irradiated in the presence of the platinum *bis*-*σ*-alkynyl precursors for approximately 8 h at room temperature, resulting in the formation of dark brown solutions of the *bis*-*σ*-borirenyl platinum complexes. Progress and completion of the reactions were ascertained by $^{31}P\{^1H\}$ and $^{11}B\{^1H\}$ NMR spectroscopic measurements of the crude reaction mixtures.

Once consumption of the platinum *bis*-*σ*-alkynyl precursor and mono *σ*-borirenyl intermediate had been confirmed *via* $^{31}P\{^1H\}$ NMR spectroscopy, photolytic irradiation of the samples was typically halted and the crude mixtures were purified

by solvent removal *in vacuo* and sublimation of unreacted [$(OC)_5CrBN(SiMe_3)_2$] (**13**) and the [$Cr(CO)_6$] byproduct. If the samples are left to rest overnight, crystallization of [$Cr(CO)_6$] out of solution will occur, making workup easier. The reaction crude (yellow/brown solids) was chromatographed over pacified silica gel[397] and dried *in vacuo* to yield the air- and moisture-sensitive platinum *bis*-σ-borirenyl complexes as yellow solids. It is important to note that the platinum *bis*-σ-borirenyl species are only stable on pacified silica gel and will readily decompose upon exposure to regular silica gel as well as Al_2O_3.

3.1.3.2 *trans*-[Pt{(μ-{B=N($SiMe_3$)$_2$}C=C)-Ph}$_2$(PEt_3)$_2$] (119/120)

trans-[Pt{(μ-{B=N($SiMe_3$)$_2$}C=C)-Ph}$_2$(PEt_3)$_2$] (**119**/**120**) was prepared by modification to the literature procedure previously outlined in Section 3.1.3.1 and in the introduction of Dr. Qing Ye's doctoral[436] work * in which *trans*-[$Pt(C{\equiv}C\text{-}Ph)_2(PEt_3)_2$] (**95**) is mixed with [$(OC)_5Cr\{BN(SiMe_3)_2\}$] (**13**) (2.2 eq. minimum) in benzene solution (Figure 3-28). The reaction is irradiated photolytically for 8 h at room temperature during which full consumption of [$(OC)_5Cr\{BN(SiMe_3)_2\}$] (**13**) is witnessed *via* $^{11}B\{^1H\}$ NMR spectroscopy ($^{11}B\{^1H\}$: δ = 92.5 ppm) with formation of the *trans*-platinum mono-σ-borirenyl and *bis*-σ-borirenyl products (the resonances appear as overlapping signals at approximately $^{11}B\{^1H\}$: δ = ~35 ppm). $^{31}P\{^1H\}$ NMR spectroscopic monitoring of the reaction mixture shows consumption of *trans*-[$Pt(C{\equiv}C\text{-}Ph)_2(PEt_3)_2$] (**95**) ($^{31}P\{^1H\}$: δ = 10.7 ppm, $^1J_{P\text{-}Pt}$ = 2,387 Hz) with formation of the *trans*-platinum mono-σ-borirenyl species *trans*-[Pt(C≡C-Ph){(μ-{B=N($SiMe_3$)$_2$}C=C)-Ph}(PEt_3)$_2$] (**118**) ($^{31}P\{^1H\}$: δ = 9.9 ppm, $^1J_{P\text{-}Pt}$ = 2,593 Hz) firstly (not isolated), and formation of the *trans*-platinum *bis*-σ-borirenyl species *trans*-[Pt{(μ-{B=N($SiMe_3$)$_2$}C=C)-Ph}$_2$(PEt_3)$_2$] (**119**/**120**) ($^{31}P\{^1H\}$: δ = 5.9 and 5.9 ppm respectively, $^1J_{P\text{-}Pt}$ = 2,765 and 2,762 Hz respectively) secondly (Figure 3-28). The resulting dark yellow reaction mixture was purified *via* pacified silica gel (SiO_2) column chromatography[397] to yield the *trans*-platinum *bis*-σ-borirenyl species *trans*-[Pt{(μ-{B=N($SiMe_3$)$_2$}C=C)-Ph}$_2$(PEt_3)$_2$] (**119**/**120**) as air-sensitive light yellow solids in 39% yield. Differential thermal analysis of these light yellow crystalline solids showed a melting point for *trans*-[Pt{(μ-{B=N($SiMe_3$)$_2$}C=C)-Ph}$_2$(PEt_3)$_2$] (**119**/**120**) at 165 °C with thermal decomposition at temperatures in excess of 282 °C.

* See the thesis of Dr. Qing Ye, Chapter 2.1 (pages 23-54) and Chapter 3 (pages 111-119) for the synthesis and characterization of platinum and iron mono-σ-borirenyl complexes.

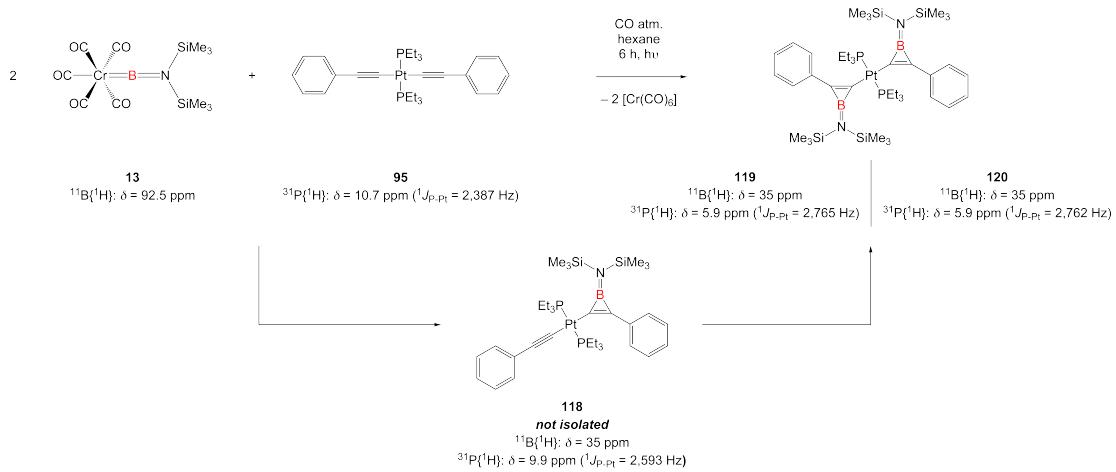

Figure 3-28. *trans*-[Pt{(*μ*-{B=N(SiMe$_3$)$_2$}C=C)-Ph}$_2$(PEt$_3$)$_2$] (**119**/**120**) synthesis from *trans*-[Pt(C≡C-Ph)$_2$(PEt$_3$)$_2$] (**95**) with the non-isolated intermediate *trans*-[Pt(C≡C-Ph){(*μ*-{B=N(SiMe$_3$)$_2$}C=C)-Ph}(PEt$_3$)$_2$] (**118**).*

After the successful synthesis of *trans*-[Pt{(*μ*-{B=N(SiMe$_3$)$_2$}C=C)-Ph}$_2$(PEt$_3$)$_2$] (**119**/**120**), analysis of the spectroscopic data revealed two sets of resonances corresponding to the purified compound. The twin sets of data were detected in ^{1}H, ^{13}C, ^{29}Si, ^{31}P, and ^{195}Pt NMR spectra and were presumed to correlate to different *syn*- and *anti*- conformations of the *trans*-platinum *bis*-*σ*-borirenyl arms relative to each other across the platinum core. The ^{31}P{^{1}H} NMR data recorded for *trans*-[Pt{(*μ*-{B=N(SiMe$_3$)$_2$}C=C)-Ph}$_2$(PEt$_3$)$_2$] (**119**/**120**) show two sets of singlets (^{31}P{^{1}H}: δ = 5.9 and 5.9 ppm, respectively) with prominent ^{195}Pt (I = ½, 33.8% natural abundance) satellites of relatively equal $^{1}J_{P\text{-}Pt}$ coupling values ($^{1}J_{P\text{-}Pt}$ = 2,765 and 2,762 Hz respectively). The ^{195}Pt{^{1}H} spectra also verified this signal duality (^{195}Pt{^{1}H}: δ = −4,108 and −4,110 ppm respectively) and again showed relatively equal $^{1}J_{Pt\text{-}P}$ coupling constant values between the two resolved, distinct triplet resonances ($^{1}J_{Pt\text{-}P}$ = 2,751 and 2,759 Hz respectively) (Figure 3-29). The presence of two species in solution (*syn*-/*anti*- conformations) is the reason that two different compound numbers are given for the species **119**/**120** as it is unclear which conformer correlates to which specific set of NMR resonances.

The NMR spectroscopic data (^{1}H, ^{13}C{^{1}H}, and ^{29}Si{^{1}H}) for the trimethylsilyl moiety environments also displayed this signal duality. ^{13}C-^{1}H 2D correlation spectra (^{13}C-^{1}H HSQC and HMBC) showed two distinct trimethylsilyl carbon environments appearing at 4.05 ppm and 4.02 ppm that correlated to ^{1}H NMR resonances for protons appearing at 0.603 ppm and 0.574 ppm, respectively (18H for each

* NMR spectroscopic data taken directly from reaction mixtures: ^{31}P{^{1}H} NMR (161.98 MHz, benzene, H_3PO_4, 297 K).

resonance). $^{29}Si\{^{1}H\}$ NMR spectra also showed two distinct resonances appearing at 5.46 ppm and 5.35 ppm (Figure 3-29). The only NMR spectra that did not display this duality of signals were the $^{11}B\{^{1}H\}$ spectra, however, data for *trans*-[Pt{(μ-{B=N(SiMe$_3$)$_2$}C=C)-Ph}$_2$(PEt$_3$)$_2$] (**119**/**120**) showed such broad resonances that overlap of multiple signals could not be disregarded. Interpretation of this data was clearly indicative of two distinct species existing in solution during the NMR characterization studies of *trans*-[Pt{(μ-{B=N(SiMe$_3$)$_2$}C=C)-Ph}$_2$(PEt$_3$)$_2$] (**119**/**120**).

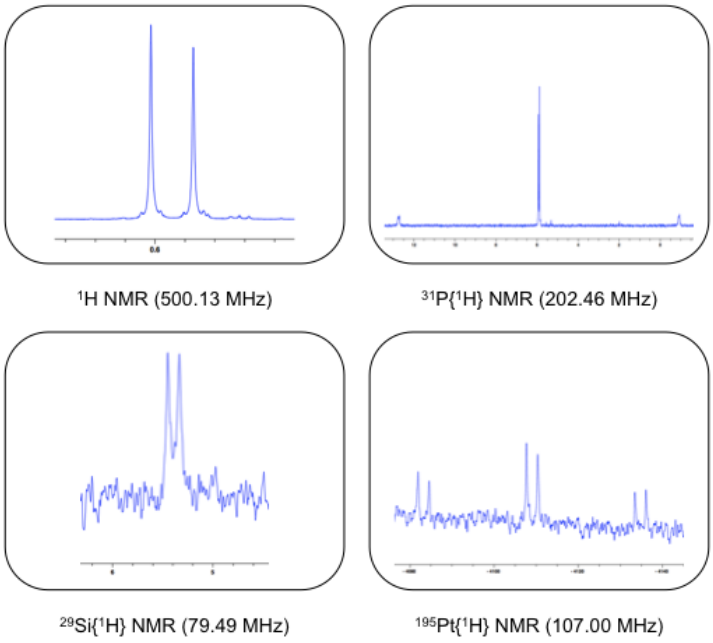

Figure 3-29. *trans*-[Pt{(μ-{B=N(SiMe$_3$)$_2$}C=C)-Ph}$_2$(PEt$_3$)$_2$] (**119**/**120**) NMR resonance duality observed in ^{1}H, $^{29}Si\{^{1}H\}$, $^{31}P\{^{1}H\}$ and $^{195}Pt\{^{1}H\}$ spectra.*

The duality of these ^{1}H, $^{13}C\{^{1}H\}$, $^{29}Si\{^{1}H\}$, $^{31}P\{^{1}H\}$, and $^{195}Pt\{^{1}H\}$ NMR resonances for pure samples of *trans*-[Pt{(μ-{B=N(SiMe$_3$)$_2$}C=C)-Ph}$_2$(PEt$_3$)$_2$] (**119**/**120**) indicates that a rotational barrier exists between the platinum core and the borirene arms in the periphery of the molecule. This rotational barrier results in two conformational isomers (*syn*- and *anti*- conformations) of the borirene-platinum-borirene system; either both being held on one side of the PtX_2L_2 plane, or a staggered conformation across this plane. The hindrance of bond rotation within this *trans*-[Pt{(μ-{B=N(SiMe$_3$)$_2$}C=C)-Ph}$_2$(PEt$_3$)$_2$] (**119**/**120**) system was hypothesized to result from two different kinds of interactions of the platinum *bis*(phosphine) core with the σ-borirenyl moieties. The pseudo-hindered rotation could be due to: (A) steric

* NMR spectroscopic data taken directly from reaction mixtures: $^{31}P\{^{1}H\}$ NMR (161.98 MHz, benzene, H_3PO_4, 297 K).

encumbrance exerted by the phosphine ligands, or (B) strong electronic conjugation between the platinum core and the twin borirene aromatic systems.

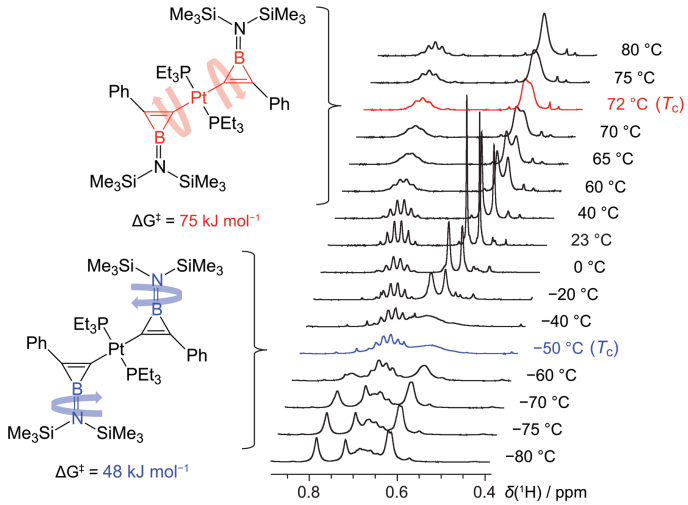

Figure 3-30. VT-NMR data of *trans*-[Pt{(μ-{B=N(SiMe$_3$)$_2$}C=C)-Ph}$_2$(PEt$_3$)$_2$] (**119**/**120**) showcasing the coalescence temperatures (T_C) of the Pt-C$_\alpha$ bond (red) and the B-N bond (blue).

$$\Delta G^{\ddagger} = 19.13 T_c \left(9.97 + \log \frac{T_c}{\delta \nu}\right) [\mathrm{Jmol}^{-1}]$$

Equation 3-1. Equation used to calculate the rotational energetic barriers (ΔG)* for the Pt-C$_\alpha$ and B-N bonds.[437]

Variable-temperature (VT) ^{1}H NMR spectroscopic data (Figure 3-30) for *trans*-[Pt{(μ-{B=N(SiMe$_3$)$_2$}C=C)-Ph}$_2$(PEt$_3$)$_2$] (**119**/**120**) yielded two separate coalescence temperatures (T_C = −50 °C and 72 °C) corresponding to two different rotational barriers of the molecule. These temperatures can be assigned to the rotational energy barriers for the B-N and Pt-C bonds, respectively. As can be seen in Figure 3-30, the upper rotational barrier (red spectra and rotational arrows) is demonstrated by the coalescence of the two independent trimethylsilyl signals into one broad singlet at 72 °C (ΔG‡ = 75 kJ/mol as calculated by Equation 3-1).[437] The lower thermal rotational barrier (blue spectra and rotational arrows) at −50 °C (ΔG‡ = 48 kJ/mol as calculated by Equation 3-1)[437] is in agreement with published data from Dr. Qing Ye's study of a platinum monoborirene species.[295,436] Data published from the study shows a VT-NMR coalescence temperature (T_C) of −55 °C (ΔG‡ = 45 kJ/mol as calculated by Equation 3-1)[437] that was also linked to the rotational energy barrier around the B-N bond.[295] Figure 3-30 shows the full VT ^{1}H NMR study (from −80 °C to 80 °C) of

* Where T_C in the coalescence temperature (K) and $\delta\nu$ is the difference in NMR resonances (Hz) at room temperature (r.t.).

trans-[Pt{(μ-{B=N(SiMe$_3$)$_2$}C=C)-Ph}$_2$(PEt$_3$)$_2$] (**119**/**120**). Structurally, the temperature-dependent rotation (or rotational hindrance) of the borirenyl and trimethylsilylamino- elements of the molecule can be explained by observation of four signals corresponding to the four different trimethylsilyl environments at low temperatures (below –50 °C). As seen in Figure 3-31, these four distinct trimethylsilyl environments corresponding to the freezing of both B-N and Pt-C bond rotations can be observed as four peaks in the ^{29}Si-^{1}H heteronuclear correlation NMR spectrum of the complex at –80 °C (two of the peaks almost overlap each other and integrate for 2:1 equivalents compared to the other two smaller peaks). Warming of this system to room temperature compromises the B-N rotational energetic barrier to yield two signals corresponding to two different trimethylsilyl environments as would be expected by the *syn*- and *anti*- conformations for the borirenyl moieties across the platinum core (matching the experimentally observed dual resonances in ^{13}C{^{1}H}, ^{31}P{^{1}H}, and ^{195}Pt{^{1}H} NMR spectra for the complex recorded at room temperature). Finally, high temperature studies (> 72 °C) of the system led to coalescence of the two signals into one broad resonance which corresponds to both rotational energetic barriers becoming compromised and both temperature dependent rotations becoming NMR indiscernible.

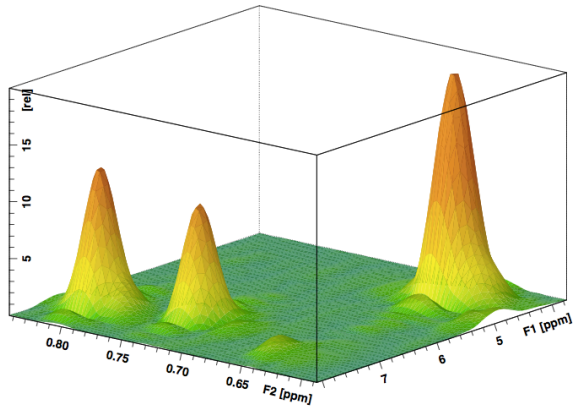

Figure 3-31. Two-dimensional correlation NMR (^{1}H-^{29}Si) spectrum acquired for *trans*-[Pt{(μ-{B=N(SiMe$_3$)$_2$}C=C)-Ph}$_2$(PEt$_3$)$_2$] (**119**/**120**) below the –50 °C rotational barrier witnessing four independent trimethylsilyl signals (two have a significant overlap but are still distinguishable).

As previously stated, the Pt-C rotational barrier was hypothesized to be due to: (A) steric encumbrance exerted by the phosphine ligands, or (B) strong electronic conjugation between the platinum core and the twin borirene aromatic systems. To probe the degree of steric encumbrance exerted by the phosphine ligands in *trans*-[Pt{(μ-{B=N(SiMe$_3$)$_2$}C=C)-Ph}$_2$(PEt$_3$)$_2$] (**119**/**120**), NOESY and ROESY experiments

were performed on the complex in an effort to detect any steric interaction between the ancillary protons of the triethylphosphine arms and the trimethylsilyl arms. Both NOESY and ROESY NMR spectroscopic experiments (performed in several solvents and with a variety of mixing times) failed to show any discernable interactions between these two proton environments in the complex *trans*-[Pt{(μ-{B=N(SiMe$_3$)$_2$}C=C)-Ph}$_2$(PEt$_3$)$_2$] (**119**/**120**). This evidence suggests that the high rotational energy barrier observed could be primarily due to an electronic interaction between the ligand and the platinum core rather than any steric hindrance from the phosphines. Discussion of this electronic interaction of the platinum core with the borirenyl moieties will be performed in Section 3.1.3.5.

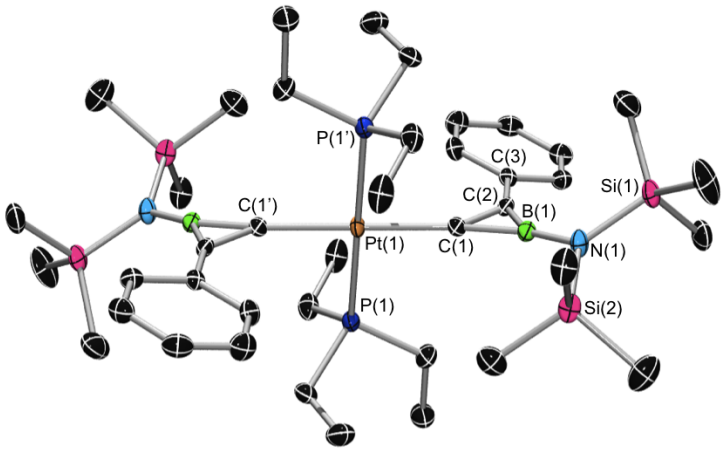

Figure 3-32. ORTEP-rendered structure of *trans*-[Pt{(μ-{B=N(SiMe$_3$)$_2$}C=C)-Ph}$_2$(PEt$_3$)$_2$] (**119**/**120**). Thermal ellipsoids set at 50% probability. All hydrogen atoms have been omitted for clarity. Selected bond distances (Å) and angles (°): Pt(1)–P(1) 2.2872(7), Pt(1)–C(1) 2.046(4), C(1)–C(2) 1.373(6), C(2)–C(3) 1.480(6), C(1)–B(1) 1.505(6), C(2)–B(1) 1.454(6), B(1)–N(1) 1.451(4), P(1)–Pt(1)–P(1) 180.00(3), C(1)–Pt(1)–C(1) 180.0(1), P(1)–Pt(1)–C(1) 93.7(1), Pt(1)–C(1)–C(2) 139.6(3), C(1)–C(2)–C(3) 134.7(4).

Crystals suitable for X-ray diffraction were grown from saturated solutions of **119**/**120** in hexamethyldisiloxane (HMDS). An ORTEP diagram for the structure* as well as some key bond distances are shown in Figure 3-32. The *trans*-[Pt{(μ-{B=N(SiMe$_3$)$_2$}C=C)-Ph}$_2$(PEt$_3$)$_2$] (**119**/**120**) species (with comparable bond distances from *trans*-[Pt(C≡C-Ph)$_2$(PEt$_3$)$_2$] (**95**) shown in brackets) displays Pt-C(1), C(1)-C(2), and C(2)-C(3) bond distances of 2.046(4) [1.98(1)], 1.373(6) [1.21(1)], and 1.480(6) [1.43(1)] Å, respectively. This data for the C(1)-C(2), C(1)-B(1), and C(2)-B(1) bond distances (1.373(6), 1.505(6) and 1.454(6) Å, respectively) are comparable† to

* $C_{40}H_{76}B_2N_2P_2PtSi_4$, M = 976.04, triclinic, space group = P–1.
† $C_{20}H_{41}BClNP_2PtSi_2$, M = 655.01, monoclinic, space group = $P2_1/c$. The structure has two independent molecules in the asymmetric unit, which feature very similar structures.

the distances listed from the *trans*-[PtCl{(μ-{BN(SiMe$_3$)$_2$}C=C)-Ph}(PMe$_3$)$_2$] (**88**) species reported by our group in 2009[295] (1.374(7), 1.511(8) and 1.482(8) Å respectively) and the values for the C(1)-C(2) bond distance are similar to these expected for a C-C double bond.

3.1.3.3 *trans*-[Pt{(μ-{B=N(SiMe$_3$)$_2$}C=C)-*p*-C$_6$H$_4$OMe}$_2$(PEt$_3$)$_2$] (122/123)

trans-[Pt{(μ-{B=N(SiMe$_3$)$_2$}C=C)-*p*-C$_6$H$_4$OMe}$_2$(PEt$_3$)$_2$] (**122**/**123**) was prepared by modification to the literature procedure previously outlined in Section 3.1.3.1 and in the doctoral thesis of Dr. Qing Ye* in which *trans*-[Pt(C≡C-*p*-C$_6$H$_4$OMe)$_2$(PEt$_3$)$_2$] (**102**) is mixed with [(OC)$_5$Cr{BN(SiMe$_3$)$_2$}] (**13**) (2.2 eq. minimum) in hexane solution (Figure 3-33). The reaction was irradiated for 8 h at room temperature during which time full consumption of [(OC)$_5$Cr{BN(SiMe$_3$)$_2$}] (**13**) was witnessed *via* ^{11}B{^{1}H} NMR spectroscopy (^{11}B{^{1}H}: δ = 92.3 ppm) with formation of the mono-σ-borirenyl and *bis*-σ-borirenyl product resonances appearing as overlapping signals at approximately ^{11}B{^{1}H}: δ = ~33 ppm. ^{31}P{^{1}H} NMR spectroscopic monitoring of the reaction mixture shows consumption of *trans*-[Pt(C≡C-*p*-C$_6$H$_4$OMe)$_2$(PEt$_3$)$_2$] (**102**) (^{31}P{^{1}H}: δ = 11.3 ppm, $^1J_{P\text{-}Pt}$ = 2,424 Hz) with formation of the mono-σ-borirenyl species *trans*-[Pt(C≡C-*p*-C$_6$H$_4$OMe){(μ-{B=N(SiMe$_3$)$_2$}C=C)-*p*-C$_6$H$_4$OMe}(PEt$_3$)$_2$] (**121**) (^{31}P{^{1}H}: δ = 9.7 ppm, $^1J_{P\text{-}Pt}$ = 2,622 Hz) firstly (not isolated), and formation of the *trans*-platinum *bis*-σ-borirenyl species *trans*-[Pt{(μ-{B=N(SiMe$_3$)$_2$}C=C)-*p*-C$_6$H$_4$OMe}$_2$(PEt$_3$)$_2$] (**122**/**123**) (^{31}P{^{1}H}: δ = 5.5 ppm and 5.4 ppm, $^1J_{P\text{-}Pt}$ = 2,791 and 2,788 Hz respectively) secondly (Figure 3-33). Purification of the reaction mixture was performed by removal of all volatiles *in vacuo* and sublimation of all unreacted borylene and [Cr(CO)$_6$] byproduct by heating to 65 °C. The resulting dark yellow reaction mixture was purified *via* pacified silica gel (SiO$_2$) column chromatography[397] to yield the *trans*-platinum *bis*-σ-borirenyl species *trans*-[Pt{(μ-{B=N(SiMe$_3$)$_2$}C=C)-*p*-C$_6$H$_4$OMe}$_2$(PEt$_3$)$_2$] (**122**/**123**) as air-sensitive light yellow solids in 45% yield.

* See the thesis of Dr. Qing Ye, Chapter 2.1 (pages 23-54) and Chapter 3 (pages 111-119) for the synthesis and characterization of platinum and iron mono-σ-borirenyl complexes.

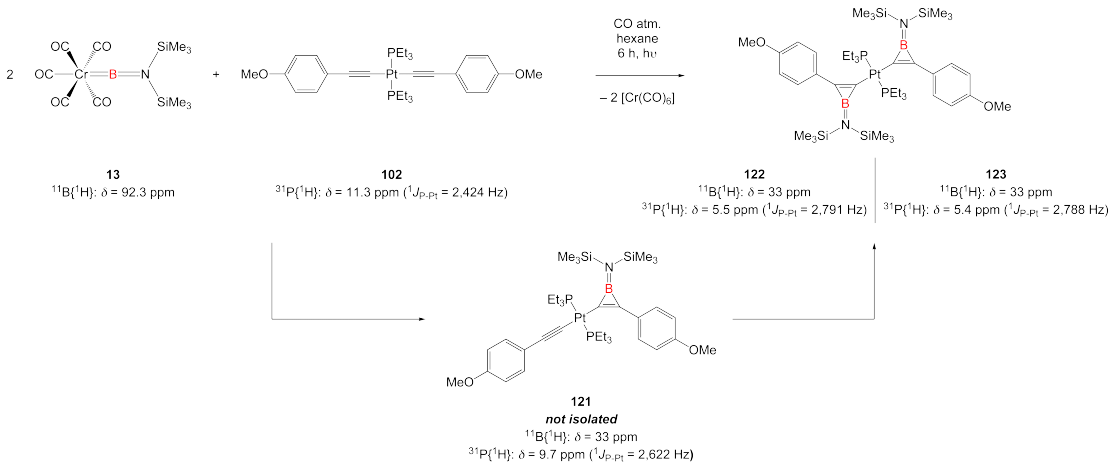

Figure 3-33. *trans*-[Pt{(μ-{B=N(SiMe$_3$)$_2$}C=C)-*p*-C$_6$H$_4$OMe}$_2$(PEt$_3$)$_2$] (**122**/**123**) synthesis from *trans*-[Pt(C≡C-*p*-C$_6$H$_4$OMe)$_2$(PEt$_3$)$_2$] (**102**) with the non-isolated intermediate **121**.*

The *trans*-[Pt{(μ-{B=N(SiMe$_3$)$_2$}C=C)-*p*-C$_6$H$_4$OMe}$_2$(PEt$_3$)$_2$] (**122**/**123**) product is witnessed *via* ^{195}Pt{^{1}H} NMR spectroscopy as dual sets of triplets appearing at –4,110 ppm and –4,111 ppm ($^1J_{Pt\text{-}P}$ = 2,755 and 2,763 Hz respectively). Crystals suitable for X-ray diffraction were grown from saturated solutions of **122**/**123** in hexamethyldisiloxane (HMDS). An ORTEP diagram for the structure† as well as some key bond distances are shown in Figure 3-34. The *trans*-[Pt{(μ-{B=N(SiMe$_3$)$_2$}C=C)-*p*-C$_6$H$_4$OMe}$_2$(PEt$_3$)$_2$] (**122**/**123**) species (with comparable bond distances from *trans*-[Pt(C≡C-*p*-C$_6$H$_4$OMe)$_2$(PEt$_3$)$_2$] (**102**) shown in brackets) displays Pt-C(1), C(1)-C(2), and C(2)-C(3) bond distances of 2.076(3) [2.000(9)], 1.384(4) [1.20(1)], and 1.476(4) [1.468(6)] Å respectively. The bond distances for the C(1)-B(1) and C(2)-B(1) bond distances were found to be 1.522(4) and 1.481(4) Å respectively and will be discussed in greater detail in Section 3.1.3.5.

* NMR spectroscopic data taken directly from reaction mixtures: ^{31}P{^{1}H} NMR (161.98 MHz, benzene, H$_3$PO$_4$, 297 K).
† C$_{42}$H$_{80}$B$_2$N$_2$O$_2$P$_2$PtSi$_4$, *M* = 1,036.09, triclinic, space group = *P*–1.

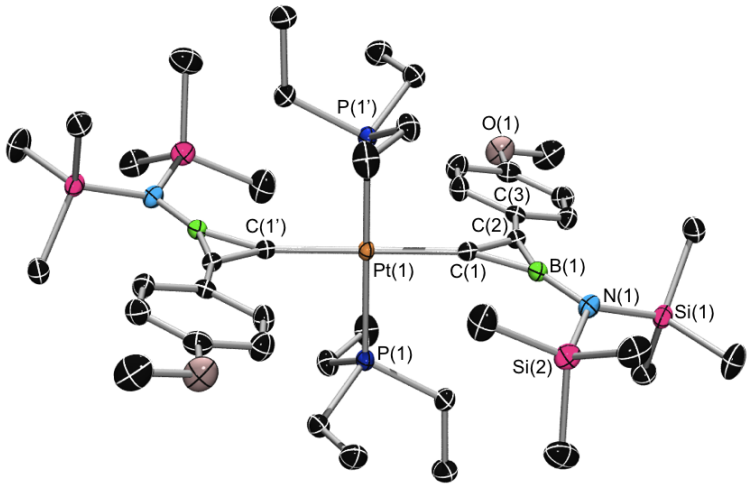

Figure 3-34. ORTEP-rendered structure of *trans*-[Pt{(μ-{B=N(SiMe$_3$)$_2$}C=C)-*p*-C$_6$H$_4$OMe}$_2$(PEt$_3$)$_2$] (**122**/**123**). Thermal ellipsoids set at 50% probability. All hydrogen atoms have been omitted for clarity. Selected bond distances (Å) and angles (°): Pt(1)–P(1) 2.314(1), Pt(1)–C(1) 2.076(3), C(1)–C(2) 1.384(4), C(2)–C(3) 1.476(4), C(1)–B(1) 1.522(4), C(2)–B(1) 1.481(4), B(1)–N(1) 1.459(4), P(1)–Pt(1)–P(1) 180.00(2), C(1)–Pt(1)–C(1) 180.0(1), P(1)–Pt(1)–C(1) 90.41(7), Pt(1)–C(1)–C(2) 138.0(2), C(1)–C(2)–C(3) 133.1(2).

3.1.3.4 *trans*-[Pt{(μ-{B=N(SiMe$_3$)$_2$}C=C)-*p*-C$_6$H$_4$CF$_3$}$_2$(PEt$_3$)$_2$] (125/126)

trans-[Pt{(μ-{B=N(SiMe$_3$)$_2$}C=C)-*p*-C$_6$H$_4$CF$_3$}$_2$(PEt$_3$)$_2$] (**125**/**126**) was prepared by modification to the literature procedure previously outlined in Section 3.1.3.1 and in the doctoral thesis of Dr. Qing Ye* in which *trans*-[Pt(C≡C-*p*-C$_6$H$_4$CF$_3$)$_2$(PEt$_3$)$_2$] (**106**) is mixed with [(OC)$_5$Cr{BN(SiMe$_3$)$_2$}] (**13**) (2.2 eq. minimum) in hexane solution (Figure 3-35). The reaction was irradiated for 8 h at room temperature during which time full consumption of [(OC)$_5$Cr{BN(SiMe$_3$)$_2$}] (**13**) was witnessed *via* ^{11}B{^{1}H} NMR spectroscopy (^{11}B{^{1}H}: δ = 92.8 ppm) with formation of the mono-σ-borirenyl and *bis*-σ-borirenyl product resonances appearing as overlapping signals at approximately ^{11}B{^{1}H}: δ = ~35 ppm. ^{31}P{^{1}H} NMR spectroscopic monitoring of the reaction mixture shows consumption of *trans*-[Pt(C≡C-*p*-C$_6$H$_4$CF$_3$)$_2$(PEt$_3$)$_2$] (**106**) (^{31}P{^{1}H}: δ = 11.3 ppm, $^1J_{P\text{-}Pt}$ = 2375 Hz) with formation of the mono-σ-borirenyl species *trans*-[Pt(C≡C-*p*-C$_6$H$_4$CF$_3$){(μ-{B=N(SiMe$_3$)$_2$}C=C)-*p*-C$_6$H$_4$CF$_3$}(PEt$_3$)$_2$] (**124**) (^{31}P{^{1}H}: δ = 9.8 ppm, $^1J_{P\text{-}Pt}$ = 2,618 Hz) firstly (not isolated), and formation of the *trans*-platinum *bis*-σ-borirenyl species *trans*-[Pt{(μ-{B=N(SiMe$_3$)$_2$}C=C)-*p*-C$_6$H$_4$CF$_3$}$_2$(PEt$_3$)$_2$] (**125**/**126**) (^{31}P{^{1}H}: δ = 6.1 ppm and 5.7 ppm, $^1J_{P\text{-}Pt}$ = 2,776 and 2,765 Hz respectively) secondly (Figure 3-35). Purification of the reaction mixture was performed by removal of all volatiles *in vacuo* and sublimation of all unreacted

* See the thesis of Dr. Qing Ye, Chapter 2.1 (pages 23-54) and Chapter 3 (pages 111-119) for the synthesis and characterization of platinum and iron mono-σ-borirenyl complexes.

borylene and [Cr(CO)$_6$] byproduct by heating to 65 °C. The resulting dark yellow reaction mixture was purified *via* pacified silica gel (SiO_2) column chromatography[397] to yield the *trans*-platinum *bis*-σ-borirenyl species *trans*-[Pt{(μ-{B=N(SiMe$_3$)$_2$}C=C)-*p*-C$_6$H$_4$CF$_3$}$_2$(PEt$_3$)$_2$] (**125/126**) as air-sensitive light yellow solids in 63 % yield.

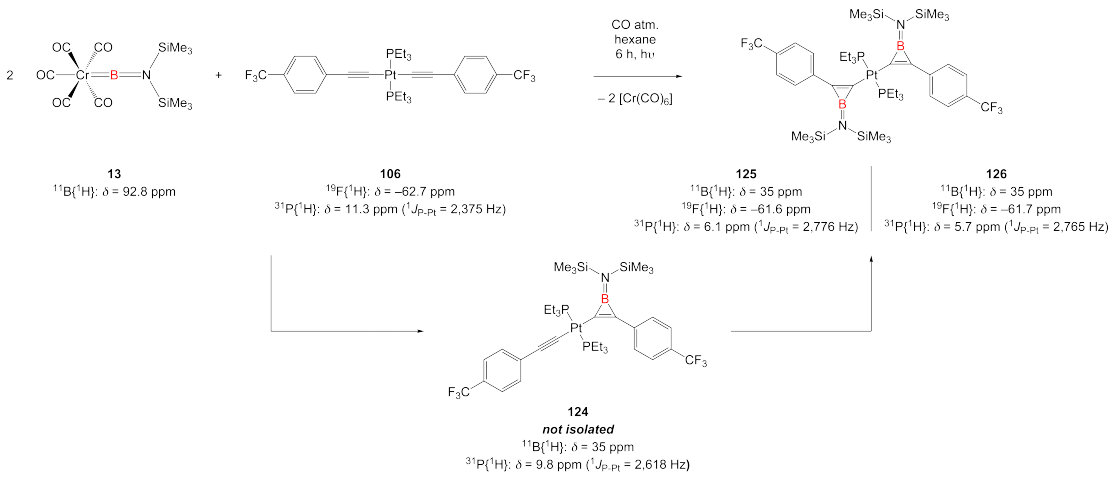

Figure 3-35. *trans*-[Pt{(μ-{B=N(SiMe$_3$)$_2$}C=C)-*p*-C$_6$H$_4$CF$_3$}$_2$(PEt$_3$)$_2$] (**125/126**) synthesis from *trans*-[Pt(C≡C-*p*-C$_6$H$_4$CF$_3$)$_2$(PEt$_3$)$_2$] (**106**) with the non-isolated intermediate **124**.*

The *trans*-[Pt{(μ-{B=N(SiMe$_3$)$_2$}C=C)-*p*-C$_6$H$_4$CF$_3$}$_2$(PEt$_3$)$_2$] (**125/126**) product is witnessed *via* ^{195}Pt{^{1}H} NMR spectroscopy as dual sets of triplets appearing at –4,100 ppm and –4,111 ppm ($^1J_{Pt\text{-}P}$ = 2,719 and 2,737 Hz respectively). Crystals suitable for X-ray diffraction were grown from saturated solutions of **125/126** in hexamethyldisiloxane (HMDS). An ORTEP diagram for the structure† is shown in Figure 3-36, however, as with the *trans*-[Pt(C≡C-*p*-C$_6$H$_4$CF$_3$)$_2$(PEt$_3$)$_2$] (**106**) species, the presence of two trifluoromethyl groups on the periphery of the complex make the structure highly disordered and the bond distances could not be accurately compared to similar species.

* NMR spectroscopic data taken directly from reaction mixtures: ^{31}P{^{1}H} NMR (161.98 MHz, benzene, H_3PO_4, 297 K).
† $C_{42}H_{74}B_2F_6N_2P_2PtSi_4$, *M* = 1,112.04, monoclinic, space group = *Cc*.

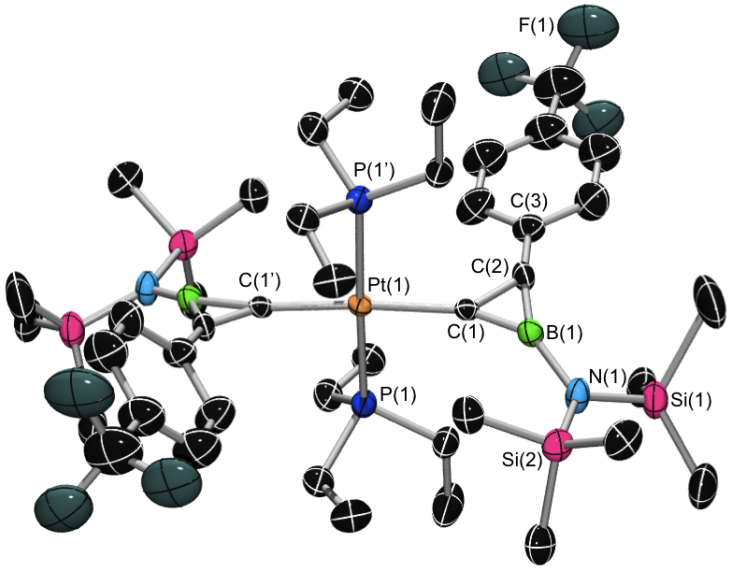

Figure 3-36. ORTEP-rendered structure of *trans*-[Pt{(μ-{B=N(SiMe$_3$)$_2$}C=C)-*p*-C$_6$H$_4$CF$_3$}$_2$(PEt$_3$)$_2$] (**125**/**126**). Thermal ellipsoids set at 50% probability. All hydrogen atoms have been omitted for clarity.

3.1.3.5 Discussion and Theory

As previously stated, the NMR spectra for all compounds reported in Section 3.1.3: (*trans*-[Pt{(μ-{B=N(SiMe$_3$)$_2$}C=C)-Ph}$_2$(PEt$_3$)$_2$] (**119**/**120**), *trans*-[Pt{(μ-{B=N(SiMe$_3$)$_2$}C=C)-*p*-C$_6$H$_4$OMe}$_2$(PEt$_3$)$_2$] (**122**/**123**), and *trans*-[Pt{(μ-{B=N(SiMe$_3$)$_2$}C=C)-*p*-C$_6$H$_4$CF$_3$}$_2$(PEt$_3$)$_2$] (**125**/**126**)) show dual sets of resonances. As can be seen below in Table 3-6, the dual signals appear in the ^{1}H, ^{13}C{^{1}H}, ^{29}Si{^{1}H}, ^{31}P{^{1}H}, and ^{195}Pt{^{1}H} NMR spectra. This duality of compound signals is also believed to exist in the ^{11}B{^{1}H} NMR spectroscopic data; however, due to the severe quadrupolar broadening of the signals, the resonances appear to overlap with each other, forming a broad singlet. A ^{1}H VT-NMR NMR experiment showed two energetic rotational barriers (T_C = −50 °C (ΔG = 48 kJ/mol) and 72 °C = ΔG = 75 kJ/mol)* for the complex *trans*-[Pt{(μ-{B=N(SiMe$_3$)$_2$}C=C)-Ph}$_2$(PEt$_3$)$_2$] (**119**/**120**). The upper rotational energetic barrier (ΔG = 75 kJ/mol) appeared to be due to hindered rotation around the Pt-C bond because the previous platinum mono-borirenyl species showed the lower rotational energetic barrier (ΔG = 48 kJ/mol) to correspond to hindered rotation around the B-N bond.[295,436] Two explanations for this Pt-C rotational energy barrier were hypothesized: either (A) steric bulk from the triethylphosphine arms, or (B) strong electronic interactions from the platinum metal d orbitals with the σ-borirenyl arms. As previously discussed, NOESY and ROESY NMR spectroscopy failed to discern any interactions between the arms of the

* Values for ΔG are calculated by Equation 3-1.

triethylphosphine moieties and the trimethylsilyl moieties, making this steric explanation seem implausible. What follows in this section are detailed studies aimed at explaining the electronic interactions from the platinum d orbitals responsible for hindering rotation around the *σ*-borirenyl arms of the molecule.

	$^{1}H_{TMS}$ [ppm]	^{11}B [ppm]	$^{13}C_{TMS}$ [ppm]	$^{29}Si_{TMS}$ [ppm]	^{31}P [ppm] ($^{1}J_{P\text{-}Pt}$) [Hz]	^{195}Pt [ppm] ($^{1}J_{Pt\text{-}P}$) [Hz]
119/120	0.603 0.574	35.3	4.05 4.02	5.46 5.35	5.9 (2,765) 5.9 (2,762)	−4,108 (2,751) −4,110 (2,759)
122/123	0.625 0.603	35.4	4.11 4.06	– –	6.0 (2,773) 6.0 (2,765)	−4,110 (2,755) −4,111 (2,763)
125/126	0.535 0.525	35.1	3.94 3.85	5.98 5.79	6.2 (2,743) 5.8 (2,728)	−4,100 (2,719) −4,111 (2,737)

Table 3-6. Comparative ^{1}H, ^{11}B, ^{13}C, ^{29}Si, ^{31}P, and ^{195}Pt NMR spectroscopic data for the platinum *bis*-*σ*-borirenyl **119/120**, **122/123**, and **125/126** reported in Section 3.1.3.

As can be seen in the above Table 3-6, the effect of the electron-donating methoxy substituent and the electron-withdrawing trifluoromethyl substituent effect the electronic shielding of the measured nuclei in divergent manners. Using *trans*-[Pt{(*μ*-{B=N(SiMe$_3$)$_2$}C=C)-Ph}$_2$(PEt$_3$)$_2$] (**119/120**) as a "neutral" or unsubstituted species, the methoxy-functionalized species *trans*-[Pt{(*μ*-{B=N(SiMe$_3$)$_2$}C=C)-*p*-C$_6$H$_4$OMe}$_2$(PEt$_3$)$_2$] (**122/123**) can be seen to shift the ^{1}H and ^{13}C NMR resonance for the trimethylsilyl moieties downfield compared to an upfield shift witnessed for the trifluoromethyl-functionalized species *trans*-[Pt{(*μ*-{B=N(SiMe$_3$)$_2$}C=C)-*p*-C$_6$H$_4$CF$_3$}$_2$(PEt$_3$)$_2$] (**125/126**). This data is exactly what would be expected from the perturbation of the neutral electronic structure with increased electronic shielding (**122/123**) and decreased electronic shielding (**125/126**). This shifting of the electronic structure of the molecule is also witnessed in the coupling constants observed during $^{31}P\{^{1}H\}$ and $^{195}Pt\{^{1}H\}$ NMR spectroscopic characterization of the systems with an increase in the coupling constants for the electron-donating methoxy-functionalized species (**122/123**) and a decrease in the coupling constants with the electron-withdrawing trifluoromethyl-substituted species (**125/126**).

Comparisons in the X-ray structural data for compounds **119/120**, **122/123**, and **125/126** is another manner for quantifying the degree of interaction between the platinum metal center and the *σ*-borirenyl arms; however, the structure for **125/126** was once again highly disordered due to the trifluoromethyl moieties present on the periphery of the complex. To discuss this structure, the bonds will be averaged for

trend establishment only and not discussed in highly accurate terms. Although VT-NMR data indicates fluxional rotation around the platinum-carbon bond at temperatures in excess of 72 °C, all obtained crystalline samples from this class of *trans*-platinum *bis*-*σ*-borirenes were observed to crystallize with *anti*-configured *σ*-borirenyl arms. Of key interest in comparative studies between species **119**/**120**, **122**/**123**, and **125**/**126** are the Pt-C(1) and borirene C(1)-C(2) bond lengths (Table 3-7), which indicate the degree of delocalization across both the individual borirene rings as well as the *bis*-*σ*-borirenyl conjugation across the platinum center. For compounds **88** and **119**/**120**, the respective borirene C(1)-C(2) distances were found to be nearly identical (1.373(1) and 1.374(5) Å respectively). These distances indicate that similar degrees of delocalization are possessed by both of these compounds. The respective Pt(1)-C(1) distances for (**122**/**123**) and (**125**/**126**) were found to be 2.046(1) and 2.076(7) Å respectively.

The X-ray crystallographic geometric examination of these solid-state structures also confirmed a coplanar arrangement of the *σ*-borirenyl arms in two of the three species ((**119**/**120**) and (**122**/**123**)). The geometric arrangement of the borirenyl arms around the platinum center is difficult to discern on the species **125**/**126** due to disorder in the crystal structure due to the trifluoromethyl substituents on the phenyl ring. The coplanar framework between the twin heteroaromatic ring systems across the platinum core is indicative of strong exocyclic conjugation between aromatic systems; however, disorder within the refined data combined with near identical structural bond distances and angles make extrapolation of trends within these electron-withdrawing and -donating variants of the *trans*-platinum *bis*-*σ*-borirene frameworks difficult to discern. However, what can be confirmed is the close structural similarity (bond distances and angles) of all three *trans*-platinum *bis*-*σ*-borirene systems (**119**/**120**, **122**/**123**, and **125**/**126**) investigated in this work with the previously reported platinum mono-*σ*-borirene species **88**.

	88[295]	**119/120**	**122/123**	**125/126**
Space Group	$P2_1/c$	$P\bar{1}$	$P\bar{1}$	$P\bar{1}$
Pt_1–P_1 [Å]	2.279(2)	2.287(1)	2.314(1)	2.279
Pt_1–C_α [Å]	1.974(5)	2.046(4)	2.076(3)	2.042(6)
C_α–C_β [Å]	1.374(7)	1.373(6)	1.384(4)	1.363(9)
C_β–C_γ [Å]	1.466(7)	1.480(6)	1.476(4)	1.455(7)
C_α–B_1 [Å]	1.511(8)	1.505(6)	1.522(4)	1.494(9)
C_β –B_1 [Å]	1.482(8)	1.454(6)	1.481(4)	1.456(9)
B_1–N_1 [Å]	1.428(7)	1.451(4)	1.459(4)	1.437(9)
$\Sigma*$(B) [°]	359.9	359.6	359.3	359.2
$\Sigma*$(N) [°]	360.0	359.0	357.0	359.9

Table 3-7. Comparative X-ray structural data for the platinum *bis*-σ-borirenyl species *trans*-[Pt{(μ-{B=N(SiMe$_3$)$_2$}C=C)-Ph}$_2$(PEt$_3$)$_2$] (**119/120**), *trans*-[Pt{(μ-{B=N(SiMe$_3$)$_2$}C=C)-*p*-C$_6$H$_4$OMe}$_2$(PEt$_3$)$_2$] (**122/123**), and *trans*-[Pt{(μ-{B=N(SiMe$_3$)$_2$}C=C)-*p*-C$_6$H$_4$CF$_3$}$_2$(PEt$_3$)$_2$] (**125/126**) reported in Section 3.1.3.

The UV-vis data for compounds **119/120**, **122/123**, and **125/126** were recorded in hexane to discern the bathochromic or hypsochromic shifting influence on the system by the augmentation of the aryl substituents. As the UV-vis absorption shifting was previously theorized by Dr. Alfredo Vargas in Chapter 3.1.1.1, the ability of these *trans*-platinum *bis*-σ-borirenes to have tunable absorption spectra comprises a fundamental point of emphasis for this research project.

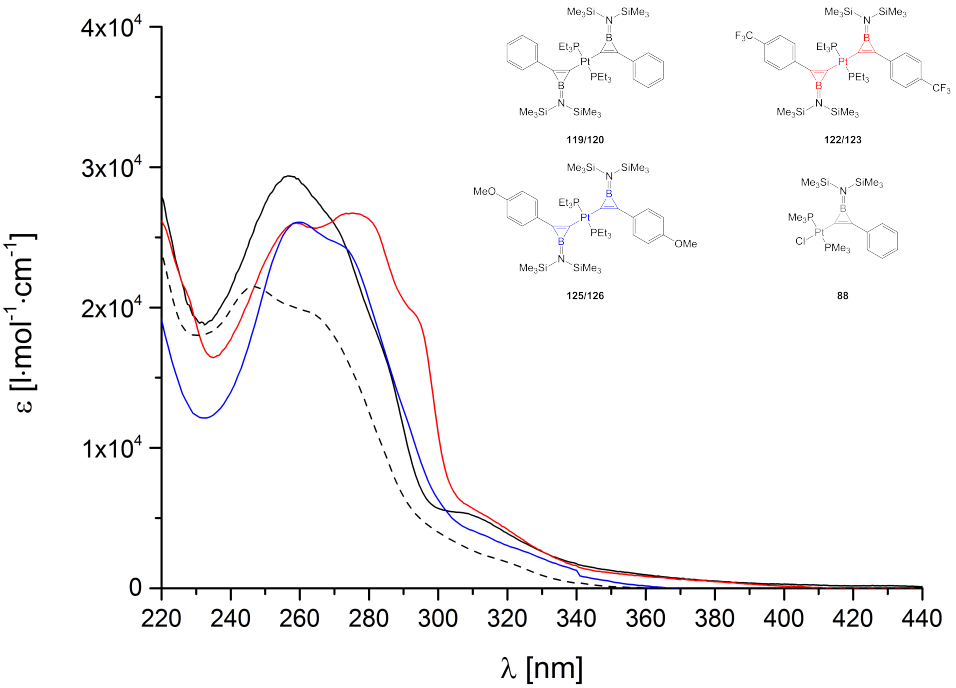

Figure 3-37. UV-vis absorption spectra of *trans*-platinum *bis*-σ-alkynyl species *trans*-[Pt{(μ-{B=N(SiMe$_3$)$_2$}C=C)-Ph}$_2$(PEt$_3$)$_2$] (**119/120**, black), *trans*-[Pt{(μ-{B=N(SiMe$_3$)$_2$}C=C)-*p*-C$_6$H$_4$OMe}$_2$(PEt$_3$)$_2$] (**122/123**, blue), and *trans*-[Pt{(μ-{B=N(SiMe$_3$)$_2$}C=C)-*p*-C$_6$H$_4$CF$_3$}$_2$(PEt$_3$)$_2$] (**125/126**, red) compared to *trans*-[PtCl{(μ-{BN(SiMe$_3$)$_2$}C=C)-Ph}(PMe$_3$)$_2$] (**88**, dashed) as measured in hexane. Data is plotted as wavelength [λ] *vs*. extinction coefficient [ε].

	88[295]	**119/120 (ε)**	**122/123 (ε)**	**125/126 (ε)**
λ_{max} [nm]	247.0	256.5 (29,370)	260.0 (26,070)	275.5 (26,730)
λ_{local} [nm]	–	–	–	259.0 (26,030)

Table 3-8. UV-vis absorption maxima [λ] and extinction coefficients [ε] recorded for the compounds *trans*-[Pt{(μ-{B=N(SiMe$_3$)$_2$}C=C)-Ph}$_2$(PEt$_3$)$_2$] (**119/120**, black), *trans*-[Pt{(μ-{B=N(SiMe$_3$)$_2$}C=C)-*p*-C$_6$H$_4$OMe}$_2$(PEt$_3$)$_2$] (**122/123**, blue), and *trans*-[Pt{(μ-{B=N(SiMe$_3$)$_2$}C=C)-*p*-C$_6$H$_4$CF$_3$}$_2$(PEt$_3$)$_2$] (**125/126**, red) compared to *trans*-[PtCl{(μ-{BN(SiMe$_3$)$_2$}C=C)-Ph}(PMe$_3$)$_2$] (**88**, dashed) as measured in hexane.

The UV-vis spectrum of compound *trans*-[Pt{(μ-{B=N(SiMe$_3$)$_2$}C=C)-Ph}$_2$(PEt$_3$)$_2$] (**119/120**, black) recorded in hexane shows an absorption maximum at 256.5 nm, which is slightly red-shifted relative to that observed for the platinum monoborirene complex *trans*-[PtCl{(μ-{BN(SiMe$_3$)$_2$}C=C)-Ph}(PMe$_3$)$_2$] (**88**, dashed) (247.0 nm, spectrum also recorded in hexane). The UV-vis spectra for compounds *trans*-[Pt{(μ-{B=N(SiMe$_3$)$_2$}C=C)-*p*-C$_6$H$_4$OMe}$_2$(PEt$_3$)$_2$] (**122/123**, blue) and *trans*-[Pt{(μ-{B=N(SiMe$_3$)$_2$}C=C)-*p*-C$_6$H$_4$CF$_3$}$_2$(PEt$_3$)$_2$] (**125/126**, red) recorded in hexane both showed red-shifted absorption maxima relative to both *trans*-[Pt{(μ-

{B=N(SiMe$_3$)$_2$}C=C)-Ph}$_2$(PEt$_3$)$_2$] (**119**/**120**) and *trans*-[PtCl{(μ-{BN(SiMe$_3$)$_2$}C=C)-Ph}(PMe$_3$)$_2$] (**88**) (Figure 3-37 and Table 3-8). Compound *trans*-[Pt{(μ-{B=N(SiMe$_3$)$_2$}C=C)-Ph}$_2$(PEt$_3$)$_2$] (**119**/**120**) was tested for solvatochromism by recording the absorption spectrum in acetonitrile; however, the spectrum appears nearly identical to that recorded in hexane, suggesting very little discernable solvatochromatic shifting of the absorption maxima. One feature of note in the spectra of compounds *trans*-[Pt{(μ-{B=N(SiMe$_3$)$_2$}C=C)-Ph}$_2$(PEt$_3$)$_2$] (**119**/**120**), *trans*-[Pt{(μ-{B=N(SiMe$_3$)$_2$}C=C)-*p*-C$_6$H$_4$OMe}$_2$(PEt$_3$)$_2$] (**122**/**123**), and *trans*-[Pt{(μ-{B=N(SiMe$_3$)$_2$}C=C)-*p*-C$_6$H$_4$CF$_3$}$_2$(PEt$_3$)$_2$] (**125**/**126**) is the presence of a significant shoulder, found at longer wavelengths from the main absorption signal.

	88	**119/120**	**119/120 ($\Delta E_{0.5}$)**
ΔE_{orb} [kcal/mol]	−138	−310	−155
ΔE_{elstat} [kcal/mol]	−171	−324	−162
ΔE_{Pauli} [kcal/mol]	237	465	233
ΔE_{int} [kcal/mol]	−72	−170	−85

Table 3-9. Energy decomposition analysis of *trans*-[PtCl{(μ-{BN(SiMe$_3$)$_2$}C=C)-Ph}(PMe$_3$)$_2$] (**88**) and *trans*-[Pt{(μ-{B=N(SiMe$_3$)$_2$}C=C)-Ph}$_2$(PEt$_3$)$_2$] (**119**/**120**) using the fragment approach.[*]

Investigation of the bonding situation in the model *trans*-platinum *bis*-σ-borirene complex *trans*-[Pt{(μ-{B=N(SiMe$_3$)$_2$}C=C)-Ph}$_2$(PEt$_3$)$_2$] (**119**/**120**) was performed using Kohn-Sham density functional theory (DFT) calculations.[†] Table 3-9 lists all bonding energy contributions observed by fragment approach analysis of the modeling of the *bis*-σ-borirene *trans*-[Pt{(μ-{B=N(SiMe$_3$)$_2$}C=C)-Ph}$_2$(PEt$_3$)$_2$] (**119**/**120**) system relative to the monoborirene *trans*-[PtCl{(μ-{BN(SiMe$_3$)$_2$}C=C)-Ph}(PMe$_3$)$_2$] (**88**) system. The bonding energy decomposition clearly shows that the borirenes are not "independently" bound to the platinum center. The orbital interactions are synergically enhanced, and as expected, the electrostatic contributions and the Pauli contributions become more independent. Furthermore, the orbital projections show that the HOMO of *trans*-[Pt{(μ-{B=N(SiMe$_3$)$_2$}C=C)-Ph}$_2$(PEt$_3$)$_2$] (**119**/**120**) consists of the borirene σ-networks, with σ-antibonding character between the platinum and α-carbon atoms. However, we were unable to

[*] The energies stated for **119**/**120** are total energies for the combination of all three fragments and must subsequently be halved to obtain the energies for each borirene fragment interacting with the platinum center (see column $\Delta E_{0.5}$).
[†] Geometry optimizations were conducted at the B3LYP/6-311+G* and OLYP/TZP levels of theory using the Gaussian03 and ADF programs.

observe any molecular orbital containing a π-interaction between d(Pt) and p(C) orbitals (Figure 3-38).

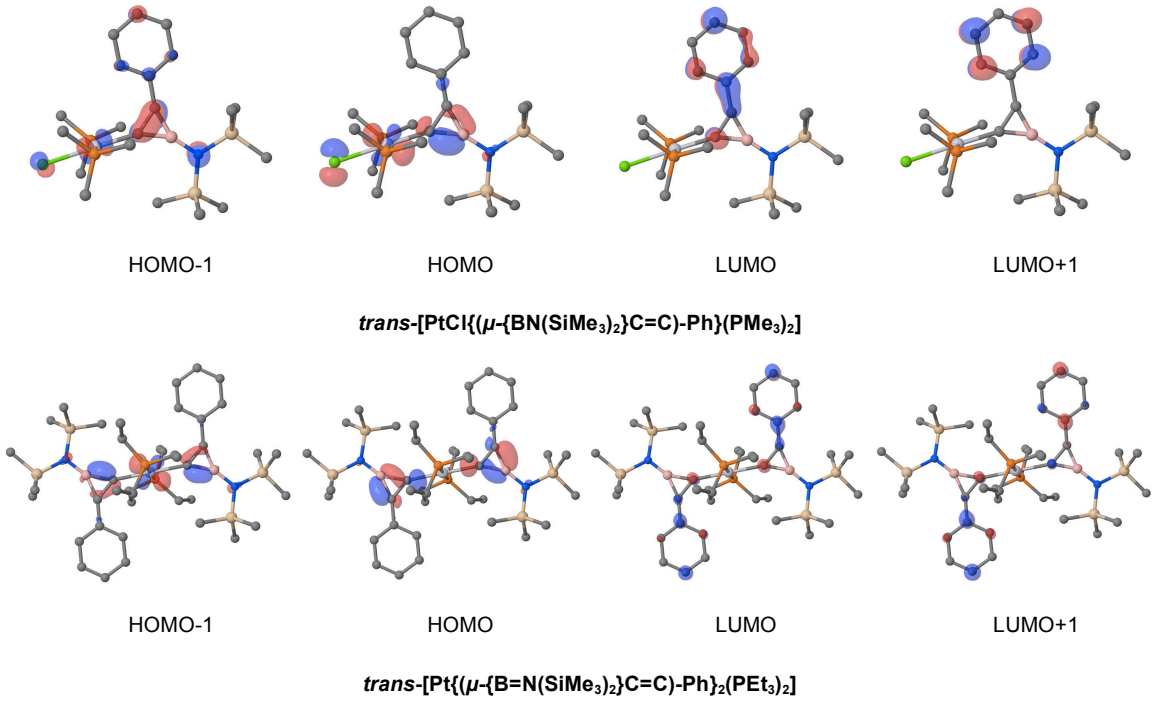

Figure 3-38. Frontier molecular orbital (MO) projections of *trans*-[PtCl{(μ-{BN(SiMe$_3$)$_2$}C=C)-Ph}(PMe$_3$)$_2$] (**88**, top) and *trans*-[Pt{(μ-{B=N(SiMe$_3$)$_2$}C=C)-Ph}$_2$(PEt$_3$)$_2$] (**119**/**120**, bottom).

Time-dependent density functional theory (TD-DFT) methods were used to model the major electronic transitions observed in the absorption spectra of the mono- and *bis*-σ-borirene complexes. These calculations indicated that in the model monoborirene compound *trans*-[Pt{(μ-{B=N(SiMe$_3$)$_2$}C=C)-Ph}$_2$(PEt$_3$)$_2$] (**119**/**120**) the major electronic transition contributing to the UV-vis profile is from an orbital consisting of borirene C=C and B=N π-bonding interactions into orbitals based predominantly on the phenyl substituents. A similar transition from a d_{z^2} orbital on Pt into the same phenyl-based orbital is also a contributor in the *bis*-σ-borirene complex *trans*-[Pt{(μ-{B=N(SiMe$_3$)$_2$}C=C)-Ph}$_2$(PEt$_3$)$_2$] (**119**/**120**). It can also be seen that in these two complexes **88** and **119**/**120**, the orbital from which the electron originates has antibonding character between the C=C π-bonds and a d-orbital predominantly based on Pt. The case of **119**/**120** strongly suggests that there is a photophysically-active π-network spanning the borirenes, albeit one containing four nodes (Figures 3-38 and Figure 3-39).

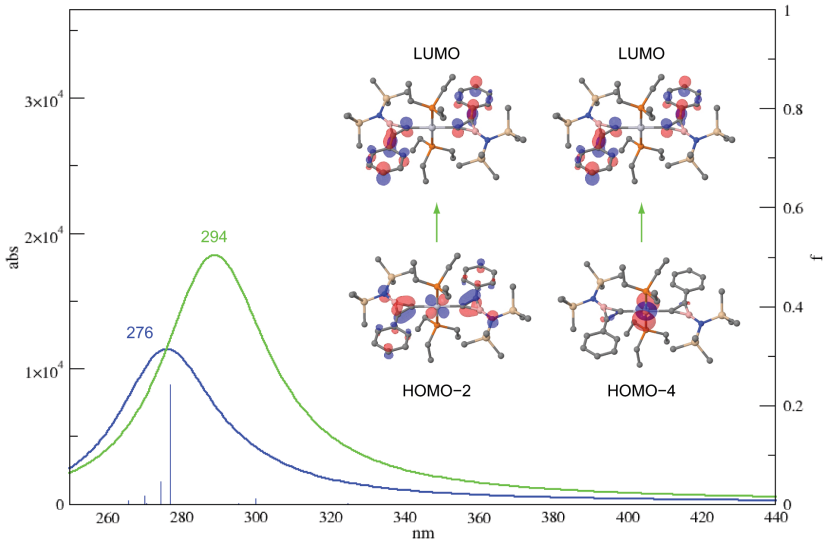

Figure 3-39. TD-DFT calculations for the absorption maxima of the platinum borirenyl complexes *trans*-[PtCl{(μ-{BN(SiMe$_3$)$_2$}C=C)-Ph}(PMe$_3$)$_2$] (**88**, blue) and *trans*-[Pt{(μ-{B=N(SiMe$_3$)$_2$}C=C)-Ph}$_2$(PEt$_3$)$_2$] (**119**/**120**, green) shown with the calculated orbital transitions for this absorption within the complex *trans*-[Pt{(μ-{B=N(SiMe$_3$)$_2$}C=C)-Ph}$_2$(PEt$_3$)$_2$] (**119**/**120**).

Finally, electron contour diagrams (taken from the calculated Laplacian environments) of both complexes *trans*-[PtCl{(μ-{BN(SiMe$_3$)$_2$}C=C)-Ph}(PMe$_3$)$_2$] (**88**) and *trans*-[Pt{(μ-{B=N(SiMe$_3$)$_2$}C=C)-Ph}$_2$(PEt$_3$)$_2$] (**119**/**120**) were projected. In these projections, the filled B-N bonding π-orbital is observed to perturb the VSCC (valence shell charge correlation) electronic environment of the boron ring component for the *trans*-platinum mono-σ-borirenyl and *bis*-σ-borirenyl interactions. Contour line diagrams have been projected (Figure 3-40) for the *trans*-platinum borirenyl complexes **88** and **119**/**120** within the *cyclo*-BC$_2$ ring plane. Solid lines indicate areas of charge concentration while dashed lines show areas of charge depletion. Examination of the boron environments show a strong B-N interaction which destabilizes the ring aromaticity and warps the circular shape of the VSCC boron environment (B-N exocyclic interaction disturbance of the ring aromaticity) which pushes the "aromatic" delocalized electron density predominantly towards the C-C system in the *cyclo*-BC$_2$ borirene ring unit. The aminoborirene species synthesized in these studies all contain this exocyclic sp^2-nitrogen-boron bond, which has the ability to donate electron density from the lone pair of electrons on the nitrogen center into the boron p$_z$-orbital. This interaction serves to stabilize the boron p$_z$-orbital, however, it subsequently pushes the aromatic electron density towards the carbons in the system.

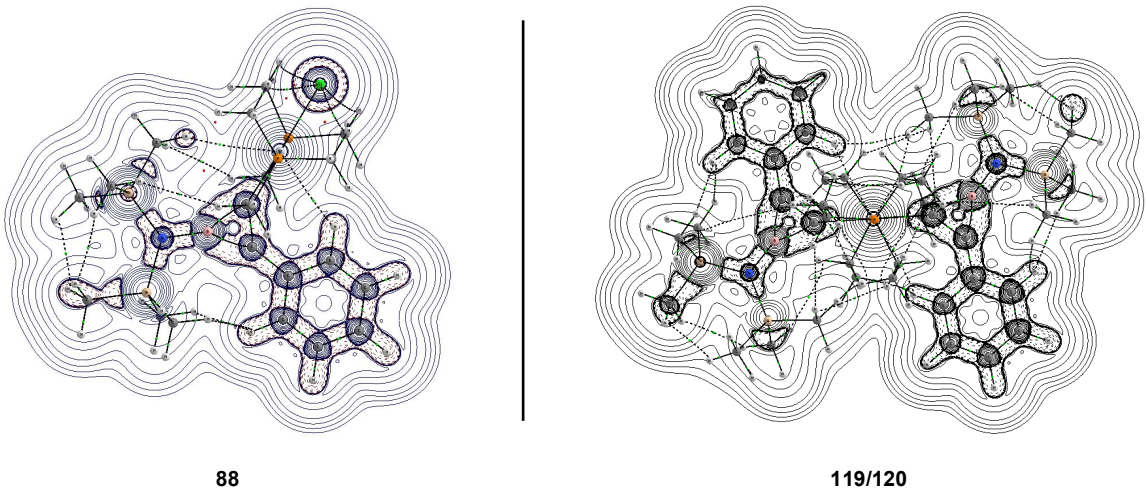

Figure 3-40. Electron contour diagrams taken from the calculated Laplacian operator functions of *trans*-[PtCl{(μ-{BN(SiMe$_3$)$_2$}C=C)-Ph}(PMe$_3$)$_2$] (**88**, left) and *trans*-[Pt{(μ-{B=N(SiMe$_3$)$_2$}C=C)-Ph}$_2$(PEt$_3$)$_2$] (**119**/**120**, right).

3.1.3.6 Attempted Borylene Transfer onto *trans*-[Pt(C≡C-9-C$_{14}$H$_9$)$_2$(PEt$_3$)$_2$] (63)

The synthesis of *trans*-[Pt{(μ-{B=N(SiMe$_3$)$_2$}C=C)-9-C$_{14}$H$_9$}$_2$(PEt$_3$)$_2$] (**127**) was attempted by modification to the literature procedure previously outlined in Section 3.1.3.1 and in the doctoral thesis of Dr. Qing Ye [*] in which *trans*-[Pt(C≡C-9-C$_{14}$H$_9$)$_2$(PEt$_3$)$_2$] (**63**) is mixed with [(OC)$_5$Cr{BN(SiMe$_3$)$_2$}] (**13**) (2.2 eq. minimum) in benzene solution (Figure 3-41). The reaction was irradiated for 8 h at room temperature during which time only one half of the [(OC)$_5$Cr{BN(SiMe$_3$)$_2$}] (**13**) appeared to be consumed *via* ^{11}B{^{1}H} NMR spectroscopy (^{11}B{^{1}H}: δ = 92.8 ppm) with evolution of only one other observable species at approximately ^{11}B{^{1}H}: δ = ~47 ppm. ^{31}P{^{1}H} NMR spectroscopic monitoring of the reaction mixture showed what appeared to be formation of free triethylphosphine at ^{31}P{^{1}H}: δ = −20.5 ppm (with decomposition of *trans*-[Pt(C≡C-9-C$_{14}$H$_9$)$_2$(PEt$_3$)$_2$] (**63**)). Purification of the reaction mixture was performed by removal of all volatiles *in vacuo* and sublimation of all unreacted borylene and [Cr(CO)$_6$] byproduct by heating to 65 °C. The resulting dark yellow reaction mixture was purified *via* pacified silica gel (SiO$_2$) column chromatography[397] to yield the unexpected product [(Pt{μ-BN(SiMe$_3$)$_2$}$_2$){Cr(μ-CO)(CO)$_4$}{Cr(μ-CO)(CO)$_3$(PEt$_3$)}] (**64**) as a yellow air and moisture sensitive crystalline solid in very poor (isolated crystals) yield (<10% yield).

[*] See the thesis of Dr. Qing Ye, Chapter 2.1 (pages 23-54) and Chapter 3 (pages 111-119) for synthesis and characterization of platinum and iron mono-σ-borirenyl complexes.

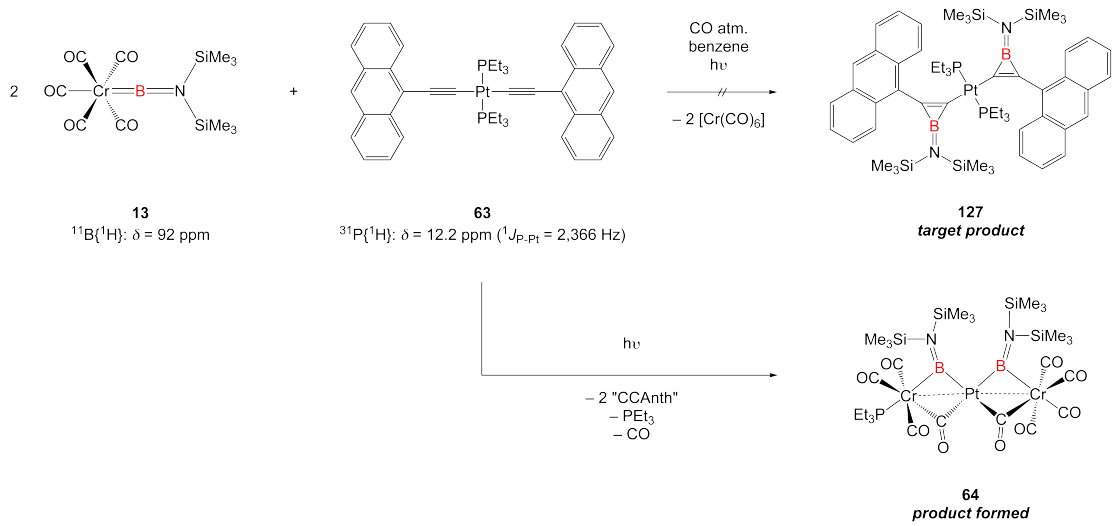

Figure 3-41. [(Pt{μ-BN(SiMe$_3$)$_2$}$_2$){Cr(μ-CO)(CO)$_4$}{Cr(μ-CO)(CO)$_3$(PEt$_3$)}] (**64**) synthesis *via* photolytic rearrangement of the platinum *bis*-σ-alkynyl species *trans*-[Pt(C≡C-9-C$_{14}$H$_9$)$_2$(PEt$_3$)$_2$] (**63**) in the presence of two equivalents of [(OC)$_5$Cr{BN(SiMe$_3$)$_2$}] (**13**).

The formation of this unexpected [(Pt{μ-BN(SiMe$_3$)$_2$}$_2$){Cr(μ-CO)(CO)$_4$}{Cr(μ-CO)(CO)$_3$(PEt$_3$)}] (**64**) Cr-Pt-Cr bowtie complex is presumably due to the reductive elimination and dissociation of some form of the coupled alkynyl-anthracene moieties to generate a ligand-depleted Pt(0) species in the presence of two equivalents of the [(OC)$_5$Cr{BN(SiMe$_3$)$_2$}] (**13**) complex. Photolytic irradiation of this terminal borylene in the presence of an electronically unsaturated platinum center allowed for the formation of the four bridging ligand interactions to the platinum center with coordination of a phosphine to the *trans*- position relative to one of the bridging borylene moieties. As the yield of this reaction was so poor, little discussion of the NMR data can be done due to the fact that uncertainty still exists if this isolated species is the favored product in this reaction or just an isolated secondary species. Structural discussion of this species can be found in Section 2.2.3.3.

3.1.3.7 Transfer attempts onto *cis*-[Pt(C≡C-Ph)$_2$(DCPE)] (112)

The synthesis of *cis*-[Pt{(μ-{B=N(SiMe$_3$)$_2$}C=C)-Ph}$_2$(DCPE)] (**128**) (DCPE = *bis*(dicyclohexylphosphino)ethane) was attempted by modification of the literature procedure previously outlined in Section 3.1.3.1 and in the doctoral thesis of Dr. Qing Ye* in which *cis*-[Pt(C≡C-Ph)$_2$(DCPE)] (**112**) is mixed with [(OC)$_5$Cr{BN(SiMe$_3$)$_2$}] (**13**) (2.2 eq. minimum) in benzene solution (Figure 3-42, top). The reaction was irradiated by photolysis for approximately 8 h at room temperature during which

* See the thesis of Dr. Qing Ye, Chapter 2.1 (pages 23-54) and Chapter 3 (pages 111-119) for the synthesis and characterization of platinum and iron mono-σ-borirenyl complexes.

time full decomposition of the *cis*-[Pt(C≡C-Ph)$_2$(DCPE)] (**112**) complex was observed *via* $^{31}P\{^1H\}$ NMR spectroscopy. Following this failed reaction another attempt was made by treatment of the *trans*-[Pt{(μ-{B=N(SiMe$_3$)$_2$}C=C)-Ph}$_2$(PEt$_3$)$_2$] (**119**/**120**) with DCPE to attempt a bidentate phosphine exchange for two monodentate phosphines (Figure 3-42, bottom) similar to the reported synthesis of the species reported in Section 3.1.2.5. This reaction also unfortunately failed to show any conversion to the *cis*-[Pt{(μ-{B=N(SiMe$_3$)$_2$}C=C)-Ph}$_2$(DCPE)] (**128**) product after irradiation and heating.

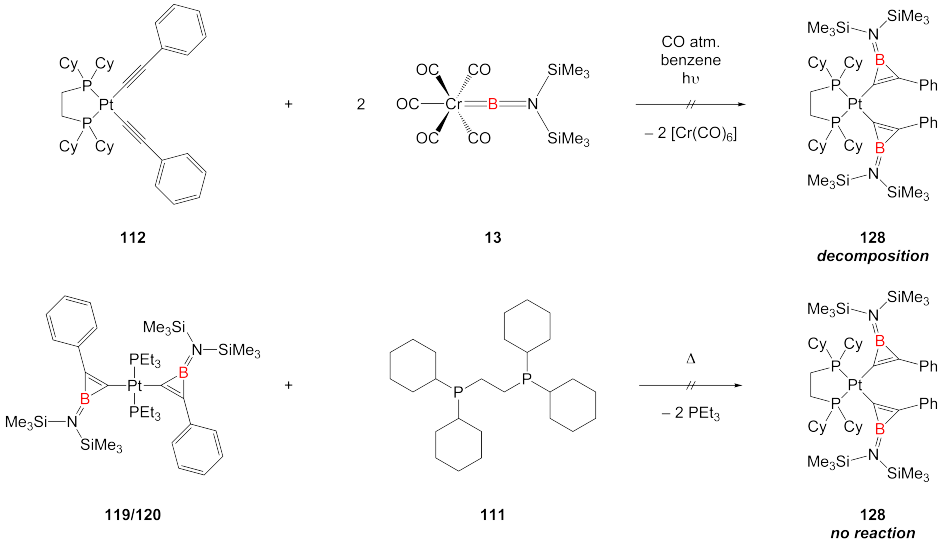

Figure 3-42. Attempts to prepare *cis*-[Pt{(μ-{B=N(SiMe$_3$)$_2$}C=C)-Ph}$_2$(DCPE)] (**128**) *via* photolytic borylene transfer (top) or coordination of a bidentate diphosphine to the *bis*(phosphine) metal center to force *trans*-/*cis*- rearrangement (bottom).

Similar reductive eliminations have been reported by Jones and coworkers[406] in which a bidentate phosphine Pt(0) π-alkynyl complex *cis*-[Pt(η^2-C$_2$Ph$_2$)(DIPPM)] (**129**) (DIPPM = *bis*(di*iso*propylphosphino)methane) can be converted to the *cis*-platinum σ-alkynyl aryl complex **130** (Pt(II)) by photolysis (Figure 3-43). This reaction was found to be reversible by heating of the *cis*-platinum σ-alkynyl aryl complex **130** to 80 °C. This reported set of reaction conditions and overall similarity between the reported complex **130** and *cis*-[Pt(C≡C-Ph)$_2$(DCPE)] (**112**) make the reductive elimination reactions observed photolytically plausible and support the idea that photolytic alkyne substituent coupling is actively decomposing the *cis*-[Pt(C≡C-Ph)$_2$(DCPE)] (**112**) precursor before borylene transfer can be accomplished in solution. A similar mechanism of reductive elimination may also be

the decomposition pathway for the *trans*-[Pt(C≡C-9-$C_{14}H_9$)$_2$(PEt_3)$_2$] (**63**) species reported in Section 3.1.3.6.

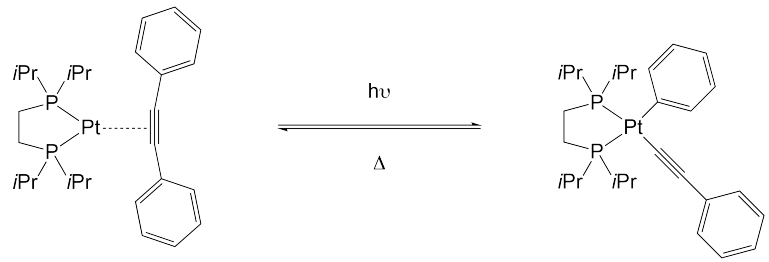

129 130

Figure 3-43. Reversible photolytic C-C single bond oxidative addition and thermal recombination of a π-alkynyl ligand in the *cis*-[Pt(η^2-C_2Ph_2)(DIPPM)] (**129**) complex as reported by Jones and coworkers.[406]

3.1.3.8 Attempted Borylene Transfer onto *trans*-[Pt{(C≡C)$_3$-Tr*}$_2$(PEt_3)$_2$] (115)

The synthesis of *trans*-[Pt({(μ-{B=N($SiMe_3$)$_2$}C=C)-Ph}$_3$-Tr*)$_2$(PEt_3)$_2$] (**131**) was attempted by modification to the literature procedure previously outlined in Section 3.1.3.1 and in the doctoral thesis of Dr. Qing Ye [*] in which *trans*-[Pt{(C≡C)$_3$-Tr*}$_2$(PEt_3)$_2$] (**115**) is mixed with [(OC)$_5$Cr{BN($SiMe_3$)$_2$}] (**13**) (6.6 eq. minimum) in benzene solution (Figure 3-44). The reaction was irradiated for 8 h at room temperature during which time full decomposition of *trans*-[Pt{(C≡C)$_3$-Tr*}$_2$(PEt_3)$_2$] (**115**) complex was witnessed. The terminal borylene species [(OC)$_5$Cr{BN($SiMe_3$)$_2$}] (**13**) ($^{11}B\{^1H\}$: δ = 92 ppm) is not witnessed to be consumed during the decomposition of *trans*-[Pt{(C≡C)$_3$-Tr*}$_2$(PEt_3)$_2$] (**115**). $^{31}P\{^1H\}$ NMR spectroscopic monitoring of the reaction mixture showed what appeared to be formation of free triethylphosphine at −20.5 ppm (with decomposition of *trans*-[Pt{(C≡C)$_3$-Tr*}$_2$(PEt_3)$_2$] (**115**)).

[*] See the thesis of Dr. Qing Ye, Chapter 2.1 (pages 23-54) and Chapter 3 (pages 111-119) for the synthesis and characterization of platinum and iron mono-σ-borirenyl complexes.

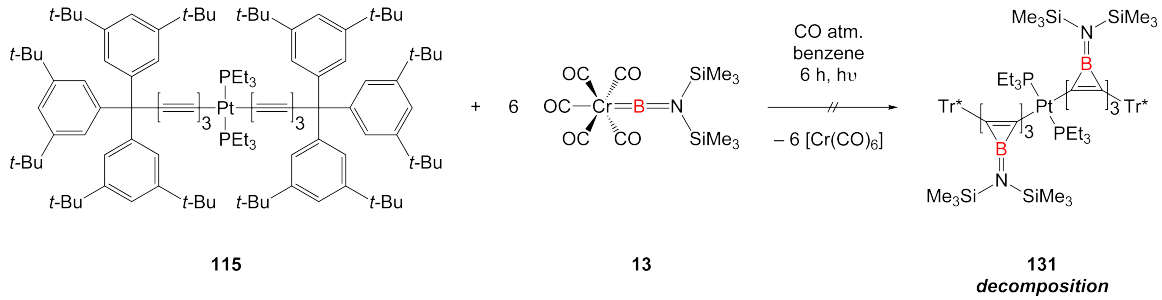

Figure 3-44. Attempted synthesis of *trans*-[Pt({(*μ*-{B=N(SiMe$_3$)$_2$}C=C)-Ph}$_3$-Tr*)$_2$(PEt$_3$)$_2$] (**131**) *via* photolytic transfer of a terminal borylene ligand from [(OC)$_5$Cr{BN(SiMe$_3$)$_2$}] (**13**) onto the alkynyl substituents of *trans*-[Pt{(C≡C)$_3$-Tr*}$_2$(PEt$_3$)$_2$] (**115**).

3.2 Gladysz-Type Platinum End-Capped Alkynyl Species

3.2.1 Synthesis of Platinum Butadiynyl Precursors

Another class of alkynes that were synthesized for use as platforms for the stabilization of transition metal conjugated borirene species are the platinum end-capped alkynes. These compounds have been prepared by a number of groups,[430,432,434] most prominantly by the group of Gladysz and coworkers.[431,433] As these chains of sp-hybridized carbons represent the simplest iteration of what could be termed as a "molecular wire", they are used to predict the physical and spectroscopic properties of carbyne (or polyalkyne). To achieve the best predictions for the properties of carbyne, Gladysz and coworkers, as well as the aforementioned group of Tykwinski and coworkers,[430,434] have tried to extend the chain lengths of "carbyne" segments to the maximum extent and study these species relative to the shorter variants. The highly energetic nature of these systems relative to the molecular weight of the carbyne fragments requires the use of extremely large sterically bulky substituents or stabilizing metals to limit their explosive nature in the solid state. As a result of the success in the synthesis of *trans*-platinum *bis*-σ-borirenyl compounds, these Gladysz-type platinum end-capped alkynyl species seemed like promising candidates to research for the generation of small borirene chains that could display exocyclic π-conjugation (coplanarity) across the platinum end-caps.

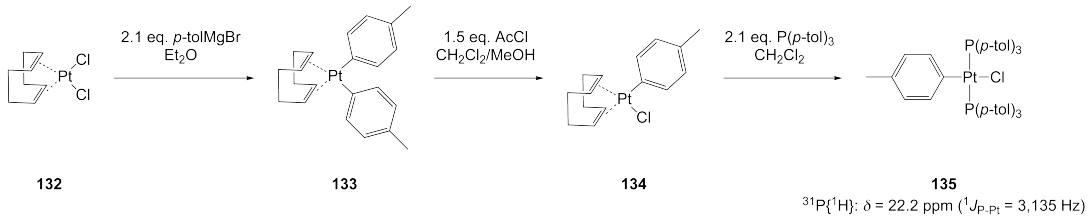

Figure 3-45. First stage of the synthetic route outlined by Gladysz and coworkers for the synthesis of the platinum end-capped octatetraynes.[431]

As can be seen by Figure 3-45, the first stage of the synthetic route employed by Gladysz and coworkers for the synthesis of the platinum end-capped alkynyl species *trans,trans*-[(*p*-tol){(*p*-tol)$_3$P}$_2$Pt(C≡C)$_4$Pt{P(*p*-tol)$_3$}$_2$(*p*-tol)] (**138**) has been outlined. This route uses [PtCl$_2$(COD)] (**132**) (COD = 1,5-cyclooctadiene) as a starting material for the generation of a *bis*(phosphine) platinum monohalide complex (**135**). The second stage of the synthetic route (Figure 3-46) starts the butadiyne heterocoupling (**137**) and homocoupling (**138**) reaction sequences. As the

fundamental starting material for all-carbon sp-hybridized chain extension and coupling reactions, the species *trans*-[PtCl(*p*-tol){P(*p*-tol)$_3$}$_2$] (**135**) must first be synthesized (Figure 3-45). The first step in this process is treatment of [PtCl$_2$(COD)] (**132**) with 2.1 eq. of *p*-tolMgBr to generate [Pt(*p*-tol)$_2$(COD)] (**133**). This platinum *bis*(aryl) species can be converted to the monohalide [PtCl(*p*-tol)(COD)] (**134**) by treatment with *in situ*-generated HCl from acetyl chloride in a mixture of MeOH/CH$_2$Cl$_2$. At this point in the synthesis, the exchange of the bidentate 1,5-cyclooctadienyl ligand (COD) for two mono-phosphine ligands can be achieved. As reported by Gladysz and coworkers, the triarylphosphine P(*p*-tol)$_3$ was used in the synthesis of the platinum halide *bis*(phosphine) complex *trans*-[PtCl(*p*-tol){P(*p*-tol)$_3$}$_2$] (**135**).

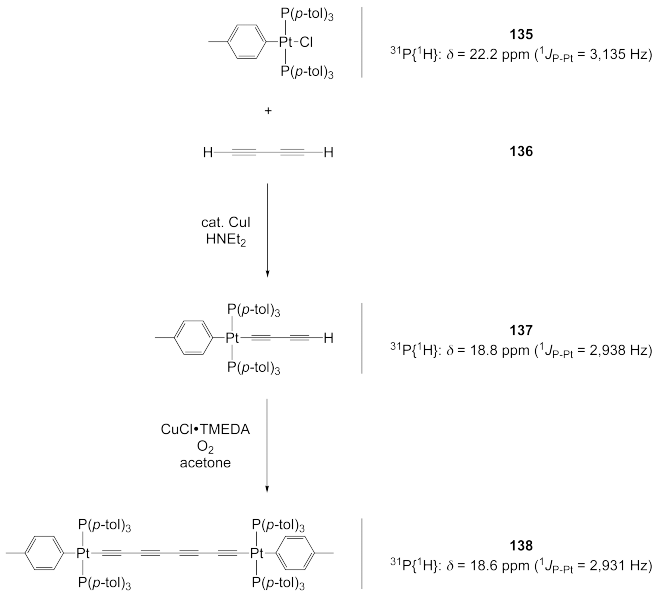

Figure 3-46. The route employed by Gladysz and coworkers for the synthesis of the platinum end-capped octatetraynyl species *trans,trans*-[(*p*-tol){(*p*-tol)$_3$P}$_2$Pt(C≡C)$_4$Pt{P(*p*-tol)$_3$}$_2$(*p*-tol)] (**138**).

Copper-iodide-catalyzed coupling of butadiyne (**136**) to the *trans*-platinum *bis*(phosphine) chloride precursor **135** was performed with formation of the *trans*-platinum butadiynyl species *trans*-[Pt{(C≡C)$_2$-H}(*p*-tol){P(*p*-tol)$_3$}$_2$](**137**) and one equivalent of the salt [H$_2$NEt$_2$]Cl. The chain extension reactions (homocoupling) were performed under Hay conditions[438] (a variation of Glaser coupling)[439,440] and proceeds *via* copper acetylide oxidative coupling with dioxygen to yield *trans,trans*-[(*p*-tol){(*p*-tol)$_3$P}$_2$Pt(C≡C)$_4$Pt{P(*p*-tol)$_3$}$_2$(*p*-tol)] (**138**) (Figure 3-46). An added benefit of the air- and moisture-stability of the platinum end-capped alkynyl compounds (at least with the short chain analogs) is the option for them to be

purified under ambient conditions; however, all platinum end-capped alkynyl products synthesized in this study were properly dried and stored in glovebox atmospheres.

3.2.1.1 *trans*-[PtCl(*p*-tol)(PCy_2Me)$_2$] (140)

trans-[PtCl(*p*-tol)(PCy_2Me)$_2$] (**140**) was prepared according to the modified literature previously discussed[431] in which [PtCl(*p*-tol)(COD)] (**134**) was mixed with methyl(dicyclohexyl)phosphine (**139**) (2.1 equivalents) and allowed to stir for 16 h at room temperature (Figure 3-47). $^{31}P\{^1H\}$ NMR spectroscopic monitoring of the reaction after 16 h saw near full conversion of free methyl(dicyclohexyl)phosphine ($^{31}P\{^1H\}$: δ = –18.1 ppm) to *trans*-[PtCl(*p*-tol)(PCy_2Me)$_2$] (**140**) species ($^{31}P\{^1H\}$: δ = 11.2 ppm, $^1J_{P\text{-}Pt}$ = 2848 Hz). Workup of the compound gave *trans*-[PtCl(*p*-tol)(PCy_2Me)$_2$] (**140**) as air-stable white crystalline solids in 90% yield. Differential thermal analysis of these white crystalline solids showed a melting point for **140** at 183 °C with no decomposition below 300 °C.

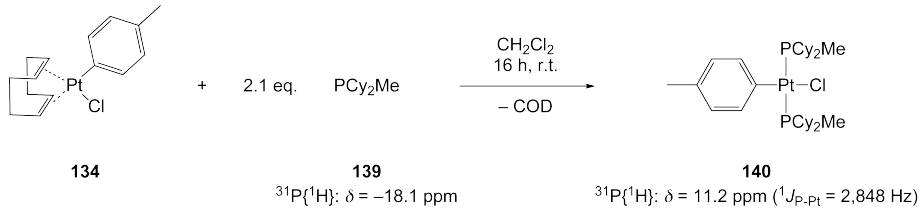

Figure 3-47. *trans*-[PtCl(*p*-tol)(PCy_2Me)$_2$] (**140**) synthesis from [PtCl(*p*-tol)(COD)] (**134**) as inspired by literature reported by Gladysz[431] and coworkers.*

Spectroscopically, the *trans*-[PtCl(*p*-tol)(PCy_2Me)$_2$] (**140**) product is witnessed *via* $^{195}Pt\{^1H\}$ NMR spectroscopy as a triplet appearing at –4,222 ppm ($^1J_{Pt\text{-}P}$ = 2,837 Hz). Crystals suitable for X-ray diffraction were grown from saturated solutions of (**140**) in benzene. An ORTEP diagram for the structure† as well as some key bond distances for *trans*-[PtCl(*p*-tol)(PCy_2Me)$_2$] (**140**) are shown in Figure 3-48. The *trans*-[PtCl(*p*-tol)(PCy_2Me)$_2$] (**140**) species displays Pt(1)-C(1) bond distances of 2.015(3) Å and a Pt(1)-Cl(1) bond distance of 2.4098(8) Å. The square planar platinum structure displays the Pt(1)-P(1) and Pt(1)-P(2) bond distances to both be 2.3021(7) Å due to the symmetry (*Pnma*) of the system.

* NMR spectroscopic data taken directly from reaction mixtures: $^{31}P\{^1H\}$ NMR (161.98 MHz, 4:1 (v:v) $C_6H_5CH_3$/$HNEt_2$, H_3PO_4, 297 K).
† $C_{33}H_{57}ClP_2Pt$, M = 746.26, orthorhombic, space group = *Pnma*.

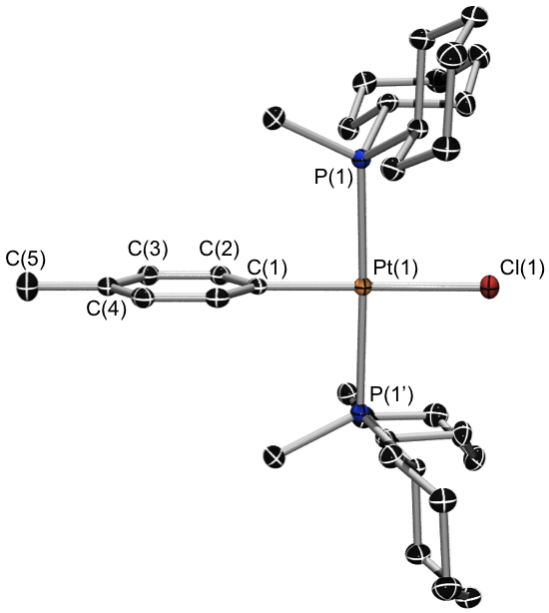

Figure 3-48. ORTEP rendered structure of *trans*-[PtCl(*p*-tol)(PCy_2Me)$_2$] (**140**). Thermal ellipsoids set at 50% probability. All hydrogen atoms have been omitted for clarity. Selected bond distances (Å) and angles (°): Pt(1)–P(1) 2.3021(7), Pt(1)–Cl(1) 2.4093(8), Pt(1)–C(1) 2.015(3), P(1)–Pt(1)–Cl(1) 88.85, C(1)–Pt(1)–Cl(1) 179.26.

3.2.1.2 *trans*-[Pt{(C≡C)$_2$-H}(*p*-tol)(PCy_2Me)$_2$] (141)

trans-[Pt{(C≡C)$_2$-H}(*p*-tol)(PCy_2Me)$_2$] (**141**) was prepared according to the modified literature procedure previously discussed* in which *trans*-[PtCl(*p*-tol)(PCy_2Me)$_2$] (**140**) is mixed with a catalytic amount of CuI in $HNEt_2$ and cooled to –45 °C (Figure 3-49). Butadiyne (0.4 M in THF) was then added to the reaction mixture with stirring and allowed to react at –45 °C for a period of 1 h. $^{31}P\{^1H\}$ NMR spectroscopic monitoring of the reaction witnessed near full conversion of *trans*-[PtCl(*p*-tol)(PCy_2Me)$_2$] (**140**) ($^{31}P\{^1H\}$: δ = 11.2 ppm, $^1J_{P\text{-}Pt}$ = 2,848 Hz) to the *trans*-[Pt{(C≡C)$_2$-H}(*p*-tol)(PCy_2Me)$_2$] (**141**) species ($^{31}P\{^1H\}$: δ = 10.0 ppm, $^1J_{P\text{-}Pt}$ = 2,658 Hz). After this time, the reaction mixture was allowed to come to room temperature and stir for an additional hour. After removal of the solvent, the crude pale yellow solid was purified by column chromatography (Al_2O_3), and dried to yield *trans*-[Pt{(C≡C)$_2$-H}(*p*-tol)(PCy_2Me)$_2$] (**141**) as pale yellow solids in 40% yield.

* See Section 3.2.1.

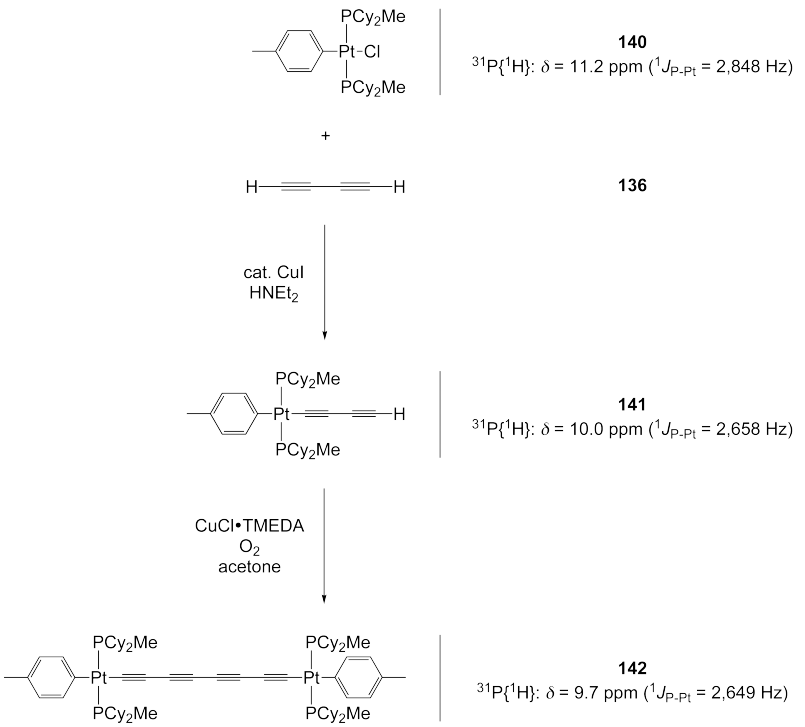

Figure 3-49. *trans*-[Pt{(C≡C)$_2$-H}(*p*-tol)(PCy$_2$Me)$_2$] (**141**) synthesis from *trans*-[PtCl(*p*-tol)(PCy$_2$Me)$_2$] (**140**) as outlined by Gladysz and coworkers.[*]

Differential thermal analysis of these light yellow crystalline solids showed an exothermic peak for **141** at 191 °C (melting point) followed by what appeared to be multiple decomposition peaks at 283 °C and 386 °C. The species **141** was then subjected to thermogravimetric analysis to ascertain if any stable decomposition product could possibly be isolated; however, only direct decomposition of the species to platinum metal was witnessed in the data analysis with no apparent stable intermediate.

The *trans*-[Pt{(C≡C)$_2$-H}(*p*-tol)(PCy$_2$Me)$_2$] (**141**) product is witnessed *via* ^{195}Pt{^{1}H} NMR spectroscopy as a triplet appearing at −4,759 ppm ($^1J_{Pt\text{-}P}$ = 2,390 Hz). Analysis of *trans*-[Pt{(C≡C)$_2$-H}(*p*-tol)(PCy$_2$Me)$_2$] (**141**) by infrared spectroscopy shows multiple observable bands that could correspond to the Pt-C stretching mode at 607 and 514 cm^{-1} and one observable $\tilde{\nu}$(C≡C) absorption at 2,132 cm^{-1}. Crystals suitable for X-ray diffraction were grown from saturated solutions of **141** in hexane. An ORTEP diagram for the structure[†] as well as some key bond distances for *trans*-[Pt{(C≡C)$_2$-H}(*p*-tol)(PCy$_2$Me)$_2$] (**141**) are shown in Figure 3-50. The *trans*-[Pt{(C≡C)$_2$-H}(*p*-tol)(PCy$_2$Me)$_2$] (**141**) species displays Pt(1)-P(1), Pt(1)-P(2),

[*] NMR spectroscopic data taken directly from reaction mixtures: ^{31}P{^{1}H} NMR (161.98 MHz, 4:1 (v:v) $C_6H_5CH_3$/HNEt$_2$, H_3PO_4, 297 K).
[†] $C_{37}H_{58}P_2Pt$, M = 759.88, monoclinic, space group = $P2_1/c$.

Pt(1)-C(1), Pt(1)-C(5) bond distances of 2.312(1), 2.308(1), 2.029(4), and 2.077(4) Å respectively.

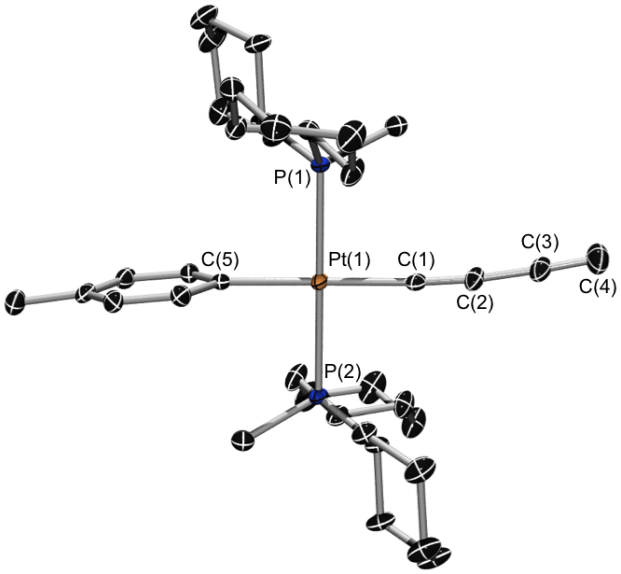

Figure 3-50. ORTEP-rendered structure of *trans*-[Pt{(C≡C)$_2$-H}(*p*-tol)(PCy$_2$Me)$_2$] (**141**). Thermal ellipsoids set at 50% probability. All hydrogen atoms have been omitted for clarity. Selected bond distances (Å) and angles (°): Pt(1)–P(1) 2.312(1), Pt(1)–P(2) 2.308(1), Pt(1)–C(1) 2.029(4), Pt(1)–C(5) 2.077(4), C(1)–C(2) 1.220(6), C(2)–C(3) 1.389(7), C(3)–C(4) 1.207(8), P(1)–Pt(1)–C(1) 89.12, C(1)–Pt(1)–C(5) 178.32.

3.2.1.3 *trans,trans*-[(*p*-tol)(Cy$_2$MeP)$_2$Pt(C≡C)$_4$Pt(PCy$_2$Me)$_2$(*p*-tol)] (142)

trans,trans-[(*p*-tol)(Cy$_2$MeP)$_2$Pt(C≡C)$_4$Pt(PCy$_2$Me)$_2$(*p*-tol)] (**142**) was prepared according to the modified literature procedure previously discussed* in which *trans*-[Pt{(C≡C)$_2$-H}(*p*-tol)(PCy$_2$Me)$_2$] (**141**) is mixed with CuCl•TMEDA in acetone (Figure 3-49). The modified Hay coupling conditions are then applied to the system and the two platinum species are coupled together through oxidation of the copper acetylenides with dioxygen. $^{31}P\{^1H\}$ NMR spectroscopic monitoring of the reaction witnessed near full conversion of *trans*-[Pt{(C≡C)$_2$-H}(*p*-tol)(PCy$_2$Me)$_2$] (**141**) ($^{31}P\{^1H\}$: δ = 10.0 ppm, $^1J_{P\text{-}Pt}$ = 2,658 Hz) to the *trans,trans*-[(*p*-tol)(Cy$_2$MeP)$_2$Pt(C≡C)$_4$Pt(PCy$_2$Me)$_2$(*p*-tol)] (**142**) species ($^{31}P\{^1H\}$: δ = 9.7 ppm, $^1J_{P\text{-}Pt}$ = 2449 Hz). Workup of the reaction mixture gave *trans,trans*-[(*p*-tol)(Cy$_2$MeP)$_2$Pt(C≡C)$_4$Pt(PCy$_2$Me)$_2$(*p*-tol)] (**142**) as a yellow solid in very poor yield (< 10%). Full characterization of the compound was not possible as

* See Section 3.2.1.

the yield was too low and the synthetic scale was always kept small due to the possibility of explosive copper acetylide side products. The low yield of the reaction only allowed for synthesis of approximately 20 mg of substance, which was used directly to test for transfer of a borylene fragment to the system (See Section 3.2.2).

3.2.2 Borylene Transfer Attempts

As can be seen below in Figure 3-51, borylene transfer reactions were tried with the *trans,trans*-platinum *bis*(phosphine) octatetraynyl complexes *trans,trans*-[(*p*-tol){(*p*-tol)$_3$P}$_2$Pt(C≡C)$_4$Pt{P(*p*-tol)$_3$}$_2$(*p*-tol)] (**138**) and *trans,trans*-[(*p*-tol)(Cy$_2$MeP)$_2$Pt(C≡C)$_4$Pt(PCy$_2$Me)$_2$(*p*-tol)] (**142**). These reactions were carried out using [(OC)$_5$Cr{BN(SiMe$_3$)$_2$}] (**13**) (4.4 equivalents) and performed photolytically. Unfortunately the yield for the complex *trans,trans*-[(*p*-tol)(Cy$_2$MeP)$_2$Pt(C≡C)$_4$Pt(PCy$_2$Me)$_2$(*p*-tol)] (**142**) was insufficient for more thorough reaction studies; however, the high yield for the complex *trans,trans*-[(*p*-tol){(*p*-tol)$_3$P}$_2$Pt(C≡C)$_4$Pt{P(*p*-tol)$_3$}$_2$(*p*-tol)] (**138**) provided sufficient amounts of precursor to attempt borylene transfer reactions on these systems. After repeated irradiation of these *trans,trans*-platinum *bis*(phosphine) octatetrayne complexes with [(OC)$_5$Cr{BN(SiMe$_3$)$_2$}] (**13**), only decomposition of these two specific products could be observed from NMR spectroscopic monitoring of these reaction mixtures under photolytic conditions.

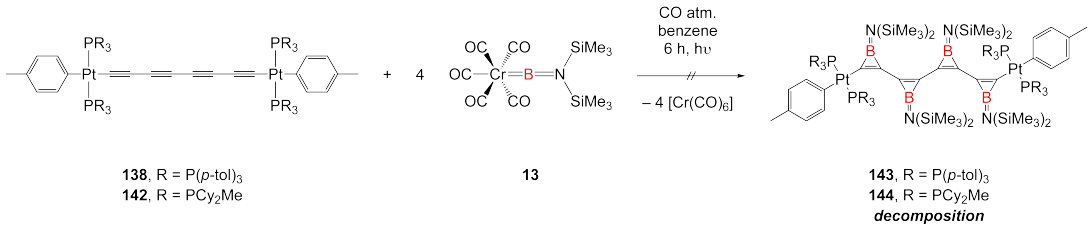

Figure 3-51. Attempts to transfer multiple terminal borylene ligands onto the *trans,trans*-platinum *bis*(phosphine) octatetraynyl complexes *trans,trans*-[(*p*-tol){(*p*-tol)$_3$P}$_2$Pt(C≡C)$_4$Pt{P(*p*-tol)$_3$}$_2$(*p*-tol)] (**138**) and *trans,trans*-[(*p*-tol)(Cy$_2$MeP)$_2$Pt(C≡C)$_4$Pt(PCy$_2$Me)$_2$(*p*-tol)] (**142**).

Borylene transfer reactions were also attempted with the *trans*-platinum *bis*(phosphine) butadienyl complexes *trans*-[Pt{(C≡C)$_2$-H}(*p*-tol){P(*p*-tol)$_3$}$_2$] (**137**) and *trans*-[Pt{(C≡C)$_2$-H}(*p*-tol)(PCy$_2$Me)$_2$] (**141**) (Figure 3-51). These reactions were carried out using the terminal borylene species [(OC)$_5$Cr{BN(SiMe$_3$)$_2$}] (**13**) (2.2 equivalents) and performed photolytically. These reactions also showed unfortunate product decomposition after repeated irradiation reactions of *trans*-platinum *bis*(phosphine) butadienyl complexes with [(OC)$_5$Cr{BN(SiMe$_3$)$_2$}] (**13**). As with the transfer reaction reported in Figure 3-50, only decomposition of these two specific products could be observed from NMR spectroscopic monitoring of the reaction mixtures under photolytic conditions.

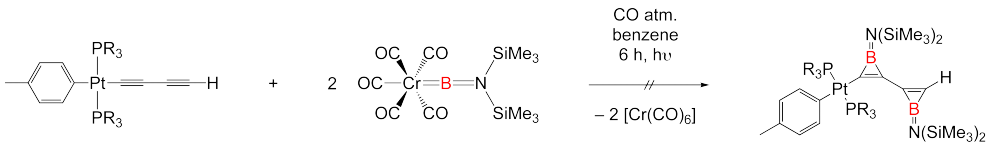

137, R = P(*p*-tol)$_3$
141, R = PCy$_2$Me

13

145, R = P(*p*-tol)$_3$
146, R = PCy$_2$Me
decomposition

Figure 3-52. Attempts to transfer multiple terminal borylene ligands onto the complexes *trans*-[Pt{(C≡C)$_2$-H}(*p*-tol){P(*p*-tol)$_3$}$_2$] (**137**) and *trans*-[Pt{(C≡C)$_2$-H}(*p*-tol)(PCy$_2$Me)$_2$] (**141**).

3.3 Synthesis of Monoborirene Adducts

As part of the continued studies of the asymmetric borylene ligand complexes developed in Section 2.1.2, the Group 6 unsymmetrical terminal pentacarbonyl borylene complexes [(OC)$_5$M{BN(SiMe$_3$)(*t*-Bu)}] (M = Cr (**19**), Mo (**20**), and W (**21**)) were tested for photolytic and thermolytic transfer reactions (Figure 3-53). The basis for all of these reactions was taken from previous literature publications by Braunschweig and coworkers.[173,174,295,297] The chromium terminal unsymmetrical borylene [(OC)$_5$Cr{BN(SiMe$_3$)(*t*-Bu)}] (**19**) was tested for photolytic transfer ability to a simple phenyl-substituted alkyne substrate (**147**). The tungsten unsymmetrical terminal pentacarbonyl borylene [(OC)$_5$W{BN(SiMe$_3$)(*t*-Bu)}] (**21**) was tested for transfer to a *trans*-platinum mono-σ-alkynyl species *trans*-[PtCl(C≡C-Ph)(PEt$_3$)$_2$] (**99**). Finally, the molybdenum unsymmetrical terminal pentacarbonyl borylene [(OC)$_5$Mo{BN(SiMe$_3$)(*t*-Bu)}] (**20**) was tested for thermal transfer to the pentamethylcyclopentadienyl iron dicarbonyl σ-alkynyl complex [(η^5-C$_5$Me$_5$)(OC)$_2$Fe(C≡C-Ph)][441] (**89**). These transfer studies were designed to establish precedence for all three members of this unsymmetrical Group 6 borylene family of complexes in displaying similar reactivity patterns to the symmetrical *bis*(trimethylsilyl)aminoborylene complexes [(OC)$_5$M{BN(SiMe$_3$)$_2$}] (M = Cr (**13**), Mo (**14**), and W (**15**)) previously discussed in Section 2.1.1.

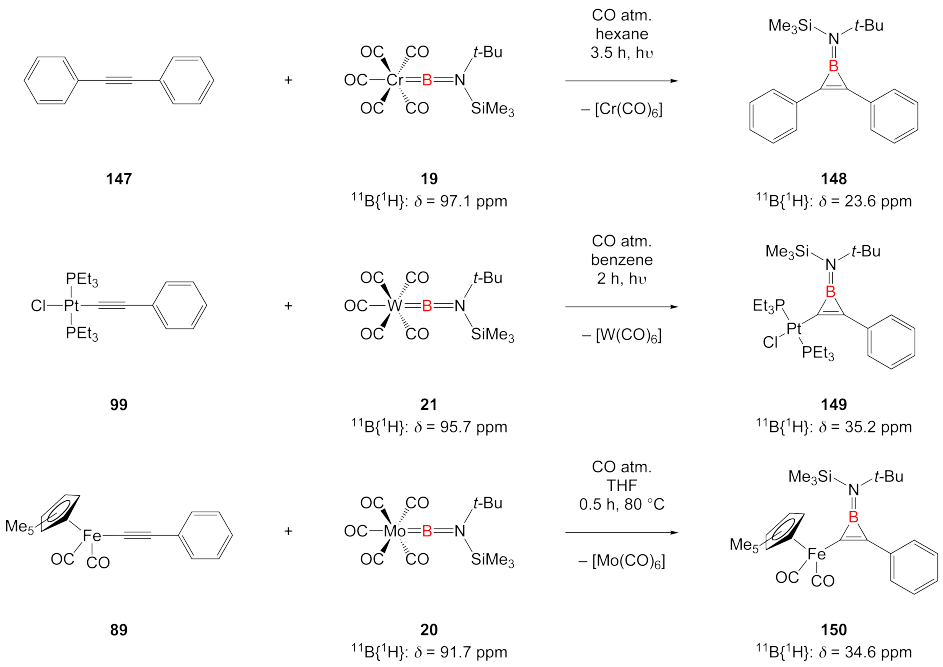

Figure 3-53. Borylene transfer reactions performed using all three members of the Group 6 terminal unsymmetrical borylene complexes ((**19**), (**20**), and (**21**)) (Section 2.1.1) to alkynyl species either under photolytic or thermolytic conditions.

The generation of the diphenyl-substituted borirene (**148**) (Figure 3-53) was conducted *via* photolytic transfer of the borylene ligand from [(OC)$_5$Cr{BN(SiMe$_3$)(*t*-Bu)}] (**19**) onto diphenylacetylene (**147**). The reaction was observed to be complete after approximately 3.5 h of irradiation with consumption of **19** witnessed in ^{11}B{^{1}H} NMR spectroscopy (^{11}B{^{1}H}: δ = 97.1 ppm) and growth of the borirene product resonance at (^{11}B{^{1}H}: δ = 23.6 ppm) corresponding to the (trimethylsilyl)(*tert*-butyl)amino-2,3-diphenylborirene (**148**). The generation of the *trans*-platinum mono-σ-borirenyl complex (**149**) was conducted *via* photolytic transfer of the borylene ligand from [(OC)$_5$W{BN(SiMe$_3$)(*t*-Bu)}] (**21**) onto *trans*-[PtCl(C≡C-Ph)(PEt$_3$)$_2$] (**99**). As in the case of the reaction of compound **148**, the reaction was observed to be completed after an irradiation time of approximately 2 h with complete consumption of [(OC)$_5$W{BN(SiMe$_3$)(*t*-Bu)}] (**21**) witnessed in ^{11}B{^{1}H} NMR spectroscopy (^{11}B{^{1}H}: δ = 95.7 ppm) and growth of the borirene resonance at (^{11}B{^{1}H}: δ = 35.2 ppm) corresponding to *trans*-[PtCl{(μ-{BN(SiMe$_3$)(*t*-Bu)}C=C)-Ph}(PEt$_3$)$_2$] (**149**).

The generation of the pentamethylcyclopentadienyl iron mono-σ-borirenyl complex [(η^5-C$_5$Me$_5$)(OC)$_2$Fe(μ-{BN(SiMe$_3$)(*t*-Bu)}C=C)Ph] (**150**) was conducted *via* thermolytic transfer of the borylene ligand from [(OC)$_5$Mo{BN(SiMe$_3$)(*t*-Bu)}] (**20**) onto the iron precursor [(η^5-C$_5$Me$_5$)(OC)$_2$FeC≡C-Ph] (**89**). The thermolytic borylene transfer from [(OC)$_5$Mo{BN(SiMe$_3$)(*t*-Bu)}] (**20**) onto [(η^5-C$_5$Me$_5$)(OC)$_2$FeC≡C-Ph] (**89**) was observed to be complete after approximately 0.5 h of heating of the reaction mixture to 80 °C with consumption of [(OC)$_5$Mo{BN(SiMe$_3$)(*t*-Bu)}] (**20**) witnessed in ^{11}B{^{1}H} NMR spectroscopy (^{11}B{^{1}H}: δ = 91.7 ppm) and growth of the borirene product resonance at (^{11}B{^{1}H}: δ = 34.6 ppm) corresponding to formation of [(η^5-C$_5$Me$_5$)(OC)$_2$Fe(μ-{BN(SiMe$_3$)(*t*-Bu)}C=C)Ph] (**150**).

Workup of the three new borirenes was attempted as outlined in Section 3.1.3; however, purification of these species was difficult as they all appear to be oils (at room temperature), making single-crystal X-ray structural diffraction studies difficult. Purification of the reaction mixtures was performed by removal of all volatiles *in vacuo* and sublimation of all unreacted borylene and [M(CO)$_6$] (M = Cr, Mo, and W) byproduct by heating to 65 °C under high vacuum (0.001 Torr). The resulting dark yellow reaction mixtures were purified *via* pacified silica gel (SiO$_2$) column chromatography[397] to yield products **148**, **149**, and **150** as air-sensitive light yellow oils. One difference in the purification of these new borirene species relative to

the *trans*-platinum *bis*(borirenyl) species discussed in Section 3.1.3 is that a small remainder of terminal group 6 unsymmetrical borylene is always observed to exist in the product fraction after the sublimation of the $[M(CO)_6]$ (M = Cr, Mo, and W) byproducts. The $[(OC)_5M\{BN(SiMe_3)(t\text{-Bu})\}]$ (M = Cr (**19**), Mo (**20**), and W (**21**)) products in their pure state sublime or distill as highly viscous oils while the symmetrical *bis*(trimethylsilyl)aminoborylene species $[(OC)_5M\{BN(SiMe_3)_2\}]$ (M = Cr (**13**), Mo (**14**), and W (**15**)) are witnessed to be solids when sublimed, so full extraction from the reaction crude material is made much more difficult for these new borylene species. The main point of these test reactions was to verify that this new class of borylene ligand $\{BN(SiMe_3)(t\text{-Bu})\}$ will react in a similar manner to the previously published *bis*(trimethylsilyl)aminoborylene ligands $\{BN(SiMe_3)_2\}$ and they have been witnessed to fulfill this requirement.

3.4 Expansion Reaction of a Borirene to a Borole

Initial studies of borirene systems by Eisch and coworkers[263] revealed an interesting ring expansion of a borirene system (*cyclo*-BC_2) to a Lewis-base-quarternized borole system (*cyclo*-BC_4). To our knowledge this reaction had not been attempted by members of our group and was probed to see if the route is actually feasible. As can be seen below in Figure 3-54, the reported reaction starts with the pyridine-quarternized triphenylborirene (**151**). Photolytic irradiation of this quarternized borirene with another equivalent of free alkyne (diphenylacetylene) was reported to force a ring expansion of the quarternized borirene system resulting in the formation of the quarternized borole (**153**). Interestingly, the alkyne was found to insert into a B-C bond, rather than the C-C bond (Figure 3-54). As the number of substituents available for stabilizing free boroles are still severely limited in scope, the ability to quarternize borirenes and expand them with substituted alkynes to yield new classes of boroles seemed to be a highly desirable research topic. Borirene systems are known to be capable of functionalization with a much broader range of substituents compared to boroles and through this ring expansion reaction boroles could not only be synthesized bearing new substituents, but synthesized in unsymmetrical functionalized fashions.

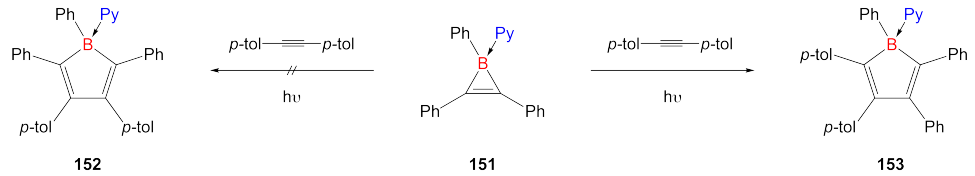

Figure 3-54. Reaction reported by Eisch and coworkers[263] for ring expansion of a quarternized borirene to a quarternized borole by photolysis with an alkyne.

As a starting point for these studies of borirene ring expansion the *bis*(trimethylsilyl)amino-2,3-diphenylborirene (**154**) was chosen due to its structural similarity to the borirene used in the previously reported ring-expansion reaction as well as the compound's relative convenience in preparation and purification. The species is also easy to detect and follow in reaction studies by $^{11}B\{^1H\}$ NMR spectroscopic monitoring ($^{11}B\{^1H\}$: δ = 24.6 ppm). Figure 3-55 shows the Lewis base coordination reaction with the *N*-heterocyclic carbene (NHC) IMeMe (1,3,4,5-tetramethylimidazol-2-ylidene) to form the quarternized borirene species **155** ($^{11}B\{^1H\}$: δ = −18.6 ppm). Reactions of **155** with one additional equivalent of diphenylacetylene yielded a new product that was witnessed in $^{11}B\{^1H\}$ NMR spectroscopy as a peak at $^{11}B\{^1H\}$: δ = −4.1 ppm and assumed to be the NHC-

quarternized borole by comparison to literature data of the DMAP (dimethylaminopyridine) quarternized tetraphenyl-substituted chloroborole reported by Braunschweig and coworkers in 2008.[282] Interestingly, this reaction was witnessed to occur without photolytic irradiation of the mixture, and upon sitting overnight the reaction yielded a color change from light yellow to an intensely red colored (opaque) solution.

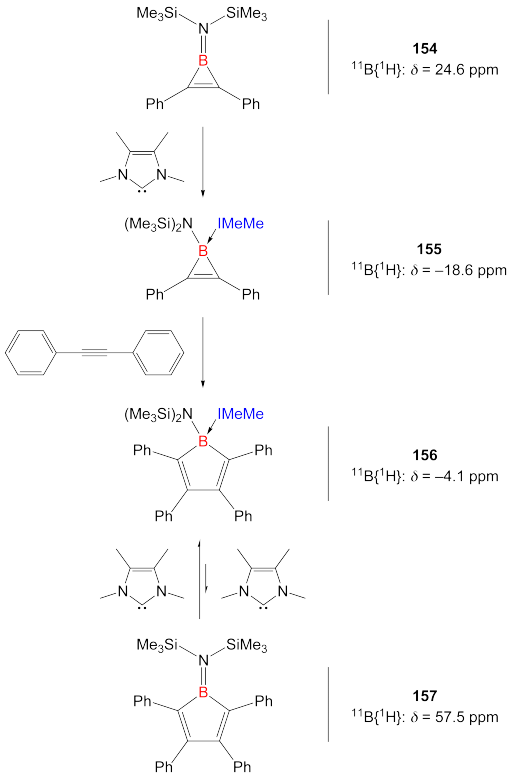

Figure 3-55. Borirene expansion *via* quarternization of **154** with the *N*-heterocyclic carbene IMeMe and reaction with a functionalized alkyne to yield **156**.

$^{11}B\{^{1}H\}$ NMR spectroscopic data from this reaction mixture witnessed a new, extremely broad resonance appearing at ($^{11}B\{^{1}H\}$: δ = 57.5 ppm) correlates very well with the literature-reported NMR resonance for a tetraphenyl-functionalized *bis*(trimethylsilyl)aminoborole (**157**) ($^{11}B\{^{1}H\}$: δ = 59.5 ppm).[282] $^{11}B\{^{1}H\}$ NMR spectroscopic monitoring of this reaction over a three day period inexplicably showed conversion of all NHC-quarternized borirene to the "free" borole with almost no witnessed NHC-quarternzied borole in solution. The only other product observed in the $^{11}B\{^{1}H\}$ NMR spectra during monitoring of the reaction is unquarternized borirene (**154**), which was present during the entire reaction study as the NHC was used as a limiting reagent in these reactions. Unfortunately, nothing was able to be isolated after repeated attempts; however, the NMR spectra for these reactions are all reproducible and indicate the same products being formed with the evolution of an

intense red-colored solution. This intensely colored wine-red/black, solution is also strongly indicative of the formation of the free borole, which has been previously reported to be this color.[282]

3.5 Alkynylborane Oligomerization Studies

Inspired by work from Chujo and coworkers, a project was established to attempt to prepare an oligo(alkynylborane). As Chujo elegantly demonstrated by utilizing a hydroboration route to polymerize three-coordinate boron centers into π-conjugated organic and organometallic backbones (see Section 1.2.2), a halostannane elimination route could also be feasible by utilizing our dihaloborane precursors and *bis*(trimethylstannyl)acetylene[442] to yield a boron-functionalized alkynylborane oligomer. Equimolar mixing of these reagents resulted in formation of the monomeric species $XB\{N(SiMe_3)_2\}C{\equiv}CSnMe_3$. However, pure fractions of this species gave only oily material and are very difficult to purify from the unreacted haloborane precursors.

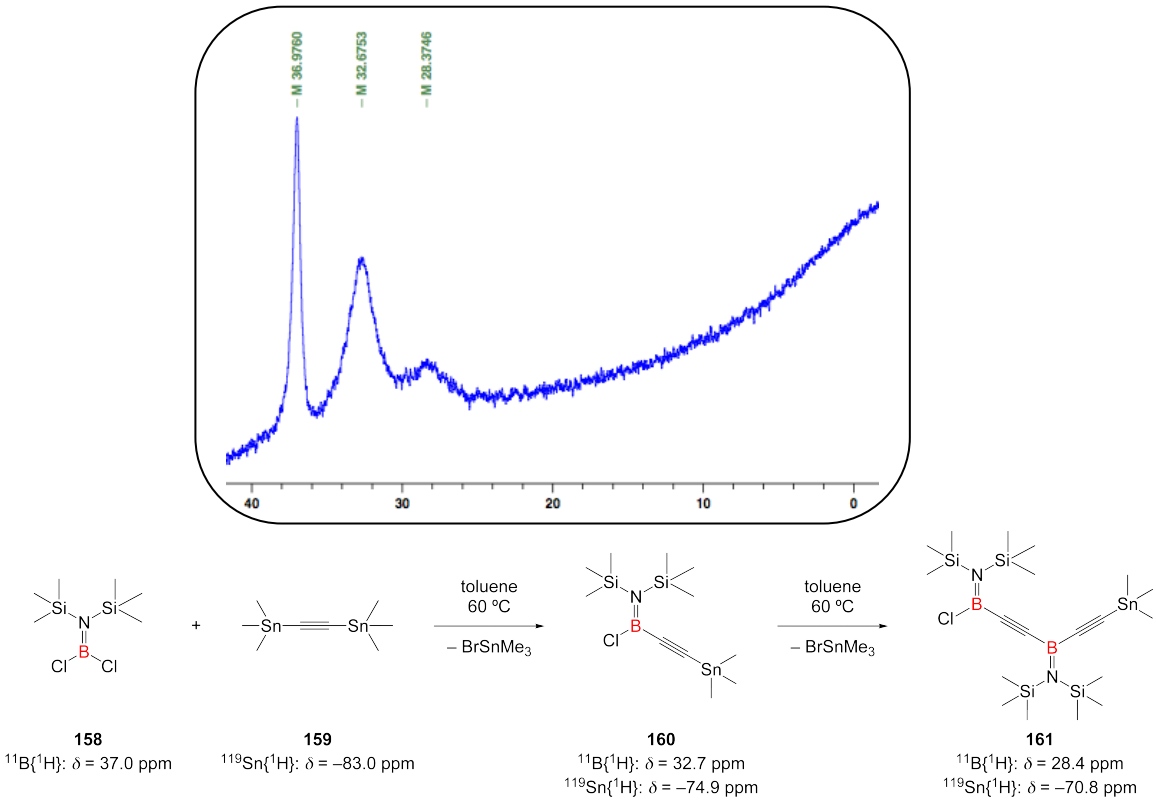

Figure 3-56. $^{11}B\{^1H\}$ NMR data (top) and reaction scheme (bottom) for the first series of test reactions in the synthesis of an alkynylborane.

As can be seen in Figure 3-56 (bottom), the first test reaction for the synthesis of these monomeric stannyl-functionalized haloboranes was conducted with $Cl_2BN(SiMe_3)_2$[443] (**158**) and $Me_3SnC{\equiv}CSnMe_3$ (**159**).[442] Upon heating this mixture to 60 °C, halostannane elimination was observed *via* $^{119}Sn\{^1H\}$ NMR spectroscopic[444] monitoring ($^{119}Sn\{^1H\}$: δ = 157.2 ppm). $^{11}B\{^1H\}$ NMR spectroscopic monitoring of the system witnessed three resonances which progressively shifted

upfield and became broader, suggesting formation of $ClB\{N(SiMe_3)_2\}C{\equiv}CSnMe_3$ (**160**) ($^{11}B\{^1H\}$: δ = 32.7 ppm) and one combination step to yield the product **161** ($^{11}B\{^1H\}$: δ = 28.4 ppm) (Figure 3-56, top).

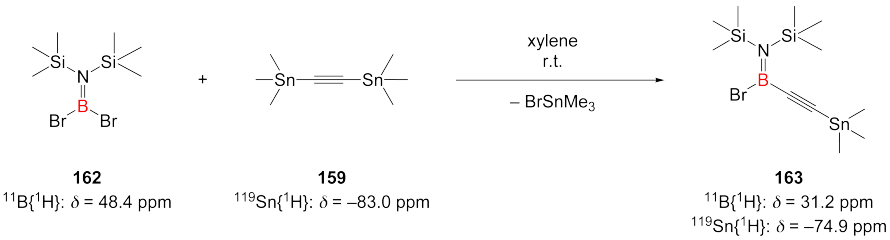

Figure 3-57. Synthesis of a monomeric stannane-functionalized alkynylhaloborane $BrB\{N(SiMe_3)_2\}C{\equiv}CSnMe_3$ (**163**) upon mixing of $Br_2BN(SiMe_3)_2$ (**162**) and $Me_3SnC{\equiv}CSnMe_3$ (**159**) at room temperature.

The initial synthesis of $Cl(B\{N(SiMe_3)_2\}C{\equiv}C)_2SnMe_3$ (**161**) was encouraging; however, in order to achieve maximum chain length in these combination studies, formation of the monomer had to be possible at room temperature to enable thermally-induced polymerization at reasonable temperatures (<160 °C) and in normal laboratory solvents (xylene). The reaction outlined in Figure 3-56 was reproduced with the dibromoborane $Br_2BN(SiMe_3)_2$ (**162**) and was found to successfully produce the monomeric stannyl-functionalized haloborane $BrB\{N(SiMe_3)_2\}C{\equiv}CSnMe_3$ (**163**) at room temperature (Figure 3-57). Controlled heating studies of this species in xylene saw decrease of the $^{11}B\{^1H\}$ NMR resonance observed for the monomeric species **163** ($^{11}B\{^1H\}$: δ = 31.2 ppm) and formation of multiple broad signals which eventually converged to one signal in $^{11}B\{^1H\}$ NMR spectra after heating to 150 °C for one week ($^{11}B\{^1H\}$: δ = 28.4 ppm). The rationalization for the multiple NMR signals converting to one extremely broad resonance is that upon heating of the monomer **163** and other small chain variants, combination will eventually drive all of these small species to a maximum chain length (Figure 3-58). This major product was observed to precipitate out of solution upon cooling of the reaction mixtures as a white solid and could be isolated by filtration.

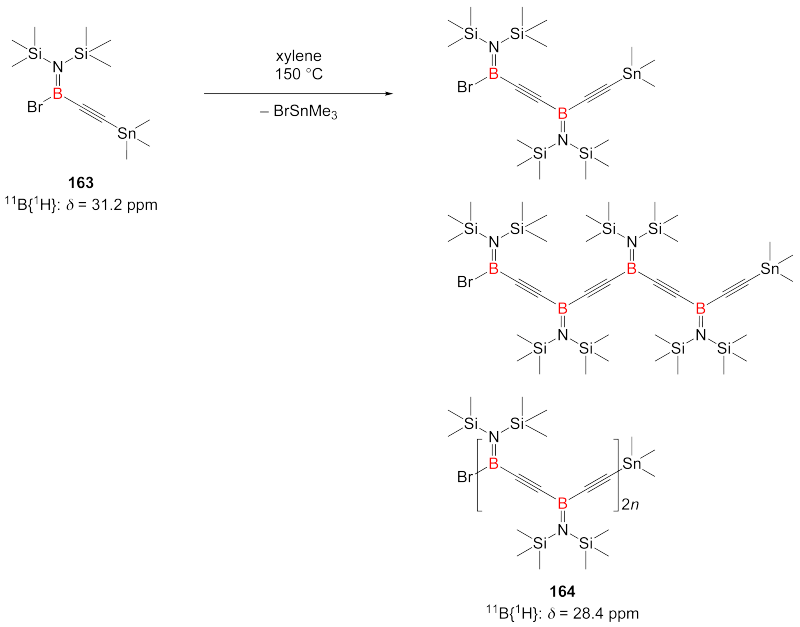

Figure 3-58. Controlled heating of $BrB\{N(SiMe_3)_2\}C{\equiv}CSnMe_3$ (**163**) and several proposed combination routes which are eventually witnessed to form a single $^{11}B\{^1H\}$ NMR resonance for a maximum chain length **164**.

This white solid was analyzed by gel permeation chromatography (GPC) and found to have a maximum molecular weight of approximately ~1,500 Da. Unfortunately the instrument is designed to analyze material of a much higher molecular weight and was unable to give a more accurate maximum weight for the analyzed species. Figure 3-59 shows the recorded spectrum for two separate detectors that was used to estimate the molecular weight of the main product (1,000 Da). Examination of the blue line spectrum in Figure 3-59 shows maxima correlating to approximately ~450, ~700, and ~1,100 Da, which could correspond to chain doubling due to combination from halostannane elimination. The repeating unit ($BN(SiMe_3)_2C{\equiv}C$) molecular weight is 195 Da with the molecular weight of the end groups (Br and $SnMe_3$) being 244 Da. This yields the equation ($M = (195)n + (244)$) where n is the number of repeating units and M is the calculated molecular weight. This equation indicates that all three of these species observed *via* GPC are plausible combinations of smaller alkynylborane monomers (1, 2, and 4 repeating unit combinations, respectively). Presumably this $BrB\{N(SiMe_3)_2\}C{\equiv}CSnMe_3$ (**163**) monomeric species begins to combine with itself under heating and will form a dimer, tetramer, and octomer. The $^{11}B\{^1H\}$ NMR data for this compound is also as expected for this type of combination with severe broadening of the boron resonance observed for the transition of the monomer to higher molecular weight analogs and formation of increasingly broad resonances which eventually collapse into one extremely broad resonance at ($^{11}B\{^1H\}$: δ = 28.4 ppm).

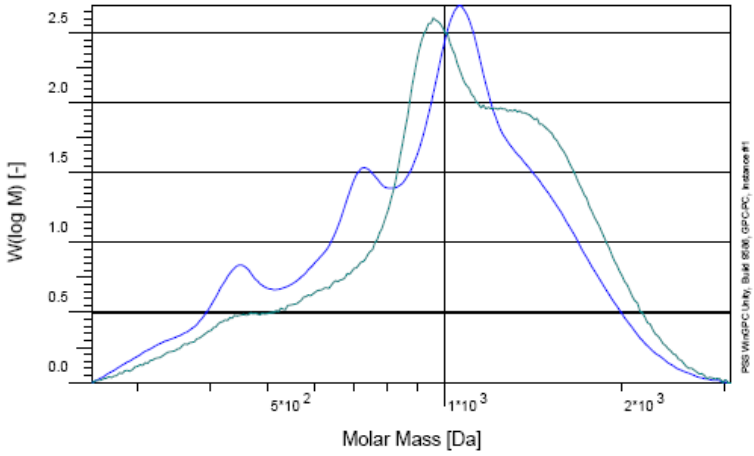

Figure 3-59. GPC data taken from the characterization of the white precipitate isolated from controlled heating of $BrB\{N(SiMe_3)_2\}C{\equiv}CSnMe_3$ (**163**).

Finally, borylene transfer reactions were also attempted with $BrB\{N(SiMe_3)_2\}C{\equiv}CSnMe_3$ (**163**) and the white precipitate **164** isolated from the controlled heating experiments of the monomer. The stoichiometry of these transfer reactions were ascertained from a 1:1 ratio of $Me_3SnC{\equiv}CSnMe_3$ (**159**) used in the initial synthesis of the monomer. Unfortunately, no photolytic borylene transfer could be confirmed by these studies and only decomposition of the terminal borylene complex was observed (Figure 3-60). Additionally, photolysis of **163** was attempted to check for photolytic rearrangment of the alkyne to the borirene in a similar manner to that reported by Eisch and coworkers for their aryl-substituted alkynylboranes. Unfortunately, this also failed to show any stable photolytic rearrangement of these species to a borirenyl species **166**.

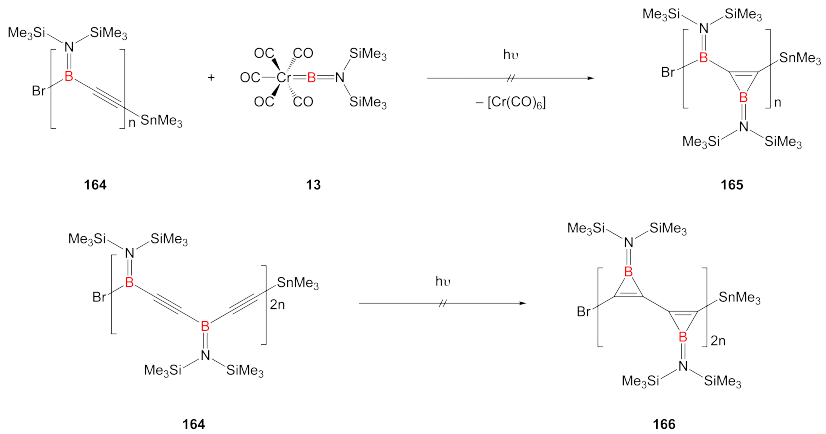

Figure 3-60. Borylene transfer reactions with $[(OC)_5Cr\{BN(SiMe_3)_2\}]$ (**13**) and photo-rearrangements attempted with the white precipitate **164** isolated from controlled heating experiments of the system.

3.6 Project Borirene Summary

In this chapter, the synthesis of the first platinum *bis*(borirene) complexes are presented along with findings from structural and electronic examination of the role of platinum in allowing increased coplanarity and conjugation of twin borirene systems. This series of *trans*-platinum linked *bis*(borirene) complexes (**119**/**120**, **122**/**123**, and **125**/**126**) all show coplanarity in the twin ring systems and stand as the first verified structural representations of two coplanar borirene systems across a linking unit. The role of a platinum atom in mediating communication between chromophoric ligands can be generalized by an expected bathochromic (red) shift in the absorption spectrum due to an increase in the electronic delocalization between the formerly independent aromatic systems when compared to the platinum mono-*σ*-borirenyl systems. The *trans*-platinum *bis*(borirene) scaffold serves as a simplified monomeric system that allows not only study of the effects of transition metals in mitigating electronic conjugation, but also the tunability of the overall photophysical profile of the system by exocyclic augmentation of the three-membered aromatic ring.

Three *trans*-platinum *bis*(borirene) complexes were successfully prepared by borylene transfer to *trans*-platinum *bis*(alkynyl) complexes. Although a host of other variants of platinum alkynyl species were prepared and attempted, these three were the only ones that successfully yielded *trans*-platinum *bis*(borirenyl) units. Attempts were also made to create a *cis*- variant for direct UV-vis comparison to the *trans*-platinum *bis*(borirenyl) variants, however these attempts were not successful. Gladysz-type platinum end-capped alkynyl species were also synthesized to serve as transfer platforms for borirene synthesis in sequential order; however, these species were shown to not be photolytically stable.

A host of new monoborirenes were synthesized by photolytic and thermolytic transfer of the unsymmetrical {$BN(SiMe_3)(t\text{-Bu})$} ligand from the complexes $[(OC)_5M\{BN(SiMe_3)(t\text{-Bu})\}]$ (M = Cr (**19**), Mo (**20**), and W (**21**)) to organic and organometallic alkynyl species to check that the complexes display the same reactivity as reported for $[(OC)_5M\{BN(SiMe_3)_2\}]$ (M = Cr (**13**), Mo (**14**), and W (**15**)). These species are all found to be oils when in pure states and X-ray structural determination was impossible for these species.

A ring expansion reaction previously reported by Eisch and coworkers was investigated and reproduced using the *bis*(trimethylsilyl)aminoborirene (**154**). The study found strong NMR spectroscopic evidence that the ring expansion does occur with mixing of a functionalized alkyne with a quarternized boron center (NHC) but does not require photolytic irradiation as reported in the publication. Also, with this particular *bis*(trimethylsilyl)aminoborole system, dissociation of the NHC from the borole appears to occur in solution over time to yield NMR spectral data that is in strong agreement with the previously reported Lewis-base-free *bis*(trimethylsilyl)aminoborole. This data is in agreement with the X-ray structure published for *bis*(trimethylsilyl)aminoborole which shows a B-N bond distance correlating to a double bond, hence an electronically-saturated boron center without the carbene stabilizing interaction.

Finally, a study of halostannane elimination for the creation of alkynylborane chains was conducted to probe the feasibility of this synthetic route in creating small boron-containing oligoalkynyl species. The preliminary results in this study indicate chain doubling due to thermal halosilane eliminations in a 1, 2, to 4 pattern as indicated by GPC data for the solid precipitate isolated from test reactions. This material contains two trimethylsilyl groups per repeating unit to promote solubility of the chain, while the thermal release of trimethylstannylbromide is a controllable process, as opposed to radical or hydroboration polymerization mechanisms as in the case of Chujo and coworkers.

Chapter 4 – Project Boratabenzene

4.1 *bis*(Boratabenzene) Synthesis

As stated in the introduction,* boratabenzene systems are aromatic monoboron-containing six-membered anionic isoelectronic analogs to cyclopentadienyl anions and are typically witnessed to coordinate to metal centers in similar manners (albeit in an η^6-manner). With the development of a reliable procedure for the synthesis of tetrabromodiborane (B_2Br_4) by our research group,[445] a new reaction was conceived to synthesize a 1,1'-*bis*(boratabenzene) ligand system [(*cyclo*-C_5H_5B)-(*cyclo*-BC_5H_5)]$^{2-}$ that would constitute a new bicyclic, dianionic variant of this ligand system. Using the well-known method developed by Herberich and coworkers,[300,301,344,345] augmentation of the boratabenzene boron atom with a boron substituent (a second boratabenzene ring) would now become possible. As only neutral or Lewis basic substituents have been previously shown to be valid candidates for stabilizing boratabenzene systems, this boron-functionalized boratabenzene species would stand alone as the only example of a Lewis acidic boron-functionalized boratabenzene compound. The cited synthetic process utilized by Herberich has already been discussed in detail in Section 1.3.3. The following chapter focuses on the development and modification of this protocol towards the reliable synthesis of a *bis*(boratabenzene) complex, the reactivity of the complex, and the interesting conjugative properties this new ligand system can enable for metal-metal magnetic and electronic communication.

* See Section 1.3.3 for details.

4.1.1 Previous Work

The synthesis of ferrocene[446,447] is viewed as a milestone in organometallic chemistry as the discovery ushered in a tremendous amount of interest in aromatic, anionic ligands that can occupy multiple coordination sites of a metal center. This discovery initiated a host of debates (as transcribed by Pauling)[448] corresponding to the metal/ligand bonding situation as well as the electron counting rules corresponding to these systems. As the boratabenzene ligand can be rationalized as a boron-containing η^6-coordinating variant of the cyclopentadienyl ligand, study of these ligands and their communicative properties with exocyclic substituents were subsequently researched heavily following the discovery of the metallocene class of compounds.[300,301,344,345]

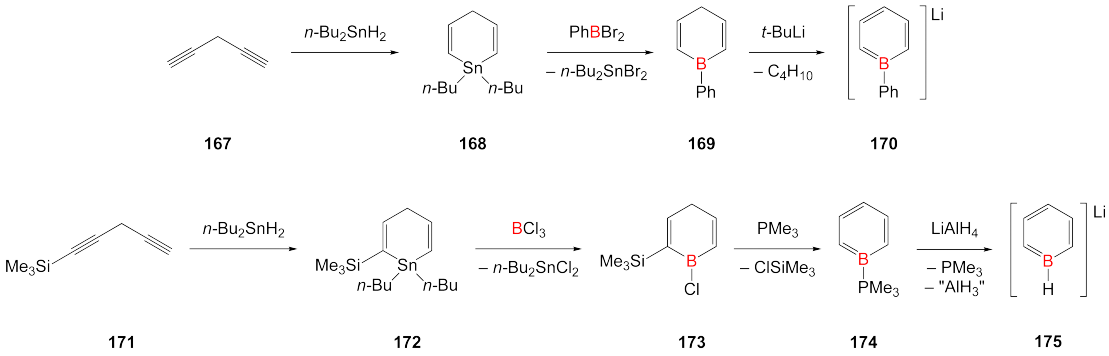

Figure 4-1. Reactions reported by Ashe *et al.* (top) and Fu *et al.* (bottom) providing an alternate route to lithium salts of the boratabenzene anions.[322,350]

In the realm of modern transition metal boratabenzene chemistry, the predominant route for synthesis of boratabenzene transition metal complexes is structured around the initial synthesis of a cation-stabilized boratabenzene salt (Figure 4-1, (**170**) and (**175**)), followed by salt elimination reactions with an appropriate transition metal halide precursor to yield the ligand η^6-coordinated to the transition metal.[300,301] This final step, although relatively efficient in terms of yield, relies on the synthesis and reduction of boracyclic precursors (boracyclohexa-2,5-dienes (**169**) and borabenzenes (**174**)) traditionally made through tin-boron exchange reactions from highly toxic stannacyclic derivatives (Figure 4-1, (**168**) and (**172**)).[273,318,319] Herberich was able to avoid this tedious method in his pioneering synthesis of the first boratabenzene complex by developing a dibromoborane induced "ring-expansion" reaction of cobaltocene (**176**) (Figure 4-2). This reported reaction is unique in that two equivalents of cobaltocene are required to provide the reductant as well as the reagent for the synthesis of $[(\eta^5\text{-}C_5H_5)Co(\eta^6\text{-}C_5H_5B\text{-}Ph)][X]$ (X = 0.5 $[SnBr_6]^{2-}$ (**178**) or $[PF_6]^-$ (**179**)).[344,345] Analysis of the reaction shows the

consumption of one equivalent of cobaltocene and 0.5 equivalents of $SnBr_4$ in the reduction of the boron-halide bonds (forming one equivalent of cobaltocenium bromide and 0.5 equivalents of $SnBr_6$), with the final equivalent remaining to "ring-expand" to the boratabenzene product $[(\eta^5\text{-}C_5H_5)Co(\eta^6\text{-}C_5H_5B\text{-}Ph)][SnBr_6]_{0.5}$ (**178**).

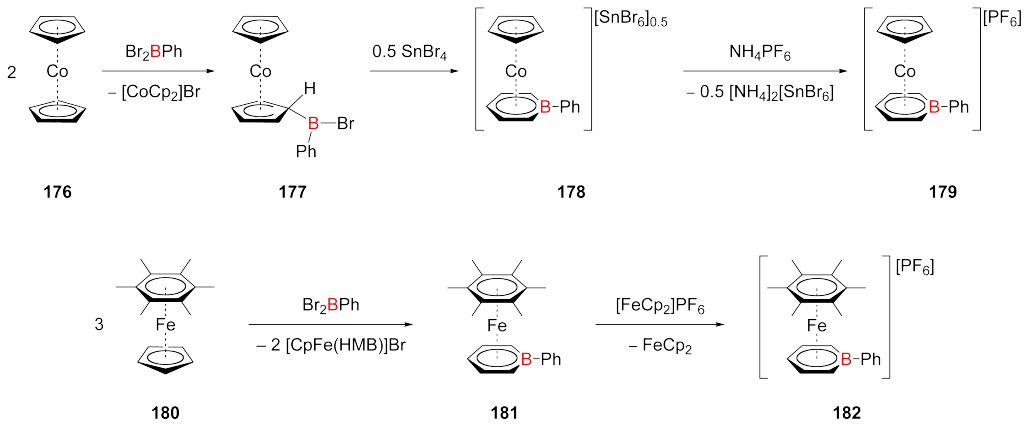

Figure 4-2. Reactions published by Herberich *et al.* for the synthesis of boratabenzene complexes, through ring expansion of the 19-electron metallocenes (**176**) and (**180**) with a functionalized dibromoborane.[344,345,449]

Research by Herberich and coworkers also found alternative 19-electron metal scaffolds such as $[(\eta^5\text{-}C_5H_5)Fe(HMB)]$ (HMB = hexamethylbenzene) (**180**) suited to carry out these boratabenzene syntheses processes as they possess the ability to also function as a reductant in solution in a similar role played by cobaltocene to yield the iron boratabenzene complex $[(HMB)Fe(\eta^6\text{-}C_5H_5B\text{-}Ph)]$ (**182**) (Figure 4-2).[449] Previous work by the groups of Heck,[327,335] O'Hare,[450] and others[334,338,341] have examined the relationship of spatially close transition metal centers tethered either through direct functionalization (**185**) or through π-linking intermediaries (**188**) respectively. The synthesis of these species were accomplished in similar manners to those reported by Herberich[344,345] (Figure 4-3), by treatment of three and six equivalents of cobaltocene with the respective dibromoboranes (**183**) and (**186**).[327,350] Spectroscopic, magnetic and electrochemical data pertaining to these studied compounds have been used to quantify the effects of the boratabenzene ligand framework in mitigating communication *via* the boron empty p_z orbital with the exocyclic substituent. Conclusions drawn from examination of these systems have indicated an increase in communication between the metal centers through incorporation of boratabenzene ligands into these metal-metal spanning ligand systems. The preparation of a 1,1'-*bis*(boratabenzene) dicobalt complex with a direct boratabenzene-boratabenzene B–B single bond can now allow for assessment of this

new ligand system upon metal-metal electronic and magnetic communicative abilities relative to these previously published complexes.

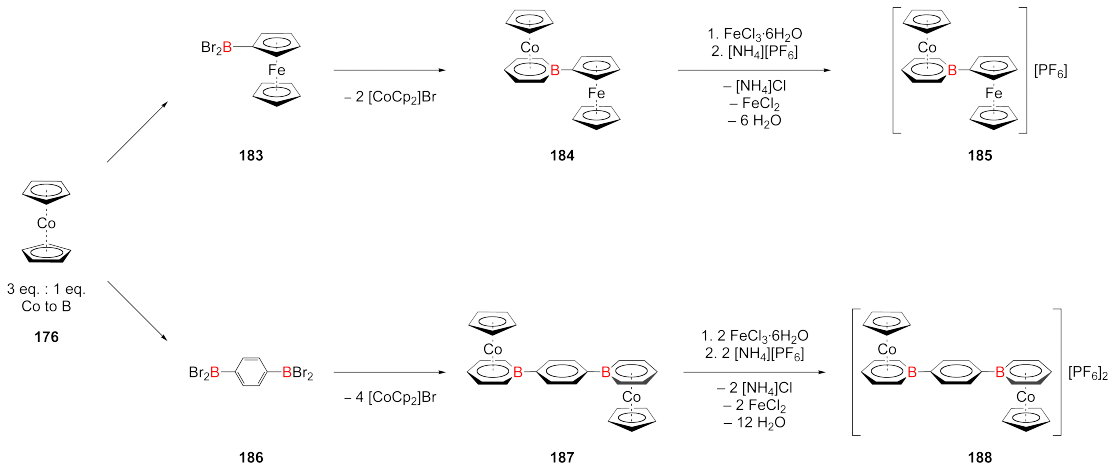

Figure 4-3. Reactions published by Heck[327] (top) and O'Hare[450] (bottom) for the synthesis of boratabenzene-linked sandwich complexes.

4.1.2 Synthesis and Purification of a 1,1'-*bis*(Boratabenzene) Complex

The 1,1'-*bis*(boratabenzene) complex [{(η^5-C_5H_5)Co}$_2${μ:η^6,η^6-(BC_5H_5)$_2$}] (**189**) was prepared by treatment of cobaltocene (**176**) with tetrabromodiborane (**65**). Successful yields of these preparatory scale reactions for the 1,1'-*bis*(boratabenzene) complex must be done with freshly prepared reagents as the stoichiometric ratios for the reagents used in the synthesis must be as close to exact as possible. The reactions were typically run by combination of ~1.2 g of tetrabromodiborane (one full batch as outlined in the doctoral thesis of Dr. Jan Mies)[445] and ~4.0 g of cobaltocene. Preparation of the cobaltocene reagent required for the synthesis was undertaken in approximately ~30 g scales by the route outlined by Cordes[451] although alternative routes are available from Wilkinson, Pauson, and Cotton[452] (Figure 4-4). In this route, freshly-prepared sodium cyclopentadienide (**190**) in THF is mixed with cobaltdichloride hexaammine (**191**) and heated to eliminate two equivalents of NaCl with the release of six equivalents of ammonia gas. Workup of the mixture gave the cobaltocene complex in yields close to literature values (~86% yield).

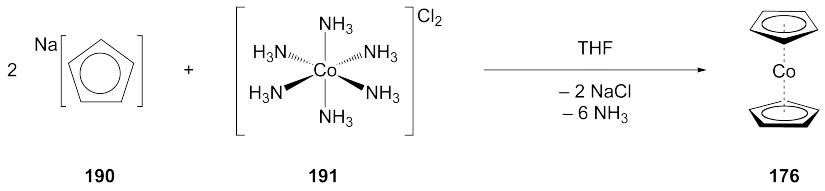

Figure 4-4. Synthesis of cobaltocene (**176**) from cobaltdichloride hexaammine ([$CoCl_2(NH_3)_6$]) (**191**) and two equivalents of sodium cyclopentadienylide (**190**).[451]

Tetrabromodiborane (**65**) was also prepared fresh before each reaction as the species is not stable for prolonged periods of time even at low temperatures (–78 °C) and the concentration of the reagent is essential for adequate yields of the *bis*(boratabenzene) complex. Figure 4-5 shows the synthetic route reported to tetrabromodiborane (**65**) by Nöth and coworkers,[453] which requires treatment of tetramethoxydiborane (**192**) with excess BBr_3 (**193**) in dichloromethane. Workup of the crude mixture by multiple distillations gave the tetrabromodiborane (**65**) reagent in fair yields (~35%).

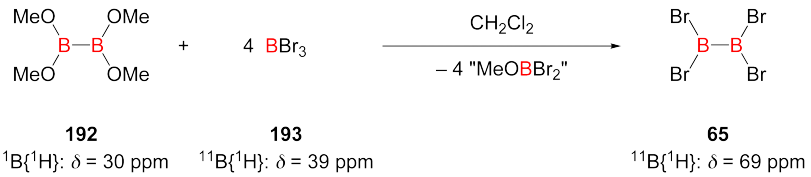

Figure 4-5. Synthesis of tetrabromodiborane (**65**) from tetramethoxydiborane (**192**) and excess BBr_3 (**193**).

4.1.2.1 [{(η^5-C_5H_5)Co}$_2${μ:η^6,η^6-(BC_5H_5)$_2$}] (189)

Treatment of six equivalents of cobaltocene (**176**) in dichloromethane at −78 °C with tetrabromodiborane (**65**) led to the formation of the double-ring-expanded *bis*(boratabenzene) species [{(η^5-C_5H_5)Co}$_2${μ:η^6,η^6-(BC_5H_5)$_2$}] (**189**) (Figure 4-6). The reaction mixture is witnessed to start as a deep red/violet solution that slowly turns black with a brown precipitate as four equivalents of cobaltocenium bromide ([(η^5-C_5H_5)$_2$Co]Br) are formed during the progress of the reaction. The reaction was kept at −78 °C for one hour and was slowly allowed to warm to room temperature during the course of another hour. Workup of the product gave [{(η^5-C_5H_5)Co}$_2${μ:η^6,η^6-(BC_5H_5)$_2$}] (**189**) (yield = 39%) as a dark violet crystalline solid with a melting point of 145 °C, and thermal decomposition in excess of 223 °C.

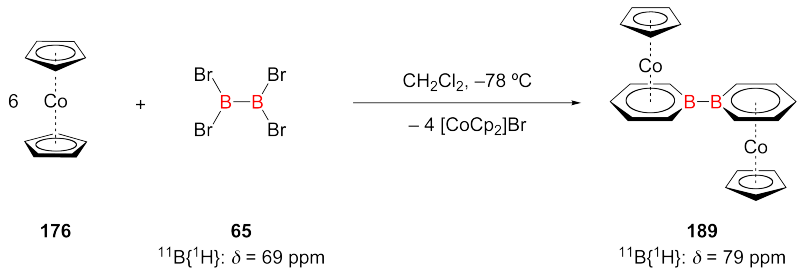

Figure 4-6. Synthesis of the *bis*(boratabenzene) complex [{(η^5-C_5H_5)Co}$_2${μ:η^6,η^6-(BC_5H_5)$_2$}] (**189**) from tetrabromodiborane (**65**) and six equivalents of cobaltocene (**176**).

Analysis of a broad chemical shift region of the ^{1}H NMR spectrum (400.13 MHz, C_6D_6, 297 K) for [{(η^5-C_5H_5)Co}$_2${μ:η^6,η^6-(BC_5H_5)$_2$}] (**176**) (Figure 4-7) exhibits three broad singlet resonances at 32 (*para*-), 28 (*meta*- or *ortho*-), and −51 (*meta*- or *ortho*-) ppm corresponding to the boratabenzene ring protons and a broad singlet at −57 ppm which corresponds to the cyclopentadienyl ring protons. The ^{11}B{^{1}H} NMR resonance for the compound is observed at δ = 79 ppm (^{10}B{^{1}H}: δ = 77 ppm (br s)). This resonance is shifted downfield from the typical region for transition metal boratabenzene complexes as a result of the paramagnetic influences of 19-electron cobalt metal centers.[300,301] A magnetic susceptibility measurement was performed on [{(η^5-C_5H_5)Co}$_2${μ:η^6,η^6-(BC_5H_5)$_2$}] (**189**) in toluene solution (Evans method; μ_{eff} = 2.3 μ_B) and is consistent with the cobalt centers both being in a low-spin d^7 electronic state (each cobalt center containing one unpaired electron).[327,350]

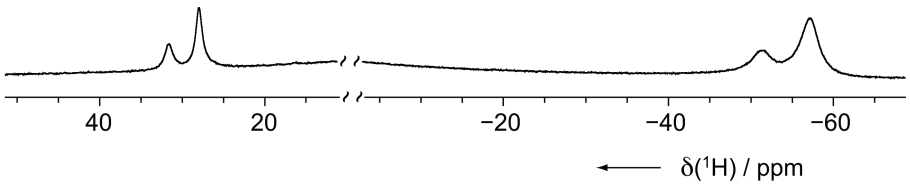

Figure 4-7. Paramagnetic NMR chemical shifts for the *bis*(boratabenzene) complex (**189**).

Isolation of crystals suitable for single-crystal X-ray diffraction of [{(η^5-C_5H_5)Co}$_2${μ:η^6,η^6-(BC_5H_5)$_2$}] (**189**) * were possible from storage of a saturated hexane solution of the compound in a −30 °C freezer for 2 weeks. Diffraction of the deep red crystals showed the desired *bis*(boratabenzene) system within a monoclinic $P2_1/c$ symmetry lattice. An ORTEP diagram for the structure as well as some key bond distances for [{(η^5-C_5H_5)Co}$_2${μ:η^6,η^6-(BC_5H_5)$_2$}] (**189**) are shown in Figure 4-8.

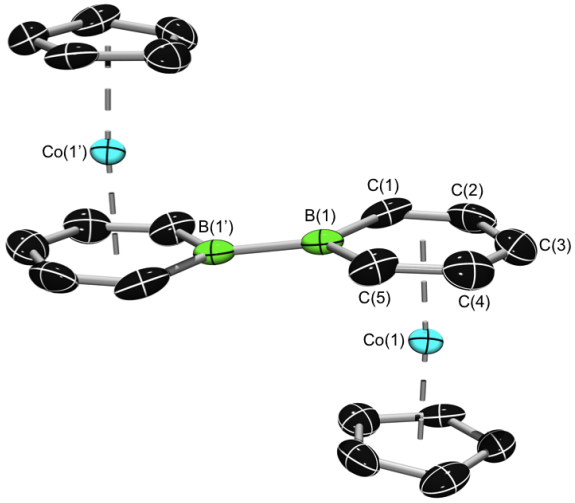

Figure 4-8. ORTEP-rendered structure of [{(η^5-C_5H_5)Co}$_2${μ:η^6,η^6-(BC_5H_5)$_2$}] (**189**). Thermal ellipsoids set at 50% probability. All hydrogen atoms have been omitted for clarity. Selected bond distances (Å) and angles (°): B(1)–B(1)' 1.71(1), B(1)–Co(1) 2.277(8), C(3)–Co(1) 2.09(1), Co(1)–Co(1)' 5.76, Avg. B(1)–C_{ortho} 1.57, Avg. C_{ortho}–C_{meta} 1.38, Avg. C_{meta}–C(3) 1.425.

Analysis of the structure shows the two cobalt centers coordinated to opposite sides of the C_5H_5B-BC_5H_5 rings. The BC_5H_5 ring bond distances for this system are comparable to other similar η^6-boratabenzene transition metal systems[300,301] with average B-C(1) and B-C(5) distances of 1.57 Å and an average C-C ring distance of 1.4025 Å (Figure 4-8). The boron-boron distance between the *bis*(boratabenzene) rings is difficult to discuss with accuracy due to an inversion center lying between the B-B unit; however, the B-B bond distance is found to be 1.71(1) Å, which is typically

* $C_{20}H_{20}B_2Co_2$, M = 399.86, monoclinic, space group = $P2_1/c$.

classified in the range of B-B single bond distances[454,455] with a cobalt-cobalt distance of 5.76 Å. The cobalt-cobalt distance in the *trans*-configured structure is thus slightly longer (~0.66 Å) than in the cyclopentadienyl-cyclopentadienyl linked bicobaltocene analog (~5.1 Å).[456] Examination of the BC_5H_5 ring shows a bending of the boron atom *towards* the metal center by approximately 6° (C(1)-B(1)-C(5) plane relative to C(1)-C(3)-C(5) plane), which is contrary to related boratabenzene complexes in which the boron atom is displaced *away* from the metal.[300,301] This can be attributed to the absence of a π-donating boron substituent (*e.g.* amino) and thus a more pronounced electron-deficiency at the boron atom. Figure 4-9 lists all pertinent bond distances in the boratabenzene ring system relative to the cobalt center with relevant bond angles (°) and lengths (Å). Examination of these distances shows the cobalt metal center positioned away from the boron substituent and closer to the *para*-carbon of the boratabenzene ring. This positioning of the cobalt center is what subsequently causes the bending in the ring between the B(1)-C_{ortho}-C_{meta} atoms and shows that the boron atom still prefers an interaction with the cobalt center rather than "slip-distorting" away from the metal center.

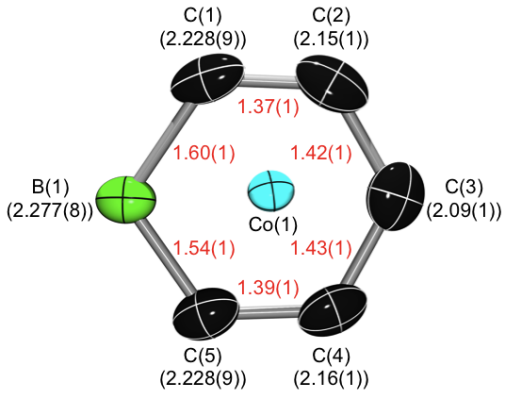

Figure 4-9. ORTEP-rendered structure of one boratabenzene unit within the structure of [{(η^5-C_5H_5)Co}$_2${μ:η^6,η^6-(BC_5H_5)$_2$}] (**189**). Thermal ellipsoids set at 50% probability. All hydrogen atoms have been omitted for clarity. Intra-ring bond distances (Å) are reported in red while the cobalt-boratabenzene ring bond distances (Å) are reported in parenthesis (black).

The EPR spectrum of [{(η^5-C_5H_5)Co}$_2${μ:η^6,η^6-(BC_5H_5)$_2$}] (**189**) was measured in toluene glass at 20 K (Figure 4-10). The species exhibits a broad resonance centered at approximately g = 2, with superimposed ^{59}Co (I = 7/2) hyperfine coupling and a broad low-field signal at g = ~4.6. The resolved spectroscopic lines were simulated with rhombic spin Hamiltonian parameters (g_1 = 1.863, g_2 = 2.022, and g_3 = 2.117; A_1 = 161, A_2 = 84, and A_3 = 424 MHz), which are in line with EPR data of similar low-spin boratabenzene Co(II) complexes.[327]

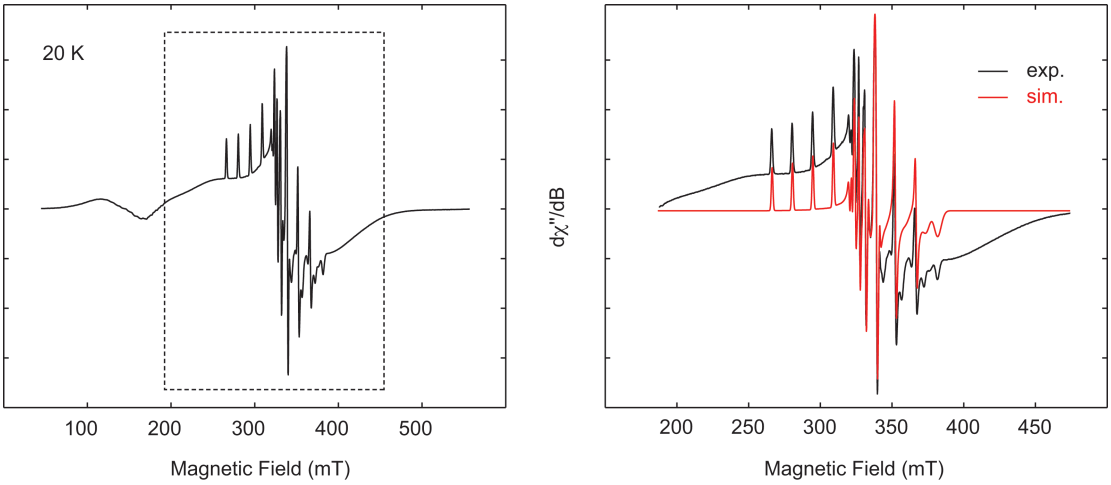

Figure 4-10. Frozen-solution X-band EPR spectrum of [{(η^5-C_5H_5)Co}$_2${μ:η^6,η^6-(BC_5H_5)$_2$}] (**189**) at 20 K (black). An expanded view of the g = ~2 region is shown on the right together with a simulated spectrum (red). The overall spectral profile remains unchanged in the temperature range of 10-120 K.

Although the observed broad features (especially the signal with zero crossing at around g = 4.5) suggest a triplet state for the two cobalt centers in the complex and thus ferromagnetically-coupled Co(II) atoms; they are likely due to a high-spin Co(II) impurity in solution. This interpretation of the data is also supported by solid-state SQUID magnetic measurements (Figure 4-11), which suggest that the cobalt ions in [{(η^5-C_5H_5)Co}$_2${μ:η^6,η^6-(BC_5H_5)$_2$}] (**189**) have a doublet ground state (S = 1/2) and are only weakly coupled by antiferromagnetic exchange (J = −6.0 cm^{-1}). This relatively small magnetic interaction is surprising considering the close metal-metal spatial proximity, but it illustrates the effect of the B-B unit in mitigating the magnitude of the antiferromagnetic coupling. As a result of the B-B units effect on the antiferromagnetic coupling of the two cobalt metal centers, the observed coupling constant is significantly smaller than in a closely related *para*-phenylene-bridged *bis*(boratabenzene) dicobalt species (J = ca. −28 cm^{-1}).[450] In order to describe accurately the temperature dependencies of the magnetic moments of [{(η^5-C_5H_5)Co}$_2${μ:η^6,η^6-(BC_5H_5)$_2$}] (**189**) in the measured range (2-300 K), intermolecular interactions have to be taken into account (Weiss's constant: Θ = −8.3 K). This may be related to the molecular packing, which shows a perpendicular arrangement of neighboring molecules that is held together by a network of close C–H---B contacts (~3.18 Å).

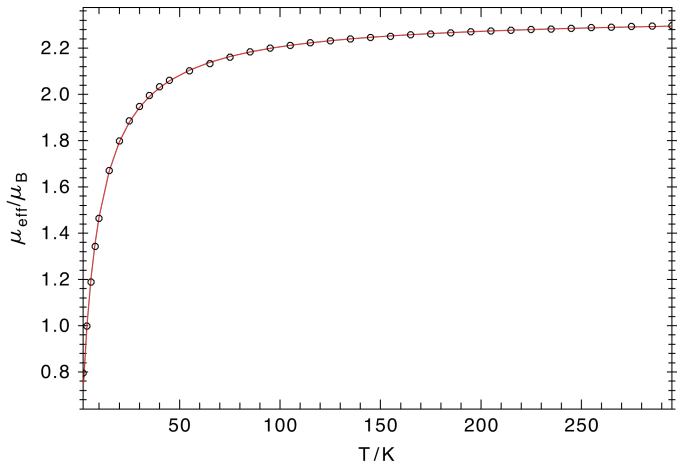

Figure 4-11. SQUID plot of μ_{eff} (in Bohr magnetons) *vs.* *T* for [{(η^5-C_5H_5)Co}$_2$\{μ:η^6,η^6-(BC_5H_5)$_2$\}] (**189**).

The two formally independent paramagnetic transition metal centers can theoretically communicate electronically by linkage of a B-B σ-bond, which bear a bonding LUMO that can manifest electronic delocalization across both metal ligand scaffolds when filled. The redox properties of [{(η^5-C_5H_5)Co}$_2$\{μ:η^6,η^6-(BC_5H_5)$_2$\}] (**189**) were studied using cyclic voltammetry (CV) and differential pulse voltammetry (DPV) (Figure 4-12). [{(η^5-C_5H_5)Co}$_2$\{μ:η^6,η^6-(BC_5H_5)$_2$\}] (**189**) displayed two closely-spaced oxidation waves and two well-resolved reduction waves, corresponding to the [(**189**)]$^{0/+1}$, [(**189**)]$^{+1/+2}$, [(**189**)]$^{0/-1}$, and [(**189**)]$^{-1/-2}$ redox couples, respectively. The oxidation processes are identified as Co(II)/Co(III) and the reduction processes as Co(II)/Co(I) couples by the similarity of their *E* values to those of related complexes (**185**)[327] and (**188**).[450] The separation of the two oxidation events in the cyclic voltammogram of [{(η^5-C_5H_5)Co}$_2$\{μ:η^6,η^6-(BC_5H_5)$_2$\}] (**189**) (ΔE = 102 mV) suggests an approximate comproportionation constant of $K_c = 10^{1.7}$ (Equation 4-1), whereas the second pair of redox couples associated with the reduction features a markedly higher comproportionation constant of $K_c = 10^{4.6}$ (ΔE = 272 mV).[457] These findings reveal clear evidence for interaction between the metal centers and display more pronounced electronic coupling in the mixed-valent monoanion than in the monocation.[458] When applied to Robin-Day classification the comproportionation constant for the two oxidation events ($K_c = 10^{1.7}$) is slightly less than the benchmark of $K_c = 10^2$ (barrier between class I and class II Robin-Day systems), which describes the complex as a class I Robin-Day system.[457] The reduction comproportionation constant of $10^{4.6}$, however, is directly in the range of a class II Robin-Day system ($10^2 < K_c < 10^6$). This classification is simply another means of experimentally quantifying partial electronic delocalization between the well-defined reduction events.[457] When

compared to boratabenzene complex (**188**), the electronic interaction for complex (**189**) is stronger (more delocalized) than in the related bimetallic cobalt complex with a *para*-phenylene bridge between the two [(η^5-C_5H_5)Co(η^6-C_5H_5B)] fragments **188**. Examination of the cyclic voltammetry data for complex **188** shows no resolvable separations between the Co(III)/Co(II) and Co(II)/Co(I) redox couples indicating low communication between the centers. However, it should be noted that the ΔE value for complexes **188** and **189** is still considerably weaker than in dicobaltocene (ΔE = 395 mV for the Co(III)/Co(II) couple).[456] This evidence suggests that due to the comparatively electron-deficient boron atoms in **189** the delocalization of positive charge is reduced, leading to a more localized structure.

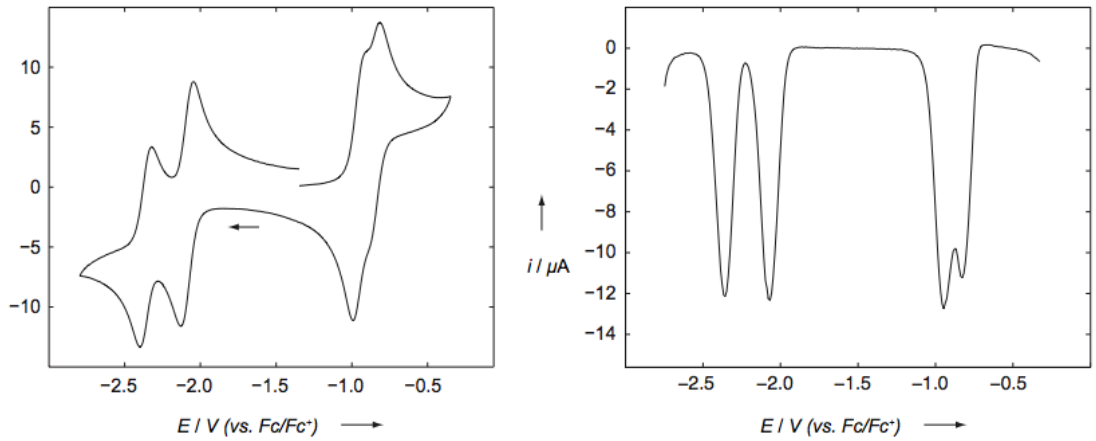

Figure 4-12. Cyclic voltammogram (left) and differential pulse voltammogram (right) of [{(η^5-C_5H_5)Co}$_2$\{μ:η^6,η^6-(BC_5H_5)$_2$\}] (**189**) in THF with 0.1 M [nBu$_4$N][PF_6] as the supporting electrolyte. Formal potentials: $E_{1/2}(1)$ = −0.84 V, $E_{1/2}(2)$ = −0.94 V, $E_{1/2}(3)$ = −2.09 V, and $E_{1/2}(4)$ = −2.36 V (relative to the Fc/Fc$^+$ couple).

$$K_c = 10^{(F\cdot\Delta E^\circ/2.303\cdot R\cdot T)} \quad \equiv \quad K_c = 10^{(16.90\cdot\Delta E^\circ)}$$

Equation 4-1. Equation used to calculate the comproportionation constants (K_c)* for complexes **188** and **189** (full equation on left and standard temperature and pressure variant on right).[457]

* Where F and R correspond to the Faraday and ideal gas constants, respectively, with T and ΔE^o calculated in Kelvin and Volts, respectively.

4.1.3 Oxidation Studies of [{(η^5-C_5H_5)Co}$_2${μ:η^6,η^6-(BC_5H_5)$_2$}] (189)

Analysis of the cyclic voltammetry data showed the viability for the compound to be stable in either a mixed oxidation state or a dicationic state. We attempted to quantify this data experimentally by isolation of the mono- and dicationic analogs of the *bis*(boratabenzene) species. Oxidation of **189** was performed with either one or two equivalents of ferrocenium hexafluorophosphate ([(η^5-C_5H_5)$_2$Fe][PF_6]) in 1,2-difuorobenzene yielding the mono- and dicationic species [{(η^5-C_5H_5)Co}$_2${μ:η^6,η^6-(BC_5H_5)$_2$}][PF_6] (**194**) and [{(η^5-C_5H_5)Co}$_2${μ:η^6,η^6-(BC_5H_5)$_2$}][PF_6]$_2$ (**195**) respectively. Both species are poorly soluble in 1,2-difluorobenzene and could only be completely dissolved using acetonitrile and nitromethane solvents; however, both species are unstable in these solvents and will eventually decompose in solution over prolonged periods of time.

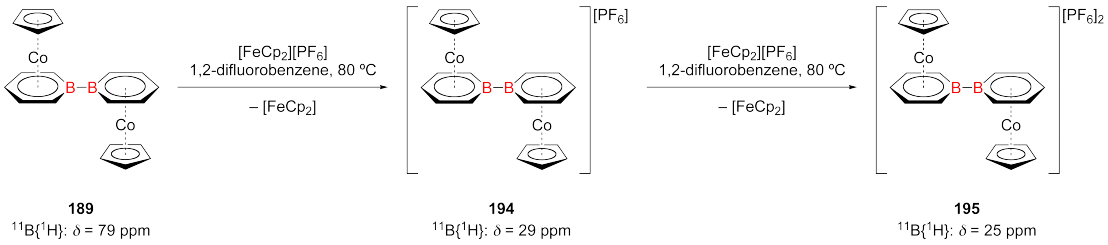

Figure 4-13. Oxidation reactions of the *bis*(boratabenzene) complex **189** with one and two equivalents of [(η^5-C_5H_5)$_2$Fe][PF_6] yielding the monocationic and dicationic complexes **194** and **195** respectively.

4.1.3.1 [{(η^5-C_5H_5)Co}$_2${μ:η^6,η^6-(BC_5H_5)$_2$}][PF_6]$_2$ (195)

In synthesis mimicking the work reported by Heck[327] and O'Hare[450] (Figure 4-3) for the oxidation of boratabenzene transition metal systems using iron trichloride hexahydrate, ferrocenium hexafluorophosphate ([(η^5-C_5H_5)$_2$Fe][PF_6]) was used as an oxidant for the synthesis of the monocationic (**194**) and dicationic (**195**) *bis*(boratabenzene) species. The original synthesis by oxidation with iron trichloride hexahydrate was impossible to reproduce due to the release of up to six equivalents of water from the reagent, which led to decomposition of the *bis*(boratabenzene) complex. Species **194** and **195** were found to be poorly soluble in 1,2-difluorobenzene and could only be redissolved in either acetonitrile or nitromethane, however, both mono- and dicationic forms are not stable in these solvents and will gradually decompose over the course of a few hours. Spectroscopically the ^{1}H NMR data for **195** displayed characteristic signals for the cyclopentadienyl protons (^{1}H: δ = 5.77 ppm) and boratabenzene ligands (δ = 6.97, 6.77 and 6.19 ppm) indicate a

diamagnetic ground state of the dication $[\{(\eta^5\text{-}C_5H_5)Co\}_2\{\mu{:}\eta^6,\eta^6\text{-}(BC_5H_5)_2\}]^{2+}$ with the cobalt ions in a low-spin d^6 configuration and the formation of only one isomer. The ^{11}B NMR chemical shift is at δ = 24.5 ppm, which is in the typical range for η^6-boratabenzene transition metal complexes.[300,301] Preparative oxidation of **195** supports the voltammetric conclusions of successive one-electron, metal-centered oxidation events leading to a closed-shell dicobalt(III) complex.

4.1.3.2 $[\{(\eta^5\text{-}C_5H_5)Co\}_2\{\mu{:}\eta^6,\eta^6\text{-}(BC_5H_5)_2\}][PF_6]$ (194)

Synthesis and isolation of the monocationic *bis*(boratabenzene) species (**194**) proved exceedingly difficult as the compound is only soluble in acetonitrile and nitromethane and is much less stable than compound **195** while dissolved in these solvents. The best spectroscopic method for identification of the compound is *via* EPR spectroscopy (see Figure 4-14). EPR spectra for the compound in a frozen toluene solution at 20 K witnesses the mixed-valent Co(II)/(III) species (**194**) as a broad resonance at g = 2 with superimposed hyperfine couplings that are not sufficiently well resolved in order to obtain all of the rhombic g and A tensor values (g_z = 2.120 and A_z = 413 MHz is the only resolved hyperfine coupling observed). The absence of clearly resolved ^{59}Co hyperfine coupling might be indicative of some delocalization of the unpaired electron across both metal ions mediated by the B-B unit. The mixed-valent monocation (**194**) could only be identified by EPR spectroscopy, whereas the dication (**195**) allowed characterization by NMR and elemental analysis. One other characterization technique that could show interesting characteristics for the stepwise oxidation of compound **189** was UV-vis spectroscopy (absorption) of the neutral species relative to the monocation (**194**) and dication (**195**). Comparisons of the absorption spectra for all three species in acetonitrile universally showed local absorptions at λ = 262 nm, while compound **189** was the only species to display an absorption maxima (λ_{max}) at 359 nm. Both the monocationic (**194**) and dicationic (**195**) compounds did not display any other well-defined absorption maxima besides the absorption at λ = 262 nm, however, further examination of the UV-vis absorption spectra for compound (**194**) showed a shoulder around λ = 290 nm, while the spectra for compound (**195**) displayed complete absence of this shoulder and only a well-defined absorption maximum at λ_{max} = 262 nm. This data indicates that the neutral species (**189**) displays an absorption maximum that is witnessed to shift hypsochromically in the spectra for the monocation (**194**) and is completely lost in the spectra for the dication (**195**), providing further evidence for an increased energetic gap (HOMO-LUMO gap) when

transitioning between the oxidation states in the *bis*(boratabenzene) complexes **189**, **194**, and **195** respectively.

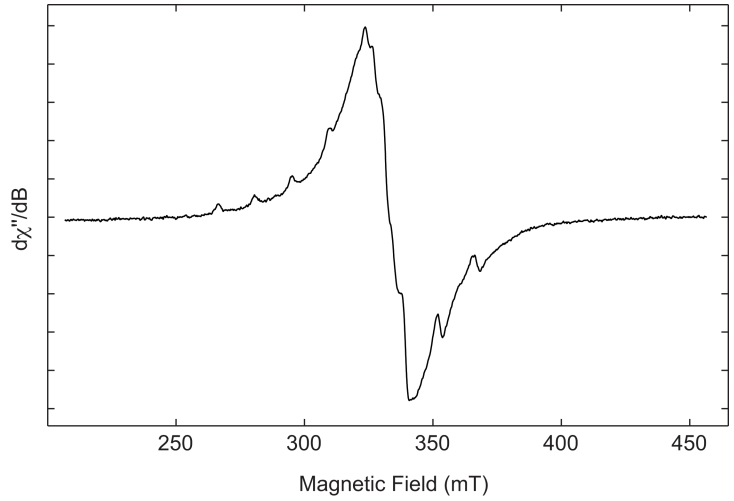

Figure 4-14. Frozen-solution continuous-wave X-band EPR spectrum of [{(η^5-C_5H_5)Co}$_2${μ:η^6,η^6-(BC_5H_5)$_2$}]$^+$ (**194**) at 10 K.

4.2 Reactivity Studies of [{(η^5-C_5H_5)Co}$_2${μ:η^6,η^6-(BC_5H_5)$_2$}] (189)

Studies were conducted on the *bis*(boratabenzene) complex in order to test for useful reactivity by either: (A) cleaving the actual *bis*(boratabenzene) ring system from one or both cobalt centers, or (B) oxidatively adding the system to a transition metal to effect an L_xM-η^1-(BC_5H_5) interaction, which to our knowledge has never been experimentally confirmed.[300,301] Although no known oxidative additions of boratabenzene systems to transition metals are known, the ring cleavage reactions were thoroughly researched by Herberich and coworkers in a 1976 publication.[351]

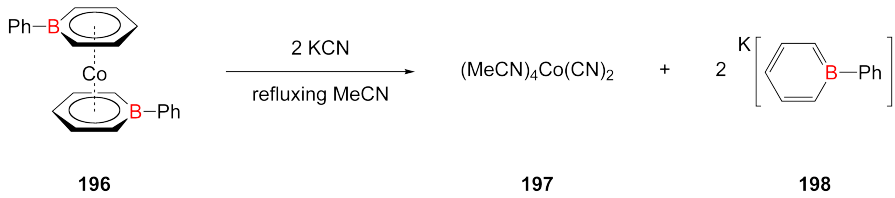

Figure 4-15. Cleavage of a boratabenzene ring system from a cobalt metal center published by Herberich and coworkers. [351]

Herberich and coworkers[351] were able to show ring cleavage of a boratabenzene ligand from the cobalt scaffold by treatment of a cobalt boratabenzene complex (**196**) with potassium cyanide in refluxing acetonitrile (Figure 4-15). The reaction proceeds by utilizing the cyano ligands in acetonitrile to displace the boratabenzene ligands, resulting in formation of the complex [$(MeCN)_4Co(CN)_2$] (**197**) and two equivalents of the liberated potassium boratabenzene salt (**198**).

4.2.1 [{(η^5-C_5H_5)Co}$_2${μ:η^6,η^6-(BC_5H_5)$_2$}] (189) Ring-Cobalt Cleavage Attempts with MCN

The ring cleavage reaction published by Herberich was repeated using essentially the same ratios of sodium cyanide to boratabenzene rings (Figure 4-16). As can be seen below, the neutral cobalt *bis*(boratabenzene) complex (**189**) was treated with two equivalents of sodium cyanide in refluxing acetonitrile in a reaction designed to displace the potassium *bis*(boratabenzene) salt (**200**) with formation of two equivalents of the three-legged piano stool cobalt complex [(η^5-C_5H_5)Co(CN)(NCMe)$_2$] (**199**).

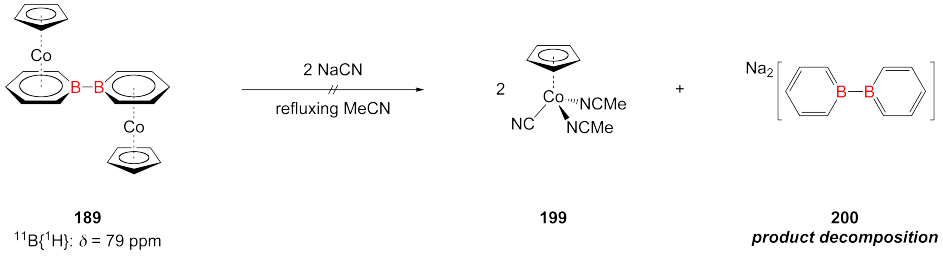

Figure 4-16. Reaction designed to reproduce the reported boratabenzene ring-cleavage reaction with the *bis*(boratabenzene) species (**189**) yielding the hypothetical *bis*(boratabenzene) salt (**200**).

Unfortunately, for this particular reaction, the nature of the B-B Lewis acidic sites seems to allow for coordination of the acetonitrile solvent and decomposition of the complex. Analysis of the reaction mixtures is further complicated by the presence of a paramagnetic cobalt byproduct. The coordination of acetonitrile is further confirmed by the compound's instability in acetonitrile as witnessed in the oxidation studies of the complex. Workup of all these ring cleavage attempts gave no compounds that could be confirmed as formation of either the monoboratabenzene ring-cobalt cleavage or the *bis*(boratabenzene) ring-cobalt cleavage products (**200**).

4.2.2 Attempted Boron-Boron Bond Cleavage by Oxidative Addition of [{(η^5-C_5H_5)Co}$_2${μ:η^6,η^6-(BC_5H_5)$_2$}] (189) to Transition Metals

Finally, the *bis*(boratabenzene) B-B bond in compound **189** was tested for reactivity by oxidative addition to transition metal scaffolds previously shown to be active in the B-B bond activation of diboranes. As shown in the introduction,* a variety of transition metal phosphine and carbene complexes have been shown to be capable of oxidatively adding diborane B-B bonds,[47] which typically result in the displacement of one or more of the L-type ligands with formation of two transition metal boryl bonds. As many of these reactions utilize B_2Cat_2 and B_2Pin_2 as diborane precursors, the similarity of these diboranes to the neutral *bis*(boratabenzene) complex (**189**) seemed like a logical candidate to test for their oxidative addition reactivity. This reactivity was predicted by realization that the diboranes B_2Cat_2 and B_2Pin_2 both contain oxygen substituents to stabilize the Lewis acidic boron environments, which is similar to the anionic ring-delocalized electrons in the anionic boratabenzene systems.

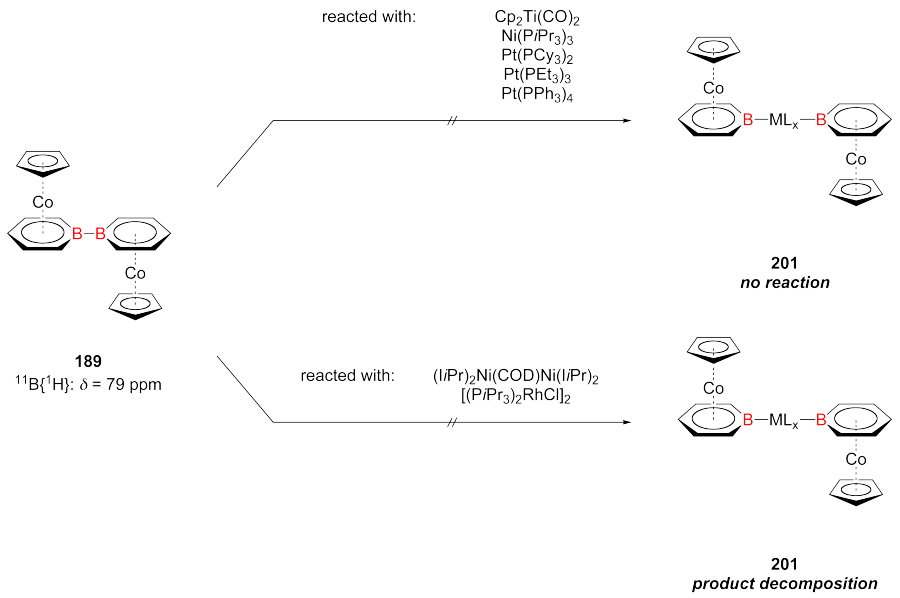

Figure 4-17. Test reactions for the oxidative addition of the *bis*(boratabenzene) B-B bond in complex (**189**) with a wide variety of transition metals. The reactions all yielded either no reaction (top) or decomposition of the *bis*(boratabenzene) complex (**189**) (bottom).

As can be seen in Figure 4-17, the *bis*(boratabenzene) complex was reacted with a wide variety of transition metal phosphine and carbene complexes to test for any reactivity indicative of B-B bond cleavage. After testing the reactivity with all of these transition metal species, no transition metal scaffold was found that resulted in a

* See Section 1.1.3 for details.

stable L_xM-η^1-(BC_5H_5) complex and as can be seen in Figure 4-17, all reactions typically witnessed no reactivity with the metal systems. Two of the complexes showed sufficient reactivity to decompose the *bis*(boratabenzene) complex; however, it is unclear if any oxidative addition of the B-B bond ever occurred during these reactivity studies.

4.3 Project Boratabenzene Summary

To summarize the results of Chapter 4, the *bis*(boratabenzene) complex (**189**) was successfully prepared by treatment of tetrabromodiborane with six equivalents of cobaltocene in a unique reaction that utilized cobaltocene as both a reagent and reductant. The bimetallic transition metal complex features a new bridging *bis*(boratabenzene) ligand linked through a boron-boron single bond that can manifest delocalization of electron density by providing an accessible LUMO orbital for π-communication between the cobalt centers and heteroaromatic rings.

This dianionic diboron ligand was shown to facilitate electronic coupling between the cobalt metal sites, as evidenced by the potential separations between successive single-electron redox events in the cyclic voltammogram. The extent of metal-metal communication thereby depends on the charge of the metal atoms, with the negative charge being more efficiently delocalized across the *bis*(boratabenzene) unit (class II Robin-Day system). Magnetic studies indicate that the Co(II) ions are weakly antiferromagnetically coupled across the B-B bridge.

While reduction of the *bis*(boratabenzene) system resulted in decomposition of the complex, oxidation of the system by one and two electron steps resulted in isolable stable monocationic (**194**) and dicationic (**195**) forms of the *bis*(boratabenzene) complex. Study of these systems verifies the experimentally-observed cyclic voltammetry studies performed on the neutral species. These species are unfortunately not stable in acetonitrile or nitromethane solutions, which until this point are the only solvents that have been observed to dissolve the cationic species. Unfortunately, this instability in solution complicates reactivity studies of these cationic complexes.

Finally, reactivity studies were performed on the neutral *bis*(boratabenzene) complex (**189**) in which the compound was tested for: (A) cleavage of the boratabenzene (cyclo-BC_5H_5) ring from the cobalt center, and (B) oxidative addition of the B-B bond to a transition metal scaffold to attempt synthesis of the first ever L_xM-η^1-(BC_5H_5) complex. Both of these reactivity studies, however, proved unsuccessful and typically witnessed decomposition of the *bis*(boratabenzene) complex or no reactivity. After repeated attempts of these synthetic studies, no confirmed reactivity of the *bis*(boratabenzene) besides oxidation of the system could be confirmed.

Chapter 5 – Summary

Project Borylene

A new borylene ligand ({BN(SiMe$_3$)(*t*-Bu)}) has been successfully synthesized bound in a terminal manner to base metal scaffolds of the type [M(CO)$_5$] (M = Cr, Mo, and W), yielding complexes [(OC)$_5$Cr{BN(SiMe$_3$)(*t*-Bu)}] (**19**), [(OC)$_5$Mo{BN(SiMe$_3$)(*t*-Bu)}] (**20**), and [(OC)$_5$W{BN(SiMe$_3$)(*t*-Bu)}] (**21**) (Figure 5-1). Synthesis of complexes **19**, **20**, and **21** was accomplished by double salt elimination reactions of Na$_2$[M(CO)$_5$] (M = Cr (**11**), Mo (**1**), and W (**12**)) with the dihaloborane Br$_2$BN(SiMe$_3$)(*t*-Bu) (**18**). This new "first generation" unsymmetrical borylene ligand is closely akin to the *bis*(trimethylsilyl)aminoborylene ligand and has been shown to display similar structural characteristics and reactivity. The unsymmetrical borylene ligand {BN((SiMe$_3$)(*t*-Bu)} does display some individual characteristics of note and has experimentally been shown to undergo photolytic transfer to transition metal scaffolds in a more rapid manner, and appears to be a more reactive borylene ligand, than the previously published symmetrical {BN(SiMe$_3$)$_2$} ligand, based on NMR and IR spectroscopic evidence.

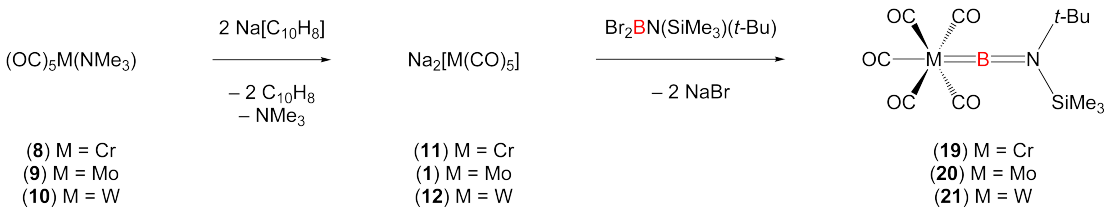

Figure 5-1. [(OC)$_5$M{BN(SiMe$_3$)(*t*-Bu)}] synthesis by reaction of the corresponding transition metal dianionic complexes with Br$_2$BN(SiMe$_3$)(*t*-Bu) (**18**).

Photolytic transfer reactions with this new borylene ligand ({BN((SiMe$_3$)(*t*-Bu)}) were conducted with other metal scaffolds, resulting in either complete borylene transfer or partial transfer to form bridging borylene ligand interactions between the two transition metals. The unsymmetrical ligand's coordination to early transition metals (up to Group 6) indicates a preference for a terminal coordination motif while bound to these highly Lewis acidic species. The ligand appears to form more energetically stable bridging coordination modes when bound to transition metals with high Lewis basicity (beyond Group 9) and has been witnessed to transfer to transition metal scaffolds in a terminal manner and subsequently rearrange in order to achieve a more energetically stable bridging final state.

Figure 5-2 lists the four different transfer reactions conducted between the chromium borylene species [(OC)$_5$Cr{BN(SiMe$_3$)(*t*-Bu)}] (**19**) and the transition metal

complexes [(η^5-C_5H_5)V(CO)$_4$] (**51**), [(η^5-C_5Me_5)Ir(CO)$_2$] (**56**), [(η^5-C_5H_4Me)Co(CO)$_2$] (**59**), and [{(η^5-C_5H_5)Ni}$_2$(μ-(CO)$_2$}] (**53**). These reactions successfully yielded the new "second generation" borylene complexes [(η^5-C_5H_5)(OC)$_3$V{BN(SiMe$_3$)(*t*-Bu)}] (**55**), [(η^5-C_5Me_5)Ir{BN(SiMe$_3$)(*t*-Bu)}$_2$] (**58**), [{(η^5-C_5H_4Me)Co}$_2$(μ-CO)$_2$(μ-BN(SiMe$_3$)(*t*-Bu)}] (**61**), and [{(η^5-C_5H_5)Ni}$_2$(μ-CO){μ-BN(SiMe$_3$)(*t*-Bu)}] (**62**), respectively.

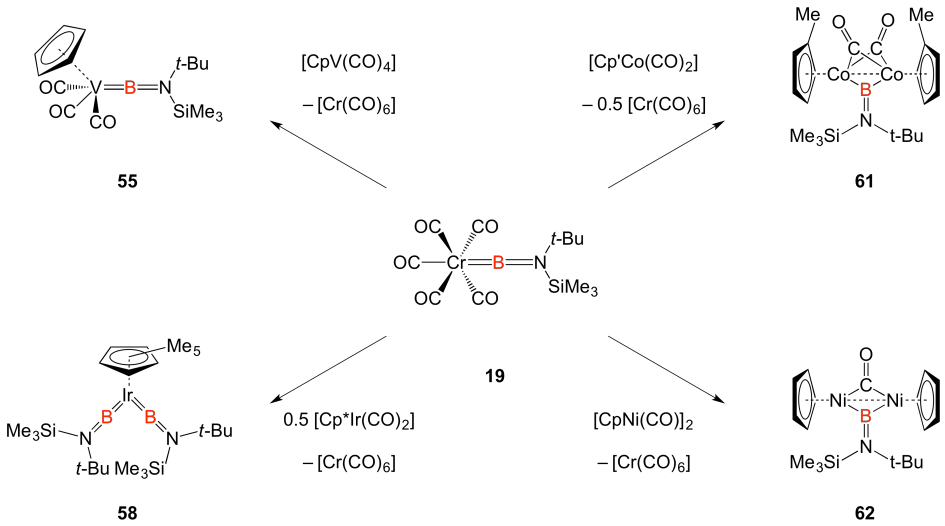

Figure 5-2. Synthesis of second-generation transition metal borylene species by photolytic borylene transfer from [(OC)$_5$Cr{BN(SiMe$_3$)(*t*-Bu)}] (**19**).

Analysis of the accumulated data for all of the terminal borylene species discussed in this section, particularly bond distances, infrared spectroscopy, and $^{11}B\{^1H\}$ NMR spectroscopic data, has been performed, and a trend in the data has led to the following conclusions:

[1] NMR spectroscopic data for the $^{11}B\{^1H\}$ boron and $^{13}C\{^1H\}$ carbonyl environments of the first generation borylene species ([(OC)$_5$M{BN(SiMe$_3$)(*t*-Bu)}] (M = Cr (**19**), Mo (**20**), and W (**21**))) all show progressive up-field shifting as the Group 6 metal becomes heavier (Cr (**19**) to Mo (**20**) to W (**21**)), indicating maximum deshielding for these nuclei in the [(OC)$_5$Cr{BN(SiMe$_3$)(*t*-Bu)}] (**19**) complex.

[2] The boron-metal-*trans*-carbon (B-M-C$_{trans}$) axes of the first generation borylene complexes [(OC)$_5$M{BN(SiMe$_3$)(*t*-Bu)}] (M = Mo (**20**), and W (**21**)) are not completely linear, preventing direct IR spectroscopic comparison. The chromium analog [(OC)$_5$Cr{BN(SiMe$_3$)(*t*-Bu)}] (**19**), however, is essentially linear and displays the expected three carbonyl IR stretching frequencies, all at higher energy than those of the chromium *bis*(trimethylsilyl)aminoborylene complex [(OC)$_5$Cr{BN(SiMe$_3$)$_2$}] (**13**), indicating that the ({BN(SiMe$_3$)(*t*-Bu)}) ligand is either a stronger σ-donor or a poorer π-acceptor compared to the chromium metal center.

[3] In transfer reactions, the {$BN(SiMe_3)(t\text{-Bu})$} fragment appears to be more stable as a terminal ligand when bound to more Lewis acidic first row transition metals and appears to prefer coordination in a bridging motif when coordinated to more Lewis basic first row transition metals.

Project Borirene

The synthesis of the first platinum *bis*(borirene) complexes are presented along with findings from structural and electronic examination of the role of platinum in allowing increased coplanarity and conjugation of twin borirene systems. This series of *trans*-platinum-linked *bis*(borirene) complexes (**119**/**120**, **122**/**123**, and **125**/**126**) all show coplanarity in the twin ring systems and stand as the first verified structural representations of two coplanar borirene systems across a linking unit. The role of a platinum atom in mediating communication between chromophoric ligands can be generalized by an expected bathochromic (red) shift in the absorption spectrum due to an increase in the electronic delocalization between the formerly independent aromatic systems when compared to the platinum mono-σ-borirenyl systems. The *trans*-platinum *bis*(borirene) scaffold serves as a simplified monomeric system that allows not only study of the effects of transition metals in mitigating electronic conjugation, but also the tunability of the overall photophysical profile of the system by exocyclic augmentation of the three-membered aromatic ring.

A series of *trans*-platinum *bis*(alkynyl) complexes were prepared (Figure 5-3) to serve as stable platforms to transfer terminal borylene ligands {$BN(SiMe_3)_2$} onto **95**, **102**, **106**, and **63**. Mixing of *cis*-[$PtCl_2(PEt_3)_2$] (**93**) with two equivalents of corresponding alkynes in diethylamine solutions successfully yielded *trans*-[$Pt(C{\equiv}C\text{-}Ph)_2(PEt_3)_2$] (**95**), *trans*-[$Pt(C{\equiv}C\text{-}p\text{-}C_6H_4OMe)_2(PEt_3)_2$] (**102**), *trans*-[$Pt(C{\equiv}C\text{-}p\text{-}C_6H_4CF_3)_2(PEt_3)_2$](**106**), and *trans*-[$Pt(C{\equiv}C\text{-}9\text{-}C_{14}H_9)_2(PEt_3)_2$] (**63**) through salt elimination reactions.

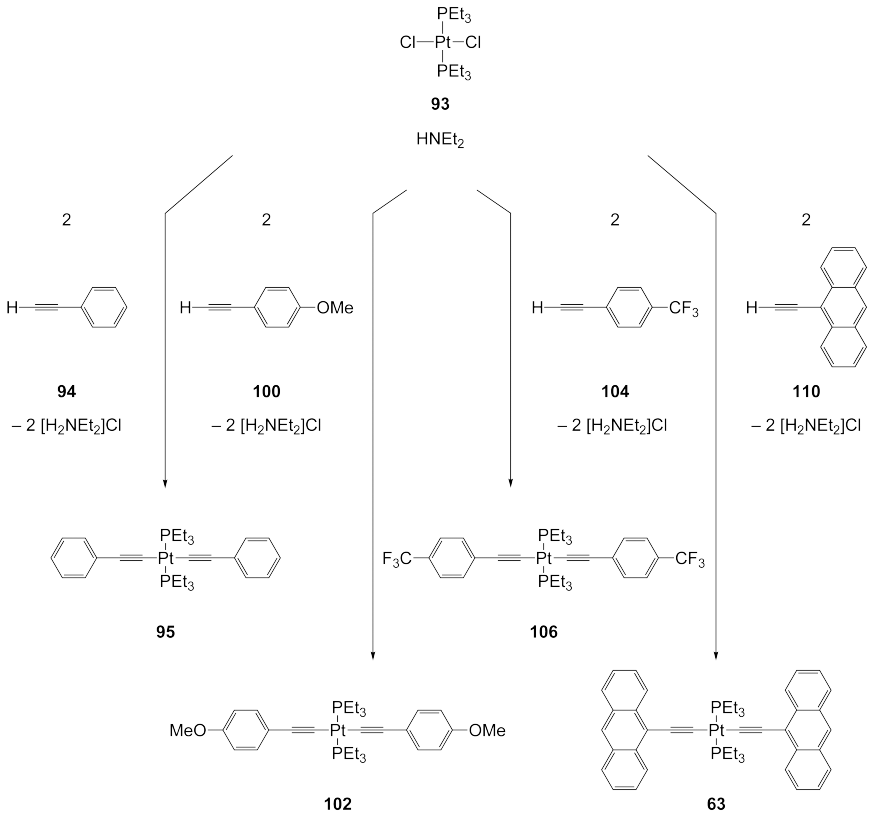

Figure 5-3. Synthesis of four *trans*-platinum *bis*(alkynyl) complexes from *trans*-$[PtCl_2(PEt_3)_2]$.

Three of the *trans*-platinum *bis*(alkynyl) complexes (**95**, **102**, and **106**) successfully yielded *trans*-platinum *bis*(borirenyl) complexes **119**/**120**, **122**/**123**, and **125**/**126** through photolytic transfer of two equivalents of the terminal borylene ligand $\{BN(SiMe_3)_2\}$ from $[(OC)_5Cr\{BN(SiMe_3)_2\}]$ (**13**) (Figure 5-4). Attempted borylene transfer reactions to the *trans*-platinum *bis*(alkynyl) complex *trans*-$[Pt(C{\equiv}C\text{-}9\text{-}C_{14}H_9)_2(PEt_3)_2]$ (**63**) failed due to the complex's photoinstability. Although a host of other variants of platinum alkynyl species were prepared and attempted, these three were the only ones that successfully yielded *trans*-platinum *bis*(borirenyl) units. Attempts were also made to create a *cis* variant for direct UV-vis comparison to the *trans*-platinum *bis*(borirenyl) variants, however, these attempts were also not successful. Gladysz-type platinum end-capped alkynyl species were also synthesized to serve as transfer platforms for borirene synthesis in sequential order, however, these species were also shown to not be photolytically stable.

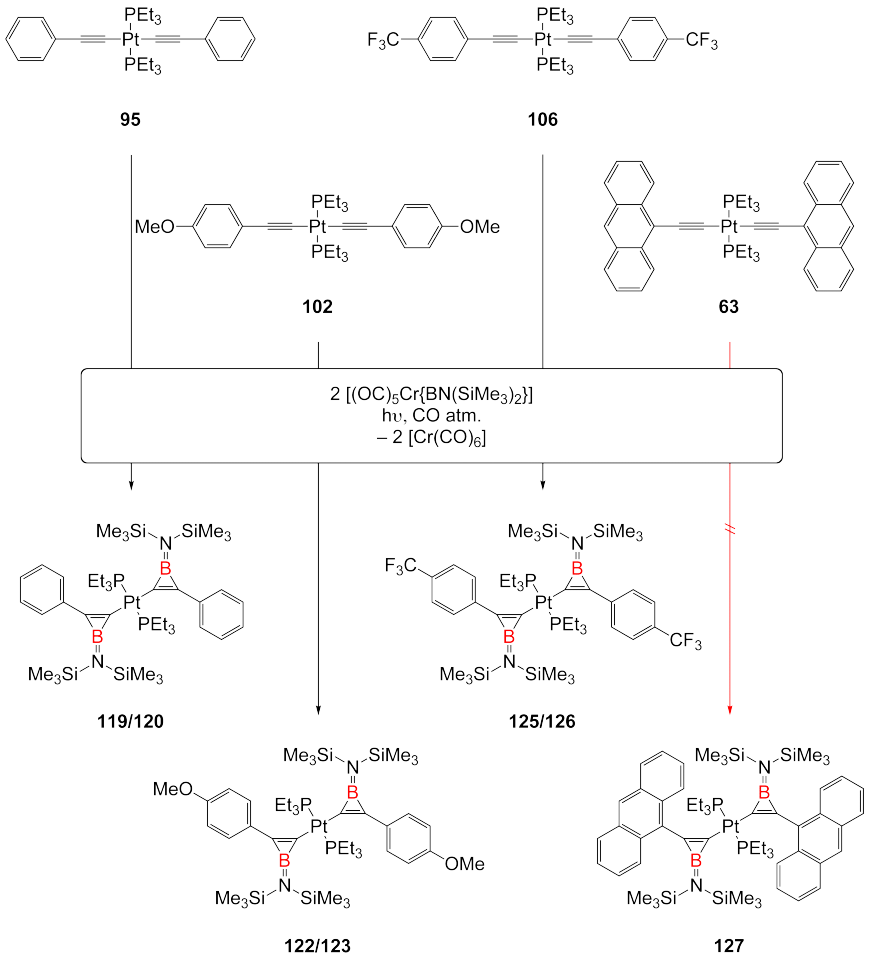

Figure 5-4. Three *trans*-platinum *bis*(borirenyl) complexes synthesized from dual borylene ligand transfers of {$BN(SiMe_3)_2$} from [$(OC)_5Cr\{BN(SiMe_3)_2\}$] (**13**) to the *trans*-platinum *bis*(alkynyl) substituents.

A host of new monoborirenes: Ph-(μ-{$BN(SiMe_3)(t\text{-Bu})$}C=C)-Ph (**148**), *trans*-[$PtCl\{(\mu\text{-}\{BN(SiMe_3)(t\text{-Bu})\}C{=}C)\text{-}Ph\}(PEt_3)_2$] (**149**), and [($\eta^5$-$C_5Me_5$)$(OC)_2Fe$($\mu$-{$BN(SiMe_3)(t\text{-Bu})$}C=C)Ph] (**150**) were synthesized by photo- and thermolytic transfer of the unsymmetrical {$BN(SiMe_3)(t\text{-Bu})$} ligand from the complexes [$(OC)_5M\{BN(SiMe_3)(t\text{-Bu})\}$] (M = Cr (**19**), Mo (**20**), and W (**21**)) to organic and organometallic alkynyl species to verify that the borylene complexes all display similar reactivity to the symmetrical terminal borylenes of the type [$(OC)_5M\{BN(SiMe_3)_2\}$] (M = Cr (**13**), Mo (**14**), and W (**15**)). These monoborirenes are all found to be oils when in their pure states and X-ray structural determination was impossible for these species.

Project Boratabenzene

The *bis*(boratabenzene) complex [{(η^5-C_5H_5)Co}$_2${μ:η^6,η^6-(BC_5H_5)$_2$}] (**189**) was successfully prepared by treatment of tetrabromodiborane (**65**) with six equivalents of cobaltocene (**176**) in a unique reaction that utilized cobaltocene as both a reagent and reductant (Figure 5-5). The bimetallic transition metal complex features a new bridging *bis*(boratabenzene) ligand linked through a boron-boron single bond that can manifest delocalization of electron density by providing an accessible LUMO orbital for π-communication between the cobalt centers and heteroaromatic rings.

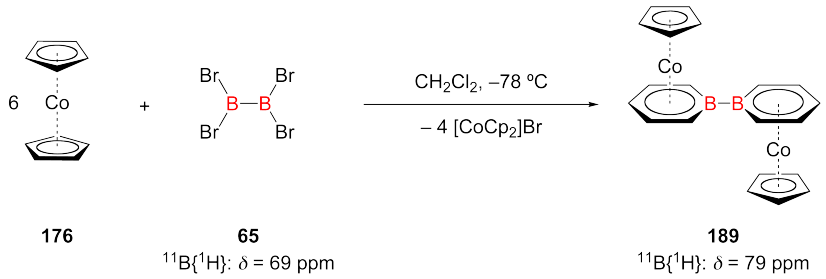

Figure 5-5. Synthesis of the *bis*(boratabenzene) complex [{(η^5-C_5H_5)Co}$_2${μ:η^6,η^6-(BC_5H_5)$_2$}] (**189**) from tetrabromodiborane (**65**) and six equivalents of cobaltocene (**176**).

This dianionic diboron ligand was shown to facilitate electronic coupling between the cobalt metal sites, as evidenced by the potential separations between successive single-electron redox events in the cyclic voltammogram. Four formal redox potentials for complex **189** were found: $E_{1/2}(1)$ = −0.84 V, $E_{1/2}(2)$ = −0.94 V, $E_{1/2}(3)$ = −2.09 V, and $E_{1/2}(4)$ = −2.36 V (relative to the Fc/Fc$^+$ couple) (Figure 5-6). These potentials correlate to two closely-spaced oxidation waves and two well-resolved reduction waves ([(**189**)]$^{0/+1}$, [(**189**)]$^{+1/+2}$, [(**189**)]$^{0/-1}$, and [(**189**)]$^{-1/-2}$ redox couples, respectively). The extent of metal-metal communication was found to be relative to the charge of the metal atoms, with the negative charge being more efficiently delocalized across the *bis*(boratabenzene) unit (class II Robin-Day system). Magnetic studies indicate that the Co(II) ions are weakly antiferromagnetically coupled across the B-B bridge.

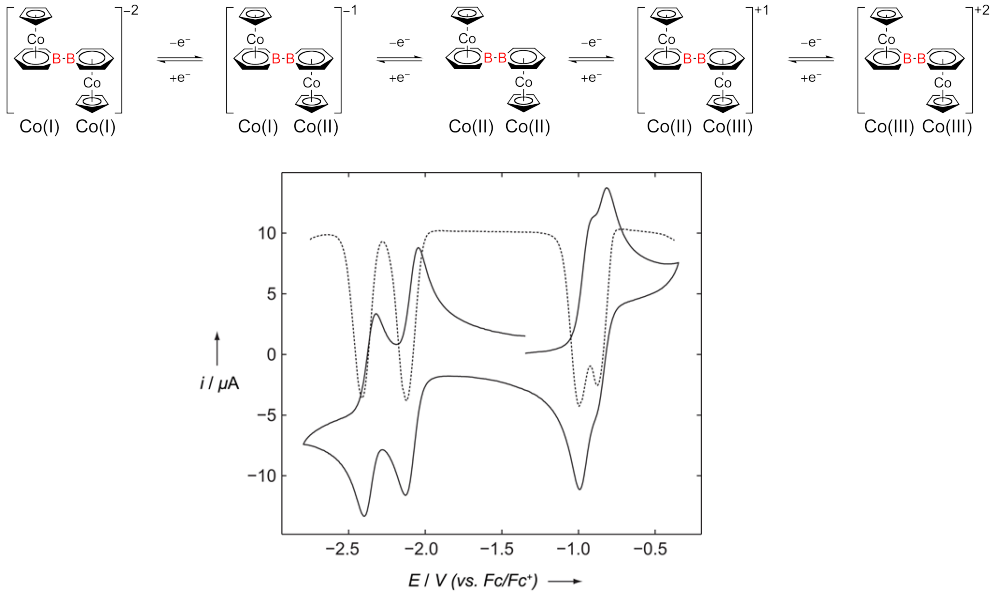

Figure 5-6. Cyclic voltammogram (solid line) and differential pulse voltammogram (dashed line) of [{(η^5-C_5H_5)Co}$_2${μ:η^6,η^6-(BC_5H_5)$_2$}] (**189**) with the redox states illustrated above the figure.

While reduction of the *bis*(boratabenzene) system resulted in decomposition of the complex, oxidation of the system by one- and two-electron steps resulted in isolable stable monocationic (**194**) and dicationic (**195**) forms of the *bis*(boratabenzene) complex (Figure 5-7). Study of these systems verified the results of the cyclic voltammetry studies performed on the neutral species. These species are unfortunately not stable in acetonitrile or nitromethane solutions, which until this point are the only solvents that have been observed to dissolve the cationic species. Unfortunately, this instability in solution complicates reactivity studies of these cationic complexes.

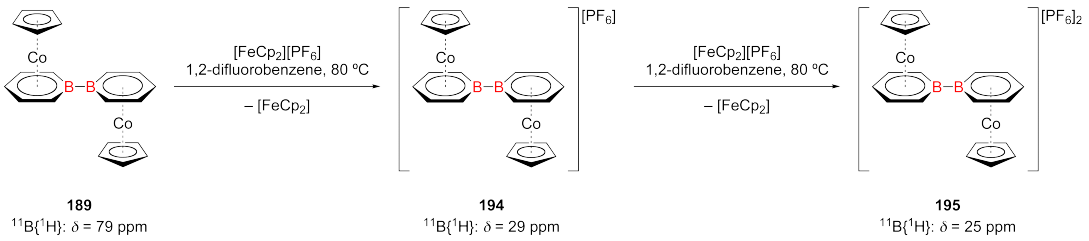

Figure 5-7. Oxidation reactions of the *bis*(boratabenzene) complex **189** with one and two equivalents of [(η^5-C_5H_5)$_2$Fe][PF_6] yielding the monocationic and dicationic complexes **194** and **195** respectively.

Finally, reactivity studies were performed on the neutral *bis*(boratabenzene) complex **189** in which the compound was tested for: (A) cleavage of the boratabenzene (cyclo-

BC_5H_5) ring from the cobalt center, and (B) oxidative addition of the B-B bond to a transition metal scaffold to attempt synthesis of the first ever L_xM-η^1-(BC_5H_5) complex. Both of these reactivity studies, however, proved unsuccessful and typically witnessed decomposition of the *bis*(boratabenzene) complex or no reactivity. After repeated attempts of these reactions, no oxidative addition of the *bis*(boratabenzene) system could be confirmed.

Chapter 6 – Zusammenfassung

Projekt: Borylene

Ein neuer Borylen-Ligand ({BN(SiMe$_3$)(*t*-Bu)}) konnte dargestellt werden, der terminal an Metallfragmente der Form [M(CO)$_5$] (M = Cr, Mo, und W) bindet. Die Komplexe [(OC)$_5$Cr{BN(SiMe$_3$)(*t*-Bu)}] (**19**), [(OC)$_5$Mo{BN(SiMe$_3$)(*t*-Bu)}] (**20**), und [(OC)$_5$W{BN(SiMe$_3$)(*t*-Bu)}] (**21**) konnten durch doppelte Salzeliminierung von Na$_2$[M(CO)$_5$] (M = Cr (**11**), Mo (**1**), und W (**12**)) mit dem Dihalogenboran Br$_2$BN(SiMe$_3$)(*t*-Bu) (**18**) erfolgreich dargestellt werden (Abbildung 6-1). Der neue, unsymmetrische Borylen-Ligand der "ersten Generation" ist eng verwandt mit dem Bis(trimethylsilyl)aminoborylen-Liganden, zu dem er, wie gezeigt werden konnte, ähnliche Strukturmerkmale und Reaktivitäten aufweist. Der unsymmetrische Borylen-Ligand {BN((SiMe$_3$)(*t*-Bu)} zeigt jedoch auch einige Besonderheiten. So verläuft der photolytische Transfer auf Übergangsmetallfragmente im Vergleich zum symmetrischen {BN(SiMe$_3$)$_2$}-Liganden schneller, was ihn auf der Grundlage von NMR- und IR-spektroskopischen Daten zu einem reaktiveren Borylen macht.

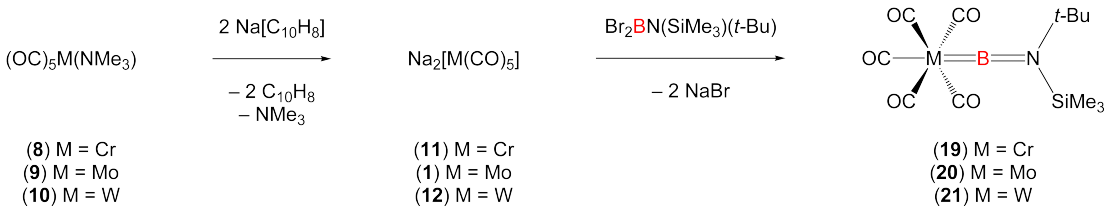

Abbildung 6-1. Synthese von [(OC)$_5$M{BN(SiMe$_3$)(*t*-Bu)}] durch die Reaktion entsprechender dianionischer Übergangsmetall-Komplexe mit Br$_2$BN(SiMe$_3$)(*t*-Bu) (**18**).

Photolytische Transferreaktionen des neuen Borylens ({BN((SiMe$_3$)(*t*-Bu)}) mit verschiedenen Metallkomplexen verlaufen entweder unter vollständigem oder teilweisem Transfer zu verbrückenden Borylen-Komplexen. Im Falle von Lewis-aciden, frühen Übergangsmetallkomplexen (bis zur Gruppe 6) wird eine terminale Koordination bevorzugt. Bei Lewis-basischen Übergangsmetallen (jenseits der Gruppe 9) hingegen scheint der verbrückende Koordinationsmodus energetisch bevorzugt zu sein. Es wurde beobachtet, dass bei Transferreaktionen anfänglich terminale Borylen-Komplexe gebildet werden, die sich in Komplexe mit verbrückenden Borylen-Liganden umlagern.

Abbildung 6-2 gibt eine Übersicht über die durchgeführten Transferreaktionen zwischen der Chromborylen-Spezies [(OC)$_5$Cr{BN(SiMe$_3$)(*t*-Bu)}] (**19**) und den Übergangsmetallkomplexen [(η^5-C$_5$H$_5$)V(CO)$_4$] (**51**), [(η^5-C$_5$Me$_5$)Ir(CO)$_2$] (**56**), [(η^5-

$C_5H_4Me)Co(CO)_2]$ (**59**), und $[\{(\eta^5\text{-}C_5H_5)Ni\}_2\{\mu\text{-}(CO)_2\}]$ (**53**). Bei diesen Umsetzungen konnten die Borylen-Komplexe der "zweiten Generation" $[(\eta^5\text{-}C_5H_5)(OC)_3V\{BN(SiMe_3)(t\text{-}Bu)\}]$ (**55**), $[(\eta^5\text{-}C_5Me_5)Ir\{BN(SiMe_3)(t\text{-}Bu)\}_2]$ (**58**), $[\{(\eta^5\text{-}C_5H_4Me)Co\}_2(\mu\text{-}CO)_2\{\mu\text{-}BN(SiMe_3)(t\text{-}Bu)\}]$ (**61**), und $[\{(\eta^5\text{-}C_5H_5)Ni\}_2(\mu\text{-}CO)\{\mu\text{-}BN(SiMe_3)(t\text{-}Bu)\}]$ (**62**) erfolgreich erhalten werden.

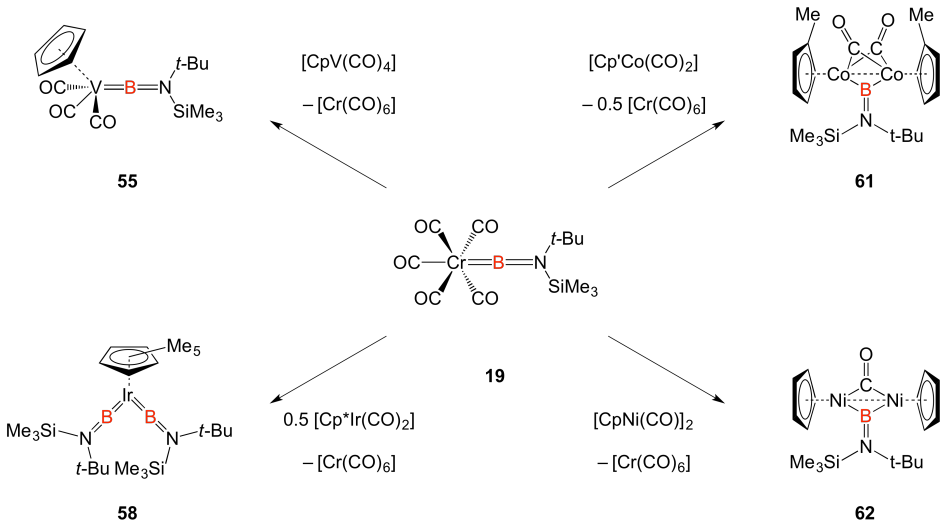

Abbildung 6-2. Synthese von Übergangsmetallborylen-Komplexen der "zweiten Generation" durch photolytischen Borylentransfer von $[(OC)_5Cr\{BN(SiMe_3)(t\text{-}Bu)\}]$ (**19**).

Eine Analyse der gesammelten spektroskopischen (NMR, IR) und strukturellen Daten erlaubt folgende Schlussfolgerungen für die terminalen Borylen-Komplexe:

[1] Die NMR-spektroskopischen Daten für die Gruppe-6-Metall-Komplexe der "ersten Generation" $[(OC)_5M\{BN(SiMe_3)(t\text{-}Bu)\}]$ (M = Cr (**19**), Mo (**20**), und W (**21**)) zeigen, dass die $^{11}B\{^1H\}$- und $^{13}C\{^1H\}$-NMR Signale für die Carbonyle bei Gang zu den schwereren Homologen zu höherem Feld verschoben sind. Daraus resultiert die größte Entschirmung der Kerne für den Komplex $[(OC)_5Cr\{BN(SiMe_3)(t\text{-}Bu)\}]$ (**19**).

[2] Die Bor-Metall-*trans*-Kohlenstoff-Achse (B-M-C_{trans}) in den Borylen-Komplexen der "ersten Generation" $[(OC)_5M\{BN(SiMe_3)(t\text{-}Bu)\}]$ (M = Mo (**20**) und W (**21**)) ist nicht linear, was einen direkten Vergleich der IR-Schwingungsbanden miteinander verhindert. Die Chrom-Verbindung ist nahezu linear und zeigt die erwarteten drei IR-Schwingungsbanden für die Carbonyle, die im Vergleich zum Chrom-Bis(trimethylsilyl)aminoborylen-Komplex $[(OC)_5Cr\{BN(SiMe_3)_2\}]$ (**13**) zu höheren Energien verschoben sind. Die Befunde deuten darauf hin, dass der $\{BN(SiMe_3)(t\text{-}Bu)\}$-Ligand ein etwas stärkerer σ-Donor ist.

[3] Wie in Transferreaktionen gezeigt werden konnte, bevorzugt der Borylen-Ligand {BN(SiMe$_3$)(*t*-Bu)} einen terminalen Koordinationsmodus bei Lewis-aciden, frühen Übergangsmetallen und einen verbrückenden Koordinationsmodus bei Lewis-basischen, späten Übergangsmetallen.

Projekt: Borirene

Die Synthese der ersten Bis(borirenyl)platin-Komplexe wurde vorgestellt, zusammen mit strukturellen und elektronischen Auswirkungen der koplanar angeordneten Borirenringe. Die Reihe der *trans*-Bis(borirenyl)platin-Komplexe **119**/**120**, **122**/**123**, und **125**/**126** stellt die ersten Beispiele für Bis(boriren)-Komplexe dar, in denen die Ringsysteme koplanar zueinander angeordnet sind (Abbildung 6-4). Die Rolle des Platinatoms als Vermittler elektronischer Kommunikation zwischen den chromophoren, aromatischen Borliganden manifestiert sich in einem bathochromen Shift der Boriren-Absorptionsbanden im Vergleich zu Mono-*σ*-Borirenyl-Systemen, als Folge einer ausgedehnten Elektronendelokalisierung. Das *trans*-Bis(boriren)platin-Gerüst dient dabei als vereinfachtes monomeres System, um sowohl die Effekte des Übergangmetallatoms in der Vermittlung elektronischer Konjugation als auch die Abstimmbarkeit der photophysikalischen Eigenschaften in Abhängigkeit der dreigliedrigen, aromatischen Ringe zu studieren.

Eine Reihe von *trans*-Bis(alkinyl)platin-Komplexen (**95**, **102**, **106**, und **63**) wurde als Plattform für den Borylentransfer von {BN(SiMe$_3$)$_2$} dargestellt (Abbildung 6-3). Durch Salzeliminierungsreaktionen von *cis*-[PtCl$_2$(PEt$_3$)$_2$] (**93**) mit zwei Äquivalenten des entsprechenden Alkins in Diethylamin ließen sich die Komplexe *trans*-[Pt(C≡C-Ph)$_2$(PEt$_3$)$_2$] (**95**), *trans*-[Pt(C≡C-*p*-C$_6$H$_4$OMe)$_2$(PEt$_3$)$_2$] (**102**), *trans*-[Pt(C≡C-*p*-C$_6$H$_4$CF$_3$)$_2$(PEt$_3$)$_2$] (**106**), und *trans*-[Pt(C≡C-9-C$_{14}$H$_9$)$_2$(PEt$_3$)$_2$] (**63**) synthetisieren.

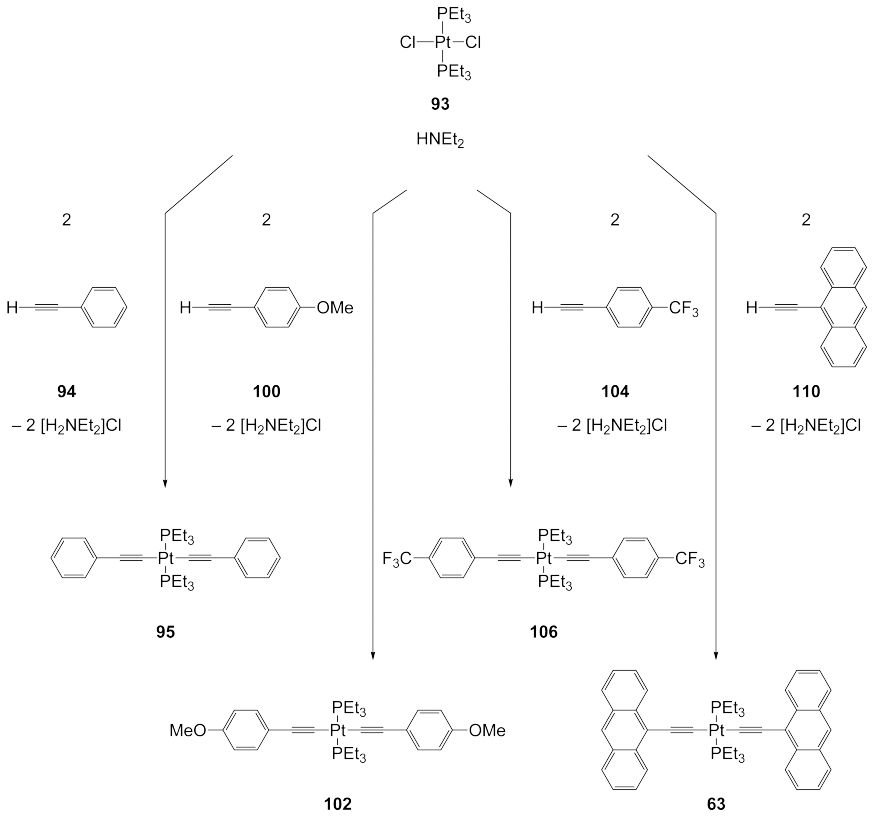

Abbildung 6-3. Synthese von vier *trans*-Bis(alkinyl)platin-Komplexen ausgehend von *trans*-[$PtCl_2(PEt_3)_2$].

Drei *trans*-Bis(borirenyl)platin-Komplexe (**119**/**120**, **122**/**123**, und **125**/**126**) konnten erfolgreich durch photolytischen Transfer des terminalen Borylen-Liganden {$BN(SiMe_3)_2$} vom Chrom-Komplex [$(OC)_5Cr\{BN(SiMe_3)_2\}$] (**13**) auf die *trans*-Bis(alkinyl)platin-Komplexe (**95**, **102**, und **106**) dargestellt werden (Abbildung 6-4). Versuche des Borylentransfers auf den *trans*-Bis(alkinyl)platin-Komplex *trans*-[$Pt(C{\equiv}C\text{-}9\text{-}C_{14}H_9)_2(PEt_3)_2$] (**63**) scheiterten an der Photoinstabilität des Komplexes. Obwohl eine weitere Vielzahl an Platin-Alkinyl-Komplexen dargestellt wurde, verlief der Borylentransfer nur bei den drei eben erwähnten Komplexen erfolgreich. Weitere Bestrebungen, ein *cis*-Isomer zum direkten Vergleich mit den *trans*-konfigurierten Komplexen darzustellen, verliefen ebenfalls erfolglos. Außerdem wurden terminal funktionalisierte Platin-Komplexe vom Gladysz-Typ als Plattform zum Borylentransfer synthetisiert, zeigten sich aber ebenfalls instabil unter photolytischen Bedingungen.

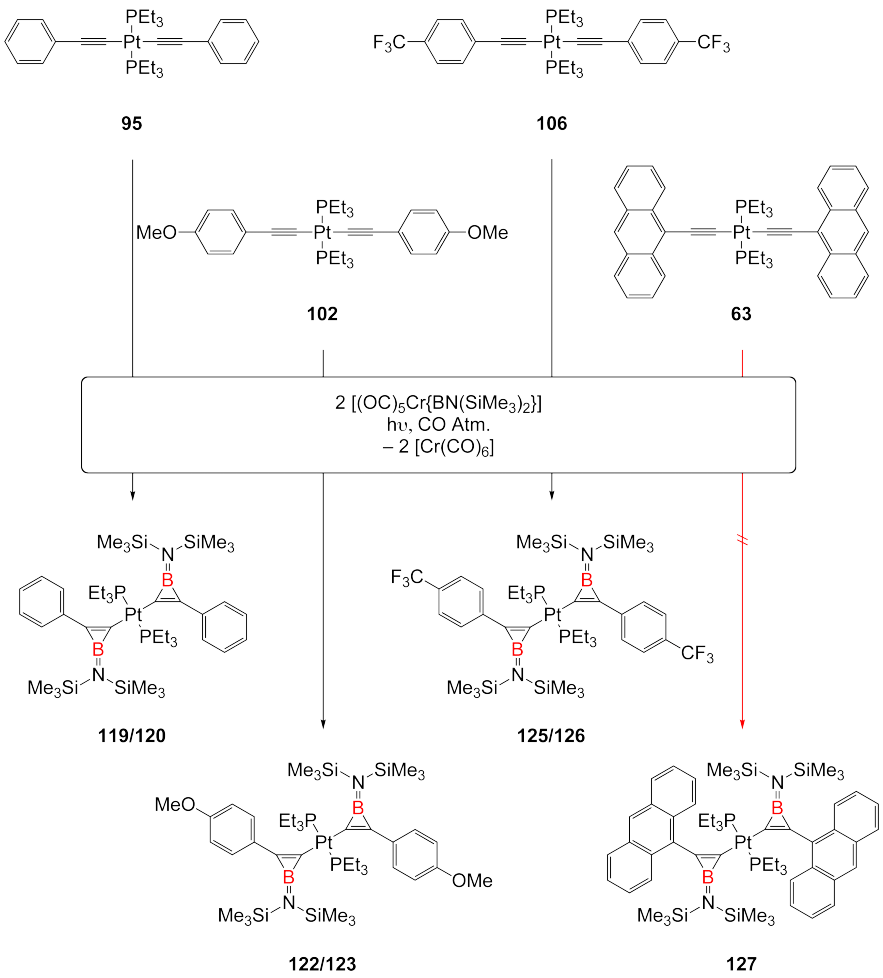

Abbildung 6-4. Synthese von drei *trans*-Bis(borirenyl)platin-Komplexen durch doppelten {BN(SiMe$_3$)$_2$}-Borylentransfer von [(OC)$_5$Cr{BN(SiMe$_3$)$_2$}] (**13**) auf die *trans*-Bis(alkinyl)platin-Substituenten.

Eine Reihe neuer Monoborirene Ph-(μ-{BN(SiMe$_3$)(*t*-Bu)}C=C)-Ph (**148**), *trans*-[PtCl{(μ-{BN(SiMe$_3$)(*t*-Bu)}C=C)-Ph}(PEt$_3$)$_2$] (**149**), und [(η^5-C$_5$Me$_5$)(OC)$_2$Fe(μ-{BN(SiMe$_3$)(*t*-Bu)}C=C)Ph] (**150**) wurde durch photolytischen und thermischen Transfer des unsymmetrischen {BN(SiMe$_3$)(*t*-Bu)}-Liganden ausgehend von den Komplexen [(OC)$_5$M{BN(SiMe$_3$)(*t*-Bu)}] (M = Cr (**19**), Mo (**20**), und W (**21**)) auf organische und organometallische Alkin-Substrate dargestellt. Ziel dieser Umsetzungen war es zu untersuchen, ob der unsymmetrische Borylen-Ligand eine andere Reaktivität im Vergleich zu den symmetrischen, terminalen Borylenen der Form [(OC)$_5$M{BN(SiMe$_3$)$_2$}] (M = Cr (**13**), Mo (**14**), und W (**15**)) aufweist. Die entsprechenden Monoborirene wurden als analytisch reine Öle isoliert. Zur Röntgenstrukturanalyse geeignete Einkristalle konnten demnach nicht erhalten werden.

Projekt: Boratabenzole

Der Bis(boratabenzol)-Komplex [{(η^5-C_5H_5)Co}$_2${μ:η^6,η^6-(BC_5H_5)$_2$}] (**189**) wurde durch Umsetzung von Tetrabromdiboran (**65**) mit sechs Äquivalenten Cobaltocen erfolgreich dargestellt. Die Reaktion ist in der Hinsicht besonders, da Cobaltocen (**176**) sowohl als Reagens als auch als Reduktionsmittel fungiert (Abbildung 6-5). Der bimetallische Übergangsmetallkomplex besteht aus einem verbrückenden Bis(boratabenzol)-Liganden, der die beiden Metallzentren durch eine Bor-Bor-Einfachbindung verbindet. Es konnte gezeigt werden, dass der neuartige Ligand eine Delokalisierung der π-Elektronen zwischen den Cobaltatomen ermöglicht, begünstigt durch das zur Bor-Bor-Bindung zugehörige LUMO.

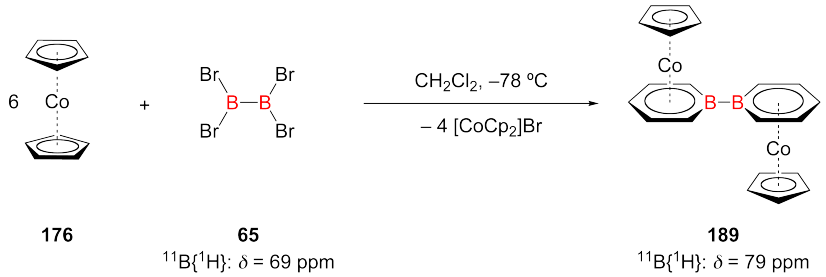

Abbildung 6-5. Darstellung des Bis(boratabenzol)-Komplexes [{(η^5-C_5H_5)Co}$_2${μ:η^6,η^6-(BC_5H_5)$_2$}] (**189**) durch Umsetzung von Tetrabromdiboran (**65**) mit sechs Äquivalenten Cobaltocen (**176**).

Wie durch die Separation aufeinanderfolgender Redoxprozesse im Cyclovoltammogramm gezeigt werden konnte, vermittelt der dianionische Diborligand die elektronische Kopplung zwischen den Cobaltatomen. Vier verschiedene Redoxpotentiale wurden für Komplex **189** gefunden: $E_{1/2}(1)$ = −0.84 V, $E_{1/2}(2)$ = −0.94 V, $E_{1/2}(3)$ = −2.09 V, und $E_{1/2}(4)$ = −2.36 V (referenziert gegen das Fc/Fc$^+$-Paar) (Abbildung 6-6). Die Potentiale können zwei dicht beieinander liegenden Oxidationsprozessen ([(**189**)]$^{0/+1}$ und [(**189**)]$^{+1/+2}$) und zwei gut getrennten Reduktionsprozessen ([(**189**)]$^{0/-1}$ und [(**189**)]$^{-1/-2}$) zugeordnet werden. Das Ausmaß der Metall-Metall-Kommunikation ist dabei abhängig von der Ladung der Metallatome. Die negative Ladung wird effektiver durch die Bis(boratabenzol)-Einheit delokalisiert (Robin-Day-Klasse II). Magnetische Messungen deuten darauf hin, dass die Cobalt(II)-Ionen schwach antiferromagnetisch über die B-B-Brücke gekoppelt sind.

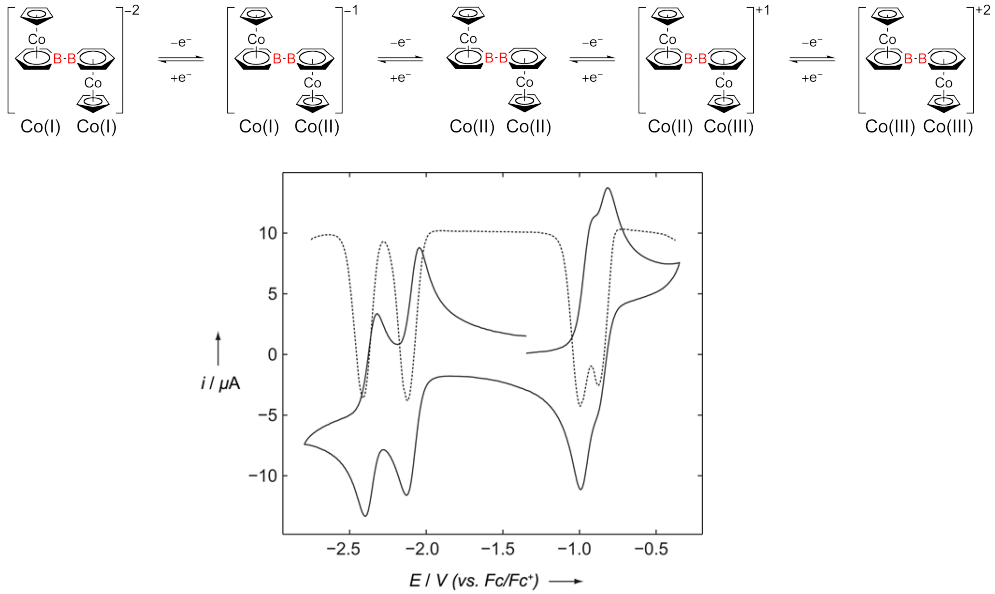

Abbildung 6-6. Cyclovoltammogramm (ausgezogene Linie) und differentielles Pulsvoltammogramm (gestrichelte Linie) von [{(η^5-C_5H_5)Co}$_2${μ:η^6,η^6-(BC_5H_5)$_2$}] (**189**), zusammen mit den korrespondierenden Redoxzuständen (über dem Diagramm).

Während die Reduktion des Bis(boratabenzol)-Systems zur Zersetzung des Komplexes führte, resultierte die Ein- und Zwei-Elektronen-Oxidation in isolierbaren, stabilen monokationischen (**194**) bzw. dikationischen (**195**) Formen des Bis(boratabenzol)-Komplexes (Abbildung 6-7). Die präparativen Arbeiten bestätigen damit die elektrochemischen Ergebnisse an der neutralen Verbindung. Die kationischen Spezies zeigten sich instabil in Acetonitril oder Nitromethan, den einzigen Lösungsmitteln worin sie sich lösten, was weitere Reaktivitätsstudien erschwerte.

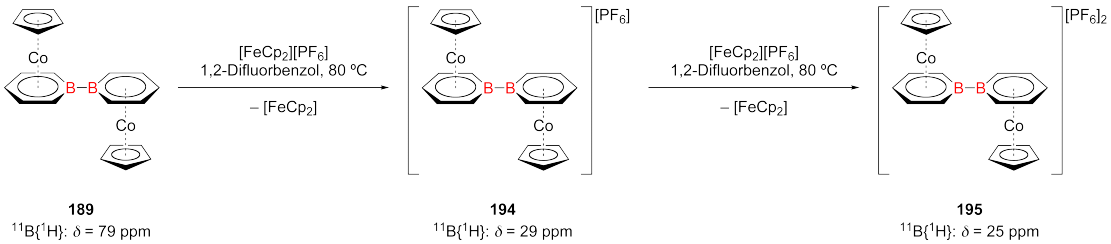

Abbildung 6-7. Oxidationsreaktionen des Bis(boratabenzol)-Komplexes **189** mit einem und zwei Äquivalenten [(η^5-C_5H_5)$_2$Fe][PF_6], die zu den entsprechenden monokationischen (**194**) bzw. dikationischen Komplexen (**195**) führen.

Schließlich wurde die Reaktivität des neutralen Bis(boratabenzol)-Komplexes **189** eingehender untersucht. Versuche zur (A) Abspaltung des freien Bis(boratabenzol)-

Liganden durch Dekomplexierung der Cyclopentadienylcobalt-Fragmente und zur (B) oxidativen Addition von Übergangsmetall-Komplexen an die B-B-Bindung, um die ersten L_xM-η^1-(BC_5H_5)-Komplexe darzustellen, wurden unternommen. Alle Versuche zeigten jedoch, dass die eingesetzten Reagenzien entweder zu keinen Umsetzungen oder zur Zersetzung des Bis(boratabenzol)-Komplexes führten. Bisher konnten somit noch keine Hinweise auf eine oxidative Addition der B-B-Bindung im Bis(boratabenzol)-Komplex erhalten werden.

Chapter 7 – Experimental

7.1 General Considerations

All manipulations were performed either under an atmosphere of dry argon or *in vacuo* using standard Schlenk line or glovebox techniques. Pentane and hexane were dried and degassed by refluxing over NaK amalgam under an atmosphere of dry argon. Diethylether (Et_2O) and tetrahydrofuran (THF) were dried and degassed by refluxing over Na/benzophenone complex and K/benzophenone complex (ketyl), respectively, under an atmosphere of dry argon. Toluene and benzene were dried and degassed by refluxing over molten sodium and potassium, respectively, under an atmosphere of dry argon. Dichloromethane and chloroform were dried and degassed by refluxing over CaH_2 under an atmosphere of dry argon. Hexamethyldisiloxane ($C_6H_{18}OSi_2$) was dried over molecular sieves (4 Å) and degassed by three freeze-pump-thaw cycles before use. Water (H_2O) and EtOH were degassed under an atmosphere of dry argon. MeOH and acetone were dried and degassed by refluxing over P_2O_5 under an atmosphere of dry argon. Deuterated benzene (C_6D_6) was dried and degassed by refluxing over $LiAlH_4$ under an atmosphere of dry argon. Deuterated toluene (C_7D_8) was dried over molecular sieves (4 Å) and degassed by three freeze-pump-thaw cycles before use. Deuterated chloroform ($CDCl_3$) was dried and degassed by refluxing over CaH_2 under an atmosphere of dry argon. Deuterated nitromethane (CD_3NO_2) and acetonitrile (CD_3CN) were dried over molecular sieves (3 Å) and degassed by three freeze-pump-thaw cycles before use. Diethylamine ($C_4H_{11}N$) and triethylamine ($C_6H_{15}N$) were dried by refluxing over CaH_2 under an atmosphere of dry argon. All dried solvents (both deuterated and non-deuterated) were stored under argon over activated molecular sieves.

Photolytic experiments were performed in quartz Schlenk flasks or J. Young tubes. The light source was a LOT-Oriel photolysis apparatus with a 500 W Hg/Xe arc lamp equipped with infrared filters, irradiating at 210-600 nm. NMR spectra of isolated compounds were either acquired on a Bruker Avance 500 NMR spectrometer or a Bruker Avance 400 NMR spectrometer. Chemical shifts (δ) are given in ppm. ^{1}H and $^{13}C\{^{1}H\}$ NMR spectra were referenced to external $SiMe_4$ by residual proton solvent (^{1}H) or the solvent itself (^{13}C). $^{11}B\{^{1}H\}$ and $^{10}B\{^{1}H\}$ NMR spectra were referenced to external $BF_3{\bullet}OEt_2$. $^{19}F\{^{1}H\}$ NMR spectra were references to external $CFCl_3$. $^{29}Si\{^{1}H\}$ NMR spectra were referenced to external $SiMe_4$. $^{31}P\{^{1}H\}$ NMR spectra were referenced to external H_3PO_4. $^{119}Sn\{^{1}H\}$ NMR spectra were referenced to external $SnMe_4$. $^{195}Pt\{^{1}H\}$ NMR spectra were referenced to external K_2PtCl_6. Assignment of the

carbon nuclei was aided by ^{13}C-^{1}H NMR correlation spectroscopy (HSQC and HMBC). IR data were acquired on a JASCO FT/IR-6200typeA apparatus. UV-vis spectra were acquired on a JASCO-V660 UV-vis spectrometer. Differential thermoanalysis (DTA) were performed on an Elementar Vario MICRO cube elemental analyser. Cyclic voltammetry experiments were performed using a Gamry Instruments Reference 600 potentiostat. EPR measurements at X-band (9.4 GHz) were carried out using a Bruker ELEXSYS E580 EPR spectrometer equipped with an Oxford Instruments helium cryostat (ESR900) and a MercuryiTC temperature controller. All chemicals not specifically referenced in this experimental work were purchased from commercial sources.

Transition metal complexes were synthesized according to literature: $Na_2[Mo(CO)_5]$ (**1**),[354] $Na_2[Cr(CO)_5]$ (**11**),[354] $Na_2[W(CO)_5]$ (**12**),[354] $[(OC)_5Cr\{BN(SiMe_3)_2\}]$ (**13**),[118,119] $[(OC)_5Mo\{BN(SiMe_3)_2\}]$ (**14**),[152] $[(OC)_5W\{BN(SiMe_3)_2\}]$ (**15**),[118,119] $[(\eta^5\text{-}C_5H_5)_2Zr\{Si(SiMe_3)_3\}_2]$ (**28**),[372] $[(\eta^5\text{-}C_5H_5)_2Hf\{Si(SiMe_3)_3\}_2]$ (**29**),[372] $[\{(\eta^5\text{-}C_5H_5)Ni\}_2(\mu\text{-}CO)_2]$ (**53**),[459] $K[(\eta^5\text{-}C_5H_5)Mn(CO)_2H]$ (**68**),[460] $[(Cy_3P)_2Cl_2Ru\{=CHCH_3\}]$ (**71**),[461] $[(\eta^5\text{-}C_5Me_5)(OC)_2Fe(C{\equiv}C\text{-}Ph)]$ (**89**),[441] *trans*-$[Pt(C{\equiv}C\text{-}Ph)_2(PEt_3)_2]$ (**95**),[419] *cis*-$[PtCl_2(PEt_3)_2]$ (**98**),[424] *trans*-$[PtCl(C{\equiv}C\text{-}Ph)(PEt_3)_2]$ (**99**),[423] $[PtCl_2(COD)]$ (**132**),[462] $[(\eta^5\text{-}C_5H_5)_2Co]$ (**176**),[451] $[Co(NH_3)_6]Cl_2$ (**191**),[462] $[(\eta^5\text{-}C_5H_5)_2Ti(CO)_2]$,[463] $[Pt(PCy_3)_2]$,[464] $[(I\textit{i}Pr)_2Ni(COD)Ni(I\textit{i}Pr)_2]$,[465] $[(P\textit{i}Pr_3)_2RhCl]_2$.[466]

Main-group precursors were synthesized according to literature: $Cl_2B\{2,6\text{-}(2,4,6\text{-}\textit{i}Pr_3C_6H_2)_2C_6H_3\}$ (**2**),[467] $HN(SiMe_3)(\textit{t}\text{-}Bu)$ (**16**),[468] $Si(SiMe_3)_4$ (**24**),[469,470] $K[Si(SiMe_3)_3]$ (**25**),[372] $(Br_2BPPh_2)_2$ (**42**),[385] $Cy_2P\text{-}PCy_2$ (**49**),[387,394] B_2Br_4 (**65**),[453] $(IMe)(C_4H_2S\text{-}2\text{-}SiMe_3)B{=}B(C_4H_2S\text{-}2\text{-}SiMe_3)(IMe)$ (**70**) (IMe = 1,3-dimethylimidazol-2-ylidene),[407,408] $H\text{-}C{\equiv}C\text{-}\textit{p}\text{-}C_6H_4CF_3$ (**104**),[428] $H\text{-}C{\equiv}C\text{-}9\text{-}C_{14}H_9$ (**110**),[429] $Cy_2PCH_2CH_2PCy_2$ (**111**) (DCPE),[471] $H\text{-}(C{\equiv}C)_3\text{-}Tr^*$ (**113**),[430] $H\text{-}(C{\equiv}C)_2\text{-}H$ (**136**),[472,473] PCy_2Me (**139**),[474] $Ph\text{-}(\mu\text{-}\{BN(SiMe_3)_2\}C{=}C)\text{-}Ph$ (**154**),[173,174] $Me_3SnC{\equiv}CSnMe_3$ (**159**),[442] $Br_2BN(SiMe_3)_2$ (**162**),[443] $Na[C_5H_5]$ (**190**),[451] $B_2(OMe)_4$ (**192**),[475] $Cl_2BN(SiMe_3)_2$,[443] $P(\textit{p}\text{-}tol)_3$,[476] IMeMe (1,3,4,5-tetramethylimidazol-2-ylidene).[477]

7.2 Project Borylene Experimental

7.2.1 $Br_2BN(SiMe_3)(t\text{-Bu})$ (18)

A solution of $HN(SiMe_3)(t\text{-Bu})$ (20.0 g, 138 mmol) in hexane (50 mL) was treated with *n*-BuLi (1.6 M in hexane, 86 mL, 140 mmol) at 0 °C for a period of 3 h. After the 3 h period, the reaction was allowed to warm to room temperature and stir for a period of 21 h. BBr_3 (13.1 mL, 34.6 g, 138 mmol) was then added dropwise to the reaction mixture over the course of 3 h with stirring for an additional period of 24 h at room temperature. Workup of this reaction mixture was undertaken by filtration of the solids and removal of all volatiles from the filtrate under high vacuum (0.001 Torr). The residual oil was distilled under high vacuum (0.001 Torr) at 43 °C to yield $Br_2BN(SiMe_3)(t\text{-Bu})$ (27.8 g, 88.3 mmol) as a clear colorless oil in 64% yield.

^{1}H NMR (500.13 MHz, $CDCl_3$, 297 K) [ppm]: δ = 1.49 (s, 9H, C-(CH_3)$_3$), 0.41 (s, 9H, Si-(CH_3)$_3$, $^2J_{H\text{-}Si}$ = 6.6 Hz).
^{13}C{^{1}H} NMR (125.77 MHz, $CDCl_3$, 297 K) [ppm]: δ = 57.6 (s, 1C, *C*-$(CH_3)_3$), 32.7 (s, 3C, C-(*C*H_3)$_3$), 5.8 (s, 3C, Si-(*C*H_3)$_3$, $^1J_{C\text{-}Si}$ = 58 Hz).
^{11}B{^{1}H} NMR (160.47 MHz, $CDCl_3$, BF_3•OEt_2, 297 K) [ppm]: δ = 36.4 (s).
^{29}Si{^{1}H} NMR (79.49 MHz, $CDCl_3$, $SiMe_4$, 297 K) [ppm]: δ = 7.8 (s).

7.2.2 $[(OC)_5Cr\{BN(SiMe_3)(t\text{-Bu})\}]$ (19)

A solution of $[(OC)_5Cr(NMe_3)]$ (1.03 g, 4.10 mmol) in THF (5 mL) was cooled to −78 °C and a solution of $Na[C_{10}H_8]$ (41 mL, 0.20 M in THF) was added dropwise over a period of 10 min. After the addition was completed, all volatile materials were removed under high vacuum (o °C/0.001 Torr) and the remaining brown/yellow solids were dissolved with Et_2O (20 mL) and triturated in an ultrasonic bath for 2 min to extract the remaining naphthalene from the crude material. The reaction mixture was separated by centrifugation to concentrate $Na_2[Cr(CO)_5]$ as a yellow solid with a Et_2O supernatant. The supernatant was subsequently decanted and the process repeated two additional times (2 x 20 mL Et_2O) in order to remove residual naphthalene. The remaining solid precipitate was dried briefly to yield $Na_2[Cr(CO)_5]$ as a light brown/yellow powder. This powder was then suspended in toluene and cooled to −78 °C, after which $Br_2BN(SiMe_3)(t\text{-Bu})$ (1.3 g, 4.1 mmol) was added dropwise by syringe. The reaction mixture was then stirred at −78 °C for one hour after which the color of the reaction mixture changed from light yellow to dark brown. The reaction flask was removed from the cold bath and allowed to stir for an additional hour while slowly warming to room temperature. Over the course of this

additional hour the reaction color could be witnessed to change to a completely opaque black suspension. All volatiles were then removed under high vacuum (0.001 Torr) and the black solid was dissolved in pentane (20 mL). This pentane suspension was triturated in an ultrasonic bath for a period of 2 min and separated by centrifugation to concentrate the salt elimination byproduct from a black pentane supernatant. Filtration of the supernatant yielded a black pentane filtrate, which precipitated colorless crystalline solids upon storage at −78 °C after a period of 24 h. These colorless crystalline solids correspond to a crude sample of [(OC)$_5$Cr{BN(SiMe$_3$)(*t*-Bu)}], which could be further purified by redissolving the crude material in pentane and storage in a −78 °C freezer for an additional period of 24 h. Removal of the supernatant from the subsequent crystalline material and drying of the product under high vacuum yielded analytically pure [(OC)$_5$Cr{BN(SiMe$_3$)(*t*-Bu)}] (0.555 g, 1.60 mmol) in 39% yield. Crystals suitable for X-ray diffraction were grown from saturated solutions of [(OC)$_5$Cr{BN(SiMe$_3$)(*t*-Bu)}] in hexane.

^{1}H NMR (500.13 MHz, C_6D_6, 297 K) [ppm]: δ = 1.15 (s, 9H, C-(CH_3)$_3$), 0.16 (s, 9H, Si-(CH_3)$_3$, $^1J_{H\text{-}Si}$ = 6.7 Hz).
^{13}C{^{1}H} NMR (125.77 MHz, C_6D_6, 297 K) [ppm]: δ = 218.4 (s, 1C, *trans-C*O to B), 217.9 (s, 4C, *cis-C*O to B), 58.4 (s, 1C, *C*-(CH$_3$)$_3$), 33.6 (s, 3C, C-(*C*H$_3$)$_3$), 3.3 (s, 3C, Si-(*C*H$_3$)$_3$).
^{13}C{^{1}H}-DEPT135 NMR (125.77 MHz, C_6D_6, 297 K) [ppm]: δ = 33.6 (s, 3C, C-(*C*H$_3$)$_3$), 3.3 (s, 3C, Si-(*C*H$_3$)$_3$).
^{11}B{^{1}H} NMR (160.47 MHz, C_6D_6, BF_3•OEt_2, 297 K) [ppm]: δ = 97.0 (br s).
^{29}Si{^{1}H} NMR (79.49 MHz, C_6D_6, $SiMe_4$, 297 K) [ppm]: δ = 3.4 (s).
IR (solid) [cm^{-1}]: $\tilde{\nu}$ = 3,255, 2,981, 2,058, 1,969, 1,900, 1,383, 1,255, 1,171.
EA [%]: calculated for $C_{12}H_{18}BCrNO_5Si$: C 41.52, H 5.23, N 4.03; found: C 41.58, H 5.25, N 3.93.
DTA [°C]: mp = 60, decomp. ≥ 211.

7.2.3 [(OC)$_5$Mo{BN(SiMe$_3$)(*t*-Bu)}] (20)

A solution of [(OC)$_5$Mo(NMe$_3$)] (0.93 g, 3.2 mmol) in THF (5 mL) was cooled to −78 °C and a solution of Na[$C_{10}H_8$] (32 mL, 0.20 M in THF) was added dropwise over a period of 10 min. After the addition was completed, all volatile materials were removed under high vacuum (o °C/0.001 Torr) and the remaining brown/yellow solids were dissolved in Et_2O (20 mL) and triturated in an ultrasonic bath for 2 min to extract the remaining naphthalene from the crude material. The reaction mixture

was separated by centrifugation to concentrate $Na_2[Mo(CO)_5]$ as a yellow solid with a Et_2O supernatant. The supernatant was subsequently decanted and the process repeated two additional times (2 x 20 mL Et_2O) in order to remove residual naphthalene. The remaining solid precipitate was dried briefly to yield $Na_2[Mo(CO)_5]$ as a light brown/yellow powder. This powder was suspended in toluene and cooled to −78 °C after which $Br_2BN(SiMe_3)(t\text{-Bu})$ (1.00 g, 3.17 mmol) was added dropwise by syringe. The reaction mixture was stirred at −78 °C for one hour after which the color of the reaction mixture changed from light yellow to dark brown. The reaction flask was subsequently removed from the cold bath and allowed to stir for an additional hour while slowly warming to room temperature. Over the course of this additional hour the reaction mixture changed to a completely opaque black suspension. All volatiles were then removed under high vacuum and the black solids were dissolved in pentane (20 mL). This pentane suspension was triturated in an ultrasonic bath for a period of 2 min and separated by centrifugation to concentrate the salt elimination byproduct from a black pentane supernatant. Filtration of the supernatant yielded a black pentane fraction, which precipitated colorless crystalline solids upon storage in the −78 °C freezer after a period of 24 h. These colorless crystalline solids correspond to a crude sample of $[(OC)_5Mo\{BN(SiMe_3)(t\text{-Bu})\}]$, which could be further purified by redissolving the crude material in pentane and storage at −78 °C for an additional period of 24 h. Removal of the supernatant from the subsequent crystalline material and drying of the product under high vacuum yielded analytically pure $[(OC)_5Mo\{BN(SiMe_3)(t\text{-Bu})\}]$ (0.080 g, 0.21 mmol) in <10% yield. Crystals suitable for X-ray diffraction were grown from saturated solutions of $[(OC)_5Mo\{BN(SiMe_3)(t\text{-Bu})\}]$ in hexane.

^{1}H NMR (500.13 MHz, C_6D_6, 297 K) [ppm]: δ = 1.14 (s, 9H, C-(CH_3)$_3$), 0.14 (s, 9H, Si-(CH_3)$_3$, $^2J_{H\text{-}Si}$ = 6.6 Hz).

^{13}C{^{1}H} NMR (125.77 MHz, C_6D_6, 297 K) [ppm]: δ = 207.5 (s, 4C, *cis-C*O to B), 206.9 (s, 1C, *trans-C*O to B), 58.3 (s, 1C, *C*-(CH_3)$_3$), 33.9 (s, 3C, C-(CH_3)$_3$), 3.5 (s, 3C, Si-(CH_3)$_3$).

^{13}C{^{1}H}-DEPT135 NMR (125.77 MHz, C_6D_6, 297 K) [ppm]: δ = 33.9 (s, 3C, C-(CH_3)$_3$), 3.5 (s, 3C, Si-(CH_3)$_3$).

^{11}B{^{1}H} NMR (160.47 MHz, C_6D_6, BF_3•OEt_2, 297 K) [ppm]: δ = 95.7 (br s).

^{29}Si{^{1}H} NMR (79.49 MHz, C_6D_6, $SiMe_4$, 297 K) [ppm]: δ = 3.4 (s).

IR (solid) [cm^{-1}]: $\tilde{\nu}$ = 2,981, 2,065, 1,896, 1,383, 1,254, 1,171.

EA [%]: calculated for $C_{12}H_{18}BMoNO_5Si$: C 36.85, H 4.64, N 3.58; found: C 36.98, H 4.64, N 3.62.
DTA [°C]: decomp. ≥ r.t.

7.2.4 [(OC)$_5$W{BN(SiMe$_3$)(*t*-Bu)}] (21)

A solution of [(OC)$_5$W(NMe$_3$)] (0.67 g, 1.8 mmol) in THF (5 mL) was cooled to −78 °C and a solution of Na[$C_{10}H_8$] (18 mL, 0.20 M in THF) was added dropwise over a period of 10 min. After the addition was completed, all volatile materials were removed under high vacuum (0 °C/0.001 Torr) and the remaining brown/yellow solids were dissolved in Et_2O (20 mL) and triturated in an ultrasonic bath for a period of 2 min to extract the remaining naphthalene from the crude material. The reaction mixture was separated by centrifugation to concentrate $Na_2[W(CO)_5]$ as a yellow solid with an Et_2O supernatant. The supernatant was subsequently decanted and the process repeated two additional times (2 x 20 mL Et_2O) to remove residual naphthalene. The remaining solid precipitate was dried briefly to yield $Na_2[W(CO)_5]$ as a light brown/yellow powder. This powder was suspended in toluene and cooled to −78 °C after which $Br_2BN(SiMe_3)$(*t*-Bu) (0.59 g, 1.9 mmol) was added dropwise by syringe. The reaction mixture was then stirred at −78 °C for one hour after which the color of the reaction mixture was witnessed to change from light yellow to dark brown. The reaction flask was removed from the cold bath and allowed to stir for an additional hour while slowly warming to room temperature. Over the course of this additional hour the reaction color could be witnessed to change to a completely opaque black suspension. All volatiles were then removed under high vacuum and the black solids were dissolved in pentane (20 mL). This pentane suspension was triturated in an ultrasonic bath for 2 min and separated by centrifugation to concentrate the salt elimination byproduct from a black pentane supernatant. Filtration of the supernatant yielded a black pentane fraction, which precipitated colorless crystalline solids upon storage at −78 °C after a period of 24 h. These colorless crystalline solids correspond to a crude fraction of [(OC)$_5$W{BN(SiMe$_3$)(*t*-Bu)}], which could be further purified by redissolving the crude material in pentane and storage in a −78 °C freezer for an additional 24 h. Removal of the supernatant from the subsequent crystalline material and drying of the product under high vacuum yielded analytically pure [(OC)$_5$W{BN(SiMe$_3$)(*t*-Bu)}] (0.293 g, 0.612 mmol) in 35% yield. Crystals suitable for X-ray diffraction were grown from saturated solutions of [(OC)$_5$W{BN(SiMe$_3$)(*t*-Bu)}] in hexane.

^{1}H NMR (500.13 MHz, C_6D_6, 297 K) [ppm]: δ = 1.14 (s, 9H, C-(CH_3)$_3$), 0.15 (s, 9H, Si-(CH_3)$_3$, $^{2}J_{H\text{-}Si}$ = 6.8 Hz).
^{13}C{^{1}H} NMR (125.77 MHz, C_6D_6, 297 K) [ppm]: δ = 197.7 (s, 4C, *cis-C*O to B, $^{1}J_{C\text{-}W}$ = 121 Hz), 191.2 (s, 1C, *trans-C*O to B, $^{1}J_{C\text{-}W}$ = 126 Hz), 58.0 (s, 1C, *C*-(CH$_3$)$_3$), 34.0 (s, 3C, C-(*C*H$_3$)$_3$), 3.5 (s, 3C, Si-(*C*H$_3$)$_3$).
^{13}C{^{1}H}-DEPT135 NMR (125.77 MHz, C_6D_6, 297 K) [ppm]: δ = 34.0 (s, 3C, C-(*C*H$_3$)$_3$), 3.50 (s, 3C, Si-(*C*H$_3$)$_3$).
^{11}B{^{1}H} NMR (160.47 MHz, C_6D_6, BF_3•OEt_2, 297 K) [ppm]: δ = 91.7 (br s).
^{29}Si{^{1}H} NMR (79.49 MHz, C_6D_6, $SiMe_4$, 297 K) [ppm]: δ = 2.5 (s).
IR (solid) [cm^{-1}]: $\tilde{\nu}$ = 3,735, 3,053, 2,985, 2,065, 1,898, 1,441, 1,369, 1,254, 1,167.
EA [%]: calculated for $C_{12}H_{18}BWNO_5Si$: C 30.09, H 3.79, N 2.92; found: C 29.72, H 3.46, N 2.79.
DTA [°C]: mp = 73, endo. = 150, decomp. ≥ 233.

7.2.5 HCy_2P•BBr_3 (48)

A solution of $HPCy_2$ (0.59 g, 3.0 mmol) in pentane (50 mL) was treated with BBr_3 (0.68 g, 2.7 mmol) at room temperature. Upon addition of the trihaloborane, an immediate white precipitate was observed resulting in a white suspension. The reaction was stirred for a period of 2 h after which the solution was filtered over a sintered glass frit. The filtered white precipitate was washed with hexane (3 x 20 mL) and dried under high vacuum (0.001 Torr) to yield the Lewis pair HCy_2P•BBr_3 (1.10 g, 2.45 mmol) as a white powder in 91% yield. Crystals suitable for X-ray diffraction were grown from saturated solutions of HCy_2P•BBr_3 in benzene.

^{1}H NMR (500.13 MHz, C_6D_6, 297 K) [ppm]: δ = 4.31 (d, 1H, P-*H*, $^{1}J_{H\text{-}P}$ = 405 Hz), 1.59 (m, 22H, P(C$_6$*H*$_{11}$)$_2$).
^{13}C{^{1}H} NMR (125.77 MHz, C_6D_6, 297 K) [ppm]: δ = 31.2 (d, 2C, P(*C*$_6$H$_{11}$)$_2$, $^{1}J_{C\text{-}P}$ = 32 Hz), 30.0 (d, 2C, P(*C*$_6$H$_{11}$)$_2$, $J_{C\text{-}P}$ = 4.3 Hz), 29.3 (d, 2C, P(*C*$_6$H$_{11}$)$_2$, $J_{C\text{-}P}$ = 3.5 Hz), 26.9 (m, 4C, P(*C*$_6$H$_{11}$)$_2$), 25.5 (d, 2C, P(*C*$_6$H$_{11}$)$_2$, $J_{C\text{-}P}$ = 1.4 Hz).
^{11}B{^{1}H} NMR (160.47 MHz, C_6D_6, BF_3•OEt_2, 297 K) [ppm]: δ = –18.3 (d, $^{1}J_{B\text{-}P}$ = 137 Hz).
^{31}P{^{1}H} NMR (202.46 MHz, C_6D_6, H_3PO_4, 297 K) [ppm]: δ = 1.7 (q, $^{1}J_{P\text{-}B}$ = 138 Hz).
IR (solid) [cm^{-1}]: $\tilde{\nu}$ = 2,933, 2,852, 1,446, 1,296, 1,179.
EA [%]: calculated for $C_{12}H_{23}BBr_3P$: C 32.66, H 5.13; found: C 32.61, H 5.15.
DTA [°C]: mp = 168.

7.2.6 [(η^5-C_5H_5)(OC)$_3$V{BN(SiMe$_3$)(*t*-Bu)}] (55)

A solution of [(OC)$_5$W{BN(SiMe$_3$)(*t*-Bu)}] (45 mg, 0.096 mmol) and [(η^5-C_5H_5)V(CO)$_4$] (23 mg, 0.10 mmol) in benzene was irradiated with a high-pressure Hg lamp at room temperature for approximately 14 h. After completion of the reaction was ascertained *via* monitoring by $^{11}B\{^1H\}$ NMR spectroscopy, all volatiles were removed under high vacuum (0.001 Torr). The resulting solid material was redissolved in hexamethyldisiloxane and filtered through a column (0.5 x 2.0 cm) of pacified silica gel.[397] Storage of this filtered solution at –30 °C for a week yielded [(η^5-C_5H_5)(OC)$_3$V{BN(SiMe$_3$)(*t*-Bu)}] as an orange crystalline solid. The supernatant was subsequently decanted and the crystalline material dried under vacuum to give [(η^5-C_5H_5)(OC)$_3$V{BN(SiMe$_3$)(*t*-Bu)}] (29 mg, 0.081 mmol) in 84% yield. Crystals suitable for X-ray diffraction were grown from saturated solutions of [(η^5-C_5H_5)(OC)$_3$V{BN(SiMe$_3$)(*t*-Bu)}] in hexane.

^{1}H NMR (500.13 MHz, C_6D_6, 297 K) [ppm]: δ = 4.64 (s, 5H, η^5-C_5H_5), 1.37 (s, 9H, C-(CH_3)$_3$), 0.26 (s, 9H, Si-(CH_3)$_3$, $^2J_{H\text{-}Si}$ = 6.7 Hz).
$^{13}C\{^1H\}$ NMR (125.77 MHz, C_6D_6, 297 K) [ppm]: δ = 197.7 (s, 3C, *C*-O), 91.3 (s, 5C, η^5-C_5H_5), 57.8 (s, 1C, *C*-(CH$_3$)$_3$), 33.1 (s, 3C, C-(*C*H$_3$)$_3$), 2.8 (s, 3C, Si-(*C*H$_3$)$_3$, $^1J_{C\text{-}Si}$ = 58 Hz).
$^{13}C\{^1H\}$-DEPT135 NMR (125.77 MHz, C_6D_6, 297 K) [ppm]: δ = 91.3 (s, 5C, η^5-C_5H_5), 33.1 (s, 3C, C-(*C*H$_3$)$_3$), 2.8 (s, 3C, Si-(*C*H$_3$)$_3$).
$^{11}B\{^1H\}$ NMR (160.47 MHz, C_6D_6, BF_3•OEt_2, 297 K) [ppm]: δ = 100.3 (br s).
$^{29}Si\{^1H\}$ NMR (79.49 MHz, C_6D_6, $SiMe_4$, 297 K) [ppm]: δ = 3.6 (s).
EA [%]: calculated for $C_{15}H_{23}BNO_3SiV$: C 50.72, H 6.53, N 3.94; found: C 46.98, H 6.30, N 3.40.
DTA [°C]: mp = 74, decomp. ≥ 259.

7.2.7 [(η^5-C_5Me_5)Ir{BN(SiMe$_3$)(*t*-Bu)}$_2$] (58)

A solution of [(η^5-C_5Me_5)Ir(CO)$_2$] (23 mg, 0.060 mmol) and [(OC)$_5$Cr{BN(SiMe$_3$)(*t*-Bu)}] (46 mg, 0.13 mmol) in hexane (2 mL) was irradiated with a high-pressure Hg lamp at room temperature for approximately 12 h. After completion of the reaction was ascertained *via* monitoring by $^{11}B\{^1H\}$ NMR spectroscopy, all volatiles were removed under high vacuum (0.001 Torr). The resulting solid material was redissolved in hexamethyldisiloxane and filtered through a column (0.5 x 2.0 cm) of pacified silica gel.[397] Storage of this filtered solution in the –30 °C freezer for a week yielded [(η^5-C_5Me_5)Ir{BN(SiMe$_3$)(*t*-Bu)}$_2$] as a light yellow crystalline solid. The supernatant was subsequently decanted and the crystalline material dried under

vacuum to give [(η^5-C_5Me_5)Ir{BN($SiMe_3$)(*t*-Bu)}$_2$] (22 mg, 0.035 mmol) in 58% yield. Crystals suitable for X-ray diffraction were grown from saturated solutions of [(η^5-C_5Me_5)Ir{BN($SiMe_3$)(*t*-Bu)}$_2$] in hexane.

^{1}H NMR (500.13 MHz, C_6D_6, 297 K) [ppm]: δ = 2.35 (s, 15H, η^5-$C_5(CH_3)_5$), 1.45 (s, 18H, C-(CH_3)$_3$), 0.44 (s, 18H, Si-(CH_3)$_3$, $^2J_{H\text{-}Si}$ = 6.7 Hz).
^{13}C{^{1}H} NMR (125.77 MHz, C_6D_6, 297 K) [ppm]: δ = 94.7 (s, 5C, η^5-$C_5(CH_3)_5$), 52.0 (s, 2C, *C*-(CH_3)$_3$), 34.0 (s, 6C, C-(*C*H_3)$_3$), 11.8 (s, 5C, η^5-C_5(*C*H_3)$_5$), 4.5 (s, 6C, Si-(*C*H_3)$_3$, $^1J_{C\text{-}Si}$ = 57 Hz).
^{13}C{^{1}H}-DEPT135 NMR (125.77 MHz, C_6D_6, 297 K) [ppm]: δ = 34.0 (s, 6C, C-(*C*H_3)$_3$), 11.8 (s, 5C, η^5-C_5(*C*H_3)$_5$), 4.5 (s, 6C, Si-(*C*H_3)$_3$).
^{11}B{^{1}H} NMR (160.47 MHz, C_6D_6, BF_3•OEt_2, 297 K) [ppm]: δ = 70.8 (br s).
^{29}Si{^{1}H} NMR (79.49 MHz, C_6D_6, $SiMe_4$, 297 K) [ppm]: δ = –1.2 (s).
IR (solid) [cm^{-1}]: $\tilde{\nu}$ = 3,749, 3,249, 2,964, 2,897, 2,002, 1,653, 1,408, 1,363, 1,252.
EA [%]: calculated for $C_{15}H_{23}BNO_3SiV$: C 45.20, H 8.06, N 4.39; found: C 45.24, H 8.05, N 4.38.
DTA [°C]: mp = 128, decomp. ≥ 301.

7.2.8 [{(η^5-C_5H_4Me)Co}$_2${μ-(CO)}$_2${μ-BN($SiMe_3$)(*t*-Bu)}] (61)

A solution of [(η^5-C_5H_4Me)Co(CO)$_2$] (42 mg, 0.22 mmol) and [(OC)$_5$Cr{BN($SiMe_3$)(*t*-Bu)}] (30 mg, 0.086 mmol) in hexane (2 mL) was irradiated with a high-pressure Hg lamp at room temperature for approximately 8 h. Monitoring of the reaction mixture was undertaken *via* ^{11}B{^{1}H} NMR spectroscopy which showed the formation of two distinct products at δ = 81 ppm and δ = 104 ppm which are proposed to correspond to the terminal and bridging borylene ligand coordination modes in solution. Once complete consumption of the [(OC)$_5$Cr{BN($SiMe_3$)(*t*-Bu)}] was observed, photolytic irradiation was halted and all volatiles were removed under high vacuum (0.001 Torr). The resulting solid material was redissolved in hexamethyldisiloxane and filtered through a column (0.5 x 2.0 cm) of pacified silica gel.[397] Storage of this filtered solution at –30 °C for a week yielded [{(η^5-C_5H_4Me)Co}$_2${μ-(CO)}$_2${μ-BN($SiMe_3$)(*t*-Bu)}] as a dark red crystalline solid. The supernatant was subsequently decanted and the crystalline material dried under vacuum to give [{(η^5-C_5H_4Me)Co}$_2${μ-(CO)}$_2${μ-BN($SiMe_3$)(*t*-Bu)}] (27 mg, 0.056 mmol) in 65% yield. Crystals suitable for X-ray diffraction were grown from saturated solutions of [{(η^5-C_5H_4Me)Co}$_2$(μ-CO)$_2${μ-BN($SiMe_3$)(*t*-Bu)}] in hexane.

^{1}H NMR (500.13 MHz, C_6D_6, 297 K) [ppm]: δ = 4.75 (s, 4H, η^5-$C_5H_4CH_3$), 4.49 (s, 4H, η^5-$C_5H_4CH_3$), 1.94 (s, 6H, η^5-$C_5H_4CH_3$), 1.40 (s, 9H, C-$(CH_3)_3$), 0.34 (s, 9H, Si-$(CH_3)_3$).
^{13}C{^{1}H} NMR (125.77 MHz, C_6D_6, 297 K) [ppm]: δ = 103.2 (s, 2C, *ipso-C* of η^5-$C_5H_4CH_3$), 88.6 (s, 4C, η^5-$C_5H_4CH_3$), 88.3 (s, 4C, η^5-$C_5H_4CH_3$), 56.8 (s, 1C, *C*-$(CH_3)_3$), 33.6 (s, 3C, C-$(CH_3)_3$), 13.2 (s, 2C, η^5-$C_5H_4CH_3$), 5.9 (s, 3C, Si-$(CH_3)_3$, $^{1}J_{C\text{-}Si}$ = 57 Hz).
^{13}C{^{1}H}-DEPT135 NMR (125.77 MHz, C_6D_6, 297 K) [ppm]: δ = 88.6 (s, 4C, η^5-$C_5H_4CH_3$), 88.3 (s, 4C, η^5-$C_5H_4CH_3$), 33.6 (s, 3C, C-$(CH_3)_3$), 13.2 (s, 2C, η^5-$C_5H_4CH_3$), 5.9 (s, 3C, Si-$(CH_3)_3$, $^{1}J_{C\text{-}Si}$ = 57 Hz).
^{11}B{^{1}H} NMR (160.47 MHz, C_6D_6, BF_3•OEt_2, 297 K) [ppm]: δ = 103.6 (br s).
^{29}Si{^{1}H} NMR (79.49 MHz, C_6D_6, $SiMe_4$, 297 K) [ppm]: δ = −2.8 (s).
IR (solid) [cm^{-1}]: $\tilde{\nu}$ = 3,738, 2,927, 2,851, 2,224, 1,762, 1,713, 1,686, 1,594, 1,495, 1,445, 1,354, 1,300, 1,254.
EA [%]: calculated for $C_{21}H_{32}BCo_2NO_2Si$: C 51.76, H 6.62, N 2.87; found: C 51.12, H 6.43, N 2.59.

7.2.9 [{(η^5-C_5H_5)Ni}$_2$(μ-CO){μ-BN(SiMe$_3$)(*t*-Bu)}] (62)

A solution of [(η^5-C_5H_5)$_2$Ni$_2$(CO)$_2$] (16 mg, 0.054 mmol) and [(OC)$_5$W{BN(SiMe$_3$)(*t*-Bu)}] (27 mg, 0.056 mmol) in hexane (2 mL) was irradiated with a high-pressure Hg lamp at room temperature for approximately 7 h. After completion of the reaction was ascertained *via* monitoring by ^{11}B{^{1}H} NMR spectroscopy, all volatiles were removed under high vacuum (0.001 Torr). The resulting solid material was redissolved in hexamethyldisiloxane and filtered through a column (0.5 x 2.0 cm) of pacified silica gel.[397] Storage of this filtered solution at –30 °C for a week yielded [{(η^5-C_5H_5)Ni}$_2$(μ-CO){μ-BN(SiMe$_3$)(*t*-Bu)}] as a dark red crystalline solid. The supernatant was subsequently decanted and the crystalline material dried under vacuum to give [{(η^5-C_5H_4Me)Co}$_2$(μ-(CO)}$_2${μ-BN(SiMe$_3$)(*t*-Bu)}] (17 mg, 0.040 mmol) in 74% yield. Crystals suitable for X-ray diffraction were grown from saturated solutions of [{(η^5-C_5H_5)Ni}$_2$(μ-CO){μ-BN(SiMe$_3$)(*t*-Bu)}] in hexane.

^{1}H NMR (500.13 MHz, C_6D_6, 297 K) [ppm]: δ = 5.32 (s, 10H, η^5-C_5H_5), 1.18 (s, 9H, C-$(CH_3)_3$), 0.24 (s, 9H, Si-$(CH_3)_3$, $^{2}J_{H\text{-}Si}$ = 6.6 Hz).
^{13}C{^{1}H} NMR (125.77 MHz, C_6D_6, 297 K) [ppm]: δ = 92.5 (s, 10C, η^5-C_5H_5), 56.9 (s, 1C, *C*-$(CH_3)_3$), 33.2 (s, 3C, C-$(CH_3)_3$), 4.0 (s, 3C, Si-$(CH_3)_3$, $^{1}J_{C\text{-}Si}$ = 57 Hz).
^{13}C{^{1}H}-DEPT135 NMR (125.77 MHz, C_6D_6, 297 K) [ppm]: δ = 92.5 (s, 10C, η^5-C_5H_5), 33.2 (s, 3C, C-$(CH_3)_3$), 4.0 (s, 3C, Si-$(CH_3)_3$).

$^{11}B\{^1H\}$ NMR (160.47 MHz, C_6D_6, BF_3•OEt_2, 297 K) [ppm]: δ = 94.1 (br s).

$^{29}Si\{^1H\}$ NMR (79.49 MHz, C_6D_6, $SiMe_4$, 297 K) [ppm]: δ = −2.8 (s).

IR (solid) [cm^{-1}]: $\tilde{\nu}$ = 3,248, 2,968, 2,085, 2,002, 1,817, 1,541, 1,469, 1,392, 1,360, 1,317, 1,252.

EA [%]: calculated for $C_{18}H_{28}BNNi_2NOSi$: C 50.20, H 6.55, N 3.25; found: C 50.29, H 6.62, N 3.20.

DTA [°C]: mp = 114, decomp. ≥ 235.

7.2.10 [(Pt{μ-BN(SiMe$_3$)$_2$}$_2$){Cr(μ-CO)(CO)$_4$}{Cr(μ-CO)(CO)$_3$(PEt$_3$)}] (64)

A solution of *trans*-[Pt(C≡C-9-$C_{14}H_9$)$_2$(PEt_3)$_2$] (10 mg, 0.012 mmol) and [$(OC)_5$Cr{BN($SiMe_3$)$_2$}] (30 mg, 0.083 mmol) in benzene (2 mL) was irradiated with a high-pressure Hg lamp at room temperature for approximately 18 h. Monitoring of the reaction mixture was undertaken *via* $^{11}B\{^1H\}$ NMR spectroscopy which showed consumption of [$(OC)_5$Cr{BN($SiMe_3$)(*t*-Bu)}] with formation of two products at δ = 92 ppm and δ = 47 ppm. Irradiation was halted and all volatiles were removed under high vacuum (0.001 Torr). The resulting solid material was redissolved in hexamethyldisiloxane and filtered through a column (0.5 x 2.0 cm) of pacified silica gel.[397] Storage of this filtered solution at −30 °C for a week yielded [(Pt{μ-BN($SiMe_3$)$_2$}$_2$){Cr(μ-CO)(CO)$_4$}{Cr(μ-CO)(CO)$_3$(PEt_3)}] as a light yellow crystalline solid. The supernatant was subsequently decanted and the crystalline material dried under vacuum to give [(Pt{μ-BN($SiMe_3$)$_2$}$_2$){Cr(μ-CO)(CO)$_4$}{Cr(μ-CO)(CO)$_3$(PEt_3)}] (isolated crystals) in <10% yield (the species could not be properly characterized). Isolated crystals suitable for X-ray diffraction were grown from a hexane solution of [(Pt{μ-BN($SiMe_3$)$_2$}$_2$){Cr(μ-CO)(CO)$_4$}{Cr(μ-CO)(CO)$_3$(PEt_3)}] stored in the glovebox freezer (−40 °C) for one week.

$^{11}B\{^1H\}$ NMR (128.38 MHz, C_6D_6, BF_3•OEt_2, 297 K) [ppm]: δ = 92 (br s), 47 (br s).

7.3 Project Borirene Experimental

7.3.1 *trans*-[Pt(C≡C-Ph)$_2$(PEt$_3$)$_2$] (95)[419]

^{1}H NMR (500.13 MHz, C_6D_6, 297 K) [ppm]: δ = 7.57 (m, 4H, *o*-C*H* of C_6H_5), 7.16 (m, 4H, *m*-C*H* of C_6H_5), 7.02 (m, 2H, *p*-C*H* of C_6H_5), 1.99 (m, 12H, P-CH_2), 1.08 (m, 18H, P-CH_2CH_3).

^{13}C{^{1}H} NMR (125.77 MHz, C_6D_6, 297 K) [ppm]: δ = 131.3 (t, *o*-*C* of C_6H_5, $^5J_{C\text{-}P}$ = 1.3 Hz), 130.1 (t, *ipso*-*C* of C_6H_5, $^3J_{C\text{-}Pt}$ = 24 Hz, $^4J_{C\text{-}P}$ = 1.3 Hz), 128.5 (s, *m*-*C* of C_6H_5), 125.3 (s, *p*-*C* of C_6H_5), 110.1 (t, *β*-*C*-C-Pt, $^2J_{C\text{-}Pt}$ = 270 Hz, $^3J_{C\text{-}P}$ = 1.3 Hz), 108.5 (t, *α*-*C*-Pt, $^1J_{C\text{-}Pt}$ = 961 Hz, $^2J_{C\text{-}P}$ = 15 Hz), 16.9 (vquin, Pt-P-*C*H_2, N_1 = 72 Hz), 8.5 (vt, P-CH_2*C*H_3, N_2 = 24 Hz).

$N_1 = |^1J_{C\text{-}P} + {}^3J_{C\text{-}P}|$

$N_2 = |^2J_{C\text{-}P} + {}^4J_{C\text{-}P}|$

^{13}C{^{1}H}-DEPT135 NMR (125.77 MHz, C_6D_6, 297 K) [ppm]: δ = 131.3 (t, *o*-*C* of C_6H_5, $^5J_{C\text{-}P}$ = 1.3 Hz), 128.5 (s, *m*-*C* of C_6H_5), 125.3 (s, *p*-*C* of C_6H_5), 8.5 (vt, P-CH_2*C*H_3, N = 23 Hz).

$N = |^2J_{C\text{-}P} + {}^4J_{C\text{-}P}|$

^{31}P{^{1}H} NMR (202.46 MHz, C_6D_6, H_3PO_4, 297 K) [ppm]: δ = 11.4 (s, $^1J_{P\text{-}Pt}$ = 2,387 Hz, $^1J_{P\text{-}C}$ = 18 Hz).

^{195}Pt{^{1}H} NMR (107.00 MHz, C_6D_6, K_2PtCl_6, 297 K) [ppm]: δ = −4,755 (t, $^1J_{Pt\text{-}P}$ = 2,376 Hz, $^1J_{Pt\text{-}C}$ = 957 Hz, $^2J_{Pt\text{-}C}$ = 266 Hz).

UV-vis (hexane) [nm]: λ = 327.

7.3.2 *trans*-[Pt(C≡C-*p*-C$_6$H$_4$OMe)$_2$(PEt$_3$)$_2$] (102)

A solution of *cis*-[$PtCl_2(PEt_3)_2$] (34 mg, 0.068 mmol) in 2.5 mL of dry 4:1 (v:v) toluene/$HNEt_2$ was triturated in an ultrasonic bath until the platinum precursor dissolved. 4-Ethynylanisole (61 mg, 0.46 mmol) was then added to the reaction mixture. The reaction was heated at 80 °C for 72 h, after which a color change was observed from colorless to light yellow. After removing the volatiles *in vacuo*, the residue was extracted with toluene (3 x 2 mL), concentrated, and chromatographed on a silica gel column (1 x 10 cm) using toluene as an eluent (R_f = 0.6). The product was discerned as a dark non-ultraviolet-active spot on TLC plates. The product fraction was collected and solvent evaporated *in vacuo* yielding *trans*-[Pt(C≡C-*p*-$C_6H_4OMe)_2(PEt_3)_2$] as an air-stable yellow crystalline solid (45 mg, 0.065 mmol) in 96% yield. Crystals suitable for X-ray diffraction were grown by slow evaporation of a saturated toluene solution of *trans*-[Pt(C≡C-*p*-$C_6H_4OMe)_2(PEt_3)_2$] at room temperature.

^{1}H NMR (500.13 MHz, C_6D_6, 297 K) [ppm]: δ = 7.50 (m, 4H, *o*-C*H* of $C_6H_4OCH_3$), 6.78 (m, 4H, *m*-C*H* of $C_6H_4OCH_3$), 3.29 (s, 6H, *p*-$C_6H_4OCH_3$), 2.04 (m, 12H, P-CH_2), 1.12 (m, 18H, P-CH_2CH_3).

^{13}C{^{1}H} NMR (125.77 MHz, C_6D_6, 297 K) [ppm]: δ = 158.0 (s, *p*-*C* of $C_6H_4OCH_3$), 132.3 (t, *o*-*C* of $C_6H_4OCH_3$, $^{5}J_{C\text{-}P}$ = 1.3 Hz), 122.8 (t, *ipso*-*C* of $C_6H_4OCH_3$, $^{3}J_{C\text{-}Pt}$ = 21 Hz, $^{4}J_{C\text{-}P}$ = 1.3 Hz), 114.2 (s, *m*-*C* of $C_6H_4OCH_3$), 109.3 (t, *β*-*C*-C-Pt, $^{2}J_{C\text{-}Pt}$ = 270 Hz, $^{3}J_{C\text{-}P}$ = 2.5 Hz), 105.7 (t, *α*-*C*-Pt, $^{1}J_{C\text{-}Pt}$ = 958 Hz, $^{2}J_{C\text{-}P}$ = 15 Hz), 54.8 (s, $C_6H_4OCH_3$), 16.9 (vquin, Pt-P-*C*H_2, N_1 = 69 Hz), 8.6 (vt, P-CH_2CH_3, N_2 = 23 Hz).

$N_1 = |^{1}J_{C\text{-}P} + {}^{3}J_{C\text{-}P}|$

$N_2 = |^{2}J_{C\text{-}P} + {}^{4}J_{C\text{-}P}|$

^{13}C{^{1}H}-DEPT135 NMR (125.77 MHz, C_6D_6, 297 K) [ppm]: δ = 158.0 (s, *p*-*C* of $C_6H_4OCH_3$), 132.3 (t, *o*-*C* of $C_6H_4OCH_3$, $^{5}J_{C\text{-}P}$ = 1.3 Hz), 114.2 (s, *m*-*C* of $C_6H_4OCH_3$), 54.8 (s, $C_6H_4OCH_3$), 8.6 (vt, P-CH_2CH_3, N = 23 Hz).

$N = |^{2}J_{C\text{-}P} + {}^{4}J_{C\text{-}P}|$

^{31}P{^{1}H} NMR (202.46 MHz, C_6D_6, H_3PO_4, 297 K) [ppm]: δ = 11.4 (s, $^{1}J_{P\text{-}Pt}$ = 2,402 Hz, $^{1}J_{P\text{-}C}$ = 18 Hz).

^{195}Pt{^{1}H} NMR (107.00 MHz, C_6D_6, K_2PtCl_6, 297 K) [ppm]: δ = -4,759 (t, $^{1}J_{Pt\text{-}P}$ = 2,390 Hz, $^{1}J_{Pt\text{-}C}$ = 952 Hz).

IR (solid) [cm^{-1}]: $\tilde{\nu}$ = 2,961, 2,930, 2,875, 2,102, 1,600, 1,564, 1,502, 1,453, 1,412, 1,376, 1,301, 1,279.

UV-vis (hexane) [nm]: λ = 339.

EA [%]: calculated for $C_{30}H_{44}O_2P_2Pt$: C 51.94, H 6.39; found: C 52.24, H 6.36.

DTA [°C]: mp = 156.

7.3.3 *trans*-[Pt(C≡C-*p*-$C_6H_4CF_3$)$_2$(PEt_3)$_2$] (106)

A solution of *cis*-[$PtCl_2(PEt_3)_2$] (32 mg, 0.064 mmol) in 2.5 mL of dry 4:1 (v:v) toluene/$HNEt_2$ was triturated in an ultrasonic bath until the platinum precursor dissolved. 4-Ethynyl-*α*,*α*,*α*-trifluorotoluene (120 mg, 0.705 mmol) was then added to the reaction mixture. The reaction was heated at 80 °C for 72 h, after which a color change was observed from colorless to light yellow. After removing the volatiles *in vacuo*, the residue was extracted with toluene (3 x 2 mL), concentrated, and chromatographed on a silica gel column (1 x 10 cm) using toluene as an eluent (R_f = 0.75). The product was discerned as a dark non-ultraviolet-active spot on TLC plates. The product fraction was collected and solvent evaporated *in vacuo* yielding air-stable yellow crystalline solids of *trans*-[Pt(C≡C-*p*-$C_6H_4CF_3$)$_2$(PEt_3)$_2$] (42 mg, 0.055

mmol) in 86% yield. Crystals suitable for X-ray diffraction were grown by slow evaporation of a saturated toluene solution of *trans*-[Pt(C≡C-*p*-$C_6H_4CF_3$)$_2$(PEt_3)$_2$] at room temperature.

^{1}H NMR (500.13 MHz, C_6D_6, 297 K) [ppm]: δ = 7.35 (m, 8H, *m*- and *o*-C*H* of $C_6H_4CF_3$), 1.94 (m, 12H, P-CH_2), 1.05 (m, 18H, P-CH_2CH_3).
^{13}C{^{1}H} NMR (125.77 MHz, C_6D_6, 297 K) [ppm]: δ = 133.3 (br s, *ipso-C* of $C_6H_4CF_3$), 131.2 (br s, *o-C* of $C_6H_4CF_3$), 128.4 (s, *m-C* of $C_6H_4CF_3$), 127.0 (q, $C_6H_4CF_3$, $^1J_{C\text{-}F}$ = 31 Hz), 125.5 (q, *p-C* of $C_6H_4CF_3$, $^2J_{C\text{-}F}$ = 3.8 Hz), 113.1 (t, *α-C*-Pt, $^1J_{C\text{-}Pt}$ = 969 Hz, $^2J_{C\text{-}P}$ = 15 Hz), 109.6 (br s, *β-C*-C-Pt, $^2J_{C\text{-}Pt}$ = 272 Hz), 16.9 (vquin, Pt-P-*C*H_2, N_1 = 69 Hz), 8.5 (vt, P-CH_2*C*H_3, N_2 = 24 Hz).
$N_1 = |^1J_{C\text{-}P} + {}^3J_{C\text{-}P}|$
$N_2 = |^2J_{C\text{-}P} + {}^4J_{C\text{-}P}|$
^{13}C{^{1}H}-DEPT135 NMR (125.77 MHz, C_6D_6, 297 K) [ppm]: δ = 131.2 (br s, *o-C* of $C_6H_4CF_3$), 128.4 (s, *m-C* of $C_6H_4CF_3$), 125.5 (q, *p-C* of $C_6H_4CF_3$, $^2J_{C\text{-}F}$ = 3.8 Hz), 8.5 (vt, P-CH_2*C*H_3, N = 21 Hz).
$N = |^2J_{C\text{-}P} + {}^4J_{C\text{-}P}|$
^{19}F{^{1}H} NMR (376.50 MHz, C_6D_6, $CFCl_3$, 297 K) [ppm]: δ = –61.8 (s).
^{31}P{^{1}H} NMR (202.46 MHz, C_6D_6, H_3PO_4, 297 K) [ppm]: δ = 11.6 (s, $^1J_{P\text{-}Pt}$ = 2,360 Hz, $^1J_{P\text{-}C}$ = 14 Hz).
^{195}Pt{^{1}H} NMR (107.00 MHz, C_6D_6, K_2PtCl_6, 297 K) [ppm]: δ = –4,748 (t, $^1J_{Pt\text{-}P}$ = 2,350 Hz, $^1J_{Pt\text{-}C}$ = 959 Hz).
IR (solid) [cm^{-1}]: $\tilde{\nu}$ = 2,972, 2,939, 2,885, 2,100, 1,678, 1,604, 1,562, 1,508, 1,456, 1,406, 1,377, 1,317, 1,259.
UV-vis (hexane) [nm]: λ = 327.
EA [%]: calculated for $C_{30}H_{38}F_6P_2Pt$: C 46.82, H 4.98; found: C: 47.68, H: 5.10.
DTA [°C]: mp = 138.

7.3.4 *trans*-[Pt(C≡C-9-$C_{14}H_9$)$_2$(PEt_3)$_2$] (63)

A solution of *cis*-[$PtCl_2$(PEt_3)$_2$] (27 mg, 0.054 mmol) in 2.5 mL of dry 4:1 (v:v) toluene/$HNEt_2$ was triturated in an ultrasonic bath until the platinum precursor dissolved. 9-Ethynylanthracene (218 mg, 1.08 mmol) was then added to the reaction mixture. The reaction was heated at 80 °C for 24 h, after which a color change was observed from colorless to light yellow. After removing the volatiles *in vacuo*, the residue was extracted with toluene (3 x 2 mL), concentrated, and chromatographed on a silica gel column (1 x 10 cm) using toluene as an eluent (R_f = 0.55). The product

was discerned as a bright yellow ultraviolet-active spot on TLC plates. The product fraction was collected and solvent evaporated *in vacuo* to yield *trans*-[Pt(C≡C-9-$C_{14}H_9$)$_2$(PEt_3)$_2$] as an unstable yellow crystalline solid (12 mg, 0.014 mmol) in 27% yield. Crystals suitable for X-ray diffraction were grown by slow evaporation of a saturated toluene solution of *trans*-[Pt(C≡C-9-$C_{14}H_9$)$_2$(PEt_3)$_2$] at room temperature.

^{1}H NMR (500.13 MHz, C_6D_6, 297 K) [ppm]: δ = 9.28 (d, 4H, $^1J_{H\text{-}H}$ = 7.7 Hz, $C_{14}H_9$), 8.06 (s, 2H, 10-C*H* of $C_{14}H_9$), 7.86 (d, 4H, $^1J_{H\text{-}H}$ = 8.5 Hz, $C_{14}H_9$), 7.51 (m, 4H, $C_{14}H_9$), 7.33 (m, 4H, $C_{14}H_9$), 2.02 (m, 12H, P-CH_2), 1.11 (m, 18H, P-CH_2CH_3).
^{13}C{^{1}H} NMR (125.77 MHz, C_6D_6, 297 K) [ppm]: δ = 132.7 (s, 4C), 132.5 (s, 4C), 129.1 (s, 4C), 128.6 (s, 2C), 128.4 (s, 4C), 125.6 (s, 4C), 125.4 (s, 4C), 123.8 (s, 2C), 123.5 (s, 2C), 123.3 (s, 2C), 17.1 (vt, 6C, Pt-P-*C*H_2, N_1 = 35 Hz), 8.6 (vt, 6C, P-CH_2*C*H_3, N_2 = 6 Hz).
$N_1 = |^1J_{C\text{-}P} + {}^3J_{C\text{-}P}|$
$N_2 = |^2J_{C\text{-}P} + {}^4J_{C\text{-}P}|$
^{13}C{^{1}H}-DEPT135 NMR (125.77 MHz, C_6D_6, 297 K) [ppm]: δ = 129.1 (s, 4C), 128.6 (s, 2C), 128.4 (s, 4C), 125.7 (s, 4C), 125.4 (s, 4C), 8.6 (6C, P-CH_2*C*H_3).
^{31}P{^{1}H} NMR (202.46 MHz, C_6D_6, H_3PO_4, 297 K) [ppm]: δ = 12.1 (s, $^1J_{P\text{-}Pt}$ = 2,364 Hz).
^{195}Pt{^{1}H} NMR (107.00 MHz, C_6D_6, K_2PtCl_6, 297 K) [ppm]: δ = −4,721 (t, $^1J_{Pt\text{-}P}$ = 2,356 Hz).

7.3.5 *cis*-[Pt(C≡C-Ph)$_2$(DCPE)] (112)

A J. Young tube was charged with *trans*-[Pt(C≡C-Ph)$_2$(PEt_3)$_2$] (20 mg, 0.032 mmol) and DCPE (13 mg, 0.032 mmol). The solids were dissolved in dry toluene (2.5 mL) and the mixture was heated to 80 °C for 24 h. Analysis of the mixture by ^{31}P NMR spectroscopy after 24 h showed full conversion of *trans*-[Pt(C≡C-Ph)$_2$(PEt_3)$_2$] species to the bidentate *cis*-[Pt(C≡C-Ph)$_2$(DCPE)] complex. The mixture was transferred to a Schlenk flask and all volatiles were removed *in vacuo* to yield a light yellow solid. The residue was extracted with toluene (3 x 2 mL), concentrated, and chromatographed on a silica gel column (1 x 10 cm) using toluene as an eluent (R_f = 0.6). The product was discerned as a dark non-ultraviolet-active spot on TLC plates. The product fraction was collected and solvent evaporated *in vacuo* yielding *cis*-[Pt(C≡C-Ph)$_2$(DCPE)] as a light-sensitive yellow crystalline solid (19 mg, 0.023 mmol) in 72% yield. Further purification of the compound was accomplished by

crystallization of a saturated toluene solution. These crystals were not suitable for X-ray diffraction study, however, the crystalline material was subjected to elemental analysis and NMR characterization. These studies showed the presence of one stoichiometric amount of toluene in the crystalline solid.

^{1}H NMR (500.13 MHz, C_6D_6, 297 K) [ppm]: δ = 7.68 (m, 4H, *o*-C*H* of C_6H_5), 7.11 (m 4H, *m*-C*H* of C_6H_5), 6.95 (m, 2H, *p*-C*H* of C_6H_5), 2.31 (br d, 4H, P-(C_6H_{11})$_2$ $^{1}J_{H\text{-}H}$ = 12 Hz), 2.23 (m, 4H, P-(C_6H_{11})$_2$), 1.60 (m, 20H, P-(C_6H_{11})$_2$), 1.15 (m, 20H, P-(C_6H_{11})$_2$), 1.15 (m, 4H, P-(C_2H_4)-P).
^{13}C{^{1}H} NMR (125.77 MHz, C_6D_6, 297 K) [ppm]: δ = 131.5 (s, 4C, *o*-*C* of C_6H_5), 130.1 (s, 2C, *ipso*-*C* of C_6H_5), 128.3 (s, 4C, *m*-*C* of C_6H_5), 125.1 (s, 2C, *p*-*C* of C_6H_5), 110.8 (m, 2C, α-*C* or β-*C* of Pt-CC-C_6H_5), 110.6 (m, 2C, α-*C* or β-*C* of Pt-CC-C_6H_5), 34.7 (d, 8C, P-(C_6H_{11})$_2$, $^{1}J_{C\text{-}P}$ = 31 Hz), 29.3 (s, 4C, P-(C_6H_{11})$_2$), 28.7 (s, 4C, P-(C_6H_{11})$_2$), 27.3 (m, 4C, P-(C_6H_{11})$_2$), 26.4 (s, 4C, P-(C_6H_{11})$_2$), 23.8 (m, 2C, P-(C_2H_4)-P).
^{13}C{^{1}H}-DEPT135 NMR (125.77 MHz, C_6D_6, 297 K) [ppm]: δ = 131.5 (s, 4C, *o*-*C* of C_6H_5), 128.3 (s, 4C, *m*-*C* of C_6H_5), 125.1 (s, 2C, *p*-*C* of C_6H_5), 34.7 (d, 8C, P-(C_6H_{11})$_2$).
^{31}P{^{1}H} NMR (202.46 MHz, C_6D_6, H_3PO_4, 297 K) [ppm]: δ = 61.9 (s, $^{1}J_{P\text{-}Pt}$ = 2,231 Hz).
^{195}Pt{^{1}H} NMR (107.00 MHz, C_6D_6, K_2PtCl_6, 297 K) [ppm]: δ = −4,891 (t, $^{1}J_{Pt\text{-}P}$ = 2,220 Hz).
EA [%]: calculated for $C_{42}H_{58}P_2Pt$ + C_7H_8: C 64.53, H 7.29; found: C: 64.35, H: 7.27.

7.3.6 *trans*-[Pt(PEt$_3$)$_2${(C≡C)$_3$-Tr*}$_2$] (115)

A solution of *cis*-[$PtCl_2(PEt_3)_2$] (8 mg, 0.02 mmol) in 2.5 mL of dry 4:1 (v:v) toluene/$HNEt_2$ was triturated in an ultrasonic bath until the platinum precursor had dissolved. H-(C≡C)$_3$-Tr* (22 mg, 0.034 mmol) was then added to the reaction mixture. The reaction was kept at room temperature for 24 h, after which a color change was observed from colorless to light yellow. After removing the volatiles *in vacuo*, the residue was extracted with toluene (3 x 2 mL), concentrated, and chromatographed on a silica gel column (1 x 10 cm) using toluene as an eluent (R_f = 0.8). The product was discerned as an ultraviolet-active spot on TLC plates. The product fraction was collected and solvent evaporated *in vacuo* yielding *trans*-[Pt{(C≡C)$_3$-Tr*}$_2$(PEt_3)$_2$] as air-stable yellow crystalline solids (20 mg, 0.012 mmol) in 72% yield. Crystals suitable for X-ray diffraction were grown by slow evaporation of a saturated toluene solution of *trans*-[Pt{(C≡C)$_3$-Tr*}$_2$(PEt_3)$_2$] at room temperature.

^{1}H NMR (500.13 MHz, C_6D_6, 297 K) [ppm]: δ = 7.45 (d, 12H, *o*-C*H* of $C_6H_3(C_4H_9)_2$, $^{4}J_{H\text{-}H}$ = 1.7 Hz), 7.43 (t, 6H, *p*-C*H* of $C_6H_3(C_4H_9)_2$, $^{4}J_{H\text{-}H}$ = 1.7 Hz), 1.71 (m, 12H, P-CH_2CH$_3$), 1.20 (s, 108H, $C_6H_3(C_4H_9)_2$), 0.85 (m, 18H, P-CH$_2$CH_3).
^{13}C{^{1}H} NMR (125.77 MHz, C_6D_6, 297 K) [ppm]: δ = 150.5 (s, 12C, *m-C* of $C_6H_3(C_4H_9)_2$), 145.5 (s, 6C, *ipso-C* of $C_6H_3(C_4H_9)_2$), 124.6 (s, 12C, *o-C* of $C_6H_3(C_4H_9)$, 120.4 (s, 6C, *p-C* of $C_6H_3(C_4H_9)_2$), 100.3 (s, 2C), 93.5 (s, 2C), 83.4 (s, 2C), 71.7 (s, 2C), 67.7 (s, 2C), 58.2 (s, 2C), 56.9 (s, 2C), 35.0 (s, 12C, *C*(CH$_3$)$_3$), 31.6 (s, 36C, C(*C*H$_3$)$_3$), 16.5 (vt, 6C, N_1 = 35 Hz, P-*C*H$_2$CH$_3$), 8.2 (s, 6C, P-CH$_2$*C*H$_3$).
N_1= $|^{1}J_{C\text{-}P} + {}^{3}J_{C\text{-}P}|$
^{13}C{^{1}H}-DEPT135 NMR (125.77 MHz, C_6D_6, 297 K) [ppm]: δ = 124.6 (s, 12C, *o-C* of $C_6H_3(C_4H_9)$, 120.4 (s, 6C, *p-C* of $C_6H_3(C_4H_9)_2$), 31.6 (s, 36C, C(*C*H$_3$)$_3$), 8.2 (s, 6C, P-CH$_2$*C*H$_3$).
^{31}P{^{1}H} NMR (202.46 MHz, C_6D_6, H_3PO_4, 297 K) [ppm]: δ = 12.5 (s, $^{1}J_{P\text{-}Pt}$ = 2,283 Hz).
^{195}Pt{^{1}H} NMR (107.00 MHz, C_6D_6, K_2PtCl_6, 297 K) [ppm]: δ = −4,743 (t, $^{1}J_{Pt\text{-}P}$ = 2,281 Hz).
IR (solid) [cm^{-1}]: $\tilde{\nu}$ = 3,251, 2,960, 2,904, 2,868, 2,137, 2,031, 1,591, 1,475, 1,454, 1,431, 1,392, 1,361, 1,248.
UV-vis (benzene) [nm]: λ = 387.
EA [%]: calculated for $C_{110}H_{156}P_2Pt$: C 76.13, H 9.06; found: C 76.97, H 9.30.
DTA [°C]: mp = 322, decomp = 325.

7.3.7 *trans*-[Pt{(μ-{B=N(SiMe$_3$)$_2$}C=C)-Ph}$_2$(PEt$_3$)$_2$] (119/120)

In a quartz J. Young NMR tube, [(OC)$_5$Cr=B=N(SiMe$_3$)$_2$] (30 mg, 0.083 mmol) and *trans*-[Pt(C≡C-Ph)$_2$(PEt$_3$)$_2$] (21 mg, 0.033 mmol) were dissolved in 1.5 mL of benzene. The NMR tube was then irradiated for 6 h at room temperature after which full conversion to the *bis*(borirene) was confirmed by ^{31}P{^{1}H} NMR spectroscopy. The volatile components of the reaction mixture were removed *in vacuo* and the brown residue was extracted with hexane and filtered through a column of pacified silica gel (0.5 x 2 cm.).[397] The light yellow fraction was collected and dried *in vacuo* to yield *trans*-[Pt{(μ-{B=N(SiMe$_3$)$_2$}C=C)-Ph}$_2$(PEt$_3$)$_2$] (13 mg, 0.013 mmol) as a light yellow crystalline solid in 40% yield. Crystals suitable for X-ray diffraction were grown by slow evaporation of a hexamethyldisiloxane solution of *trans*-[Pt{(μ-{B=N(SiMe$_3$)$_2$}C=C)-Ph}$_2$(PEt$_3$)$_2$] stored at −30 °C for 1 week.

^{1}H NMR (500.13 MHz, C_6D_6, 297 K) [ppm]: δ = 8.51 (m, 4H, *m*- or *o*-C*H* of C_6H_5), 7.50 (m, 4H, *m*- or *o*-C*H* of C_6H_5), 7.26 (m, 2H, *p*-C*H* of C_6H_5), 1.41 (m, 12H, P-CH_2), 0.72 (m, 18H, P-CH_2CH_3), 0.60 (s, 18H, Si-CH_3), 0.57 (s, 18H, Si-CH_3).
^{13}C{^{1}H} NMR (125.77 MHz, C_6D_6, 297 K) [ppm]: δ = 130.0 (s, *m*-*C* of C_6H_5), 129.6 (s, *o*-*C* of C_6H_5), 128.6 (s, *p*-*C* of C_6H_5), 128.6 (br s, *ipso*-*C* of C_6H_5), 16.7 (vt, Pt-P-*C*H_2, *N* = 34 Hz), 16.7 (vt, Pt-P-*C*H_2, *N* = 34 Hz), 8.2 (br s, P-CH_2*C*H_3), 4.1 (s, 18H, Si-*C*H_3), 4.0 (s, 18H, Si-*C*H_3).
$N = |{}^{1}J_{C\text{-}P} + {}^{3}J_{C\text{-}P}|$
^{11}B{^{1}H} NMR (160.47 MHz, C_6D_6, BF_3•OEt_2, 297 K) [ppm]: δ = 35.5 (br s, μ-(*B*=N($SiMe_3$)$_2$)C=C).
^{29}Si{^{1}H} NMR (79.49 MHz, C_6D_6, $SiMe_4$, 297 K) [ppm]: δ = 5.5 (s, N-*Si*-CH_3), 5.4 (s, N-*Si*-CH_3).
^{31}P{^{1}H} NMR (202.46 MHz, C_6D_6, H_3PO_4, 297 K) [ppm]: δ = 5.9 (s, Pt-*P*-CH_2, $^{1}J_{Pt\text{-}P}$ = 2,765 Hz), 5.9 (s, Pt-*P*-CH_2, $^{1}J_{Pt\text{-}P}$ = 2,762 Hz).
^{195}Pt{^{1}H} NMR (107.00 MHz, C_6D_6, K_2PtCl_6, 297 K) [ppm]: δ = –4,108 (t, *Pt*-P-CH_2, $^{1}J_{Pt\text{-}P}$ = 2,751 Hz), –4110 (t, *Pt*-P-CH_2, $^{1}J_{Pt\text{-}P}$ = 2,759 Hz).
IR (solid) [cm^{-1}]: $\tilde{\nu}$ = 2,956, 2,925, 2,854, 2,042, 1,965, 1,932, 1,894, 1,610, 1,485, 1,456, 1,415, 1,375, 1,292, 1,248.
UV-vis (hexane) [nm]: λ = 257.
EA [%]: calculated for $C_{40}H_{76}B_2N_2P_2PtSi_4$: C 49.22, H 7.85, N 2.87; found: C 49.64, H 8.10, N 2.52.
DTA [°C]: mp = 165.

7.3.8 *trans*-[Pt{(μ-{B=N($SiMe_3$)$_2$}C=C)-*p*-C_6H_4OMe}$_2$(PEt_3)$_2$] (122/123)

In a quartz J. Young NMR tube, [(OC)$_5$Cr=B=N($SiMe_3$)$_2$] (23 mg, 0.063 mmol) and *trans*-[Pt(C≡C-*p*-C_6H_4OMe)$_2$(PEt_3)$_2$] (15 mg, 0.022 mmol) were dissolved in 1.5 mL of hexane. The NMR tube was then irradiated for 6 h at room temperature after which full conversion to the *bis*(borirene) was confirmed by ^{31}P{^{1}H} NMR spectroscopy. The volatile components of the reaction mixture were removed *in vacuo* and the brown residue was extracted with hexane and filtered through a column of pacified silica gel (0.5 x 2 cm.).[397] The light yellow fraction was collected and dried *in vacuo* to yield *trans*-[Pt{(μ-{B=N($SiMe_3$)$_2$}C=C)-*p*-C_6H_4OMe}$_2$(PEt_3)$_2$] (10 mg, 0.010 mmol) as a light yellow crystalline solid in 45% yield. Crystals suitable for X-ray diffraction were grown by slow evaporation of a hexamethyldisiloxane

solution of *trans*-[Pt{(μ-{B=N(SiMe$_3$)$_2$}C=C)-*p*-C$_6$H$_4$OMe}$_2$(PEt$_3$)$_2$] stored at −30 °C for 1 week.

^{1}H NMR (500.13 MHz, C$_6$D$_6$, 297 K) [ppm]: δ = 8.55 (m, 4H, *o*-C*H* of C$_6$H$_4$OCH$_3$), 7.14 (m, 4H, *m*-C*H* of C$_6$H$_4$OCH$_3$), 3.39 (s, 3H, C$_6$H$_4$OC*H*$_3$), 3.39 (s, 3H, C$_6$H$_4$OC*H*$_3$), 1.44 (m, 12H, P-C*H*$_2$), 0.75 (m, 18H, P-CH$_2$C*H*$_3$), 0.63 (s, 18H, Si-C*H*$_3$), 0.60 (s, 18H, Si-C*H*$_3$).
^{13}C{^{1}H} NMR (125.77 MHz, C$_6$D$_6$, 297 K) [ppm]: δ = 159.8 (s, *p*-*C* of C$_6$H$_4$OCH$_3$), 131.7 (s, *o*-*C* of C$_6$H$_4$OCH$_3$), 128.6 (s, *ipso*-*C* of C$_6$H$_4$OCH$_3$), 114.0 (s, *m*-*C* of C$_6$H$_4$OCH$_3$), 54.9 (s, C$_6$H$_4$OCH$_3$), 16.7 (vt, Pt-P-*C*H$_2$, *N* = 33 Hz), 16.7 (vt, Pt-P-*C*H$_2$, *N* = 34 Hz), 8.2 (br s, P-CH$_2$*C*H$_3$), 4.1 (s, 18H, Si-*C*H$_3$), 4.1 (s, 18H, Si-*C*H$_3$).
$N = |{}^1J_{C\text{-}P} + {}^3J_{C\text{-}P}|$
^{13}C{^{1}H}-DEPT135 NMR (125.77 MHz, C$_6$D$_6$, 297 K) [ppm]: δ = 131.7 (s, *o*-*C* of C$_6$H$_4$OCH$_3$), 114.0 (s, *m*-*C* of C$_6$H$_4$OCH$_3$), 54.9 (s, C$_6$H$_4$OCH$_3$), 8.3 (br s, P-CH$_2$*C*H$_3$), 4.1 (s, 18H, Si-*C*H$_3$), 4.1 (s, 18H, Si-*C*H$_3$).
^{11}B{^{1}H} NMR (160.47 MHz, C$_6$D$_6$, BF$_3$•OEt$_2$, 297 K) [ppm]: δ = 35.4 (br s, μ-(*B*=N(SiMe$_3$)$_2$)C=C).
^{31}P{^{1}H} NMR (202.46 MHz, C$_6$D$_6$, H$_3$PO$_4$, 297 K) [ppm]: δ = 6.0 (s, Pt-*P*-CH$_2$, $^1J_{Pt\text{-}P}$ = 2,773 Hz), 6.0 (s, Pt-*P*-CH$_2$, $^1J_{Pt\text{-}P}$ = 2,765 Hz).
^{195}Pt{^{1}H} NMR (107.00 MHz, C$_6$D$_6$, K$_2$PtCl$_6$, 297 K) [ppm]: δ = −4,110 (t, *Pt*-P-CH$_2$, $^1J_{Pt\text{-}P}$ = 2,755 Hz), −4,111 (t, *Pt*-P-CH$_2$, $^1J_{Pt\text{-}P}$ = 2,763 Hz)
IR (solid) [cm^{-1}]: $\tilde{\nu}$ = 3,248, 3,107, 3,053, 2,015, 1,734, 1,701, 1,651, 1,556, 1,541, 1,508, 1,456, 1,419.
UV-vis (hexane) [nm]: λ = 270.
EA [%]: calculated for C$_{42}$H$_{80}$B$_2$N$_2$O$_2$P$_2$PtSi$_4$: C 48.69, H 7.78, N 2.70; found: C 48.16, H 7.91, N 2.54.

7.3.9 *trans*-[Pt{(μ-{B=N(SiMe$_3$)$_2$}C=C)-*p*-C$_6$H$_4$CF$_3$}$_2$(PEt$_3$)$_2$] (125/126)

In a quartz J. Young NMR tube, [(OC)$_5$Cr=B=N(SiMe$_3$)$_2$] (18 mg, 0.050 mmol) and *trans*-[Pt(C≡C-*p*-C$_6$H$_4$CF$_3$)$_2$(PEt$_3$)$_2$] (12 mg, 0.016 mmol) were dissolved in 1.5 mL of hexane. The NMR tube was then irradiated for 6 h at room temperature after which full conversion to the *bis*(borirene) was confirmed by ^{31}P{^{1}H} NMR spectroscopy. The volatile components of the reaction mixture were removed *in vacuo* and the brown residue was extracted with hexane and filtered through a column of pacified silica gel (0.5 x 2 cm.).[397] The light yellow fraction was collected and dried *in vacuo* to yield *trans*-[Pt{(μ-{B=N(SiMe$_3$)$_2$}C=C)-*p*-C$_6$H$_4$CF$_3$}$_2$(PEt$_3$)$_2$] (11 mg, 0.010 mmol) as a light

yellow crystalline solid in 63% yield. Crystals suitable for X-ray diffraction were grown by slow evaporation of a hexamethyldisiloxane solution of *trans*-[Pt{(*μ*-{B=N(SiMe$_3$)$_2$}C=C)-*p*-C$_6$H$_4$CF$_3$}$_2$(PEt$_3$)$_2$] stored at −30 °C for 1 week.

^{1}H NMR (500.13 MHz, C$_6$D$_6$, 297 K) [ppm]: δ = 8.32 (m, 4H, *o*-C*H* of C$_6$H$_4$CF$_3$), 7.73 (m, 4H, *m*-C*H* of C$_6$H$_4$CF$_3$), 1.29 (m, 12H, P-C*H*$_2$), 0.64 (m, 18H, P-CH$_2$C*H*$_3$), 0.54 (s, 18H, Si-C*H*$_3$), 0.53 (s, 18H, Si-C*H*$_3$).
^{13}C{^{1}H} NMR (125.77 MHz, C$_6$D$_6$, 297 K) [ppm]: δ = 139.9 (s, *ipso*-*C* of C$_6$H$_4$CF$_3$), 129.6 (s, *o*-*C* of C$_6$H$_4$CF$_3$), 129.1 (s, *p*-C$_6$H$_4$*C*F$_3$), 128.8 (s, *m*-*C* of C$_6$H$_4$CF$_3$), 125.7 (s, *p*-*C* of C$_6$H$_4$CF$_3$), 16.6 (m, Pt-P-*C*H$_2$), 8.1 (m, P-CH$_2$*C*H$_3$), 3.9 (s, 18H, Si-*C*H$_3$), 3.9 (s, 18H, Si-*C*H$_3$).
^{13}C{^{1}H}-DEPT135 NMR (125.77 MHz, C$_6$D$_6$, 297 K) [ppm]: δ = 129.6 (s, *o*-*C* of C$_6$H$_4$CF$_3$), 128.8 (s, *m*-*C* of C$_6$H$_4$CF$_3$), 125.7 (s, *p*-*C* of C$_6$H$_4$CF$_3$), 8.1 (m, P-CH$_2$*C*H$_3$), 3.9 (s, 18H, Si-*C*H$_3$), 3.9 (s, 18H, Si-*C*H$_3$).
^{11}B{^{1}H} NMR (160.47 MHz, C$_6$D$_6$, BF$_3$•OEt$_2$, 297 K) [ppm]: δ = 35.1 (br s, *μ*-(*B*=N(SiMe$_3$)$_2$)C=C).
^{19}F{^{1}H} NMR (376.50 MHz, C$_6$D$_6$, CFCl$_3$, 297 K) [ppm]: δ = −61.6 (s, *p*-C$_6$H$_4$C*F*$_3$), −61.7 (s, *p*-C$_6$H$_4$C*F*$_3$).
^{29}Si{^{1}H} NMR (79.49 MHz, C$_6$D$_6$, SiMe$_4$, 297 K) [ppm]: δ = 6.0 (s, N-*Si*-CH$_3$), 5.8 (s, N-*Si*-CH$_3$).
^{31}P{^{1}H} NMR (202.46 MHz, C$_6$D$_6$, H$_3$PO$_4$, 297 K) [ppm]: δ = 6.2 (s, Pt-*P*-CH$_2$, $^1J_{Pt\text{-}P}$ = 2,743 Hz), 5.8 (s, Pt-*P*-CH$_2$, $^1J_{Pt\text{-}P}$ = 2,728 Hz).
^{195}Pt{^{1}H} NMR (107.00 MHz, C$_6$D$_6$, K$_2$PtCl$_6$, 297 K) [ppm]: δ = −4,100 (t, *Pt*-P-CH$_2$, $^1J_{Pt\text{-}P}$ = 2,719 Hz), −4,111 (t, *Pt*-P-CH$_2$, $^1J_{Pt\text{-}P}$ = 2,737 Hz).
IR (solid) [cm^{-1}]: $\tilde{\nu}$ = 2,987, 2,954, 2,906, 2,837, 1,911, 1,603, 1,406, 1,313, 1,248.
UV-vis (hexane) [nm]: λ = 275.
EA [%]: calculated for C$_{42}$H$_{74}$B$_2$F$_6$N$_2$P$_2$PtSi$_4$: C 45.36, H 6.71, N 2.52; found: C 45.37, H 6.74, N 2.52.

7.3.10 *trans*-[PtCl(*p*-tol)(PCy$_2$Me)$_2$] (140)

A Schlenk flask was charged with a solution of [PtCl(COD)(*p*-C$_6$H$_4$CH$_3$)] (0.701 g, 1.63 mmol) in dry CH$_2$Cl$_2$ (30 mL). After solvation of the platinum complex, PCy$_2$Me (0.73 g, 3.4 mmol) was added to the flask and the mixture was stirred for 16 h. Analysis of the reaction mixture subsequently showed complete conversion to the product by ^{31}P NMR spectroscopy. The solvent was removed *in vacuo* to yield an oily solid with an off-white color. This solid material was dissolved in 10 mL of dry CH$_2$Cl$_2$

and dried two additional times *in vacuo* to remove as many volatile components as possible from the crude material. The product was then dissolved in 10 mL of dry CH_2Cl_2 and transferred to a round-bottomed flask. The solvent was removed *via* rotary evaporation and left to dry in a 40 °C bath for 1 h. The white crystalline residue was scraped from the flask and suspended in cold MeOH. The suspended product was collected on a sintered glass frit and washed repeatedly (3 x 3 mL) with cold hexane. The product was collected and dried *in vacuo* for a period of 3 h (0.001 Torr) to yield *trans*-[PtCl(*p*-tol)(PCy_2Me)$_2$] as an air-stable white crystalline solid (1.09 g, 1.46 mmol) in 90% yield. Crystals suitable for X-ray diffraction were grown by slow evaporation of a saturated benzene solution of *trans*-[PtCl(*p*-tol)(PCy_2Me)$_2$] at room temperature.

^{1}H NMR (500.13 MHz, C_6D_6, 297 K) [ppm]: δ = 7.49 (d, 2H, *o*-C*H* of $C_6H_4CH_3$, $^3J_{H\text{-}H}$ = 7.9 Hz, $^3J_{H\text{-}Pt}$ = 62 Hz), 6.97 (d, 2H, *m*-C*H* of $C_6H_4CH_3$, $^3J_{H\text{-}H}$ = 7.6 Hz), 2.51 (br d, 4H, P-(C_6H_{11})$_2$, $^1J_{H\text{-}H}$ = 13 Hz), 2.35 (m, 4H, P-(C_6H_{11})$_2$), 2.27 (s, 3H, $C_6H_4CH_3$), 1.68 (m, 20H, P-(C_6H_{11})$_2$), 1.25 (m, 16H, P-(C_6H_{11})$_2$), 0.58 (vt, 6H, P-CH_3, N = 6.5 Hz, $^3J_{H\text{-}Pt}$ = 33 Hz).

$N = |^2J_{C\text{-}P} + {}^4J_{C\text{-}P}|$

^{1}H{^{31}P} NMR (500.13 MHz, C_6D_6, 297 K) [ppm]: δ = 7.49 (d, 2H, *o*-C*H* of $C_6H_4CH_3$, $^3J_{H\text{-}H}$ = 8.0 Hz, $^3J_{H\text{-}Pt}$ = 62 Hz), 6.97 (d, 2H, *m*-C*H* of $C_6H_4CH_3$, $^3J_{H\text{-}H}$ = 7.5 Hz), 2.51 (br d, 4H, P-(C_6H_{11})$_2$, $^1J_{H\text{-}H}$ = 13 Hz), 2.35 (m, 4H, P-(C_6H_{11})$_2$), 2.27 (s, 3H, $C_6H_4CH_3$), 1.69 (m, 20H, P-(C_6H_{11})$_2$), 1.25 (m, 16H, P-(C_6H_{11})$_2$), 0.58 (s, 6H, P-CH_3, $^3J_{H\text{-}Pt}$ = 33 Hz).

^{13}C{^{1}H} NMR (125.77 MHz, C_6D_6, 297 K) [ppm]: δ = 138.3 (t, 2C, *o*-*C* of $C_6H_4CH_3$, $^2J_{C\text{-}Pt}$ = 26 Hz, $^3J_{C\text{-}P}$ = 2 Hz), 137.0 (t, 1C, *ipso*-*C* of $C_6H_4CH_3$, $^2J_{C\text{-}P}$ = 9 Hz), 130.3 (s, 1C, *p*-*C* of $C_6H_4CH_3$, $^5J_{C\text{-}P}$ = 2 Hz), 129.0 (s, 2C, *m*-*C* of $C_6H_4CH_3$), 34.2 (vt, 4C, P-(C_6H_{11})$_2$, N_1 = 31 Hz), 29.2 (s, 4C, P-(C_6H_{11})$_2$), 28.3 (s, 4C, P-(C_6H_{11})$_2$), 27.4 (vt, 4C, P-(C_6H_{11})$_2$, N_2 = 13 Hz), 27.2 (vt, 4C, P-(C_6H_{11})$_2$, N_3 = 10 Hz), 26.9 (s, 4C, P-(C_6H_{11})$_2$), 21.1 (s, 1C, Pt-$C_6H_4CH_3$), 2.3 (vt, 2C, P-CH_3, N_1 = 33 Hz).

$N_1 = |^1J_{C\text{-}P} + {}^3J_{C\text{-}P}|$

$N_2 = |^2J_{C\text{-}P} + {}^4J_{C\text{-}P}|$

$N_3 = |^3J_{C\text{-}P} + {}^5J_{C\text{-}P}|$

^{13}C{^{1}H}-DEPT135 NMR (125.77 MHz, C_6D_6, 297 K) [ppm]: δ = 138.3 (s, 2C, *o*-*C* of $C_6H_4CH_3$), 129.0 (s, 2C, *m*-*C* of $C_6H_4CH_3$), 34.2 (vt, 4C, P-(C_6H_{11})$_2$), 21.1 (s, 1C, Pt-$C_6H_4CH_3$), 2.3 (vt, 2C, P-CH_3).

^{31}P{^{1}H} NMR (202.46 MHz, C_6D_6, H_3PO_4, 297 K) [ppm]: δ = 11.2 (s, $^1J_{P\text{-}Pt}$ = 2,849 Hz).

^{195}Pt{^{1}H} NMR (107.00 MHz, C_6D_6, K_2PtCl_6, 297 K) [ppm]: δ = –4,222 (t, $^{1}J_{Pt\text{-}P}$ = 2,837 Hz).

IR (solid) [cm^{-1}]: $\tilde{\nu}$ = 2,924, 2,912, 2,840, 1,586, 1,483, 1,443, 1,411, 1,344, 1,328, 1,291, 1,263.

EA [%]: calculated for $C_{33}H_{57}ClP_2Pt$: C 53.11, H 7.70; found: C: 53.23, H: 7.85.

DTA [°C]: mp = 183.

7.3.11 *trans*-[Pt{(C≡C)$_2$-H}(*p*-tol)(PCy$_2$Me)$_2$] (141)

A Schlenk flask was charged with *trans*-[PtCl(*p*-tol)(PCy$_2$Me)$_2$] (118 mg, 0.158 mmol) and CuI (10 mg, 0.053 mmol). The reagents were then dissolved and suspended in dry $HNEt_2$ (7 mL) and cooled to –45 °C. Once the desired temperature had been reached, butadiyne (0.81 M solution in THF, 7.0 mL, 5.7 mmol) was added dropwise to the reaction mixture over 10 min. The mixture was stirred for a period of 1 h after which the cooling bath was removed and the flask was allowed to slowly warm to room temperature. The reaction mixture was stirred for an additional hour during which the color changed from clear to light yellow. The reaction mixture was transferred to a round-bottomed flask and ~80% of the solvent removed *via* rotary evaporation. As this reaction generates copper acetylide species as byproducts (black solids), any solid products in the reaction flasks must be kept covered in solvent as they are known to be explosive in the solid state. This remaining solution was extracted with toluene (4 x 5 mL) and the extracts were passed through an 8 cm column of silica gel (R_f = 1). The product fractions were collected and the solvent removed *via* rotary evaporation. The final product was collected as a pale tan powder and dried *in vacuo* to give *trans*-[Pt{(C≡C)$_2$-H}(*p*-tol)(PCy$_2$Me)$_2$] (48 mg, 0.063 mmol) in 40% yield. The product was stored under argon in a dark environment as it is light sensitive (the product is air stable). Crystals suitable for X-ray diffraction were grown by slow evaporation of a saturated benzene solution of *trans*-[Pt{(C≡C)$_2$-H}(*p*-tol)(PCy$_2$Me)$_2$] at room temperature.

^{1}H NMR (500.13 MHz, C_6D_6, 297 K) [ppm]: δ = 7.43 (d, 2H, *o*-C*H* of $C_6H_4CH_3$, $^{3}J_{H\text{-}H}$ = 7.1 Hz, $^{3}J_{H\text{-}Pt}$ = 39 Hz), 7.09 (d, 2H, *m*-C*H* of $C_6H_4CH_3$, $^{3}J_{H\text{-}H}$ = 7.2 Hz), 2.37 (br d, 4H, P-(C_6H_{11})$_2$, $^{1}J_{H\text{-}H}$ = 13 Hz), 2.30 (s, 3H, $C_6H_4CH_3$), 2.19 (m, 4H, P-(C_6H_{11})$_2$), 1.66 (m, 20H, P-(C_6H_{11})$_2$), 1.69 (s, 1H, Pt-CC-CC-*H*), 1.20 (m, 16H, P-(C_6H_{11})$_2$), 0.73 (vt, 6H, P-CH_3, *N* = 6 Hz, $^{3}J_{H\text{-}Pt}$ = 32 Hz).

$N = |^{2}J_{H\text{-}P} + {}^{4}J_{H\text{-}P}|$

^{1}H{^{31}P} NMR (500.13 MHz, C_6D_6, 297 K) [ppm]: δ = 7.43 (d, 2H, *o*-C*H* of $C_6H_4CH_3$, $^{3}J_{H\text{-}H}$ = 6.7 Hz, $^{3}J_{H\text{-}Pt}$ = 39 Hz), 7.09 (d, 2H, *m*-C*H* of $C_6H_4CH_3$, $^{3}J_{H\text{-}H}$ = 7.2 Hz), 2.37 (br d, 4H, P-(C_6H_{11})$_2$, $^{1}J_{H\text{-}H}$ = 13 Hz), 2.30 (s, 3H, $C_6H_4CH_3$), 2.19 (m, 4H, P-(C_6H_{11})$_2$), 1.66 (m, 20H, P-(C_6H_{11})$_2$), 1.69 (s, 1H, Pt-CC-CC-*H*), 1.21 (m, 16H, P-(C_6H_{11})$_2$), 0.73 (s, 6H, P-CH_3, $^{3}J_{H\text{-}Pt}$ = 32 Hz).

^{13}C{^{1}H} NMR (125.77 MHz, C_6D_6, 297 K) [ppm]: δ = 152.3 (t, 1C, *ipso-C* of $C_6H_4CH_3$, $^{2}J_{C\text{-}P}$ = 9 Hz), 139.9 (t, 2C, *o-C* of $C_6H_4CH_3$, $^{2}J_{C\text{-}Pt}$ = 26 Hz, $^{3}J_{C\text{-}P}$ = 2 Hz), 130.4 (t, 1C, *p-C* of $C_6H_4CH_3$, $^{5}J_{C\text{-}P}$ = 2 Hz), 128.8 (s, 2C, *m-C* of $C_6H_4CH_3$), 106.2 (t, 1C, *α-C* of Pt-*C*C-CC-H, $^{2}J_{C\text{-}P}$ = 15 Hz), 94.8 (s, 1C, *β-C* or *γ-C* of Pt-C*C*-*C*C-H), 73.7 (s, 1C, *β-C* or *γ-C* of Pt-C*C*-*C*C-H), 59.1 (s, 1C, Pt-CC-C*C*-H), 35.2 (vt, 4C, P-(C_6H_{11})$_2$, N_1 = 33 Hz), 29.3 (s, 4C, P-(C_6H_{11})$_2$), 28.4 (s, 4C, P-(C_6H_{11})$_2$), 27.4 (vt, 4C, P-(C_6H_{11})$_2$, N_2 = 13 Hz), 27.2 (vt, 4C, P-(C_6H_{11})$_2$, N_3 = 11 Hz), 26.8 (s, 4C, P-(C_6H_{11})$_2$), 21.3 (s, 1C, Pt-C_6H_4CH$_3$), 3.5 (vt, 2C, P-*C*H$_3$, N_1 = 34 Hz).

$N_1 = |^{1}J_{C\text{-}P} + {}^{3}J_{C\text{-}P}|$

$N_2 = |^{2}J_{C\text{-}P} + {}^{4}J_{C\text{-}P}|$

$N_3 = |^{3}J_{C\text{-}P} + {}^{5}J_{C\text{-}P}|$

^{13}C{^{1}H}-DEPT135 NMR (125.77 MHz, C_6D_6, 297 K) [ppm]: δ = 139.9 (s, 2C, *o-C* of $C_6H_4CH_3$), 128.8 (s, 2C, *m-C* of $C_6H_4CH_3$), 59.1 (s, 1C, Pt-CC-C*C*-H), 35.2 (vt, 4C, P-(C_6H_{11})$_2$), 21.3 (s, 1C, Pt-C_6H_4CH$_3$), 3.5 (vt, 2C, P-*C*H$_3$).

^{31}P{^{1}H} NMR (202.46 MHz, C_6D_6, H_3PO_4, 297 K) [ppm]: δ = 10.0 (s, Pt-(*P*MeCy$_2$)$_2$, $^{1}J_{P\text{-}Pt}$ = 2,658 Hz).

^{195}Pt{^{1}H} NMR (107.00 MHz, C_6D_6, K_2PtCl_6, 297 K) [ppm]: δ = −4,572 (t, *Pt*-(PMeCy$_2$)$_2$, $^{1}J_{Pt\text{-}P}$ = 2,645 Hz).

IR (solid) [cm^{-1}]: $\tilde{\nu}$ = 3,259, 2,922, 2,849, 2,200, 2,132, 1,484, 1,443, 1,342, 1,290, 1,270.

EA [%]: calculated for $C_{37}H_{58}P_2Pt$: C 58.48, H 7.69; found: C: 58.83, H: 7.77.

DTA [°C]: mp = 191.

7.3.12 *trans,trans*-[(*p*-tol)(Cy$_2$MeP)$_2$Pt(C≡C)$_4$Pt(PCy$_2$Me)$_2$(*p*-tol)] (142)

A three-necked flask was charged with *trans*-[Pt{(C≡C)$_2$-H}(*p*-tol)(PCy$_2$Me)$_2$] (0.105 g, 0.138 mmol), acetone (25 mL), and fitted with a gas dispersion tube and a condenser. A separate Schlenk flask was charged with CuCl (45 mg, 0.46 mmol), and TMEDA (0.025 mL, 19 mg, 0.17 mmol) was added with stirring. After 0.5 h, stirring was halted, and a grayish solid separated from a blue supernatant. O_2 was then bubbled through the three-necked flask with stirring. After about 5 min, the solution

was heated to 40 °C (oil bath) and the blue supernatant was added in portions. After 6 h, the solvent was removed by rotary evaporation. The residue was extracted with toluene (4 x 25 mL). The extracts were filtered through an alumina column (2 x 7 cm). The solvent was subsequently removed by rotary evaporation and the residue suspended in MeOH (20 mL) and collected by filtration. The collected solid was dried under high vacuum (0.001 Torr) to give *trans,trans*-[(*p*-tol)(Cy_2MeP)$_2$Pt($C{\equiv}C$)$_4$Pt(PCy_2Me)$_2$(*p*-tol)] as a light yellow solid (isolated crystals) in <10% yield.

$^{31}P\{^1H\}$ NMR (161.98 MHz, C_6D_6, H_3PO_4, 297 K) [ppm]: δ = 9.7 (s, $^1J_{P\text{-}Pt}$ = 2,649 Hz).

7.3.13 Ph-(μ-{BN($SiMe_3$)(*t*-Bu)}C=C)-Ph (148)

A pale yellow solution of [$(OC)_5$Cr{BN($SiMe_3$)(*t*-Bu)}] (39 mg, 0.112 mmol) and 1,2-diphenylethyne (20 mg, 0.11 mmol) in hexane was irradiated with a high-pressure Hg lamp for approximately 3.5 h at room temperature. After completion of the reaction was ascertained *via* monitoring by $^{11}B\{^1H\}$ NMR spectroscopy, all volatiles were removed under high vacuum (0.001 Torr). The resulting solid material was redissolved in hexamethyldisiloxane and filtered through a column (0.5 cm x 2.0 cm) of pacified silica gel.[397] Evaporation of hexamethyldisiloxane under high vacuum gave Ph-(μ-{BN($SiMe_3$)(*t*-Bu)}C=C)-Ph as a light yellow oil.

$^{11}B\{^1H\}$ NMR (128.38 MHz, C_6D_6, $BF_3{\bullet}OEt_2$, 297 K) [ppm]: δ = 23.6 (br s).

7.3.14 *trans*-[PtCl{(μ-{BN($SiMe_3$)(*t*-Bu)}C=C)-Ph}(PEt_3)$_2$] (149)

A pale yellow solution of [$(OC)_5$W{BN($SiMe_3$)(*t*-Bu)}] (12 mg, 0.025 mmol) and *trans*-[PtCl($C{\equiv}C$-Ph)(PEt_3)$_2$] (14 mg, 0.025 mmol) in hexane was irradiated photolytically with a high-pressure Hg lamp for approximately 2 h at room temperature. After completion of the reaction was ascertained *via* monitoring by $^{11}B\{^1H\}$ NMR spectroscopy, all volatiles were removed under high vacuum (0.001 Torr). The resulting solid material was redissolved in hexamethyldisiloxane and filtered through a column (0.5 x 2.0 cm) of pacified silica gel.[397] Evaporation of hexamethyldisiloxane under high vacuum gave *trans*-[PtCl{(μ-{BN($SiMe_3$)(*t*-Bu)}C=C)-Ph}(PEt_3)$_2$] as a light yellow colored oil.

$^{11}B\{^1H\}$ NMR (128.38 MHz, C_6D_6, $BF_3{\bullet}OEt_2$, 297 K) [ppm]: δ = 35.2 (br s).

7.3.15 [(η^5-C_5Me_5)(OC)$_2$Fe(μ-{BN(SiMe$_3$)(*t*-Bu)}C=C)Ph] (150)

A pale yellow solution of [(OC)$_5$Mo{BN(SiMe$_3$)(*t*-Bu)}] (18 mg, 0.046 mmol) and [(η^5-C_5Me_5)(OC)$_2$FeC≡C-Ph] (16 mg, 0.046 mmol) in THF was heated to 80 °C for approximately 0.5 h. After completion of the reaction was ascertained *via* monitoring by $^{11}B\{^1H\}$ NMR spectroscopy, all volatiles were removed under high vacuum (0.001 Torr). The resulting solid material was redissolved in hexamethyldisiloxane and filtered through a column (0.5 cm x 2.0 cm) of pacified silica gel.[397] Evaporation of hexamethyldisiloxane under high vacuum gave [(η^5-C_5Me_5)(OC)$_2$Fe(μ-{BN(SiMe$_3$)(*t*-Bu)}C=C)Ph] as a yellow colored oil.

$^{11}B\{^1H\}$ NMR (128.38 MHz, C_6D_6, BF_3•OEt_2, 297 K) [ppm]: δ = 34.6 (br s).

7.3.16 Ph-(μ-{BN(SiMe$_3$)$_2$}C=C)-Ph•IMeMe (155)

A light yellow solution of *bis*(trimethylsilyl)amino-2,3-diphenylborirene (19 mg, 0.055 mmol) in benzene was mixed with a solution of IMeMe (7 mg, 0.06 mmol) in benzene (0.5 mL). Immediate formation of the Lewis pair was witnessed with the light yellow solution turning colorless. The reaction was used immediately for generation of product Ph-(μ-{BN(SiMe$_3$)$_2$}C=C)-Ph•IMeMe without isolation.

$^{11}B\{^1H\}$ NMR (128.38 MHz, C_6D_6, BF_3•OEt_2, 297 K) [ppm]: δ = –18.6 (s, (*B*(N(SiMe$_3$)$_2$)(IMeMe)).

7.3.17 Ph$_4$C$_4$B{N(SiMe$_3$)$_2$}•IMeMe (156)

A solution of Ph-(μ-{BN(SiMe$_3$)$_2$}C=C)-Ph•IMeMe (26 mg, 0.055 mmol) in benzene (2.5 mL) was mixed with a solution of 1,2-diphenylethyne (9 mg, 0.05 mmol) in benzene (0.5 mL) and allowed to react at room temperature for 24 h. Monitoring of the reaction after this period by $^{11}B\{^1H\}$ NMR spectroscopy showed the formation of two separate products at δ = –4.6 ppm Ph$_4$C$_4$B{N(SiMe$_3$)$_2$}•IMeMe (**156**) and δ = 57.5 ppm Ph$_4$C$_4$BN(SiMe$_3$)$_2$ (**157**). After this period the reaction color had been witnessed to evolve from an essentially colorless solution to a deep red (almost black) reaction mixture. Isolation of one of these products was attempted by removal of all volatiles under high vacuum (0.001 Torr); however, purification of this residue did not yield any isolated products.

$^{11}B\{^1H\}$ NMR (128.38 MHz, C_6D_6, BF_3•OEt_2, 297 K) [ppm]: δ = 57.5 (s, (BN($SiMe_3$)$_2$), –4.6 (s, (BN($SiMe_3$)$_2$)(IMeMe)).

7.3.18 ClBN(SiMe$_3$)$_2$C≡CSnMe$_3$ (160)

A colorless solution of $Me_3SnC{\equiv}CSnMe_3$ (20 mg, 0.057 mmol) in toluene (1.0 mL) was mixed with a solution of $Cl_2BN(SiMe_3)_2$ (14 mg, 0.058 mmol) in toluene (0.5 mL). The reaction was heated to 60 °C overnight which saw the formation of the halostannane elimination product (Me_3SnCl) and formation of $ClBN(SiMe_3)_2C{\equiv}CSnMe_3$ *via* $^{119}Sn\{^1H\}$ NMR spectroscopy. Isolation of this species was attempted by removal of all volatiles under high vacuum (0.001 Torr), however, purification of this residue did not yield any isolated products.

$^{11}B\{^1H\}$ NMR (128.38 MHz, C_6D_6, BF_3•OEt_2, 297 K) [ppm]: δ = 32.7 (br s).
$^{119}Sn\{^1H\}$ NMR (149.21 MHz, C_6D_6, $SnMe_4$, 297 K) [ppm]: δ = –74.9 (s).

7.3.19 Cl{BN(SiMe$_3$)$_2$C≡C}$_2$SnMe$_3$ (161)

A colorless solution of $Me_3SnC{\equiv}CSnMe_3$ (20 mg, 0.057 mmol) in toluene (1.0 mL) was mixed with a solution of $Cl_2BN(SiMe_3)_2$ (14 mg, 0.058 mmol) in toluene (0.5 mL). Continued heating at 60 °C for one week saw conversion to $Cl\{BN(SiMe_3)_2C{\equiv}C\}_2SnMe_3$ and final combination of two equivalents of these species with elimination of another equivalent of the halostannane (Me_3SnCl) *via* $^{119}Sn\{^1H\}$ NMR spectroscopy. Isolation of this species was attempted by removal of all volatiles under high vacuum (0.001 Torr), however, purification of this residue did not yield any isolated products.

$^{11}B\{^1H\}$ NMR (128.38 MHz, C_6D_6, BF_3•OEt_2, 297 K) [ppm]: δ = 28.4 (br s).
$^{119}Sn\{^1H\}$ NMR (149.21 MHz, C_6D_6, $SnMe_4$, 297 K) [ppm]: δ = –70.8 (s).

7.3.20 BrBN(SiMe$_3$)$_2$C≡CSnMe$_3$ (163)

A colorless solution of $Me_3SnC{\equiv}CSnMe_3$ (20 mg, 0.057 mmol) in toluene (1.0 mL) was mixed with a solution of $Br_2BN(SiMe_3)_2$ (19 mg, 0.057 mmol) in toluene (0.5 mL). The reaction was kept at room temperature overnight which saw the formation of the halostannane elimination product (Me_3SnCl) and formation of $BrBN(SiMe_3)_2C{\equiv}CSnMe_3$ *via* $^{119}Sn\{^1H\}$ NMR spectroscopy. Isolation of this species was attempted by removal of all volatiles under high vacuum (0.001 Torr), however, purification of this residue did not yield any isolated products.

$^{11}B\{^1H\}$ NMR (128.38 MHz, C_6D_6, BF_3•OEt_2, 297 K) [ppm]: δ = 31.2 (br s).

$^{119}Sn\{^1H\}$ NMR (149.21 MHz, C_6D_6, $SnMe_4$, 297 K) [ppm]: δ = –74.9 (s).

7.4 Project Boratabenzene Experimental

7.4.1 [{(η^5-C_5H_5)Co}$_2${μ:η^6,η^6-(BC_5H_5)$_2$}] (189)

Into a 250 mL three-necked flask fitted with a sidearm and Schlenk frit, cobaltocene ([(η^5-C_5H_5)$_2$Co]) (4.60 g, 24.3 mmol) was added and dissolved in 50 mL of dichloromethane. Immediately following solvation, the flask was cooled to −78 °C and a solution of B_2Br_4 (1.36 g, 3.99 mmol, in 5 mL of dichloromethane) previously cooled to −78 °C was added dropwise over 5 minutes. The reaction was kept at −78 °C for a full hour after which the bath was removed and the reaction was allowed to slowly warm to room temperature over another hour. All volatiles were then removed under vacuum and the brown solid suspended in refluxing hexane. The hot suspension was then filtered and cooled to −78 °C overnight to yield crystalline material. After removal of the supernatant, the dark violet crystalline product was placed under high vacuum (1.0 x 10^{-6} Torr) for a period of 10 h to remove any traces of unreacted cobaltocene from the mixture. The material was collected to yield [{(η^5-C_5H_5)Co}$_2${μ:η^6,η^6-(BC_5H_5)$_2$}] (0.618 g, 1.55 mmol) as a dark violet crystalline solid in 39% yield. Crystals suitable for X-ray diffraction were grown by slow evaporation of a saturated hexane solution of [{(η^5-C_5H_5)Co}$_2${μ:η^6,η^6-(BC_5H_5)$_2$}] stored at −30 °C for 1 week.

^{1}H NMR (400.13 MHz, C_6D_6, 297 K) [ppm]: δ = 31.7 (br s, 2H, *p*-C*H* of η^6-BC_5H_5), 28.0 (br s, 4H, *m*-C*H* or *o*-C*H* of η^6-BC_5H_5), −50.9 (br s, 4H, *o*-C*H* of η^6-BC_5H_5), −57.3 (br s, 10H, C*H* of η^5-C_5H_5).

^{11}B{^{1}H} NMR (128.38 MHz, C_6D_6, BF_3•OEt_2, 297 K) [ppm]: δ = 79.1 (br s).

^{10}B{^{1}H} NMR (42.99 MHz, C_6D_6, BF_3•OEt_2, 297 K) [ppm]: δ = 77.0 (br s).

^{1}H NMR (Evans method experiment) (400.13 MHz, C_6D_6, $C_{10}H_{10}Fe$, 297 K) [Bohr Magnetons]: μ_{eff} = 2.3.

Cyclic Voltammetry (THF, [*n*-Bu_4N][PF_6], [(η^5-C_5H_5)$_2$Fe]) [V]: −0.94/−0.84 (Oxidation Co(II)/Co(III)), −2.10/−2.36 (Reduction Co(II)/Co(I)).

EPR (toluene, 20 K) [MHz]: g_x = 2.12 (A_x(^{59}Co) = 150), g_y = 2.03 (A_y(^{59}Co) = 80), g_z = 1.86 (A_z(^{59}Co) = 430).

IR (solid) [cm^{-1}]: $\tilde{\nu}$ = 3,350, 2,927, 2,852, 1,643, 1,444, 1,281.

UV-vis (acetonitrile) [nm]: λ = 262, 359.

DTA [°C]: endo. = 145, endo. = 223.

EA [%]: calculated for $C_{20}H_{20}B_2Co_2$: C 60.07, H 5.04; found: C 59.90, H 5.75.

EI–MS (*m/z*) [%]: 400.0 (100, M^+), 399.0 (66.9, $M-1^+$), 189.0 (76.3, [Cp_2Co]$^+$), 123.9 (65.8, [CpCo]$^+$), 68.9 (71.2), 58.7 (90.2, Co^+).

7.4.2 [{(η^5-C_5H_5)Co}$_2${μ:η^6,η^6-(BC_5H_5)$_2$}][PF_6]$_2$ (195)

In a J. Young NMR tube, [{(η^5-C_5H_5)Co}$_2${μ:η^6,η^6-(BC_5H_5)$_2$}] (29 mg, 0.072 mmol) and [(η^5-C_5H_5)$_2$Fe][PF_6] (51 mg, 0.15 mmol) was dissolved/suspended in 1,2-difluorobenzene (1.5 mL). The NMR tube was then heated for 8 h at 80 °C after which full conversion to the dicationic species [{(η^5-C_5H_5)Co}$_2${μ:η^6,η^6-(BC_5H_5)$_2$}][PF_6]$_2$ was confirmed by $^{11}B\{^1H\}$ NMR spectroscopy. The volatile components of the reaction mixture were removed *in vacuo* and the brown residue was washed with diethylether. The product was collected and dried *in vacuo* to yield [{(η^5-C_5H_5)Co}$_2${μ:η^6,η^6-(BC_5H_5)$_2$}][PF_6]$_2$ (45 mg, 0.065 mmol) as a light yellow-brown powder in 90% yield.

^{1}H NMR (500.13 MHz, CD_3CN, 297 K) [ppm]: δ = 6.97 (m, 2H, *p*-C*H* of η^6-BC_5H_5), 6.77 (m, 4H, *o*-C*H* or *m*-C*H* of η^6-BC_5H_5), 6.19 (m, 4H, *o*-C*H* or *m*-C*H* of η^6-BC_5H_5), 5.77 (s, 10H, C*H* of η^5-C_5H_5).
$^{13}C\{^1H\}$ NMR (125.77 MHz, CD_3CN, 297 K) [ppm]: δ = 107.0 (s, *m*-*C* or *o*-*C* of η^6-BC_5H_5), 92.8 (s, *p*-*C* of η^6-BC_5H_5), 87.9 (s, *C* of η^5-C_5H_5), 68.7 (s, *m*-*C* or *o*-*C* of η^6-BC_5H_5).
$^{11}B\{^1H\}$ NMR (160.47 MHz, CD_3CN, BF_3•OEt_2, 297 K) [ppm]: δ = 24.5 (br s, η^6-*B*C_5H_5).
IR (solid) [cm^{-1}]: $\tilde{\nu}$ = 3,282, 3,124, 1,417, 1,395.
UV-vis (acetonitrile) [nm]: λ = 262.
EA [%]: calculated for $C_{20}H_{20}B_2Co_2F_{12}P_2$: C 34.82, H 2.92; found: C 34.75, H 2.59.
DTA [°C]: br. exo. = 136, exo. = 212, exo. = 221.

7.4.3 [{(η^5-C_5H_5)Co}$_2${μ:η^6,η^6-(BC_5H_5)$_2$}][PF_6] (194)

In a J. Young NMR tube, [{(η^5-C_5H_5)Co}$_2${μ:η^6,η^6-(BC_5H_5)$_2$}] (18 mg, 0.045 mmol) and [(η^5-C_5H_5)$_2$Fe][PF_6] (12 mg, 0.036 mmol) were dissolved/suspended in 1.5 mL of 1,2-difluorobenzene. The NMR tube was then heated for 8 h at 80 °C after which full conversion to the dicationic species [{(η^5-C_5H_5)Co}$_2${μ:η^6,η^6-(BC_5H_5)$_2$}][PF_6] was confirmed by $^{11}B\{^1H\}$ NMR spectroscopy. The volatile components of the reaction mixture were removed *in vacuo* and the brown residue was washed with diethylether. The product was collected and dried *in vacuo* to yield [{(η^5-C_5H_5)Co}$_2${μ:η^6,η^6-(BC_5H_5)$_2$}][PF_6] (14 mg, 0.026 mmol) as a light yellow-brown powder in 71%.

$^{11}B\{^{1}H\}$ NMR (160.47 MHz, CD_3CN, BF_3•OEt_2, 297 K) [ppm]: δ = 28.9 (br s, η^6-*B*C_5H_5).

EPR (toluene, 10 K) [MHz]: g_x = not resolved, g_y = not resolved, g_z = 2.12 ($A_z(^{59}Co)$ = 413).

UV-vis (acetonitrile) [nm]: λ = 262.

EA [%]: calculated for $C_{20}H_{20}B_2Co_2P_2F_{12}$: C 44.09, H 3.70; found: C 37.09, H 2.37.

7.5 Computational Details

7.5.1 Synthetic Attempts at a Group 6 Terminal Phosphinoborylene (Section 2.1.4)

Geometry optimizations and Density Functional Theory (DFT) calculations were carried out upon the neutral compounds **38** and **39** using the Gaussian09[478] program at the B3LYP/6-311G* level of theory and to predict the geometry and electronic structures of two proposed terminal Group 6 pentacarbonyl phosphinoborylene species. The Jmol[479] program was used to visualize the structural geometry and frontier orbital projections for the two complexes.

7.5.2 *trans*-Platinum *bis*-σ-Borirene Complex Discussion and Theory (Section 3.1.3.5)

Geometry optimizations, frequency, and excitation calculations for compounds **88**, **90**, **91**, and **119/120** were carried out using the Gaussian09[478] and Amsterdam Density Functional (ADF)[480,481] program at the B3LYP/Def2-SVP[482,483] and OLYP/TZP[484-488] levels. All calculations using ADF were conducted within the zeroth-order regular approximation (ZORA) formalism.[489-492] The nature of the bonding in the theoretical models were described using the energy decomposition analysis (EDA)[481,493] according to the methods of Morokuma[494] and Ziegler and Rauk.[495] The Jmol[479] program was used to visualize the structural geometry of the reported complexes.

7.6 Published X-ray Structural Data

The crystal data of **102**, **106**, **122/123, 125/126**, and **189** were collected on a Bruker X8-APEX II diffractometer with a CCD area detector. Those of **119/120** were collected on a Bruker D8-QUEST diffractometer with a CMOS camera. Both systems use multi-layer mirror monochromated $Mo_{K\alpha}$ radiation. The structures were solved using direct methods, refined with the Shelx software package[496] and expanded using Fourier techniques. All non-hydrogen atoms were refined anisotropically. Hydrogen atoms were included in structure factor calculations. All hydrogen atoms were assigned to idealised geometric positions.

	102	**106**	**119/120**
CCDC Number	1022256	1022257	1022258
Temperature (K)	100(2)	100(2)	100(2)
Radiation, λ (Å)	MoK_α 0.71073	MoK_α 0.71073	MoK_α 0.71073
Crystal system	Triclinic	Triclinic	Triclinic
Space group	*P*–1	*P*–1	*P*–1
***a* (Å)**	8.764(3)	11.286(3)	10.2688(5)
***b* (Å)**	9.2460(17)	24.271(8)	11.3730(6)
***c* (Å)**	9.820(2)	27.394(9)	12.3937(6)
***α* (°)**	84.970(8)	107.848(8)	89.809(2)
***β* (°)**	89.473(7)	99.385(10)	73.603(2)
***γ* (°)**	70.726(4)	95.652(10)	65.791(2)
Volume (Å^3)	748.0(3)	6958(4)	1255.94(11)
Z	1	9	1
Calculated density (Mg·m^{-3})	1.540	1.653	1.290
Absorption coefficient (mm^{-1})	4.820	4.695	2.979
***F*(000)**	348	3420	504
Theta range for collection	2.082° - 26.372°	1.379° - 26.022°	2.45° to 26.02°
Reflections collected	13436	22675	18010
Independent reflections	3055	20117	4920
Minimum/maximum transmission	0.2195/0.4856	0.6113/0.7454	0.3932/0.4920
Refinement method	Full-matrix least-squares on F^2	Full-matrix least-squares on F^2	Full-matrix least-squares on F^2
Data / parameters / restraints	3055 / 289 / 330	20117 / 617 / 1482	4920 / 238 / 0
Goodness-of-fit on F^2	1.064	0.913	1.120
Final R indices [I>2σ(I)]	R_1 = 0.0154, wR^2 = 0.0379	R_1 = 0.0827, wR^2 = 0.1935	R_1 = 0.0327, wR^2 = 0.0591
R indices (all data)	R_1 = 0.0154, wR^2 = 0.0379	R_1 = 0.2699, wR^2 = 0.2922	R_1 = 0.0374, wR^2 = 0.0612

	122/123	**125/126**	**189**
CCDC Number	1022259	1022260	1470487
Temperature (K)	100(2)	100(2)	100(2)
Radiation, λ (Å)	MoK_α 0.71073	MoK_α 0.71073	MoK_α 0.71073
Crystal system	Triclinic	Monoclinic	Monoclinic
Space group	*P*1	*Cc*	$P2_1/c$
***a* (Å)**	9.512(4)	23.002(8)	7.85(2)
***b* (Å)**	12.460(6)	11.372(4)	10.75(3)
***c* (Å)**	12.710(7)	20.732(5)	10.62(3)
***α* (°)**	105.18(2)	90	90
***β* (°)**	111.954(19)	101.270(13)	103.51(4)
***γ* (°)**	98.862(17)	90	90
Volume (Å^3)	1293.9(11)	5319(3)	871(4)
Z	1	4	2
Calculated density (Mg·m^{-3})	1.330	1.389	1.524
Absorption coefficient (mm^{-1})	2.899	2.839	1.899
***F*(000)**	536	2272	408
Theta range for collection	1.76° to 26.78°	1.805° to 26.369°	2.668° to 26.786°
Reflections collected	21007	29934	11531
Independent reflections	5444	10836	1839
Minimum/maximum transmission	0.6185/0.7454	0.6622/0.7455	0.6170/0.7454
Refinement method	Full-matrix least-squares on F^2	Full-matrix least-squares on F^2	Full-matrix least-squares on F^2
Data / parameters / restraints	5444 / 257 / 0	10836 / 318 / 536	1839 / 109 / 0
Goodness-of-fit on F^2	1.039	1.039	1.125
Final R indices [I>2σ(I)]	R_1 = 0.0230, wR^2 = 0.0495	R_1 = 0.0509, wR^2 = 0.1204	R_1 = 0.0768, wR^2 = 0.1676
R indices (all data)	R_1 = 0.0234, wR^2 = 0.0496	R_1 = 0.0685, wR^2 = 0.1315	R_1 = 0.1090, wR^2 = 0.1817

Chapter 8 – References

1. F. A. Cotton, G. Wilkinson, C. A. Murillo, M. Bochmann, *Advanced Inorganic Chemistry*, 6th Ed.; John Wiley & Sons, Inc: New York, **1999**; pp 131–174.
2. A. Stock, C. Massenez, *Ber. Dtsch. Chem. Ges.* **1912**, *45*, 3539–3568.
3. S. G. Shore, R. W. Parry, *J. Am. Chem. Soc.* **1955**, *77*, 6084–6085.
4. E. L. Muetterties, *Chem. Boron Its Compd.* **1967**, 1–24.
5. E. L. Muetterties, *Boron Hydride Chem.* **1975**, 1–37.
6. W. N. Lipscomb, *Boron Hydride Chem.* **1975**, 39–78.
7. V. I. Bregadze, *Chem. Rev.* **1992**, *92*, 209–223.
8. N. Miyaura, A. Suzuki, *Chem. Rev.* **1995**, *95*, 2457–2483.
9. R. B. King, *Chem. Rev.* **2001**, *101*, 1119–1152.
10. N. Miyaura, *Top. Curr. Chem.* **2002**, *219*, 11–59.
11. K. Fagnou, M. Lautens, *Chem. Rev.* **2003**, *103*, 169–196.
12. I. A. I. Mkhalid, J. H. Barnard, T. B. Marder, J. M. Murphy, J. F. Hartwig, *Chem. Rev.* **2010**, *110*, 890–931.
13. P. P. Power, *Nature* **2010**, *463*, 171–177.
14. D. W. Stephan, *Org. Biomol. Chem.* **2008**, *6*, 1535–1539.
15. D. W. Stephan, *Dalton Trans.* **2009**, 3129–3136.
16. D. W. Stephan, G. Erker, *Angew. Chem. Int. Ed.* **2010**, *49*, 46–76.
17. D. W. Stephan, G. Erker, *Angew. Chem.* **2010**, *122*, 50–81.
18. H. Braunschweig, *Angew. Chem. Int. Ed.* **1998**, *37*, 1786–1801.
19. H. Braunschweig, *Angew. Chem.* **1998**, *110*, 1882–1898.
20. H. Braunschweig, M. Colling, *Coord. Chem. Rev.* **2001**, *223*, 1–51.
21. H. Braunschweig, C. Kollann, D. Rais, *Angew. Chem. Int. Ed.* **2006**, *45*, 5254–5274.
22. H. Braunschweig, C. Kollann, D. Rais, *Angew. Chem.* **2006**, *118*, 5380–5400.
23. H. Braunschweig, R. D. Dewhurst, A. Schneider, *Chem. Rev.* **2010**, *110*, 3924–3957.
24. H. C. Brown, *Tetrahedron* **1961**, *12*, 117–138.
25. D. Männig, H. Nöth, *Angew. Chem. Int. Ed. Engl.* **1985**, *24*, 878–879.
26. D. Männig, H. Nöth, *Angew. Chem.* **1985**, *97*, 854–855.
27. H. C. Brown, M. Zaidlewicz, *Organic Syntheses via Boranes, Vol. 2.*; Aldrich Chemical Company: Milwaukee, WI, **2001**.
28. "The Nobel Prize in Chemistry 1976". *Nobelprize.org*. Nobel Media AB 2014. Web. 20 Jul 2015. <http://www.nobelprize.org/nobel_prizes/chemistry/laureates/1976/>
29. "The Nobel Prize in Chemistry 1979". *Nobelprize.org*. Nobel Media AB 2014. Web. 20 Jul 2015. <http://www.nobelprize.org/nobel_prizes/chemistry/laureates/1979/>
30. "The Nobel Prize in Chemistry 1981". *Nobelprize.org*. Nobel Media AB 2014. Web. 20 Jul 2015. <http://www.nobelprize.org/nobel_prizes/chemistry/laureates/1981/>
31. "The Nobel Prize in Chemistry 2010". *Nobelprize.org*. Nobel Media AB 2014. Web. 20 Jul 2015. <http://www.nobelprize.org/nobel_prizes/chemistry/laureates/2010/>
32. M. F. Hawthorne, *Mol. Med. Today* **1998**, 174–181.
33. M. F. Hawthorne, A. Maderna, *Chem. Rev.* **1999**, *99*, 3421–3434.
34. S. Vepřek, *J. Vac. Sci. Technol. A* **1999**, *17*, 2401–2420.

35. E. J. M. Hamilton, S. E. Dolan, C. M. Mann, H. O. Colijn, C. A. McDonald, S. G. Shore, *Science* **1993**, *260*, 659–661.
36. H. Nöth, G. Schmid, *Angew. Chem. Int. Ed. Engl.* **1963**, *2*, 623.
37. H. Nöth, G. Schmid, *Angew. Chem.* **1963**, *75*, 861–862.
38. R. T. Baker, D. W. Ovenall, J. C. Calabrese, S. A. Westcott, N. J. Taylor, I. D. Williams, T. B. Marder, *J. Am. Chem. Soc.* **1990**, *112*, 9399–9400.
39. J. R. Knorr, J. S. Merola, *Organometallics* **1990**, *9*, 3008–3010.
40. G. O. Spessard, G. L. Miessler, *Organometallic Chemistry*; Prentice-Hall, Inc: Upper Saddle River, NJ, **1997**; pp 71–75.
41. G. Parkin, *Organometallics* **2006**, *25*, 4744–4747.
42. A. F. Hill, *Organometallics* **2006**, *25*, 4741–4743.
43. H. Braunschweig, R. D. Dewhurst, *Dalton Trans.* **2011**, *40*, 549–558.
44. G. Bouhadir, A. Amgoune, D. Bourissou, *Adv. Organomet. Chem.* **2010**, *58*, 1–107.
45. I. Kuzu, I. Krummenacher, J. Meyer, F. Armbruster, F. Breher, *Dalton Trans.* **2008**, 5836–5865.
46. H. Kameo, Y. Hashimoto, H. Nakazawa, *Organometallics* **2012**, *31*, 3155–3162.
47. G. J. Irvine, M. J. G. Lesley, T. B. Marder, N. C. Norman, C. R. Rice, E. G. Robins, W. R. Roper, G. R. Whittell, L. J. Wright, *Chem. Rev.* **1998**, *98*, 2685–2722.
48. S. Aldridge, D. L. Coombs, *Coord. Chem. Rev.* **2004**, *248*, 535–559.
49. D. L. Kays, S. Aldridge, *Struct. Bond.* **2008**, *130*, 29–122.
50. S. A. Westcott, E. Fernández, *Adv. Organomet. Chem.* **2015**, *63*, 39–89.
51. H. Braunschweig, M. Colling, *Eur. J. Inorg. Chem.* **2003**, 393–403.
52. H. Braunschweig, *Adv. Organomet. Chem.* **2004**, *51*, 163–192.
53. H. Braunschweig, D. Rais, *Heteroat. Chem.* **2005**, *16*, 566–571.
54. C. E. Anderson, H. Braunschweig, R. D. Dewhurst, *Organometallics* **2008**, *27*, 6381–6389.
55. H. Braunschweig, C. Kollann, F. Seeler, *Struct. Bond.* **2008**, *130*, 1–27.
56. D. Vidovic, G. A. Pierce, S. Aldridge, *Chem. Commun.* **2009**, 1157–1171.
57. H. Braunschweig, R. D. Dewhurst, V. H. Gessner, *Chem. Soc. Rev.* **2013**, *42*, 3197–3208.
58. H. Braunschweig, G. R. Whittell, *Chem. Eur. J.* **2005**, *11*, 6128–6133.
59. G. O. Spessard, G. L. Miessler, *Organometallic Chemistry*; Prentice-Hall, Inc: Upper Saddle River, NJ, **1997**; pp 65–68.
60. R. H. Crabtree, *The Organometallic Chemistry of the Transition Metals*, 5th Ed.; John Wiley & Sons, Inc: Hoboken, NJ, **2009**; pp 88–98.
61. H. Braunschweig, K. Radacki, F. Seeler, G. R. Whittell, *Organometallics* **2004**, *23*, 4178–4180.
62. D. F. Shriver, *Acc. Chem. Res.* **1970**, *3*, 231–238.
63. H. Werner, *Pure & Appl. Chem.* **1982**, *54*, 177–188.
64. D. F. Shriver, *J. Am. Chem. Soc.* **1963**, *85*, 3509–3510.
65. M. P. Johnson, D. F. Shriver, *J. Am. Chem. Soc.* **1966**, *88*, 301–304.
66. K. B. Gilbert, S. K. Boocock, S. G. Shore, *Comprehensive Organometallic Chemistry, Vol. 6.*; E. W. Abel, F. G. A. Stone, G. Wilkinson, eds.; Pergamon: Oxford, **1982**; pp 879–945.
67. H. Braunschweig, T. Wagner, *Chem. Ber.* **1994**, *127*, 1613–1614.

68. W. Ruf, M. Fueller, W. Siebert, *J. Organomet. Chem.* **1974**, *64*, C45–C47.
69. H. Braunschweig, T. Wagner, *Z. Naturforsch.* **1996**, *51b*, 1618–1620.
70. H. Braunschweig, C. Kollann, *Z. Naturforsch.* **1999**, *54b*, 839–842.
71. J. M. Burlitch, J. H. Burk, M. E. Leonowicz, R. E. Hughes, *Inorg. Chem.* **1979**, *18*, 1702–1709.
72. A. F. Hill, G. R. Owen, A. J. P. White, D. J. Williams, *Angew. Chem. Int. Ed.* **1999**, *38*, 2759–2761.
73. A. F. Hill, G. R. Owen, A. J. P. White, D. J. Williams, *Angew. Chem.* **1999**, *111*, 2920–2923.
74. J. S. Figueroa, J. G. Melnick, G. Parkin, *Inorg. Chem.* **2006**, *45*, 7056–7058.
75. M. R. St.-J. Foreman, A. F. Hill, A. J. P. White, D. J. Williams, *Organometallics* **2004**, *23*, 913–916.
76. D. J. Mihalcik, J. L. White, J. M. Tanski, L. N. Zakharov, G. P. A. Yap, C. D. Incarvito, A. L. Rheingold, D. Rabinovich, *Dalton Trans.* **2004**, 1626–1634.
77. I. R. Crossley, M. R. St.-J. Foreman, A. F. Hill, A. J. P. White, D. J. Williams, *Chem. Commun.* **2005**, 221–223.
78. I. R. Crossley, A. F. Hill, A. C. Willis, *Organometallics* **2005**, *24*, 1062–1064.
79. M. Sircoglou, S. Bontemps, G. Bouhadir, N. Saffon, K. Miqueu, W. Gu, M. Mercy, C.-H. Chen, B. M. Foxman, L. Maron, O. V. Ozerov, D. Bourissou, *J. Am. Chem. Soc.* **2008**, *130*, 16729–16738.
80. S. Bontemps, G. Bouhadir, W. Gu, M. Mercy, C.-H. Chen, B. M. Foxman, L. Maron, O. V. Ozerov, D. Bourissou, *Angew. Chem. Int. Ed.* **2008**, *47*, 1481–1484.
81. S. Bontemps, G. Bouhadir, W. Gu, M. Mercy, C.-H. Chen, B. M. Foxman, L. Maron, O. V. Ozerov, D. Bourissou, *Angew. Chem.* **2008**, *120*, 1503–1506.
82. A. A. Dickinson, D. J. Willock, R. J. Calder, S. Aldridge, *Organometallics* **2002**, *21*, 1146–1157.
83. D. G. Musaev, K. Morokuma, *J. Phys. Chem.* **1996**, *100*, 6509–6517.
84. T. R. Cundari, Y. Zhao, *Inorg. Chim. Acta* **2003**, *345*, 70–80.
85. K. C. Lam, W. H. Lam, Z. Lin, T. B. Marder, N. C. Norman, *Inorg. Chem.* **2004**, *43*, 2541–2547.
86. J. H. Brewster, E.-I. Negishi, *Science* **1980**, *207*, 44–46.
87. T. Ishiyama, N. Matsuda, N. Miyaura, A. Suzuki, *J. Am. Chem. Soc.* **1993**, *115*, 11018–11019.
88. T. Ishiyama, N. Matsuda, M. Murata, F. Ozawa, A. Suzuki, N. Miyaura, *Organometallics* **1996**, *15*, 713–720.
89. K. M. Waltz, J. F. Hartwig, *Science* **1997**, *277*, 211–213.
90. I. Beletskaya, A. Pelter, *Tetrahedron* **1997**, *53*, 4957–5026.
91. G. Schmid, *Angew. Chem. Int. Ed. Engl.* **1970**, *9*, 819–916.
92. G. Schmid, *Angew. Chem.* **1970**, *82*, 920–930.
93. J. F. Hartwig, S. Huber, *J. Am. Chem. Soc.* **1993**, *115*, 4908–4909.
94. P. Nguyen, G. Lesley, N. J. Taylor, T. B. Marder, N. L. Pickett, W. Clegg, M. R. J. Elsegood, N. C. Norman, *Inorg. Chem.* **1994**, *33*, 4623–4624.
95. H. Braunschweig, B. Ganter, M. Koster, T. Wagner, *Chem. Ber.* **1996**, *129*, 1099–1101.
96. A. Kerr, T. B. Marder, N. C. Norman, A. G. Orpen, M. J. Quayle, C. R. Rice, P. L. Timms, G. R. Whittell, *Chem. Commun.* **1998**, 319–320.

97. W. Clegg, F. J. Lawlor, T. B. Marder, P. Nguyen, N. C. Norman, A. G. Orpen, M. J. Quayle, C. R. Rice, E. G. Robins, A. J. Scott, F. E. S. Souza, G. Stringer, G. R. Whittell, *J. Chem. Soc., Dalton Trans.* **1998**, 301–309.
98. N. Arnold, H. Braunschweig, P. Brenner, J. O. C. Jimenez-Halla, T. Kupfer, K. Radacki, *Organometallics* **2012**, *31*, 1897–1907.
99. H. Braunschweig, P. Brenner, R. D. Dewhurst, F. Guethlein, J. O. C. Jimenez-Halla, K. Radacki, J. Wolf, L. Zöllner, *Chem. Eur. J.* **2012**, *18*, 8605–8609.
100. H. Braunschweig, K. Radacki, F. Seeler, G. R. Whittell, *Organometallics* **2006**, *25*, 4605–4610.
101. L. Weber, *Eur. J. Inorg. Chem.* **2012**, 5595–5609.
102. Y. Segawa, M. Yamashita, K. Nozaki, *Science* **2006**, *314*, 113–115.
103. Y. Segawa, Y. Suzuki, M. Yamashita, K. Nozaki, *J. Am. Chem. Soc.* **2008**, *130*, 16069–16079.
104. M. Yamashita, Y. Suzuki, Y. Segawa, K. Nozaki, *J. Am. Chem. Soc.* **2007**, *129*, 9570–9571.
105. T. Terabayashi, T. Kajiwara, M. Yamashita, K. Nozaki, *J. Am. Chem. Soc.* **2009**, *131*, 14162–14163.
106. Y. Segawa, M. Yamashita, K. Nozaki, *Angew. Chem. Int. Ed.* **2007**, *46*, 6710–6713.
107. Y. Segawa, M. Yamashita, K. Nozaki, *Angew. Chem.* **2007**, *119*, 6830–6833.
108. T. Kajiwara, T. Terabayashi, M. Yamashita, K. Nozaki, *Angew. Chem. Int. Ed.* **2008**, *47*, 6606–6610.
109. T. Kajiwara, T. Terabayashi, M. Yamashita, K. Nozaki, *Angew. Chem.* **2008**, *120*, 6708–6712.
110. H. Braunschweig, K. Radacki, A. Schneider, *Science* **2010**, *328*, 345–347.
111. S. Bertsch, J. Brand, H. Braunschweig, F. Hupp, K. Radacki, *Chem. Eur. J.* **2015**, *21*, 6278–6285.
112. H. Braunschweig, K. Radacki, D. Rais, K. Uttinger, *Angew. Chem. Int. Ed.* **2006**, *45*, 162–165.
113. H. Braunschweig, K. Radacki, D. Rais, K. Uttinger, *Angew. Chem.* **2006**, *118*, 169–172.
114. J. Brand, H. Braunschweig, R. D. Dewhurst, F. Hupp, K. Lang, *Eur. J. Inorg. Chem.* **2015**, 2592–2595.
115. J. Brand, H. Braunschweig, F. Hupp, A. K. Phukan, K. Radacki, S. S. Sen, *Angew. Chem. Int. Ed.* **2014**, *53*, 2240–2244.
116. J. Brand, H. Braunschweig, F. Hupp, A. K. Phukan, K. Radacki, S. S. Sen, *Angew. Chem.* **2014**, *126*, 2273–2277.
117. J. Brand, H. Braunschweig, S. S. Sen, *Acc. Chem. Res.* **2014**, *47*, 180–191.
118. H. Braunschweig, C. Kollann, U. Englert, *Angew. Chem. Int. Ed.* **1998**, *37*, 3179–3180.
119. H. Braunschweig, C. Kollann, U. Englert, *Angew. Chem.* **1998**, *110*, 3355–3357.
120. F. Dahcheh, D. Martin, D. W. Stephan, G. Bertrand, *Angew. Chem. Int. Ed.* **2014**, *53*, 13159–13163.
121. F. Dahcheh, D. Martin, D. W. Stephan, G. Bertrand, *Angew. Chem.* **2014**, *126*, 13375–13379.
122. F. Dahcheh, D. W. Stephan, G. Bertrand, *Chem. Eur. J.* **2015**, *21*, 199–204.

123. H. Braunschweig, R. D. Dewhurst, F. Hupp, M. Nutz, K. Radacki, C. W. Tate, A. Vargas, Q. Ye, *Nature* **2015**, *522*, 327–330.
124. P. L. Timms, *J. Am. Chem. Soc.* **1967**, *89*, 1629–1632.
125. P. L. Timms, *Acc. Chem. Res.* **1973**, *6*, 118–123.
126. B. Pachaly, R. West, *Angew. Chem. Int. Ed. Engl.* **1984**, *23*, 454–455.
127. B. Pachaly, R. West, *Angew. Chem.* **1984**, *96*, 444–445.
128. A. W. Ehlers, E. J. Baerends, F. M. Bickelhaupt, U. Radius, *Chem. Eur. J.* **1998**, *4*, 210–221.
129. U. Radius, F. M. Bickelhaupt, A. W. Ehlers, N. Goldberg, R. Hoffmann, *Inorg. Chem.* **1998**, *37*, 1080–1090.
130. B. Wrackmeyer, *Angew. Chem. Int. Ed.* **1999**, *38*, 771–772.
131. B. Wrackmeyer, *Angew. Chem.* **1999**, *111*, 817–818.
132. C. L. B. Macdonald, A. H. Cowley, *J. Am. Chem. Soc.* **1999**, *121*, 12113–12126.
133. C. Boehme, J. Uddin, G. Frenking, *Coord. Chem. Rev.* **2000**, *197*, 249–276.
134. J. Uddin, C. Boehme, G. Frenking, *Organometallics* **2000**, *19*, 571–582.
135. J. Uddin, G. Frenking, *J. Am. Chem. Soc.* **2001**, *123*, 1683–1693.
136. Y. Chen, G. Frenking, *J. Chem. Soc., Dalton Trans.* **2001**, 434–440.
137. K. K. Pandey, D. G. Musaev, *Organometallics* **2010**, *29*, 142–148.
138. L. Xu, Q.-S. Li, Y. Xie, R. B. King, H. F. Schaefer, III, *Inorg. Chem.* **2010**, *49*, 1046–1055.
139. G. Bénac-Lestrille, U. Helmstedt, L. Vendier, G. Alcaraz, E. Clot, S. Sabo-Etienne, *Inorg. Chem.* **2011**, *50*, 11039–11045.
140. K. H. Fischer, M. Schneider, I. Fischer, B. Pfaffinger, H. Braunschweig, B. Sztáray, A. Bodi, *Chem. Eur. J.* **2012**, *18*, 4533–4540.
141. J. F. Hartwig, *Organotransition Metal Chemistry: From Bonding to Catalysis*; University Science Books: Mill Valley, CA, **2010**; pp 27–33.
142. F. A. Cotton, *Chemical Applications of Group Theory*; John Wiley & Sons, Inc.: New York, NY, **1990**; pp 17–67.
143. U. Flierler, M, Burzler, D. Leusser, J. Henn, H. Ott, H. Braunschweig, D. Stalke, *Angew. Chem. Int. Ed.* **2008**, *47*, 4321–4325.
144. U. Flierler, M. Burzler, D. Leusser, J. Henn, H. Ott, H. Braunschweig, D. Stalke, *Angew. Chem.* **2008**, *120*, 4393–4397.
145. K. Götz, M. Kaupp, H. Braunschweig, D. Stalke, *Chem. Eur. J.* **2009**, *15*, 623–632.
146. H. Braunschweig, T. Wagner, *Angew. Chem. Int. Ed. Engl.* **1995**, *34*, 825–826.
147. H. Braunschweig, T. Wagner, *Angew. Chem.* **1995**, 107, 904–905.
148. A. H. Cowley, V. Lomelí, A. Voigt, *J. Am. Chem. Soc.* **1998**, *120*, 6401–6402.
149. D. Vidovic, M. Findlater, G. Reeske, A. H. Cowley, *Chem. Commun.* **2006**, 3786–3787.
150. H. Braunschweig, M. Colling, C. Kollann, H. G. Stammler, B. Neumann, *Angew. Chem. Int. Ed.* **2001**, *40*, 2298–2300.
151. H. Braunschweig, M. Colling, C. Kollann, H. G. Stammler, B. Neumann, *Angew. Chem.* **2001**, *113*, 2359–2361.
152. B. Blank, M. Colling-Hendelkens, C. Kollann, K. Radacki, D. Rais, K. Uttinger, G. R. Whittell, H. Braunschweig, *Chem. Eur. J.* **2007**, *13*, 4770–4781.
153. H. Braunschweig, M. Colling, C. Kollann, K. Merz, K. Radacki, *Angew. Chem. Int. Ed.* **2001**, *40*, 4198–4200.

154. H. Braunschweig, M. Colling, C. Kollann, K. Merz, K. Radacki, *Angew. Chem.* **2001**, *113*, 4327–4329.
155. H. Braunschweig, R. D. Dewhurst, C. Hörl, K. Radacki, C. W. Tate, A. Vargas, Q. Ye, *Angew. Chem. Int. Ed.* **2013**, *52*, 10120–10123.
156. H. Braunschweig, R. D. Dewhurst, C. Hörl, K. Radacki, C. W. Tate, A. Vargas, Q. Ye, *Angew. Chem.* **2013**, *125*, 10307–10310.
157. H. Braunschweig, R. D. Dewhurst, K. Radacki, C. W. Tate, A. Vargas, *Angew. Chem. Int. Ed.* **2014**, *53*, 6263–6266.
158. H. Braunschweig, R. D. Dewhurst, K. Radacki, C. W. Tate, A. Vargas, *Angew. Chem.* **2014**, *126*, 6378–6381.
159. G. Alcaraz, E. Clot, U. Helmstedt, L. Vendier, S. Sabo-Etienne, *J. Am. Chem. Soc.* **2007**, *129*, 8704–8705.
160. G. Alcaraz, U. Helmstedt, E. Clot, L. Vendier, S. Sabo-Etienne, *J. Am. Chem. Soc.* **2008**, *130*, 12878–12879.
161. D. L. Coombs, S. Aldridge, C. Jones, D. J. Willock, *J. Am. Chem. Soc.* **2003**, *125*, 6356–6357.
162. D. L. Coombs, S. Aldridge, A. Rossin, C. Jones, D. J. Willock, *Organometallics* **2004**, *23*, 2911–2926.
163. G. A. Pierce, D. Vidovic, D. L. Kays, N. D. Coombs, A. L. Thompson, E. D. Jemmis, S. De, S. Aldridge, *Organometallics* **2009**, *28*, 2947–2960.
164. D. L. Kays (*née* Coombs), J. K. Day, L.-L. Ooi, S. Aldridge, *Angew. Chem. Int. Ed.* **2005**, *44*, 7457–7460.
165. D. L. Kays (*née* Coombs), J. K. Day, L.-L. Ooi, S. Aldridge, *Angew. Chem.* **2005**, *117*, 7623–7626.
166. H. Braunschweig, K. Radacki, R. Shang, C. W. Tate, *Angew. Chem. Int. Ed.* **2013**, *52*, 729–733.
167. H. Braunschweig, K. Radacki, R. Shang, C. W. Tate, *Angew. Chem.* **2013**, *125*, 757–761.
168. H. Braunschweig, M. Burzler, K. Radacki, F. Seeler, *Angew. Chem. Int. Ed.* **2007**, *46*, 8071–8073.
169. H. Braunschweig, M. Burzler, K. Radacki, F. Seeler, *Angew. Chem.* **2007**, *119*, 8217–8219.
170. J. Bauer, H. Braunschweig, A. Damme, J. O. C. Jimenez-Halla, T. Kramer, K. Radacki, R. Shang, E. Siedler, Q. Ye, *J. Am. Chem. Soc.* **2013**, *135*, 8726–8734.
171. H. Braunschweig, M. Burzler, T. Kupfer, K. Radacki, F. Seeler, *Angew. Chem. Int. Ed.* **2007**, *46*, 7785–7787.
172. H. Braunschweig, M. Burzler, T. Kupfer, K. Radacki, F. Seeler, *Angew. Chem.* **2007**, *119*, 7932–7934.
173. H. Braunschweig, T. Herbst, D. Rais, F. Seeler, *Angew. Chem. Int. Ed.* **2005**, *44*, 7461–7463.
174. H. Braunschweig, T. Herbst, D. Rais, F. Seeler, *Angew. Chem.* **2005**, *117*, 7627–7629.
175. H. Braunschweig, T. Herbst, D. Rais, S. Ghosh, T. Kupfer, K. Radacki, A. G. Crawford, R. M. Ward, T. B. Marder, I. Fernández, G. Frenking, *J. Am. Chem. Soc.* **2009**, *131*, 8989–8999.
176. H. Braunschweig, A. Damme, R. D. Dewhurst, S. Ghosh, T. Kramer, B. Pfaffinger, K. Radacki, A. Vargas, *J. Am. Chem. Soc.* **2013**, *135*, 1903–1911.

177. H. Braunschweig, R. D. Dewhurst, T. Herbst, K. Radacki, *Angew. Chem. Int. Ed.* **2008**, *47*, 5978–5980.
178. H. Braunschweig, R. D. Dewhurst, T. Herbst, K. Radacki, *Angew. Chem.* **2008**, *120*, 6067–6069.
179. H. Braunschweig, M. Colling, C. Hu, K. Radacki, *Angew. Chem. Int. Ed.* **2003**, *42*, 205–208.
180. H. Braunschweig, M. Colling, C. Hu, K. Radacki, *Angew. Chem.* **2003**, *115*, 215–218.
181. H. Braunschweig, B. Christ, M. Colling-Hendelkens, M. Forster, K. Götz, M. Kaupp, K. Radacki, F. Seeler, *Chem. Eur. J.* **2009**, *15*, 7150–7155.
182. S. Bertsch, H. Braunschweig, B. Christ, M. Forster, K. Schwab, K. Radacki, *Angew. Chem. Int. Ed.* **2010**, *49*, 9517–9520.
183. S. Bertsch, H. Braunschweig, B. Christ, M. Forster, K. Schwab, K. Radacki, *Angew. Chem.* **2010**, *122*, 9707–9710.
184. H. Braunschweig, Q. Ye, A. Vargas, R. D. Dewhurst, K. Radacki, A. Damme, *Nature Chem.* **2012**, *4*, 563–567.
185. H. Braunschweig, Q. Ye, A. Vargas, K. Radacki, A. Damme, *Angew. Chem. Int. Ed.* **2013**, *52*, 10657–10660.
186. H. Braunschweig, Q. Ye, A. Vargas, K. Radacki, A. Damme, *Angew. Chem.* **2013**, *125*, 10851–10854.
187. C. D. Entwistle, T. B. Marder, *Angew. Chem. Int. Ed.* **2002**, *41*, 2927–2931.
188. C. D. Entwistle, T. B. Marder, *Angew. Chem.* **2002**, *114*, 3051–3056.
189. F. Jäkle, *Coord. Chem. Rev.* **2006**, *250*, 1107–1121.
190. S. Yamaguchi, A. Wakamiya, *Pure Appl. Chem.* **2006**, *78*, 1413–1424.
191. M. J. D. Bosdet, W. E. Piers, *Can. J. Chem.* **2009**, *87*, 8–29.
192. F. Jäkle, *Chem. Rev.* **2010**, *110*, 3985–4022.
193. Z. Zhang, R. M. Edkins, J. Nitsch, K. Fucke, A. Steffen, L. E. Longobardi, D. W. Stephan, C. Lambert, T. B. Marder, *Chem. Sci.* **2015**, *6*, 308–321.
194. Z. Zhang, R. M. Edkins, M. Haehnel, M. Wehner, A. Eichhorn, L. Mailänder, M. Meier, J. Brand, F. Brede, K. Müller-Buschbaum, H. Braunschweig, T. B. Marder, *Chem. Sci.* **2015**, *6*, 5922–5927.
195. S. Saito, K. Matsuo, S. Yamaguchi, *J. Am. Chem. Soc.* **2012**, *134*, 9130–9133.
196. Y. Shirota, *J. Mater. Chem.* **2000**, *10*, 1–25.
197. Y. Shirota, H. Kageyama, *Chem. Rev.* **2007**, *107*, 953–1010.
198. Z. Yuan, J. C. Collings, N. J. Taylor, T. B. Marder, C. Jardin, J.-F. Halet, *J. Solid State Chem.* **2000**, *154*, 5–12.
199. C. D. Entwistle, T. B. Marder, *Chem. Mater.* **2004**, *16*, 4574–4585.
200. M. Elbing, G. C. Bazan, *Angew. Chem. Int. Ed.* **2008**, *47*, 834–838.
201. M. Elbing, G. C. Bazan, *Angew. Chem.* **2008**, *120*, 846–850.
202. N. Matsumi, Y. Chujo, *Polym. J.* **2008**, *40*, 77–89.
203. T. W. Hudnall, Y.-M. Kim, M. W. P. Bebbington, D. Bourissou, F. P. Gabbaï, *J. Am. Chem. Soc.* **2008**, *130*, 10890–10891.
204. Y. Kim, F. P. Gabbaï, *J. Am. Chem. Soc.* **2009**, *131*, 3363–3369.
205. T. W. Hudnall, C.-W. Chiu, F. P. Gabbaï, *Acc. Chem. Res.* **2009**, *42*, 388–397.
206. C. R. Wade, A. E. J. Broomsgrove, S. Aldridge, F. P. Gabbaï, *Chem. Rev.* **2010**, *110*, 3958–3984.
207. Z. M. Hudson, S. Wang, *Acc. Chem. Res.* **2009**, *42*, 1584–1596.
208. Z. M. Hudson, S. Wang, *Dalton Trans.* **2011**, *40*, 7805–7816.

209. A. Wakamiya, K. Mori, S. Yamaguchi, *Angew. Chem. Int. Ed.* **2007**, *46*, 4273–4276.
210. A. Wakamiya, K. Mori, S. Yamaguchi, *Angew. Chem.* **2007**, *119*, 4351–4354.
211. Y. Nagata, Y. Chujo, *J. Organomet. Chem.* **2009**, *694*, 1723–1726.
212. A. Iida, S. Yamaguchi, *J. Am. Chem. Soc.* **2011**, *133*, 6952–6955.
213. C. Hoffend, F. Schödel, M. Bolte, H.-W. Lerner, M. Wagner, *Chem. Eur. J.* **2012**, *18*, 15394–15405.
214. W. Kaim, A. Schulz, *Angew. Chem. Int. Ed. Engl.* **1984**, *23*, 615–616.
215. W. Kaim, A. Schulz, *Angew. Chem.* **1984**, *96*, 611–612.
216. Z. Yuan, N. J. Taylor, R. Ramachandran, T. B. Marder, *Appl. Organomet. Chem.* **1996**, *10*, 305–316.
217. A. G. Crawford, A. D. Dwyer, Z. Liu, A. Steffen, A. Beeby, L.-O. Pålsson, D. J. Tozer, T. B. Marder, *J. Am. Chem. Soc.* **2011**, *133*, 13349–13362.
218. Z. Liu, Y. Wang, Y. Chen, J. Liu, Q. Fang, C. Kleeberg, T. B. Marder, *J. Org. Chem.* **2012**, *77*, 7124–7128.
219. T. Noda, Y. Shirota, *J. Am. Chem. Soc.* **1998**, *120*, 9714–9715.
220. T. Noda, H. Ogawa, Y. Shirota, *Adv. Mater.* **1999**, *11*, 283–285.
221. T. Noda, Y. Shirota, *J. Lumin.* **2000**, *87–89*, 1168–1170.
222. K. Tanaka, Y. Chujo, *Macromol. Rapid Commun.* **2012**, *33*, 1235–1255.
223. R. J.-P. Corriu, T. Deforth, W. E. Douglas, G. Guerrero, W. S. Siebert, *Chem. Commun.* **1998**, 963–964.
224. J. C. Doty, B. Babb, P. J. Grisdale, M. Glogowski, J. L. R. Williams, *J. Organomet. Chem.* **1972**, *38*, 229–236.
225. Z. Yuan, N. J. Taylor, T. B. Marder, I. D. Williams, S. K. Kurtz, L.-T. Cheng, *J. Chem. Soc., Chem. Commun.* **1990**, 1489–1492.
226. Z. Yuan, N. J. Taylor, Y. Sun, T. B. Marder, I. D. Williams, L.-T. Cheng, *J. Organomet. Chem.* **1993**, *449*, 27–37.
227. Y. Shirota, M. Kinoshita, T. Noda, K. Okumoto, T. Ohara, *J. Am. Chem. Soc.* **2000**, *122*, 11021–11022.
228. C.-H. Zhao, A. Wakamiya, Y, Inukai, S. Yamaguchi, *J. Am. Chem. Soc.* **2006**, *128*, 15934–15935.
229. Y.-F. Li, Y. Kang, S.-B. Ko, Y. Rao, F. Sauriol, S. Wang, *Organometallics*, **2013**, *32*, 3063–3068.
230. E. Sakuda, A. Funahashi, N. Kitamura, *Inorg. Chem.* **2006**, *45*, 10670–10677.
231. S.-B. Ko, J.-S. Lu, Y. Kang, S. Wang, *Organometallics*, **2013**, *32*, 599–608.
232. M. Melaimi, F. P. Gabbaï, *J. Am. Chem. Soc.* **2005**, *127*, 9680–9681.
233. Y.-L. Rao, S. Wang, *Inorg. Chem.* **2009**, *48*, 7698–7713.
234. C. R. Wade, F. P. Gabbaï, *Inorg. Chem.* **2010**, *49*, 714–720.
235. P. Nguyen, G. Lesley, T. B. Marder, *Chem. Mater.* **1997**, *9*, 406–408.
236. Z. M. Hudson, C. Sun, M. G. Helander, H. Amarne, Z.-H. Lu, S. Wang, *Adv. Funct. Mater.* **2010**, *20*, 3426–3439.
237. Y. Sun, S. Wang, *Inorg. Chem.* **2010**, *49*, 4394–4404.
238. Y. Chujo, I. Tomita, N. Murata, H. Mauermann, T. Saegusa, *Macromolecules* **1992**, *25*, 27–32.
239. Y. Chujo, I. Tomita, T. Saegusa, *Polym. Bull.* **1993**, *31*, 547–552.
240. Y. Chujo, I. Tomita, T. Saegusa, *Polym. Bull.* **1993**, *31*, 553–558.
241. Y. Chujo, I. Tomita, T. Saegusa, *Macromolecules* **1994**, *27*, 6714–6717.
242. N. Matsumi, K. Naka, Y. Chujo, *Polym. J.* **1998**, *30*, 833–837.

243. N. Matsumi, K. Kotera, K. Naka, Y. Chujo, *Macromolecules* **1998**, *31*, 3155–3157.
244. N. Matsumi, K. Kotera, Y. Chujo, *Macromolecules* **2000**, *33*, 2801–2806.
245. N. Matsumi, T. Umeyama, Y. Chujo, *Macromolecules* **2000**, *33*, 3956–3957.
246. N. Matsumi, Y. Chujo, *Macromolecules* **2000**, *33*, 8146–8148.
247. N. Matsumi, T. Umeyama, Y. Chujo, *Macromolecules* **2001**, *34*, 3510–3511.
248. M. Miyata, N. Matsumi, Y. Chujo, *Macromolecules* **2001**, *34*, 7331–7335.
249. N. Matsumi, K. Naka, Y, Chujo, *J. Am. Chem. Soc.* **1998**, *120*, 5112–5113.
250. N. Matsumi, M. Miyata, Y. Chujo, *Macromolecules* **1999**, *32*, 4467–4469.
251. N. Matsumi, Y. Chujo, O. Lavastre, P. H. Dixneuf, *Organometallics* **2001**, *20*, 2425–2427.
252. F. Matsumoto, N. Matsumi, Y. Chujo, *Polym. Bull.* **2001**, *46*, 257–262.
253. N. Matsumi, K. Naka, Y. Chujo, *J. Am. Chem. Soc.* **1998**, *120*, 10776–10777.
254. C.-H. Zhao, A. Wakamiya, S. Yamaguchi, *Macromolecules* **2007**, *40*, 3898–3900.
255. Y. Qin, G. Cheng, O. Achara, K. Parab, F. Jäkle, *Macromolecules* **2004**, *37*, 7123–7131.
256. A. Sundararaman, M. Victor, R. Varughese, F. Jäkle, *J. Am. Chem. Soc.* **2005**, *127*, 13748–13749.
257. J. B. Heilmann, M. Scheibitz, Y. Qin, A. Sundararaman, F. Jäkle, T. Kretz, M. Bolte, H.-W. Lerner, M. C. Holthausen, M. Wagner, *Angew. Chem. Int. Ed.* **2006**, *45*, 920–925.
258. J. B. Heilmann, M. Scheibitz, Y. Qin, A. Sundararaman, F. Jäkle, T. Kretz, M. Bolte, H.-W. Lerner, M. C. Holthausen, M. Wagner, *Angew. Chem.* **2006**, *118*, 934–939.
259. A. Nagai, T. Murakami, Y. Nagata, K. Kokado, Y, Chujo, *Macromolecules* **2009**, *42*, 7217–7220.
260. H. Braunschweig, V. Dyakonov, J. O. C. Jimenez-Halla, K. Kraft, I. Krummenacher, K. Radacki, A. Sperlich, J. Wahler, *Angew. Chem. Int. Ed.* **2012**, *51*, 2977–2980.
261. H. Braunschweig, V. Dyakonov, J. O. C. Jimenez-Halla, K. Kraft, I. Krummenacher, K. Radacki, A. Sperlich, J. Wahler, *Angew. Chem.* **2012**, *124*, 3031–3034.
262. C. Elschenbroich, *Organometallchemie*, 4th ed.; B. G. Teubner Verlag / GWV Fachverlage GmbH: Wiesbaden, **2003**; pp 84–107.
263. J. J. Eisch, F. Shen, K. Tamao, *Heterocycles* **1982**, *18*, 245–250.
264. A. J. Ashe, III, F. J. Drone, C. M. Kausch, J. Kroker, S. M. Al-Taweel, *Pure & Appl. Chem.* **1990**, *62*, 513–517.
265. R. N. Grimes, *Chem. Rev.* **1992**, *92*, 251–268.
266. H. Braunschweig, I. Fernández, G. Frenking, T. Kupfer, *Angew. Chem. Int. Ed.* **2008**, *47*, 1951–1954.
267. H. Braunschweig, I. Fernández, G. Frenking, T. Kupfer, *Angew. Chem.* **2008**, *120*, 1977–1980.
268. H. Braunschweig, T. Kupfer, *Chem. Commun.* **2011**, *47*, 10903–10914.
269. H. Bönnemann, W. Brijoux, R. Brinkmann, W. Meurers, *Helv. Chim. Acta.* **1984**, *67*, 1616–1624.
270. A. J. Ashe, III, F. J. Drone, *J. Am. Chem. Soc.* **1987**, *109*, 1880–1881.
271. K. Komatsu, T. Kitagawa, *Chem. Rev.* **2003**, *103*, 1371–1427.

272. J. J. Eisch, B. Shafii, J. D. Odom, A. L. Rheingold, *J. Am. Chem. Soc.* **1990**, *112*, 1847–1853.
273. D. A. Hoic, J. R. Wolf, W. M. Davis, G. C. Fu, *Organometallics* **1996**, *15*, 1315–1318.
274. A. J. Ashe, III, W. Klein, R. Rousseau, *Organometallics* **1993**, *12*, 3225–3231.
275. E. Hückel, *Z. Phys.* **1931**, *70*, 204–286.
276. H. Sashida, A. Kuroda, T. Tsuchiya, *Chem. Commun.* **1998**, 767–768.
277. J. M. Schulman, R. L. Disch, *Organometallics* **2000**, *19*, 2932–2936.
278. R. E. Messersmith, J. D. Tovar, *J. Phys. Org. Chem.* **2015**, *28*, 378–387.
279. R. Breslow, *Chem. Eng. News* **1965**, *43*, 90–100.
280. R. Breslow, J. Brown, J. Gajewski, *J. Am. Chem. Soc.* **1967**, *89*, 4383–4390.
281. R. Breslow, *Acc. Chem. Res.* **1973**, *6*, 393–398.
282. H. Braunschweig, T. Kupfer, *Chem. Commun.* **2008**, 4487–4489.
283. H. Braunschweig, I. Fernández, G. Frenking, K. Radacki, F. Seeler, *Angew. Chem. Int. Ed.* **2007**, *46*, 5215–5218.
284. H. Braunschweig, I. Fernández, G. Frenking, K. Radacki, F. Seeler, *Angew. Chem.* **2007**, *119*, 5307–5310.
285. J. J. Eisch, *Adv. Organomet. Chem.* **1996**, *39*, 355–391.
286. H. Braunschweig, C.-W. Chiu, D. Gamon, K. Gruß, C. Hörl, T. Kupfer, K. Radacki, J. Wahler, *Eur. J. Inorg. Chem.* **2013**, 1525–1530.
287. H. Braunschweig, I. Krummenacher, J. Wahler, *Adv. Organomet. Chem.* **2013**, *61*, 1–53.
288. Y.-G. Byun, S. Saebo, C. U. Pittman, Jr., *J. Am. Chem. Soc.* **1991**, *113*, 3689–3696.
289. J. J. Eisch, B. Shafii, J. D. Odom, A. L. Rheingold, *J. Am. Chem. Soc.* **1990**, *112*, 1847–1853.
290. P. L. Timms, *J. Am. Chem. Soc.* **1968**, *90*, 4585–4589.
291. C. Pues, A. Berndt, *Angew. Chem. Int. Ed. Engl.* **1984**, *23*, 313–314.
292. C. Pues, A. Berndt, *Angew. Chem.* **1984**, *96*, 306–307.
293. C. Habben, A. Meller, *Chem. Ber.* **1984**, *117*, 2531–2537.
294. J. J. Eisch, B. Shafii, A. L. Rheingold, *J. Am. Chem. Soc.* **1987**, *109*, 2526–2528.
295. H. Braunschweig, Q. Ye, K. Radacki, *Chem. Commun.* **2009**, 6979–6981.
296. H. Braunschweig, Q. Ye, K. Radacki, T. Kupfer, *Dalton Trans.* **2011**, *40*, 3666–3670.
297. H. Braunschweig, Q. Ye, K. Radacki, P. Brenner, *Inorg. Chem.* **2011**, *50*, 62–71.
298. H. Braunschweig, T. Herbst, K. Radacki, G. Frenking, M. A. Celik, *Chem. Eur. J.* **2009**, *15*, 12099–12106.
299. H. Braunschweig, P. Brenner, R. D. Dewhurst, I. Krummenacher, B. Pfaffinger, A. Vargas, *Nature Commun.* **2012**, *3*, 872.
300. G. E. Herberich, H. Ohst, *Adv. Organomet. Chem.* **1986**, *25*, 199–236.
301. G. C. Fu, *Adv. Organomet. Chem.* **2001**, *47*, 101–119.
302. B. Y. Lee, S. Wang, M. Putzer, G. P. Bartholomew, X. Bu, G. C. Bazan, *J. Am. Chem. Soc.* **2000**, *122*, 3969–3970.
303. D. J. H. Emslie, W. E. Piers, M. Parvez, *Angew. Chem. Int. Ed.* **2003**, *42*, 1251–1255.
304. D. J. H. Emslie, W. E. Piers, M. Parvez, *Angew. Chem.* **2003**, *115*, 1289–1293.

305. C. A. Jaska, D. J. H. Emslie, M. J. D. Bosdet, W. E. Piers, T. S. Sorenson, M. Parvez, *J. Am. Chem. Soc.* **2006**, *128*, 10885–10896.
306. T. K. Wood, W. E. Piers, B. A. Keay, M. Parvez, *Angew. Chem. Int. Ed.* **2009**, *48*, 4009–4012.
307. T. K. Wood, W. E. Piers, B. A. Keay, M. Parvez, *Angew. Chem.* **2009**, *121*, 4069–4072.
308. A. Languérand, S. S. Barnes, G. Bélanger-Chabot, L. Maron, P. Berrouard, P. Audet, F.-G. Fontaine, *Angew. Chem. Int. Ed.* **2009**, *48*, 6695–6698.
309. A. Languérand, S. S. Barnes, G. Bélanger-Chabot, L. Maron, P. Berrouard, P. Audet, F.-G. Fontaine, *Angew. Chem.* **2009**, *121*, 6823–6826.
310. I. A. Cade, A. F. Hill, *Organometallics* **2012**, *31*, 2112–2115.
311. M.-A. Légaré, G. Bélanger-Chabot, G. D. Robillard, A. Languérand, L. Maron, F.-G. Fontaine, *Organometallics* **2014**, *33*, 3596–3606.
312. G. Maier, H. P. Reisenauer, J. Henkelmann, C. Kliche, *Angew. Chem. Int. Ed. Engl.* **1988**, *27*, 295–296.
313. G. Maier, H. P. Reisenauer, J. Henkelmann, C. Kliche, *Angew. Chem.* **1988**, *100*, 303.
314. R. Boese, N. Finke, J. Henkelmann, G. Maier, P. Paetzold, H. P. Reisenauer, G. Schmid, *Chem. Ber.* **1985**, *118*, 1644–1654.
315. R. Boese, N. Finke, T. Keil, P. Paetzold, G. Schmid, *Z. Naturforsch.* **1985**, *40b*, 1327–1332.
316. M. C. Amendola, K. E. Stockman, D. A. Hoic, W. M. Davis, G. C. Fu, *Angew. Chem. Int. Ed. Engl.* **1997**, *36*, 267–269.
317. M. C. Amendola, K. E. Stockman, D. A. Hoic, W. M. Davis, G. C. Fu, *Angew. Chem.* **1997**, *109*, 278–281.
318. D. A. Hoic, W. M. Davis, G. C. Fu, *J. Am. Chem. Soc.* **1995**, *117*, 8480–8481.
319. S. Qiao, D. A. Hoic, G. C. Fu, *J. Am. Chem. Soc.* **1996**, *118*, 6329–6330.
320. A. J. Ashe, III, J. W. Kampf, C. Müller, M. Schneider, *Organometallics* **1996**, *15*, 387–393.
321. D. A. Hoic, M. DiMare, G. C. Fu, *J. Am. Chem. Soc.* **1997**, *119*, 7155–7156.
322. J. S. Rogers, G. C. Bazan, C. K. Sperry, *J. Am. Chem. Soc.* **1997**, *119*, 9305–9306.
323. D. H. Woodmansee, X. Bu, G. C. Bazan, *Chem. Commun.* **2001**, 619–620.
324. G. Bélanger-Chabot, P. Rioux, L. Maron, F.-G. Fontaine, *Chem. Commun.* **2010**, *46*, 6816–6818.
325. A. J. Ashe, III, S. Al-Ahmad, X. Fang, *J. Organomet. Chem.* **1999**, *581*, 92–97.
326. D. A. Hoic, W. M. Davis, G. C. Fu, *J. Am. Chem. Soc.* **1996**, *118*, 8176–8177.
327. U. Hagenau, J. Heck, E. Hendrickx, A. Persoons, T. Schuld, H. Wong, *Inorg. Chem.* **1996**, *35*, 7863–7866.
328. B. B. Macha, J. Boudreau, L. Maron, T. Maris, F.-G. Fontaine, *Organometallics* **2012**, *31*, 6428–6437.
329. A. J. Ashe, III, J. W. Kampf, J. R. Waas, *Organometallics* **1997**, *16*, 163–167.
330. J. S. Rogers, R. J. Lachicotte, G. C. Bazan, *J. Am. Chem. Soc.* **1999**, *121*, 1288–1298.
331. G. E. Herberich, U. Englert, A. Fischer, J. Ni, A. Schmitz, *Organometallics* **1999**, *18*, 5496–5501.
332. J. S. Rogers, X. Bu, G. C. Bazan, *J. Am. Chem. Soc.* **2000**, *122*, 730–731.

333. Z. J. A. Komon, J. S. Rogers, G. C. Bazan, *Organometallics* **2002**, *21*, 3189–3195.
334. G. E. Herberich, T. S. B. Baul, U. Englert, *Eur. J. Inorg. Chem.* **2002**, 43–48.
335. U. Behrens, T. Meyer-Friedrichsen, J. Heck, *Z. Anorg. Allg. Chem.* **2003**, *629*, 1421–1430.
336. P. Cui, Y. Chen, X. Zeng, J. Sun, G. Li, W. Xia, *Organometallics* **2007**, *26*, 6519–6521.
337. P. Cui, Y. Chen, G. Wang, G. Li, W. Xia, *Organometallics* **2008**, *27*, 4013–4016.
338. D. A. Loginov, D. V. Muratov, D. S. Perekalin, Z. A. Starikova, E. A. Petrovskaya, E. I. Gutsul, A. R. Kudinov, *Inorg. Chim. Acta* **2008**, *361*, 1715–1721.
339. Y. Yuan, Y. Chen, G. Li, W. Xia, *Organometallics* **2010**, *29*, 3722–3728.
340. P. Cui, Y. Chen, Q. Zhang, G. Li, W. Xia, *J. Organomet. Chem.* **2010**, *695*, 2713–2719.
341. I. A. Cade, A. F. Hill, *Dalton Trans.* **2011**, *40*, 10563–10567.
342. S. S. Barnes, M.-A. Légaré, L. Maron, F.-G. Fontaine, *Dalton Trans.* **2011**, *40*, 12439–12442.
343. A. Mushtaq, W. Bi, M.-A. Légaré, F.-G. Fontaine, *Organometallics* **2014**, *33*, 3173–3181.
344. G. E. Herberich, G. Greiss, H. F. Heil, *Angew. Chem. Int. Ed. Engl.* **1970**, *9*, 805–806.
345. G. E. Herberich, G. Greiß, H. F. Heil, *Angew. Chem.* **1970**, *82*, 838–839.
346. G. E. Herberich, G. Greiss, H. F. Heil, J. Müller, *J. Chem. Soc. D* **1971**, 1328–1329.
347. G. E. Herberich, G. Greiß, *Chem. Ber.* **1972**, *105*, 3413–3423.
348. A. J. Ashe, III, E. Meyers, P. Shu, T. V. Lehmann, J. Bastide, *J. Am. Chem. Soc.* **1975**, *97*, 6865–6866.
349. G. E. Herberich, H. J. Becker, B. Hessner, L. Zelenka, *J. Organomet. Chem.* **1985**, *280*, 147–151.
350. A. J. Ashe, III, P. Shu, *J. Am. Chem. Soc.* **1971**, *93*, 1804–1805.
351. G. E. Herberich, H. J. Becker, K. Carsten, C. Engelke, W. Koch, *Chem. Ber.* **1976**, *109*, 2382–2388.
352. H. Braunschweig, Q. Ye, K. Radacki, *Chem. Commun.* **2012**, *48*, 2701–2703.
353. H. Braunschweig, R. D. Dewhurst, K. Radacki, B. Wennemann, Q. Ye, *Chem. Commun.* **2015**, *15*, 15465–15468.
354. J. M. Maher, R. P. Beatty, N. J. Cooper, *Organometallics* **1985**, *4*, 1354–1361.
355. N. Koelle, *J. Organomet. Chem.* **1977**, *133*, 53–58.
356. P. Geymayer, E. G. Rochow, U. Wannagat, *Angew. Chem. Int. Ed.* **1964**, *3*, 633.
357. P. Geymayer, E. G. Rochow, U. Wannagat, *Angew. Chem.* **1964**, *76*, 499–500.
358. O. A. Gansow, B. Y. Kimura, G. R. Dobson, R. A. Brown, *J. Am. Chem. Soc.* **1971**, *93*, 5922–5924.
359. P. S. Braterman, D. W. Milne, E. W. Randall, E. Rosenburg, *J. Chem. Soc., Dalton Trans.* **1973**, 1027–1031.
360. F. A. Cotton, C. S. Kraihanzel, *J. Am. Chem. Soc.* **1962**, *84*, 4432–4438.
361. C. S. Kraihanzel, F. A. Cotton, *Inorg. Chem.* **1963**, *2*, 533–540.

362. F. A. Cotton, *Inorg. Chem.* **1964**, *3*, 702–711.
363. G. D. Frey, K. Öfele, H. G. Krist, E. Herdtweck, W. A. Herrmann, *Inorg. Chim. Acta* **2006**, *359*, 2622–2634.
364. G. O. Spessard, G. L. Miessler, *Organometallic Chemistry*; Prentice-Hall, Inc: Upper Saddle River, NJ, **1997**; pp 63–64.
365. J. D. Pérez, G. I. Yranzo, L. M. Phagouapé, *Bull. Soc. Chim. Fr.* **1986**, 129–132.
366. V. Metail, S. Joanteguy, A. Chrostowska-Senio, G. Pfister-Guillouzo, A. Systermans, J. L. Ripoll, *Inorg. Chem.* **1997**, *36*, 1482–1487.
367. V. Lefèvre, J. L. Ripoll, Y. Dat, S. Joantéguy, V. Métail, A. Chrostowska-Senio, G. Pfister-Guillouzo, *Organometallics* **1997**, *16*, 1635–1640.
368. J. Levillain, G. Pfister-Guillouzo, J. L. Ripoll, *Eur. J. Org. Chem.* **2000**, 3253–3259.
369. H. Braunschweig, K. Geetharani, J. O. C. Jimenez-Halla, M. Schäfer, *Angew. Chem. Int. Ed.* **2014**, *53*, 3500–3504.
370. H. Braunschweig, K. Geetharani, J. O. C. Jimenez-Halla, M. Schäfer, *Angew. Chem.* **2014**, *126*, 3568–3572.
371. S. Bertsch, *Dissertation*, Julius-Maximilians-Universität Würzburg, **2014**.
372. C. Kayser, D. Frank, J. Baumgartner, C. Marschner, *J. Organomet. Chem.* **2003**, *667*, 149–153.
373. M. Zirngast, M. Flock, J. Baumgartner, C. Marschner, *J. Am. Chem. Soc.* **2009**, *131*, 15952–15962.
374. H. Arp, M. Zirngast, C. Marschner, J. Baumgartner, K. Rasmussen, P. Zark, T. Müller, *Organometallics* **2012**, *31*, 4309–4319.
375. A. J. Blakeney, J. A. Gladysz, *J. Organomet. Chem.* **1980**, *202*, 263–267.
376. J. A. Gladysz, *Acc. Chem. Res.* **1984**, *17*, 326–332.
377. T. D. Tilley, *Organometallics* **1985**, *4*, 1452–1457.
378. T. D. Tilley, *J. Am. Chem. Soc.* **1985**, *107*, 4084–4085.
379. J. Arnold, T. D. Tilley, *J. Am. Chem. Soc.* **1985**, *107*, 6409–6410.
380. J. Arnold, D. N. Shina, T. D. Tilley, A. M. Arif, *Organometallics* **1986**, *5*, 2037–2044.
381. J. Arnold, T. D. Tilley, A. L. Rheingold, *J. Am. Chem. Soc.* **1986**, *108*, 5355–5356.
382. B. D. Campion, J. Falk, T. D. Tilley, *J. Am. Chem. Soc.* **1987**, *109*, 2049–2056.
383. L. Nyulászi, *Chem. Rev.* **2001**, *101*, 1229–1246.
384. J. M. Breunig, A. Hübner, M. Bolte, M. Wagner, H.-W. Lerner, *Organometallics* **2013**, *32*, 6792–6799.
385. W. Gee, R. A. Shaw, B. C. Smith, G. J. Bullen, *Proc. Chem. Soc.* **1961**, 432.
386. J.-N. Li, L. Liu, Y. Fu, Q.-X. Guo, *Tetrahedron* **2006**, *62*, 4453–4462.
387. K. Issleib, W. Seidel, *Chem. Ber.* **1959**, *92*, 2681–2694.
388. H. Niebergall, *Angew. Chem.* **1960**, *72*, 210.
389. G. E. Coates, J. G. Livingstone, *J. Chem. Soc.* **1961**, 1000–1008.
390. H. Nöth, W. Schrägle, *Z. Naturforsch.* **1961**, *16b*, 473–474.
391. H. Nöth, W. Schrägle, *Chem. Ber.* **1964**, *97*, 2218–2229.
392. H. Nöth, W. Schrägle, *Chem. Ber.* **1964**, *97*, 2374–2384.
393. H. Nöth, W. Schrägle, *Chem. Ber.* **1965**, *98*, 352–362.
394. E. Fluck, K. Issleib, *Chem. Ber.* **1965**, *98*, 2674–2680.

395. W. Becker, H. Nöth, *Chem. Ber.* **1972**, *105*, 1962–1971.
396. X. Pan, Y. Su, X. Chen, Y. Zhao, Y. Li, J. Zuo, X. Wang, *J. Am. Chem. Soc.* **2013**, *135*, 5561–5564.
397. H. Staub, R. Guillet-Nicolas, N. Even, L. Kayser, F. Kleitz, F.-G. Fontaine, *Chem. Eur. J.* **2011**, *17*, 4254–4265.
398. H. Braunschweig, D. Rais, K. Uttinger, *Angew. Chem. Int. Ed.* **2005**, *44*, 3763–3766.
399. H. Braunschweig, D. Rais, K. Uttinger, *Angew. Chem.* **2005**, *117*, 3829–3832.
400. H. Braunschweig, K. Radacki, D. Rais, K. Uttinger, *Organometallics* **2006**, *25*, 5159–5164.
401. H. Braunschweig, K. Radacki, K. Uttinger, *Eur. J. Inorg. Chem.* **2007**, 4350–4356.
402. H. Braunschweig, P. Brenner, R. D. Dewhurst, M. Kaupp, R. Müller, S. Östreicher, *Angew. Chem. Int. Ed.* **2009**, *48*, 9735–9738.
403. H. Braunschweig, P. Brenner, R. D. Dewhurst, M. Kaupp, R. Müller, S. Östreicher, *Angew. Chem.* **2009**, *121*, 9916–9919.
404. H. Braunschweig, K. Radacki, R. Shang, *Chem. Commun.* **2013**, *49*, 9905–9907.
405. H. Braunschweig, K. Radacki, R. Shang, *Chem. Sci.* **2015**, *6*, 2989–2996.
406. C. Müller, C. N. Iverson, R. J. Lachicotte, W. D. Jones, *J. Am. Chem. Soc.* **2001**, *123*, 9718–9719.
407. H. Braunschweig, R. D. Dewhurst, C. Hörl, A. K. Phukan, F. Pinzner, S. Ullrich, *Angew. Chem. Int. Ed.* **2014**, *53*, 3241–3244.
408. H. Braunschweig, R. D. Dewhurst, C. Hörl, A. K. Phukan, F. Pinzner, S. Ullrich, *Angew. Chem.* **2014**, *126*, 3305–3308.
409. I. Bejan, D. Scheschkewitz, *Angew. Chem. Int. Ed.* **2007**, *46*, 5783–5786.
410. I. Bejan, D. Scheschkewitz, *Angew. Chem.* **2007**, *119*, 5885–5888.
411. J. Jeck, I. Bejan, A. J. P. White, D. Nied, F. Breher, D. Scheschkewitz, *J. Am. Chem. Soc.* **2010**, *132*, 17306–17315.
412. H. Braunschweig, V. Dyakonov, B. Engels, Z. Falk, C. Hörl, J. H. Klein, T. Kramer, H. Kraus, I. Krummenacher, C. Lambert, C. Walter, *Angew. Chem. Int. Ed.* **2013**, *52*, 12852–12855.
413. H. Braunschweig, V. Dyakonov, B. Engels, Z. Falk, C. Hörl, J. H. Klein, T. Kramer, H. Kraus, I. Krummenacher, C. Lambert, C. Walter, *Angew. Chem.* **2013**, *125*, 13088–13092.
414. K. Sonogashira, S. Takahashi, N. Hagihara, *Macromolecules* **1977**, *10*, 879–880.
415. S. Takahashi, M. Kariya, T. Yatake, K. Sonogashira, N. Hagihara, *Macromolecules* **1978**, *11*, 1063–1066.
416. M. S. Khan, A. K. Kakkar, N. J. Long, J. Lewis, P. Raithby, P. Nguyen, T. B. Marder, F. Wittmann, R. H. Friend, *J. Mater. Chem.* **1994**, *4*, 1227–1232.
417. M. Parthey, K. B. Vincent, M. Renz, P. A. Schauer, D. S. Yufit, J. A. K. Howard, M. Kaupp, P. J. Low, *Inorg. Chem.* **2014**, *53*, 1544–1554.
418. N. Wang, S.-B. Ko, J.-S. Lu, L. D. Chen, S. Wang, *Chem. Eur. J.* **2013**, *19*, 5314–5323.
419. K. Sonogashira, Y. Fujikura, T. Yatake, N. Toyoshima, S. Takahashi, N. Hagihara, *J. Organomet. Chem.* **1978**, *145*, 101–108.
420. A. Sebald, B. Wrackmeyer, W. Beck, *Z. Naturforsch.* **1983**, *38b*, 45–56.

421. J. P. Carpenter, C. M. Lukehart, *Inorg. Chim. Acta* **1991**, *190*, 7–10.
422. M. Carlsson, B. Eliasson, *Organometallics* **2006**, *25*, 5500–5502.
423. K. Haskins-Glusac, M. R. Pinto, C. Tan, K. S. Schanze, *J. Am. Chem. Soc.* **2004**, *126*, 14964–14971.
424. G. W. Parshall, *Inorg. Synth.* **1970**, *12*, 26–33.
425. F. R. Hartley, *Organomet. Chem. Rev. A* **1970**, *6*, 119–137.
426. E. Matern, J. Pikies, G. Fritz, *Z. Anorg. Allg. Chem.* **2000**, *626*, 2136–2142.
427. D. E. Berry, *J. Chem. Educ.* **1994**, *71*, 899–902.
428. B. Alameddine, O. F. Aebischer, W. Amrein, B. Donnio, R. Deschenaux, D. Guillon, C. Savary, D. Scanu, O. Scheidegger, T. A. Jenny, *Chem. Mater.* **2005**, *17*, 4798–4807.
429. Q. Xiao, R. T. Ranasinghe, A. M. P. Tang, T. Brown, *Tetrahedron* **2007**, *63*, 3483–3490.
430. W. A. Chalifoux, R. R. Tykwinski, *Nature Chem.* **2010**, *2*, 967–971.
431. Q. Zheng, J. C. Bohling, T. B. Peters, A. C. Frisch, F. Hampel, J. A. Gladysz, *Chem. Eur. J.* **2006**, *12*, 6486–6505.
432. T. Gibtner, F. Hampel, J.-P. Gisselbrecht, A. Hirsch, *Chem. Eur. J.* **2002**, *8*, 408–432.
433. W. Mohr, J. Stahl, F. Hampel, J. A. Gladysz, *Chem. Eur. J.* **2003**, *9*, 3324–3330.
434. S. Eisler, A. D. Slepkov, E. Elliot, T. Luu, R. McDonald, F. A. Hegmann, R. R. Tykwinski, *J. Am. Chem. Soc.* **2005**, *127*, 2666–2676.
435. B. Wrackmeyer, A. Sebald, *J. Organomet. Chem.* **1997**, *544*, 105–114.
436. Q. Ye, *Dissertation*, Julius-Maximilians-Universität Würzburg, **2012**.
437. H. Günther, *NMR-Spektroskopie*, 2nd ed.; Georg Thieme Verlag: Stuttgart, **1983**.
438. A. S. Hay, *J. Org. Chem.* **1962**, *27*, 3320–3321.
439. C. Glaser, *Ber. Dtsch. Chem. Ges.* **1869**, *2*, 422–424.
440. C. Glaser, *Justus Liebigs Ann. Chem.* **1870**, *154*, 137–171.
441. M. Akita, M. Terada, S. Oyama, Y. Moro-oka, *Organometallics* **1990**, *9*, 816–825.
442. J. J. Eisch, B. W. Kotowicz, *Eur. J. Inorg. Chem.* **1998**, 761–769.
443. W. Haubold, U. Kraatz, *Z. Anorg. Allg. Chem.* **1976**, *421*, 105–110.
444. A. G. Davies, B. Wrackmeyer, *Tin Chemistry: Fundamentals, Frontiers and Applications*, 1st ed.; John Wiley & Sons, Ltd: West Sussex, **2008**; pp 1–52.
445. J. Mies, *Dissertation*, Julius-Maximilians-Universität Würzburg, **2013**.
446. T. J. Kealy, P. L. Pauson, *Nature* **1951**, *168*, 1039–1040.
447. S. A. Miller, J. A. Tebboth, J. F. Tremaine, *J. Chem. Soc.* **1952**, 632–635.
448. L. Pauling, *The Nature of the Chemical Bond*, 3rd ed.; Cornell University Press: Ithaca, New York, **1960**.
449. G. E. Herberich, W. Klein, T. P. Spaniol, *Organometallics* **1993**, 12, 2660–2667.
450. T. Hascall, V. Beck, S. Barlow, A. R. Cowley, D. O'Hare, *Organometallics* **2004**, *23*, 3808–3813.
451. J. F. Cordes, *Chem. Ber.* **1962**, *95*, 3084–3085.
452. G. Wilkinson, P. L. Pauson, F. A. Cotton, *J. Am. Chem. Soc.* **1954**, *76*, 1970–1974.
453. H. Nöth, H. Pommerening, *Chem. Ber.* **1981**, *114*, 398–399.

454. P. P. Power, *Chem. Rev.* **1999**, *99*, 3463–3503.
455. R. C. Fischer, P. P. Power, *Chem. Rev.* **2010**, *110*, 3877–3923.
456. G. E. McManis, R. M. Nielson, M. J. Weaver, *Inorg. Chem.* **1988**, *27*, 1827–1829.
457. P. Zanello, *Inorganic Electrochemistry: Theory, Practice, and Applications*, 1st ed.; RSC Publishing: Cambridge, **2003**.
458. R. F. Winter, *Organometallics* **2014**, *33*, 4517–4536.
459. P. McArdle, A. R. Manning, *J. Chem. Soc. A* **1971**, 717–719.
460. H. Braunschweig, B. Ganter, *J. Organomet. Chem.* **1997**, *545*, 163–167.
461. W. Stüer, B. Weberndörfer, J. Wolf, H. Werner, *Dalton Trans.* **2005**, 1796–1803.
462. D. Drew, J. R. Doyle, *Inorg. Synth.* **1990**, *28*, 346–351.
463. J. E. Bercaw, R. H. Marvich, L. G. Bell, H. H. Brintzinger, *J. Am. Chem. Soc.* **1972**, *94*, 1219–1238.
464. S. Otsuka, T. Yoshida, M. Matsumoto, K. Nakatsu, *J. Am. Chem. Soc.* **1976**, *98*, 5850–5858.
465. T. Schaub, U. Radius, *Chem. Eur. J.* **2005**, *11*, 5024–5030.
466. H. Werner, J. Wolf, U. Schubert, K. Ackermann, *J. Organomet. Chem.* **1983**, *243*, C63–C70.
467. W. J. Grigsby, P. P. Power, *J. Am. Chem. Soc.* **1996**, *118*, 7981–7988.
468. D. A. Gaul, O. Just, W. S. Rees, Jr, *Inorg. Chem.* **2000**, *39*, 5648–5654.
469. H. Gilman, C. L. Smith, *J. Am. Chem. Soc.* **1964**, *86*, 1454.
470. H. Gilman, C. L. Smith, *J. Organomet. Chem.* **1967**, *8*, 245–253.
471. K. Issleib, K. Krech, K. Gruber, *Chem. Ber.* **1963**, *96*, 2186–2192.
472. H. D. Verkruijsse, L. Brandsma, *Synth. Commun.* **1991**, *21*, 657–659.
473. L. Brandsma, *Synthesis of Acetylenes, Allenes, and Cumulenes: Methods and Techniques*; Elsevier Academic Press: Oxford, UK, **2004**; pp 212–213.
474. E. Payet, A. Auffrant, X. F. L. Goff, P. L. Floch, *J. Organomet. Chem.* **2010**, *695*, 1499–1506.
475. R. J. Brotherton, A. L. McCloskey, J. L. Boone, H. M. Manasevit, *J. Am. Chem. Soc.* **1960**, *82*, 6245–6248.
476. E. L. Gall, K. B. Aïssi, I. Lachaise, M. Troupel, *Synlett* **2006**, 954–956.
477. N. Kuhn, T. Kratz, *Synthesis* **1993**, 561–562.
478. M. J. Frisch, G. W. Trucks, H. B. Schlegel, G. E. Scuseria, M. A. Robb, J. R. Cheeseman, J. A. Montgomery, Jr., T. Vreven, K. N. Kudin, J. C. Burant, J. M. Millam, S. S. Iyengar, J. Tomasi, V. Barone, B. Mennucci, M. Cossi, G. Scalmani, N. Rega, G. A. Petersson, H. Nakatsuji, M. Hada, M. Ehara, K. Toyota, R. Fukuda, J. Hasegawa, M. Ishida, T. Nakajima, Y. Honda, O. Kitao, H. Nakai, M. Klene, X. Li, J. E. Knox, H. P. Hratchian, J. B. Cross, V. Bakken, C. Adamo, J. Jaramillo, R. Gomperts, R. E. Stratmann, O. Yazyev, A. J. Austin, R. Cammi, C. Pomelli, J. W. Ochterski, P. Y. Ayala, K. Morokuma, G. A. Voth, P. Salvador, J. J. Dannenberg, V. G. Zakrzewski, S. Dapprich, A. D. Daniels, M. C. Strain, O. Farkas, D. K. Malick, A. D. Rabuck, K. Raghavachari, J. B. Foresman, J. V. Ortiz, Q. Cui, A. G. Baboul, S. Clifford, J. Cioslowski, B. B. Stefanov, G. Liu, A. Liashenko, P. Piskorz, I. Komaromi, R. L. Martin, D. J. Fox, T. Keith, M. A. Al-Laham, C. Y. Peng, A. Nanayakkara, M. Challacombe, P. M. W. Gill, B. Johnson, W. Chen, M. W. Wong, C. Gonzalez, J. A. Pople, Gaussian 03, Revision E.01. Gaussian, Inc., Wallingford, CT, **2004**.

479. Jmol: an open-source Java viewer for chemical structures in 3D. <http://www.jmol.org>
480. G. te Velde, F. M. Bickelhaupt, E. J. Baerends, C. Fonseca Guerra, S. J. A. van Gisbergen, J. G. Snijders, T. Ziegler, *J. Comp. Chem.* **2001**, *22*, 931–967.
481. Amsterdam Density Functional, Theoretical Chemistry, Vrije Universiteit, Amsterdam, The Netherlands. <http://www.scm.com>
482. A. D. Becke, *J. Chem. Phys.* **1993**, *98*, 1372–1377.
483. F. Weigend, R. Ahlrichs, *Phys. Chem. Chem. Phys.* **2005**, *7*, 3297–3305.
484. N. C. Handy, A. J. Cohen, *Mol. Phys.* **2001**, *99*, 403–412.
485. R. C. Raffenetti, *J. Chem. Phys.* **1973**, *59*, 5936–5950.
486. D. P. Chong, E. van Lenthe, S. J. A. van Gisbergen, E. J. Baerends, *J. Comp. Chem.* **2004**, *25*, 1030–1036.
487. E. van Lenthe, E. J. Baerends, *J. Comp. Chem.* **2003**, *24*, 1142–1156.
488. D. P. Chong, *Mol. Phys.* **2005**, *103*, 749–761.
489. E. van Lenthe, E. J. Baerends, J. G. Snijders, *J. Chem. Phys.* **1993**, *99*, 4597–4610.
490. E. van Lenthe, E. J. Baerends, J. G. Snijders, *J. Chem. Phys.* **1994**, *101*, 9783–9792.
491. E. van Lenthe, A. E. Ehlers, E. J. Baerends, *J. Chem. Phys.* **1999**, *110*, 8943–8953.
492. R. Bouten, E. J. Baerends, E. van Lenthe, L. Visscher, G. Schreckenbach, T. Ziegler, *J. Phys. Chem. A* **2000**, *104*, 5600–5611.
493. F. M. Bickelhaupt, E. J. Baerends, Kohn-Sham Density Functional Theory: Predicting and Understanding Chemistry. In *Reviews in Computational Chemistry*; K. B. Lipkowitz, D. B. Boyd, Eds.; Wiley-VCH: New York, **2000**.
494. K. Morokuma, *Acc. Chem. Res.* **1977**, *10*, 294–300.
495. T. Ziegler, A. Rauk, E. J. Baerends, *Theo. Chim. Acta* **1977**, *43*, 261–271.
496. G. Sheldrick, *Acta Crystallogr. Sect. A* **2008**, *A64*, 112–122.